# SULPHATED AND NON-SULPHATED DISACCHARIDES: CELLULAR AND MOLECULAR MECHANISMS OF ACTION IN MACROPHAGE FUNCTION

**Prabhjot Bajwa**

**School of Health Sport and Bioscience, University of East London**

**December 2021**

**A thesis submitted in partial fulfilment of the requirements of the University of East London for the degree of Doctor of Philosophy**

**Abstract**

Sulphated disaccharides are degradation products of heparinase that are released by inflammatory cells at sites of inflammation. Recent studies have shown that heparin derived sulphated disaccharides inhibit macrophage TNF-α synthesis, delayed-type hypersensitivity, rat adjuvant and rat and mouse collagen induced arthritis, with indications that they act on T-cell and macrophage function. The mechanisms by which these occur are unknown. Therefore, this study aims to investigate the mechanism of action of sulphated disaccharides through which they produce an inhibitory effect. In this study, the impact of sulphated disaccharides was tested on monocyte-macrophage functions *in vitro.*

In this study, it was established that sulphated disaccharides inhibit PMA-stimulated macrophage-like cell differentiation ($10^{-11}$ – $10^{-4}$ M). The reduced numbers of adherent macrophages cells leads to the reduction of pro-inflammatory macrophages. Inhibition of phosphorylation of p38 and ERK1/2 was found and was directly proportional to sulphated disaccharide structural features, namely selective (HDS-I, HDS-III) or oligosulphation (SOS, DOS). Pre-incubation of monocytes with sulphated disaccharides inhibited PMA-induced calcium mobilisation. In addition, this study demonstrated that treatment with sulphated disaccharides induces a phenotypic switch of differentiated macrophages into an anti-inflammatory phenotype and also the pro-inflammatory phenotype into an anti-inflammatory phenotype.

The current study provides an insight into the possibility of targeting inhibition of monocyte-macrophage-differentiation through inhibition of calcium mobilisation, leading to de-activation of p38 and ERK1/2 MAPK, TNF-α production, and ultimately inhibition of cell-differentiation induced cell surface adhesion molecule expression. In addition, sulphated disaccharides promote macrophage divergence towards an anti-inflammatory phenotype. The findings of this study indicate that sulphate disaccharides exhibit their inhibitory action even at very low concentrations, especially the oligosulphated compounds. Thus, suggesting a novel molecular mechanism for the treatment of macrophage-dependent chronic inflammatory diseases.

## Table of Contents

## List of tables

## List of figures

## Abbreviations

| | |
|---|---|
| AEBSF | 4-(2-aminoethyl) benzenesulfonyl fluoride |
| APC | Antigen presenting cell |
| BSA | Bovine Serum Albumin |
| CDx | Cluster of differentiation x, where x=number. |
| COX-# | Cyclooxygenase-#, where #=number. |
| DMSO | Dimethyl sulfoxide |
| DOS | diGaS; Di-glucopyranosylamine oligosulphate. |
| DMARD | Disease modifying anti-rheumatic drug |
| dNTPs | deoxyribose-nucleoside triphosphate |
| dATP | deoxyribose-adenosine triphosphate |
| dGTP | deoxyribose-guanosine triphosphate |
| dCTP | deoxyribose-cytidine triphosphate |
| dTTP | deoxyribose-thymidine triphosphate |
| E64 | 4-(2-aminoethyl) benzenesulfonyl fluoride (AEBSF), pepstatin A, bestatin, leupeptin, aprotinin and trans-epoxysuccinyl-L-leucyl-amido(4-guanidino)-butane |
| ECACC | European Collection of Cell Culture |
| EDTA | Ethylenediaminetetraacetic acid |
| ELAM-1 Selectin | Endothelial-leucocyte adhesion molecule, CD62e, E- |
| ERK-1 | Extracellular signal-regulated kinase-1, Mitogen-activated protein kinase 3, MAPK3 |
| ERK-2 | Extracellular signal-regulated kinase-2, Mitogen-activated protein kinase 1, also MAPK1, p42MAPK |
| FACS | Fluorescence activated cell sorter |
| FBS | Foetal bovine serum |
| FCS | Foetal calf serum |
| FITC | Fluorescein isothiocyanate |

| | |
|---|---|
| Fluo-4 AM | Fluo-4 acetoxymethyl ester |
| fMLP | formyl-Met-Leu-Phe |
| HDS-I | HDS-1S; C12H15NNa4O19S3 ; Heparin disaccharide I-S sodium salt; tetrasodium;(2R,3R,4S)-2-[(2R,3S,4R,5R)-4,6-dihydroxy-5-(sulfonatoamino)-2-(sulfonatooxymethyl)oxan-3-yl]oxy-4-hydroxy-3-sulfonatooxy-3,4-dihydro-2H-pyran-6-carboxylate |
| HDS-III | HDS-IIIH; C12H18NNa2O13S ; heparin disaccharide III-H sodium salt; sodium;(2R,3R,4S)-2-[(2R,3S,4R,5R)-5-azaniumyl-4,6-dihydroxy-2-(hydroxymethyl)oxan-3-yl]oxy-4-hydroxy-3-sulfonatooxy-3,4-dihydro-2H-pyran-6-carboxylate |
| HRP | Horse radish peroxidase |
| ICAM-# | Intercellular adhesion molecule class #, where #=number |
| IkBα | NFκBI, NFκB inhibitor |
| IL-# | Interleukin-#, where x = number |
| LPS | lipopolysaccharide; endotoxin |
| MAPK | MAP Kinase, p38 |
| MAPK-1 | ERK-2, extracellular signal-regulated kinase-1, Mitogen-activated protein kinase 1, p42MAPK |
| MAPK-3 | Mitogen-activated protein kinase 3, Extracellular signal-regulated kinase-1 |
| MHC | Major Histocompatibility Complex |
| MTT bromide | 3-(4,5-dimethythiazol-2-yl)-2,5-diphenyl tetrazolium |
| NF-κB | Nuclear factor kappa B |
| p38 | p38 MAP Kinase (MAPK), comprising p38-α (MAPK14), -β (MAPK11), -γ (MAPK12 / ERK6), and -δ (MAPK13 / SAPK4 |
| PD98059 | $C_{16}H_{13}NO_3$ ; 2'-Amino-3'-methoxyflavone |
| PBS | Phosphate buffered saline |
| PCR | Polymerase chain reaction |
| PE | Phycoerythrin |

| | |
|---|---|
| PMA | Phorbol myristate acetate |
| PRR | Pattern recognition receptor |
| RA | Rheumatoid arthritis |
| RPMI-1640 | Roswell Park Memorial Institute -1640 cell culture medium |
| RT-PCR | Real-time polymerase chain reaction |
| SB203580 | $C_{21}H_{16}FN_3OS$ ; 4-[4-(4-fluorophenyl)-2-(4-methylsulfinylphenyl)-1*H*-imidazol-5-yl]pyridine. |
| SDS | sodium dodecyl sulphate |
| SOS | Sucrose octasulphate; C12H14Na8O35S8 ; octasodium;[(2R,3R,4S,5R,6R)-2-[(2S,3S,4R,5R)-3,4-disulfonatooxy-2,5- bis(sulfonatooxymethyl)oxolan-2-yl]oxy-3,5-disulfonatooxy-6-(sulfonatooxymethyl)oxan-4-yl] sulphate |
| TAE buffer | 40 mM Tris, 20 mM acetic acid, 1 mM EDTA |
| TBS | Tris buffered saline |
| Th0 | T-helper cell |
| Th# | T-helper cell subclass x, where # = number |
| THP-1 | Human monocyte; DSMZ; catalogue number: ACC-16 |
| TMED | N,N,N',N'- tetramethylethylenediamine |
| Treg | T regulatory cell |
| Tris | Trizma; 2-Amino-2-(hydroxymethyl)propane-1,3-dio |
| Trizol | Guanidinium thiocyanate; guanidinium isothiocyanate |
| TLR | Toll like receptor |
| TNF-α | Tumour necrosis factor |
| U937 | Human histiocytic monocytes; ECACC; catalogue number: 85011440 |
| VCAM-1 | Vascular cell adhesion molecule-1, CD106 |

## Acknowledgements

I would like to acknowledge the guidance, encouragement, and inspiration provided by Prof Michael Seed, Dr Samir Ayoub, and Dr Natividad Garrido Mesa without whom this thesis would not have been possible.

I would like to acknowledge the kind gift of di-glucopyranosylamine (DOS) from Dr M Burnet, Synovo GmH, Germany.

I would like to thank my parents, brother, and husband for their constant encouragement and support.

# CHAPTER 1: INTRODUCTION

# 1. Introduction

Rheumatoid arthritis (RA) is a systemic chronic inflammatory auto-immune disease accompanied by severe disability, significant morbidity and mortality. It has a 20$^{th}$ century pedigree, with 19$^{th}$ century roots. The term rheumatoid arthritis was coined by Garrod in 1859 (Storey, *et al*., 1994). Research into the aetiology and pathology of RA started in earnest in the 1960s and has accelerated rapidly during the past decades to the point where RA is now accepted as the prototypic inflammatory disease. One of the major advances in our understanding of RA has been the development of animal models of this disease. The first model, adjuvant arthritis, was developed in the mid-1950s, and the other models such as antigen-induced arthritis, and collagen-induced arthritis have been used in a large number of investigations ranging from fundamental studies of the aetiology and pathogenesis of RA to their response to known or novel drugs. The presently available therapeutics are rather unsatisfactory, being suboptimally effective and having considerable, and sometimes severe and life-threatening side effects (Pincus *et al*., 1992). As the current study bears relevance to RA. the clinical picture of RA is reviewed followed by a discussion of current and future therapeutics for this condition. It is anticipated that this study will contribute to the development of more effective therapeutic interventions.

## 1.1 Pathogenesis of Rheumatoid Arthritis

RA has a worldwide distribution but most epidemiological surveys have used the criteria defined by Ropes *et al.*, in 1958. As per Ropes criteria, RA affects 1:100 of the global population with a female preponderance to male ratio of 3:1 (Edwards, *et al.,* 1999). It is caused by the body's immune system erroneously attacking its healthy tissues. It can affect diarthrodial joints, lungs, eyes, blood vessels, skin, and heart. It has become a significant socio-economic burden on society as it increases the risk of other potential diseases such as cardiovascular disease, depression, and fatigue (Dayer & Choy, 2010 and Pollard *et al.,* 2005). The mortality rate of RA patients is greater (Buch and Emery 2002, Wolfe *et al.,* 1994).

Without knowing the causative agent, it is impossible to describe accurately how RA is initiated. Rheumatoid arthritis is characterized by persistent synovitis, systemic inflammation, and autoantibodies. RA is a disease with a wide clinical spectrum and is often difficult to diagnose in the early stage of onset. Many patients may present with non-specific systemic features such as malaise, weight loss, and, a low-grade fever associated with the onset of pain, stiffness, and swelling of one or more joints. Characteristically the small joints of the hands, wrists, and feet are affected first in a symmetrical fashion but any synovial joint can be involved. There are three major pathological entities in RA; local tissue inflammation (which is consists of a mixed inflammatory cell infiltrate in which lymphocytes, plasma cells, and macrophages predominate. It is associated with local tissue damage and reparative fibrosis, the rheumatoid nodule which is serpiginous consisting of tissue necrosis surrounded by rapidly orientated lines of macrophages. When the nodule occurs in fibrous connective tissues, as it most commonly does, the collagen necrosis appears to be complete, but when viewed with crossed polarizing microscopy residual collagen fibre can be seen traversing the areas of necrosis). Vasculitis in RA may also affect the arterial or venous sides of the circulation (Collins, 1937 and Scott *et al*., 1981). Within the diarthrodial joints of patients with RA, chronic tissue inflammation is the predominant mechanism leading to the tissue changes, rheumatoid nodule formation, and vasculitis being rare (Cruikshank, 1954 and Gardner, 1972). In any individual the disease may be in different stages of evolution in different

joints. There are three forms of clinical presentation in which most cases of RA can broadly be recognized. A chronic progressive form of the disease begins with minimal joint involvement and then progresses slowly over years to multiple joint diseases with severe functional limitations. This is the most common pattern of arthritis seen. The second is an intermittent course that is punctuated by acute episodes of arthritis with periods of remission in between. The third form is an explosive onset with multiple joint involvements and acute synovitis which may go into partial remission after three years or so. This pattern of RA is more commonly seen when RA begins in the elderly patient (Henderson *et al*., 1995).

Cells of the myelomonocytic lineage differentiate into numerous cell types that are involved in RA disease, for instance monocytes, macrophages, osteoclasts and dendritic cells. Activation of these cells leads to the production of cytokines and mediators responsible for inflammation. Monocytes are central to the RA pathology as they accumulate in the blood and continuously migrate into the inflamed joints where they acquire an activated phenotype and can differentiate into inflammatory macrophages, dendritic cells, and osteoclasts (Ammari *et al.,* 2018 and Goudot *et al.,* 2017). As a consequence of their marked plasticity, the differentiation pathways can be influenced by an excess or imbalance of particular pathophysiological stimuli such as cytokines or growth factors, resulting in altered differentiation or maturation if regulatory mechanisms fail. Different immune modulators such as cytokines and effector cells and signalling pathways are known to be involved in the pathophysiology of RA. The complex interactions of cytokines and effector cells result in the joint damage that begins at the synovial membrane (Smolen and Steiner, 2003).

A hallmark of RA pathology is the remarkable increase of cellularity accompanied by angiogenesis in the synovial membrane. The RA joint RA is typified as exhibiting pannus formation, synovitis, bone erosions, and joint destruction. Synovial inflammation is usually a defensive cellular response against invading pathogens but defects in normal mechanisms give rise to RA (Fig.1.1 and Fig.1.2). The major characteristic of RA is symmetric polyarticular inflammation of the synovial membrane which is a connective tissue that lines the inner surface of joint capsules (Kunisch *et al.*, 2004).

The normal joint consists of the bone end covered by articular cartilage and surrounded by a fibrous capsule. The stability of the joint depends upon the structural integrity of the capsule and its ligamentous thickening. The capsule is lined by synovium which is a vascular fibrous or adipose tissue covered, in the normal joint, by an incomplete layer of specialised synovial cells of two types, the type A and type B synoviocytes, which have a special phagocytic and biosynthetic properties respectively. The synovium is involved in producing the synovial fluid which provides lubrication and nourishment for joint movement. The synovial fluid is produced by macrophage-like synoviocytes cells termed type A synoviocytes, which contain 25% of synovial lining cluster of differentiation (CD) cells that include CD14, CD18, and CD68 macrophages. Type B, fibroblast-like cells which express high levels of uridine diphosphoglucose dehydrogenase, play an important role in the synthesis of hyaluronan, a glycosaminoglycan (Edwards and Willoughby 1982).

Depending upon the phase of the disease the rheumatoid synovium contains a mixed inflammatory cell infiltrate in which the major cell types are polymorphs, lymphocytes, plasma cells, and macrophages. Normal cartilage consists of a meshwork of type II collagen fibres that encapsulates aggregates of partially hydrated, hydrophilic glycosaminoglycans. The expansion of the glycosaminoglycans by ingress of water from the synovial fluid is resisted by the collagen fibres, making the cartilage turgid. In RA the inflamed synovium is no longer under the normal homeostatic mechanisms that inhibit the synovial overgrowth of cartilage. The synovium starts to encroach upon the edge of the cartilage at the periphery of the joint. As the synovium overgrows, there is destruction and loss of cartilage. As a consequence this leads to joint space narrowing.

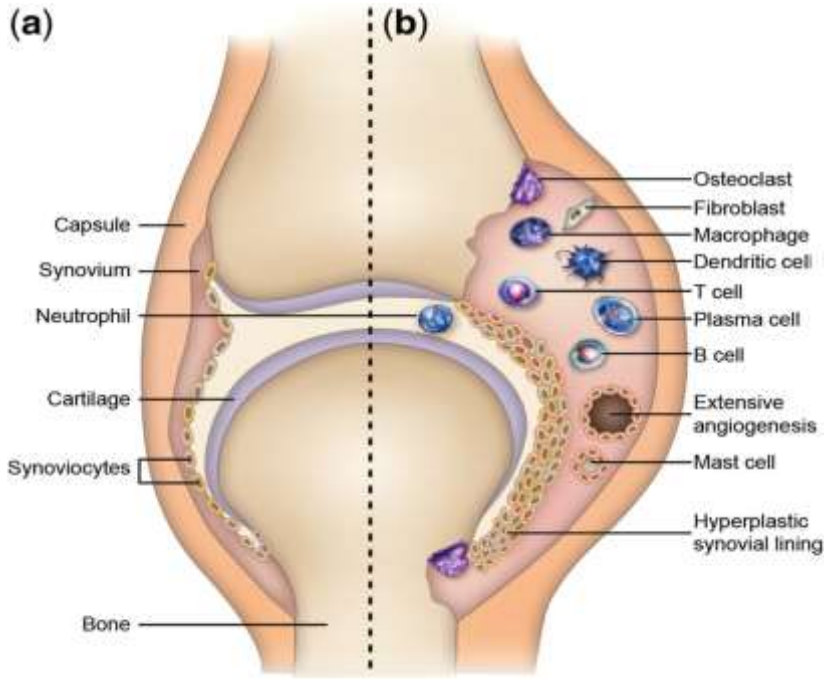


**Figure 1. 1*. Pathology of RA.***

*Schematic view of a normal joint (a) and a RA affected joint (b). In rheumatoid arthritis the synovial membrane becomes thickened. A defect in the immune system allows some B cells and T cells to recognise tissue antigens as foreign. The cells infiltrate the joint and release cytokines. B cells produce auto-antibodies such as Rheumatoid Factor, which target the joint. Pro-inflammatory cytokines stimulate the recruitment and priming of other immune cells including macrophages and neutrophils, that attack the joint. Neutrophils and macrophages release digestive enzymes, which contribute to joint damage including cartilage. (Adapted from, Smolen and Steiner, 2003).*

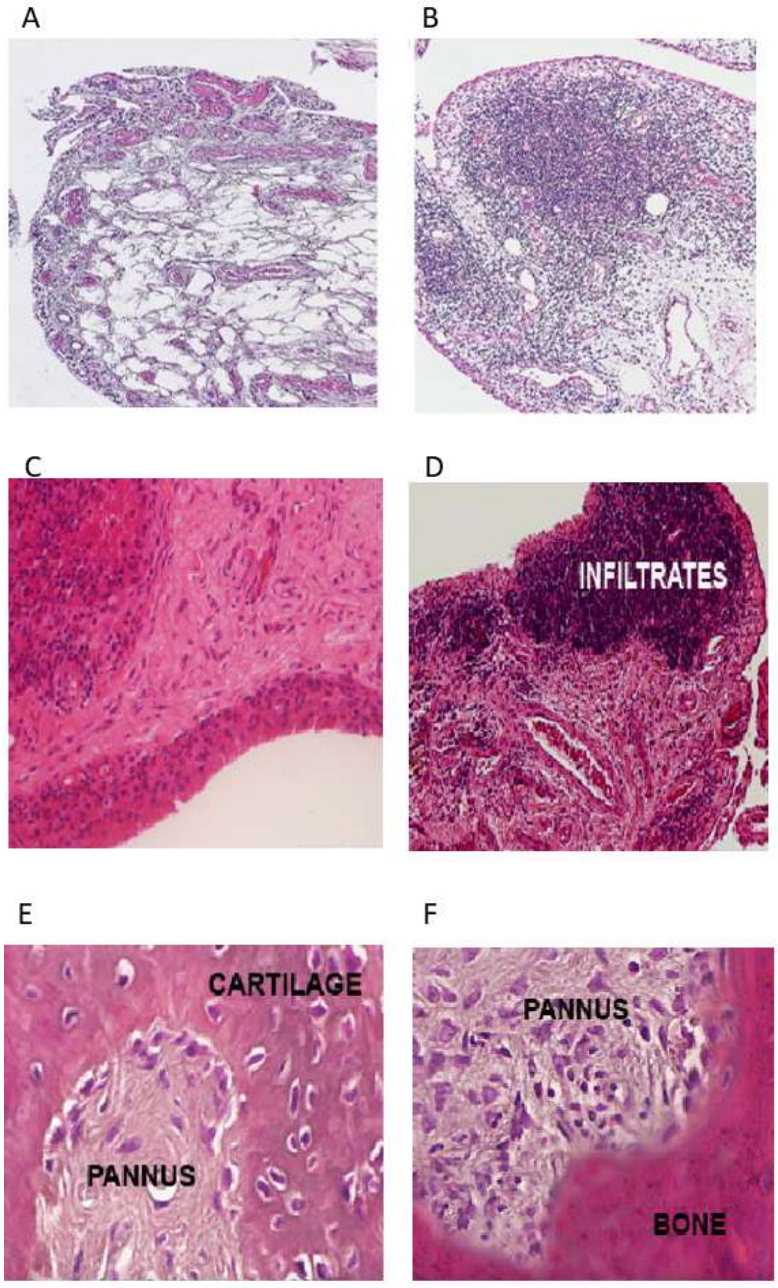


**Figure 1. 2*. Inflammation of Synovium membrane in RA.***

*A) A normal synovium membrane. B) Synovium membrane of a Rheumatoid arthritis patient. C) Synovial lining hyperplasia in RA. D) Macrophage and lymphocyte infiltrate in RA. E) Pannus invasion into cartilage in RA. F) Pannus invasion into the bone in RA The inflammatory auto-immune process takes place primarily in the synovial membrane, but also in the synovial fluid (Figure adapted from, Pitzalis et al., 2013).*

The innate immune response is activated immediately following infection, adaptive immunity as a consequence of reinfection. The synovial CD68 macrophages express major histocompatibility complex II (MHC II) as do antigen presenting cells (APCs) $CD4^+$ T- helper (Th) cells on their surface. MHC II molecules are only found on the surface of APCs, these include macrophages, dendritic cells, and B cells. APCs trigger innate immunity by different mechanisms (Fig.1.3). In humans, the MHC is a cluster of genes located on chromosome 6 that code for MHC proteins also called Human Leukocyte Antigen (HLA). There are two classes of MHC molecules involved in adaptive immunity, MHC I and MHC II. Both types of MHC molecules are transmembrane glycoproteins that assemble as dimers in the cytoplasmic membrane of cells, but their structures are quite different (Fig.1.4). In the innate immune system, the recognition of extracellular pathogens is mainly mediated by macrophages and dendritic cells in the mononuclear phagocyte system. They recognise pathogen-associated molecular patterns (PAMPs) brought by microbes and damage-associated molecular patterns (DAMPs) produced by damaged host cells through antigen-specific surface receptors, including pattern recognition receptors (PRRs) (ten Broeke *et al*., 2013). Toll-like receptors (TLRs) represent a major PRR family. Once their extracellular domains bind PAMPs or DAMPs, the TLRs trigger an intracellular signalling pathway to activate various transcription factors such as nuclear factor-κB (NF-κB). After recognising their specific molecular patterns, APCs internalize antigens by phagocytosis, process them, and display peptide antigen fragments on their surface with MHC II for recognition by the appropriate T-cells (Steinman, 1991; Gaudino and Kumar, 2019).

The synovium is believed to be the seat of the changes that occur in the joint. Normal synovial fluid is present in small amounts, is viscid, and contains less than 100 cells per cubic millimetre. However, in RA the volume of synovial fluid often increases, and its composition and cellularity changes. Some of the cellular changes are typical of RA disease and others reflect the degree of disease activity. In RA, the central process is the presentation of an antigen by APC to T cells to produce a T-helper 1 cells (Th1) and T-helper 17 (Th17) response. The majority of T cells in the synovium carry the CD4 T cells and express class II antigens, indicating that they are activated. However, T cells in the synovial fluid are mostly $CD8^+$. $CD4^+$ T cells are stimulated by interleukin-4 (IL-4) to

develop into Th1/Th17 cells (control-cell mediated responses) and Th2 cells (control antibody-mediated responses) and Treg cells (regulate immune reactions) (Kinne *et al.*, 2002). The main Th1 cytokine is the interferon-gamma (IFN-y). Th17 cells require exact cytokines, i.e. transformation multiplication factor-β (TGF-β) mixed with IL-6 or IL-21 for its differentiation. They are responsible for producing pro-inflammatory cytokines such as tumour necrosis factor (TNF)-α, IL-6, and IL-1. Th1 and Th17 cells are produced parallel to each other and can cause inflammation and autoimmune disease.

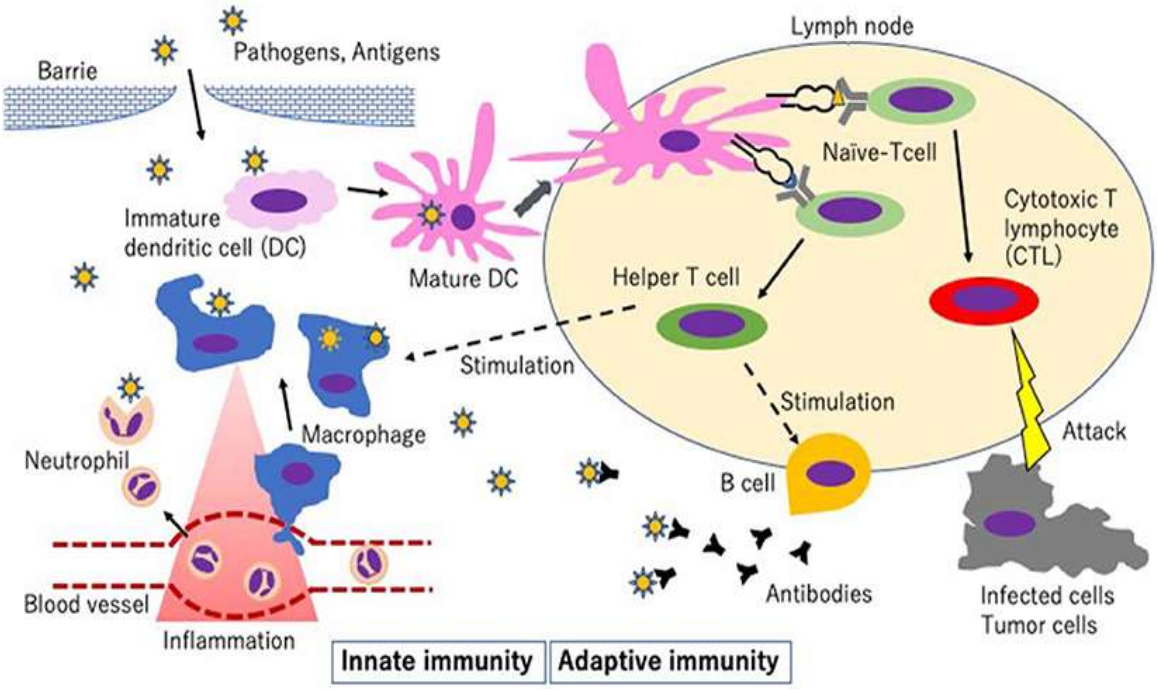


**Figure 1. 3*. A schematic diagram of innate immunity and adaptive immunity.***

*Activation of pattern recognition receptors on tissue-resident macrophages and/or dendritic cells by pathogen-associated molecular patterns resulting in activation of the innate immune response and migration of monocytes (that mature into recruited macrophages and neutrophils in the systemic circulation) and maturation of dendritic cells (which then migrate to the lymph node). Processing of the antigens and their presentation on MHC-I or MHC-II to the T cell receptor on T cells. This leads to the development of adaptive immunity. Figure adapted from (Hatano and Watanabe, 2020).*

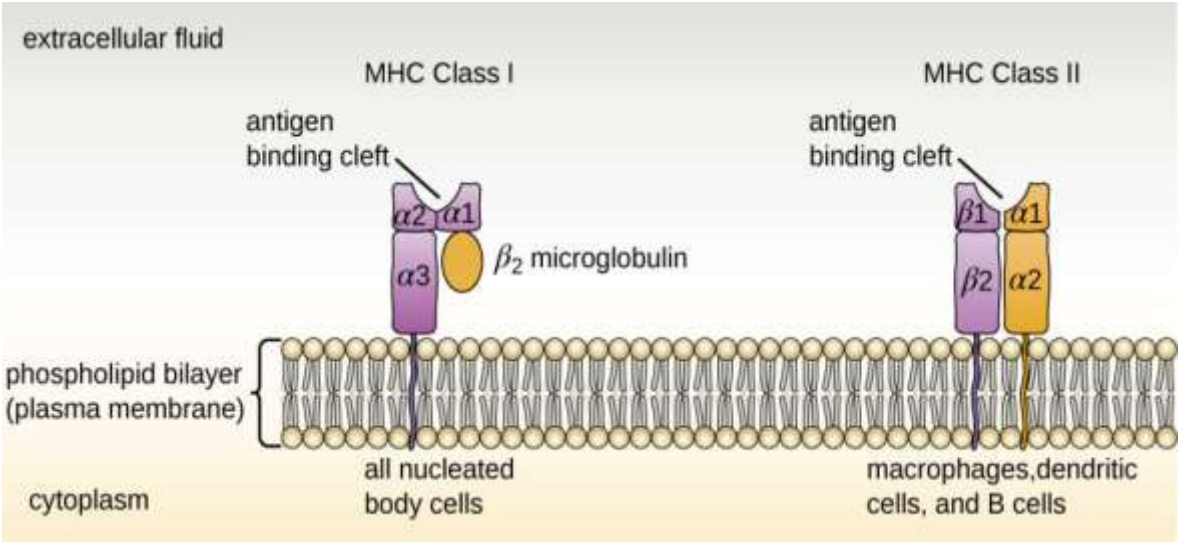


**Figure 1. 4*. MHC I are found on all nucleated body cells, and MHC II are found on macrophages, dendritic cells, and B cells (along with MHC I).***

*MHC I molecules are composed of an α protein chain coupled with a smaller $\beta_2$ microglobulin protein, and only the α chain spans the cytoplasmic membrane. The α chain of the MHC I molecule folds into three separate domains: $\alpha_1$, $\alpha_2$ and $\alpha_3$. MHC II molecules are composed of two protein chains (an α and a β chain) that are approximately similar in length. Both chains of the MHC II molecule possess portions that span the plasma membrane, and each chain folds into two separate domains: $\alpha_1$ and $\alpha_2$, and $\beta_1$, and $\beta_2$. To present abnormal or non-self-antigens to T cells, MHC molecules have a cleft that serves as the antigen-binding site near the outermost portion of the MHC-I or MHC-II dimer. For MHC I, the antigen-binding cleft is formed by the $\alpha_1$ and $\alpha_2$ domains, whereas for MHC II, the cleft is formed by the $\alpha_1$ and $\beta_1$ domains. Figure adapted from (Microbiology, 2021).*

In RA, the synovial membrane is invaded by undifferentiated peripheral blood mononuclear cells including plasma cells, neutrophils, mast cells, dendritic cells, $CD4^+$ T-cells (Th1 cells, Th17 cells, and Th2 cells), B cells, immune-regulatory Treg cells, synovial fibroblast-like cells, and resident synovial macrophages. These in turn induce monocyte adhesion to extracellular matrix molecules (ECM) such as intercellular adhesion molecule-1 (ICAM-1 or CD54) (Dustin *et al;* 1986) and their expression can be up-regulated by IL-1 and TNF-α (Abbot *et al.,* 1992), CD102 (ICAM-2) (de Fougerolles *et al;* 1991) and CD50 (ICAM-3) (Fawcett *et al;* 1992, de Fougerolles *et al;* 1992), CD62e endothelial-leucocyte adhesion molecule-1 (ELAM-1, E-selectin) (Carlos *et al;*1991) and CD106 vascular cell adhesion molecule-1 (VACM-1) (Elices *et al*; 1990) to initiate migration of circulating monocytes to promote synovial inflammation. Several immuno-histochemical staining studies have shown that ICAM-1, VCAM-1, and ELAM-1 are all highly expressed by rheumatoid synovial vascular endothelial cells and cells in the lining layer (Koch *et al.*, 1991; Morales-Ducret *et al.*, 1992; Wilkinson *et al.*, 1993). Monocytes express $\beta_2$-integrin complex CD11/CD18 (CD11a, CD11b, CD11c) on their surface, which is the receptor for the endothelial ligands CD54, CD102 (deFougerolles *et* al; 1991 & 1992 and Marlin, 1987) and CD50 (Fawcett *et al;* 1992, Campanero *et al*; 1993 and El- Gabalawy *et al*; 1994) and this binding facilitates monocyte adhesion to the endothelium.

Subsequently, monocytes differentiate into macrophages. As a result, the synovial lining becomes hyperplastic leading to inflammation of the synovium membrane (Smolen and Steiner, 2003). It is generally accepted that an increased number of macrophages in the synovial tissue mostly arises from the infiltration of circulating monocytes and initiate the acute inflammatory arthritic response (Udalova *et al.*, 2016). However, like macrophages, monocytes also display phenotypical and functional heterogeneity. The increase of soluble CD14 in RA relates to monocyte-macrophage activation (Bas *et al.*, 2004 and Yu *et al.*, 1998).

The initial event leading to RA is a breakdown of immune tolerance, resulting in autoantibody production via antigen-specific T and B cell activation. B lymphocytes express cell-surface proteins, including immunoglobulin and

differentiation antigens such as CD20 and CD22. The autoantibodies can form larger immune complexes that can further stimulate the production of pro-inflammatory cytokines through complement and Fc-receptor activation (Smolen *et al.,* 2007). T-cell and B-cell activation results in increased production of cytokines and chemokines, leading to a feedback loop for additional T-cell, macrophage, and B-cell interactions (Smolen and Steiner, 2003; Smolen *et al.,* 2007). TNF-α and IL-6 play a dominant role in the pathogenesis of RA (McInnes and Schett, 2007; Firestein, 2003) and IL-1 increases synovial fibroblast cytokines and chemokines and is involved in endothelial cell adhesion molecule expression (McInnes and Schett, 2007) as well as VEGF expression. This induces angiogenesis contributing to pannus formation (Paleolog, 2002). IL-17 expression is enhanced which stimulates the recruitment of monocytes and neutrophils by increasing local chemokine production, facilitating T-cell infiltration and activation, and amplifying immune responses by inducing IL-6 production (Nalbandian and Crispin, 2009), also has a significant impact on the RA disease process.

The presence of autoantibodies is a hallmark of the rheumatoid disease, among these, are rheumatoid factors (polyreactive IgM antibodies produced by a subset of B lymphocytes and bind to the Fc portion of the IgG molecule), anti-citrullinated protein antibodies (ACPA), and anti-carbamylated protein (anti-CarP) antibodies (Fig.1.5). These autoantibodies can predominantly be detected in serum and synovial fluid of RA patients (Trouw *et al*., 2017). They may form immune complexes in the joints, leading to the attraction of immune cells through for example; complement activation or direct activation of immune cells leading to the secretion of cytokines and chemokines (Daha, *et al.*, 2011 and Trouw *et al*., 2009) which can augment the immune response and contribute to chronic inflammation and bone destruction.

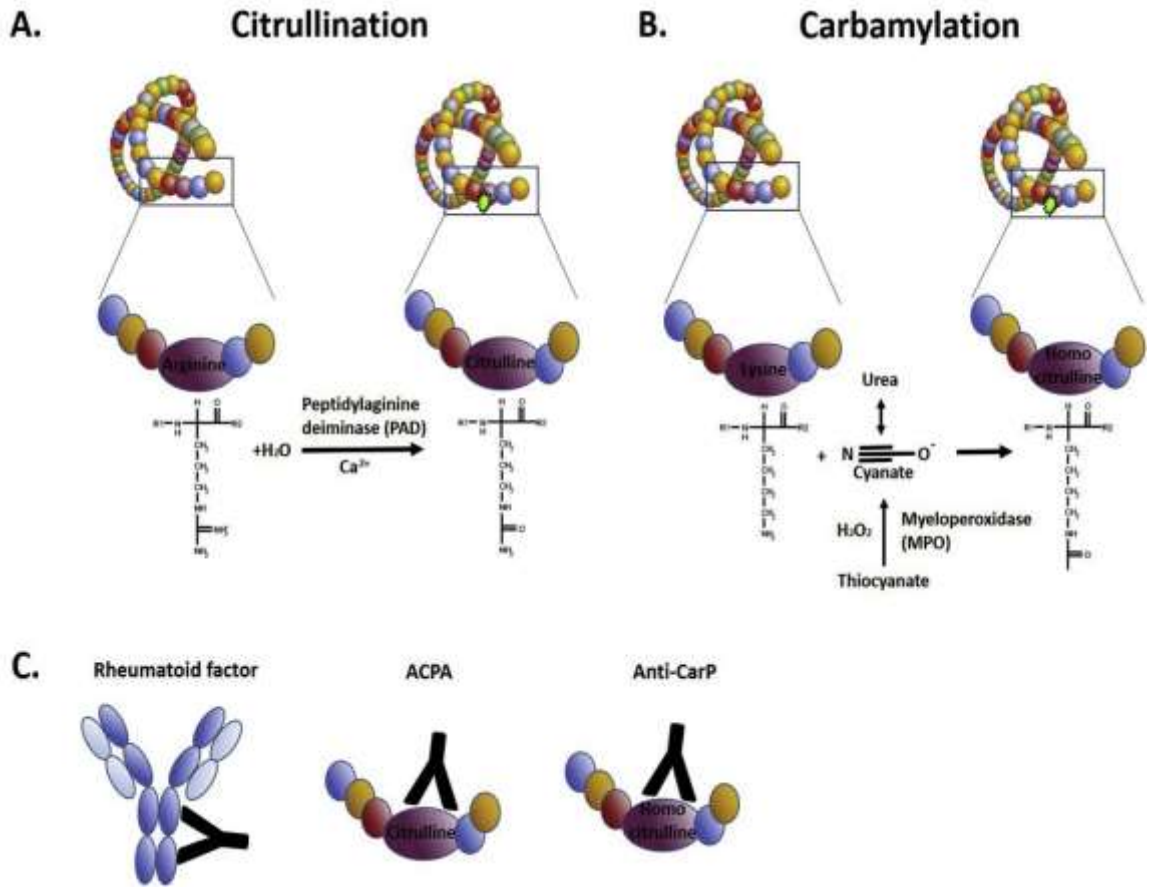


**Figure 1. 5*. Post-translational modifications and autoantibodies in RA.***

*Citrullination is the conversion of an arginine into a* citrulline *by an enzymatic reaction with Peptidylarginine deiminase (A) which can be released by neutrophils or originate from bacteria. Carbamylation is the conversion of a lysine into homocitrulline by a chemical reaction with cyanate (B). Various conditions can lead to an elevated cyanate level, such as renal disease, inflammation and smoking. These post translational modifications can be recognised by autoantibodies. The best-known antibodies in rheumatoid arthritis are rheumatoid factor, anti-citrullinated protein antibody (ACPA) and anti-carbamylated protein antibody (anti-CarP antibodies) (C). Figure adapted from (Shi et al., 2014 and Derksen et al., 2017).*

## 1.2 Macrophages in Synovial Inflammation

Resident macrophages are present in normal synovium both in the intimal layer and within the subintima. Macrophages play an important role in the pathogenesis of RA . The of number macrophages increases significantly in the inflamed synovial membrane and at the cartilage-pannus junction and their range of marker expression varies at different sites in the tissue (Mulherin *et al.*, 1996; Hogg *et al*., 1985; Salisbury *et al*., 1987 and Broker *et al*., 1990). Several studies linked the increased number of macrophages in affected joints compared to normal joints (Kraan *et al*., 1998). The degree of monocyte infiltration, which then differentiate into macrophages which subsequently become activated, correlates not only with the joint pain and inflammatory status of the patient (Tak *et al.,* 1997) but also with the radiological progression of permanent joint damage (Mulherin *et al.,* 1996) and the disease features that eventually defines the quality of life. The expression of CD14 and CD68 is predominant in synovial macrophages compared to peripheral blood monocytes (Yoon *et al.,* 2004). Macrophages at all sites in the tissue are $CD68^{+}$, and other cells are negative. High expression of CD68 on synovial macrophages has been found to be pre-dominantly accountable for the production of an increased expression of TNF- α, IL-1 particularly at the cartilage–pannus junction (Chu *et al.*, 1991) where cartilage damage takes place and chondrocytes express TNF receptors (Deleuran *et al.*, 1992) correlating with joint disease severity (Firestein *et al.,*1990, Zamani, *et al.,* 2013 and reviewed in: Pitzalis *et al.*, 2014). This suggests that TNF-α and IL-1 both have a direct involvement in cartilage destruction.

Cytokines produced by monocytes and macrophages are pro-inflammatory and induce tissue destruction. TNF-α, IL-1, and IL-8 have all been shown to cause synovitis (Pettipher *et al.*, 1986; Henderson and Pettipher, 1989; O' Bryne *et al.*, 1990; Endo *et al.*, 1991), and TNF-α and IL-1 can also cause cartilage degradation when injected intra-articularly in rabbit knee joints. Transgenic mice bearing a human TNF-α transgene modified in the 3'-region express higher levels of TNF-α and develop chronic arthritis resembling RA which is prevented by anti-TNF-α treatment (Keffer *et al.*, 1991). In human RA, TNF-α and IL-1 are likely to be important cytokines that are responsible for cartilage

destruction. Both TNF-α and IL-1 can stimulate synovial cells and chondrocytes to produce metalloproteinases which destroy the extracellular matrix components such as collagen and proteoglycan (reviewed by Firestein, 1992; Dinarello, 1992). They also inhibit matrix synthesis.

A study by Gracie *et al.,* 1999 reported that in the RA synovial membrane IL-18, a cytokine of the IL-1 family (Dinarello, 1999), is expressed most prominently in CD68+ macrophages that are contained in lymphoid aggregates. CD14+ macrophages of the RA synovial fluid also express the IL-18 receptor and IL-18, either alone or in concert with IL-12 and IL-15, strongly enhances the production of IFN-γ, TNF-α, GM-CSF, and NO by cultured synovial cells. Treatment with recombinant murine IL-18 markedly aggravates experimental arthritis (Gracie *et al.,* 1999), indicating that IL-18 has pro-inflammatory effects on this disorder.

These inflammatory responses act as the major orchestrator of synovial membrane inflammation. This leads to the establishment of pannus in the joint capsule, morning stiffness, and pain of joints with progressive bone erosion resulting in deformity and loss of mobility of the joint (reviewed in: Pitzalis *et al.*, 2014). The *in vitro* studies show that synovial fluid monocyte cells have round-shaped adherent $CD68^{+}$ cells and could differentiate into macrophages that produce TNF-α (Panayi *et al.,* 1974). TNF- α has a central role in regulating the action of downstream pro-inflammatory cytokine signalling cascades (Brennan *et al.,* 1989).

These studies suggest that RA arises from the differentiation of monocyte cells into macrophages and postulate that TNF-α is a pivotal cytokine in the pathogenesis of RA based on the fact that TNF-α is a pro-inflammatory cytokine causing arthritis and it is required for other inflammatory cytokines for example; IL-1 and GM-CSF production by RA synovial cells (Brennan *et al.*, 1989) and present in abundance in rheumatoid joints (di Giovine *et al.*, 1988).

Investigations have not revealed what starts the RA process. It is, however, associated with genetic composition. The disease is not carried in the genes, but genes can increase the likelihood of body reaction to the environmental factors, i.e. viruses and bacteria, which may stimulate the disease. During inflammation, reactive oxygen species (ROS) production is induced by inflammatory cells to kill

pathogens. ROS formation is a pathological event in which the pool of reactive oxygen species increases over time, either by the reduction in antioxidant defences, their augmented production, or a combination of both. ROS plays an important part in cellular activities such as signalling transduction, gene transcription, and responses to the immune (Jones *et al.*, 2012). The increased generation of ROS likely causes oxidative stress, which damages protein, matrix components, lipids, and nucleic acids. ROS also serves as essential intracellular signal molecules to amplify synovial inflammation. ROS play a big role in macrophage-mediated immunity. They facilitate antimicrobial activity from bacteria alongside parasites and redox-regulation of an immune signal. They induce inflammatory activation; this assists the host response against pathogens.

### 1.3 Macrophage Polarization

Monocytes (Mo) alongside macrophages (Mϕ) are vital cellular components comprising the innate immune system that actively regulate development, and resolution of many inflammatory illnesses. Macrophages derive from monocytes that have migrated into body tissues from the bloodstream (Jablonski, *et al.*, 2015). Macrophages in the body tissues become activated and lead to inflammation of the synovial membrane.

Macrophage polarisation produces distinct functional phenotypes as a reaction to specific micro-environmental stimuli. Macrophages can be polarized into M1 macrophages and then activated into M2 macrophages (Fig.1.6). The differentiated naïve macrophages (M0) can further mature and activate into pro-inflammatory (M1) and anti-inflammatory (M2) macrophages (Mills *et al.,* 2000) in response to interferon regulatory factor (IRF), signal transducers, and activators of transcription (STAT) pathway and suppressor of cytokine signalling (SOCS) proteins (Sica and Bronte, 2007). M1 and M2 macrophages are characterised by their functional properties such as cytokine production, gene expression, and phenotypic such as surface markers properties (Gordon and Martinez *et al.,* 2010, Mantovani *et al.,* 2007).

The IRF-STAT pathways are activated (Fig.1.7) by interferon gamma-γ (IFNγ), LPS, Interleukin-4 (IL-4) and IL-13 (Mills *et al.,* 2000, Nathan *et al.,* 1983 and Stein *et al.,* 1992). IFNγ TLR binding signalling activates IRF, signal transducers, and activators of the transcription pathway to polarize M0 macrophage to M1 macrophage via STAT1 (Sica and Bronte, 2007). LPS and TLR4 signalling pathways can also polarize M0 macrophages to M1 macrophages by activating STAT1-α and STAT1-β in a Myeloid differentiation primary response 88 (MyD88) independent manner (Toshchakov *et al.,*2002*).* In addition, SOCS3 proteins activate nuclear factor kappa B (NF-κB)-phosphatidyl inositol 3 kinase (PI3) pathways to produce nitric oxide via G-protein coupled receptor P2Y(2)R nitric oxide synthase-2 (*NOS2)* (Eun *et al.,* 2014), cell growth and cell differentiation factor Activin A (Arnold *et al.,* 2014*)* to promote M1 markers expression and down-regulate IL-10 production (Sierra-Filardi *et.,* 2011). Bruton's tyrosine Kinase (Btk) has been indicated as critical for M1 polarization as an absence of Btk polarized M1 macrophages to M2 macrophages in response to LPS stimulation (Ni *et al.,* 2014). The hypoxia inducible factor HIF-1α regulates M1 polarization by regulating *NOS2* expression and the M1 state (Takeda *et al.*, 2010).

In contrast, M0 macrophages are polarized toward M2 macrophages by IL-4 and IL-13 by binding to their surface receptors via STAT6 (Sica and Bronte, 2007). This signalling activates STAT6 (Fig.1.8) to transcribe anti-inflammatory gene expression such as Arginase-1, and CD206 (reviewed in: Lawrence and Natoli, 2011, Tugal *et al.,* 2013). Kruppel-like factor 4 (KLF-4) synchronises with STAT6 to induce Arginase-1, Peroxisome proliferator-activated receptor-γ (PPAR-γ) and inhibit TNF-α, COX-2 and NOS2 by sequestering essential co-activators of NF-κB (Liao *et al.,* 2011). IRF4 and NF-κB p50 subunit has also been shown to play a role in M2 polarization (Satoh *et al.,* 2013, Porta *et al.,* 2009). The hypoxia inducible factor HIF-2α regulates M2 polarization by arginase 1 expression and the M2 state (Takeda *et al.*, 2010). Additionally, the cytokine IL-21 mediates M2 polarization by decreasing NOS2 expression and increasing STAT3 phosphorylation, and bone morphogenetic protein *(*BMP)-7 induces M2 polarization *in vitro* via activation of the SMAD-PI3K-Akt-mTOR pathway (Li *et al.*, 2013).

M1 macrophages express high levels of MHC II, CD68, CD86, and CD80 surface markers and secrete high levels of TNF-α, IL-6, IL-12, and IL-18 (Martinez *et al.*, 2008; Mosser and Edwards, 2008). In a disease context, M1 macrophages initiate and sustain inflammation and cause joint erosion and therefore can be harmful to health. M1 macrophages release nitric oxide (NO) to protect from viruses and bacteria (Murray, *et al.*, 2014). M2 macrophages express high levels of CD200R, CD206, CD163, and Arginase-1 surface markers and produce high levels of IL-10 and low levels of IL-12 (Duluc *et al.*, 2007 and Roszer *et al.,* 2015) and contribute to vasculogenesis, tissue remodelling, and repair. M2 phenotypes generate either proline to stimulate collagen production or polyamines to trigger proliferation. They do not produce Nitric Oxide but facilitate the formation of the extracellular matrix.

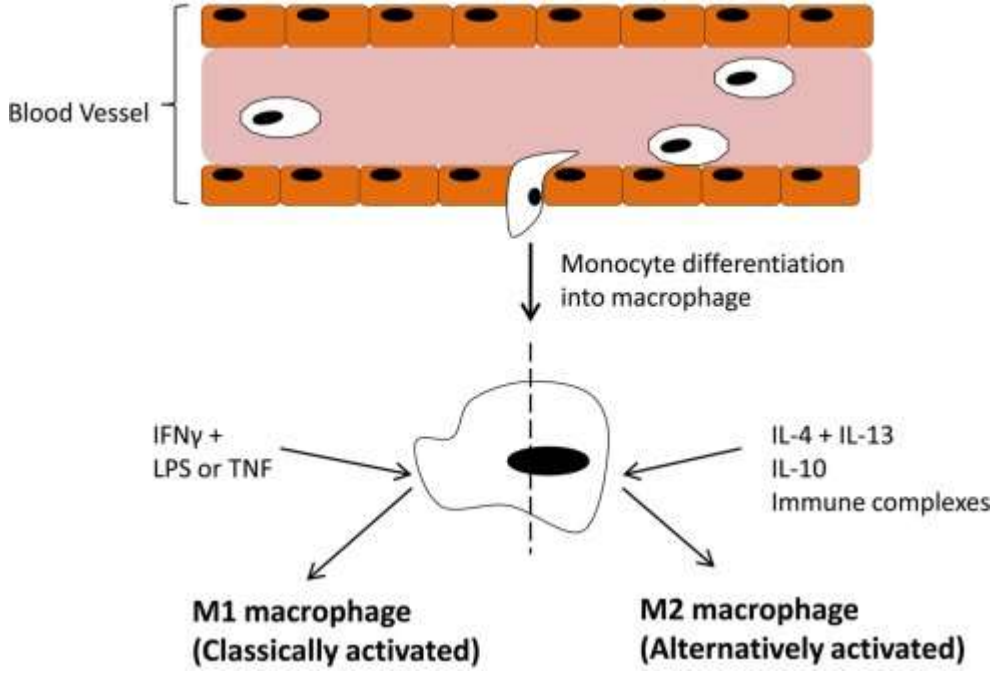


**Figure 1. 6*. Blood-borne monocytes exit the blood stream and differentiate into macrophages.***

*The macrophage differentiation depends on the stimulus provided by the microenvironment. IFNγ along with LPS or TNFα drive M1 (classically activated) macrophages polarization which participate in pro-inflammatory activities. On the other hand, IL-4 + IL-13, IL-10, or immune complexes drive M2 (alternatively activated) macrophages, which participate in anti-inflammatory responses. (Figure adapted from Kennedy et al., 2011).*

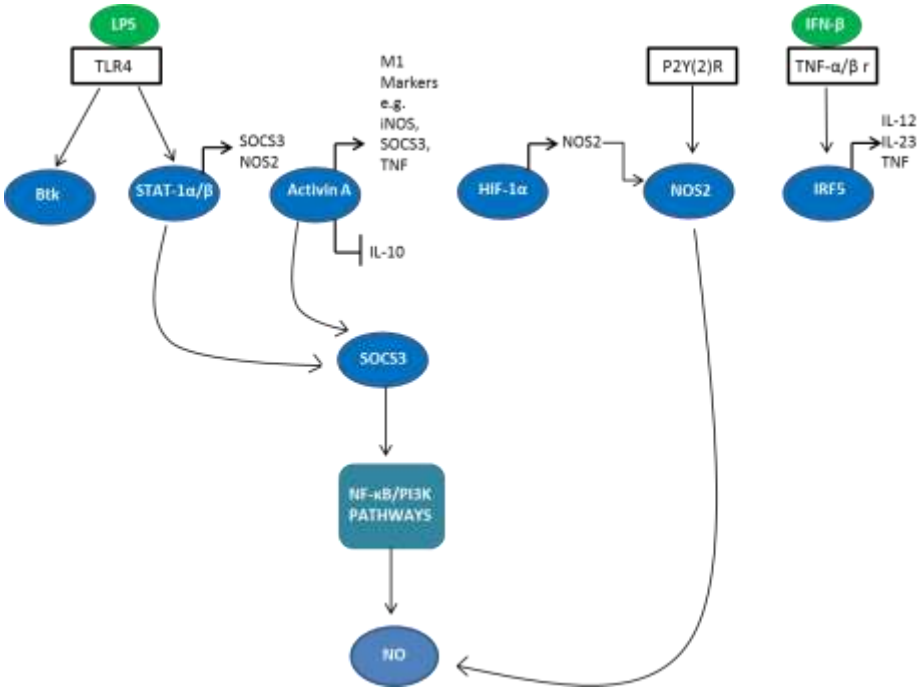


**Figure 1. 7*. Schematic representation of the signalling molecules involved in M1 polarization*.**

*The interferon regulatory factor- signal transducers and activators of transcription (IRF-STAT) pathways are activated by IFNγ, LPS, IL-4 and IL-13. IFNγ TLR binding signalling activates IRF-STAT to polarize M0 macrophage to M1 macrophage via STAT1. LPS and TLR4 signalling pathway can also polarize M0 macrophages to M1 macrophages by activating STAT1-α and STAT1-β in MyD88 independent manner. Suppressor of cytokine signalling (SOCS)-3 proteins activates NF-κB- PI3 pathways to produce nitric oxide via P2Y(2)R NOS2, Activin A to promote M1 markers expression and down-regulate IL-10 production. M1 macrophages release NO to provide protection from viruses and bacteria. Bruton's tyrosine kinase (Btk) has been indicated as critical for M1 polarization as the absence of Btk polarized M1 macrophages to M2 macrophages in response to LPS stimulation. The hypoxia inducible factor (HIF)-1α regulates M1 polarization by regulating* NOS2 *expression and the M1 state.*

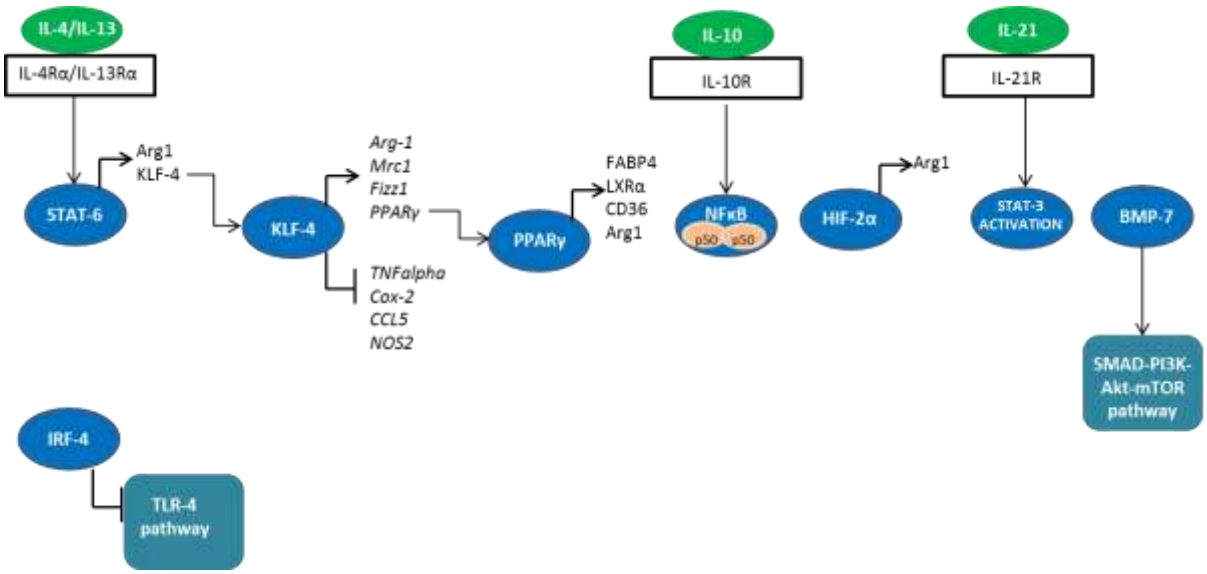


**Figure 1. 8.** ***Schematic representation of the signalling molecules involved in M2 polarization***.

*M0 macrophages are polarized toward M2 macrophage by IL-4 and IL-13 by binding to their surface receptors via signal transducers and activators of transcription (STAT) 6. This signalling activates STAT6 to transcribe Arginase-1, CD206. Kruppel-like factor 4 (KLF-4) synchronises with STAT6 to induce Arginase-1, Peroxisome proliferator-activated receptor (PPAR)-γ and inhibit TNF-α, COX-2 and NOS2 by sequestering essential co-activators of NF-κB. IRF4 and NF-κB p50 subunit has also shown to play a role in M2 polarization. The hypoxia inducible factor (HIF)-2α regulates M2 polarization by arginase 1 expression and the M2 state. Furthermore, the cytokine IL-21 mediates M2 polarization by decreasing NOS2 expression and increasing STAT3 phosphorylation and bone morphogenetic protein (BMP)-7 induces M2 polarization in vitro via activation of the SMAD-PI3K-Akt-mTOR pathway.*

Some studies suggest that M2 macrophages can be further classified into M2a, M2b, M2c, and M2d subsets based on the applied stimuli and the induced transcriptional changes (Mantovani *et al.*, 2004; Martinez and Gordon, 2014; Murray *et al.*, 2014, Colin *et al.*, 2014; Ferrante and Leibovich, 2012). M2a subtype is induced by IL-4 and IL-13 and expresses high levels of CD206, IL-1R, CD163, IL-6, and chemokine ligand (CCL)-17 (Martinez *et al.*, 2008; Mosser and Edwards, 2008). M2b subtype activation is elicited by immune complexes, IL-1 receptor ligands, and bacterial LPS and expresses IL-1, IL-10, TNF-α, CD86, IL-6, CCL-1 (Martinez *et al.*, 2008; Mosser and Edwards, 2008), and the M2c subtype activation is initiated in response to IL-10, glucocorticoids, and TGF-β and express CD206, C163, IL-10, TGF-β, CXCL13, CCL-2 (Martinez *et al.*, 2008). The M2d subtype activation is caused in response to IL-6 and adenosines and expresses VEGF, IL-10, IL-12, TGF-β, CCL-5, and CXCL-16 (Wang *et al.*, 2010 and Ferrante *et al.*, 2013; Martinez *et al.*, 2008).

A study by Miossec *et al.,* 1990 suggests that the anti-inflammatory cytokine IL-4 plays a protective role in arthritis, its virtual absence from synovial samples points to a lack of protective mechanisms, rather than active regulation. This Th2-like cytokine down-regulates monocyte-macrophage cytotoxicity and cytokine production (Isomaki, *et al.*, 1996) including that of TNF-α (Hart *et al.*, 1996). Furthermore, Allen *et al.*, 1993 reported that IL-4 decreases IL-1β production while increasing IL-1 receptor antagonist production, thus suggesting a synchronised anti-inflammatory approach. IL-10 is a macrophage-derived cytokine (Abbas *et al.,* 1996) that reduces HLA-DR expression and antigen presentation in monocytes and inhibits the production of pro-inflammatory cytokines, granulocyte-macrophage colony-stimulating factor (GM-CSF), and Fcγ receptors by synovial macrophages (Isomaki, *et al.*, 1996). Consistently with cytokine and chemokine down-regulation, IL-10 suppressed experimental arthritis (Abbas *et al.*, 1996). A study by Bessis *et al.,* 1996 suggested that IL-13 exerts suppressive effects in experimental arthritis, probably through a selective effect on monocytes-macrophages. In RA, IL-13 is produced by synovial fluid mononuclear cells, which, when exposed to exogenous IL-13, reduce their production of IL-1 and TNF-α (Isomaki *et al.*, 1996).

Targeting monocyte-macrophage differentiation should thus be a powerful way of inhibiting inflammation and bone erosion in arthritis. Their plasticity is a major property that helps the switch from the M1 phenotype to the M2 phenotype (Mantovani *et al.*, 2004). The polarity balance between M1 and M2 is essential for adequate immune function as dysfunction between them causes excessive production of pro-inflammatory cytokines. Fukui *et al.*, (2017) and Zhu *et al.*, (2015) confirmed that M1/M2 macrophage subset ratios disequilibrium is higher in RA patients' synovial fluid compared to osteoclast patients.

The synovial CD68 macrophages play a central role in the pathology of RA (Yanni *et al.*, 1994). In a double-immunofluorescence staining study by Ambarus *et al.*, (2012) and Wiktor-Jedrzejczak and Gordon (1996), the $CD68^{+}$ marker was found to be co-localised with the IFN-γ dependent polarization markers, IL-4 dependent polarized markers, and IL-10 dependent polarized markers. Kennedy *et al.,* (2011) suggest that depletion of macrophages from RA synovial cell cultures can significantly reduce TNF- α levels.

Soler *et al.*, (2015) suggest that the degree of joint erosion and the contribution to hyperplasia of the intimal synovial lining layer could also be linked to the increased number in the synovial tissue. For example, Fukui *et al.,* (2017) and Zhu *et al.*, (2015) suggested that the intimal lining layer contains mainly mature resident macrophage markers CD163 and CD32 co-localised with $CD68^{+}$, whereas the synovial sub-lining contains more mixed phenotypes $CD68^{+}$ co-localized with CD163 and CD32 and CD64, and the CD200R and $CD14^{+}$, proposing that it is actively infiltrated with immature monocytes derived macrophages. Furthermore, Ambarus *et al.*, (2012) concluded that disease activity in RA seemed associated with the number of synovial sub-lining macrophages, but not with intimal lining layer macrophages.

Some studies suggest that surface markers for both M1 and M2 phenotypes may coexist on the same cell (Trombetta *et al.*, 2018 and Cutolo *et al.*, 2018). For example, to evaluate *ex-vivo* and *in vitro* polarization markers of M1 and M2 macrophage cellular compartments Ambarus *et al.*, (2012) purified $CD14^{+}$ monocytes from the peripheral blood of RA patients and compared them with the same cells from healthy donors. Conversely, CD64, CD200R, and CD16 labelling did not show a significant difference between the two phenotypes. A

study by Quero *et al.*, (2017) did not show any specific difference in M1 or M2 marker expression where GM-CSF M1 macrophages expressed CD163 and CD206 which should be M2 markers. Similarly, Zhao *et al.*, (2017) analysed M1 ($CD68^{+}CD192^{+}$) and M2 ($CX3CR1^{+}CD163^{+}$) but no significant difference was found and concluded that RA peripheral blood seems to be composed of mixed M1 and M2 monocyte sub-populations. However, contrary to these studies, a gene expression study by Hofkens *et al.*, (2013) from rodents during antigen-induced arthritis, indicated, that the up-regulation of M1 markers (IL-1β, IL-6, FcγRI, and CD86) even though M2 markers (Arg1 and Ym1), remained high and constant throughout the disease period.

Literature review therefore indicates that disequilibrium of M1 and M2 markers is present in RA patients. Therefore, agents with the potential to inhibit pro-inflammatory cytokine production or promote anti-inflammatory cytokine production may be useful in treating arthritis and other inflammatory diseases. For that reason, monocyte-macrophage differentiation has a great potential as a new model of inflammatory diseases and that alteration of this pathway may reduce distortion of a synovial membrane. To understand the early events that lead to monocyte-macrophage differentiation in RA, it is important to understand the molecular signalling pathways involved in monocyte-macrophage differentiation.

## 1.4 Intracellular Signalling Pathways

Literature suggests that once a receptor protein of the monocytes binds a ligand, it undergoes a conformational change which in turn launches a series of biochemical reactions within the cell. These intracellular signalling pathways, also called signal transduction cascades, typically amplify the message, producing multiple intracellular signals for every receptor that is bound. As a result, activation of receptors triggers the synthesis of small molecules called second messengers (cyclic nucleotides, such as cAMP and other soluble molecules that signal within the cytosol; lipid messengers that signal within cell membranes; ions that signal within and between cellular compartments; and gases and free radicals that can signal throughout the cell and even to neighbouring cells), which initiate and coordinate intracellular signalling pathways (Heldin *et al*., 2016). Figure 1.9 illustrates second message pathways. Activation of adenylyl cyclase by G-protein-coupled receptors (GPCRs) generates the cyclic nucleotide second messenger 3′-5′-cyclic adenosine monophosphate (cAMP).

It was first identified in 1957 as the first intracellular second messenger of extracellular ligand action (Sutherland and Rall, 1958). It is considered a universal regulator of metabolism and gene expression (Beavo and Brunton, 2002). In the immune system, cAMP regulates both innate and adaptive immune cell activities (Serezani *et al*., 2008). Dent *et al.,* (1994 and Wall *et al.,* (2009) studies reported that increased cAMP levels appear to generally weaken monocyte inflammatory functions. Gilbert and Hoffmann, (1985), Levy *et al*.,1(996) and Wortis *et al*., (1995) reported that cAMP is required for the induction of antigen-stimulated cell activation but subsequently limits activation by negatively regulating signalling through B cell and T cell receptors. Several studies reported that in B cells it provides an essential signal in the induction of antigen-stimulated proliferation and antibody production. A study by Cekic *et al*., (2013) and Vag *et al*., (2001) reported that in T cells, cAMP participates in the regulation of nearly all functional activities ranging from peripheral maintenance of naïve T cells to their activation via the T cell receptors acquisition of effector function and memory (Liopeta *et* al., 2009, Hedrich *et al*., 2012; Vig *et al*., 2002). Bopp *et al*., (2007) and Bacher *et al*., (2013) studies have shown that cAMP forms an essential component of the

suppressive mechanism in Treg. Bopp *et al*., (2007 and 2009) studies suggest that Treg contain increased levels of cytosolic cAMP, further upregulates their cAMP level upon activation, and consigns cAMP to target cells via gap junctions and Vahl *et* al., (2014) indicated that increased cAMP formation in Treg is a prerequisite for their suppressive activity (Fig.1.10). The inhibition of cAMP formation abrogates the suppressive function of Treg (Klein *et al*., 2012).

Several studies have shown that by increasing levels of intracellular cAMP, PDE4 inhibitors induce anti-inflammatory effects in almost all inflammatory and immune cells and are known to suppress a multitude of inflammatory responses, including proliferation, chemotaxis, phagocytosis, and release of pro-inflammatory mediators, such as cytokine and chemokines, reactive oxygen species, lipid mediators, and hydrolytic enzymes (Serezani *et al*., 2008; Torphy *et al*., 1998; Press and Banner *et al*., 2009).

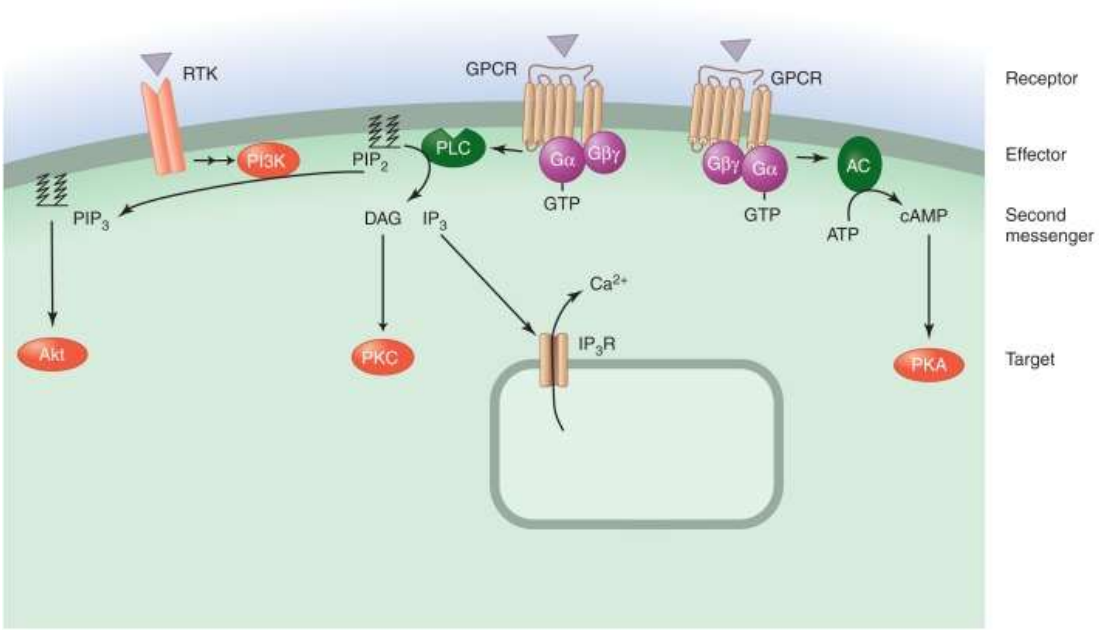


**Figure 1. 9*. Second messengers disseminate information received from cell-surface receptors.***

*Indicated are three examples of a receptor activating an effector to produce a second messenger that modulates the activity of a target. On the right, binding of agonists to a GPCR (the receptor) can activate adenylyl cyclase (the effector) to produce cAMP (the second messenger) to activate protein kinase A (PKA; the target). On the left, binding of growth factors to a receptor tyrosine kinase (RTK; the receptor) can activate PI3K (the effector) to generate PIP3 (the second messenger), which activates Akt (the target). In the center, binding of ligands to a GPCR (receptor) activates phospholipase C (PLC; the effector), to generate two second messengers, DAG and IP3, which activate protein kinase C (PKC; the target) and release calcium from intracellular stores, respectively. (Figure adapted from Newton et al., 2016).*

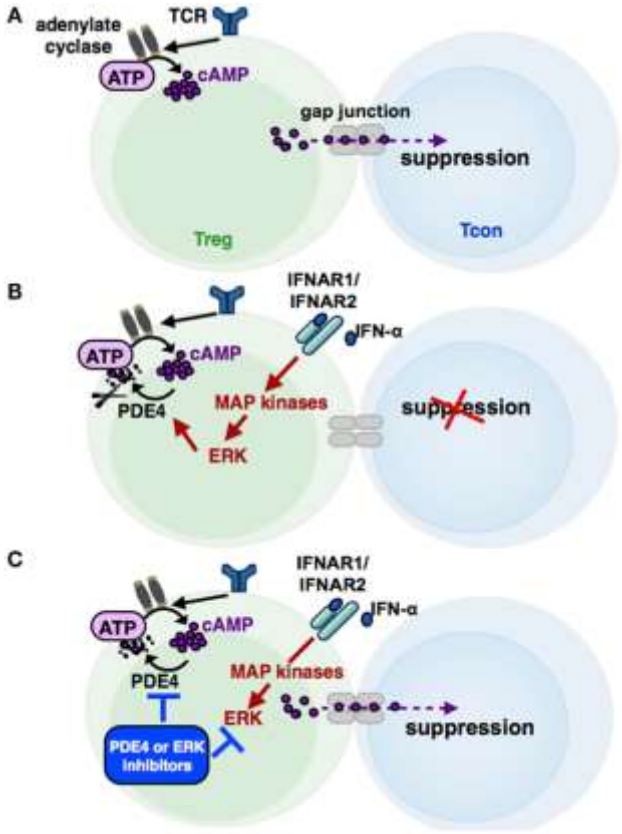


**Figure 1. 10.** ***The cAMP pathway in Treg and its regulation by IFN-α.***

*Signalling via the T cell receptor (TCR) leads to an activation of adenylate cyclases, resulting in high cAMP levels in regulatory T cells (Treg). cAMP can be transferred via gap junctions into conventional T cells (Tcon), thereby mediating the suppressive activity of Treg (A). Phosphodiesterase 4 (PDE4), which can be activated by MAP kinase ERK-related pathways, reduces cAMP in Treg by enzymatic cleavage, impairing the regulatory activity of Treg (B). IFN-α abolishes the suppressive function of Treg by cAMP reduction, restoring the Tcon activation. Inhibition of the ERK or PDE4 pathway, respectively, results in a renewed suppressive capacity of IFN-α treated Treg (C) (Figure adapted from Raker et al., 2016).*

As illustrated in figure 1.9, the stimulation of phosphoinositide 3-kinase (PI3K) by growth factor receptor activation generates the lipid second messenger phosphatidylinositol 3,4,5-trisphosphate (PIP3). In addition, activation of phospholipase C by GPCRs generates the two second messengers, membrane-bound messenger diacylglycerol (DAG) and soluble messenger inositol 1,4,5-trisphosphate (IP3), which bind to receptors on subcellular organelles to release calcium into the cytosol. Together, DAG and $Ca^{2+}$ activate another enzyme called protein kinase C (PKC).

The intracellular signalling pathway is considered to play an important role in the induction and maintenance of chronic inflammation. PKC is a family of proline-directed serine-threonine kinases which is activated by diacylglycerol (DAG) and calcium ions for translocation from the cytosol to the plasma membrane. The PKC signalling pathway activates a network of extracellular signal-regulated protein kinases I and 2 (ERK1/2) Mitogen-activated protein kinases (MAPKs), c-Jun-N-terminal kinases (JNKs), and p38 MAPKs. MAPKs comprise p38-α (MAPK14), -β (MAPK11), -γ (MAPK12 / ERK6), and -δ (MAPK13 / SAPK4 and participate in the transduction of signals to regulate cell cycle progression, cell migration, cell proliferation, cell survival, cell differentiation and apoptosis (Tanaka and Nishizuka, 1994; Newton, 2001 and reviewed in: Seger *et al.,* 1995 and Kyriakis *et al.,* 1996). These pathways are approximately 60-70 % identical to each other but differ in sequence, size, and their activation in response to stimuli. Mitogen-catalysed protein kinases (MAPKs) are serine-threonine protein kinases that transduce the signal from the cell surface to the nucleus. They are activated by cellular stresses*,* i.e., UV irradiation, high osmotic stress, heat shock, lipopolysaccharide, protein synthesis inhibitors, and pro-inflammatory cytokines. ERK1/2 MAPKs are activated by growth-related stimuli (Cobb *et al.*, 1991 and Sugden and Clerk, 1997) whereas the JNKs and p38 MAPKs are activated in response to cellular stresses (Ip and Davis, 1998). Some studies suggest that the MAPK signal is an important modulator of M2b macrophage polarization as the activation of p38, ERK1/2, and JNK is enhanced in M2b macrophages induced by granulin or administration of activated Lymphocyte –Derived DNA (Chen *et al.*, 2013 and Zhang *et al.*, 2010).

The gonadotropin-releasing hormone (GnRH) receptor is involved in the activation of MAPK Pathways. It utilizes Gq protein to facilitate downstream signalling. GnRH facilitates all MAPK cascades through a mechanism known as the PKC-dependent as mentioned above. MKPs are involved in the inactivation of MAPK to avoid the excessive and inappropriate signalling that may result in a defect in the normal cellular operations. MAPK pathway helps in the regulation of cellular growth, gene expansion, and survival. However, abnormal MAPK signalling may result in increased or uncontrolled cell proliferation and resistance to apoptosis (Morrison, 2012). p38 is the major MAPK involved in RA. It makes a big contribution to the production of inflammatory mediators ERK1/2 is also a constituent of mitogen.

Protein phosphorylation plays a central role in controlling cell cycle processes and once MAPKs signalling pathways are activated in response to stimuli, they activate the cell cycle regulating Cyclin D1 and $p21^{WAF1}$ genes expression for cell proliferation and differentiation. These cell cycle regulating genes plays a critical role in cell cycle progression and cell differentiation where the cyclin D1 gene bind to cyclin-dependent kinase (ckd)-4 and cdk6 to promote cell cycle progression from growth (G1) phase to S phase (DNA replication) by Rb protein phosphorylation for cell cycle progression. On the other hand, the $p21^{WAF1}$ gene binds to the cdk-2-cyclin complex to inhibit the G1 phase transition to S phase by inhibiting phosphorylation of Rb to promote monocyte-macrophage differentiation (Matsumoto *et al.,* 2006).

ERK1/2 MAPK signalling pathway normally participates in cell proliferation and cell survival (Xia *et al.,* 1995) whereas p38 MAPK signalling promotes cell differentiation. However, recent studies suggest that in addition to the ERK1/2 effect on cell proliferation and cell survival, the ERK1/2 signalling pathway can also regulate cell differentiation (Miranda *et al.,* 2001, Kawamura *et al.,* 1999 and Tokuda *et al.,* 1999) through cross-talk with p38 MAPK (Shimo *et al.,* 2007). In addition, there are some reports which suggest that $p21^{WAF1}$ is regulated by ERK1/2 MAPK and ERK1/2 specific inhibitor PD98059 is reported to inhibit the expression of $p21^{WAF1}$ in the leukemic and cancer cell lines (Agadir *et al.,* 1999, Das *et al.,* 2000, Dufourny *et al.,* 1997, Sato *et al.,* 2000, Sugibayashi *et al.,* 2001 *and* Miranda *et al.,* 2001).

The ERK1/2 and p38 signalling pathways are activated by phosphorylation at specific sites and their activation can be monitored *in vitro* using a phosphorylated-specific antibody (Miranda *et al.,* 2001). ERK1/2 consists of 44 kDa ERK1 and 42 kDa ERK2, which share approximately 84% sequence homology. The two phosphorylation events, first on tyrosine residue and a second on a proximal threonine residue are required for ERK1/2 full activation. However, ERK1/2 can even enter and exit the nucleus of a cell in the absence of an activated signalling pathway due to its interaction with nuclear pore proteins. ERK is involved in the regulation of IL-6, IL-12, IL-23, and TNF-α synthesis (Goodridge *et al.*, 2003; Feng *et al.*, 1999). ERK1/2 activity is inhibited by its specific PD98059 inhibitor (Kosako *et al.,* 2009 and Whitehust *et al.,* 2002).

A study by Schett *et at.*, 2000 suggests that p38 MAPK, JNK, and ERK, are expressed in the rheumatoid synovium and have been implicated in the pathogenesis of RA. ERK MAPK inhibitors (for example; PD098059) have been found to reduce nociceptive responses in an adjuvant-induced monoarthritis in rats (Cruz *et al.*, 2005) and inflammation in an ear oedema model in mice and an experimental osteoarthritis model in rabbits (Jaffee *et al.*, 2000; Pelletier *et al.*, 2003), suggesting that ERK plays an important role in chronic inflammation. In Schett *et al.*, (2000) ERK MAPK has been shown to be activated in synovial fibroblasts following stimulation with IL-1, TNF-α, and fibroblast growth factor and is also found to be activated in mononuclear cell infiltrates and synovial fibroblasts in synovial tissue from RA patients, suggesting involvement of ERK in joint damage associated with pro-inflammatory cytokine production by macrophages.

p38 MAPK signalling pathway is involved in human inflammatory disease and is activated in the rheumatoid synovium (Feldmann *et al.*, 2001). Due to the presence of different stress factors and increased pro-inflammatory cytokines in the synovium, the activation of the p38MAPK signalling pathway in RA joints is conceivable. p38α is a 38 kDa protein that regulates LPS-induced TNF-α and IL-1β from monocyte cells (Han *et al.,* 1993, Lee *et al.,* 1994) and it has pro-inflammatory properties in RA synovial fluid (Korb *et al.,* 2006). In another study Schett *et al.,* 2008 reported that Phospho-p38α (p-p38α) is localised to the RA synovial intimal lining, which includes fibroblast-like synoviocytes and monocytes that produce IL-6 and a variety of other pro-inflammatory mediators. A study by

Zwerina *et al.*, (2006) suggests that activation of p38 MAPK is an important step in TNF-α mediated inflammatory bone destruction, and inhibition of p38MAPK in animal models leads to reduced inflammation, which correlates with reduced expression of IL1, IL6, and RANKL cytokines. p38α activity can be inhibited by its specific inhibitor SB203580 which acts as a specific competitive ATP binding inhibitor (Davies *et.,* 2000) and reduces pro-inflammatory cytokine TNF-α expression in RA animal models (Sweeney, Firestein, 2006; Hammaker, Firestein, 2010; Kumar *et al.,* 2003).

T cell activation, p38 MAPK activation, and calcium mobilisation are also a feature of the linkage of purinergic signalling via P2X1, P2Y2 receptor subtypes in different inflammatory cells (Yip *et al*., 2009 and Falzoni *et al.,* 1995). Purinergic receptors are ATP receptors. They are split into two types, P2Y and P2X. The latter are ATP-activated receptor channels that allow the passage of the ions across membranes of the cell, while P2Y and GPCRs are ATP-activated. P2Y receptors can both be anti-inflammatory as well as pro-inflammatory. They control macrophage inflammatory responses. Receptors that sense stress includes P2X and P2Y receptors. They play a significant role in macrophage responses to various stresses in response to extracellular nucleotides and their sugar derivatives.

3′-5′-cyclic guanosine monophosphate (cGMP) is another cyclic nucleotide that serves as a second messenger. cGMP is often synthesised by receptor guanylyl cyclases and it can also be produced by soluble cytoplasmic guanylyl cyclases, which are stimulated by nitric oxide (Newton *et al*., 2016).

## 1.5 Anti-Rheumatic Drugs

Several existing drugs (Table 1.1) are available to treat inflammatory rheumatic disease to reduce pain, and inflammation in the joints, and slow disease progression. The National Institute for Health and Care Excellence (NICE, 2021) guidelines recommend the use of cyclooxygenase inhibitors (for example; naproxen, and ibuprofen) to reduce RA symptoms like pain and inflammation and recommend using disease-modifying antirheumatic drugs (DMARDs) for example; methotrexate, leflunomide, sulfasalazine as first-line treatments within 3 months of the onset of persistent RA symptoms to slow the progression of RA. Their efficacy has been established in placebo-controlled trials (Fig.1.11) (Donahue *et al.*, 2008; Suarez-Almazor *et al*., 2000 and Osiri *et al.*, 2003). NICE guidelines recommend a combination of DMARDs and corticosteroids (prednisolone or azathioprine) for patients who are unresponsive to DMARD monotherapy. The glucocorticoids slow the disease progression by inhibiting the transcription of cytokines gene expression.

Biologics such as anti-IL-6 (sarilumab, tocilizumab), anti-IL-12 anti-IL-23 ( ustekinumab), and Janus-associated kinase inhibitors (tofacitinib, baricitinib, cytokine modulators (adalimumab, etanercept, infliximab, certolizumab pegol, golimumab) are used in combination with methotrexate as options for unresponsive patients to DMARDs and corticosteroid combination therapy (NICE, 2021).

According to NICE (2021), the long-term side effects of DMARDs include nausea, hair loss, liver toxicity and prolonged use of corticosteroids can induce immunosuppression against infection, osteoporosis, hyperglycaemia, and hypertension (Salliot *et al*., 2009 and Alcorn *et al*., 2009). Similarly, biologics, Janus-associated kinase inhibitors, and cytokine modulators also have unwanted side effects such as hypersensitivity, gastrointestinal symptoms, headache, upper respiratory infections, common cold, congested nose sore throat, and injection site reactions.

**Table 1. 1.** ***Pharmacologic therapies for rheumatoid arthritis*****.**

| DMARDs | | | | |
|---|---|---|---|---|
| **Classification** | **Name** | **Mechanism of action** | **Potential mechanisms** | **Reference** |
| Conventional synthetic DMARDs | Methotrexate | Analog of folic acid | Folate-dependent processes; Adenosine signaling; Methyl-donor production; Reactive oxygen species; Adhesion-molecule expression; Cytokine profiles Eicosanoids and MMPs. | (Brown *et al.*, 2016) |
| | Leflunomide/ Teriflunomide | Pyrimidine synthesis inhibitor | DHODH-dependent pathway; Leukocyte adhesion; Rapidly dividing cells; NF-kB; Kinases; Interleukins; TGF-β. | (Kasarello *et al.*, 2017) |
| | Sulfasalazine | Anti-inflammatory and immunosuppression | Cyclooxygenase and PGE2; Leukotriene production and chemotaxis; Inflammatory cytokines (IL-1, IL-6, TNF-α); Adenosine signaling; NF-kB activation. | (Linares *et al.*, 2011) |
| | Chloroquine /Hydroxychloroquine | Immunomodulatory effects | Toll-like receptors; Lysosomotropic action; Monocyte-derived pro-inflammatory cytokines; Anti-inflammatory effects; Cellular immune reactions; T cell responses; Neutrophils; Cartilage metabolism and degradation. | (Rainsford *et al.*, 2015) |
| **Antibody-based therapies** | | | | |
| **Classification** | **Name** | **Mechanism of action** | **Potential mechanisms** | **Reference** |
| TNF-α targeted therapy | Infliximab | TNF-α inhibitor | Phagocytosis and pro-inflammatory cytokines; Chemoattractant; Adhesion molecules and chemokines; Treg cell function; Function of osteoclasts, leukocytes, endothelial and synovial fibroblasts. | (Kim and Moudgil, 2017) |
| | Adalimumab | | | |
| | Etanercept | | | |
| | Golimumab | | | |
| | Certolizumab pegol | | | |
| B-cell targeted therapy | Rituximab | B cell depleting | Fc receptor gamma-mediated antibody-dependent cytotoxicity and phagocytosis; Complement-mediated cell lysis; antigen presentation; B cell apoptosis; Depletion of CD4+ T cells. | (Mota *et al.*, 2017) |
| | Ofatumumab | | | |
| | Belimumab | Inhibitors of B cell function | | |
| | Atacicept | | | |
| | Tabalumab | | | |
| T-cell targeted therapy | Abatacept | CD28/CTLA4 system | Autoantigen recognition; Immune cell infiltrate; T cells activation. | (Mellado *et al.*, 2015) |
| | Belatacept | CD80/CD86 | | |
| Interleukin targeted therapy | Tocilizumab | IL-6 inhibition | Innate and the adaptive immune system perturbation; Acute-phase proteins. | (Raimondo *et al.*, 2017) |
| | Anakinra | IL-1 inhibition | Inflammatory responses; Matrixenzyme. | (Cavalli and Dinarello, 2015) |
| | Canakinumab | | | |
| | Rilonacept | | | |
| | Secukinumab | IL-17 inhibition | Mitochondrial function; Autophagosome formation. | (Kim *et al.*, 2017) |
| | Ixekizumab | | | |
| Growth and differentiation factors | Denosumab | RANKL inhibitor | Maturation and activation of osteoclast. | (Fassio *et al.*, 2017) |
| | Mavrilimumab | GM-CSF inhibitor | Activation, differentiation, and survival of macrophages, dendritic cells, and neutrophils; T helper 1/17 cell; modulation of pain pathways. | (Burmester *et al.*, 2017) |
| **Small molecules** | | | | |
| **Classification** | **Name** | **Mechanism of action** | **Potential mechanisms** | **Reference** |
| JAK pathway | Tofacitinib | JAK1 and JAK3 inhibitor | T-cell activation, pro-inflammatory cytokine production, synovial inflammation, and structural joint damage. | (Yamaoka, 2016; Winthrop *et al.*, 2017) |
| | Baricitinib | JAK1 and JAK2 inhibitor | | |
| | Filgotinib | JAK1 inhibitor | | |

## 1.6 Sulphated Disaccharides

In spite of the dramatic improvements seen with the biologics, 40% of patients remain unresponsive to available treatments. Some patients have to undergo regular changes to therapeutics to maintain responsiveness. For these reasons, there is an intense global effort to develop more potent and effective orally active anti-inflammatory drugs which can cure disorders like RA from their first diagnosis (Scott *et al.,* 2010). Therefore, sulphated disaccharides may pose as potential new anti-inflammatory therapeutic for the treatment of RA. Sulphated disaccharides are generated during inflammation by heparanase enzyme activity and are located within inflamed tissues (Cahalon *et al.,* 1997). Literature reports suggest that these compounds play an important role in the inhibition of rat adjuvant and collagen-induced rat and mouse arthritis and hypersensitivity responses *in vivo* through an unknown mechanism. Lees *et al.*, (2009) reported that orally active sulphated disaccharides may provide the basis for new oral anti-rheumatic therapeutics.

It has been reported that large sulphated polysaccharides (found in marine algae include carrageenan from red algae, ulvan isolated from green algae, and fucoidan from brown algae (Mclachlan, 1985)) such as calcium pentosan polysulphate have been found to be mildly anti-inflammatory but not anti-rheumatic. However, glycosaminoglycan polysaccharides with repeat disaccharide subunits possessing 2-amino and 6'-carboxylate groups have been found to possess anti-inflammatory and anti-rheumatic activity (Smith *et al.,* 1994). For example, chondroitin sulphate has been shown to have anti-arthritic activity when administered orally in rats and humans (Ronca *et al.,*1998).

Similarly, the anti-coagulant heparin is a polyanionic sulphated polysaccharide (Young, 2008), which is generally found in mast cells and is co-released with histamine into the vasculature during infection at injured tissues. At sites of tissue injury, it dissociates from its protein core to exist as free glycosaminoglycan chains (Nader *et al.*, 1999). It has been found to possess weak anti-asthma activity when given locally by inhalation (Lever *et al.*, 2001). However, heparin physiological analogues, heparan sulphates, have been found to inhibit T cell-

mediated immune responses in adjuvant-induced arthritis and delayed-type hypersensitivity in rodents when given orally in nanogram quantities (Cahalon *et al*; 1997 and Lider *et al.,* 1995).

The extracellular matrix heparan derived sulphate disaccharides differ from the heparin derived sulphate disaccharides in their backbone composition. As shown in Fig.9A and 9B, the heparin-derived sulphated disaccharides backbone is composed of iduronic acid and glucosamine moieties whereas the heparan sulphate disaccharide backbone is composed of glucuronic acid and glucosamine moieties having either a glycosidic -O- linkage or -N-linkage (Salmivirta *et al.,* 1996). Heparan sulphates are composed of glycosaminoglycan chains that are negatively charged under physiological conditions through the presence of sulphate and uronic moieties. They are present throughout the cellular surface and reside in most cell membranes and are prominent in extracellular matrix. Various degrees of sulphation occurs on each monosaccharide unit, ranging from zero to tri-sulphation (Salmivirta *et al.,* 1996, Cahalon *et al.,* 1997 and Chowers *et al.*, 2001). Cahalon *et al.,* (1997) suggest that sulphate group of sulphated disaccharides may be functionally important for their inhibitory action. Heparan and heparin glycosaminoglycan consist of heterogeneous mixtures of repeating units of D- glucosamine and L-iduronic acids or D-glucuronicacids, sulphation at each residue varies (Fig.1.11) (Salmivirta *et al.,* 1996).

Glycosaminoglycans (GAGs) are molecules made of long, un-branched chains of negatively charged sugars. They are made up of a repeating disaccharide unit. They are found throughout the body, including joints, blood plasma, skin, and various organs' mucous membranes. Each GAG has its function and benefit in the body. They play a big part in the cell signalling process, for example, controlled cell growth, facilitating cell adhesion, wound repair, anticoagulation, proliferation, and skin generation. The most common GAGs are heparin, heparan sulphate, chondroitin sulphate, and keratan sulphate with chondroitin sulphate, being the most abundant GAG in the body. GAGs trigger autoimmune dysfunctions which involve the success of GAG-combined cells. These cells shift to anatomical places predominant within GAGs promoting inflammation and pathology seen in human RA (Powell, 2004). Chondroitin

Sulphate (CS) is the major sulphated disaccharide formed in the joints. CS is a vital component of joint ECM and assumes a crucial task in developing and facilitating joint/cartilage pathologies. CS forms a vital part of cartilage. It gives elasticity to the cartilage by helping it retain water and reduces the activity of enzymes and substances that break down collagen in joints. It helps manage osteoarthritis, a common bone disorder that affects the cartilage surrounding your joints. Taking CS supplements increases the synthesis of various cartilage components while also preventing cartilage breakdown. (Eymard, *et al.*, 2017). In cases of inflammation, CS elicits an anti-inflammatory effect at the chondral and synovial levels preventing joint swelling and effusion. Studies show that CS affects inflammatory processes by inhibiting NF-κB signalling (Xu *et al*., 2008 and Jomphe *et al*., 2008) and also inhibits IL-1β-induced liberation of pro-inflammatory genes, for example, IL-6, NOS-2, and prostaglandin E2 synthase (da Cunha *et al*., 2017 and Gouze *et al*., 2006). Furthermore, CS was found to block LPS binding to CD44 on rat bone marrow-derived macrophages to inhibit the LPS/CD44/NF-κB pathway (Taraballi *et al*., 2016).

A study on the effects of CS and its oligosaccharides on TLR-mediated IL-6 secretion by macrophages like J774.1 cells (Jin *et al.*, 2011) suggested that TLR1/TLR2, TLR4, and TLR9 are different in terms of the structures of the ligand-binding domains. Unlike TLR1/TLR2 and TLR4, TLR9 contains an additional cysteine-rich motif that is possibly in charge of CpG binding (Jin *et al*., 2010; West *et al*., 2006; Bell *et al*., 2003 and Lee *et al*., 2001). This study proposed that the presence of this additional cysteine-rich domain in the TLR9 molecule might account for the CpG-induced IL-6 secretion mediated by TLR9 is most markedly suppressed by CS-C and Di-CSs, as compared with TLR1/TLR2- and TLR4-mediated IL-6 secretion (Jin *et al*., 2010). Thus, receptors for the sulphated disaccharides can be receptors displaying toll-like properties TLR9 ligands which get activated in response to DNA. It detects rare DNA signatures TLR9 sense, hence determining either some viruses or bacteria within the cell resulting in stimulation of an immune response. TLR9 assumes an important role in the activation of both immunes alongside inflammatory responses to different microbial components. It combines DNA in viruses alongside bacteria which triggers signal cascading that leads to a response of pro-inflammatory cytokine.

Sulphation as discussed above is the process that involves conjugation, in which different body processes, starting from biotransformation/detox pathways up to the biosynthesis of various proteins. Hormone sulphation allows the transportation of hormones through the blood to aim tissues. It enhances the binding of DNA present in bacteria and viruses, triggering pro-inflammatory responses. Studies suggest that only TLR9 receptors have demonstrated anti-inflammatory properties of Sulphated disaccharides. The other TRLs –ranging from TLR1 to TLR8 have not demonstrated any anti-inflammatory properties of Sulphated.

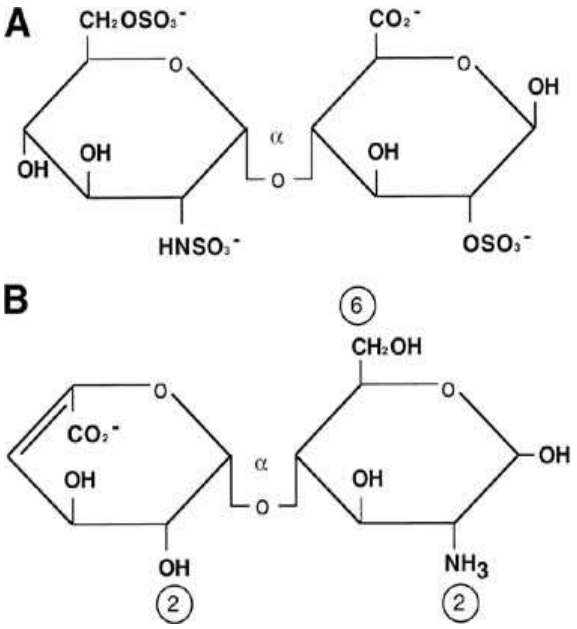


C

| | Iduronic Acid | Glucosamine | | Sigma Cat. No. |
|---|---|---|---|---|
| | *Position 2* | *Position 2 (N)* | *Position 6 (OH)* | |
| **3 Sulfates** | | | | |
| SSS-2 | S | S | S | H-9267 |
| **2 Sulfates** | | | | |
| SSH-3 | S | S | H | H-9392 |
| HSS-4 | H | S | S | H-1020 |
| SHS-5 | S | H | S | H-8892 |
| SActS-6 | S | COCH3 | S | H-9517 |
| **1 Sulfate** | | | | |
| SHH-7 | S | H | H | H-9142 |
| HHS-8 | H | H | S | H-9017 |
| HSH-9 | H | S | H | H-1145 |
| HActS-10 | H | COCH3 | S | H-8642 |
| SActH-11 | S | COCH3 | H | H-8767 |
| **Non Sulfated** | | | | |
| HActH-12 | H | COCH3 | H | H-0895 |
| HHH-13 | H | H | H | H-9276 |

**Figure 1. 11*. The backbones of the heparin and heparan sulphate disaccharide molecules.***

*(*A*) Structure of heparan sulphate - derived sulphated disaccharide (SSS1-DS) composed of glucuronic acid and glucosamine moieties. (*B*) The heparin-derived sulphated disaccharide (DS) backbone is composed of an iduronic acid and a glucosamine moiety. The numbers indicate positions to which sulphate or acetyl groups are attached. (*C*) The summary of the heparin-derived sulphated disaccharide (DS) used in the study by Chowers and colleagues (2001). The positions of the sulphate and acetyl molecules are indicated. The heparan sulphate–derived SSS1 and the heparin-derived SSS2 (shown in* B*) have a similar sulphation pattern, but differ in the DS backbone. Figure adapted from* (Chowers *et al.*, *2001).*

At the site of infection, macrophages synthesise cytokines that activate endothelial cells, whilst heparin sulphate on endothelial cells binds to leukocyte L-selectins leading to leukocyte rolling (Parish, 2006). Macrophages also release considerable amounts of chemokines that bind to GAGs on the endothelial surface (Webb *et al*., 1993). Leukocytes adhere to endothelial cells firmly and then migrate through the endothelial barrier. Therefore, the roles of GAGs in inflammation and immunity are linked to chemokines due to their highly polar nature. Heparan-sulphate glycosaminoglycan chains tend to exist as proteoglycan components that are tethered to a protein core. Therefore, they are expressed on the surface of cells, giving a net negative charge to these surfaces.

During inflammation, membrane-bound heparan sulphate is released into the ECM and the bloodstream, a process known as proteoglycan shedding which occurs when the core protein part of HS proteoglycan is cleaved by proteases (Nam and Park, 2012). The shed proteoglycans can be further degraded by mammalian heparanase or heparinase I, enzymes that digest long HS chains into small oligosaccharide fragments. All of this with the effect of degrading extracellular matrix. The heparan sulphate disaccharides then negatively downregulate inflammatory responses by inhibiting macrophage TNF-α, IL-8 and IL-1β synthesis (Cahalon *et al;* 1997 and Chowers *et al.,* 2001) and T cell function (Hecht *et al.*, 2004). Intracellular signalling in neutrophils has been shown to be affected by heparin (Lever and Page, 2001) and heparan sulphated disaccharides inhibit the transcription factor NF-κB. This in turn regulates the synthesis of TNF-α and leukocyte adhesion to the endothelium (Hershkoviz *et al.,* 2000). These heparan sulphate fragments are important mediators of inflammation (Collins and Troeberg, 2019), chemotaxis (Crijns *et al*., 2020) coagulation (Oduah *et al*., 2016), and infection (Aquino *et* al., 2020 and Hayashida *et* al., 2008) by interacting with signalling molecules (Fig. 1.13).

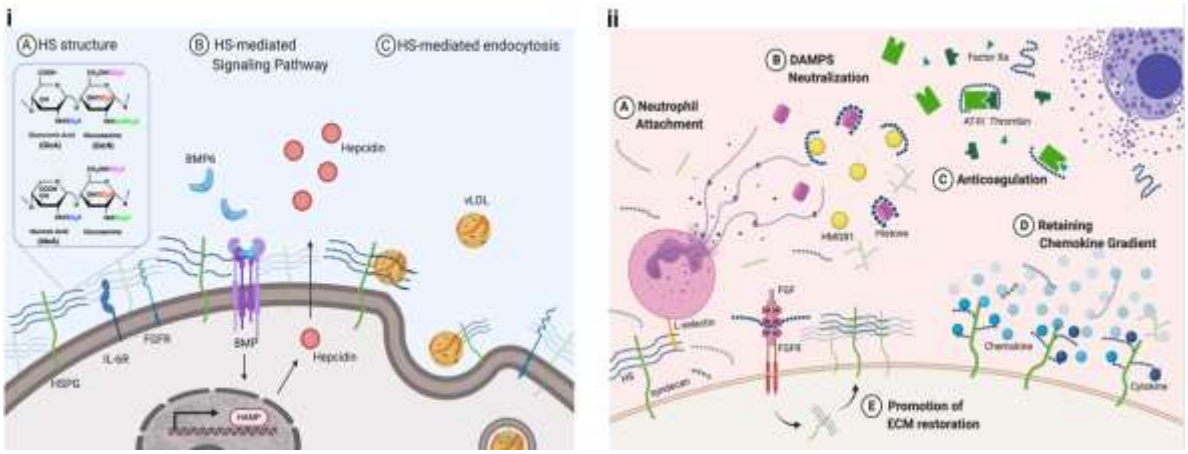


**Figure 1. 12*. Endogenous heparan sulphate (HS) on the cell surface in a healthy state (ii) and a disease state (ii).***

*(**A**) Membrane-bound HS is usually attached to a core protein in the form of heparan sulphate proteoglycan (HSPG), such as syndecan or glypican. (**B**) Membrane-bound heparan sulphate acts as a co-receptor for various ligands, for example, BMP6. In hepatocytes, heparan sulphate mediates hepcidin expression by modulating BMP6/BMP binding. (**C**) Membrane-bound heparan sulphate acts as a receptor to facilitate lipid clearance, for example, vLDL in the liver. In figure **ii.** (**A**) shows that membrane-bound heparan sulphate can bind to adhesion molecules on neutrophils, supporting their attachment and rolling on the cell surface. (**B**) Shed heparan sulphate fragments can bind to damage associate molecular patterns (DAMPs) (for example, histones and HMGB1 release by neutrophils) during inflammation, neutralize them, and prevent DAMPs from potentiating inflammatory response. (**C**) Highly sulphated heparan sulphate, heparin, is released by activated mast cells and simultaneously binds to antithrombin III (AT-III) and thrombin to inhibit coagulation cascades. Circulating heparan sulphate fragments can also bind to AT-III and inhibit factor Xa activity; however, they are usually not long enough to inhibit thrombin. (**D**) Heparan sulphate binds to chemokines (ex. CXCL-10, CXCL-12, CCL-2) and cytokines (ex. IL-8, IL-10, IL-12), maintaining their concentration gradients to recruit more immune cells. (**E**) Shed heparan sulphate fragments act as co-receptors for various ligands, for example, FGF. The formation of HS-FGF-FGFR complex induces downstream signalling pathways for ECM restoration. (Figure adapted from Arnold et al., 2020).*

Cahalon and colleagues (1997) produced heparin tri-sulphated disaccharides, di-sulphated disaccharides and non-sulphated disaccharides by the action of bacteria (*Flavobacterium heparium)* heparinase I on porcine intestinal mucosa heparin sodium salt and separated by high-performance liquid chromatography (HPLC). They studied the impact of the sulphated disaccharide molecules on TNF-α production *in vitro* by incubating mouse peritoneal macrophages of C57BL/6 mice with saline or with different concentrations (0.001 ng/mL to 100 ng/mL) of tri-sulphated disaccharides, di-sulphated disaccharides and non-sulphated disaccharides for 20 h and stimulated the mouse peritoneal macrophages with LPS. The percent inhibition of TNF-α production was determined in comparison to cultures of macrophages incubated with saline. The results demonstrated that tri-sulphated disaccharide and di-sulphated disaccharide produce a bell-shaped inhibition curve. The non-sulphated disaccharides did not inhibit macrophage TNF-α production.

Furthermore, Cahalon *et al.,* (1997) used an *in vivo* model to study the effects of sulphated disaccharides on cell-mediated inflammation in mice and rats. Groups of BALB/c mice were sensitized topically to oxazolone and the degree of delayed-type hypersensitivity reactivity was assessed 6 days later by applying oxazolone to the ears and measuring the increase in ear thickness 24 h later. The mice were treated by a s.c. injection of the indicated amounts of D-DS, T-DS or 0-DS given 1 day before primary sensitization. Dexamethasone, 40 µg, given 1 day before challenge, was used as a positive control for an anti-inflammatory effect. The percent inhibition was calculated in comparison to control sensitized mice that had been treated with saline. Percent inhibitions of 20% or more were significantly different ($P < 0.01$) from the saline control. They showed that the inhibitory effect of di-sulphated disaccharide was bell-shaped where higher concentrations of tri-sulphated disaccharide and di-sulphated disaccharide were found be less effective. The non-sulphated disaccharide was not effective compared to tri-sulphated disaccharide and di-sulphated disaccharide.

In addition, Cahalon *et al.,* (1997) tested sulphated disaccharides on adjuvant arthritis in female Lewis rats induced by with *M.tuberculosis* in oil. Rats were treated 12 days after the development of limbs swelling with di-sulphated disaccharides (subcutaneous route; s.c) non-sulphated disaccharides

(administered s.c.) or tri-sulphated disaccharide (administrated orally) and repeated at weekly intervals for 4 weeks. The doses of s,c. di-sulphated disaccharides were 30 ng, 120 ng or 240 ng. The dose of 120 ng produced significant differences from the saline control ($P < 0.01$) at days 20, 25, 30 and 35. The doses of s.c. non-sulphated disaccharides were 30 ng, 60 ng, 120 ng or 240 ng, none of these doses affected arthritis significantly. The doses of oral tri-sulphated disaccharide were 120 ng, 500 ng, 1200 ng or 5000 ng. The dose of 1200 ng produced significant differences for the saline control ($P < 0.01$) at days 17, 19, 21, 23 and 26. The di-sulphated disaccharides demonstrated bell-shaped inhibition dose-response curves. The non-sulphated disaccharide was less effective. The tri-sulphated disaccharides and di-sulphated disaccharides inhibited adjuvant arthritis more effectively when administered orally, and in nanogram amounts.

In another study, Chowers *et al.,* (2001) tested the effect of the various sulphated disaccharides on cytokine secretion from epithelial cells. In this study monolayers of HT-29 cells were incubated with a panel of sulphated disaccharide molecules at concentrations of 50 or 100 ng/mL. The sulphated disaccharide molecules reduced the spontaneous IL-8 secretion from the epithelial cells. Dose-dependent inhibition of IL-8 secretion was observed at concentrations as low as 0.01 ng/mL. The sulphated disaccharides had no effect or only a partial, non-dose-dependent effect on IL-8 and IL-1β secretion from HT-29 cells and sulphated disaccharides inhibited both IL-8 and IL-1β secretion. Similar effects were produced by the sulphated disaccharides on the Caco-2 cells.

Furthermore, the effect of sulphated disaccharide molecules was tested on the secretion of pro-inflammatory mediators by epithelial cells under TNF-α stimulation. The SSS-2 sulphated disaccharide with 3 sulphates inhibited the TNF-α – induced secretion of both IL-8 and IL-1β in a dose-dependent manner. This study suggested that the side residues attached to the sulphated disaccharide molecules determine these molecules inhibitory action and affinity with the cells. This study indicated that the number and position of sulphate molecules had an important effect on sulphated disaccharides activity where sulphate disaccharide molecules with 3 and 2 sulphates were inhibitory, but the molecules with only 1 sulphate were non-inhibitory. This study concluded that the

position of the sulphate and acetyl groups plays an important role in the biological activity of the different sulphated disaccharide molecules (Chowers *et al.,* 2001).

### 1.7 Rational for this study

Inflammation is a defensive cellular mechanism in response to harmful stimuli but uncontrolled inflammation leads to inflammatory diseases such as RA. The synovial CD68 macrophages are accountable for excessive pro-inflammatory TNF-α release. In spite of available therapies, there is still a need for orally active anti-inflammatory drugs. Hence, compounds with the potential to prevent the accumulation of macrophages, and to polarize CD68 pro-inflammatory macrophages to anti-inflammatory macrophages to inhibit TNF-α production may be useful in treating chronic inflammatory diseases.

Heparin derived sulphated disaccharide molecules have been reported to be synthesised in inflammation and reported to inhibit macrophage TNF-α production, delayed-type hypersensitivity, adjuvant arthritis, and rat collagen-induced arthritis with unknown mechanisms of action. When given *in vivo* they are anti-rheumatic and have a tentative mechanism for T-cells. Studies by Hiebert *et al*., (2002) and Lees *et al*., (2008) reported that sucrose octasulphate (SOS) is orally absorbed. Lees *et al*., (2008) used a 100mg/kg oral administration route once or twice a day for rat and mouse collagen-induced arthritis. In addition, Lees *et al*., (2008) attempted to convert Di-glucopyranosylamine (diGa) parenteral anti-rheumatic activity to oral activity through the suppression of gastric acid by the administration of sucralfate and lansoprazole. The study reported that SOS but not diGa reduces collagen arthritis. SOS treatment was effective during the sensitisation period in rats. Normally orally administered highly charged molecules are thought not to be effectively absorbed, but it seems that sulphated disaccharides are absorbed through the jejunum, from where blood bypasses the hepatic portal vein to the liver, into the general circulation. This suggests that heparin-derived sulphated disaccharides which are released during inflammation can be used as molecular regulators of inflammation if given orally.

Additionally, preliminary data (Bajwa and Seed, 2015 unpublished observations) indicated that these compounds have a distinct effect on the monocyte-macrophage differentiation *in vitro* and formed the basis of this study. In this study, U937 human monocytic cells were grown to confluence in RPMI 1640 and seeded into 96 well or 24 well plates at 107 cells/ml. U937 cells were incubated with PMA at 0.8, 8.0 or 80 nM for periods of 72 hours. Non-adherent cells were washed away, and the residual adherent cells were incubated with Trypsin/EDTA, aspirated, and counted with a haemocytometer. Flat, granular, viable cells (assessed by Trypan Blue exclusion) were then counted. Once a concentration of PMA and time of incubation were determined, cells were incubated with either sucrose octasulphate, diglucopyranosylamine octa-sulphate, heparin disaccharide-IIIH or heparin disaccharide-IS for two hours and PMA added for 72 hours. Differentiation into adherent cells was assayed as before. U937 cells were differentiated with 8 nM PMA for 72 hours as previously reported by us. 96 well plate data elicited erratic results. Incubation of U927 cells in 24-well plates elicited reproducible findings. SOS, DOS and HDS-IIIH exhibited bell shaped inhibition curves characteristic of these chemicals, with a maximal inhibition seen at $10^{-11}$ M. HDS-IS elicited a different shape, with inhibition of U937 cell differentiation reaching a maximum at 100 μM. This indicates that a single sulphate on each sugar is required for potent activity, as a three sulphate group as found with HDS-IS results in a great reduction in activity. SDS with a minimum of one sulphate per sugar inhibits PMA induced differentiation of U937 cells to adherent macrophage like cells. These preliminary findings led to the research aims and objectives listed below as further investigations on the mechanisms of anti-inflammatory actions of the sulphated disaccharide compounds could pave the way for the development of these compounds as potent therapeutics for RA.

The studies directed at specific molecules will contribute to an understanding of the pathogenesis of RA and the development of more effective therapies and preventive measures. Therefore, in this study, four sulphated disaccharides with different sulphation patterns were used to investigate the unknown cellular and molecular mechanisms of action of sulphated disaccharides on macrophage function. This study relates to sulphated disaccharide compounds sucrose octasulphate (SOS), diglucopyranosylamine octa-sulphate (diGaS, or DOS), heparin disaccharide-IS and heparin disaccharide-IIIH (HDS-IIIH) containing one

to eight sulphates (Fig. 4.01 in Chapter 4) at concentrations of $10^{-11}$ M to $10^{-4}$ M. This study relates to methods of testing the impact of sulphated disaccharides to investigate cell surface markers, cellular signalling pathways by which macrophage polarization may be affected by sulphated disaccharides for a deeper understanding of the mechanism of action of these compounds.

**Importance of the research:** The information of this thesis will directly inform the design of the protocols for the inhibition of monocyte-macrophage inhibition in the context of inflammation. In the future, if successful, this strategy may open the door for a new therapeutic approach.

**Overall, this study could contribute to the phase 1 trials of sulphated disaccharides aimed at inhibiting inflammation.**

## 1.8 Aim and Objectives

The work presented in this thesis aimed to investigate the unknown molecular mechanism of action of sulphated disaccharides through which they inhibit collagen and antigen-induced arthritis and TNF-α synthesis.

Macrophages play important roles in the initiation, propagation, and resolution of inflammation, and inflammation-related pathogenesis such as RA. Therefore, monocyte-macrophage differentiation is central to inflammation, none of the current biotherapies specifically target monocyte-macrophage differentiation in RA. Their plasticity (Mantovani *et al*., 2004; Mosser and Edwards, 2008) makes them an ideal target for the treatment of inflammation, especially arthritis. This study focused on small molecules to induce or inhibit monocyte-macrophage differentiation and polarization.

The specific objectives of this investigation are:

- To characterise and establish an *in vitro* monocyte-macrophage differentiation system.
- To identify the impact of sulphated disaccharides on differentiated macrophage cell surface marker and whether this contributes to cell functional outcomes.
- To study the impact of sulphated disaccharides on p38 and ERK1/2 MAPK signalling pathways and intracellular calcium mobilisation.
- To determine whether sulphated disaccharide compounds induce a phenotypic switch of differentiated macrophage (M0) phenotype into activated pro-inflammatory (M1) phenotype macrophage or anti-inflammatory (M2) phenotype macrophage or switch from M1 phenotype into M2 phenotype.

# CHAPTER 2: MATERIALS AND METHODS

## 2.1 Cell culture

Human monocytic U937 (ECACC; catalogue number: 85011440) and THP-1 (DSMZ; catalogue number: ACC-16) cell lines were obtained from the European Collection of Cell Culture (ECACC) and German Collection of Microorganisms and Cell Cultures (DSMZ) respectively. Both cell lines were maintained in 1X Roswell Park Memorial Institute (RPMI)-1640 medium containing L-Glutamine (Gibco; 11530586) supplemented with 10% heat-inactivated foetal bovine serum or FBS (Gibco; 11550356) and 1% penicillin (5,000 Unites/mL) and streptomycin (5,000 µg/mL) antibiotic (Gibco; 11528876). Cells were sub-cultured every 48 h to 72 h in $75cm^2$ (T75) flasks (JetBiofil; catalogue number: TCF-012-250) at 80–90% confluence in an environment of 5% $CO_2$ incubated at 37°C, at a density of $2x10^5$ cells/ml and $2x10^6$ cells/ml as recommended by supplier's instructions and cell viability (>95%) was confirmed by trypan blue (Sigma-Aldrich; TB154) dye exclusion using an automated cell counter Countess™ II FL (Invitrogen; AMQAF1000). Changes to cellular morphology were routinely checked and recorded by using a digital inverted microscope for transmitted light (AMG- EVOSxl). Routine testing of U937 and THP-1 cell cultures for Mycoplasma infection (Appendix Fig.1) was carried out by using the American Type Culture Collection Universal Mycoplasma detection kit according to manufacturer's instructions (ATCC, catalogue number: 30-1012K; Lot: 64021178).

## 2.2 Estimation of cell differentiation

To induce *in vitro* monocyte differentiation into macrophage-like cells, U937 and THP-1 cells were cultured in 24-well tissue culture plates to an initial density of $2x10^5$ cells/mL in a total volume of 2 mL per well with and without PMA (Sigma-Aldrich; P8139) to a final concentration of 0.8 nM, 8 nM or 80 nM (PMA stock concentration was prepared in DMSO; final concentration of DMSO was <0.01%) for a different time of 24 h, 48 h and 72 h at 37 $^0$C under standard culture conditions. For negative controls, the cells were incubated in the absence of

PMA, in an RPMI-1640 supplemented medium. After PMA stimulation, PMA-containing media and non-adherent cells were collected and centrifuged at 252 x *g* for 5 minutes at 4 $^{0}$C, resuspended in RPMI- 1640 supplemented medium, and counted by using Countess™ II FL. The residual adhered cells were washed twice with 1X Dulbecco's phosphate-buffered saline (PBS) [(-) CaCl2, (-) MgCl2)] (Gibco; 11530486) at room temperature without disturbing the cell layer and rested in PMA-free RPMI-1640 (10% FBS, 1% Penicillin and Streptomycin) supplemented media for additional 72 h to mature adherent cells. Cells were harvested, and subsequently washed twice in ice-cold PBS. Cells were detached by incubation with a 0.25% Ethylenediaminetetraacetic acid or EDTA (Sigma-Aldrich; E5134) solution for 5 min at 4°C and adherent cells were collected using a cell scraper (Greiner bio-one; 541070). The adherent cells were centrifuged, resuspended in RPMI 1640 supplemented medium, and counted by using Countess™ II FL. The U937 and THP-1 cells were visualised before and after monocyte differentiation by using a digital inverted light microscope at 40x magnification. Images were taken of the untreated cells and PMA treated macrophage-like cells. The 48 h and 72 h test groups were compared to their corresponding 24 h test group. The differentiation was calculated as the number of adherent cells that were alive after the trypan blue exclusion from the total number of cells counted by the Cell countess FLII cell counter bright field and was expressed as the number of adherent cells per mL. PMA-differentiated cells were further stimulated with 1µg/mL (Murthy *et al.*, 2000) LPS from Escherichia coli 0111:B4 (Sigma-Aldrich; catalogue number: L2630-25MG; Lot: 095M4165V) and 10 ng/ml (Bonder *et al.*, 1999) of IL-4 (Bio-legend) except one set of unstimulated negative control and PMA-stimulated alone positive control for 6 h cytokine analysis (6 h was chosen as optimal concentrations for stimulation of cytokine production in subsequent experiments (Appendix Fig.105 and Appendix Fig.106).

## 2.3 Cell treatment

To test the impact of sulphated disaccharide compounds (Table 2.01) on U937 and THP-1 differentiation, a monolayer of cells (2 x$10^5$ cell/mL) was incubated in a 24-well plate with SOS, DOS, HDS-I, and HDS-III at concentrations of $10^{-11}$ M to $10^{-4}$ M (concentrations were based on *in vivo* results as outlined in chapter 1) in the absence and presence of 8 nM PMA (2h before PMA addition) for 48 h. The samples were collected to determine the differentiation as described in section 2.2. The sulphated disaccharide compounds-treated cells in the absence and presence of PMA were compared to unstimulated (negative) control cells and PMA-stimulated (positive) control cells for morphological characteristics difference.

**Table 2.0 1** ***Stock of sulphated disaccharides was purchased from several suppliers.***

*Sulphate disaccharides were dissolved in 1X PBS to obtain a 10 mM stock solution and were further diluted with RPMI-1640 medium to prepare $10^{-11}$ M to $10^{-4}$ M concentration solutions.*

| Stock | Manufacturer |
|---|---|
| 5g Sucrose octasulphate sodium salt or SOS | Molekula; catalogue number: 86854612; CAS: 74135-10-7; Batch number: 207028 |
| 3.5g N-Acetyl-Diosamineoctasulphate octapotassium salt or DOS | synthesised Dr M Burnet, Synovo GmbH; CSY:5500; Date:26.07.06 |
| 5mg Heparin disaccharide (HDS-I) sodium salt or HDS-I | Sigma-Aldrich; catalogue number: HP267-5MG; Lot: SLBQ5662V |
| 1mg Heparin disaccharide (HDS-III) disodium salt or HDS-III | Sigma-Aldrich; catalogue number: H9142-1MG; Lot: BCBM5964V |

## 2.4 Flow cytometry

### 2.4.1 Immunofluorescent detection of cell surface differentiation markers

U937 and THP-1 cells were incubated with sulphated disaccharides in the absence and presence of PMA as described in section 2.3. For experimental controls, U937 and THP-1 PMA-differentiated cells at 48 h were cultured as described in section 2.2. The samples were centrifuged and re-suspended in 1 mL of 1X PBS. The samples were filtered through Nitex nylon mesh (Sefar; catalogue number: 30048962) and transferred into BD Falcon round-bottom tubes (Fisher; catalogue number: 352058). Samples were re-centrifuged and re-suspended in 200 µl of FACS buffer (2% FCS and 1 mM EDTA in PBS). The FCS was used in the FACS buffer to avoid non-specific binding by blocking other sites of proteins, hence reducing the background noise. It was also used to maintain cell viability and stabilise proteins. EDTA was used to limit the cell-cell interactions to reduce the number of doublet events. The samples were kept on ice to prevent the formation of aggregates.

#### 2.4.1.1 Staining

The samples were harvested, and counted as described in section 2.2. To identify and gate out dead cells from the final analysis the cells per sample were stained with Live/Dead fixable viability eFluor™ 506 dye (eBioscience; catalogue number: 65-0866-14; Lot: 4327321) for 10 mins at 4 $^{0}$C. This dye was excited by the violet (405nm) laser line with a peak emission of 506 nm as per the manufacturer's instruction. The non-specific binding of Fc receptors on monocytes and macrophages was blocked by incubating samples with 1% purified human Fc binding inhibitor (eBioscience Affymetrix; 14-9161-73) in PBS for 10 mins at 4 $^{0}$C.

Samples were then stained for 20 mins at 4 $^{0}$C with 1 µl of a standard panel of immune-phenotyping antibodies including PE-labeled anti-human CD14, FITC-

labeled anti-human CD11a, BV650-labeled anti-human CD11b, Cyanin 7 PE-labeled anti-human CD68 and for BV711- labelled anti-human CD206, PerCP/Cy5.5 anti-human CD163 and FITC anti-human CD86 surface markers (Table 2.02) at the manufactures' recommended optimal dilution to target an epitope of interest to identify and quantify the populations of monocyte and macrophage cells and their cell surface receptors. The specificity controls were also included where samples were stained with relevant mouse isotype control (Table.2.02) antibodies which are raised against an antigen not found in the cell type. The isotype controls were used to help distinguish a true positive signal from a negative signal due to non-specific binding. The isotype controls were used to set gates to define positive or negative populations for specific surface markers. Isotype controls were purchased from the same manufacturer as the primary antibody and used at the same concentration as the primary antibody.

**Table 2.0 2** ***Summary of antibodies and isotypes used for flow cytometry***

| Antibody specificity | Fluoro-chrome | Clone | Isotype | Clone | Dilution used | Source |
|---|---|---|---|---|---|---|
| CD14 | Anti-human CD14 PE 12-0149-42 | 61D3 | Mouse IgG1 K Iso Control PE | P3.6.2.8.1 (12-4714-41) | 1:200 | Invitrogen |
| CD11a | Anti-human CD11a FITC 11-0119-41 | HI111 | Mouse IgG1 K Iso Control FITC | P3.6.2.8.1 (11-4714-41) | 1:200 | Invitrogen |
| CD11b | Anti-human CD11b BV650 301335 | ICRF44 | BV650 Mouse IgG1 K Iso Control | MOPC-21 (400163) | 1:200 | Bio-legend |
| CD68 | Anti-human CD68 PE-Cyanine 7 25-0689-41 | EBioY1/ 82A | Mouse IgG2b CD68 Iso Control PE-Cyanine 7 | eBMG2b (25- 4732-81) | 1:200 | Invitrogen |
| CD206 | Brilliant Violet 711™ 321135 | 15-2 | Brilliant Violet 711™ Mouse IgG1, κ Isotype Ctrl | MOPC-21 | 1:200 | Bio-legend |
| CD163 | PerCP/Cy5.5 anti-human CD163 326511 | RM3/1 | PerCP/Cy5 .5 Mouse IgG1, κ isotype Ctrl | MOPC-21 400149 | 1:200 | Bio-legend |
| CD86 | FITC anti-human CD86 Antibody 374203 | BU63 | FITC Mouse IgG1,κ Isotype Ctrl | MOPC-21 (400107) | 1:200 | Bio-legend |

#### 2.4.1.2 Gating strategy

After the staining period, cells were washed, centrifuged, resuspended in PBS, and analysed by BD FACSCelesta™ having BDFACS Diva software (version 6.0) and analysed using FlowJo (TreeStar, Ashland, Oregon, USA). A minimum of 5 x $10^4$ cells were analysed in each experiment. Forward and side scatter light was used to identify the non-adherent or adherent populations and to measure the size and granularity of the cells. Histograms were gated on live populations based on forward and side scatter. Auto-fluorescence was recorded by analysing unstained cells. To determine the true positive signal from PMA stimulated cells compared to unstimulated cells, biological controls were used to set gating strategies. Therefore, PMA-stimulated, unstimulated cells and unstained unstimulated or even unstained treated sample controls were used to determine the true positive signal from PMA-stimulated cells (Fig.2.1 and Fig.2.2).

The location of the negative population was determined by acquiring an unstained sample. The unstained sample was used to determine the level of background fluorescence, voltages, and negative gates appropriately. Following, the isotype controls were acquired to determine the non-specific binding of an antibody to Fc receptors. This ensured that the observed staining of cells was due to specific antibody binding to the target cell rather than an artifact.

For flow cytometry, instrument controls were used at the beginning of experiments to help set up or confirm the BD FACSCelesta™ instrument parameters: photomultiplier tube (PMT) voltage and compensation for the multiple fluorophores. The unstained sample and the single colour stained cells were used to set up PMT voltages. Compensation controls were used for each experiment to ensure accuracy. Compensation beads controls were used to apply for compensation. Beads were used with an advantage of representation necessary to populate the compensation algorithm accurately. Same antibodies were used to stain beads as stained samples for accuracy. After setting up PMT voltages and compensating all the channels used, samples were acquired.

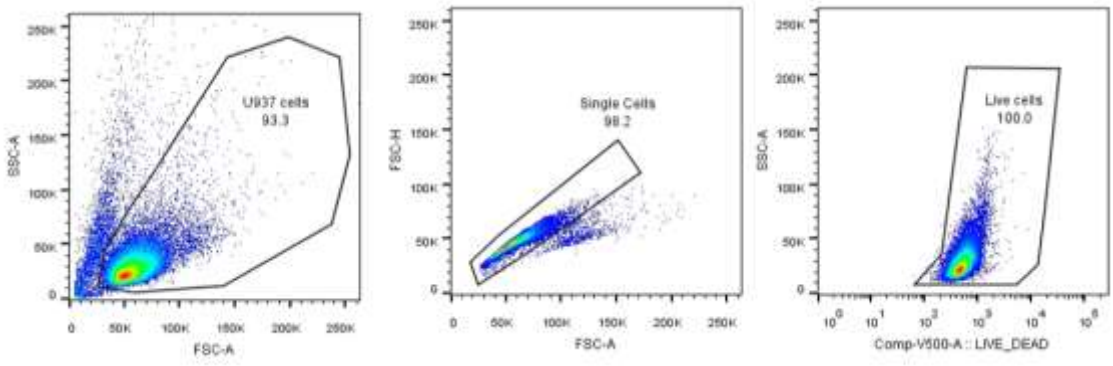


**Figure 2. 1*. Gating strategy for the analysis of U937 cells by flow cytometry.***

*U937 non-adherent cells were stained with Live/Dead fixable viability eFluor™ 506 dye. Cells were gated on live cells (FSC vs SSC) and double cells were discriminated using FSC-A versus FSC-H gating strategy. Dead cells were gated out from single live cells. FACS plot is representative of one out of 3 experiments.*

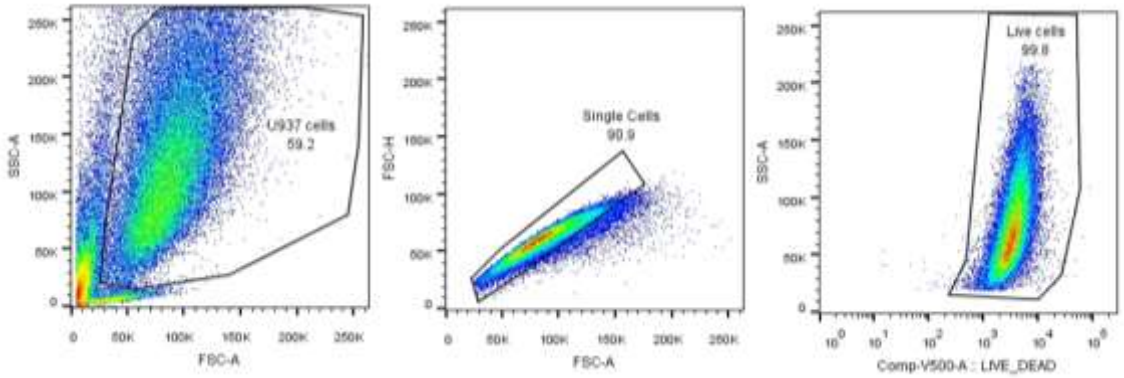


**Figure 2. 2*. Gating strategy for the analysis of PMA differentiated U937 cells by flow cytometry.***

*U937 PMA differentiated adherent cells were stained with Live/Dead fixable viability eFluor™ 506 dye and with anti-CD68 specific antibodies. Cells were gated on live cells (FSC vs SSC) and double cells were discriminated using FSC-A versus FSC-H gating strategy. Dead cells were gated out from single live cells using live/dead fixable viability dye. FACS plot is representative of one out of 3 experiments.*

### 2.4.2 Calcium measurements with Fluo-4 AM

THP-1 and U937 cells were cultured in a T75 flask overnight and were centrifuged at ~200 × *g* for 3 minutes. The cell pellet was resuspended in Fluo-4 Direct™ calcium assay buffer to a density of 2.5 x$10^5$ cells/100 µL per sample in Eppendorf tubes. The Eppendorf samples were incubated at 37°C and 5% $CO_2$ for 60 minutes. Following the incubation period, an equal volume of 2X Fluo-4 Direct™ calcium reagent loading solution (prepared as per manufacturer's instructions) was added directly into Eppendorf's and incubated for further 60 minutes. Changes in intracellular calcium levels were determined using the Fluo-4 Direct™ calcium assay kit (Invitrogen; F10471). The Flou-4 AM labelled U937 and THP-1 cell fluorescence intensity was measured using BD Accuri C6™ flow cytometer FL1-A FITC channel filters for excitation at 494 nm and emission at 516 nm and analysed using BD Accuri C6 software. The total acquisition time was 5 minutes. The cells were stimulated with sulphated disaccharides 10 minutes before the acquisition and stimulated with PMA for approximately 1 minute from the beginning of the measurement. Pre-treatment time was chosen as the optimal time for sulphated disaccharides in subsequent experiments (Appendix Fig.92 to Appendix Fig.96).

The gating was set by acquiring the unstained sample (not stained for Flou-4AM dye) on BD Accuri C6 flow cytometry. The no-cell control Flou-4AM buffer was also included as a negative control. The dead cells were excluded in flow cytometric analysis by gating out cells that show no fluorescence. Contour plots of side scatter vs. forward scatter were created to measure fluorescence at FL-1A FITC channel (Fig.2.3). In an optimisation experiment, the samples were stimulated with 1µM A23187 calcium ionophore (Andrews *et al.*, 2002) to test the impact of 8 nM PMA. Ionophore A23187 stock concentration was prepared using DMSO (the final concentration of DMSO was <0.01%). The baseline of calcium levels was recorded for 1 min on the BD Accuri C6, followed by the addition of test compounds. The tested compounds were added using a gel loading pipette (Gilson), allowing for the addition of test compounds. SB203580 and PD98059 were also tested to study their impact on intracellular calcium (Appendix Fig.97 to Appendix Fig.100).

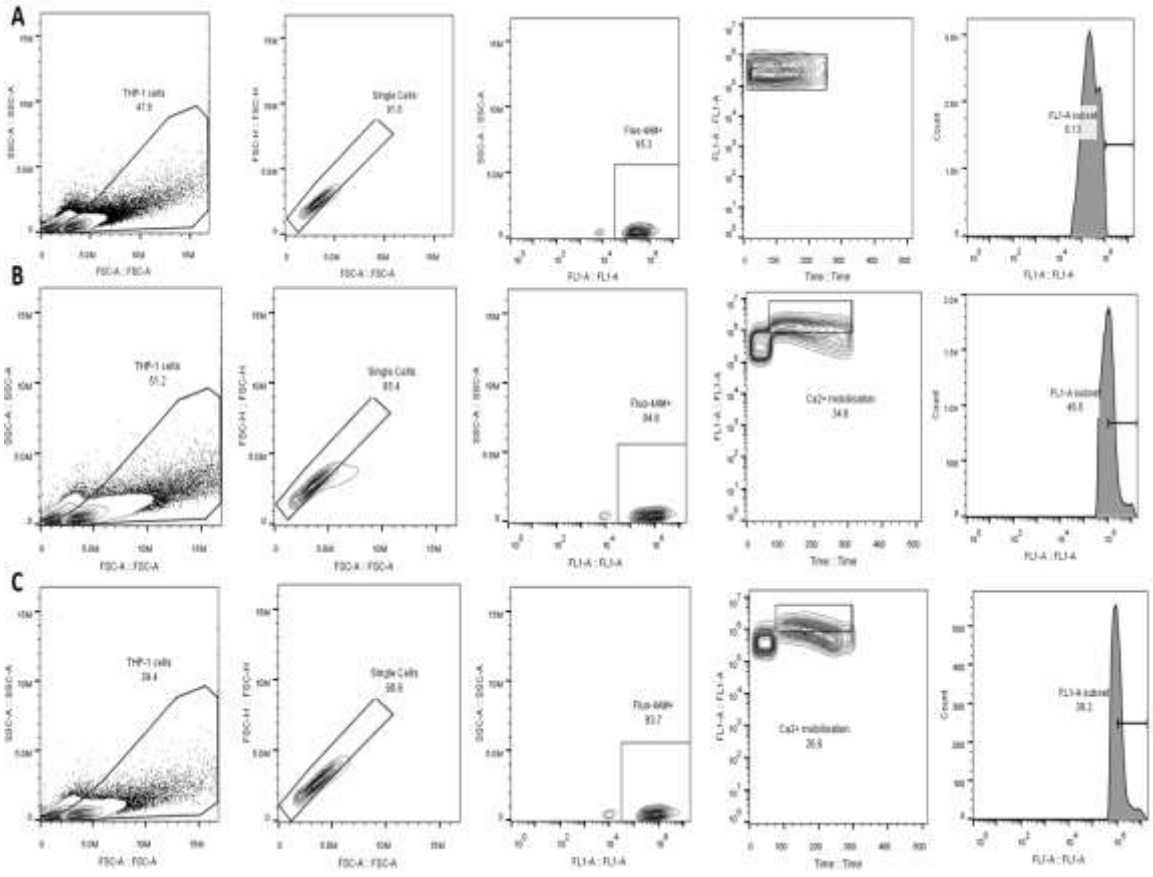

**Figure 2. 3.** ***Gating strategy for measurement of intracellular calcium ions of THP-1 cells by flow cytometry.***

*Contour plot of side scatter vs. forward scatter of Fluo-4AM stained THP-1 population in the (A) absence and (C) presence of 8 nM PMA. Fluorescence of Fluo-4AM (585/40) FL1-A FITC channel scatter vs time indicate the changes produced on fluorescence of cells by gating on side scatter vs forward scatter. Single cells were analysed by gating out doublet cells from the gate. Contour plots are representative of one out of 3 experiments. Panel (A) shows the baseline of calcium levels. (B) 1 µM Ionophore A23187 was used to compare the (C) PMA effect on $Ca^{2+}$ mobilisation. Ionophore A23187 induced a large increase in intracellular $Ca^{2+}$ mobilisation and thus higher Fluo-4 AM fluorescence. This reflected an increase in intracellular $Ca^{2+}$ of the U937 cells as would be expected with calcium Ionophore.*

## 2.5 Cell Proliferation Assay

### 2.5.1 CyQUANT® assay

Nucleic acid dye-binding CyQUANT® cell proliferation assay kit (Invitrogen; C7026) was also used to determine the number of cells in sulphated disaccharides treated samples. Briefly, a cell suspension of U937 and THP-1 with $5 \times 10^5$ cells/mL concentration was prepared in a growth medium, centrifuged for 5 minutes at 200 x *g,* and re-suspended in an RPMI medium. The volume of 200 µL of the suspended cells was added in two 96-well microplates (Jet Biofil; TCP011096; duplicate plates were prepared and labelled as *adhesion plate* and *cell number plate* for cell adhesion determination as per manufactures protocol. Samples were treated with sulphated disaccharides (Table 2.01) at concentrations of $10^{-11}$ M to $10^{-4}$ M for 1 h and 2 h before treatment with 8 nM PMA. Negative control with no cells and positive control PMA-stimulated wells were also included to compare cells adherence to plates in the presence of sulphated disaccharides. The cell suspension was incubated at 37°C for 48 h. The plate labelled as *cell number plate* was centrifuged and washed twice with 1X PBS to remove the growth medium. This plate was used to determine the total cell number in wells. The growth medium was removed from the second plate – labelled as the *adhesion plate* and washed twice with pre-warmed (37°C) 1X PBS to remove non-adherent cells. This plate was used to determine the number of adherent cells in the wells. Similarly, cell pellets of unstimulated and PMA-stimulated cells of 1 mL total volume at a density of 1 $x10^5$ cell/mL were prepared to prepare standard curves. The cells in both microplates and cell pellets in centrifuge tubes were stored at –70°C. After 24 h, microplates and cell pellets in centrifuge tubes were thawed at room temperature and 200µL of the 1X CyQUANT® GR dye/cell-lysis buffer was added to each sample well. The samples were incubated for 5 minutes at room temperature in the dark. The samples fluorescence was measured using a fluorescence micro-plate multi-mode reader Synergy/HTX (BioTek) with filters 485/20 nm excitation and 528/20 nm emission maxima. The observed fluorescence was converted to cell numbers using a standard curve according to the manufacturer's protocol. CyQUANT® GR dye/cell-lysis buffer was used to make dilution series in the wells of a microplate

corresponding to cell numbers ranging from 50 to 50,000 in 200 µL volumes. A 200 µL sample with no cells was also included as a control.

### 2.5.2 MTT assay

The colorimetric yellow 3-(4,5-dimethythiazol-2-yl)-2,5-diphenyl tetrazolium bromide (MTT) assay (Chowers *et al*; 2001 and Mosmann, 1983) was performed to study the metabolic activity of U937 and THP-1 cells in the presence of PMA and sulphate disaccharide compounds. This assay allows the yellow MTT to enter the cells and pass into the mitochondria where it reduces to an insoluble, dark purple coloured formazan product and reflects metabolic activity as the number of viable cells present in the sample. The MTT was dissolved in PBS to obtain a 0.5 mg/mL stock solution and was stored at -20 $^{0}$C.

i) To test PMA concentrations impact on the metabolic activity of U937 and THP-1 monocyte cells (2x$10^5$ cells/100µl/well) were incubated in a 96-well plate in the presence or absence of PMA (0.8 nM, 8 nM, 80 nM) as described in section 2.2.

ii) To test sulphated disaccharides ($10^{-11}$ M to $10^{-4}$ M) impact on the metabolic activity of U937 and THP-1 cells were incubated in a 96-well plate in the absence and presence of PMA as described in section 2.3.

After 48 h, 25 µl of an MTT solution (0.5 mg/ml) was added directly to each well following 4 h incubation in dark at 37 °C in 5% $CO_2$. The plates were then centrifuged at 700 × *g* for 15 minutes. The supernatants were removed from all the wells and formazan crystals were solubilised with 100 µl of DMSO and the absorbance was determined at 570 nm using an ELISA multi-mode plate reader (Synergy/HTX BioTeK). The cells treated with RPMI-1640 media were used as negative control and in the presence of PMA were used as a positive control.

The percentage of viability was calculated using the formula:

$$\text{Percentage of survival cells} = \frac{\text{The absorbance of a test sample in the absence of PMA and absence of PMA}}{\text{The absorbance of control}} \times 100$$

## 2.6 Enzyme-linked immunosorbent assay (ELISA)

U937 and THP-1 cells were treated with sulphated disaccharides 2 h before PMA treatment for 48 h as described in section 2.3 and 2 h before LPS or IL-4 treatment for 6 h (Fig.2.4) as described in section 2.2.

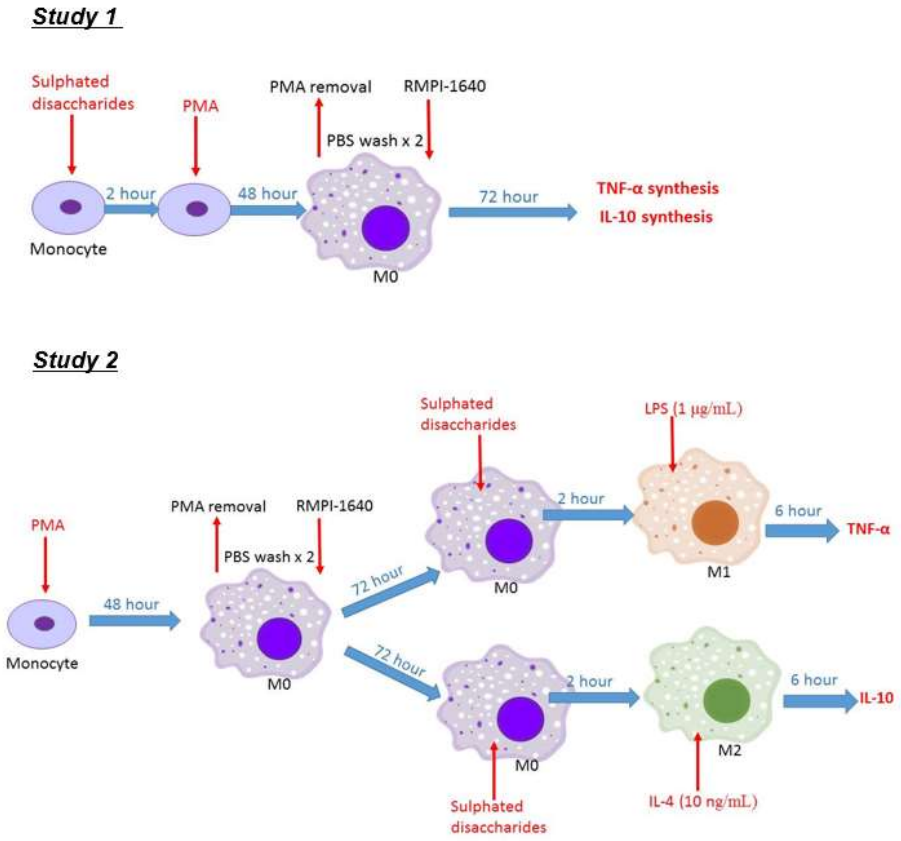


**Figure 2. 4*. In vitro study design 1 and study 2.***

*The impact of sulphated disaccharides on PMA, LPS, or IL-4 induced TNF-α and IL10 production when given 2 hours before PMA or LPS/IL-4. In a study, 1 cells were not stimulated with LPS or IL-4. The optimal time period for LPS or IL-4 was optimised in a preliminary experiment (Appendix Fig. 104 to Appendix Fig.105).*

The supernatants from experimental cultures were assessed for TNF-α and IL-10 cytokines concentration quantification by using Human TNF-α (eBioscience; 88-7346-88) and IL-10 (Invitrogen; 88-7106-88) ELISA Ready-Set-Go Kits according to manufacturer's instructions. Briefly, 96-well ELISA specific high binding plates (Jet Biofil; FEB-100-096) were coated with 100 µL diluted capture

antibody anti-human TNF- αpurified or IL-10 in coating buffer per well. The plates were sealed with adhesive plastic and incubated overnight at 4 $^{0}$C. The ELISA plate wells were aspirated and washed 3 times with >250µL/well wash buffer containing 1x PBS, 0.05% Tween® -20 (Sigma-Aldrich; P2287). The plate wells were blocked with 200 µL/well of 1x ELISA/ELISPOT diluent and covered with adhesive plastic. The plates were incubated at room temperature for 1 h. The plate wells were aspirated and washed 1 time with wash buffer.

A series of standards were prepared according to the manufacturer's instructions, and experimental samples were diluted at 1:10 or 1:20 before adding 100µL of each to the plate. The plates were incubated overnight at 4 0C. After 24 h, the wells were aspirated and washed 3-5 times with wash buffer. The diluted anti-human TNF-α biotinylated component or IL-10 (100µL/well) was added and the plates were incubated for 1 h at room temperature. The plate wells were again aspirated and washed 3-5 times with wash buffer. Enzyme Avidin-HRP (100µL/well) was added and plates were incubated for 30 minutes at room temperature. The plate wells were aspirated and washed 5-7 times with wash buffer. The detection 1X TMB solution (100 µL/well) was added and incubated at room temperature (in dark) for 15 minutes. The enzyme reaction was stopped by adding 50 µL/well stop solution 2N ($H_2SO_4$) or sulphuric acid. The absorbance of the end product was measured at 450 nm by using an ELISA multi-mode plate reader (Synergy/HTX BioTeK).

The average absorbance measurement for the duplicate wells of standards, blanks, and experimental samples (triplicates) was calculated. The average of the blank wells was subtracted from the average absorbance reading for standards and experimental samples to give the correct absorbance. The standard curve of serial dilutions for each plate was created using computer software GraphPad prism (version 4). The log of the standard concentrations was plotted on the x-axis and mean absorbance was plotted on the y-axis. The best fit line was generated by non-linear regression analysis. The concentration of the experimental samples was determined using the average absorbance value of each sample (y- value) and the equation was generated from the standard curve to solve for X (unknown) representing the concentration of cytokine in that sample.

## 2.7 Protein expression

### 2.7.1 Protein extraction

The protein was extracted using a mammalian cell lysis buffer of cell lysis kit (Sigma-Aldrich; MCL1) as per the manufacturer's instructions. Briefly, U937/THP-1 cells were seeded in T25 flasks (2 x $10^5$ cells/mL) as described in section 2.3. The cell suspension was centrifuged for 5 minutes at 420 x g, the cell pellet was washed twice with PBS and re-centrifuged. The cell pellet containing $10^6$-$10^7$ cells was resuspended in 1 mL of cell lysis buffer as per the manufacturer's instructions. The adherent cells were washed twice with 1X PBS and cell lysis buffer was added in T25 flasks. The resuspended non-adherent and adherent cell samples were incubated for 15 minutes on an orbital shaker (Stuart Scientific; STR6) at 4 $^0$C. The adherent cells were scraped gently and collected in a centrifuge conical test tube. The cellular debris for adherent and non-adherent samples was pelleted by centrifugation for 10 minutes at 12,000 x *g*. The protein-containing supernatant was transferred into an ice-cold test tube. Before the isolation was carried out, the viability of the detached cells in each subpopulation was checked to exceed 85% as determined by trypan blue exclusion using an automated cell counter.

### 2.7.2 Bradford protein assay

Quantification of purified proteins was performed utilising the colorimetric Bradford protein assay (Bradford, 1976). In this assay, an acidic protein assay dye reagent concentrate containing phosphoric acid and methanol (Bio-Rad; catalogue number: 500-0006) was used to bind to protein in solution. The lyophilized protein assay standard II bovine serum albumin (BSA) standard (Bio-Rad; catalogue number: 500-0007) serial dilutions were prepared in order to generate the standard curve from 1.2 mg/mL to 0.06mg/mL. The samples were diluted in deionised water in a 1:5 dilution. Ten microliters of standards and diluted samples were added per well in a 96 well plate. Following this, diluted Bradford dye reagent (200 µL/well) was added and incubated on an orbital

shaker at room temperature for 5 minutes as per the manufacturer's instructions. The absorbance was measured at 595 nm and a colour gradient was observed where brown colour indicated low concentration and a blue colour indicated a high concentration. The binding of proteins to the dye induces a shift in maximum absorption from 465 nm to 595 nm which is stable for one hour. The unknown concentration of protein samples was quantified by using the BSA standards by extrapolating the absorbance on the y-axis against the known concentrations of the BSA standards on the x-axis, using GraphPad prism 8.2.1.

### 2.7.3 Sodium dodecyl sulphate polyacrylamide gel electrophoresis (SDS-PAGE)

The samples in cell lysis buffer (as described in section 2.7.1) were diluted at a 3:1 ratio with 4x Laemmli sample buffer (Bio-Rad; catalogue number: 1610747) containing 277.8 mM Tris-HCl, pH 6.8 sample buffer, 44.4% (v/v) glycerol, 4.4% sodium dodecyl sulphate or SDS, 0.02% bromophenol blue, 100 µL DL-Dithiothreitol solution or DTT (Sigma-Aldrich; BCBT334). The protein samples were heated at 95 $^{0}$C for 5 minutes using heat block thermomixer comfort (Effendroff) and cooled on ice. The samples were centrifuged at 189 x *g* for 5 minutes. The protein samples were subjected to 12% sodium dodecyl sulphate-polyacrylamide gel electrophoresis (SDS- PAGE). The samples were sized resolved using the Mini-PROTEAN® Tetra-cell gel electrophoresis system (Bio-Rad).

The 10 mL of a 12% resolving gel was prepared with 4 mL protogel 30% containing 0.8% (w/v) Bis-Acrylamide stock solution (37.5:1) (National diagnostic; EC-890), 2.5 mL 4x protogel resolving buffer containing 1.5M Tris-HCl, 0.4% SDS, pH 8.8 (National diagnostic; EC-892), 3.39 mL deionized water, 0.1 mL of 10% ammonium persulphate or APS (Sigma-Aldrich; A3678) and 0.01 mL of N,N,N',N'- tetramethylethylenediamine or TEMED (Sigma-Aldrich; T9281). Similarly, 10 mL of a 4% stacking gel was prepared with 1.3 mL protogel 30%, 2.5 mL protogel stacking containing 0.5M Tris-HCl, 0.4% SDS, pH 6.8 (National diagnostic; EC-893), 6.1 mL deionized water, 0.05 mL 10% APS and 0.01 mL TEMED. The 12% acrylamide gels were transferred to an electrophoresis tank

containing 1x electrophoresis running buffer: 25 mM 2- Amino-2-(hydroxymethyl)-1,3-propanediol or Tris (Roche diagnostics; 10708976001), 250 mM glycine (Sigma-Aldrich; G8898), and 0.1% sodium dodecyl sulphate or SDS (Sigma-Aldrich; L3771). Precision Plus ProteinTM dual colour standards (10 µl) with a molecular weight range from 250 kDa – 10 kDa (Bio-Rad; 161-0374) were used to verify the electro-transfer and determine the protein molecular weight. It was loaded in the 1st lane of the gel and the remaining lanes were loaded with 20 µg experimental protein samples according to each experiment plan. The samples were run at a voltage of 50 V until the dye reached the bottom of the gel (approximately 1 hour). To avoid protein elution from the gel, the gel was immediately processed for transfer.

### 2.7.4 Transfer of proteins

A 24 mM Tris-base, 194 mM glycine, and 20% methanol (Acros organics UK; 325740025) containing transfer buffer immersed filter sandwich method was used for protein standard and protein transfer. The transfer buffer soaked three mini transfer blot filter papers (Bio-Rad; 1703932) were placed followed by 0.2 µm pore size nitrocellulose membrane (Amersham™ Protran® Premium Western blotting membrane) in the transfer cassette (Bio-Ra). On top of this, the SDS-PAGE gel was placed followed by a wet filter paper. The sandwich (filter paper/membrane/filter paper) cassettes were placed in Trans-Blot® Turbo™ transfer system (Bio-Rad) run for mixed molecular weight protocol for 7 minutes electric charge to allow migration of proteins from the gel onto a membrane. Completion of transfer was visually confirmed using a pre-stained molecular weight marker.

### 2.7.5 Blocking the membrane

The nitrocellulose membrane was washed three times with 15 mL of 1X TBS, 0.1% Tween-20 wash buffer with 5 minutes incubation period. The two blocking buffers were used in this study and optimised for different antibodies. The

nitrocellulose membrane was blocked with either 5% (w/v) non-fat dry milk (Marvel; 3023034) or 5% bovine serum albumin or BSA (w/v) (Sigma-Aldrich; A7906-100G) containing 1X TBS, 0.1% Tween-20 blocking buffer. The membrane was incubated with 25 mL of blocking buffer for 1 hour at room temperature on an orbital shaker. For antibodies raised in mouse such as β-actin and IkBα, the membrane was blocked with 5% non-fat milk blocking buffer whereas, for antibodies raised in the rabbit the membrane was blocked with 5% BSA blocking buffer. The membrane was washed three times with 15 mL of 1X TBS, 0.1% Tween-20 wash buffer for 5 minutes. The membrane was blocked with blocking buffer to achieve optimal signal of proteins by reducing the non-specific binding of the primary or secondary antibodies (Table 2.03) and to reduce background.

### 2.7.6 Incubation with the primary antibody

The primary antibody dilutions of 1:5000 for mouse anti-β- actin monoclonal antibody and 1:1000 for total and phospho p38, ERK1/2, IkBα, p65NF- kB and p21 was done in either 5% (w/v) non-fat dry milk or 5% BSA (w/v) containing 1X TBS, 0.1% Tween-20 diluent following manufacturers datasheet. The nitrocellulose membrane was incubated with 10 mL of primary antibodies overnight (to ensure specific binding of the antibody to the target protein) at 4 $^{0}$C temperature (to prevent degradation of the target protein) on an orbital shaker (to enable adequate homogenous covering of the membrane and to prevent uneven binding). Following overnight primary antibody incubation, the membrane was washed three times with 15 mL of 1X TBS-T, 0.1% Tween-20 wash buffer for 5 minutes at room temperature on an orbital shaker.

The primary antibody positive controls were also performed to assess and validate their specificity to the target protein of interest. The unstimulated and PMA stimulated samples of U937 cells were subjected to the primary antibody overnight at 4 $^{0}$C. The primary antibody control for phosphorylated form and total protein was performed in the absence of secondary antibodies.

### 2.7.7 Incubation with the secondary antibody

Following overnight primary antibody incubation, the membrane was washed three times with 15 mL of 1X TBS-T, 0.1% Tween-20 wash buffer for 5 minutes at room temperature on an orbital shaker to remove residual primary antibody. The membrane was incubated in 5% (w/v) non-fat dry milk or 5% BSA (w/v) in 1X TBS, 0.1% Tween-20 containing a 1:2000 dilution of anti-mouse IgG/HRP antibody or anti-rabbit IgG/HRP antibody for 1 hour at room temperature on an orbital shaker. The secondary antibody (Table 2.3) was used against the same species in which the primary antibody was raised. After an incubation period, the membrane was washed three times in 1X TBS-T, 0.1% Tween-20 wash buffer for 5 minutes at room temperature on an orbital shaker. The secondary antibody control for anti-mouse IgG/HRP antibody and anti-rabbit IgG/HRP antibody was also performed in the absence of the primary antibody (Appendix Fig.81). SB203580 and PD98059 were also tested to study their impact on p38, ERK1/2, and p21 (Appendix Fig.83 to Appendix Fig.91).

**Table 2.0 3** ***Summary of antibodies used to detect protein expression by immunoblotting.*** *The anti-rabbit secondary antibody was used raised against primary antibody raised in rabbit and similarly, anti-mouse secondary antibody was used raised against primary antibody raised in mouse.*

| Primary antibody | Antibody host & | Molecular weight | Dilution | Secondary antibody | Dilution |
|---|---|---|---|---|---|
| β-actin (Sigma-Aldrich, A5316) | mouse monoclonal antibody | 42 | 1:5000 | HRP-conjugate anti-mouse IgG antibody (Cell Signalling, 7076) | 1:2000 |
| Total IkBα Cell Signalling, 4814S) | Mouse monoclonal antibody | 39 | 1:1000 | | |
| Phospho-IkBα (Cell Signalling, 2859S) | Rabbit monoclonal antibody | 39 | 1:1000 | HRP-conjugate anti-rabbit IgG antibody (Cell Signalling, 7074) | 1:2000 |
| Total p38 MAPK (Cell Signalling, 8690S) | Rabbit monoclonal antibody | 38 | 1:1000 | | |
| Phospho- p38 MAPK (Cell Signalling, 4511S) | Rabbit monoclonal antibody | 38 | 1:1000 | | |
| Total p42/p44 ERK MAPK (Cell Signalling, 4695S) | Rabbit monoclonal antibody | 42 and 44 | 1:1000 | | |
| Phospho-p42/p44 ERK MAPK (Cell Signalling, 9101S) | Rabbit monoclonal antibody | 42 and 44 | 1:1000 | | |
| Total p65NF-kB (Cell Signalling, 8242S) | Rabbit monoclonal antibody | 65 | 1:1000 | | |
| Phospho-p65NF-kB (Cell Signalling, 3033S) | Rabbit monoclonal antibody | 65 | 1:1000 | | |
| Total p21WAF1/Cip1 (Cell Signalling, 2947S) | Rabbit monoclonal antibody | 21 | 1:1000 | | |
| Phospho-p21WAF1/Cip1 (Thermofisher, PA5-36677) | rabbit polyclonal antibody | 21 | 1:1000 | | |

### 2.7.8 Visualisation of membrane

The membrane was visualised by using the Amersham™ ECL Prime detection reagent (GE Healthcare; catalogue number: RPN2232). The membrane was incubated with 10 mL (5 mL Reagent A, 5 mL Reagent B) for 1 min at room temperature with gentle agitation and exposed to x-ray film (ChemiDoc, Bio-Rad). Initially, signal intensities of the protein ladder were analysed using an Image Lab 5.1 software (Bio-Rad) colometric auto-exposure setting to ensure the band analysed is of the correct molecular weight. Secondly, a high-resolution sensitivity setting was used to analyse for specific protein bands between 1 and 300 seconds of exposure. Quantification of the protein bands was performed by densitometry Image J and the signals were then normalised to control, and the results were expressed in arbitrary units.

### 2.7.9 Reprobing of membrane

Membranes were stripped of antibodies and reused (where necessary) for the detection of a second protein. After x-ray film exposure, the membrane was washed four times for 5 minutes with 15 mL of 1X TBS, 0.1% Tween-20 washing buffer to remove the chemiluminescent substrate. The membrane was incubated for 30 minutes in 1X western blot stripping buffer (Thermofisher; catalogue number: 46430) at room temperature with slight agitation. The membrane was washed for six minutes with 15 mL of 1X TBS, 0.1% Tween-20 washing buffer. The complete removal of secondary antibody was tested by incubating the membrane with a new chemiluminescent substrate working solution and exposed to x-ray film. After determining the proper stripping of the membrane, the second immunoprobing experiment was performed. The membrane was washed four times for 5 minutes with 15 mL 1X TBS, 0.1% Tween-20 washing buffer to remove the chemiluminescent substrate. The membrane was blocked and incubated with antibodies as described in sections 2.7.5- 2.7.7. The freshly prepared primary and secondary antibodies were used for the detection of a second protein to maintain the effective concentration of the diluted working solutions.

## 2.8 RNA purification

### 2.8.1 Total RNA isolation

To study the impact of sulphated disaccharides on gene expression of U937 cells, total RNA was isolated using Trizol reagent (Invitrogen; 15596026) according to the manufacturer's protocol. Briefly, U937 cells (2 x $10^5$ cells/mL/well) were grown in monolayer in 6-well plates in the presence of SOS, DOS, and PMA as described in section 2.3. Total RNA from unstimulated control U937 cells, PMA-stimulated cells, PMA + LPS-stimulated cells and PMA + IL-4 stimulated cells were also isolated. After the treatment incubation period, cell culture growth media was removed from the 6-well plates. Trizol reagent (400µL per 1mL 1x $10^5$ -$10^7$ cells) was added directly to the culture plates to lyse the cells. The lysate was incubated for 5 min at room temperature and collected in sterile Eppendorf tubes. Chloroform (80 µL per 1 mL of Trizol reagent) was added to the samples for 15 sec and incubated for 3 min at room temperature. The samples were centrifuged for 15 min at 12000 x g at 4 $^oC$. The aqueous phase collected was collected, mixed with isopropanol (200µL per 1 mL of Trizol reagent), and incubated for 10 min at room temperature. The samples were centrifuged for 10 min at 12000 x g at 4 $^oC$. The supernatant was discarded and a white gel-like pellet was washed and re-suspended with 400 µL 75% ethanol. The samples were centrifuged at 7500 x g at 4 $^oC$ for 5 min. The supernatant was discarded and the pellet was dried at room temperature for 5-10 min. The pellet was re-suspended in 20µL of nuclease-free water (Promega, catalogue number: M7505). The samples were incubated in a heat-block set at 55-60 $^oC$ for 10-15 min. The RNA samples were stored at -80 $^oC$ until needed.

The RNA concentration was quantified using NanoDrop™ Spectrophotometer (Thermo Fisher Scientific). The absorbance at 260 nm of the NanoDrop™ instrument provides total nucleic acid content and absorbance at 280 nm provides RNA sample purity. The RNA samples were diluted in RNase-free water and then the absorbance of samples was measured at 260 nm and 280 nm. A ratio of approximately 2 was considered pure.

### 2.8.2 DNase treatment of extracted RNA samples

The DNase treatment of RNA samples was performed using the RQ1 (RNA-Qualified) RNase-Free DNase kit (Promega; catalogue number: M6101) to maintain the isolated total RNA integrity. The DNase I (endonuclease) digestion reactions (Appendix Table 1) were prepared for each experimental RNA sample and were incubated at 37 $^{0}$C for 30 min. The DNase digestion reaction was terminated by adding 1 µL of RQ1 DNase stop solution (20mM EGTA, pH 8.0) and the reaction was incubated at 65 $^{0}$C for 10 min to inactivate the DNase. The concentration of treated RNA was again quantified using NanoDrop™ Spectrophotometer as described in section 2.8.1.

## 2.9 Reverse transcription–polymerase chain reaction (RT-PCR)

### 2.9.1 First-strand cDNA synthesis

The 10 ng of total RNA was reverse transcribed into full-length, random primer-primed first-single stranded complementary DNA (cDNA) using a GoScript™ reverse transcription mix, random primers (Promega; A2801) that includes the GoScript™ enzyme mix (GoScript™ reverse transcriptase and recombinant RNasin® Ribonuclease inhibitor), GoScript™ reaction buffer (random primers, $MgCl_2$ and dNTPs) and nuclease-free water. The final volume of 10 µL GoScript™ reverse transcription mix reaction for each cDNA reaction was prepared on ice by combining GoScript™ reverse buffer containing random primers, nuclease-free water, and with or without GoScript™ enzyme mix (Appendix Table 2 and Appendix Table 3). The no-RNA template control reactions in the absence of the GoScript™ enzyme mix were prepared to confirm the absence of DNA genomic in the total RNA samples.

Furthermore, the final volume of 20 µL reactions was prepared in nuclease-free, low retention PCR-compatible reaction tubes by combining 10 µL GoScript™ reverse transcription mix with experimental DNase-treated RNA samples (total RNA volume required to add in reaction to obtain 10 ng cDNA was calculated

after RNA quantification with NanoDrop (as described in section 2.8.1) and nuclease-free water as (described in Appendix Table 4). The reverse transcription reactions were incubated in a programmed thermal cycler PCR (Bio-Rad T100TM thermal cycler) for cDNA template (Appendix Table 5). Following termination of the reaction, RT-PCR products were stored at 4 $^{0}$C for immediate analysis or stored at -20 $^{0}$C for long-term storage.

### 2.9.2 Primers for cDNA amplification

For amplification of cDNA by RT-PCR (Appendix Table 6 to Appendix Table 8), the published gene-specific forward and reverse primer sequences for CD14 (Park *et al.,* 2007), CD200R (Kim *et al.,* 2016), Arginase 1 (Jimenez-Garcia *et al.,* 2015), p21WAF1/Cip1 (Matsumoto *et al.,* 2006) were used and lyophilized primers were accessed from Eurofins genomics. Published β-actin primer sequence (Park *et al.,* 2007) was used as an internal control (Table 2.04). The product size of primers was confirmed using the Primer-BLAST tool (NCBI).

To reconstitute the primers the lyophilized primer tubes were centrifuged down before opening the tube. The lyophilized primers were reconstituted in nuclease-free water to a final concentration of 100 µM stock for each primer by using the following mentioned formula:

100 µM = X nmoles lyophilized primer + (X × 10 µl RNase-free water)

To determine the amount of water to add to the lyophilized primer to make a 100 µM primer stock, the number of nmol of primer in the tube was multiple by 10. For example, in β-actin forward there was 28.7 nmol of primer, a 100 µM forward primer stock was created by adding 287 µl of water. The original primer tubes were used for 100 µM stock. The 100 µM primers suspended in RNase-free water were mixed and incubated at room temperature for 10 min before they were used for working 1:10 stock dilutions. The 100 µM stock primers were diluted with RNase-free water in a sterile PCR tube to a 10 µM working stock to reduce the number of freeze/thaw cycles and to reduce the chance of contaminating the primary source of the primer.

**Table 2.0 4** ***Summary of primers used for cDNA amplification.***

| Gene | Primer Sequence (5'-> 3') | Melting Temperature °C | Molecular weight (g/mol) | Product size (bp) |
|---|---|---|---|---|
| β-actin forward | TGAAGTCTGACGTGGACATC | 57.3 | 6157 | 246 |
| β-actin reverse | ACTCGTCATACTCCTGCTTG | 57.3 | 6019 | |
| CD14 forward | CGAGGACCTAAAGATAACC GGC | 62.1 | 6762 | 553 |
| CD14 reverse | GTTGCAGCTGAGATCGAGC AC | 61.8 | 6471 | |
| p21 forward | ACAGTTTGGCAATTGGAAGC A | 65.7 | 6392 | 321 |
| p21 reverse | CACCCAGATGACTCCAAGAT CAG | 59.8 | 6397 | |
| CD200R forward | CTTCCTGTTCCAGGTGCCAA A | 59.8 | 6357 | 245 |
| CD200R reverse | GCCTCAGATGCCTTCACCTT G | 61.8 | 6333 | |
| Arginase-1 forward | ACAGTTTGGCAATTGGAAGC A | 55.9 | 6494 | 69 |
| Arginase-1 reverse | CACCCAGATGACTCCAAGAT CAG | 62.4 | 6987 | |

### 2.9.3 Amplification of cDNA by PCR

The single-stranded cDNA template was amplified by adding 2X PCR Master Mix (Promega; M7502) ready-to-use solution [containing 50 units/mL of *Taq* DNA polymerase in a proprietary reaction buffer (pH 8.5), dNTPs (400 µM of each dATP, dGTP, dCTP, dTTP), 3mM $MgCl_2$], nuclease-free water and primers

(forward and reverse) as described in Appendix Table 2.06. The reverse transcript (RT) PCR reaction of a total 25 µL volume was prepared for each experimental sample. The PCR reaction mixture was transferred between different temperature steps where the denaturation temperature was used to break the base pairs and release single-stranded DNA to act as templates, annealing temperature was used to attach the primers to the templates and the extension temperature was used to synthesis DNA.

### 2.9.4 Gel electrophoresis of PCR products

The amplified PCR products were analysed using a 2% agarose SYBER safe stain gel electrophoresis by running them alongside a 100bp DNA ladder to determine the approximate electro-separated DNA fragment. The loading samples were prepared by mixing 10 µL of the PCR product with 2 µL of gel loading dye purple. Two micro-litre of Quick load® Purple 100bp DNA ladder and test samples were loaded onto the gel. The gel was electrophoresed at 120 V until the tracking dye migrated down to 75- 80% of gel (approximately 1 h) and the bands were visualised under UV illuminator (Bio-Rad ChemiDoc MP T100 system).

## 2.10 STATISTICAL ANALYSIS

Each experiment was performed three times with triplicates unless specified. The data were analysed as mean and standard mean error (mean ± SEM) and represent triplicate measurements made in three independent experiments. The statistical significance of differences between the groups was assessed using GraphPad prism 8.2.1 with analysis of variance (ANOVA) followed by Dunnett's post hoc test which is a multiple comparison procedure to compare each of a number of treatments with a single control to determine a difference. Statistical significance was identified by a probability (p) value; *$p<0.05$, **$p<0.01$, ***$p<0.001$, ****$p<0.0001$ compared to control. The *n* value given in the figures represents the number of separate experiments.

# CHAPTER 3: PMA INDUCES DIFFERENTIATION OF HUMAN MONOCYTES INTO MACROPHAGES

## 3.1 Introduction

In the first chapter, it has been outlined that the differentiation of peripheral blood mono-nuclear monocyte cells into macrophages is centra; to inflammation of the synovium which leads to rheumatoid disease (Ziff, 1989 and Harris, 1990). The migration of peripheral blood mononuclear cells to inflamed synovium is the result of a cascade of events that involves several adhesion molecules required for attachment to the endothelium (Carlos and Harlan, 1994). Monocyte adhesion to endothelium is a critical step in the migration process that precedes monocyte differentiation to tissue macrophages and type A synoviocytes (Cutolo *et al*., 1993). Multiple publications have shown that macrophages from synovial fluid and synovitis from RA patients have enhanced expression of $\beta_1$ – $\beta_2$ integrins, suggesting that after their migration circulating monocytes may undergo differentiation (Allen *et al*., 1989, El-Gabalawy and Wilkins, 1993 and Koch *et al*., 1991).

Several investigations have shown that activated CD68 synovial macrophages are accountable for disease development, particularly at the cartilage-pannus junction (Mulherin *et al*., 1996). The density of activated CD68 macrophages is reduced with anti-rheumatic treatment (Kraan *et al*., 2000; Barrera *et al*., 2000 and *Wong et al*., 2000). CD68, the human homologue of mouse macrosialin is 110 kDa heavily glycosylated protein (Kunisch *et al*., 2009) which is expressed in lysosomal membranes and on the cell surface of monocytes and tissue macrophages (Strobl *et al*., 1995 and Umino *et al*., 1999). CD14 is a common marker used to show the differentiation of monocytes to macrophages (Schwende *et al*., 1996 and Dobrovolskaia, and Vogel, 2002). The CD14, CD11a, and CD11b have also been reported to up-regulate to precede monocyte attachment to endothelium and differentiation to macrophages (Cutolo *et al.*, 1993; de Fougerolles *et al*., 1992, Marlin *et al*., 1987 and Torsteinsdóttir *et al*., 1999).

One study by Liote *et al.*, 1996 demonstrated that the number of adherent RA monocytes was increased two to three-fold compared with normal monocytes, both with plastic and with fibronectin-coated gelatin surfaces. RA monocytes were twice as adherent as normal monocytes to the secreted extracellular matrix.

The percentage of monocytes that adhered to plasma protein-coated surfaces was significantly higher in patients with RA than in normal subjects. This study further identified adhesion receptors of monocytes that may be involved in monocyte attachment to endothelial cells. The author demonstrated the presence of CD11a/CD18, CD11b/CD18, and CD11c/CD18 on monocytes, an increased number of circulating monocytes with CD11b molecules in RA patients, and increased expression of CD11b on monocytes from RA patients by using flow cytometry. This study concluded that up-regulation of these surface markers are related to the state of activation of monocytes.

Phorbol 12-myristate 13-acetate or PMA also known as 12-O-Tetradecanoylphorbol-13-acetate or TPA (Diageanult *et al.,* 2010) is a phorbol ester found in croton oil and is known to stimulate the synthesis of both DNA and RNA, induces growth arrest, maturation, and differentiation of hematopoietic cell lines, including leukemic cells (Cavender *et al*;1991). PMA is a natural analogue of protein kinase C (PKC) activator diacylglycerol (DAG), (Newton, 2001). PMA can activate the PKC signalling pathway (O'Brian *et* al., 1989) to further activate downstream p38 and p42/p44ERK MAPK pathways in leukemic cells (Kharbanda *et al*., 1994).

Therefore, in this study, it was hypothesised that activation of monocytes is associated with upregulation of adhesion or differentiated surface markers and increased cell adhesion.

## 3.2 Aim

To optimise the conditions for PMA to induce monocyte-macrophage differentiation.

The following objectives were undertaken to address this aim:

1. Assess the *in vitro* monocyte-macrophage differentiation at different concentrations of PMA and at different time points.
2. Determine whether PMA-differentiated macrophages demonstrate cell surface markers and signalling pathways related to cell differentiation.

To achieve the objectives, the U937 and THP-1 cell lines were chosen for *in vitro* cell differentiation. The U937 cell line was isolated from the histiocytic lymphoma of a 37-year-old male which are ovoid in shape with little to no variation in cell morphology. U937 nuclei are large and irregular in shape (Sundstrom and Nilsson, 1976). The THP-1 cell line was established in 1980 by Tsuchiya *et al*. (1980). It was derived from the blood of a patient with acute monocytic leukaemia. THP-1 cells show a large, round single-cell morphology. The U937 and THP-1 express distinct monocyte marker CD14 and respond rapidly to lipopolysaccharide to promote the macrophage phagocytosis (Wright *et al*., 1990). The basic difference between U937 and THP-1 cells is the origin and maturation stage. U937 cells are of histiocytoma tissue origin, thus at a more mature stage, whereas THP-1 cells originate from blood leukaemia origin at a less mature stage (Chanput *et al.,* 2014). As U937 and THP-1 are very frequently used, we focus our study on these two cell lines.

## 3.3 Results

### 3.3.1 PMA induces cell adhesion and the differentiation of U937 and THP-1 monocytes to macrophages

#### 3.3.1.1 PMA impact on cell morphology

This experiment was performed to test the response of U937 and THP-1 cells to the PMA to find the optimal concentration of PMA and optimise the growth incubation period required to differentiate U937 and THP-1 monocytes to macrophages to study the role of the sulphated disaccharides in cell differentiation.

In this study, the U937 and THP-1 cells were treated with PMA at 0.8 nM, 8 nM, and 80 nM for 24 h, 48 h, and 72 h in 24-well cell culture plates. Following PMA treatment, PMA-induced U937 and THP-1 cells were analysed for morphological changes, cell adherence, and phenotypic changes compared to unstimulated U937 and THP-1 cells. The growth pattern, adherence, and change in morphology of PMA-treated U937 and THP-1 cells to the 24-well cell culture plate surface at concentrations of 0.8 nM PMA, 8 nM PMA and 80 nM PMA were monitored using light microscopy at 24 h, 48 h, and 72 h based on the seeded cell density showing adherence to the 24-well plate (Appendix Fig.2 and Appendix Fig.3).

The change in morphology images was taken at 40x magnification with inverted phase-contrast microscopy. To understand the differential response of U937 and THP-1 cells, the morphology of the cell cultures before and post PMA treatment were compared (Fig.3.1). The morphological characteristics of the two cultures were remarkably different. Undifferentiated U937 (Fig.3.1a) and THP-1 (Fig.3.1c) cells were found to be spherical at 24 h, 48 h, and 72 h incubation periods. However, after 48-72 h incubation PMA-induced U937 and THP-1 monocytic cells strongly adhered to the 24-well plates and transformed from non-adherent monocyte rounded cells to an adherent flattened ‘’macrophage-like’’ cell with PMA addition (Fig.3.1b). The THP-1 transformed cells showed large

pseudopodia or elongated arms (Fig.3.01d) but the U937 cells morphology was large and round (Fig.3.1b). Based on changes in morphology it was concluded that morphological changes consist of clumping of cells and adherence to the plastic surfaces as it was observed that cells formed clumps in cell culture during differentiation and became adherent to the bottom of the 24-well plate wells.

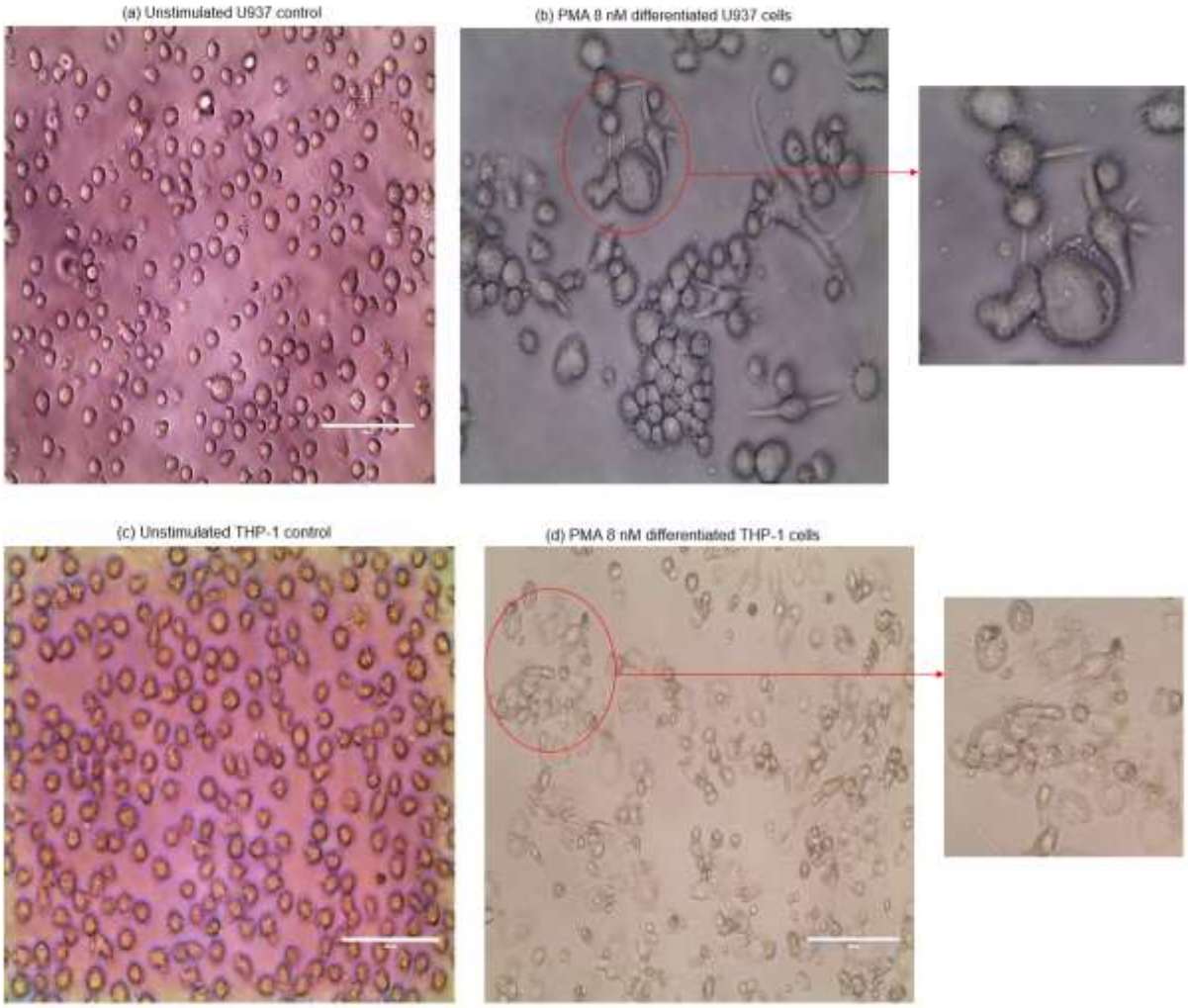


**Figure 3. 1*. PMA induced cell differentiation of U937 and THP-1 cells.***

*Representative microscopic images are from one out of 3 independent experiments. (a) Unstimulated U937, (b) PMA (8 nM) stimulated U937 (c) unstimulated THP-1, and (d) PMA (8 nM) stimulated THP-1 cells. Morphology of differentiated monocytes cultured in RPMI 1640 supplemented with 10% FCS and 8 nM PMA for 48 h showing the change in shape and increase in the size of*

*cells. The change in morphology image was taken at 40x magnification with inverted phase-contrast microscopy. Scale bar = 100um.*

### 3.3.1.2 PMA impact on cell adhesion

In this study, it was found that the adherent cell cultures comprised at least two sub-populations. Some of these cells had a macrophage-like appearance, whereas others were floating. These floating cells were referred to as non-adherent cells which represented only a very small sub-population in the PMA adherent culture. These floating non-adherent cells were initially collected carefully and counted.

The adherent cells (Fig.3.2) and non-adherent (Appendix Fig.4) were counted for each test group for cell number by cell Countess® and trypan blue exclusion. The 48 h test group was compared to their corresponding 24 h and 72 h test groups for significant differences. Significance was identified by a p-value less than 0.05.

Treatment with PMA resulted in slower proliferation of U937 (Fig.3.2a) and THP-1 cells (Fig. 3.02b) compared to unstimulated control U937 and THP-1 cells. In the presence of PMA, cell proliferation was inhibited compared to unstimulated control cells. When cells were examined microscopically, differences were also apparent within 24 h in PMA-treated cell cultures as PMA-treated cells exhibit growth arrest at 24 h after the addition of PMA and almost 90% apparent growth arrest of cells after 48 h (Appendix Fig.2 and Appendix Fig.3). Cells then tend to lose adhesiveness gradually after 72 h. The growth arrest phenotype was much less prominent with 0.8 nM PMA treated cells that continued moderate proliferation even after the addition of the reagent. It was investigated that the differentiation and maturation were induced by 8 nM PMA and 80 nM PMA and 48 h PMA-culture time effectively increase cellular adherence of macrophage-like cells. A two-fold increase in adherence was observed in the 8 nM at 48 h test group following 72 h resting period relative to the 24 and 72 h test groups (Fig.3.2a and Fig3.02b). The number of cells detected in the non-adherent population was reduced after PMA treatment (Appendix Fig.4), whilst the number of adherent cells was increased (Fig.3.2).

Out of 2 x $10^5$ cells/mL U937 or THP-1 seeded density, unstimulated control U937 cells proliferated to viable 1 x $10^6$ cells/mL at 24 h, 2.8 x $10^6$ cells/mL at 48 h and further increased to viable 3 x $10^6$ cells/mL at 72 h (Fig.3.2a). The unstimulated control THP-1 cells increased to viable 1.3 x $10^6$ cells/mL at 24 h, viable 2 x $10^6$ cells/mL at 48 h and viable 3 x $10^6$ cells/mL at 72 h (Fig. 3.02b).

As shown in Figure.3.02, out of 2 x $10^5$ cells/mL seeded density at 24 h 1.8 x $10^5$ cells/mL viable U937 cells and 3 x $10^5$ cells/mL viable THP-1 cells adhered to 24-well plate in 0.8 nM PMA cell cultures. The number of U937 or THP-1 adherent cells increased to viable 3.5 x $10^5$ cells/mL in 8 nM PMA cell cultures and 3 x $10^5$ cells/mL viable in 80 nM PMA cell cultures at 24 h. The number of U937 and THP-1 adherent cells increased to viable 6 x $10^5$ cells/mL in 8 nM PMA cell cultures at 48 h. There was no significant difference between 0.8 nM PMA cell cultures and 80 nM PMA cell cultures adherent cells compared to 8 nM PMA cell cultures adherent cells in U937 cells at 48 h. However, the number of viable THP-1 adherent cells were less in 0.8 nM PMA (3.5 x $10^5$ cells/mL) and 80 nM PMA (3.5 x $10^5$ cells/mL) cell cultures compared to 8 nM PMA cell cultures viable adherent cells at 48 h. After 48 h the number of viable U937 and THP-1 adherent cells decreased to 4 x $10^5$ cells/mL and THP-1-adherent cells decreased to 3.8 x$10^5$ cells/mL in 8 nM PMA cell cultures at 72 h.

Cell adhesion at 0.8 nM PMA was unstable and the cells were easily detached after PBS washing. This indicates that 0.8 nM PMA was not enough to differentiate the U937 and THP-1 cells stably. The stabilities of PMA differentiated cells at 24 h, 8 h, and 72 h after removing PMA from the cell cultures were analysed by incubating differentiated cells in PMA-free 10% FBS and 1% penicillin/streptomycin supplemented RPMI-1640 media for 72 h. Regardless of the PMA-free media used, adherent cell stability was found to be dependent on the PMA concentration used to induce the monocyte-macrophage differentiation.

Therefore, the minimum concentration of PMA for stable differentiation was determined to be 8 nM at 48 h. The trypan blue exclusion viability of U937 and THP-1 cells were subdued after PMA treatment in a concentration-dependent manner and the results of the experiments concluded that the viability of U937 and THP-1 cells at 80 nM PMA was significantly lower than 8 nM PMA. In a set of experiments, U937 and THP-1 cell metabolism was also determined by

measuring the reducing potential of the cells using a colorimetric MTT assay to rule out the possibility of whether the PMA was toxic for the U937 and THP-1 cells. It was found that U937 and THP-1 cells cultured with PMA did express a cytotoxic activity when compared with unstimulated control U937 and THP-1 cells, but 8 nM PMA was less toxic compared to 80 nM PMA ($p < 0.01$) in U937 and less toxic compared to 0.8 nM PMA and 80 nM PMA in THP-1 cells at 48 h. The results indicated that 80 nM PMA caused had cytotoxic effects on U937 and THP-1 cells at 24 h, 48 h, and 72 h.

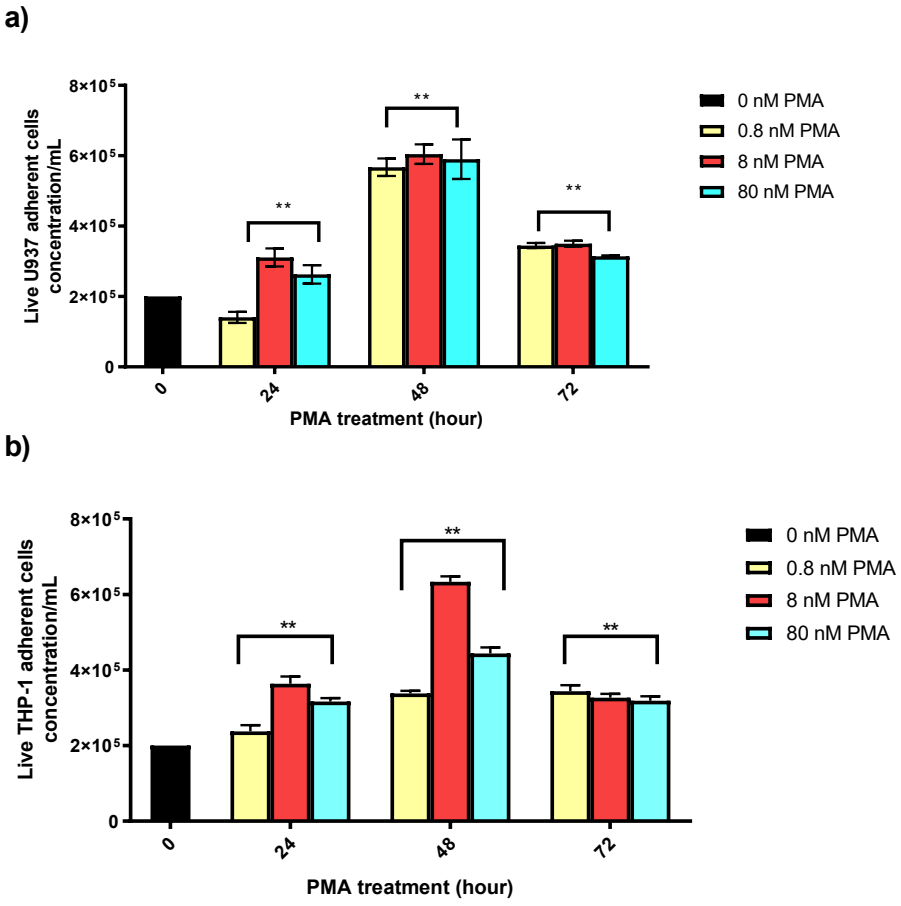


**Figure 3. 2*. Concentration and time-dependent effect of PMA on U937 and THP-1 cells.***

*The number of adherent cells increased in PMA cultures. PMA induced (a) U937 and (b) THP-1 monocyte-macrophage differentiation in a concentration (0.8 nM, 8 nM and 80 nM) and time-dependent manner (24, 48 and 72 h). 8 nM PMA induced more differentiation at 48 h compared to 24 h and 72 h. The data was analysed by Cell countess as described in section 2.2 and one-way ANOVA with post hoc Dunnett's test and is presented as mean ± SEM of viable cells (viability analysed by trypan blue exclusion) of three independent experiments. Two asterisks (**) in (a) indicates significant differences between unstimulated U937 cells to PMA stimulated cells at 24 h, 48 h, 72 h ($p < 0.01$). The reduction of MTT was also measured by mitochondrial succinate dehydrogenase in active U937 and THP-1 cells (Appendix Fig. 5).*

### 3.3.1.3 Relationship between p38 and p42/p44ERKMARK signalling pathway in PMA-induced monocyte differentiation

This study then evaluated whether 8 nM PMA concentration and 48 h time point were sufficient to activate the protein kinase C (PKC) signalling pathway and downstream p38 and p42/p44ERK MAPK pathways in U937 and THP-1 cells. This was examined by western blot analysis.

In the first set of experiments U937 cells were cultured in the presence of 0.8 nM PMA, 8 nM PMA and 0.8 nM PMA for 48 h. U937 cells treated with RPMI-1640 media were used as an unstimulated control. The expression of phosphorylated p38 protein was observed at a molecular weight of 38 kDa in PMA-stimulated U937 and unstimulated control U937 cells at 48 h (Fig.3.3a). The phosphorylation expression of p38 protein was visible with 0.8 nM PMA which increased with 8 nM PMA and decreased at 80 nM PMA at 48 h. The ratio of phosphorylated protein over total protein (Fig.303b) bands intensity for unstimulated control and PMA-stimulated U937 cells was quantified against β-actin loading control (Fig.3.3b). The quantification data analyses indicated that the phosphorylation expression level of p38 was increased after 8 nM PMA treatment at 48 h compared with unstimulated control U937 cells.

In the second set of experiments, THP-1 cells were cultured with 8 nM PMA for 24 h, 48 h, and 72 h. THP-1 cells treated with RPMI-1640 media in the absence of PMA were used as an unstimulated control. The expression of total and phosphorylated p38 and p42/p44ERKprotein was detected at a molecular weight of 38 kDa and 42/44 kDa in PMA-stimulated THP-1 cells at 24 h (Fig.3.4a). It was observed that the phosphorylation expression of p38 and p42/p44ERK in 8 nM PMA-stimulated THP-1 cells increased at 48 h which further decreased at 72 h. The ratio of phosphorylated p38 over total p38 (Fig.3.4b) and p42/p44ERK over total p42/p44ERK (Fig.3.4d) bands intensity of 8 nM PMA-stimulated THP-1 and unstimulated control THP-1 cells was quantified against β-actin loading control (Fig.3.4c & Fig.3.4e). The quantification data analyses revealed that p38 and p42/p44ERK phosphorylated at 24 h and 72 h compared to unstimulated control THP-1 cells. However, the phosphorylation expression level of p38 and

p42/p44ERK was increased after 8 nM PMA treatment at 48 h compared with unstimulated control THP-1 cells.

PMA (8 nM) induced phosphorylation of p38 in U937 (Fig.3.3 & Fig.3.4) and p42/p44ERKprotein expression in THP-1 cells at 48 h (Fig.3.4).

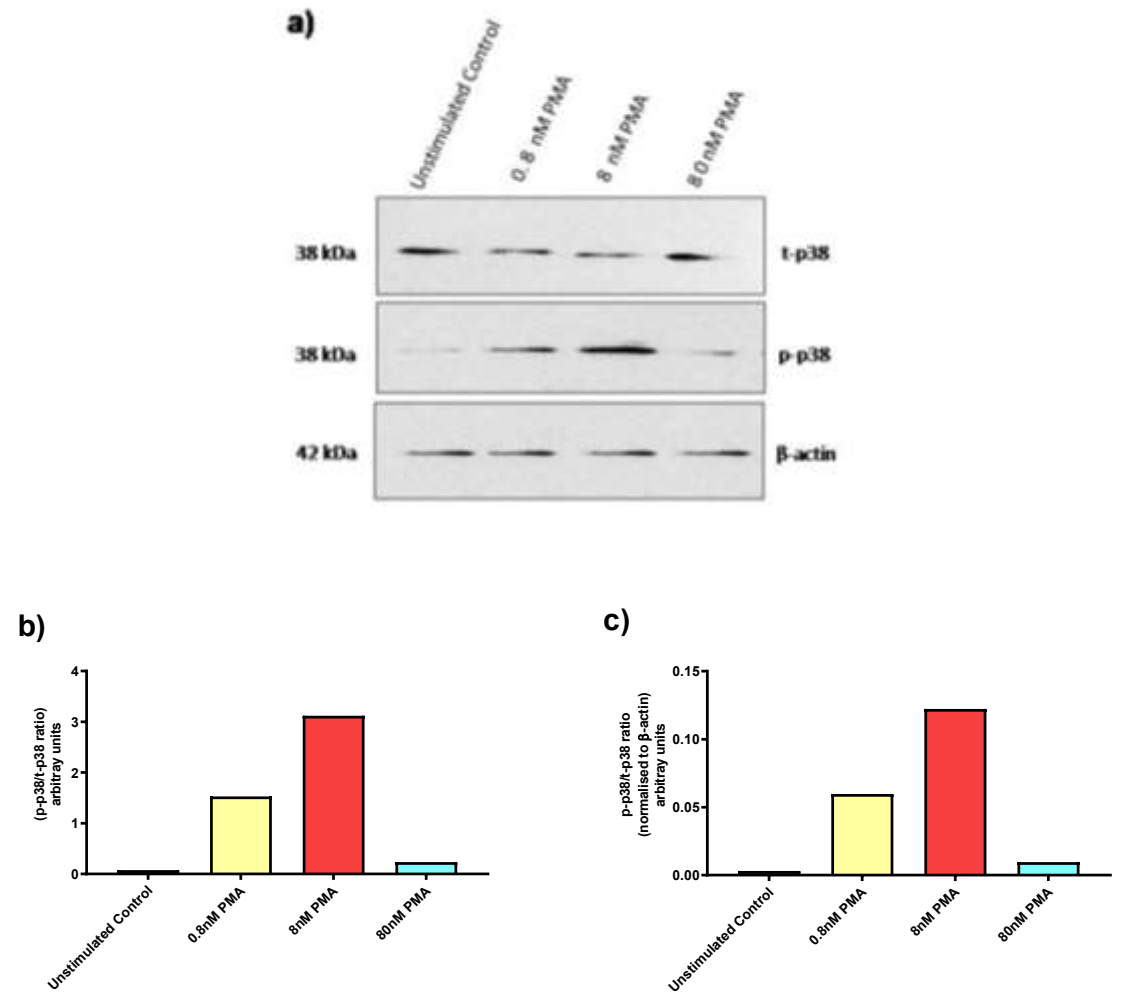


**Figure 3. 3*. PMA induced phosphorylation of p38 in U937 cells.***

*a) A representative blot of two independent experiments. b) Densitometric results for p-p38 over t-p38. c) p-p38 over t-p38 results normalised to densitometric results of β-actin respectively. U937 cells were cultured in the presence of 0.8 nM PMA, 8 nM PMA and 0.8 nM PMA for 48 h. Cells treated with RPMI-1640 media were used as a unstimulated control. The adherent cells were harvested, lysed using cell lysis kit and 20 µg of total cellular protein of unstimulated control U937 cells and PMA stimulated U937 cells were separated by SDS- PAGE on 12% gel. Protein was transferred onto nitrocellulose membrane and immunoblotted with total and phospho-rabbit monoclonal primary antibodies (dilution, 1:1000) of p38. The endogenous level of total (t) and phosphorylated (p) p38 MAPK was detected at a molecular weight of 38 kDa, in U937 cells. β-actin was used as a loading control to quantify the band intensity of total and phosphorylated proteins by Image J. The results are expressed in arbitrary units.*

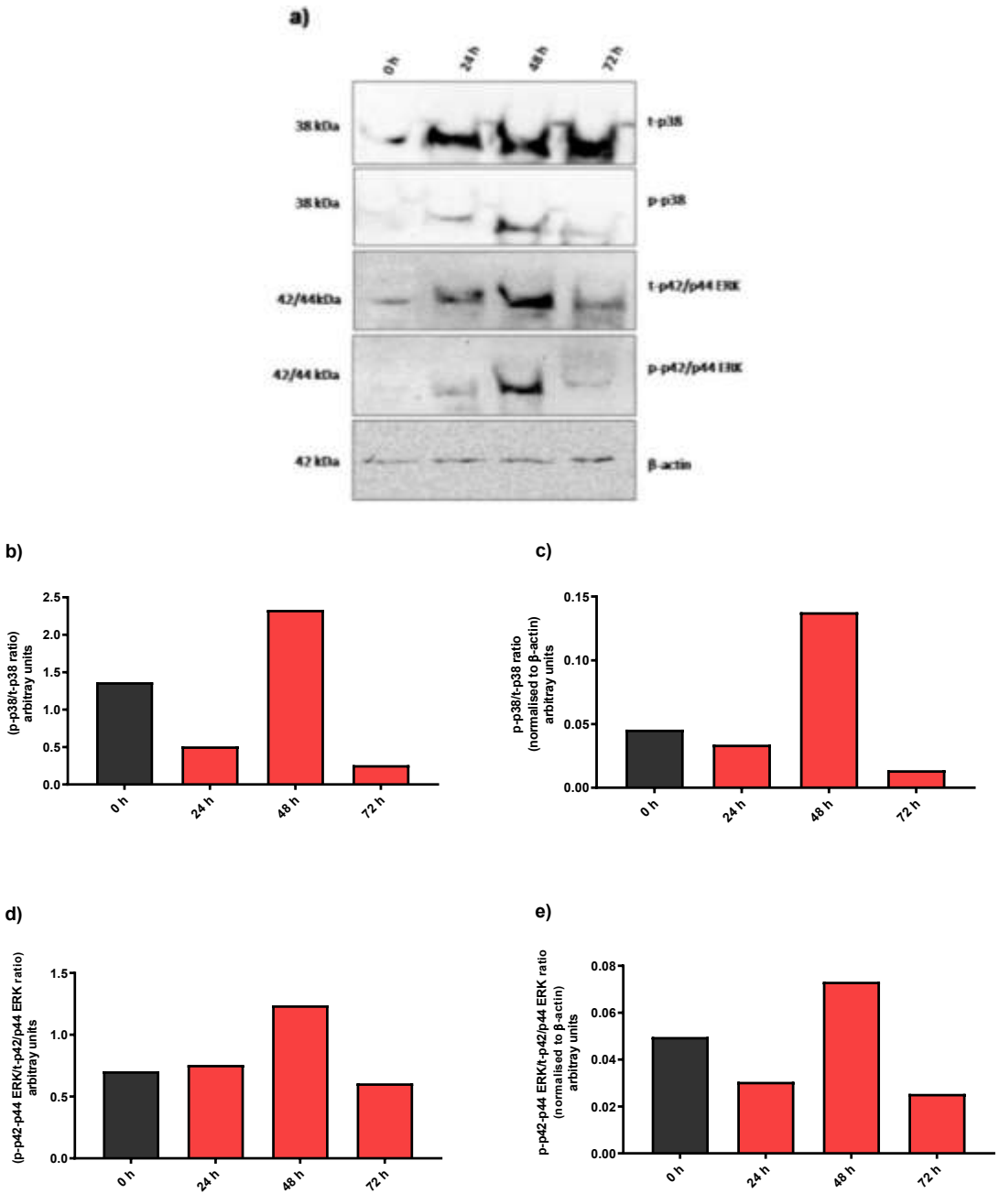


**Figure 3. 4*. PMA induced phosphorylation of p38 and ERK1/2 in THP-1 cells.***

*a): A representative blot of two independent experiments. Densitometric results for b) p-p38 over t-p38 d), p-p42/p44ERK over total p42/p44ERK c) & e): p-p38 over t-p38 and p-p42/p44ERK over total p42/p44ERK results normalised to densitometric results of β-actin respectively. THP-1 cells were treated with 8 nM PMA for 24 h, 48 h and 72 h. Cells treated with RPMI-1640 media were used as an unstimulated control. The PMA-stimulated adherent THP-1 cells were harvested, lysed, loaded (20 µg per lane) on SDS- PAGE on 12% gel, and*

*transferred onto nitrocellulose membrane and immunoblotted with (dilution, 1:1000) of p38 and p42/p44ERK. The endogenous level of total (t) and phosphorylated (p) p38 MAPK and p42/p44ERK was detected at a molecular weight of 38 kDa and 42/44 kDa in THP-1 cells. The results are expressed in arbitrary units.*

### 3.3.1.4 Phenotypic analysis of PMA-differentiated U937 and THP-1 macrophages

The preliminary study was undertaken to analyse further PMA-differentiated adherent cells for their size and complexity at 48 h (Appendix Fig.6). Furthermore, to ensure that 48 h was sufficient for the differentiation process, this study analysed the surface antigens on U937 and THP-1 cells that could be expressed or disappear when monocytes differentiate to macrophages to study the characteristic changes of monocytes differentiating into macrophages.

Therefore, to determine whether PMA-stimulated U937 and THP-1 cells adherence and differentiation were associated with CD14, CD11a, CD11b, and CD68 up-regulation, the U937, and THP-1 monocytes were stimulated with 8 nM PMA for 48 h. The U937 and THP-1 cells cultured in 10% FBS RPMI 1640 media in the absence of PMA were used as an unstimulated control. The PMA-differentiated adherent U937 and THP-1 cells were incubated with monoclonal anti-CD14, CD11a, CD11b, and CD68 antibodies as described in materials and methods section 2.4.

The optimal interpretation of experimental data was done by eliminating false positive and negative results by using the unstained, live-dead dye and isotype controls. The changes in the surface makers expression of CD14, CD11a, CD11b, and CD68 in the U937 and THP-1 cell differentiation model were carried out by using flow cytometer as described in materials and methods section 2.4. Significance was identified by a p-value less than 0.05. Before staining cells with flow cytometry antibodies U937 and THP-1 PMA-differentiated adherent cells were counted for cell count and viability at 48 h as described in materials and methods section 2.2.

For flow cytometry analysis U937 and THP-1 cell population was identified by forward and side scatter characteristics or using side scatter by drawing a gate on the dense U937 and THP-1 cells population (Fig.2.5, Fig.2.6). It was found that dead cells had lower forward scatter and higher side scatters than live cells. The dead cells, debris, clumps, or doublets were then identified and removed from the final analysis to prevent false-positive data by gating on the unstained and single population. Subsequently, the singlet gate of the height (FSC-H)

against the area (FSC-A) for forward scatter was analysed from the U937 and THP-1 cell population gate for their uptake of the Live/dead stain. Live cells were analysed by gating on the unstained live cells against Fluor 506 stained population within the total U937 and THP-1 cell population as described in materials and methods section 2.4.1.2 and Fig.2.1 and Fig.2.2.

The expression of CD14, CD11a, CD11b, and CD68 surface markers in PMA-stimulated U937 and THP-1 adherent compared to unstimulated control U937 and THP-1 cells. The expression was determined on the live $CD14^+$, $CD11a^+$, $CD11b^+$, and $CD68^+$ cells by measuring live cells mean fluorescence intensity for adherent U937 and THP-1 cells (Fig.3.5-Fig.3.8).

The shift of the PMA stimulated population onto the unstimulated control population was analysed using histograms displaying a single fluorescence on the x-axis (Appendix Fig.7) and the number of cell counts on the y- axis was plotted. The cells expressing the selected marker expression were considered a positive dataset. Histogram gates were gated for CD14, CD11a, CD11b, and CD68 positive cells expression after cells stained with isotype control antibodies.

As shown in Figures.3.05a,c – 3.08a,c, U937 and THP-1 differentiation by 0.8 nM PMA, 8 nM PMA and 80 nM PMA at 48 h significantly increase ($p < 0.01$) in percentage of $CD14^+$, $CD11a^+$, $CD11b^+$ and $CD68^+$ cells compared to the unstimulated control U937 $CD14^+$ cells (6.75%), $CD11a^+$ cells (3.90%), $CD11b^+$ cells (0.95%) and no cells were found to be $CD68^+$. The treatment with 0.8 nM PMA for 48 h was sufficient to induce CD14 expression as that of 80 nM PMA (Fig.3.5), even though 0.8 nM PMA was found to be insufficient to induce cell adhesion of PMA-differentiated U937 and THP-1 cells.

It was found that percentage of U937 adherent cells for $CD14^+$ (99.8%), $CD11a^+$ (99.2%), $CD11b^+$(99.2%) and $CD68^+$(99.5%) cells with 8 nM PMA at 48 h was higher compared to 0.8 nM PMA and 80 nM PMA. The percentage of $CD14^+$, $CD11a^+$, $CD11b^+$ and $CD68^+$ with 8 nM PMA was significantly ($p < 0.01$) higher compared to unstimulated control U937 cells (Fig.3.5a – Fig.3.8a). The percentage of U937 adherent cells with 0.8 nM PMA found to be lower for $CD14^+$ (65%), $CD11b^+$ (42.9%) and $CD68^+$ (84.7%) compared to 80 nM PMA $CD14^+$ (68.4%), $CD11b^+$ (88.6%) and $CD68^+$ (97.7%). However, percentage of $CD11a^+$

(89.3%) with 0.8 nM PMA was found to be higher compared to $CD11a^+$ (79.9%) with 80 nM PMA. The percentage of $CD14^+$, $CD11a^+$, $CD11b^+$ and $CD68^+$ was significantly higher with 0.8 nM PMA ($p < 0.01$) and 80 nM PMA ($p < 0.01$) compared to unstimulated control U937 cells (Fig.3.5a – Fig.3.8a).

The level of positive cells expression was measured as the relative mean fluorescence intensity (MFI) of live cells (Fig.3.5b,d – Fig.3.8b,d). The MFI of 0.8 nM PMA $CD14^+$ cells, 8 nM PMA $CD14^+$ cells and 80 nM PMA $CD14^+$ cells was also found be significantly ($p < 0.01$) higher compared to unstimulated control U937 cells (Fig.3.5b).The expression for 8 nM PMA $CD11a^+$and $CD68^+$cells was significantly ($p < 0.01$) higher compared to unstimulated control U937 cells, whereas there was no significant difference for expression of 0.8 nM PMA $CD11a^+$ or $CD68^+$ cells and 80 nM PMA $CD11a^+$ or $CD68^+$ cells (Fig.3.6b & Fig.308b).Similarly, there was no significant difference for expression of 0.8 nM PMA $CD11b^+$ cells but 8 nM PMA $CD11b^+$ cells and 80 nM PMA $CD11b^+$ cells had significantly ($p < 0.01$) higher expression compared to unstimulated control U937 cells (Fig.3.7b).

The interesting distribution was observed for $CD14^+$, $CD11a^+$, $CD11b^+$ and $CD68^+$ cells in PMA-stimulated THP-1 adherent cells compared to PMA-stimulated U937 adherent cells. The proportion of $CD14^+$, $CD11a^+$, $CD11b^+$ and $CD68^+$was different in both PMA-stimulated U937 and THP-1 adherent cells. In U937 cells, the high percentage of $CD14^+$, $CD11a^+$, $CD11b^+$ and $CD68^+$ was observed whereas in THP-1 cells, the low percentage of $CD14^+$, $CD11a^+$, $CD11b^+$ and $CD68^+$was observed. The percentage of $CD14^+$, $CD11a^+$, $CD11b^+$ and $CD68^+$ cells with 8 nM PMA in U937 adherent cells was increased up to 90% (Fig.3.5a – Fig3.08a) whereas in THP-1 cells it increased up to 50% for $CD14^+$, 10% for $CD11a^+$, 15% for $CD11b^+$ and 60% for $CD68^+$cells (Fig.3.5c – Fig.3.8c). The percentage of $CD14^+$ (50.9%), $CD11a^+$ (10.2%), $CD11b^+$ (14.7%) and $CD68^+$ (52%) cells of 8 nM PMA was increased significantly ($p < 0.01$) compared to unstimulated control THP-1 $CD14^+$ (0.90%), $CD11a^+$ (5.57%), $CD11b^+$(0.22%) and $CD68^+$ (1.65%) cells. The percentage of 8 nM PMA positive cells was higher compared to0.8 nM PMA $CD14^+$ (1.34%), $CD11a^+$ (2.06%), $CD11b^+$(0.99%) and $CD68^+$ (0.48%) cells of and 80 nM PMA $CD14^+$ (40.4%), $CD11a^+$ (5.57%), $CD11b^+$(6.44%), but lower percentage of $CD68^+$ compared to 80 nM PMA $CD68^+$

(60.1%) (Fig.3.5c – Fig.3.8c). The expression of 8 nM PMA $CD14^+$, $CD11a^+$, $CD11b^+$ , $CD68^+$ and 80 nM PMA $CD11b^+$, $CD68^+$ was found to be significant ($p < 0.01$) compared to unstimulated control THP-1 cells. There was no significant difference between 0.8 nM PMA positive cells and unstimulated control THP-1 cells (Fig.3.5d – Fig.3.8d).

Collectively based on the above results, it was concluded that PMA induces cell-differentiation in U937 and THP-1 cells through p38 and ERK1/2 signalling pathways and upregulation of cell surface markers expression. A concentration of 8 nM PMA at 48 h treatment period followed by a 72 h PMA free culture time interval was sufficient to yield the highest viable adherent matured macrophage-like cells. Therefore, for future studies, a concentration of 8 nM PMA at 48 h followed by 72 h maturation period was used as the optimal condition for the monocyte-macrophage differentiation.

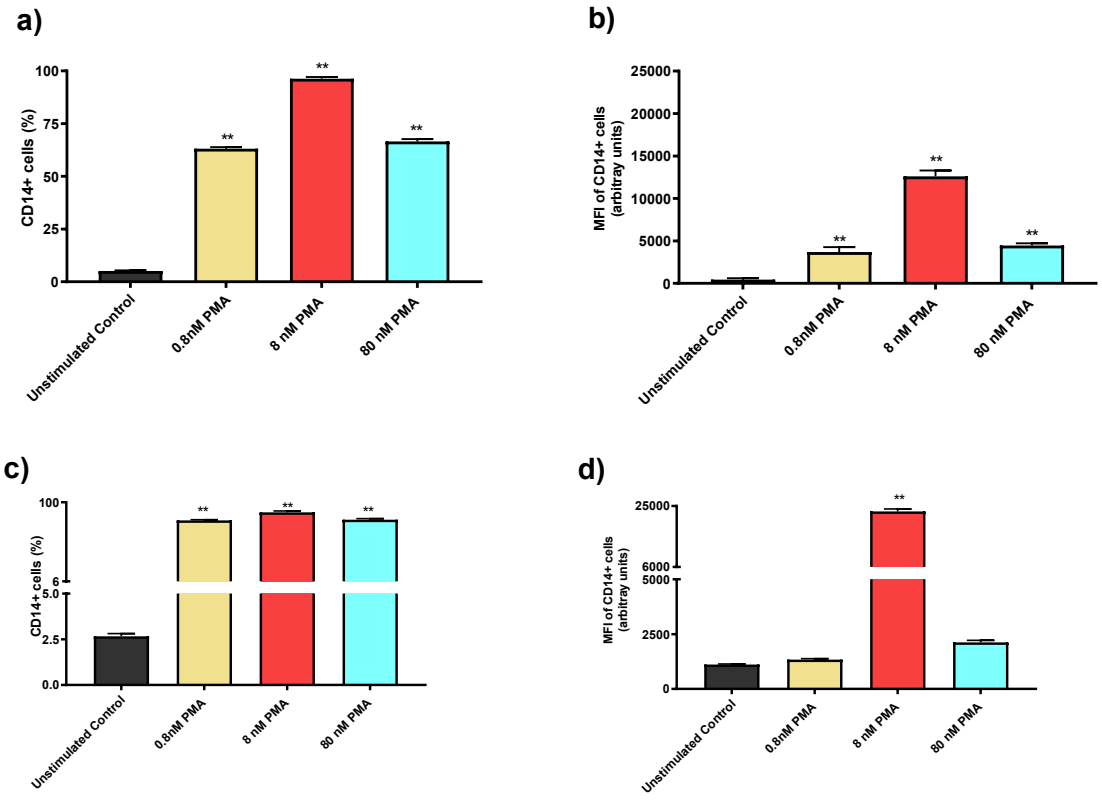


**Figure 3. 5*. PMA up-regulates CD14 surface marker in U937 and THP-1 cells.***

*Bar graph represents the percentage of CD14 positive cells of PMA – differentiated (a) U937, (c) THP-1 cells, and MFI of CD14 positive cells of (b) U937, (d) THP-1 cells. The U937 and THP-1 cells were stimulated by 0.8 nM PMA, 8 nM PMA and 80 nM PMA for 48 h. The samples were stained with PE-labeled anti-human CD14. The isotype controls were used to set gets to define positive or negative populations for CD14 surface markers from the live gate. Comparisons were made against the no PMA control (unstimulated control cells). The results were acquired by FACS, analysed by FlowJo, and statistically analysed by ANOVA, Dnunett's, mean ± SEM (n=3), **p<0.01 vs unstimulated control cells. Data presented were pooled from 3 experiments.*

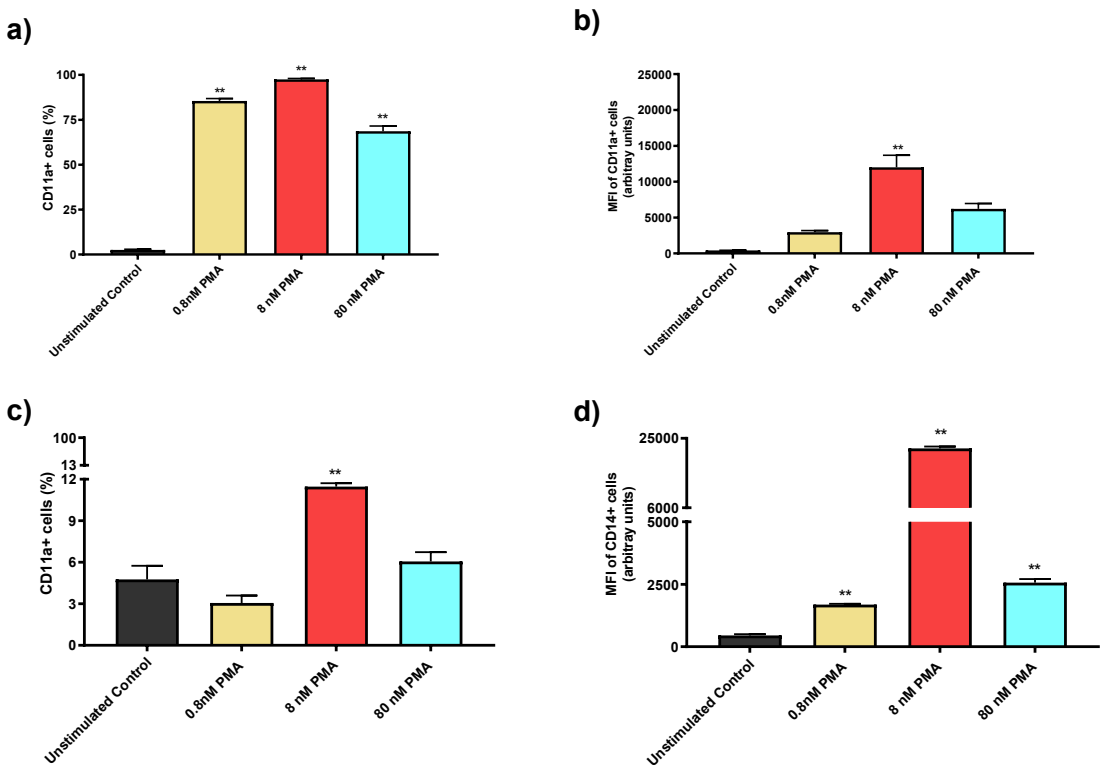


**Figure 3. 6*. PMA upregulates CD11a surface marker in U937 and THP-1 cells.***

*Bar graph represents the percentage of CD11a positive cells of PMA – differentiated (a) U937, (c) THP-1 cells, and MFI of CD11a positive cells of (b) U937, (d) THP-1 cells. The U937 and THP-1 cells were stimulated by 0.8 nM PMA, 8 nM PMA and 80 nM PMA for 48 h. The samples were stained with FITC-labeled anti-human CD11a. The isotype controls were used to set gets to define positive or negative populations for CD11a surface markers from the live gate. Comparisons were made against the no PMA control (unstimulated control cells). The results were acquired by FACS, analysed by FlowJo, and statistically analysed by ANOVA, Dunnett's, mean ± SEM (n=3), **p<0.01 vs unstimulated control cells. Data presented were pooled from 3 experiments.*

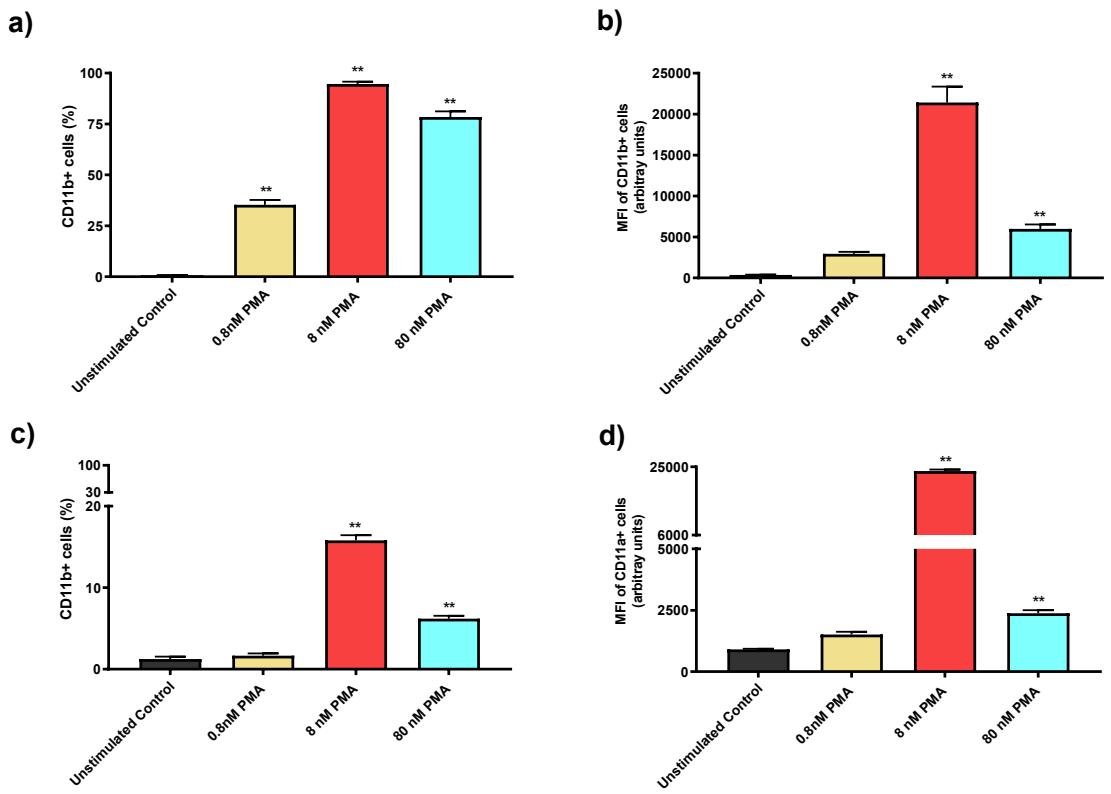


**Figure 3. 7*. PMA upregulates CD11b surface marker in U937 and THP-1 cells.***

*Bar graph represents the percentage of CD11b positive cells of PMA – differentiated (a) U937, (c) THP-1 cells, and MFI of CD11b positive cells of (b) U937, (d) THP-1 cells. The U937 and THP-1 cells were stimulated by 0.8 nM PMA, 8 nM PMA and 80 nM PMA for 48 h. The samples were stained with BV650-labeled anti-human CD11b. The isotype controls were used to set gets to define positive or negative populations for CD11b surface markers from the live gate. Comparisons were made against the no PMA control (unstimulated control cells). The results were acquired by FACS, analysed by FlowJo, and statistically analysed by ANOVA, Dunnett's, mean ± SEM (n=3), **p<0.01 vs unstimulated control cells. Data presented were pooled from 3 experiments.*

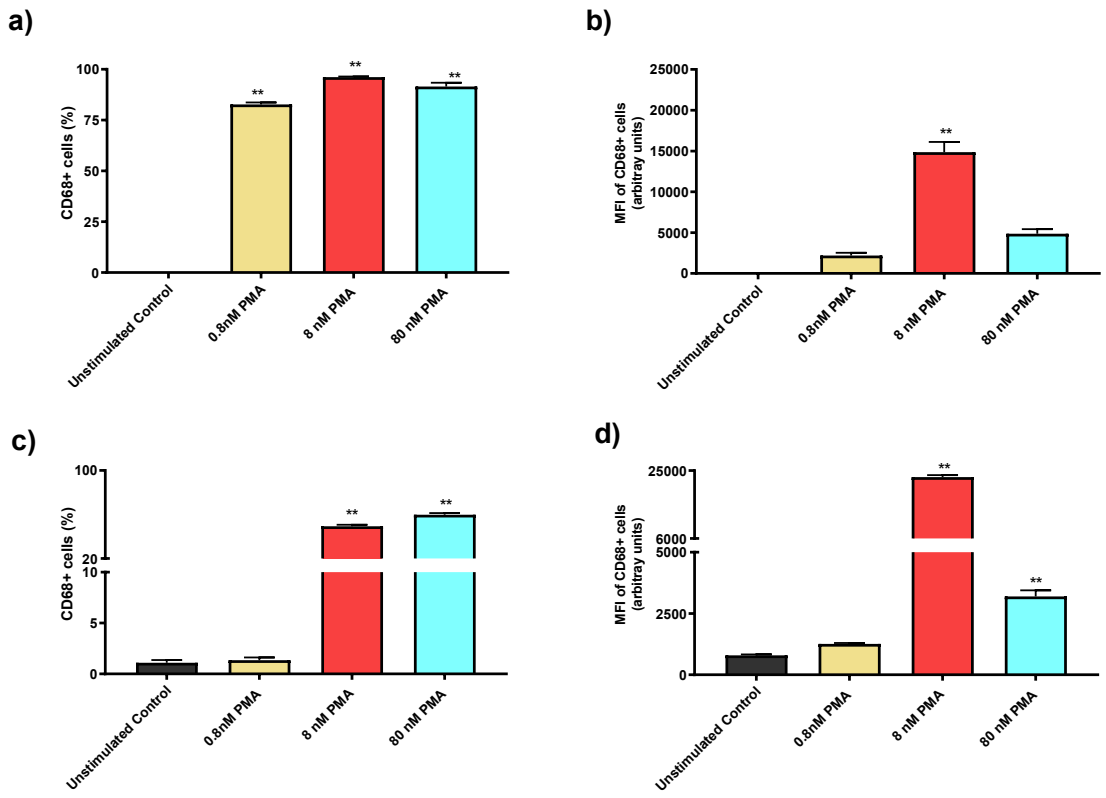


**Figure 3. 8*. PMA upregulates CD68 surface marker in U937 and THP-1 cells.***

*Bar graph represents the percentage of CD68 positive cells of PMA – differentiated (a) U937, (c) THP-1 cells, and MFI of CD68 positive cells of (b) U937, (d) THP-1 cells. The U937 and THP-1 cells were stimulated by 0.8 nM PMA, 8 nM PMA and 80 nM PMA for 48 h. The samples were stained with Cyanin 7 PE-labelled anti-human CD68. The isotype controls were used to set gets to define positive or negative populations for CD68 surface markers from the live gate. Comparisons were made against the no PMA control (unstimulated control cells). The results were acquired by FACS, analysed by FlowJo, and statistically analysed by ANOVA, Dunnett's, mean ± SEM (n=3), **p<0.01 vs unstimulated control cells. Data presented were pooled from 3 experiments.*

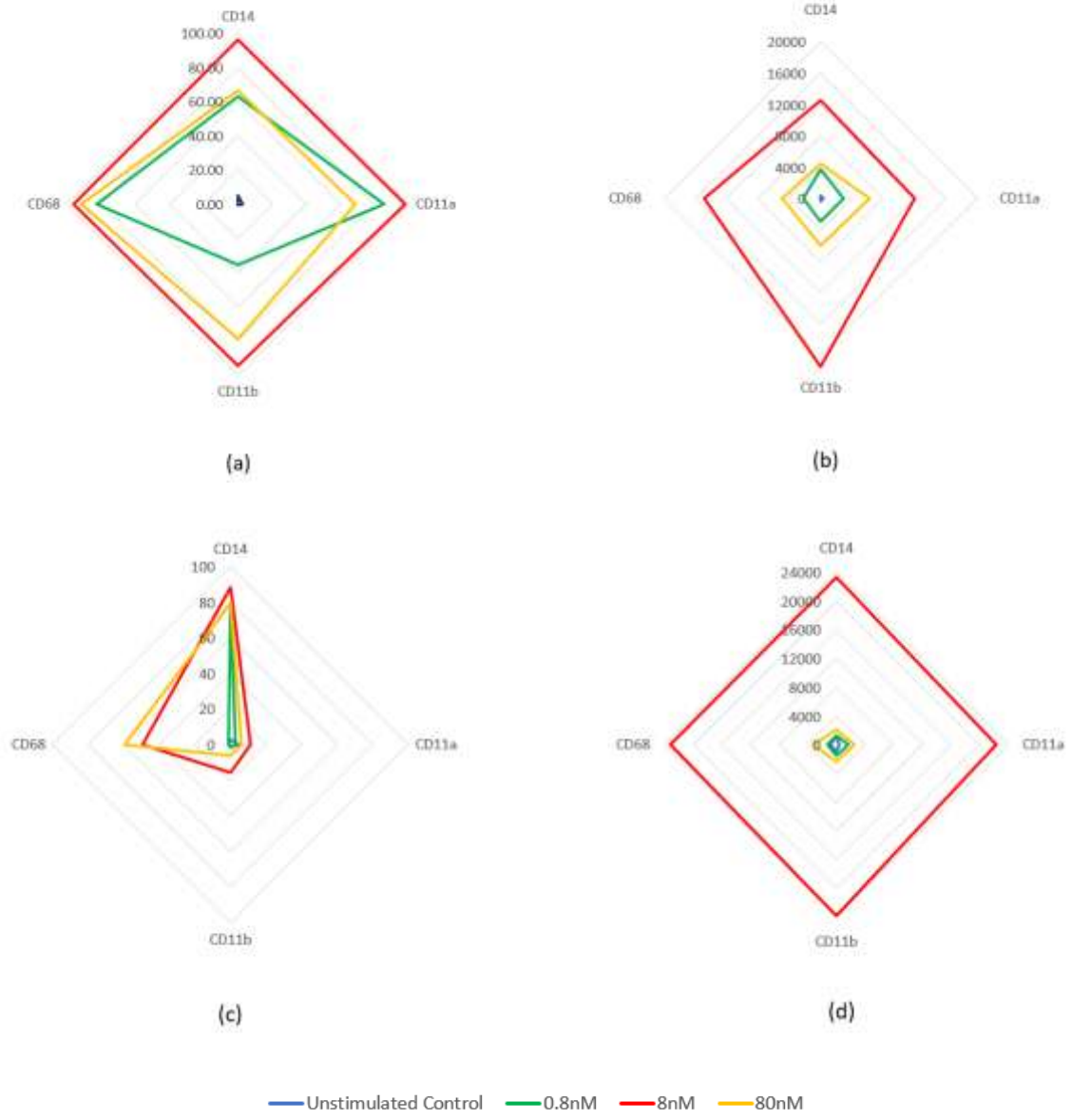


**Figure 3. 9*. Radar plots to summarise the impact of PMA on the percentage and expression of cell surface markers (Fig.3.5 – Fig.3.8) of differentiated cells.***

*Radar plots of differentiated positive surface markers (a) U937, (c) THP-1 cells and MFI of positive surface markers (b) U937, (d) THP-1 cells. 8 nM PMA upregulated percentage of CD14, CD11b, and CD68 surface markers expression in differentiated (a) U937 and (b) THP-1 cells compared to unstimulated cells. However, CD11a was almost negative in THP-1 cells of both unstimulated and PMA stimulated cells.*

## 3.4 Discussion

The main objective of this study was to optimise the PMA conditions to induce cell differentiation. There are several methods used to study macrophages *in vitro* such as peripheral blood mononuclear cells (PBMCs) and monocyte cell lines, such as U937, THP-1, or HL-60. In this study, an *in vitro* model was established by using the U937 and THP-1 monocyte human myeloid leukaemia cell lines.

The justification for using both U937 and THP-1 cells in this study was that these cells resemble primary monocytes and macrophages in morphology and differentiation properties. These leukaemia cells have been used as the experimental *in vitro* model of human macrophages to elucidate mechanisms of monocyte-macrophage differentiation, monocyte-endothelium attachment (Liu *et al*., 2004), to study macrophage role in inflammatory diseases (Abrink *et al*., 1994; Collins, 1987; Verhoeckx *et al*., 2004; Hjort *et al*., 2003; Kramer and Wray, 2002; Ueki *et al*., 2002 and Sakamoto *et al*., 2001) and monocyte-macrophage polarization (Chanput *et al.,* 2014). In addition, isolation of primary tissue macrophages required ethical approval for blood donation or collection from a specific tissue. Limited cell numbers represent a barrier to the use of these primary cells in protocols requiring very large numbers of cells. While U937 and THP-1 monocytic cell lines have obvious advantages in terms of ease of acquisition, as compared to primary macrophages.

The U937 and THP-1 cell lines treatment with PMA induces cell differentiation (Huberman *et al*., 1979). The phenotype of the cells following PMA stimulation varies between studies, with some of the differences attributed to the time of incubation or concentration used in the study. The elevated concentration of PMA is also capable of stimulating various genes in THP-1 cells (Kohro *et al*., 2004). PMA at concentrations of 16 nM to 540 nM has been used to induce cell differentiation in *in vitro* models (Chanput *et al*., 2014; Chen *et al;* 2004, Juliet *et al*; 2003 and Reyes *et al;* 1999) which in this study was considered to be significantly high. Therefore, in this study, it was considered that the PMA concentrations should be optimised in order to minimise the upregulated expression of genes and avoid the masking of the effects of the secondary stimuli by PMA.

This study initially tested the response of U937 and THP-1 cells to different concentrations of PMA and at different time points to evaluate whether PMA was able to induce monocyte-macrophage differentiation in U937 and THP-1 cells. The data in this chapter suggested that cell adhesion to culture plates; change in cell morphology (shape and size) and cell surface marker expression were the noticeable characteristics for cell differentiation in culture. This study results concluded that these cell lines are suitable as *in vitro* models for the investigation of macrophage biological activities since they can be differentiated to macrophages by activation of cell surface markers. When U937 and THP-1 monocyte cells were treated with PMA concentrations ranging from 0.8 nM to 80 nM for 24 h, 48 h, and 72 h, it was found that 8 nM PMA was appropriate to induced cell differentiation of U937 and THP-1 cells in 24-well plates. After removing PMA at 48 h, the stabilities of PMA-differentiated U937 and THP-1 cells in PMA-free 10% FCS RPMI-media during the maturation period for 72 h was found to be dependent on the PMA concentration used to induce the differentiation. A study by Park *et al;* 2006 showed that THP-1 cells became adherent after induction with 5 ng/mL PMA at 48 h.

These study results were comparable and confirm the similar observation in U937 and THP-1 with 8 nM (equal to 5 ng/mL) PMA at 48 h. Based on literature and our experience, U937 and THP-1 monocytes fully differentiated into macrophages after 48 h PMA exposure (Zhang *et al.,* 2010; Cam and de Mejia, 2012; Moreno-Navarrete *et al,* 2009 and Gillies *et al*., 2012). Liang *et al*; 2006 demonstrated that the differentiated macrophages are larger, more granular, and exert macrophage-like characteristics. These results confirm the similar observation where PMA (8 nM)-induced differentiated macrophages were larger and more granular, became adherent to cell culture plates, and exerted macrophage-like characteristic at 48 h followed by an additional 72 h resting period. The monocyte enlarges in size as it differentiates into the macrophage (Giraud *et al*; 2012). The cell morphology characteristics also confirmed the change in cell size during differentiation of U937 and THP-1 monocytes to macrophages when induced with 8 nM PMA. The increase in cell size showed the complete differentiation of monocytes to macrophages.

In addition, it was determined if PMA differentiated macrophages demonstrate signalling pathways related to cell differentiation. According to previous literature, PMA activates the protein kinase C (PKC) signalling pathway (O'Brian *et* al., 1989) and can also activate downstream p38 and p42/p44ERK MAPK pathways in leukemic cells (Kharbanda *et al*., 1994; Almog and Naor, 2008; Nomura *et al*., 2007). Therefore, this was hypothesised that PMA could activate PKC signalling pathways in U937 and THP-1 monocytic cells during cell differentiation. The U937 cells were assessed for p38 at different concentrations of PMA and THP-1 cells were assessed with 8 nM PMA for p38 and ERK1/2 at different time points by western blot. The western blot analyses revealed that the phosphorylation level of p38 and ERK1/2 was significantly increased after 8 nM PMA treatment at 48 h compared with unstimulated control U937 cells.

The results suggested that p38 and ERK1/2 pathways are involved in PMA-induced cell differentiation. A study by Jiang and Fleet, 2012 suggested that p38 is a downstream signal of another PMA-regulated signal transduction pathway as they confirmed that treatment with 100 nM PMA can activate both ERK1/2 which occurred within 5 minutes, and p38 which was seen 1 hour after PMA treatment. Our data show that PMA treatment activated the p38 and ERK1/2 in U937 and THP-1 cells. Nutchey *et al*., 2005 have previously shown that ERK1/2 is activated by PMA in HEK293T cells.

To further investigate if PMA-differentiated macrophages demonstrate cell surface markers, the cells were stained for CD14, CD11a, CD11b, and CD68 surface markers and analysed by flow cytometry. The primary purpose of this study was to confirm whether the increased cell adhesion and upregulation of cell surface markers are associated with monocyte-macrophage differentiation. The results revealed that the morphology of U937 and THP-1 cells converted to macrophage-like phenotype, with significantly increased CD14, CD11b, CD68 expression, indicating that the model of monocyte differentiation *in vitro* was successfully established. PMA treatment of non-adherent U937 and THP-1 cells was associated with the cell attachment to form three-dimensional cell aggregates, growth arrest, and monocyte-macrophage differentiation.

The up and down-regulation of surface markers expression after PMA differentiation is a strong indication that U937 and THP-1 cells used in this study

are nearly proximal to macrophages. The expression of CD14 and CD68 surface markers were used to assess the differentiation of monocytes to macrophages. CD14, CD11a, CD11b, and CD68 are induced in monocyte-derived macrophages, U937 cell-derived macrophages manifest up-regulation of all the surface markers whereas, THP-1 cells only upregulated CD14, CD11b, and CD68 alone. The inconsistency of up-regulation of CD11a was observed with PMA differentiated U937 cells contrary to PMA differentiated THP-1 cells that show down-regulation. CD11a down-regulated upon monocyte differentiation in THP-1 cells. CD11a was almost negative in THP-1 cells of both unstimulated and PMA stimulated cells. This agrees with other studies suggesting that CD11a were negative in the synovial lining cells of both control and RA (Emmrich, 1990). The basis for this difference between U937 and THP-1 cells may be due to the different origin and maturation stages of cells. U937 cells are of tissue origin (histocytic lymphoma) thus at a more mature stage. THP1 cells are of blood leukemic origin at a less mature stage.

Another explanation is that up-regulation can be the effect of U937 cells that are not equal to THP-1 cells in the first place. These findings suggested a tight regulatory relationship between cell adherence, cell growth, and surface marker expression predominant role of the CD11b and CD68 in PMA-induced adherence of U937 and THP-1 cells. The function of CD11b and CD68 appeared more pronounced by its involvement to affect the cell growth as indicated by the significantly reduced cell number in unstimulated cells where its expression was marginal compared to PMA-stimulated cells.

Previous studies have shown that PMA treatment of THP-1 cells leads to a more mature phenotype with a lower rate of proliferation, higher levels of adherence, higher rate of phagocytosis and increased cell-surface expression of CD11b and CD14 (Qin, 2012; Abrahams *et al*., 2004 and Schwende *et al*., 1996). Interestingly we found significant inconsistencies in numerous previous studies in terms of CD14 expression by THP-1 cells at basal levels as well as using the same stimuli. For example, studies by Foster *et al*., 2005 and Ciabattini *et al*., 2006 have reported almost 90% CD14 expression in unstimulated THP-1 cells while Schwende *et al*., 1996 and Tobias *et al*., 1993 have reported lower or no expression.

Similarly, various studies described THP-1 CD14 levels in response to PMA vary from poor or no response (Fleit, 1991 and Fleit and Kobasiuk, 1991) to increased levels (Park *et* al., 2007; Ding *et al*., 2009 and Schwende *et al*., 1996). Different studies by others reported that adhesion molecules are up-regulated in U937 and THP-1 cells during differentiation (Miranda *et al*., 2002). The findings of the study prove that adhesion molecules such as CD11a and CD11b on monocytes were activated during differentiation into macrophages, and the increased surface markers expression and adhesion of differentiated cells to the cell-culture surface may contribute to understanding the underlying inhibitory mechanism action of sulphated disaccharide compounds on monocyte-macrophage differentiation.

Taken together, these results indicate that U937 and THP-1 cells serve as a good *in vitro* model system with a propensity of expression of CD14, CD11a, CD11b, and CD68 cell surface markers and p38 and ERK1/2 expression following 8 nM PMA treatment.

## 3.5 Conclusion

In this chapter, it has been demonstrated that PMA differentiated U937 and THP-1 cells develop into cells with certain characteristics of monocyte-macrophages. The U937 and THP-1 cells used in this study are proved to be very close to functional monocytes. Differentiation events were documented in morphologic, phenotypic, and functional changes. The treatment with 8 nM PMA for 48 h followed by additional PMA-free 72 h incubation were optimal conditions to induce U937 and THP-1 cell differentiation and surface markers (CD14, CD11a, CD11b, CD68) expression as 0.8 nM PMA was insufficient for inducing the adhesion of differentiated cells and 80 nM lead to significant cell death.

This study proposed that the stimulating effect of the PMA on p38 and ERK1/2 signalling may be partially mediated through the activation of cell adhesion surface markers and the pathways may play an important role in the monocyte differentiation.

In summary, PMA concentration and time are extremely important to take into consideration before starting differentiation studies using U937 and THP-1 cells. We found that 8 nM PMA for 48 h induced macrophages surface marker expression that are highly increased during differentiation into macrophages. Therefore, results from this protocol would be useful to study the impact of sulphated disaccharides on cell differentiation, cell surface markers expression, and cell signalling, which may modulate macrophage activation.

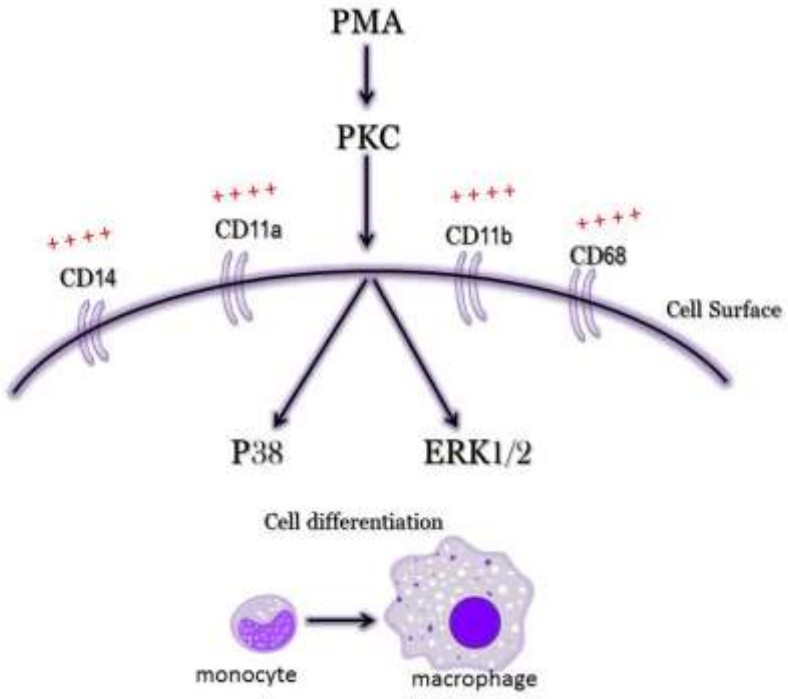


**Figure 3. 10**. ***A diagram to conclude Chapter 3.***

*Treatment of U937 and THP-1 monocyte cells with 8 nM PMA for 48 hours induced monocyte-macrophage differentiation in association with activation of p38 and p42/p45ERK MARK signalling pathway and upregulation of cell surface adhesion markers. The concentration of 8 nM PMA is optimal to induce cell differentiation in U937 and THP-1 cells.*

# CHAPTER 4: SULPHATED DISACCHARIDES INHIBIT PMA-INDUCED MONOCYTE DIFFERENTIATION TO MACROPHAGE

## 4.1 Introduction

As outlined in chapter 1, heparin and heparan sulphate are complex, linear, acidic polysaccharides belonging to the GAG family, and can be found primarily on the cell surface or in the extracellular matrix, attached to a protein core. The structural diversity of heparin and heparan sulphate lies at the core of the different range of physiological processes these molecules tend to modulate (Shriver *et al*., 2012).

Sulphated disaccharides are generated by enzymatic degradation of heparin or heparan sulphate glycosaminoglycans which have been found to inhibit T cell-mediated delayed-type hypersensitivity reaction to arthritic antigen in adjuvant arthritis in rodents at nanomolar amounts and regulate T-cell macrophages TNFα, IL-8 and IL-1β secretion (Lider *et al.,* 1989, Lider *et al;.,* 1990, Cahalon *et al.,* 1997, Hecht *et al.,* 2004). Cahalon *et al.,* (1997) studies suggest that the sulphate group of sulphated disaccharides may be functionally important for their inhibitory action. A study by Hecht *et al.,* (2004) reported inhibition of NF-κB activation with 10 ng/mL tri-sulphated disaccharide treatment in human anti-CD3-activated T-cells. Inhibition of NF-κB led to inhibition of TNF-α and IFN-y. Mono-sulphated disaccharide did not inhibit T cells-induced TNF-α and IFN-y production. Salmivirta *et al*., (1996) suggest that heparan is less sulphated than heparin.

Heparin disaccharide I-S sodium salt (HDS I-S) and Heparin disaccharide III-H sodium salt (HDS III-H) are unsaturated heparin salts. HDS I-S contains three sulphates (Fig.4.1a) whilst, HDS III-H contains one sulphate (Fig.4.1b). Both are obtained by the enzymatic dissociation of heparan sulphate and heparin by various heparinises (Cahalon *et al.,* 1997). The enzyme action results in a C4-C5 double bond in uronic acid. Heparin disaccharide salt has been used as a non-naphthalene, negatively charged, bivalent compound to test its ability to induce liquid-liquid phase separation (Babinchak *et al*., 2020). It is a bivalent compound with less hydrophobic nature and known to elevate the cytosolic calcium ($Ca^{2+}$) extrusion rate and may serve as a potential drug for the activation of $Na^{+}$ /$Ca^{2+}$ exchanger ( Shinjo *et al*., 2002).

Sucrose octasulphate (SOS) is liberated from the mucoadhesive anti-ulcer, anti-inflammatory bowel disease drug sucralfate by gastric acid hydrolyzation (Maddison, *et al*., 2008). Sucralfate is a complex salt composed of SOS and aluminium hydroxide. A series of studies suggest that sucralfate polymerizes to a viscous adhesive gel under acidic conditions which adheres to inflammatory sites and creates a strong protective gel layer against pepsin, acid, and bile acid (Itoh *et al*., 2004; Nagashima *et al*., 1980; Nakazawa *et al*., 1981 and Steiner *et al*., 1982). SOS is an oligosulphated disaccharide with eight sulphates, O-linked glycosyl, and furanyl moieties (Fig.4.1c). It has been found to downregulate joint inflammation, LPS induced TNF-α synthesis, collagen arthritis, and bone erosion in mice *in vivo* by suppressing TNF- α and IL-2α with an unknown mechanism of action (Lees *et al*., 2008). A study by Fannon *et al*., (2008), demonstrated that SOS shares some characteristics of heparin including an ability to inhibit tumour growth and growth factor binding to cells yet does not possess the potent anticoagulation activity that has limited the use of heparin for cancer therapy.

Di-glucopyranosylamine octasulphate sulphate or DOS which has oral anti-rheumatic activities (Bolton *et al.,* 2005) inhibits collagen and antigen-induced arthritis in mice with an unknown mechanism of action (Lees *et al.,* 2008). DOS is composed of N-linked glucuronic acid and glucosamine moieties linked through N-Acetylglucosamine (Ac group) with eight sulphates (Fig.4.1d).

As outlined in chapter 1, in a preliminary study (Bajwa and Seed, 2015) these compounds exhibited bell-shaped inhibition curves with a maximal inhibition seen at $10^{-11}$ M. HDS-IS elicited a different shape, with inhibition of U937 cell differentiation reaching a maximum at $10^{-4}$ M. This indicates that a single sulphate can elicit potent activity equivalent to the octa-sulphated compounds. However, the addition of a single sulphate to HDS-III radically alters the inhibition profile.

Given the findings from Chapter 3 demonstrating that PMA induced monocyte-macrophage differentiation in U937 and THP-1 cells. Therefore, in this study, it was hypothesised that sulphated disaccharides inhibit PMA-induced monocyte-macrophage differentiation. The structure-function relationship further strengthened the hypothesis of this study that the different sulphation within these sulphated disaccharides encodes information that forms the basis for regulating cell differentiation. This study focused on lower concentrations ranging from $10^{-}$

$^{11}$ M – $10^{-4}$ M to investigate the mechanism of action of sulphated disaccharides in inflammation by examining their impact on PMA-induced cell differentiation.

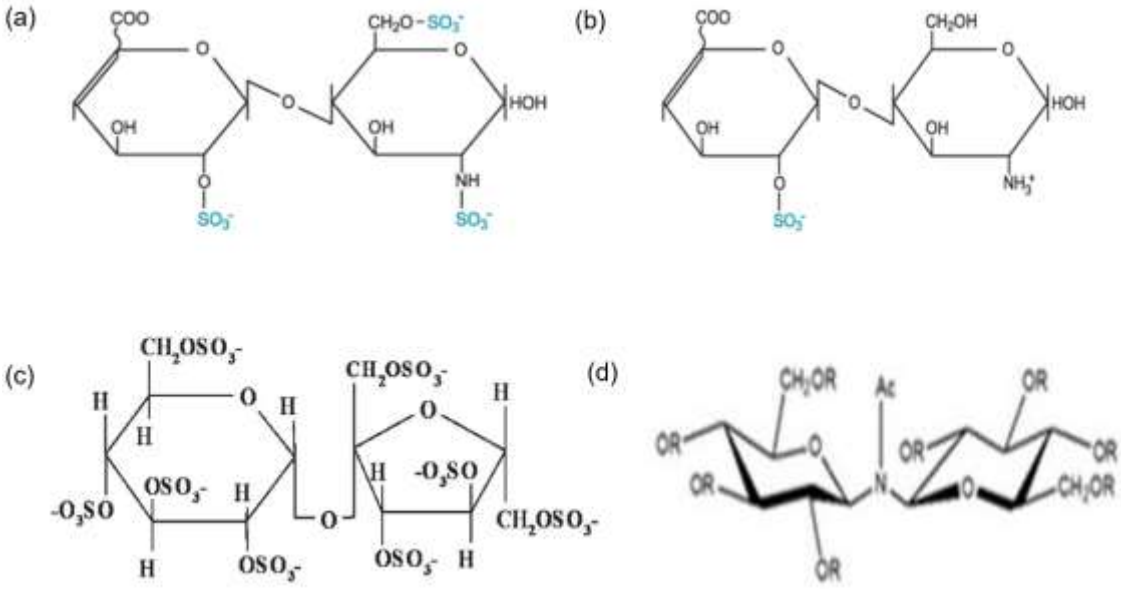


**Figure 4. 1*. Chemical structures of natural and synthetic heparin disaccharides.***

***(a)*** *Heparin disaccharide I-S sodium salt (HDS* ***I-S), (b)*** *Heparin disaccharide III-H sodium salt (HDS III-H),* ***(c)*** *Sucrose octasulphate (SOS) and* ***(d)*** *Di-glucosylamine octasulphate (DOS). 'R'* ***in DOS*** *indicates* ***the*** *presence of* ***the*** *number of sulphates.*

## 4.2 Aim

This chapter aimed to identify the impact of sulphated disaccharides on differentiated macrophage cell surface markers and whether this impact contributes to the inhibition of surface markers expression outcome.

The first question addressed in this study was *how much time to allow* for sulphated disaccharides exposure to U937 and THP-1 cells. Once optimal pre-incubation duration was achieved, this study investigated how sulphated disaccharides would impact PMA-induced cell differentiation of U937 and THP-1 cells. The different concentrations for sulphated disaccharides were prepared ranging from $10^{-11}$ M to $10^{-4}$ M.

## 4.3 Results

### 4.3.1 Sulphated disaccharides impact on cell adhesion

To optimise the pre-incubation duration of sulphated disaccharides these compounds were tested by using a cell proliferation assay as described in materials and methods section 2.5.

Sulphated disaccharide compounds produced a significant reduction in the proportion of cell adhesion and the number of adherent cells when given 2 h before 8 nM PMA compared to 1 h before 8 nM PMA at 48 h. The results of this study were useful for optimising the time point suitable for screening sulphated disaccharides impact on cell count and cell adhesion. The percentage of cell adhesion of U937 and THP-1 in the presence of PMA was up to 80%.

As shown in Fig.4.1 and Fig.4.2, U937 and THP-1 adherent cells of 8 nM PMA decreased significantly ($p < 0.01$) in the presence of $10^{-11}$ M to $10^{-4}$ M SOS and DOS when given 2 hour before (Fig.4.1b, Fig.4.1d, Fig.4.2b & Fig.4.2d) PMA compared to given 1 hour before (Fig.4.1a, Fig.4.1c, Fig.4.2a & Fig.4.2c) PMA. This resulted in significant ($p < 0.01$) inhibition of PMA-induced cell adhesion of up to 50% at concentrations of $10^{-11}$ M to $10^{-4}$ M. No significant difference in the number of adherent cells and percentage of cell adhesion of U937 and THP-1 cells was found when SOS and DOS were given 1 hour before PMA.

PMA (8 nM)-induced number of adherent cells were significantly ($p < 0.01$) reduced in the presence of HDS-I at concentrations of $10^{-9}$ M to $10^{-4}$ M when given 2 hour before (Fig.4.3b & Fig.4.3d) PMA compared to 1 hour before PMA (Fig.4.3a & Fig.4.3c). The lower concentrations $10^{-11}$ M and $10^{-10}$ M of HDS-I had no significant impact on PMA-induced cell adhesion. As shown in Fig.4.3, HDS-I significantly ($p < 0.01$) inhibited PMA-induced cell adhesion up to 30% in U937 cells and approximately 50% in THP-1 cells at concentrations of $10^{-9}$ M to $10^{-4}$ M when given 2 hours before PMA.

HDS-III reduced PMA-induced cell adhesion from 80% to 20% in U937 cells and 30% in THP-1 cells at concentrations of $10^{-7}$ M to $10^{-4}$ M when given 2 hours

before (Fig.4.4b & Fig.4.4d) PMA compared to 1 hour before (Fig.4.4a & Fig.4.4c). PMA. The number of adherent cells were reduced ($p < 0.01$) in U937 and THP-1 cells in the presence of HDS-III at concentrations of $10^{-8}$ M to $10^{-4}$ M. The lower concentrations $10^{-11}$ M, $10^{-10}$ M and $10^{-9}$ M of HDS-III showed no significant effect on PMA-induced cell adhesion (Fig.4.4b & Fig.4.4d).

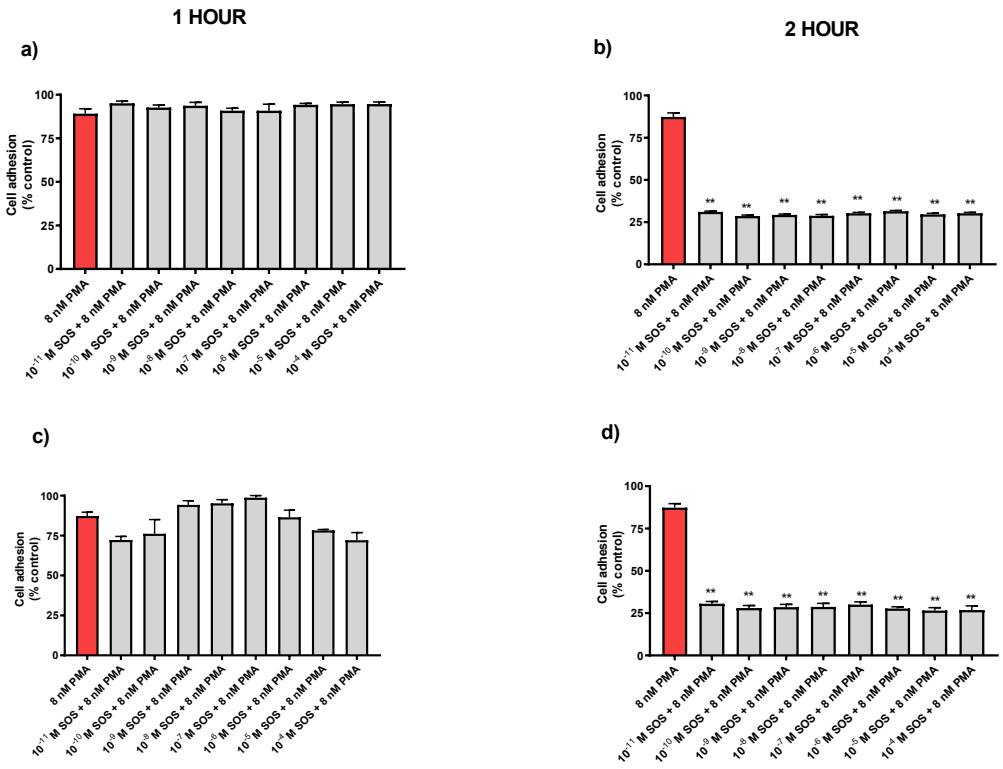


**Figure 4. 2*. SOS impact on impact on U937 and THP-1 cell adhesion.***

*SOS ($10^{-11}$ to $10^{-4}$ M) given at 1 h on (a) U937 and (c) THP-1 and at 2 h on (b) U937 and (d) THP-1 before PMA for 48 h. The adherence of U937 and THP-1 cells to 96-well cell culture plates was determined using the CyQUANT® cell proliferation assay kit proprietary green fluorescent CyQUANT® GR dye. Briefly, U937 and THP-1 cells with cell density of 5 x $10^5$cells/mL were seeded in 96-well plate. SOS at concentrations of $10^{-11}$ M to $10^{-4}$ M were administered to 96-well plates at 1 h and 2h prior to 8 nM PMA at 48 h. A blank well with no cells was used as a negative control and cells in the presence of PMA alone were used as a positive control. Data analysed using One Way ANOVA with Dunnett's post hoc test (n=3), mean ± SEM, **p<0.01 vs PMA. Data presented was pooled from three experiments.*

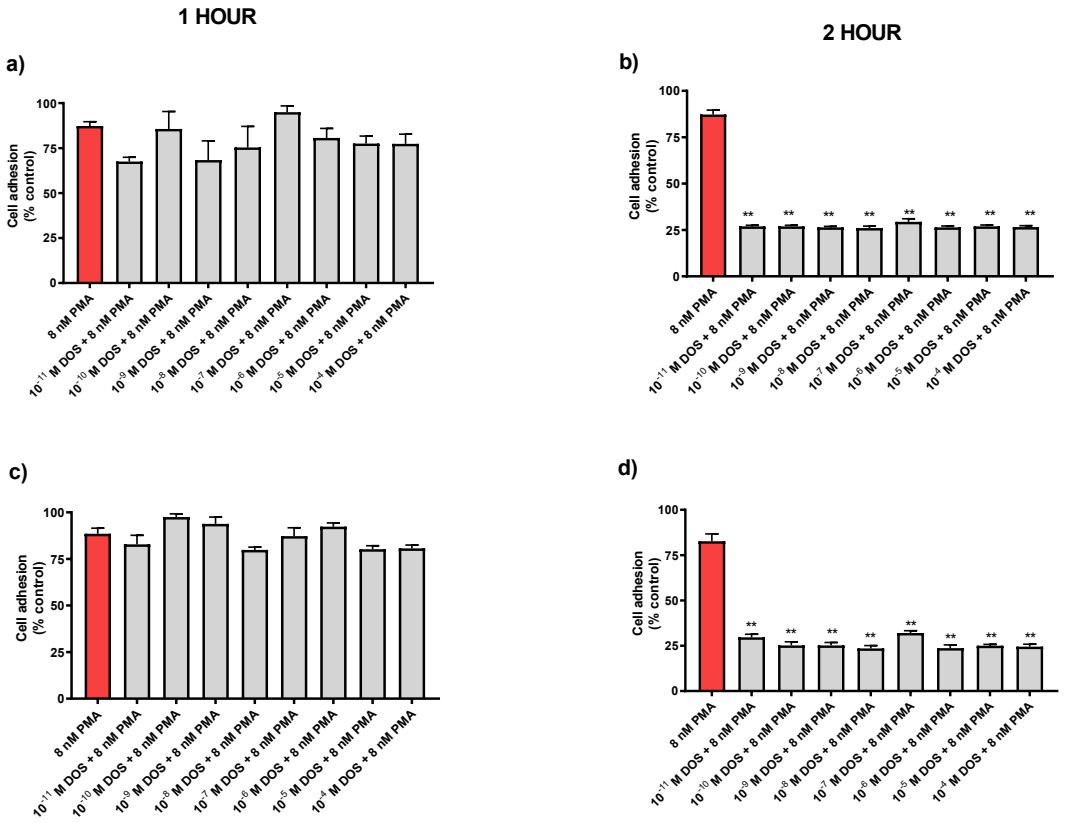


**Figure 4. 3*. DOS impact on U937 and THP-1 cell adhesion.***

*DOS (10-11 to 10-4 M) given at 1 h on (a) U937 and (c) THP-1 and at 2 h on (b) U937 and (d) THP-1 before PMA for 48 h. The adherence of U937 and THP-1 cells to 96-well cell culture plates was determined using the CyQUANT® cell proliferation assay kit proprietary green fluorescent CyQUANT® GR dye. Briefly, U937 and THP-1 cells with cell density of 5 x 105cells/mL were seeded in 96-well plate. DOS at concentrations of 10-11 M to 10-4 M were administered to 96-well plates at 1 h and 2h prior to 8 nM PMA at 48 h. A blank well with no cells was used as a negative control and cells in the presence of PMA alone were used as a positive control. Data analysed using One Way ANOVA with Dunnett's post hoc test (n=3), mean ± SEM, **p<0.01 vs PMA. Data presented was pooled from three experiments.*

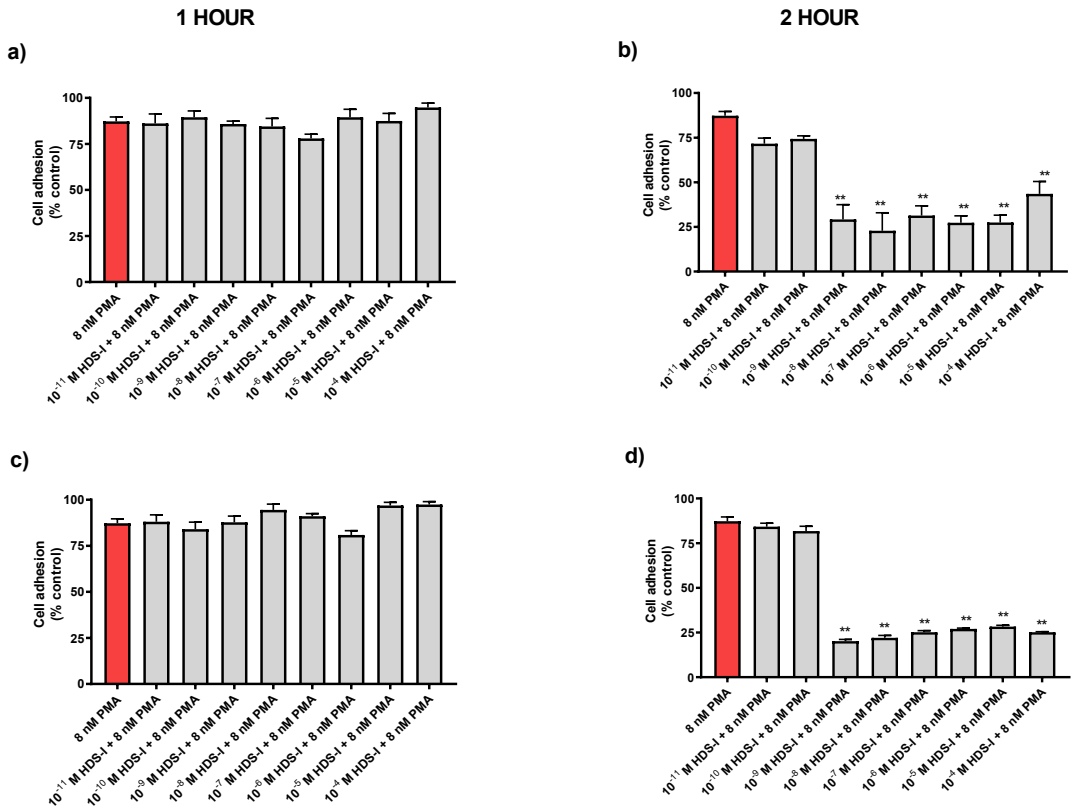


**Figure 4. 4*. HDS-I impact on U937 and THP-1 cell adhesion.***

*HDS-I ($10^{-11}$ to $10^{-4}$ M) given at 1 h on (a) U937 and (c) THP-1 and at 2 h on (b) U937 and (d) THP-1 before PMA for 48 h. The adherence of U937 and THP-1 cells to 96-well cell culture plates was determined using the CyQUANT® cell proliferation assay kit proprietary green fluorescent CyQUANT® GR dye. Briefly, U937 and THP-1 cells with cell density of 5 x $10^5$cells/mL were seeded in 96-well plate. HDS-I at concentrations of $10^{-11}$ M to $10^{-4}$ M were administered to 96-well plates at 1 h and 2h prior to 8 nM PMA at 48 h. A blank well with no cells was used as a negative control and cells in the presence of PMA alone were used as a positive control. Data analysed using One Way ANOVA with Dunnett's post hoc test (n=3), mean ± SEM, **p<0.01 vs PMA. Data presented was pooled from three experiments. HDS-I ($10^{-11}$ to $10^{-4}$ M) given at 1 h (a,b) and at 2 h (c,d) before PMA for 48 h. Cell proliferation was determined using cell proliferation assay (see methods section 2.4). Data analysed using One Way ANOVA with Dunnett's post hoc test (n=3), mean ± SEM, **p<0.01 vs PMA.*

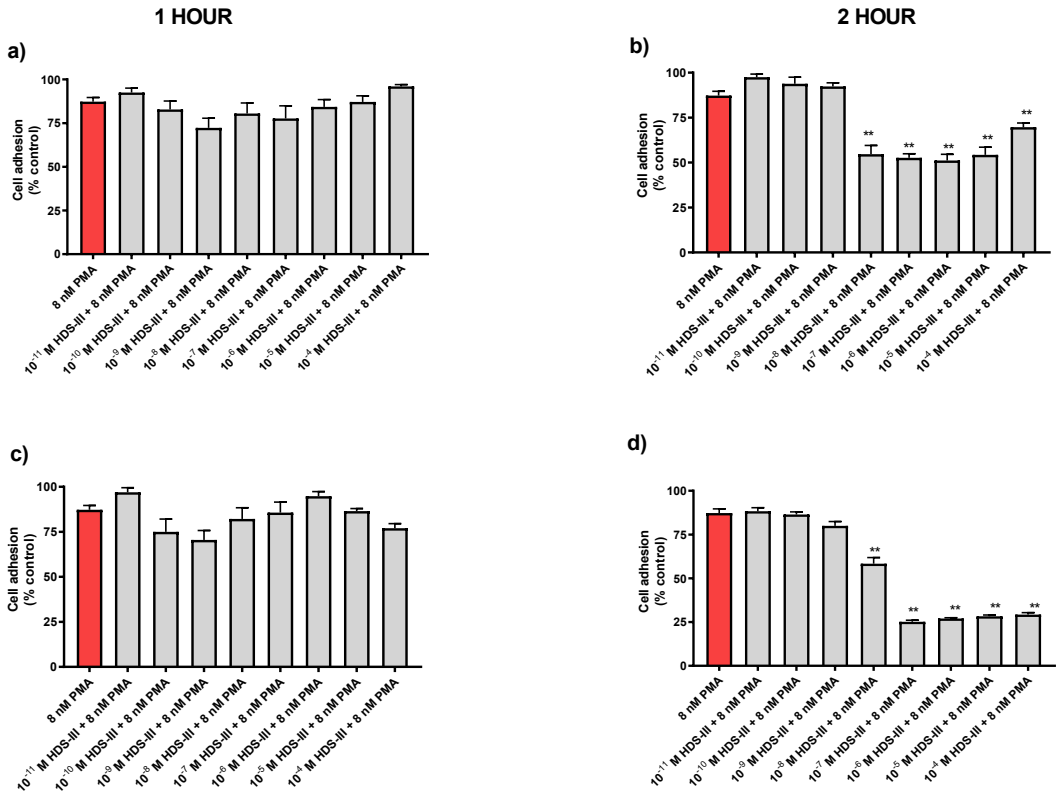


**Figure 4. 5*. HDS-III impact on U937 and THP-1 cell adhesion.***

*HDS-III ($10^{-11}$ to $10^{-4}$ M) given at 1 h on (a) U937 and (c) THP-1 and at 2 h on (b) U937 and (d) THP-1 before PMA for 48 h. The adherence of U937 and THP-1 cells to 96-well cell culture plates was determined using the CyQUANT® cell proliferation assay kit proprietary green fluorescent CyQUANT® GR dye. Briefly, U937 and THP-1 cells with cell density of 5 x $10^5$cells/mL were seeded in 96-well plate. HDS-III at concentrations of $10^{-11}$ M to $10^{-4}$ M were administered to 96-well plates at 1 h and 2h prior to 8 nM PMA at 48 h. A blank well with no cells was used as a negative control and cells in the presence of PMA alone were used as a positive control. Data analysed using One Way ANOVA with Dunnett's post hoc test (n=3), mean ± SEM, **p<0.01 vs PMA. Data presented was pooled from three experiments.*

### 4.3.2 Sulphated disaccharides reduced number of adherent cells in PMA cell culture

In this study, the impact of sulphated disaccharides on PMA-induced adherent cells was investigated by examining their effect on U937 and THP-1 cells morphology, cell count and cell viability. The impact of sulphated disaccharides on U937 and THP-1 cells was determined in the presence and absence of PMA by microscopic imaging and cell count by trypan blue exclusion using Countess™ II FL (see Appendix – Fig.9 to Fig.32 for microscopic imaging and cell count data in the absence of PMA).

SOS (Fig.4.5a & Fig.4.5b) and DOS (Fig.4.5c & Fig.4.5d) at concentrations of $10^{-11}$ M to $10^{-4}$ M inhibited PMA-induced cell adhesion of U937 and THP-1 cells to 24-well plates when given 2 h before 8 nM PMA. The number of adherent cells collected from SOS, DOS and PMA cultures were reduced significantly ($p < 0.01$) in a concentration dependent manner compared to PMA cell cultures.

In the cell culture of HDS-I and PMA the number of U937 adherent cells was inhibited at concentrations of $10^{-9}$ M and $10^{-6}$ M with significance ($p < 0.05$) and at concentrations of $10^{-8}$ M, $10^{-7}$ M, $10^{-5}$ M, $10^{-4}$ M ($p < 0.01$) when given 2 h prior to PMA (Fig.4.5e). Similarly, HDS-I at concentrations of $10^{-9}$ M to $10^{-4}$ M inhibited number of THP-1 adherent cells (Fig.4.5f).

HDS-III in the presence of PMA inhibited a noticeable number of U937 adherent cells at concentrations of $10^{-8}$ M ($p < 0.05$), $10^{-7}$ M to $10^{-4}$ M ($p < 0.01$) when given 2 h prior to PMA (Fig.4.5g). Similarly, HDS-III reduced significantly a number of THP-1 adherent cells at concentrations of $10^{-8}$ M to $10^{-4}$ M ($p < 0.01$) (Fig.4.5h).

It was observed that U937 and THP-1 cells showed a monocytic non-adherent phenotype in the presence of SOS, DOS at concentrations of $10^{-11}$ M to $10^{-4}$ M.

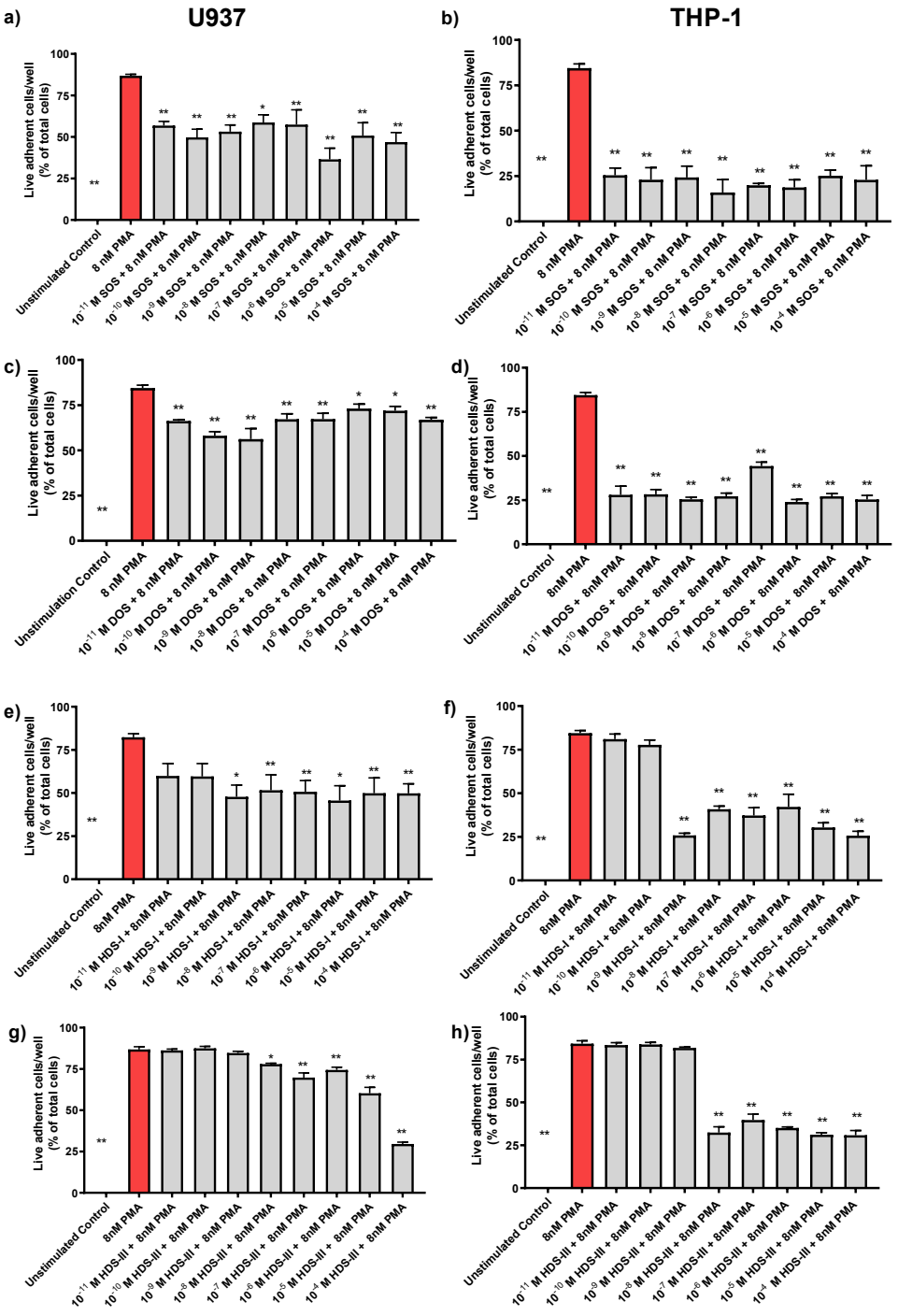


**Figure 4. 6.** ***Sulphated disaccharides impact on U937 and THP-1 cell count in the presence of PMA.***

*The U937 (a, c, e, g) and THP-1 (b, d, f, h) cells with cell density of 2 x$10^5$ cell/mL were pre-incubated in 24-well plate and were pre-treated (given 2 h before PMA) with SOS (a, b), DOS (c, d), HDS-I (e, f) and HDS-III (g, h) at concentrations of $10^{-11}$ to $10^{-4}$ M for 48 h in the presence of 8 nM PMA. Subsequently cells were visualised using inverted light microscope at 40x magnification and were counted*

*by using Countess™ II FL. Non-adherent cells were removed at 48 h and adherent cells were collected and counted at 72 h. Cell count (presented as percentage of control) for adherent cells in the presence of PMA. Results analysed by One Way ANOVA with Dunnett's post hoc test, means± SEM (n =3), *p<0.05, **p<0.01 vs PMA. Data presented was pooled from three experiments.*

### 4.3.3 Sulphated disaccharides down-regulated PMA-induced cell surface markers expression

This study was conducted to determine whether sulphated disaccharides have an impact on the PMA-induced up-regulation of cell surface markers expression. This was investigated using flow cytometry. Briefly, U937 and THP-1 cells were treated with sulphated disaccharides in the presence and absence of PMA as described in materials and methods section 2.3 and were analysed using flow cytometry as described in materials and methods section 2.4 (Appendix Fig. 33 to Appendix Fig. 80).

Flow cytometric analysis for CD14, CD11a, CD11b, CD68 positive cells and their expression revealed significant inhibition of PMA-induced cell differentiation by sulphated disaccharides when given prior to PMA induction (Fig.4.6 to Fig.4.13).

SOS significantly reduced percentage of $CD14^+$ (Fig.4.6a), $CD11b^+$ (Fig.4.7a), and $CD68^+$ (Fig.4.7e) cells and their expression (Fig.4.6b & Fig.4.7b,f,h) in SOS + PMA U937 cultures at concentrations of $10^{-11}$ M to $10^{-4}$ M ($p < 0.01$) compared to PMA-stimulated U937 cultures. $CD11a^+$cells (Fig.4.6e) was significantly reduced by SOS at concentrations of $10^{-11}$ M ($p < 0.05$), $10^{-10}$ M to $10^{-7}$ M and $10^{-5}$ M ($p < 0.01$) and expression of $CD11a^+$ cells (Fig.4.6f) was inhibited by SOS at concentrations of $10^{-11}$ M to $10^{-4}$ M ($p < 0.01$) in SOS + PMA U937 cultures compared to PMA-treated U937 cultures $CD11a^+$.

Similar results were found in THP-1 cells. SOS reduced the percentage of $CD14^+$ (Fig.4.6c), $CD11a^+$ (Fig.4.6g), $CD68^+$ (Fig.4.7g) cells and their degree of expression in SOS + PMA THP-1 cultures at concentrations of $10^{-11}$ M to $10^{-4}$ M ($p < 0.01$) compared to PMA-stimulated THP-1 cultures $CD14^+$ (Fig.4.6d), $CD11a^+$ (Fig.4.6h) and $CD68^+$ (Fig.4.7h). SOS reduced the percentage of $CD11b^+$ (Fig.4.7c) cells at concentrations of $10^{-11}$ M, $10^{-9}$ M to $10^{-4}$ M ($p < 0.01$) and $10^{-10}$ M ($p < 0.05$) and their marker expression in SOS + PMA THP-1 cultures at concentrations of $10^{-11}$ M to $10^{-4}$ M ($p < 0.01$) compared to PMA-treated THP-1 cultures $CD11b^+$ (Fig.4.7d).

DOS and HDS-I significantly reduced the percentage of $CD14^+$, $CD11a^+$, $CD11b^+$, and $CD68^+$ cells and intensity of marker expression in DOS + PMA U937

cultures and DOS + PMA THP-1 cultures at concentrations of $10^{-11}$ M to $10^{-4}$ M ($p < 0.01$ and $p < 0.05$) compared to PMA-stimulated cells U937 and THP-1 cultures at 48 h (Fig.4.8 – Fig.4.11).

HDS-III significantly reduced the percentage of $CD14^+$ cells (Fig.4.10a) in HDS-III + PMA U937 cell cultures at concentrations of $10^{-11}$ M ($p < 0.05$), $10^{-10}$ M to $10^{-6}$M ($p < 0.01$) and degree of expression of $CD14^+$ cells (Fig.4.10b) at concentrations of $10^{-11}$ M to $10^{-5}$M ($p < 0.01$) compared to PMA-U937 cell cultures at 48 h. The percentage of $CD11a^+$ cells (Fig.4.10e) was significantly lower ($p < 0.05$, $p < 0.01$) in HDS-III + PMA U937 cell cultures at HDS-III concentrations of $10^{-11}$ M to $10^{-8}$M and MFI of $CD11a^+$ cells (Fig.4.10f) at HDS-III concentrations of $10^{-11}$ M to $10^{-4}$M compared to PMA-U937 cell cultures. $CD11b^+$ cell (Fig.4.11a) percentage was increased in HDS-III + PMA U937 cultures and degree of CD11b expression (Fig.4.11b) was reduced at HDS-III concentrations of $10^{-10}$ M to $10^{-4}$ M ($p < 0.01$) compared to PMA-U937 cell cultures. The percentage of $CD68^+$ cells (Fig.4.11e) and their CD68 expression (Fig.4.11f) was reduced by HDS-III at concentrations of $10^{-11}$ M to $10^{-4}$ M ($p < 0.01$) compared to PMA-U937 cell cultures. HDS-III at concentrations of $10^{-11}$ M to $10^{-4}$ M also significantly reduced ($p < 0.01$) $CD14^+$ (Fig.4.10c), $CD11a^+$ (Fig.4.10g), $CD11b^+$ (Fig.4.11c), and $CD68^+$ (Fig.4.10g), cells and their expression (Fig.4.10d,h & Fig.4.11d,h) in HDS-III + PMA THP-1 cultures compared to PMA-THP-1 cultures.

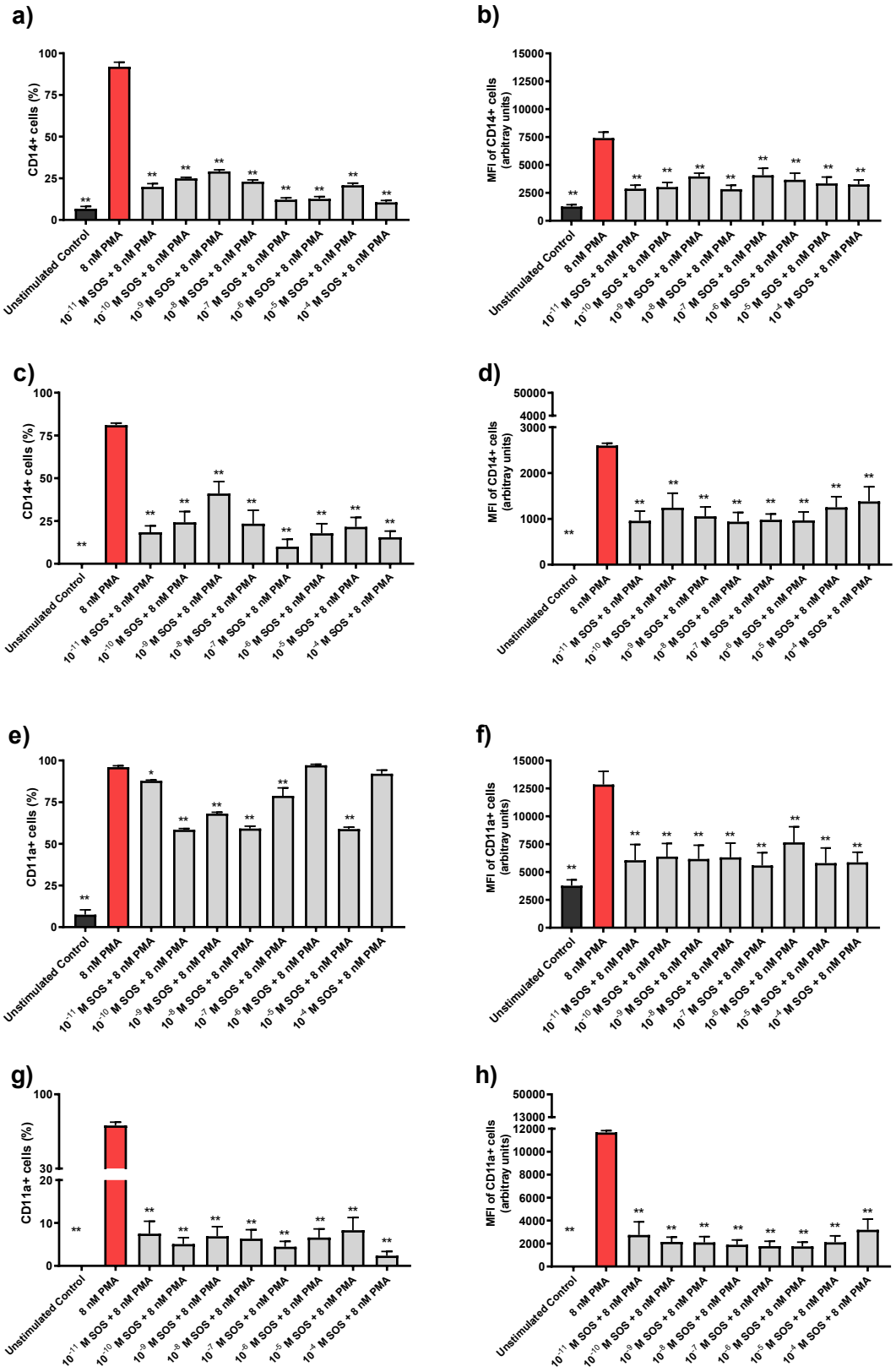


**Figure 4. 7*. The impact of SOS on U937 and THP-1 CD14 and CD11a expression in the presence of PMA.***

*Bar graph represents (a) CD14 positive U937 cells, (b) MFI of CD14 positive U937 cells, (c) CD14 positive THP-1 cells, (d) MFI of CD14 positive THP-1 cells, (e) CD11a positive U937 cells, (f) MFI of CD11a U937 positive cells, (g) CD11a positive THP-1 cells and (h) MFI of CD11a THP-1 positive cells. The impact of sulphated disaccharides was investigated in the presence of PMA. The U937 and THP-1 cells were cultured in 24-well tissue culture plates at an initial density of $2x10^5$ cells/mL per well. Cells were then incubated with SOS 2 h prior to 8 nM PMA and incubated for 48 h at 37 $^0$C with 5% $CO_2$. Non-adherent cells were removed at 48 h. The adherent cells of this experiment were left for a resting period in fresh PMA-free RPMI-1640 supplemented media for further 72 h incubation. The adherent cells from 24-well plates were harvested after 72 h subsequently washed twice in ice-cold (4 $^0$C) PBS and cells were counted and stained for CD14, CD11a cell surface markers to sulphated disaccharides impact on mature macrophages and the treated samples were analysed by flow cytometry. Isotype control on CD14-PE and CD11a-FITC channels were used to identify the positive cells. ANOVA with post hoc Dunnett's test, mean ± SEM (n=3), *p<0.05, **p < 0.01 vs PMA. The data presented was pooled from three experiments.*

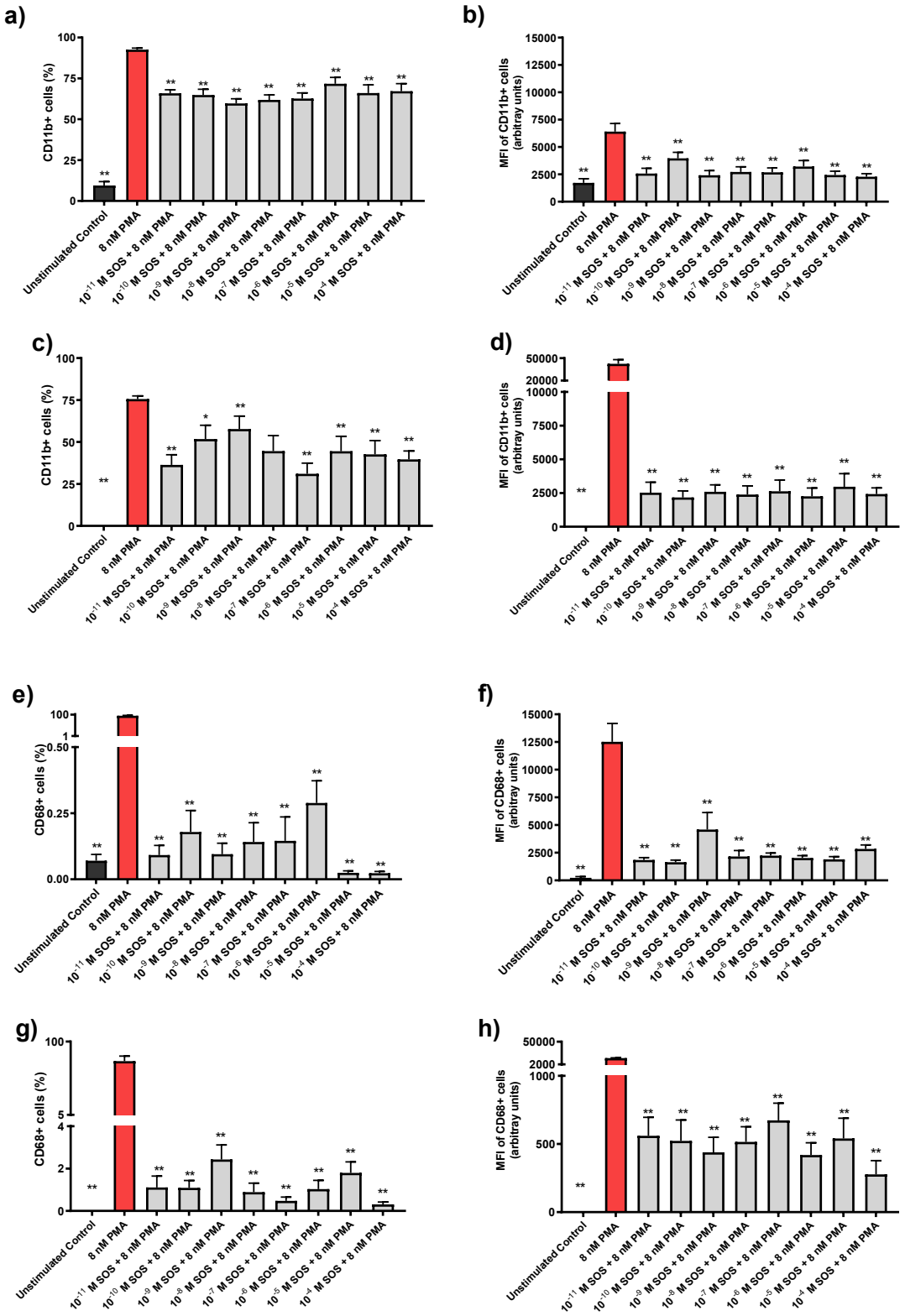


**Figure 4. 8*. The impact of SOS on U937 and THP-1 CD11b and CD68 expression in the presence of PMA.***

*Bar graph represents (a) CD11b positive U937 cells, (b) MFI of CD11b positive U937 cells, (c) CD11b positive THP-1 cells, (d) MFI of CD11b positive THP-1*

*cells, (e) CD68 positive U937 cells, (f) MFI of CD68 U937 positive cells, (g) CD68 positive THP-1 cells and (h) MFI of CD68 THP-1 positive cells. The impact of sulphated disaccharides was investigated in the presence of PMA. The U937 and THP-1 cells were cultured in 24-well tissue culture plates at an initial density of $2x10^5$ cells/mL per well. Cells were then incubated with SOS 2 h prior to 8 nM PMA and incubated for 48 h at 37 $^0$C with 5% $CO_2$. Non-adherent cells were removed at 48 h. The adherent cells of this experiment were left for a resting period in fresh PMA-free RPMI-1640 supplemented media for further 72 h incubation. The adherent cells from 24-well plates were harvested after 72 h subsequently washed twice in ice-cold (4 $^0$C) PBS and cells were counted and stained for CD11b, CD68 cell surface markers to sulphated disaccharides impact on mature macrophages and the treated samples were analysed by flow cytometry. Isotype control on CD11b-BV650 and CD68-Cyanine-7 channels were used to identify the positive cells. ANOVA with post hoc Dunnett's test, mean ± SEM (n=3), *p<0.05 **p < 0.01 vs PMA.*

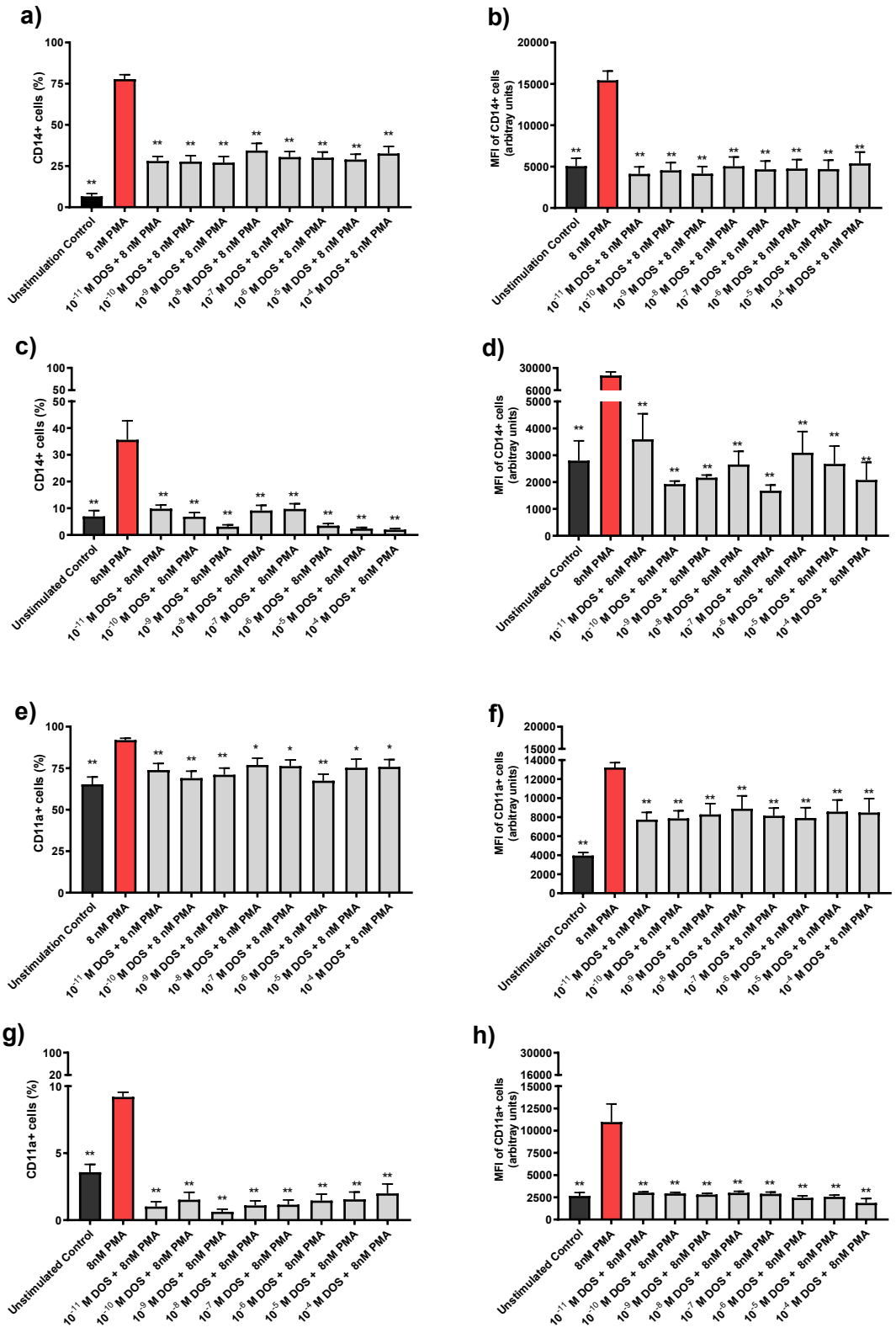


**Figure 4. 9*. The impact of DOS on U937 CD14 and CD11a expression in the presence of PMA.***

*Bar graph represents (a) CD14 positive U937 cells, (b) MFI of CD14 positive U937 cells, (c) CD14 positive THP-1 cells, (d) MFI of CD14 positive THP-1 cells,*

*(e) CD11a positive U937 cells, (f) MFI of CD11a U937 positive cells, (g) CD11a positive THP-1 cells and (h) MFI of CD11a THP-1 positive cells. The impact of sulphated disaccharides was investigated in the presence of PMA. The U937 and THP-1 cells were cultured in 24-well tissue culture plates at an initial density of $2x10^5$ cells/mL per well. Cells were then incubated with DOS 2 h prior to 8 nM PMA and incubated for 48 h at 37 $^0$C with 5% $CO_2$. Non-adherent cells were removed at 48 h. The adherent cells of this experiment left for a resting period in fresh PMA-free RPMI-1640 supplemented media for further 72 h incubation. The adherent cells from 24-well plates were harvested after 72 h subsequently washed twice in ice-cold (4 $^0$C) PBS and cells were counted and stained for CD14, CD11a cell surface markers to sulphated disaccharides impact on mature macrophages and the treated samples were analysed by flow cytometry. Isotype control on CD14-PE and CD11a-FITC channels were used to identify the positive cells. ANOVA with post hoc Dunnett's test, mean ± SEM (n=3), *p<0.05, **p < 0.01 vs PMA. The data presented was pooled from three experiments*

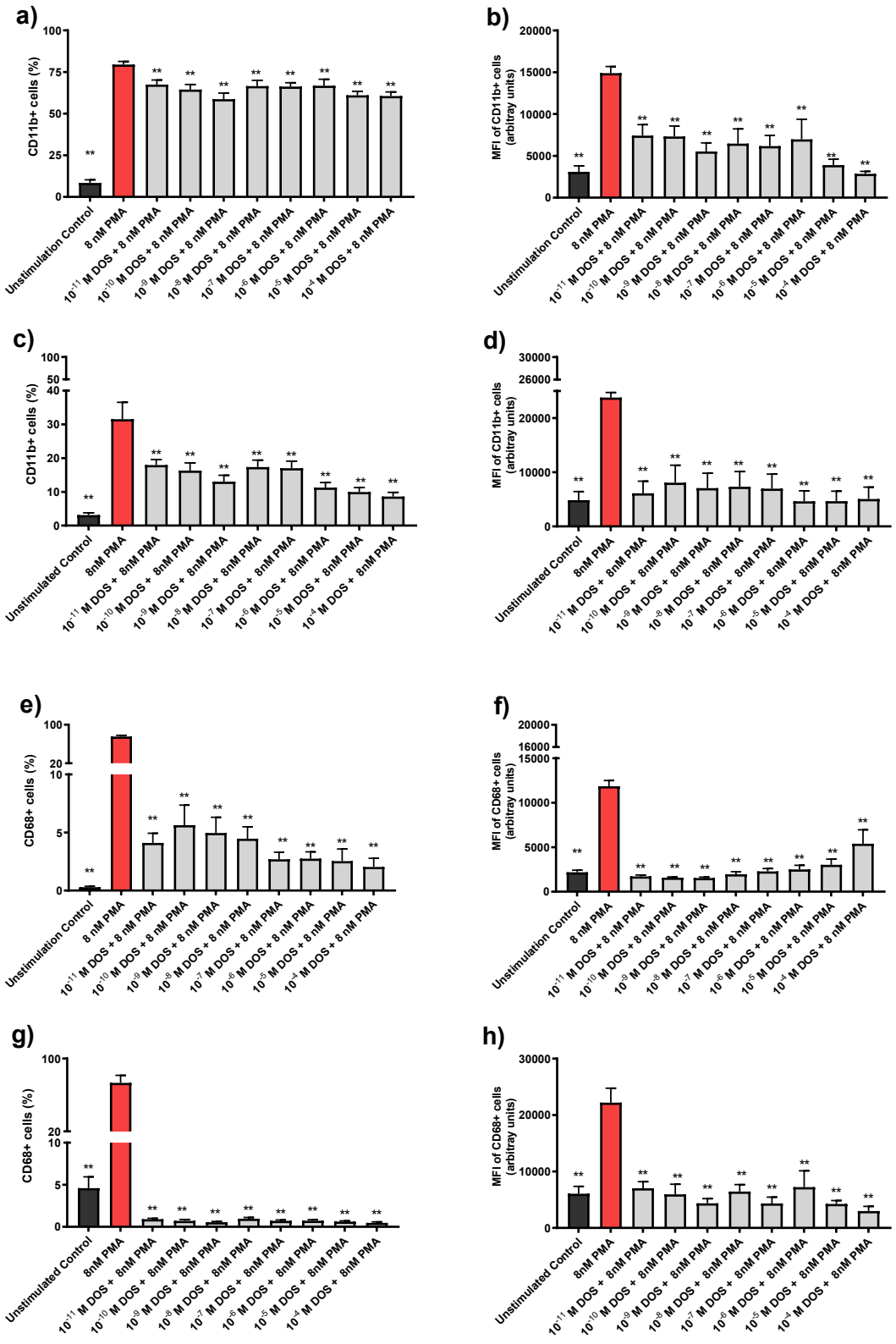


**Figure 4. 10.** ***The impact of DOS on U937 and THP-1 CD11b and CD68 expression in the presence of PMA.***

*Bar graph represents (a) CD11b positive U937 cells, (b) MFI of CD11b positive U937 cells, (c) CD11b positive THP-1 cells, (d) MFI of CD11b positive THP-1*

*cells, (e) CD68 positive U937 cells, (f) MFI of CD68 U937 positive cells, (g) CD68 positive THP-1 cells and (h) MFI of CD68 THP-1 positive cells. The impact of sulphated disaccharides was investigated in the presence of PMA. The U937 and THP-1 cells were cultured in 24-well tissue culture plates at an initial density of $2x10^5$ cells/mL per well. Cells were then incubated with DOS 2 h prior to 8 nM PMA and incubated for 48 h at 37 $^0$C with 5% $CO_2$. Non-adherent cells were removed at 48 h. The adherent cells of this experiment left for a resting period in fresh PMA-free RPMI-1640 supplemented media for further 72 h incubation. The adherent cells from 24-well plates were harvested after 72 h subsequently washed twice in ice-cold (4 $^0$C) PBS and cells were counted and stained for CD11b, CD68 cell surface markers to sulphated disaccharides impact on mature macrophages and the treated samples were analysed by flow cytometry. Isotype control on CD11b-BV650 and CD68-Cyanine-7 channels were used to identify the positive cells. ANOVA with post hoc Dunnett's test, mean ± SEM (n=3), **p < 0.01 vs PMA. The data presented was pooled from three experiments.*

.

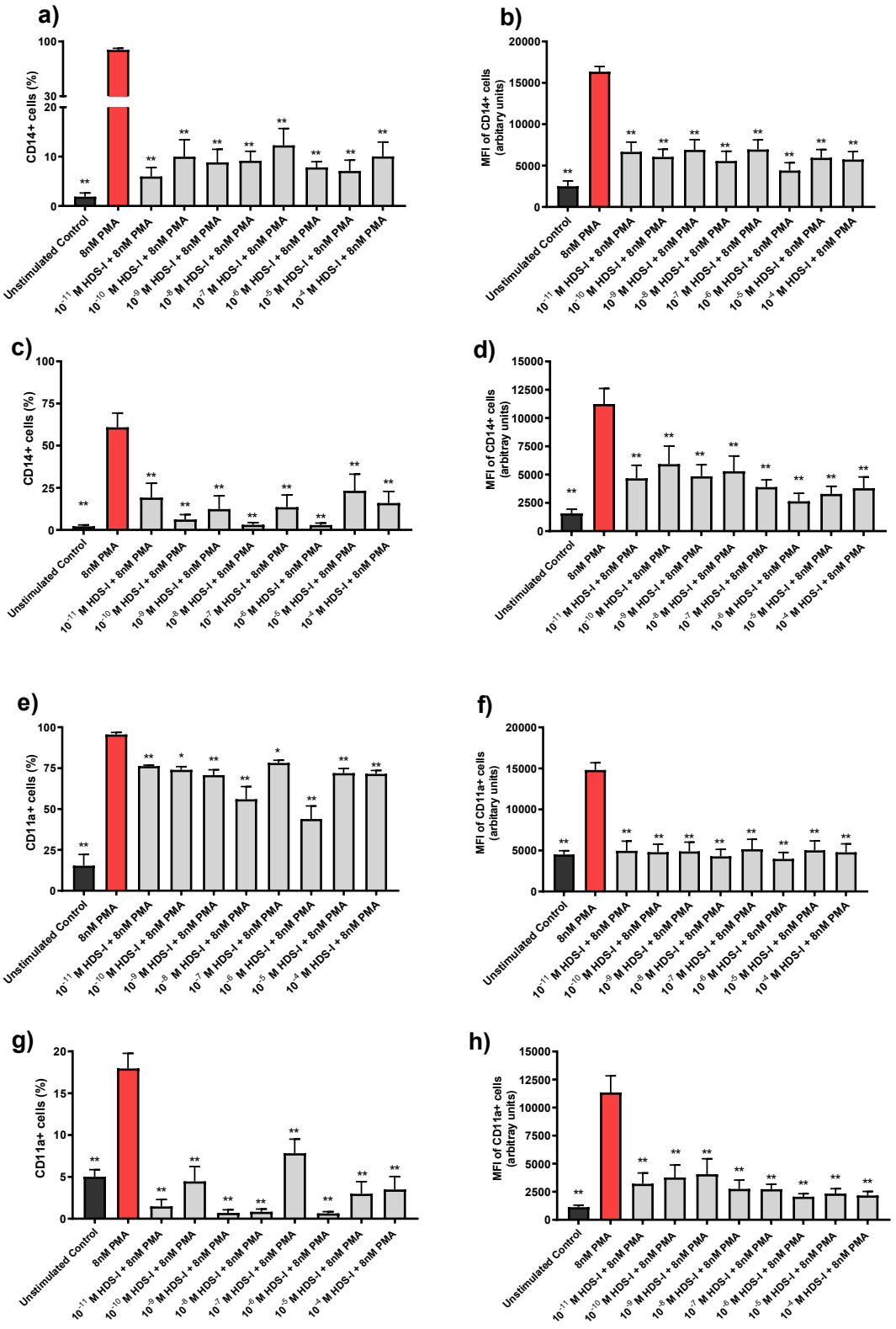


**Figure 4. 11.** ***The impact of HDS-I on U937 and THP-1 CD14 and CD11a expression in the presence of PMA.***

*Bar graph represents (a) CD14 positive U937 cells, (b) MFI of CD14 positive U937 cells, (c) CD14 positive THP-1 cells, (d) MFI of CD14 positive THP-1 cells,*

*(e) CD11a positive U937 cells, (f) MFI of CD11a U937 positive cells, (g) CD11a positive THP-1 cells and (h) MFI of CD11a THP-1 positive cells. The impact of sulphated disaccharides was investigated in the presence of PMA. The U937 and THP-1 cells were cultured in 24-well tissue culture plates at an initial density of $2x10^5$ cells/mL per well. Cells were then incubated with HDS-I 2 h prior to 8 nM PMA and incubated for 48 h at 37 $^0$C with 5% $CO_2$. Non-adherent cells were removed at 48 h. The adherent cells of this experiment were left for a resting period in fresh PMA-free RPMI-1640 supplemented media for further 72 h incubation. The adherent cells from 24-well plates were harvested after 72 h subsequently washed twice in ice-cold (4 $^0$C) PBS and cells were counted and stained for CD14, CD11a cell surface markers to sulphated disaccharides impact on mature macrophages and the treated samples were analysed by flow cytometry. Isotype control on CD14-PE and CD11a-FITC channels were used to identify the positive cells. ANOVA with post hoc Dunnett's test, mean ± SEM (n=3), *p<0.05, **p < 0.01 vs PMA. The data presented was pooled from three experiments.*

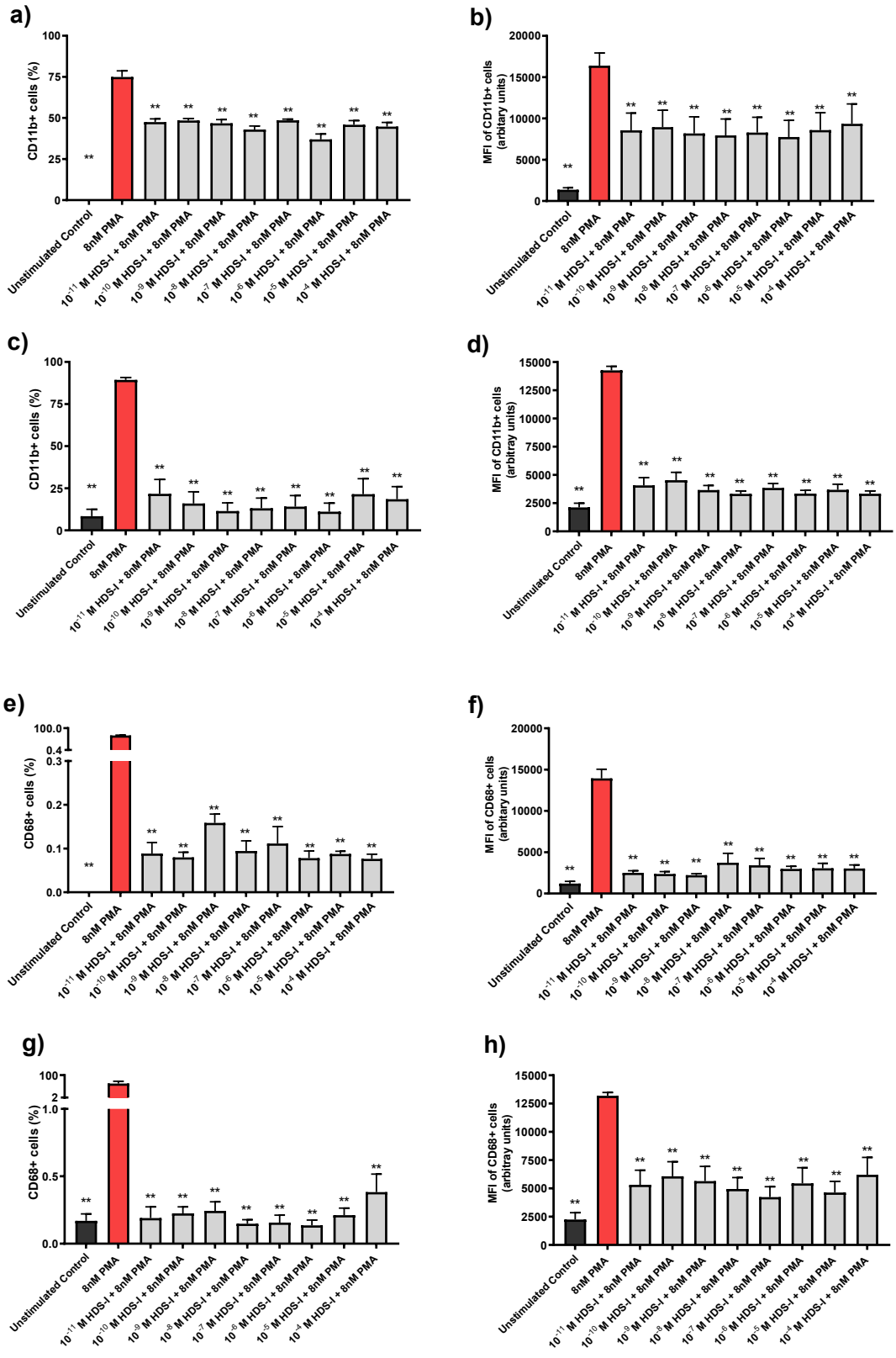


**Figure 4. 12.** ***The impact of HDS-I on U937 and THP-1 CD11b and CD68 expression in the presence of PMA.***

*Bar graph represents (a) CD11b positive U937 cells, (b) MFI of CD11b positive U937 cells, (c) CD11b positive THP-1 cells, (d) MFI of CD11b positive THP-1 cells, (e) CD68 positive U937 cells, (f) MFI of CD68 U937 positive cells, (g) CD68 positive THP-1 cells and (h) MFI of CD68 THP-1 positive cells. The impact of sulphated disaccharides was investigated in the presence of PMA. The U937 and THP-1 cells were cultured in 24-well tissue culture plates at an initial density of $2x10^5$ cells/mL per well. Cells were then incubated with HDS-I 2 h prior to 8 nM PMA and incubated for 48 h at 37 $^0$C with 5% $CO_2$. Non-adherent cells were removed at 48 h. The adherent cells of this experiment were left for a resting period in fresh PMA-free RPMI-1640 supplemented media for further 72 h incubation. The adherent cells from 24-well plates were harvested after 72 h subsequently washed twice in ice-cold (4 $^0$C) PBS and cells were counted and stained for CD11b, CD68 cell surface markers to sulphated disaccharides impact on mature macrophages and the treated samples were analysed by flow cytometry. Isotype control on CD11b-BV650 and CD68-Cyanine-7 channel were used to identify the positive cells. ANOVA with post hoc Dunnett's test, mean ± SEM (n=3), *p<0.05 **p < 0.01 vs PMA. The data presented was pooled from three experiments.*

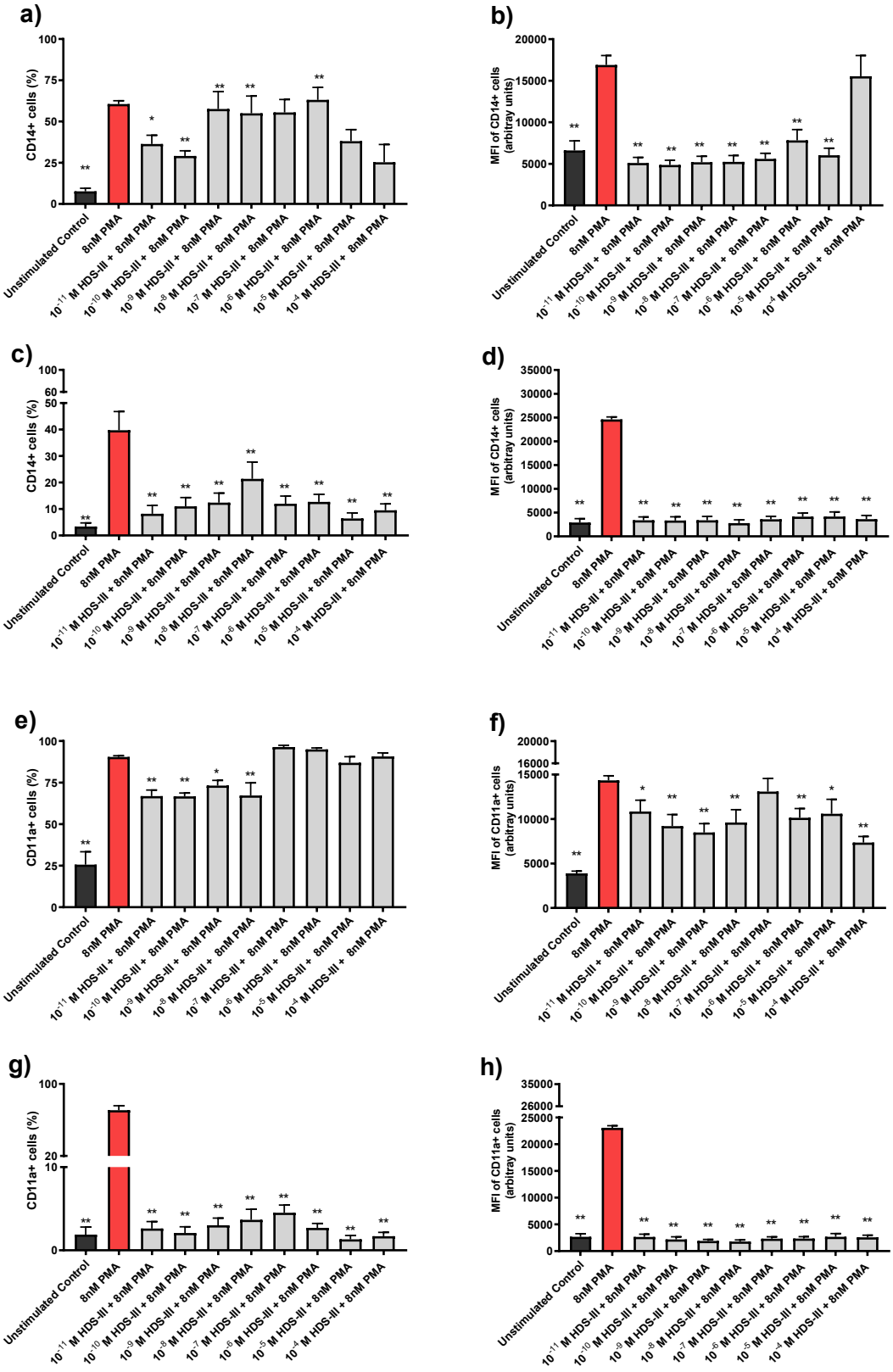


**Figure 4. 13.** ***The impact of HDS-III on U937 and THP-1 CD14 and CD11a expression in the presence of PMA.***

*Bar graph represents (a) CD14 positive U937 cells, (b) MFI of CD14 positive U937 cells, (c) CD14 positive THP-1 cells, (d) MFI of CD14 positive THP-1 cells, (e) CD11a positive U937 cells, (f) MFI of CD11a U937 positive cells, (g) CD11a positive THP-1 cells and (h) MFI of CD11a THP-1 positive cells. The impact of sulphated disaccharides was investigated in the presence of PMA. The U937 and THP-1 cells were cultured in 24-well tissue culture plates at an initial density of $2x10^5$ cells/mL per well. Cells were then incubated with HDS-III 2 h prior to 8 nM PMA and incubated for 48 h at 37 $^0$C with 5% $CO_2$. Non-adherent cells were removed at 48 h. The adherent cells of this experiment were left for a resting period in fresh PMA-free RPMI-1640 supplemented media for further 72 h incubation. The adherent cells from 24-well plates were harvested after 72 h subsequently washed twice in ice-cold (4 $^0$C) PBS and cells were counted and stained for CD14, CD11a cell surface markers to sulphated disaccharides impact on mature macrophages and treated samples were analysed by flow cytometry. Isotype control on CD14-PE and CD11a-FITC channels were used to identify the positive cells. ANOVA with post hoc Dunnett's test, mean ± SEM (n=3), *p<0.05, **p < 0.01 vs PMA. The data presented was pooled from three experiments.*

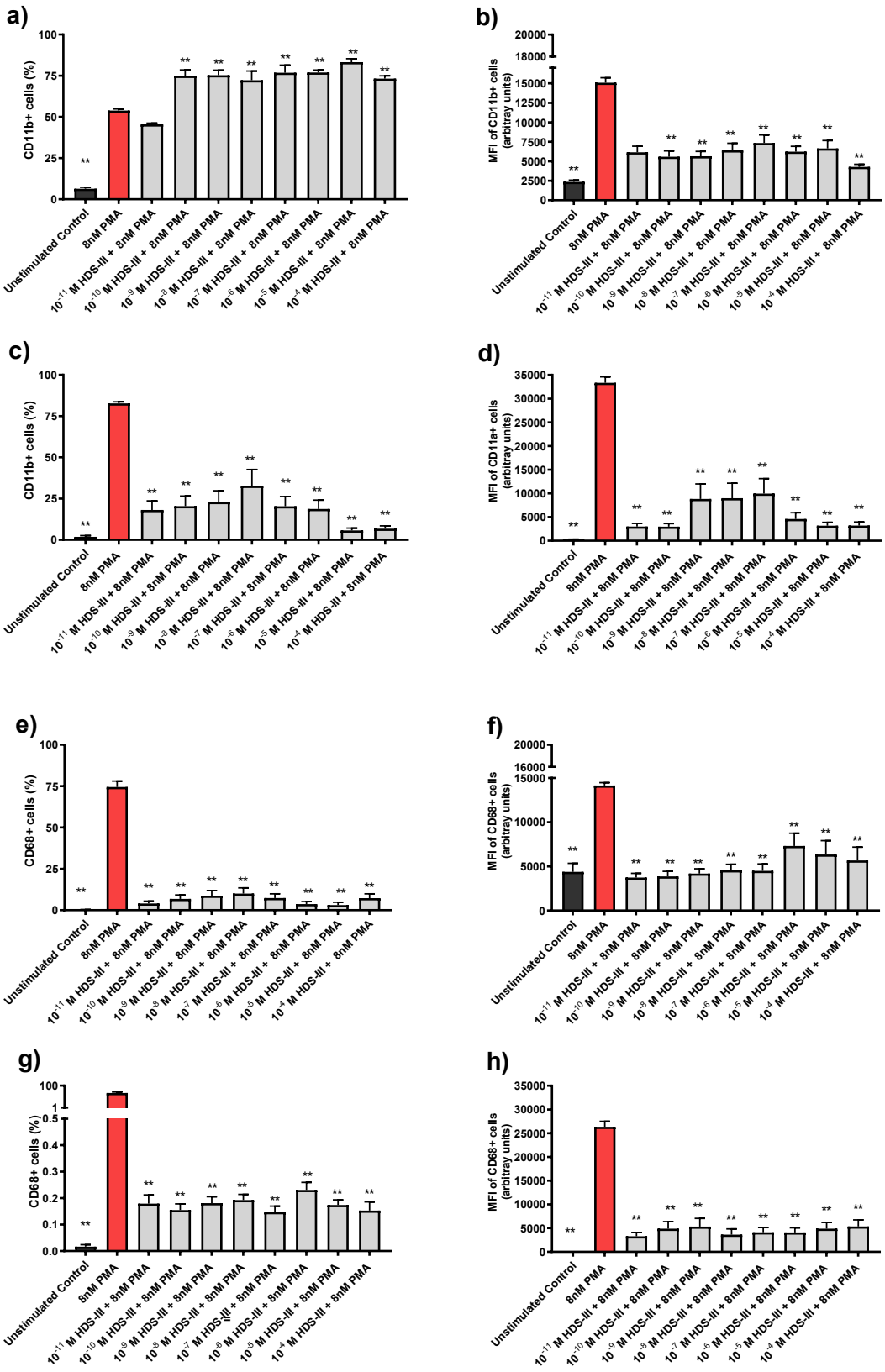


**Figure 4. 14.** ***The impact of HDS-III on U937 and THP-1 CD11b and CD68 expression in the presence of PMA.***

*Bar graph represents (a) CD11b positive U937 cells, (b) MFI of CD11b positive U937 cells, (c) CD11b positive THP-1 cells, (d) MFI of CD11b positive THP-1 cells, (e) CD68 positive U937 cells, (f) MFI of CD68 U937 positive cells, (g) CD68 positive THP-1 cells and (h) MFI of CD68 THP-1 positive cells. The impact of sulphated disaccharides was investigated in the presence of PMA. The U937 and THP-1 cells were cultured in 24-well tissue culture plates at an initial density of $2x10^5$ cells/mL per well. Cells were then incubated with HDS-III 2 h prior to 8 nM PMA and incubated for 48 h at 37 $^0$C with 5% $CO_2$. Non-adherent cells were removed at 48 h. The adherent cells of this experiment were left for a resting period in fresh PMA-free RPMI-1640 supplemented media for further 72 h incubation. The adherent cells from 24-well plates were harvested after 72 h subsequently washed twice in ice-cold (4 $^0$C) PBS and cells were counted and stained for CD11b, CD68 cell surface markers to sulphated disaccharides impact on mature macrophages and the treated samples were analysed by flow cytometry. Isotype control on CD11b-BV650 and CD68-Cyanine-7 channels were used to identify the positive cells. ANOVA with post hoc Dunnett's test, mean ± SEM (n=3), *p<0.05 **p < 0.01 vs PMA. The data presented was pooled from three experiments.*

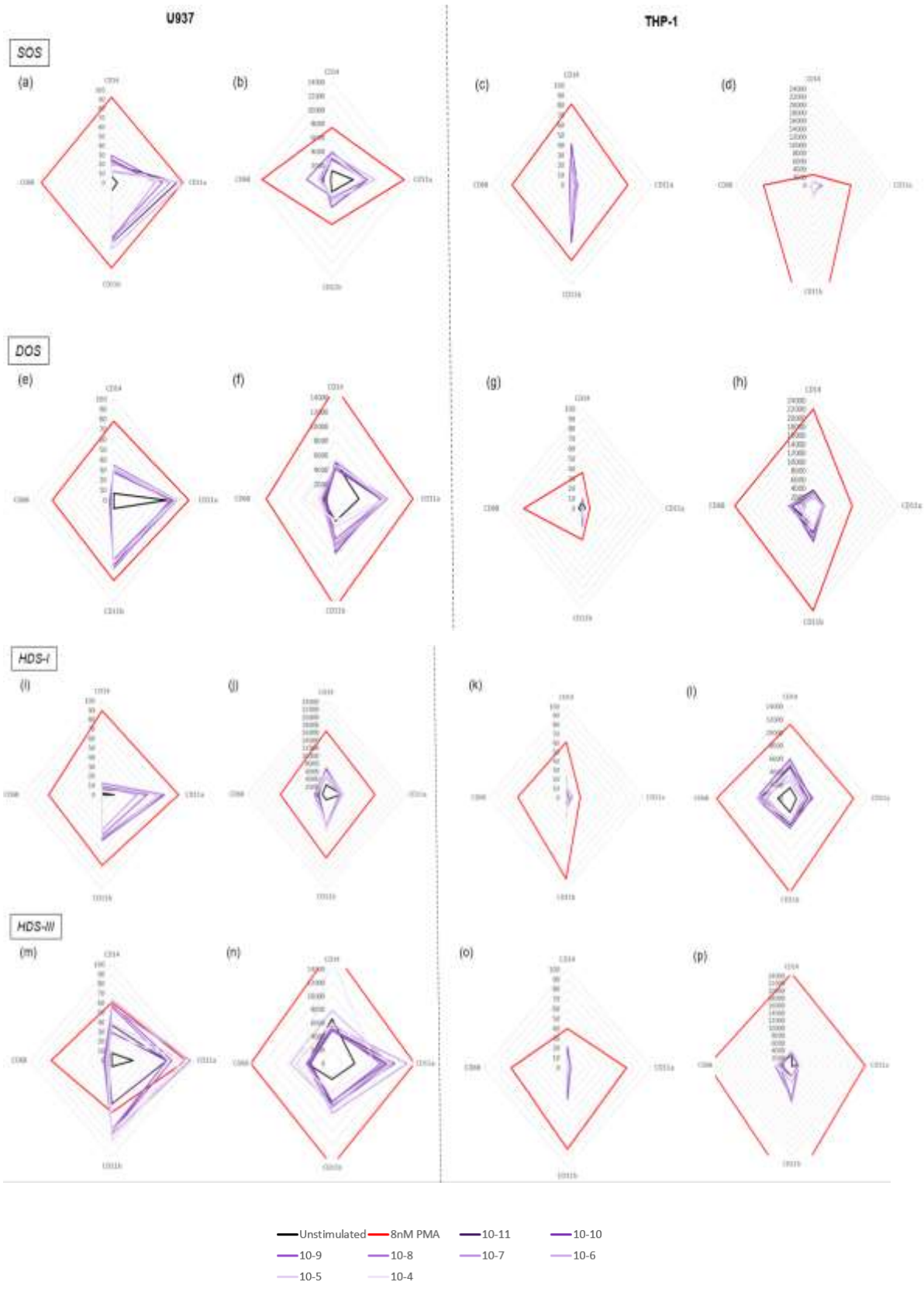


**Figure 4. 15.** ***Radar charts representing the summary of findings of Fig.4.6 – Fig.4.13.***

*Sulphated disaccharides down-regulated PMA-induced cell surface markers percentage of positive U937 and THP-1 cells and their expression. Radar charts used for seeing which surface marker expression upregulated or downregulated within a dataset. Radar plots were used to plot CD14, CD11a, CD11b and CD68 surface markers over sulphated disaccharide concentrations or MFI by giving an axis for each variable, and these axes were arranged radially around a central point and spaced equally. The data from a single observation are plotted along each axis and connected to form a polygon. The grid lines were used to connect the axes and are used as a guideline to facilitate interpretation of the data.*

**Table 4.0 1** ***Summary Data - Cell morphology.***

*Numeric = concentration (M), XX%= Max % inhibition (this is a visual approximation, not read off the graphs).*

| Treatment | Adherent Cell No. | % Cell Adhesion | % Live Adherent |
|---|---|---|---|
| PMA-SOS U937 | ↓<11 95% | ↓<11 75% | ↓<11 50% |
| PMA-SOS THP-1 | ↓<11 90% | ↓<11 75% | ↓<11 50% |
| PMA-DOS U937 | ↓<11 90 | ↓<11 75% | ↓<11 20% |
| PMA-DOS THP-1 | ↓<11 75% | ↓<11 75% | ↓<11 75% |
| PMA-HDS1 U937 | ↓9 - 4 90% | ↓9 - 4 75% | ↓9 – 4 50% |
| PMA-HDS1 THP-1 | ↓9 – 4 90% | ↓9 – 4 75% | ↓9 - 4 75% |
| PMA-HDSIII U937 | ↓8 – 4 90% | ↓8 – 4 50% | ↓8-4 70% |
| PMA-HDSIII THP-1 | ↓8 – 4 90% | ↓8 – 4 75% | ↓8 – 4 70% |

**Table 4.0 2** ***Summary Date - Cell markers, PMA stimulated % change compared to PMA control.***

*Numeric = concentration (M), XX%= Max % inhibition (this is a visual approximation, not read off the graphs).*

| Treatment | CD14 Adherent | | CD11a Adherent | | CD11b Adherent | | CD68 Adherent | |
|---|---|---|---|---|---|---|---|---|
| | % | MFI | % | MFI | % | MFI | % | MFI |
| PMA-SOS U937 | ↓<11 80% | ↓<11 70% | ↓<11 ~40% | ↓<11 70% | ↓<11 30% | ↓<11 70% | <11 99% | <11 90% |
| PMA-SOS THP-1 | ↓<11 80% | ↓<11 70% | ↓<11 90% | ↓<11 80% | ↓<11 60% | ↓<11 99% | ↓<11 95% | ↓<11 99% |
| PMA-DOS U937 | ↓<11 60% | ↓<11 100% | ↓<11 60% | ↓<11 60% | ↓<11 10% | ↓<11 70% | ↓<11 95% | ↓<11 100% |
| PMA-DOS THP-1 | ↓<11 100% | ↓<11 100% | ↓<11 100% | ↓<11 100% | ↓<11 50% | ↓<11 100% | ↓<11 100% | ↓<11 100% |
| PMA-HDS1 U937 | ↓<11 90% | ↓<11 70% | ↓<11 20% | ↓<11 100% | ↓<11 40% | ↓<11 60% | ↓<11 90% | ↓<11 95% |
| PMA-HDS1 THP-1 | ↓<11 70% | ↓<11 70% | ↓<11 100% | ↓<11 100% | ↓<11 90% | ↓<11 90% | ↓<11 100% | ↓<11 100% |
| PMA-HDSIII U937 | ↓<11 50% | ↓<11 100% | ↓<11 25% | ↓<11 20% | ↑<11 30% | ↓<11 90% | ↓<11 95% | ↓<11 100% |
| PMA-HDSIII THP-1 | ↓<11 95% | ↓<11 100% | ↓<11 100% | ↓<11 100% | ↓<11 95% | ↓<11 95% | ↓<11 95% | ↓<11 95% |

## 4.4 Discussion

Given the findings from chapter 3 demonstrating that PMA induced cell differentiation and up-regulated panel of cell surface markers CD14, CD11a, CD11b, and CD68 expression in U937 and THP-1 *in vitro* model. The main focus of this chapter was to investigate whether sulphated disaccharides have the efficacy to inhibit PMA induced changes in cell morphology and the associated changes in the expression of CD surface markers.

The efficacy of SOS was reported to be weaker than that of sucralfate in an ethanol-induced gastric injury model (Szabo and Brown, 1987). Fannon *et al.,* (2008) tested the efficacy of SOS *in vivo* study on mouse melanoma and lung carcinoma models. C57/BL6 male mice were injected subcutaneously with 1 $\times 10^6$ B16/F10 cells and treated with SOS (100 mg/kg/day). This study demonstrated inhibition of tumour growth by SOS by day 12 with the average volume of tumours treated with SOS being only 30% of those treated with saline ($P$ <0.05). A similar reduction was found on day 17 (32%). In addition, SOS potently inhibited fibroblast growth factor (FGF-2) binding to endothelial cells and stripped pre-bound FGF-2 from cells. SOS also regulated FGF-2 stimulated proliferation. Further, SOS facilitated FGF-2 diffusion through Descemet's membrane, a heparan sulphate-rich basement membrane from the cornea, suggesting a possible role in FGF-2 clearance. The results of this study suggest that SOS has the potential to remove growth factors from tumour microenvironments and the approach offers an attractive area for further study.

Several studies indicate that SOS showed therapeutic effects in different models of oesophagitis as SOS was able to suppress $H^+$ ion permeability in biopsied human oesophageal mucosa (Orlando, 1987; Orlando *et al*., 1990; Orlando *et al*., 1987 and Tobey *et al*., 1986). A study by Hayakawa *et al*., (2019), demonstrated that SOS decreases oesophagitis in a dose-dependent manner and SOS exhibited a stronger therapeutic effect than sucralfate at low doses against reflux oesophagitis. In this study, SOS and sucralfate were administered to oesophagitis-induced rats in doses of 1.8–144 μmol/kg, and the ulcer lesion size was macroscopically examined and scored. Effective pepsin activity in the gastric juices obtained from the animal model was evaluated by a casein digestion test.

The gross pathology, particularly the ulcer size, was significantly reduced, by SOS administration. The gross pathology was scored as 0, no visible lesions; 1, mucosal erosion; 2, the total area of mucosal damage, including an ulcer, was <30 mm2; 3, total area of mucosal lesions, including an ulcer, was ≥31 mm2; and 4, perforation. The *in vitro* assessments of peptic activity demonstrated that SOS inhibited peptic activity at concentrations of 5–120 μmol/L; the estimated $IC_{50}$ value was 25.4 μmol/L. In addition, this study demonstrated that SOS strongly accumulated at the inflammatory lesion sites by using imaging mass spectrometry, indicating its ability to selectively produce a protective layer at inflammation sites.

Seed *et al.,* (2007) assessed rat collagen-induced arthritis clinically for ankle joint inflammation where the degree of arthritis and bone erosion was measured by clinical score on an arbitrary scale. The oral administration of SOS at a dose of 100 mg/kg was found to be effective to reduce joint inflammation in rat collagen-induced arthritis and mouse collagen-induced arthritis. The change in volume of the hind paws was also measured in rat collagen-induced arthritis and it was inhibited by oral administration of SOS at a dose of 30 mg/kg.

In this chapter, firstly, optimal pre-incubation duration for sulphated disaccharides was addressed to inhibit PMA-induced cell differentiation. This was achieved by cell proliferation assay. This was important as increasing the exposure and concentration of a drug can cause it to affect targets other than the principal one.

Secondly, the impact of sulphated disaccharides on U937 and THP-1 morphology, cell number, and cell surface markers expression was determined in the presence and absence of PMA. To confirm the inhibition, cells were visualised using microscopic imaging, cell count and flow cytometry. The impact of sulphated disaccharides on U937 and THP-1 cells was tested in the absence of PMA to identify their action on cell proliferation and cell differentiation. The data suggested that there was no significant difference between the tested compounds compared to unstimulated control cells (Appendix Fig.9 to Appendix Fig.32).

The findings of this chapter indicate that sulphated disaccharides inhibit the cell adhesion/differentiation and expression of CD14, CD11a, CD11b and CD68 cell

surface markers on the PMA-differentiated U937 and THP-1 cells (Fig.4.14). The results of this study indicate that sulphated disaccharides have significant potential to inhibit PMA-induced cell differentiation by inhibiting the expression of cell surface adhesion markers at concentrations of $10^{-11}$ M to $10^{-4}$ M.

In this study, the difference between the different structures of SOS, DOS, HDS-I and HDS-III was observed. SOS and DOS showed inhibition of PMA-induced cell adhesion and cell surface markers expression at concentrations of $10^{-11}$ M to $10^{-4}$ M. The concentrations of $10^{-11}$ M to $10^{-10}$ M HDS-I and concentrations of $10^{-11}$ M to $10^{-9}$ M HDS-III in cell adhesion were found to be ineffective. However, PMA-induced cell surface markers expression was inhibited by HDS-I and HDS-III at concentrations of $10^{-11}$ M to $10^{-4}$ M.

Overall, the results reported in this chapter suggest that sulphated disaccharides inhibited PMA-induced cell differentiation in U937 and THP-1 cells *in vitro*, which were confirmed using microscopic imaging, cell count and flow cytometry.

Therefore, it was proposed that sulphated disaccharides inhibit monocyte-macrophage differentiation by interacting with specific monocyte cell surface molecules or receptors to inhibit their activation following inflammatory stimuli, thus inhibiting their attachment to the endothelium. Binding and activation represent two distinct steps in the generation of the receptor-mediated intracellular signalling response to inhibit the activation of DAG by PMA. In this study, the end biological response of this binding is measured by cell differentiation and changes in surface CD marker expression.

The mechanisms by which sulphated disaccharides exerted inhibition of cell adhesion are not yet fully understood. The results from this chapter would be useful to identify whether sulphated disaccharides mediate inhibition of PMA-induced intracellular signalling pathways involved in monocyte-macrophage differentiation.

## 4.5 Conclusion

The findings suggested an important role of the sulphated disaccharides on cell surface expression of CD14, CD11a, CD11b and CD68 in PMA-induced differentiated U937 and THP-1 cells to coordinate cell growth with some potential intracellular signals for inhibition of the monocytic-differentiation process.

This study proposed that the activation of cell adhesion surface markers by PMA is mediated through the p38 and ERK1/2 signalling. Therefore, this study hypothesised that sulphated disaccharides may interact with intracellular signalling p38 and ERK1/2 thereby inhibiting cell differentiation. This will be further investigated in the following chapters.

# CHAPTER 5: MODULATION OF INTRACELLULAR SIGNALLING PATHWAYS IN PMA-INDUCED MACROPHAGES AND INHIBITION OF PMA-INDUCED CALCIUM MOBILISATION IN HUMAN MONOCYTES BY SULPHATED DISACCHARIDES

## 5.1 Introduction

As outlined in chapter 1, G-protein-coupled receptors (GPCRs) are the important targets for drug development (Pierce *et al*., 2002) as approximately 30% of marketed drugs mediate their actions through GPCRs (Hopkins and Groom, 2002). GPCRs mainly signal through the cAMP and calcium pathways to regulate a variety of cellular functions. cAMP and calcium are second messengers (outlined in Chapter 1) which become elevated inside cells on activation of cell surface receptors and play a critical role in cell proliferation and differentiation.

Also, it has been outlined in chapter 1 that the cAMP signalling pathway has been reported to regulate p38 and ERK1/2 activity in a cell context-dependent manner, being either inhibitory or stimulatory (Cao *et al*., 2004; Choi *et al*., 2003; Feng *et al*., 2002; Rahman *et al*., 2004; Robidoux *et al*., 2005; Wu *et al*., 1993 and Graves *et al*., 1993). In chapter 3, it has been outlined that PKC is thought to mediate the activation of p38 and ER1/2 by PMA. The results of chapter 3 demonstrated that PMA activates the PKC signalling pathway to activate downstream p38 and ERK1/2 signalling pathways to induce cell differentiation. Studies suggest that the translocation and binding of PKC to cell membranes is catalysed by $Ca^{2+}$ (Wolf *et al*., 1985) and that $Ca^{2+}$ enhances the cofactor activity of phospholipid (Konig *et al*., 1985).

The phosphoinositide signalling pathway is one of the most important cascades that leads to the activation of PKC. Stimulation of G-protein coupled receptors activates the membrane-bound phospholipase C (PLC) enzyme (Fig.5.1). PLC activates in the cytosol by hydrolysing cell membrane phosphatidylinositol 4, 5-bisphosphate (PIP2) to generate DAG and inositol 1, 4, 5 -triphosphate (IP3). These cytosolic DAG and IP3 activate the PKC pathway where DAG recycles into the plasma membrane and IP3 diffuses into the cytoplasm to bind to an IP3 receptor which serves as an IP3-sensitive $Ca^{2+}$ channel on the endoplasmic reticulum. These channels then open and allow the higher levels of $Ca^{2+}$ that are present in the endoplasmic reticulum to flow into the cytoplasm (reviewed in: Berridge and Irvine, 1984). $Ca^{2+}$ binds to PKC to trigger its translocation to the cell membrane where it interacts with DAG, via its regulatory C1 domain. The conformational change in the structure of PKC allows it to phosphorylate its

substrates, for example, Arg-rich proteins (Wu-Zhang and Newton, 2013). Literature suggests that PKC is activated by an increase in the concentration of DAG and calcium ions (Wilson *et al*., 2015). Once activated, PKC catalyses the phosphorylation of a number of endogenous proteins (Helfman *et l*., 1983; Gennaro *et al*., 1985 and Kiyotaki *et al*., 1984) including the transferrin (Stratford *et al*., 1984) and interleukin 2 receptors (Shackelford *et al*., 1984) lipocortin (Touqui *et al*., 1986) and HLA class I antigens, in temporal association with sustained activation of the NADPH-oxidase (Gennaro *et al*., 1985 and Gennaro *et al*., 1986). The activation of PCK isoforms such α, βI, βII, and γ is calcium ions, DAG, and phospholipid dependent. The other isoforms such as the δ, ε, η, and θ isoforms, and require DAG, but do not require $Ca^{2+}$ for activation (Nishizuka, 1995).

Studies suggest that the generation of cGMP-dependent protein kinases by cGMP leads to a number of events that decrease intracellular calcium ions levels. It has been shown to phosphorylate and therefore inhibit G protein function and PLC activation and further inhibit the $IP_3$ receptor on the sarcoplasmic reticulum, thus preventing calcium release from the store (Lincoln *et al*., 1993).

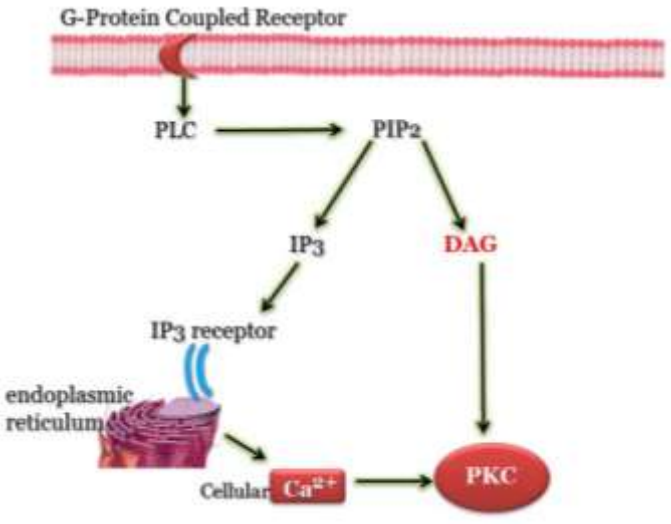


**Figure 5. 1*. A diagrammatic illustration of GPCR signalling pathways.***

*Explaining multiple signalling pathways involving PKC regulation and signal transduction indicates an increase in the cellular concentration level of $Ca^{2+}$ (adapted from Jeong-Hun Kang, 2014).*

## 5.2 Aim

In Chapter 3 it has been demonstrated that the treatment of leukemic cells U937 and THP-1 with PMA induces the activation of p38α and extracellular signal-regulated kinase (ERK) MAPK signalling pathways to promote monocyte-macrophage differentiation. Therefore, in this chapter as a step forward to verify the mechanism by which sulphated disaccharides may inhibit PMA-induced cell differentiation, the importance of p38 and ERK 1/ MAPK pathways were studied using phosphorylated specific antibodies. In addition, in this chapter, it was asked whether PMA will induce calcium mobilisation in U937 and THP-1 cells and what impact sulphated disaccharides will exhibit on calcium mobilisation.

Therefore, this chapter aimed to study the impact of sulphated disaccharides on:

- p38 and ERK1/2 MAPK protein expression by western blot.
- intracellular calcium mobilisation by flow cytometry.

## 5.3 Results

### 5.3.1 Sulphated disaccharides inhibited PMA-induced phosphorylation

To determine the impact of sulphated disaccharides on activation of p38 and ERK1/2 (Fig.5.2), the U937 cells were pre-stimulated with SOS, DOS, HDS-I and HDS-III at concentrations of $10^{-11}$ M, $10^{-7}$ M, and $10^{-4}$ M in the presence and absence of 8 nM PMA for 48 h and analysed by Western blot as described in material and methods section 2.7.

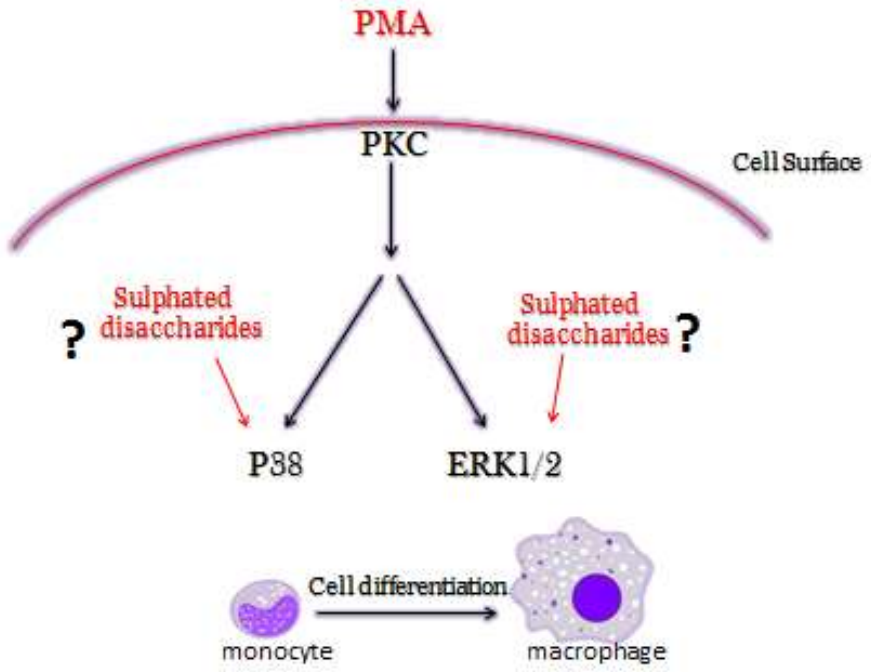


**Figure 5. 2*. A model to investigate sulphated disaccharides impact on PMA-induced p38 and ERK1/2 signalling pathways in U937 cells.***

#### 5.3.3.1 p38 and ERK expression and phosphorylation in response to SOS

SOS inhibited both p38 and ERK1/2 phosphorylation in U937 cells when given at concentrations of $10^{-11}$ M, $10^{-7}$ M, and $10^{-4}$ M for 2 h before adding 8 nM PMA for 48 h. As shown in Figure 5.3, 8 nM PMA increased the phosphorylation of p38 and ERK1/2 in U937 cells at 48 h compared to unstimulated control U937 cells and SOS inhibited PMA-induced phosphorylation of p38 and ERK1/2 in a concentration dependent manner, indicating that this activation is PMA-dependent. At a concentration of $10^{-11}$ M SOS in the presence of 8 nM PMA, higher inhibition of p38 phosphorylation, and at concentration of $10^{-4}$ M SOS in the presence of 8 nM PMA, higher inhibition of ERK1/2 was observed compared to PMA-stimulated phosphorylation.

On the other hand, the total p38 protein level was decreased in the presence of PMA compared to unstimulated control U937 cells. SOS alone did not change the level of total p38 level at 48 h compared to unstimulated control U937 cells. However, the levels of total p38 protein in PMA-stimulated U937 cells were increased in the presence of SOS compared to PMA-stimulated U937 cells. The total p38 protein level was increased in PMA-stimulated U937 cells in the presence of SOS. By contrast, there was no significant change in PMA-stimulated U937 cells total ERK1/2 protein level compared to unstimulated control U937 cells. SOS also did not have any impact on total ERK1/2 levels in the presence and absence of PMA at 48 h.

The results indicate that SOS inhibitory action is p38 and ERK1/2 dependent.

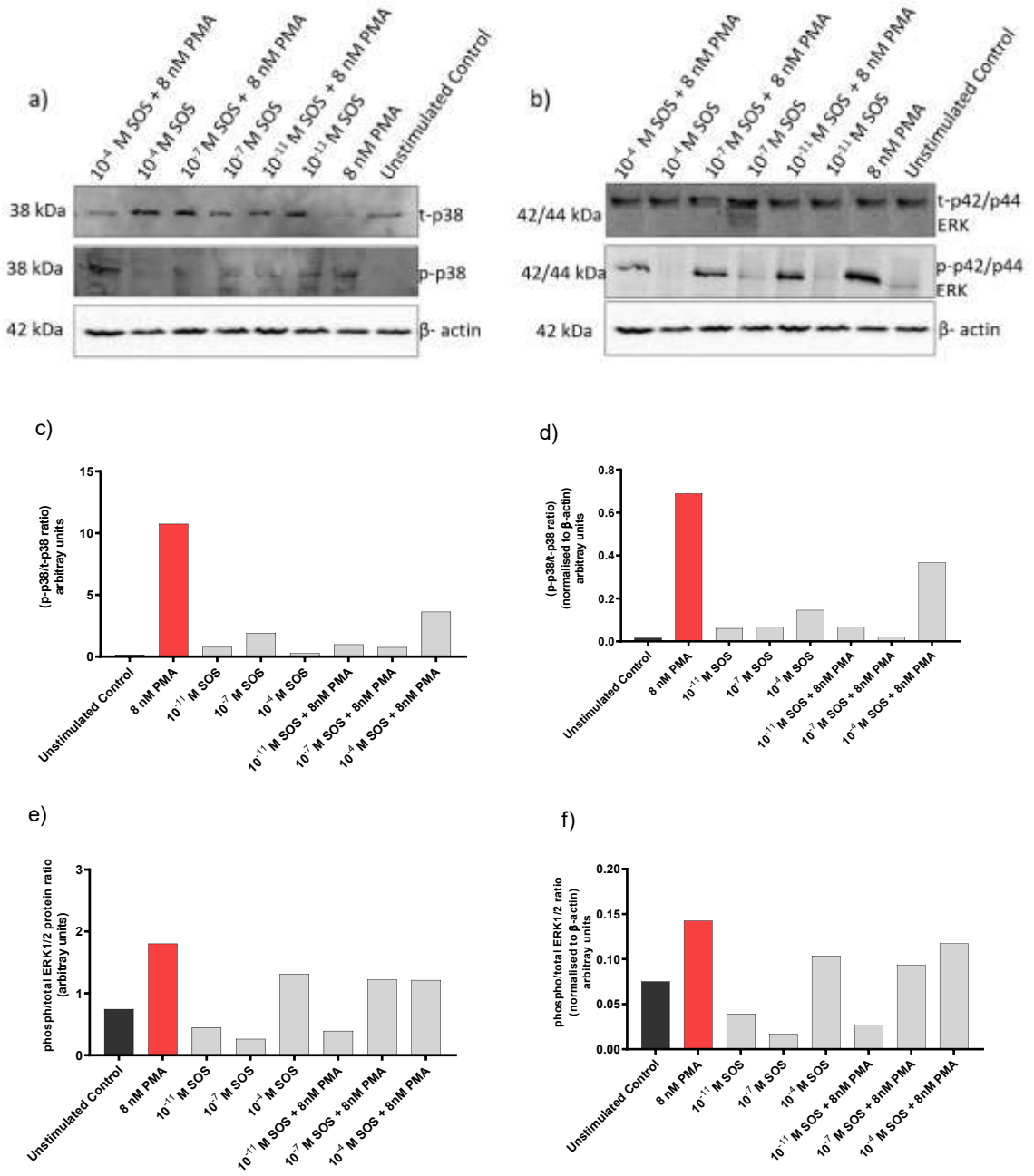


**Figure 5. 3.** ***SOS impact on p38 and ERK1/2 expression.***

*Expression and phosphorylation of p38 in U937 cells in control unstimulated and PMA (8nM, 48 hours) stimulated cells with and without 2 hours pre incubation with SOS ($10^{-11}$ M, $10^{-7}$ M, $10^{-4}$ M). After 48 h, the protein lysates were extracted using the cell lysis kit followed by protein quantification using the Bradford assay. Protein (20 µg/lane) was electrophoresed on 12% SDS/PAGE gels and transferred to nitrocellulose membranes to probe with specific antibodies. β-actin was used as a control to test the uniformity of the sample loading between all wells. Data shown are representative western blots from one out of 2 independent*

*experiments. (a) Western blots of total p38 (t-p38), phosphorylated p38 (p-p38) and β-actin. (b) Western blots of total ERK1/2 (t-p42/p44 ERK), phosphorylated ERK1/2 (p-t-p42/p44 ERK) and β-actin. (c) Bar graph representing densitometric results of phosphorylated p38 over total p38 protein. (d) Bar graph representing densitometric results of p38 from (c) normalised to β-actin controlled. (e) Bar graph representing densitometric results of phosphorylated ERK1/2 over total ERK1/2 protein. (f) Bar graph representing densitometric results of ERK1/2 from (f) normalised to β-actin controlled.*

#### 5.3.3.2 p38 and ERK expression and phosphorylation in response to DOS

The phosphorylation of p38 and ERK1/2 in U937 cells was inhibited by DOS when given at concentrations of $10^{-11}$ M, $10^{-7}$ M and $10^{-4}$ M for 2 h prior to adding 8 nM PMA for 48 h. As shown in Figure 5.4, the increase in phosphorylation of p38 and ERK1/2 in U937 cells was observed in the presence of 8 nM PMA at 48 h compared to unstimulated control U937 cells. The phosphorylation of p38 was inhibited by DOS at concentrations of $10^{-11}$ M, $10^{-7}$ M, $10^{-4}$ M and ERK1/2 phosphorylation was inhibited by DOS at concentrations of $10^{-11}$ M and $10^{-4}$ M. At concentration of $10^{-4}$ M DOS in the presence of 8 nM PMA, higher inhibition of p38 and ERK1/2 phosphorylation was observed compared to PMA-stimulated phosphorylation.

It was observed that DOS decreased the total p38 and ERK1/2 protein level compared to unstimulated control U937 cells. However, DOS in the presence of PMA increased total p38 and ERK1/2 protein level at concentrations of $10^{-11}$ M, $10^{-7}$ M and decreased total ERK1/2 protein level at concentration of $10^{-4}$ M at 48 h compared to PMA-stimulated U937 cells.

The results indicate that DOS inhibitory action is p38 and ERK1/2 dependent.

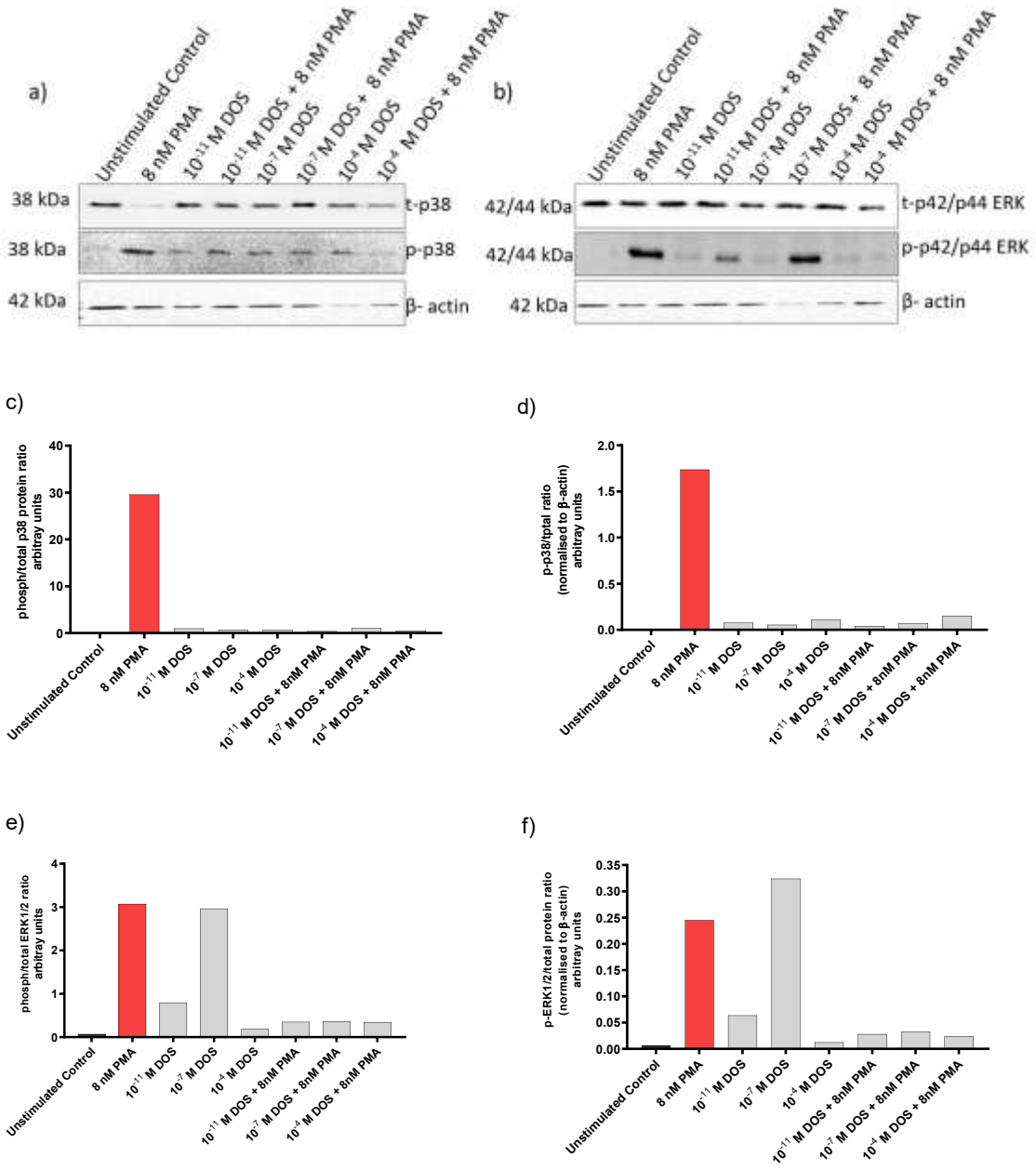


**Figure 5. 4.** ***DOS impact on p38 and ERK1/2 expression.***

*Expression and phosphorylation of p38 in U937 cells in control unstimulated and PMA (8nM, 48 hours) stimulated cells with and without 2 hours pre incubation with DOS ($10^{-11}$ M, $10^{-7}$ M, $10^{-4}$ M). After 48 h, the protein lysates were extracted using the cell lysis kit followed by protein quantification using the Bradford assay. Protein (20 µg/lane) was electrophoresed on 12% SDS/PAGE gels and transferred to nitrocellulose membranes to probe with specific antibodies. β-actin was used as a control to test the uniformity of the sample loading between all wells. Data shown are representative western blots from one out of 2 independent*

*experiments. (a) Western blots of total p38 (t-p38), phosphorylated p38 (p-p38) and β-actin. (b) Western blots of total ERK1/2 (t-p42/p44 ERK), phosphorylated ERK1/2 (p-t-p42/p44 ERK) and β-actin. (c) Bar graph representing densitometric results of phosphorylated p38 over total p38 protein. (d) Bar graph representing densitometric results of p38 from (c) normalised to β-actin controlled. (e) Bar graph representing densitometric results of phosphorylated ERK1/2 over total ERK1/2 protein. (f) Bar graph representing densitometric results of ERK1/2 from (f) normalised to β-actin controlled.*

#### 5.3.3.3 p38 and ERK expression and phosphorylation in response to HDS-I

HDS-I significantly inhibited p38 phosphorylation in U937 cells when given at concentrations of $10^{-11}$ M, $10^{-7}$ M, $10^{-4}$ M for 2 h before adding 8 nM PMA for 48 h. As shown in Figure 5.5, increase in phosphorylation of p38 in 8 nM PMA stimulated U937 cells was observed at 48 h compared to unstimulated control U937 cells. One specific band of about 38kDa in size (corresponding to the size of p38) was detected in PMA-stimulated U937 cells while no band of size and intensity (~p38 kDa], corresponding to p38 was not detected in HDS-I treated U937 cells in the presence and absence of PMA. This indicate that HDS-I completely inhibited PMA-induced phosphorylation and p38 activation is PMA-dependent. In contrast, ERK1/2 phosphorylation was only inhibited at $10^{-7}$ MHDS-I in the presence of 8 nM PMA compared to PMA-stimulated phosphorylation.

The total p38 protein level was decreased in the presence of PMA compared to unstimulated control U937 cells. The total p38 level at 48 h was decreased by HDS-I in the absence of PMA at concentrations of $10^{-11}$ M, $10^{-7}$ M compared to unstimulated control U937 cells. However, total p38 protein level in PMA-stimulated U937 cells was increased in the presence of HDS-I compared to PMA-stimulated U937 cells in a concentration dependent manner. The total ERK1/2 levels was decreased by HDS-I in the absence of PMA at concentrations of $10^{-11}$ M, $10^{-7}$ M and $10^{-4}$ M compared to unstimulated control U937 cellsat 48 h. However, total ERK1/2 protein levels in PMA-stimulated U937 cells was increased in the presence of HDS-I at concentrations of $10^{-7}$ M and $10^{-4}$ M compared to PMA-stimulated U937 cells.

The results indicate that HDS-I inhibitory action is completely p38 dependent and partially ERK1/2 dependent.

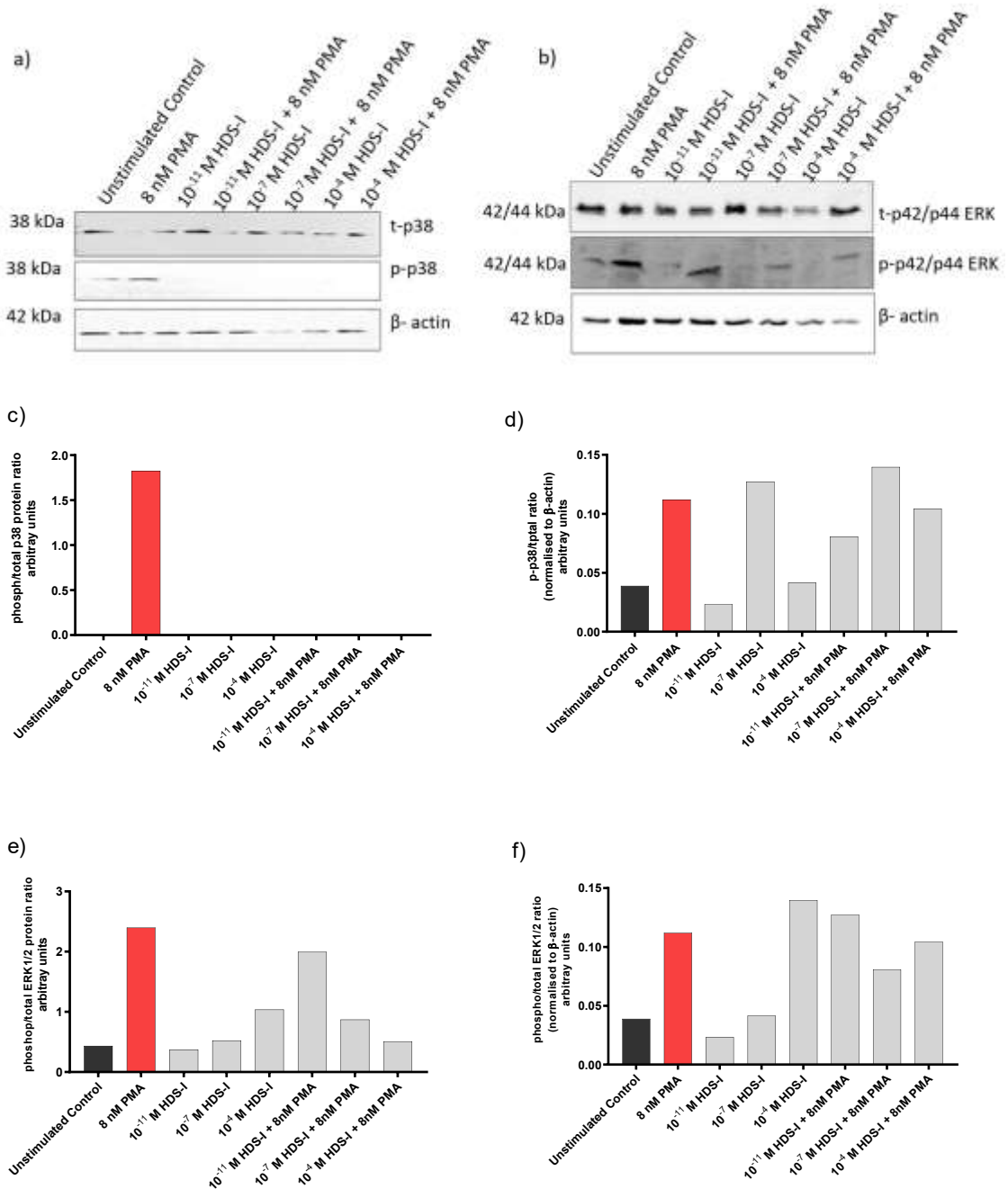


**Figure 5. 5.** ***HDS-I impact on p38 and ERK1/2 expression.***

*Expression and phosphorylation of p38 in U937 cells in control unstimulated and PMA (8nM, 48 hours) stimulated cells with and without 2 hours pre incubation with HDS-I ($10^{-11}$ M, $10^{-7}$ M, $10^{-4}$ M). After 48 h, the protein lysates were extracted using the cell lysis kit followed by protein quantification using the Bradford assay. Protein (20 µg/lane) was electrophoresed on 12% SDS/PAGE gels and transferred to nitrocellulose membranes to probe with specific antibodies. β-actin was used as a control to test the uniformity of the sample loading between all*

*wells. Data shown are representative western blots from one out of 2 independent experiments. (a) Western blots of total p38 (t-p38), phosphorylated p38 (p-p38) and β-actin. (b) Western blots of total ERK1/2 (t-p42/p44 ERK), phosphorylated ERK1/2 (p-t-p42/p44 ERK) and β-actin. (c) Bar graph representing densitometric results of phosphorylated p38 over total p38 protein. (d) Bar graph representing densitometric results of p38 from (c) normalised to β-actin controlled. (e) Bar graph representing densitometric results of phosphorylated ERK1/2 over total ERK1/2 protein. (f) Bar graph representing densitometric results of ERK1/2 from (f) normalised to β-actin controlled.*

#### 5.3.3.4 p38 and ERK expression and phosphorylation in response to HDS-III

As shown in Figure 5.6, phosphorylation of p38 was observed in 8 nM PMA stimulated U937 cells at 48 h compared to unstimulated control U937 cells. HDS-III increased phosphorylation of p38 in U937 cells at concentrations of $10^{-11}$ M, $10^{-7}$ M, $10^{-4}$ M in the absence of 8 nM PMA at 48 h compared to unstimulated control U937 cells and had no significant effect p38 phosphorylation in the presence of PMA. In contrast, HDS-III increased phosphorylation of ERK1/2 in U937 cells at concentrations of $10^{-4}$ M in the absence of 8 nM PMA at 48 h compared to unstimulated U937 cells. HDS-III inhibited ERK1/2 phosphorylation at a concentration of $10^{-7}$ M in the presence of 8 nM PMA compared to PMA-stimulated phosphorylation.

The total p38 protein level was decreased in the presence of PMA compared to unstimulated control U937 cells. HDS-III decreased the total p38 level in the absence of PMA compared to unstimulated control U937 cells and increased total p38 protein level in the presence of PMA compared to PMA-stimulated U937 cells in a concentration-dependent manner at 48 h. Similarly, the total ERK1/2 levels were decreased by HDS-III in the absence of PMA in a concentration-dependent manner compared to unstimulated control U937 cells at 48 h. However, total ERK1/2 protein levels in PMA-stimulated U937 cells was increased in the presence of HDS-III at concentrations of $10^{-11}$M and decreased at concentrations of $10^{-7}$ M and $10^{-4}$ M compared to PMA-stimulated U937 cells.

The results indicate that HDS-III inhibitory action could be ERK1/2 dependent but not p38-dependent.

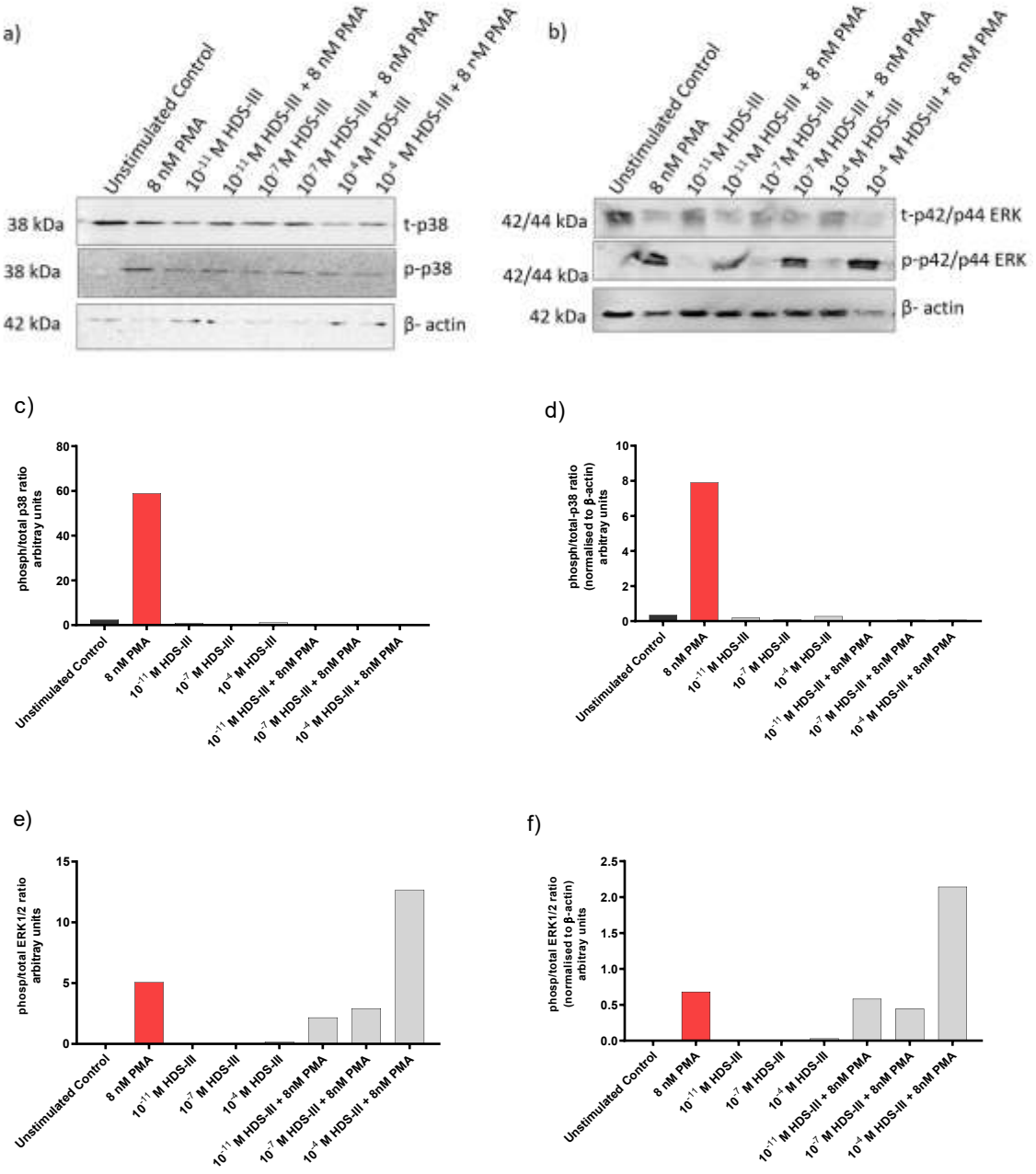


**Figure 5. 6.** ***HDS-III impact on p38 and ERK1/2 expression.***

*Expression and phosphorylation of p38 in U937 cells in control unstimulated and PMA (8nM, 48 hours) stimulated cells with and without 2 hours pre incubation with SOS ($10^{-11}$ M, $10^{-7}$ M, $10^{-4}$ M). After 48 h, the protein lysates were extracted using the cell lysis kit followed by protein quantification using the Bradford assay. Protein (20 µg/lane) was electrophoresed on 12% SDS/PAGE gels and transferred to nitrocellulose membranes to probe with specific antibodies. β-actin was used as a control to test the uniformity of the sample loading between all wells. Data shown are representative western blots from one out of 2 independent*

*experiments. (a) Western blots of total p38 (t-p38), phosphorylated p38 (p-p38) and β-actin. (b) Western blots of total ERK1/2 (t-p42/p44 ERK), phosphorylated ERK1/2 (p-t-p42/p44 ERK) and β-actin. (c) Bar graph representing densitometric results of phosphorylated p38 over total p38 protein. (d) Bar graph representing densitometric results of p38 from (c) normalised to β-actin controlled. (e) Bar graph representing densitometric results of phosphorylated ERK1/2 over total ERK1/2 protein. (f) Bar graph representing densitometric results of ERK1/2 from (f) normalised to β-actin controlled.*

### 5.3.2 Sulphated disaccharides inhibited PMA-induced intracellular $Ca^{2+}$ mobilisation

The impact of sulphated disaccharides on PMA-induced intracellular calcium mobilisation in U937 and THP-1 cells (Fig. 5.7) was investigated by flow cytometry as described in materials and methods section 2.4.2. With receptor activation, the changes in intracellular calcium release occur within nanoseconds (Alice *et al*., 2010). Therefore, to understand the change in the intracellular calcium concentration an effective *in vitro* model was required. Activation of Gq protein-coupled receptors can be monitored by measuring the increase in intracellular calcium with fluorescent dyes. The change in intracellular calcium was determined in Fluo-4-AM labelled U937/THP-1 cells where cells were pre-incubated with sulphated disaccharides 10 min prior to PMA administration at 1 min.

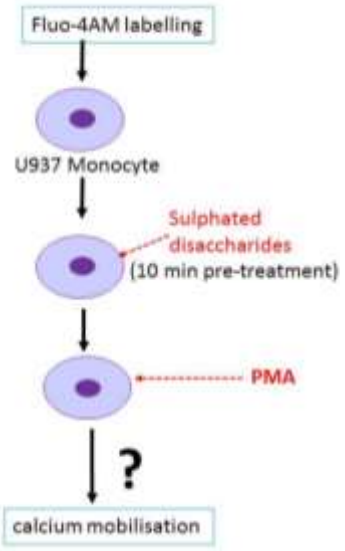


**Figure 5. 7*. The study was designed to investigate the impact of sulphated disaccharides on PMA-induced intracellular calcium changes in U937/THP-1 monocyte cell lines.***

*In this study, the impact of sulphated disaccharides on the intracellular $Ca^{2+}$ concentration was studied in the presence of PMA. The sulphated disaccharides at concentrations of $10^{-11}$ M to $10^{-4}$ M were pre-incubated with Fluo-4 AM labelled U937 and THP-1 cells for 10 min before 8 nM PMA addition. The 10 min pre-treatment time before PMA stimulation was optimised by treating THP-1 cells with SOS and DOS under different conditions (Appendix Fig.92 to Appendix Fig.95).*

Sulphated disaccharides significantly inhibited PMA-induced $Ca^{2+}$ mobilisation in U937 and THP-1 cells (Fig. 5.08- Fig.5.11). However, the level of statistical significance of disaccharides concentrations was different on both U937 and THP-1 cells. SOS inhibited U937 cells with a significance of $p<0.01$ and $p<0.0001$. However, for THP-1 cells it was also inhibited at a significance of $p<0.05$ and $p<0.001$. DOS inhibited PMA-induced $Ca^{2+}$ mobilisation in U937 cells at a significance of $p<0.0001$ and in THP-1 cells at $p<0.01$ and $p<0.0001$. HDS-I inhibited $Ca^{2+}$ mobilisation in both cells at $p<0.0001$. HDS-III statistically inhibited PMA impact on U937 cells at $p<0.01$, $p<0.001$, $p<0.0001$, and on THP-1 cells at $p<0.0001$.

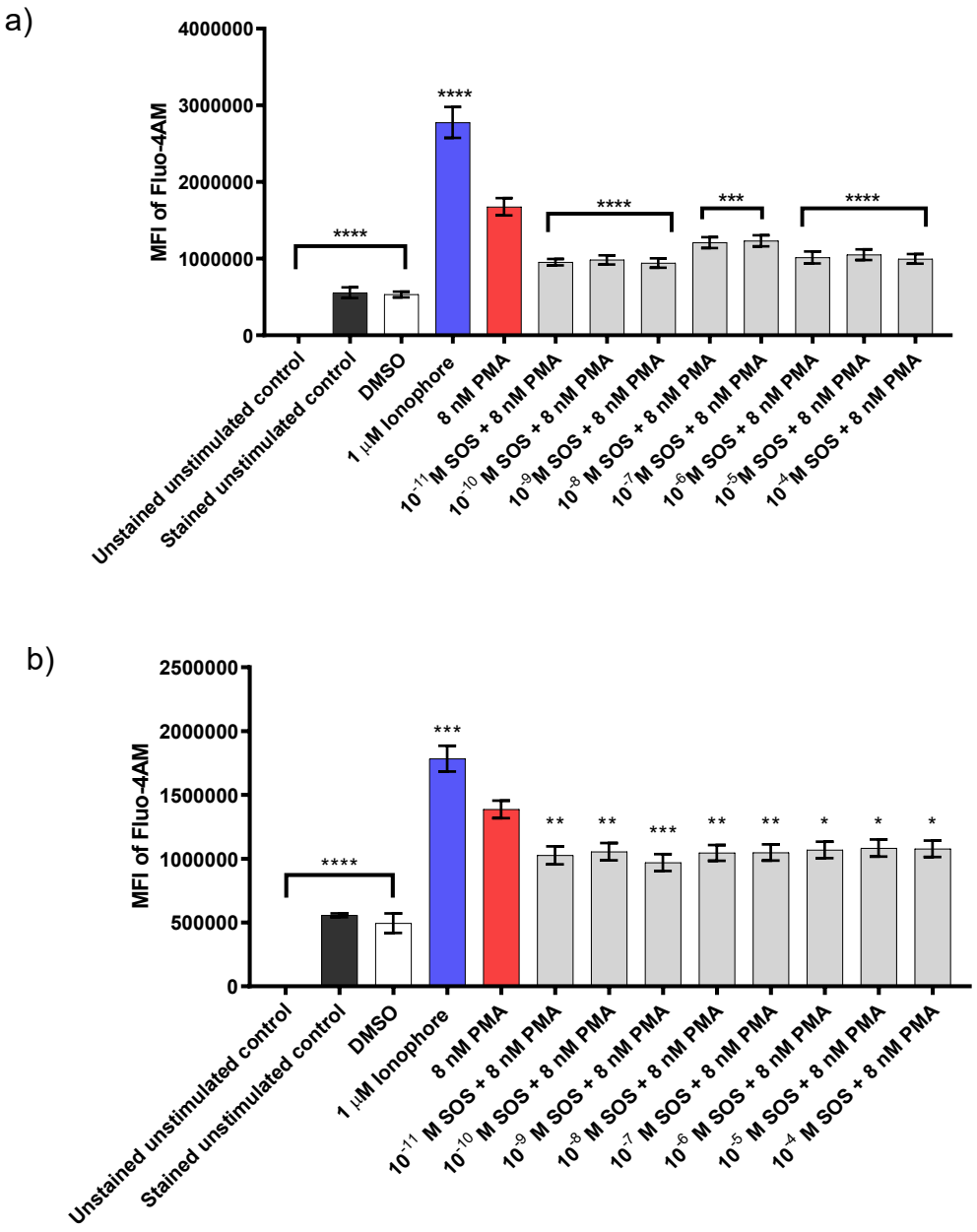


**Figure 5. 8*. Impact of SOS on PMA-induced intracellular $Ca^{2+}$ mobilisation.***

*MFI of Fluo-4AM labelled a) U937 and b) THP-1 cells on FL1-A FITC channel of BD Accuri flow cytometry. SOS at concentrations of $10^{-11}$ M to $10^{-4}$ M was pre-incubated with Fluo-4 AM labelled U937 and THP-1 cells for 10 min before 8 nM PMA addition. The MFI is represented as mean ± SEM, ****p<0.0001, **p<0.01, *p<0.05 vs PMA, Dunnett's test, mean ± SEM (n =3).*

a)

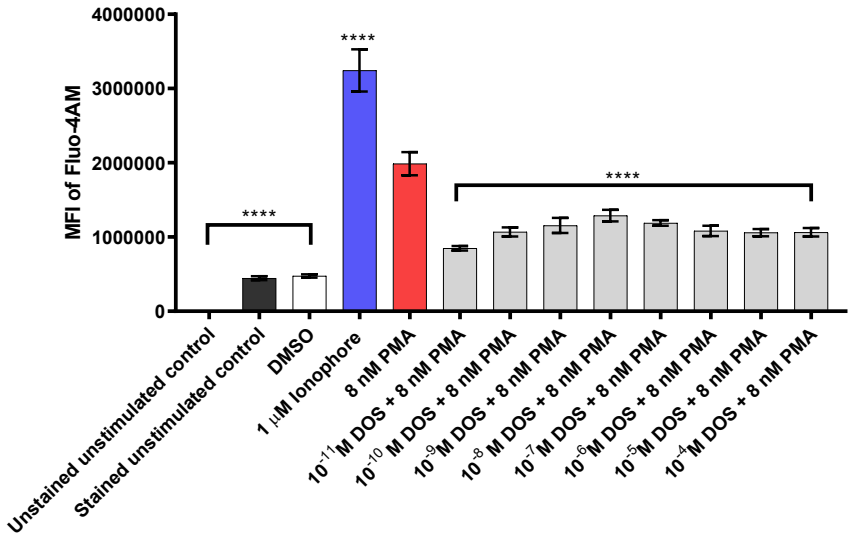


b)

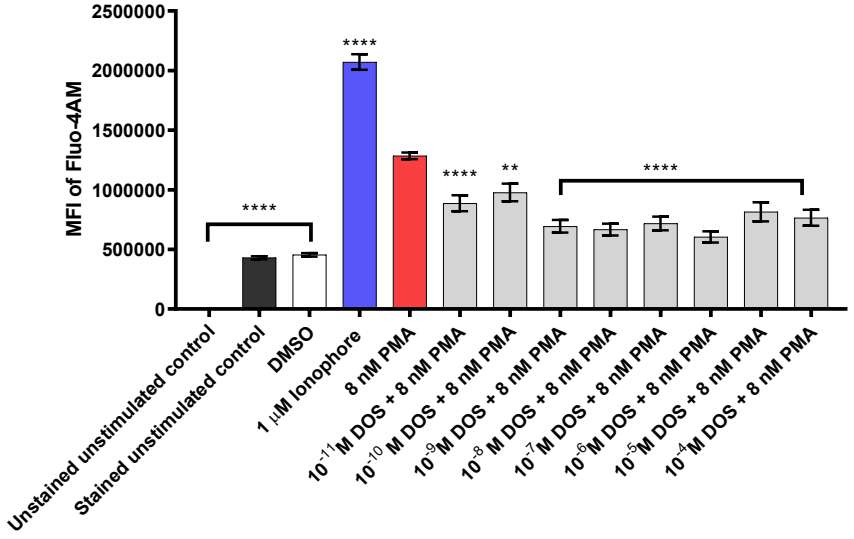


**Figure 5. 9*. Impact of DOS on PMA-induced intracellular $Ca^{2+}$ mobilisation.***

*MFI of Fluo-4AM labelled a) U937 and b) THP-1 cells on FL1-A FITC channel of BD Accuri flow cytometry. DOS at concentrations of $10^{-11}$ M to $10^{-4}$ M was pre-incubated with Fluo-4 AM labelled U937 and THP-1 cells for 10 min before 8 nM PMA addition. The MFI is represented as mean ± SEM, ****p<0.0001, **p<0.01 vs PMA, Dunnett's test, mean ± SEM (n =3).*

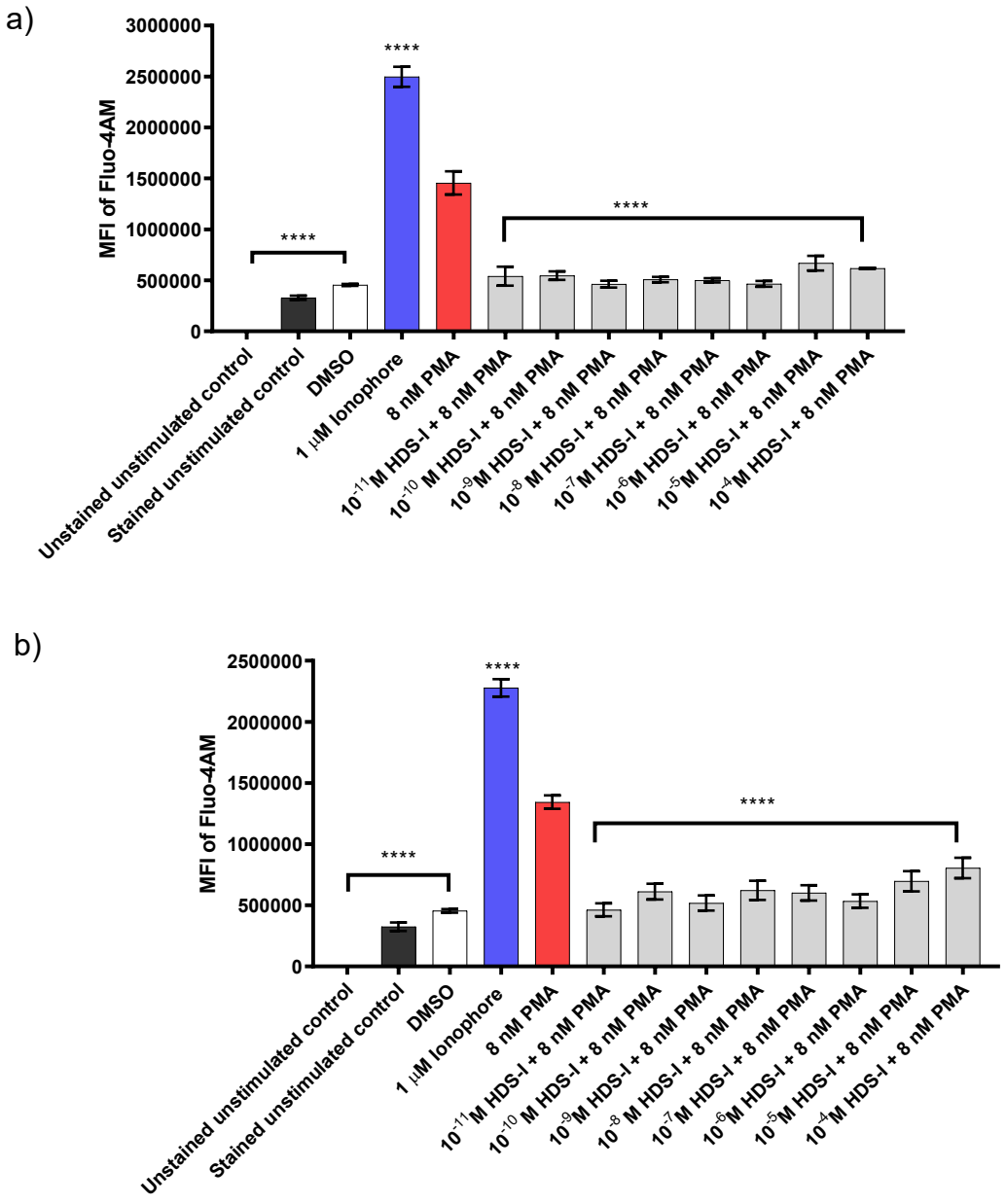


**Figure 5. 10*. Impact of HDS-I on PMA-induced intracellular $Ca^{2+}$ mobilisation.***

*MFI of Fluo-4AM labelled a) U937 and b) THP-1 cells on FL1-A FITC channel of BD Accuri flow cytometry. HDS-I at concentrations of $10^{-11}$ M to $10^{-4}$ M was pre-incubated with Fluo-4 AM labelled U937 and THP-1 cells for 10 min before 8 nM PMA addition. The MFI is represented as mean ± SEM, ****p<0.0001 vs PMA, Dunnett's test, mean ± SEM (n =3).*

a)

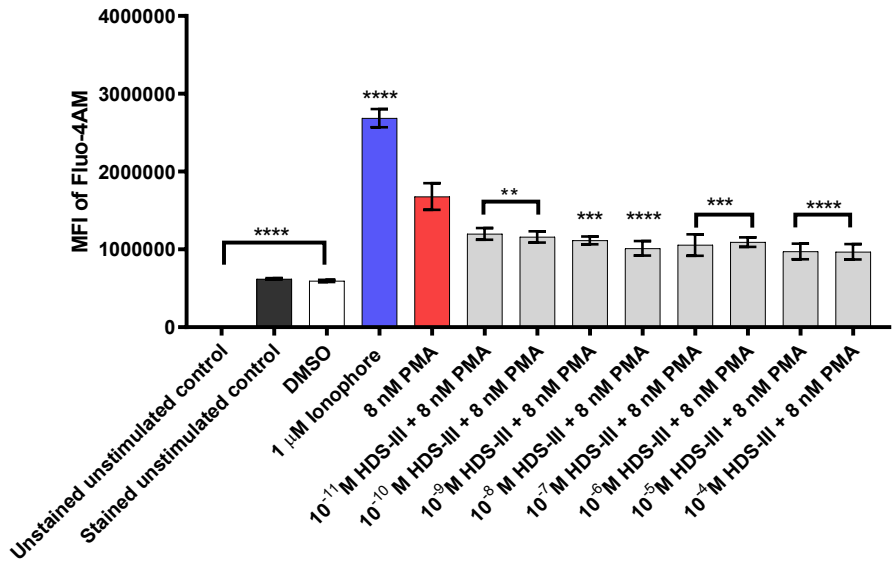


b)

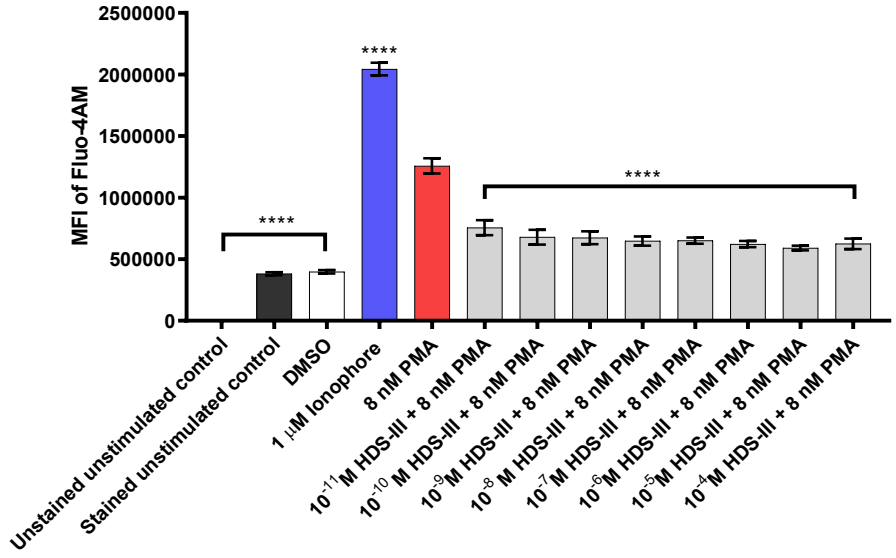


**Figure 5. 11.** ***Impact of HDS-III on PMA-induced intracellular $Ca^{2+}$ mobilisation.***

*MFI of Fluo-4AM labelled a) U937 and b) THP-1 cells on FL1-A FITC channel of BD Accuri flow cytometry. HDS-III at concentrations of $10^{-11}$ M to $10^{-4}$ M was pre-incubated with Fluo-4 AM labelled U937 and THP-1 cells for 10 min before 8 nM PMA addition. The MFI is represented as mean ± SEM, **p<0.01, ****p<0.0001 vs PMA, Dunnett's test, mean ± SEM (n =3).*

## 5.4 Discussion

As outlined in chapter 1, p38 and ERK1/2 MAPK are crucial regulators of cell differentiation. Given the findings from chapter 4, it was hypothesised that balance between the activities of p38 and ERK1/2 signalling pathways is required in PMA-induced cell differentiation and sulphated disaccharide compounds may inhibit phosphorylation of p38 and ERK1/2 MAPK.

In this study, the impact of sulphated disaccharides was examined on p38, ERK1/2 in PMA differentiated U937, and calcium mobilisation on U937/THP-1 monocytic cells. The data in this chapter suggests that sulphated disaccharides inhibited PMA-induced phosphorylation of p38 and ERK1/2 MAPK in U937 cells, as well as calcium mobilisation, suggesting the potential molecular mechanism of these compounds.

The literature suggests that the activation of p42/p44ERK (or ERK1/2) and p38α after stimulation results in de-phosphorylation on a threonine (Thr)- Glycine(Gly)-tyrosine(Tyr) motif located in the activation loop. Following activation of ERK1/2, p38 phosphorylates and activates other kinases and primary transcription factor NF-kB on serine or threonine residues (Song *et al.,* 2015). Tibbles and Woodgett (1999) in their study demonstrated that NF- κB is responsible for the transcriptional regulation of the expression of genes encoding inflammatory cytokines, such as TNF-α. NF-kB activity is mediated by translocation of its p65 (65 kDa) subunit to the nucleus in activated cells. The phosphorylation of the p65 subunit at sites Ser457, Thr458, Thr464, and Ser468 is mediated by PKC to regulate NF- κB activation, nuclear localisation, protein-protein interactions, and transcriptional activity. NF- κB itself is regulated through cytosolic inhibitory protein kinase nuclear factor of kappa light polypeptide gene enhancer in B-cells inhibitor-alpha (IkBα), which is a substrate of protein kinase IkB kinase (IKK) (Makarov, 2000). IkBα inhibits NF-kB function is inhibited by masking and isolating the nuclear localization signals of NF-κB proteins in an inactive state in the cytoplasm. NF-kB activation occurs via phosphorylation of IkBα (39 kDa) at Ser32 and Ser36, resulting in the ubiquitin-mediated proteasome-dependent degradation of IkBα and the release and nuclear translocation of active NF-kB (Jacobs and Harrison, 1998).

The results indicated that the phosphorylation of p38 at Thr180 and Tyr182 was inhibited by SOS, DOS and HDS-I. The phosphorylation of ERK1/2 at Thr202 and Tyr204 of Erk1 and Thr185 and Tyr187 of Erk2 was inhibited by SOS, DOS, HDS-III and HDS-I. The results propose that SOS and DOS may regulate the p38 and ERK1/2 signalling pathways through a negative feedback mechanism to inhibit PMA-induced cell differentiation. However, HDS-I may itself inhibit the p38 signalling pathway and partially ERK1/2 MAPK signalling pathways to inhibit PMA-induced cell differentiation.

Baeuerle and Baltimore (1988) suggest that PMA can also directly activate NF-κB as well as through the MAPK mediated pathway. Activation of ERK1/2 MAPK has been reported to be important for T cell adhesion and migration (Woods *et al.,* 2001). In addition, the cell cycle cyclin-dependent kinase inhibitor $p21^{WAF1/Cip1}$ has been reported to be up-regulated during monocyte-macrophage differentiation by ERK1/2 MAPK (Matsumoto *et al*., 2006, Steinmani *et al., 1998,* Agadir *et al*., 1999, Das *et al*., 2000, Dufourny *et al*., 1997 and Sato *et al*., 2000). A study by Zhang *et al.,* (2006), demonstrated that the inhibition of TNF-α-induced p38 activation by the cAMP pathway leads to suppression of NF-κB activation.

Several studies have reported that cAMP-elevating agents inhibit the activation of ERK and Raf-1 in fibroblasts and vascular smooth muscle cells (Wu *et al*., 1993 and Graves *et al*., 1993). In addition, some studies reported that cAMP-elevating agents do not inhibit the activation of ERKs in cells subject to cAMP-dependent inhibition of mitogenesis (Mackenzie *et al*., 1996 and Giasson *et al*., 1997). Hecht *et al.,* (2004) study suggests that tri-sulphated disaccharides interfere with ERK1/2 phosphorylation through G-protein coupled receptor activation signalling pathways which could be related to T cell adhesion and migration. Soeder *et al*., (1999), have shown that the $\beta_3$-adrenergic receptor is coupled to both $G_s$ and $G_i$ in adipocytes, leading to the activation of the PKA and ERK1/2 pathways. Furthermore, Cao *et al.,* (2001) have demonstrated that the $\beta_3$-adrenergic receptor activates the p38 pathway as a downstream consequence of the generation of cAMP and PKA activity in adipocytes and that cAMP-dependent transcription of the mitochondrial uncoupling protein 1 (UCP1) promoter by $\beta_3$AR requires p38 MAPK.

Cross talk between cAMP and MAPK pathways has been documented at multiple levels in a number of cell types (Bhat *et al*. 2007, Rey *et al*. 2007, Sengupta *et al*. 2007). Ge *et al*., (2011), postulated that cross-talk between cAMP and p38 MAPK pathway is possibly involved in the induction of leptin production by hCG in placental syncytiotrophoblasts. Stork and Schmitt (2002) suggest that the capacity of cAMP for either positive or negative regulation of the ERK cascade accounts for many of the cell type-specific actions of cAMP on cell proliferation.

Therefore, findings hypothesised a mechanism that since there is a positive feedback loop between p38 and ERK1/2 MAPK, therefore there is a possibility that sulphated disaccharide compounds block one of the two pathways and subsequently the other pathway becomes blocked. Another mechanism is hypothesised that sulphated disaccharides may inhibit ERK1/2 by inhibition or activation of ERK1/2 by cAMP. The data of this study suggest that one of these mechanisms might involve the activation of the GTPase Rap1, which can activate or inhibit ERK signalling in a cell-specific manner. These results of this study served as a source for further investigation to study the impact of sulphate disaccharides on calcium mobilisation to understand its contribution to p38 and ERK1/2 MAPK signalling pathways activation.

For the $G_q$-activated GPCRs, the binding of an agonist results in an increase in intracellular calcium. In resting cells, the cytosolic calcium concentration is much lower (∼100–200 nM) than that in the extracellular environment (∼2 mM). When the cells are excited by the activation of GPCRs, the concentration of intracellular calcium can rapidly increase to ∼100 μM (Berridge, 2006). The low basal intracellular calcium level and the rapid increase of cytosolic calcium upon receptor activation enable the use of fluorescent calcium dyes to measure transient changes in cytosolic calcium concentration. Therefore, initially an effective *in vitro* protocol was established by optimising the currently available methods. The changes in cytosolic $Ca^{2+}$ in U937 and THP-1 cells were examined by using the $Ca^{2+}$ sensitive fluorescent dye, Fluo-4 acetoxymethyl (AM) or Fluo-4 AM (Dina *et al*; 2002) initially by fluorescence spectroscopy (results showed U937 cells with varying responses and PMA failed to mobilise $Ca^{2+}$, data not presented) and then by flow cytometry to detect fluorescence from intact cells. Fluo-4 acetoxymethyl ester (Fluo-4 AM)

dyes are single wave calcium probes for which emission intensity depends on the level of bound calcium. i.e. the more calcium is present in the cell, the brighter the signal becomes (Dina *et al*; 2002). Fluo-4 AM is a high-affinity calcium indicator with an excitation at 470-490 nm and emission at 520-540 nm.

In this study, the calcium-sensitive fluorescent dye Fluo-4 (AM) was used to measure calcium mobilisation as the non-fluorescent acetoxymethyl ester group of these dyes are known to facilitate the fluorophore to cross the cell membrane. Once fluorophore reaches inside the cell, the cytoplasmic esterases hydrolyse the acetoxymethyl ester group and generate a fluorescent anionic compound within the cell (Gee *et al*., 2000). The changes in fluorescence intensity of this intracellular compound are attributed to intracellular changes in calcium ion concentration. Intracellular calcium-binding to this dye enhances the fluorescence intensity of this dye (Paul *et al*., 2011).

To test the accuracy of the flow cytometry method, U937 and THP-1 cells were exposed to Ionophore A23187, PMA and DMSO and a change in the intracellular calcium concentration were recorded as mean fluorescence intensity (MFI). PMA induced intracellular $Ca^{2+}$ mobilisation comparable to that observed with calcium ionophore A23187. The calcium ionophore A23187 (Martina *et al*; 1994 and Wang *et al*; 1994) which elevate intracellular $Ca^{2+}$ by forming calcium channels to allow calcium into cells (Przygodzki *et al*., 2005) was used in this study to confirm the calcium mobilisation in U937 and THP-1 cells to compare PMA effect on calcium mobilisation. A23187 is known to cause a rise in cytosol $Ca^{2+}$ and in concentrations between 1 and 10 µmol/l stimulates rapid activation of the NADPH-oxidase (McPhail *et al*., 1983). The results of this study confirmed that ionophore A23187 cause an increase in intracellular $Ca^{2+}$ in U937 and THP-1 cells.

In this study, it was found that the flow cytometry Accuri C6 method is a useful method for measurement of intracellular $Ca^{2+}$ concentration as it allowed identification and analysis of live individual cells within a population based on their light scatter profile and selective responsiveness to given stimuli. This accuracy of data was achieved by gating out the dead and fragmented cells from the population. This method also provided an opportunity for the use of Eppendorf's for continuous addition of test compounds to the

cell suspension. Therefore, the tested compounds were studied without pausing cell aspiration into the flow cytometer. This method was useful to test the degree of action of different tested compounds to calcium response within a single population of cells.

Further, in this chapter, the impact of sulphated disaccharides on PMA-induced intracellular $Ca^{2+}$ mobilisation was investigated. The results propose that sulphated disaccharides inhibit PMA-induced intracellular $Ca^{2+}$ mobilisation when given 10 minutes before PMA for 5 minutes. The results indicated a similar inhibitory pattern of SOS and DOS compared to HDS-I and HDS-III, suggesting that there is a possibility that they could act through a similar pathway to some extent. One explanation for the inhibitory impact of sulphated disaccharide compounds could be that these compounds may directly inhibit PMA activity. There is a possibility of competitive inhibition by sulphated disaccharide compounds which leads to inhibition of PMA ability to open a $Ca^{2+}$ influx pathway. Another mechanism is suggested by the given findings that pre-treatment of U937 and THP-1 cells with sulphated disaccharides may modify the surface receptors, thus sulphated disaccharides pre-treated U937 and THP-1 cells with PMA (8 nM) no longer showed calcium mobilisation. In contrast, the sulphated disaccharide compounds did not alter intracellular $Ca^{2+}$ mobilisation of U937 and THP-1 when given for 5 minutes in the absence of PMA compared to unstimulated control cells (Appendix Fig.92 to Appendix Fig.95). Further studies are required to investigate the importance of a 10-minute pre-incubation period for sulphated disaccharides to exert their inhibitory action on calcium mobilisation.

Increases in cAMP in leukocytes activate cAMP-dependent protein kinase (PKA). This kinase phosphorylates transcription factors that bind to the cAMP-response element on the TNFα promoter, thereby inhibiting TNFα mRNA transcription (Economou *et al*., 1989; Newell *et al*., 1994; Righi, 1993 and Zhong *et al*., 1995). Studies have reported that treatment of cell membranes with nitric oxide (NO) decreases cAMP production by inhibiting calmodulin activation of type I adenylate cyclase, presumably through thiol nitrosylation at the calmodulin-binding site (Duhe *et al*., 1994 and Vorherr *et al*., 1993). Murphy *et al*., 1998) provides evidence that increases in cGMP also lower the $Ca^{2+}$-sensitivity of cross-bridge phosphorylation. A study by Wang *et al*., (1997), demonstrated

that NO increased TNFα production in PMA-differentiated U937 cells by decreasing intracellular cAMP levels. This study indicated that NO uses cAMP, rather than cGMP as a second messenger for some of its cellular effects. This study data indicated that U937 cells lack NO-sensitive soluble guanylate cyclase and U937 cells have extremely low cGMP hydrolytic activity and do not contain the cGMP-specific PDE isoenzyme (Torphy *et al*., 1992; Barnette *et al*., 1992).

In addition, the impact of p38 MAPK inhibitor SB203580 and ERK1/2 MAPK inhibitor PD98059 was examined on U937 and THP-1 cells to confirm the PMA impact on p38 and ERK1/2. The cross-talk relationship between p38 and ERK1/2 MAPK indicated that there is a potential involvement of multiple pathways in the regulation of cell differentiation and a balance between p38 and ERK1/2 MAPK signalling pathways is required for cell differentiation. It is confirmed that the cell cycle inhibitor $p21^{WAF1/Cip1}$ is up-regulated through the ERK1/2 MAPK signalling pathway to induce monocyte-macrophage differentiation. PMA is considered to induce monocyte-macrophage differentiation through PMA → PKC → p38/ERK MAPK →$p21^{WAF1/Cip1}$ pathway (Appendix Fig.83 to Appendix Fig.91). Therefore as future work, it would be interesting to assess sulphated disaccharides impact on cyclin D1 and $p21^{WAF1/Cip1}$ expression to investigate whether expression of cell cycle-related genes is a common phenomenon in cell cycle arrest and differentiation in PMA-differentiated cells.

The impact of p38 MAPK inhibitor SB203580 and ERK1/2 MAPK inhibitor PD98059 was also examined on U937 and THP-1 cells to evaluate the participation of $Ca^{2+}$ in the PMA-induced activation of p38 and ERK1/2 MAPK signalling pathways (Appendix Fig.96 to Appendix Fig.99). It was observed that SB203580 and PD98059 had no impact on intracellular $Ca^{2+}$ mobilisation in the absence of PMA in U937 and THP-1 cells compared to unstimulated control cells. However, when SB203580 and PD98059 were given 10 minutes before PMA for 5 minutes, they inhibited PMA-induced intracellular $Ca^{2+}$ mobilisation at all the tested concentrations for 5 minutes. Thus, it concludes that p38 MAPK and ERK1/2 MAPK activation is intracellular $Ca^{2+}$ dependent.

## 5.5 Conclusion

PMA activates the PKC signalling pathway, which requires intracellular $Ca^{2+}$ to trigger its translocation to the cell membrane to activate downstream p38 and ERK1/2 signalling pathways to induce cell differentiation. The results of this study suggest that sulphated disaccharides inhibit monocyte-macrophage differentiation following inhibition of p38 and p42/44 ERK, which in turn led to inhibit the expression of adhesion molecules and adhesion to cell culture surface (as demonstrated in chapter 4). In addition, the results have shown that SOS, DOS, HDS-I and HDS-III inhibited PMA-induced intracellular $Ca^{2+}$ in a similar inhibition pattern. The results of this study support the importance of a role for intracellular calcium as a second messenger in monocytes in response to PMA. Besides the p38 and ERK1/2 pathways, our data do not exclude the possibility of additional mechanisms for the inhibition of cell differentiation by sulphated disaccharides. For example, sulphated disaccharides could inhibit other transcription factors, such as NF-κB (Baeuerle and Baltimore, 1988; Tibbles and Woodgett, 1999). This study did not focus on NF-kB but this study data further suggest that sulphated disaccharides are capable of inhibiting NF-kB in U937 and THP-1 cells. Therefore, in future work, it would be interesting to assess NF-kB phosphorylation in U937 and THP-1 cells by using a phosphorylated specific antibody. As literature suggests that elevation of cAMP inhibits p38 activity and phosphorylation and there is also a possibility of crosstalk from cAMP to the ERK1/2 cascades (Ge *et al*., 2011; Stork and Schmitt, 2002). Therefore, this chapter results hypothesise that sulphated disaccharides may inhibit p38 phosphorylation by increasing the cAMP levels in U937 cells. Also, there may act via a feedback loop within cells to stimulate NO production, which may have inhibited calcium levels through the generation of cGMP (Wang *et al*., 1997). Therefore in future work, it would be interesting to assess cAMP and cGMP in U937 and THP-1 cells (Bhat *et al*. 2007, Rey *et al*. 2007, Sengupta *et al*. 2007) by using an enzyme immunoassay. In conclusion, based on the results, this study proposes that the stimulating effect of PMA on p38 MAPK and ERK1/2 signalling may be mediated through the intracellular $Ca^{2+}$ mobilisation and sulphated disaccharides may inhibit PMA-induced cell differentiation by inhibiting this second messenger either directly or by modulating cAMP or cGMP pathways.

# CHAPTER 6: SULPHATED DISACCHARIDES AFFECTS PHENOTYPIC AND FUNCTIONAL FEATURES OF PMA-INDUCED MACROPHAGES

## 6.1 Introduction

As outlined in chapter 1, macrophages play a prominent role in the pathology of rheumatoid arthritis and other inflammatory diseases by releasing the pro-inflammatory TNF-α cytokine (Macnual *et al.,* 1990), amongst many others. TNFα is released during re-activation Herpetic keratitis, and anti-TNF therapy abrogates it (Keadle *et al,* 2000). Anti-TNF therapy is also effective in Rheumatoid arthritis. TNF-α plays a crucial role in the pathogenesis of autoimmune chronic inflammatory diseases (MacDonald *et al*., 1990), and is a proven and effective drug target. Monocyte-derived macrophages (M0) are thought to be polarized into different macrophage subsets namely, pro-inflammatory (M1) and anti-inflammatory (M2), and perhaps more. M1 and M2 macrophages are characterised based on their functional (cytokine production, gene expression) and phenotypic (surface marker) profiles (Tarique *et al*., 2015). M1 macrophages express high levels of $CD68^{+}$, $CD86^{+}$, $CD80^{+}$ and TNF-$\alpha^{high}$, whereas M2 macrophages express high levels of $CD206^{+}$, $CD200R^{+}$, $CD163^{+}$, Arginase-$1^{+}$ and IL-$10^{high}$ (Roszer, 2015 and Duluc *et al.,* 2007).

The polarization balance between these subsets is essential for adequate immune function, and dysfunction of M1 and M2 polarity is a characteristic of the pathology of autoimmune chronic inflammatory diseases (Baek *et al*., 2009). M1 macrophages have been reported to dominate at sites of infection during inflammation, and release excessive quantities of TNF-α during sepsis (Sintiprungrat *et al.,* 2010).

On the other hand, M2 macrophages have been reported to be dominant during the resolution of inflammation. In addition, Biswas *et al*., (2012) state that M2 macrophages release anti-inflammatory cytokines such as interleukin 10 (IL-10) and interleukin 4 (IL-4) which downregulate M1 activity and secrete products implicated in wound healing.

Brennan and co-workers (2008) state that anti-inflammatory macrophage IL-10 is capable of inhibiting the production of TNF-α. In inflammatory diseases, TNF-α levels rise as IL-10 levels decrease, as IL-10 regulates TNF-α converting enzyme expression. As a result, TNF-α is not regulated effectively. p38, ERK1/2 and NF-kB signalling pathways are

involved in IL-10 induction (Saraiva and O'Garra, 2010). It has been previously suggested that heparan sulphate derived sulphated disaccharide compounds, such as HDS-I and HDS-III, inhibit T cell-mediated TNF-α production in rodents and thus may function as a potent TNF-α inhibitor to regulate immune responses (Cahalon *et al.,* 2001).

M0 macrophages can be polarized into M1 and M2 macrophages *in vitro (*Davis *et al.,* 2013) by lipopolysaccharide (LPS) and interferon-gamma (IFNγ) treatment (Nathan, 1992 and Nussler *et al.,* 1993), and can be polarized to the M2 phenotype by interleukin 4 (IL-4) in the absence or presence of LPS, as well as macrophage colony-stimulating factor (MCSF-1).

In addition, M1 can be polarized to M2 and vice versa by a variety of cytokines. Macrophage interaction with T-helper 2 cells results in a release of IL-4 alone, or association with interleukin 13 (IL-13), and causes polarization of macrophages into M2 phenotypes (Mantovani *et al.,* 2006).

PMA and LPS act through NF-kB to stimulate the transcription of pro-inflammatory TNF-α (Collart *et al.,* 1990, Drouet *et al.,* 1991, Shakhov *et al.,* 1990, Takashiba *et al.,* 1995 and Trede *et al.,* 1995). In chapter 4 it has been discussed that phosphorylation of IkB activates NF-kB to translocate from the cytoplasm to the nucleus to activate TNF-α gene transcription (Bondeson *et al.,* 1999 and Trede *et al.,* 1995).

A study by Hecht *et al.,* (2004) suggests that degradation of extracellular matrix glycosaminoglycans by enzymes secreted by T cells may provide cells with regulatory signals and an increase of these degraded sulphated disaccharides in the extracellular matrix during inflammation might alert the cells to down-regulate their pro-inflammatory activity.

An understanding of sulphated disaccharides inhibitory action at the level of cytokine production will elucidate the physiological significance of the p38 and ERK1/2 MAPK signalling pathways by these compounds. Therefore, in this chapter, it was hypothesised that sulphated disaccharides inhibit M0 differentiation to M1 and also polarize M1 macrophages to M2.

Therefore, this study aimed to evaluate the impact of sulphated disaccharide compounds on macrophage activation or a shift of M1 macrophage toward M2 macrophage in PMA-induced U937/THP-1-derived macrophages.

## 6.2 Aim

This study aimed to determine whether sulphated disaccharide compounds induce a phenotypic switch of differentiated macrophage (M0) phenotype into activated pro-inflammatory (M1) phenotype macrophage or anti-inflammatory (M2) phenotype macrophage or switch from M1 phenotype into M2 phenotype.

The following objectives were undertaken to address this aim:

- To investigate the impact of sulphated disaccharides on macrophage polarization from M0 to M1 or M2 and M1 to M2 phenotypes. In the context of this, TNF-α and IL-10 cytokine production was assessed by ELISA (Fig.6.1 and Fig.6.2).

- To determine the impact of sulphated disaccharides on CD206, CD163 and CD86 surface markers expression by flow cytometry.

- To study the impact of sulphated disaccharides on gene expression of p21, CD14, CD200R and Arginase-1 by RT-PCR.

## 6.3 Results

### 6.3.1 Sulphated disaccharides impact on TNF-α and IL-10 production differentiated U937/THP-1 macrophages

To test whether sulphated disaccharides may affect TNF-α and IL-10 production by differentiated macrophages, two experimental approaches were used (Fig.6.1 & Fig.6.6). For experimental protocols, U937 and THP-1 cells at a density of $2x10^5$ cells/ml per well were grown as confluent monolayer overnight on a 24-well tissue culture plate. The supernatants from cell culture were collected and analysed for TNF-α and IL-10 production by ELISA as described in the materials and methods section 2.6.

SOS, DOS, HDS-I and HDS-III demonstrated down-regulation of PMA- induced TNF-α production in a concentration-dependent manner compared to PMA when given 2 h before PMA. Significant concentration-dependent inhibition of TNF-α production was observed with sulphated disaccharides at concentrations as low as $10^{-11}$ M. As shown in Figures (6.02a,b-6.05a,b), sulphated disaccharides that inhibited TNF-α also up-regulated IL-10 production. However, the intensity of inhibition at low concentrations was different between sulphated disaccharides, indicating differences in potency. To test whether sulphated disaccharide action was cell-specific, similar experiments were performed using THP-1 cells. As shown in Figures 6.02c,d-6.05c,d, the same pattern of inhibition was produced in THP-1 cells compared to U937 cells. Sulphated disaccharides were inhibitory for TNF-α production and promoter for IL-10 production in a concentration-dependent manner for both U937 and THP-1 cell lines.

The results of this study suggested that PMA induce macrophages are M1 phenotype. Sulphated disaccharides inhibit PMA-induced TNF-α production by polarising M1 macrophages to M2 macrophages.

In the second study, SOS, DOS, HDS-I and HDS-III significantly inhibited LPS-induced TNF- α production when given 2 h before LPS stimulation (Fig.6.7a,b- Fig.6.10a,b). These

compounds produced less IL-10 compared to IL-4 stimulated U937 or THP-1 derived M2 macrophages (Fig. 6.07c,d-Fig.6.10c,d).

Based on both studies it was concluded that sulphate disaccharides can inhibit PMA-induced and LPS-induced TNF-α production and increase IL-10 production and these compounds also inhibit both LPS stimulated TNF-α and IL-4 stimulated IL-10 synthesis when given 2 h before PMA.

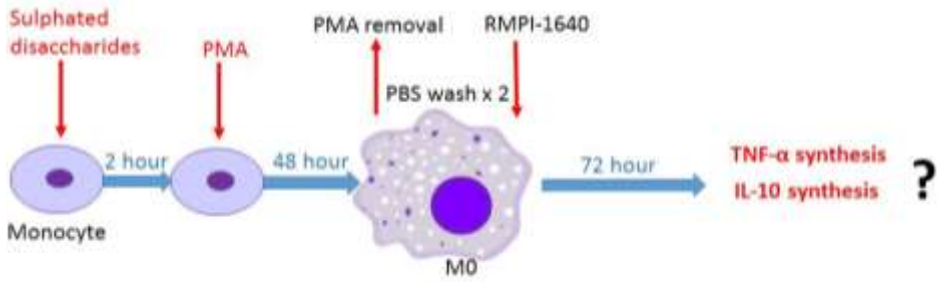


**Figure 6. 1*. In vitro study design 1 - Sulphated disaccharides given 2 h before PMA.***

*To study the impact of sulphated disaccharides on PMA-induced TNF-α and IL10 production. In this study, the cell cultures of U937 and THP-1 were pre-incubated with SOS, DOS, HDS-I and HDS-III at concentrations of $10^{-11}$ M to $10^{-4}$ M for 2 hour prior 8 nM PMA stimulation for 48 h. PMA-induced M0 macrophages were considered as a control to compare sulphated disaccharides + PMA macrophages cytokines production.*

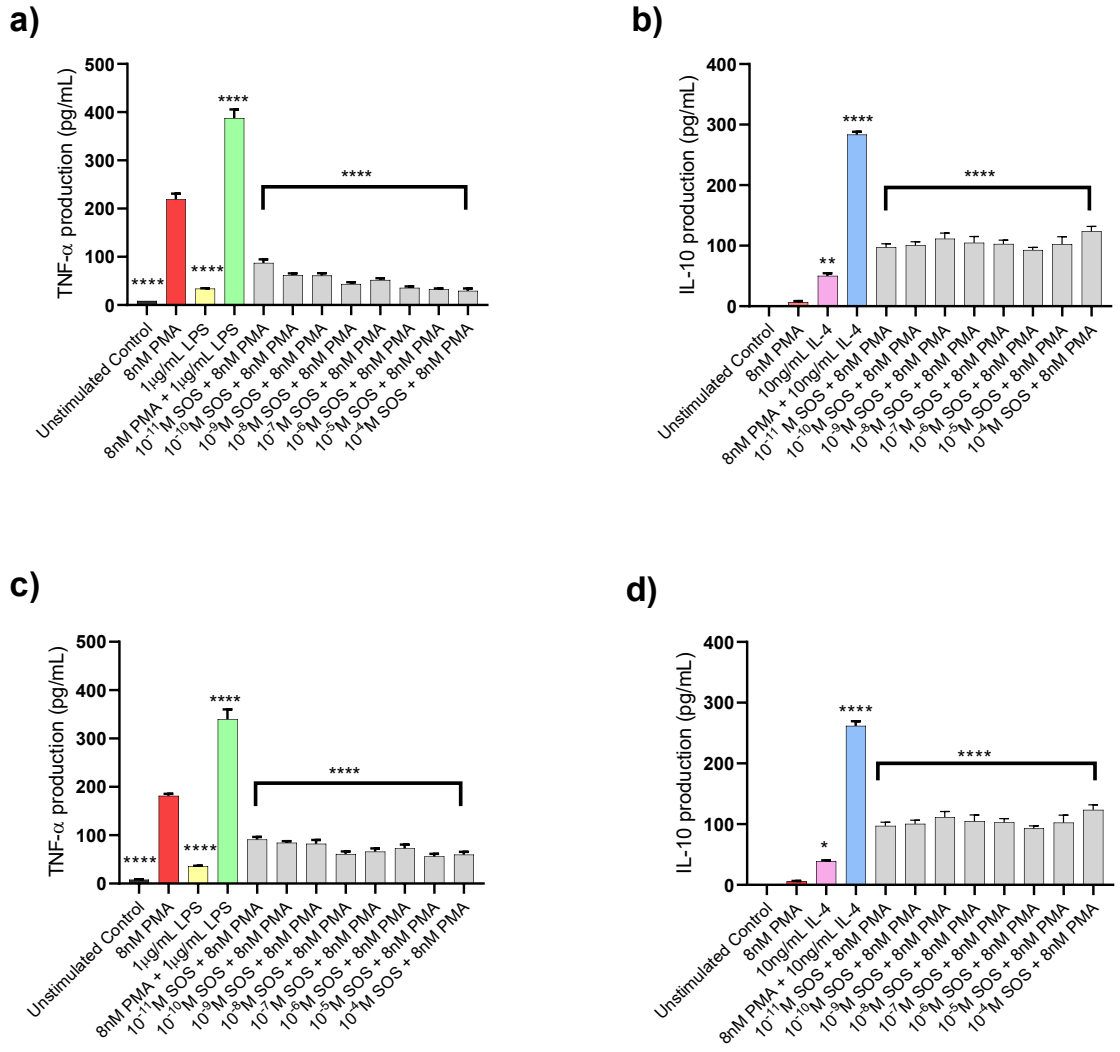


**Figure 6. 2**. ***Impact of SOS on TNF-α and IL-10 synthesis when given 2 h before PMA.***

*The U937 (a,b) and THP-1 (c,d) were pre-incubated with SOS at concentrations of $10^{-11}$ M to $10^{-4}$ M for 2 hour prior 8 nM PMA stimulation for 48 h (followed by 72 h rest). PMA-induced M0 macrophages were considered as a control to compare SOS + PMA macrophages TNF-α and IL-10 production. In this study, cells were not stimulated with LPS or IL-4. ANOVA followed by Dunnett's Test, mean ± SEM (n=3), ****p<0.001, **p<0.0001, *p<0.05 vs. PMA. TNF-α and IL-10 production was assessed by ELISA.*

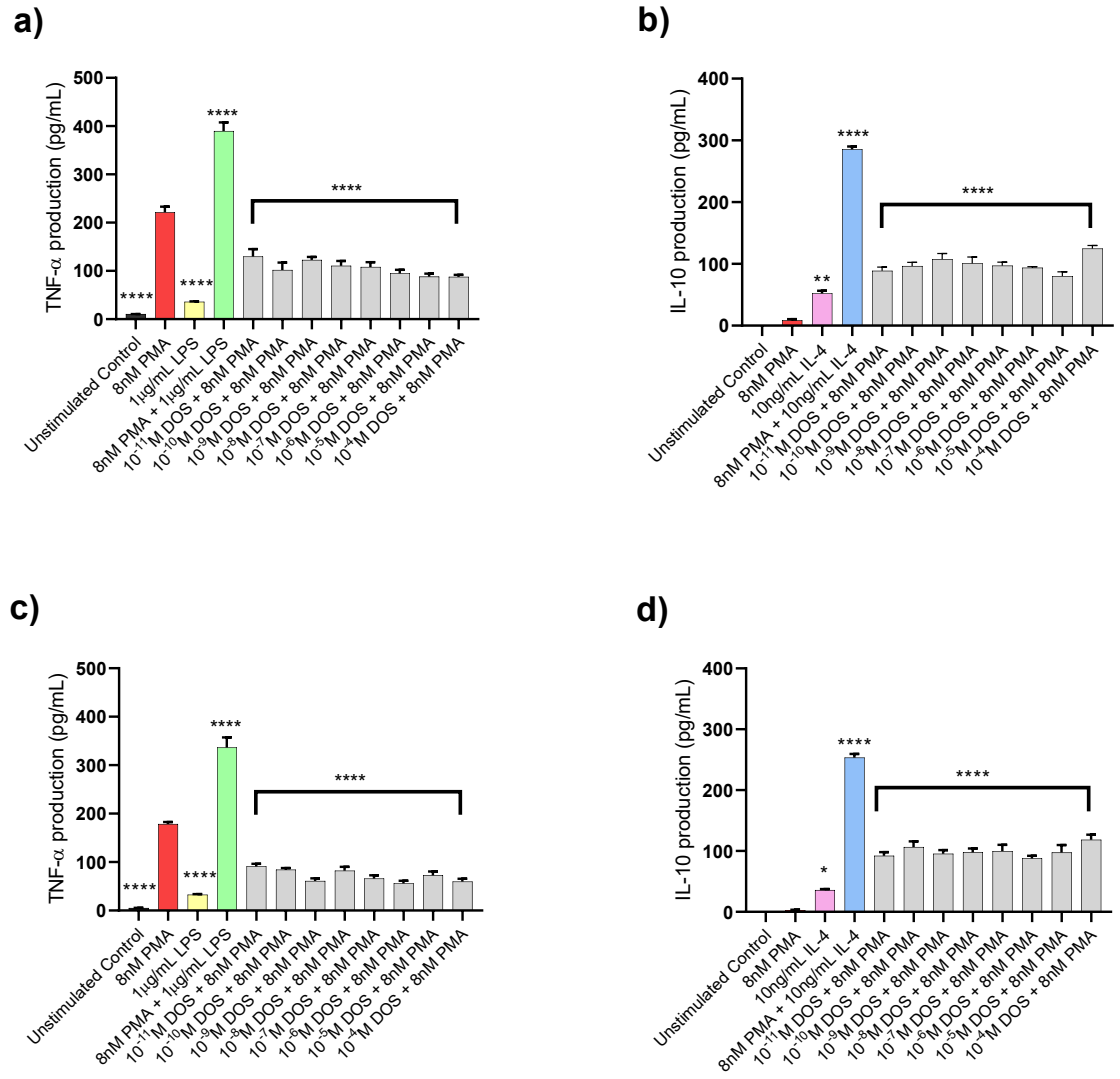


**Figure 6. 3**. ***Impact of DOS on TNF-α and IL-10 synthesis when given 2 h before PMA.***

*The U937 (a,b) and THP-1 (c,d) were pre-incubated with DOS at concentrations of $10^{-11}$ M to $10^{-4}$ M for 2 hour prior 8 nM PMA stimulation for 48 h (followed by 72 h rest). PMA-induced M0 macrophages were considered as a control to compare DOS + PMA macrophages TNF-α and IL-10 production. In this study, cells were not stimulated with LPS or IL-4. ANOVA followed by Dunnett's Test, mean ± SEM (n=3), ****p<0.001, **p<0.0001, *p<0.05 vs. PMA. TNF-α and IL-10 production was assessed by ELISA.*

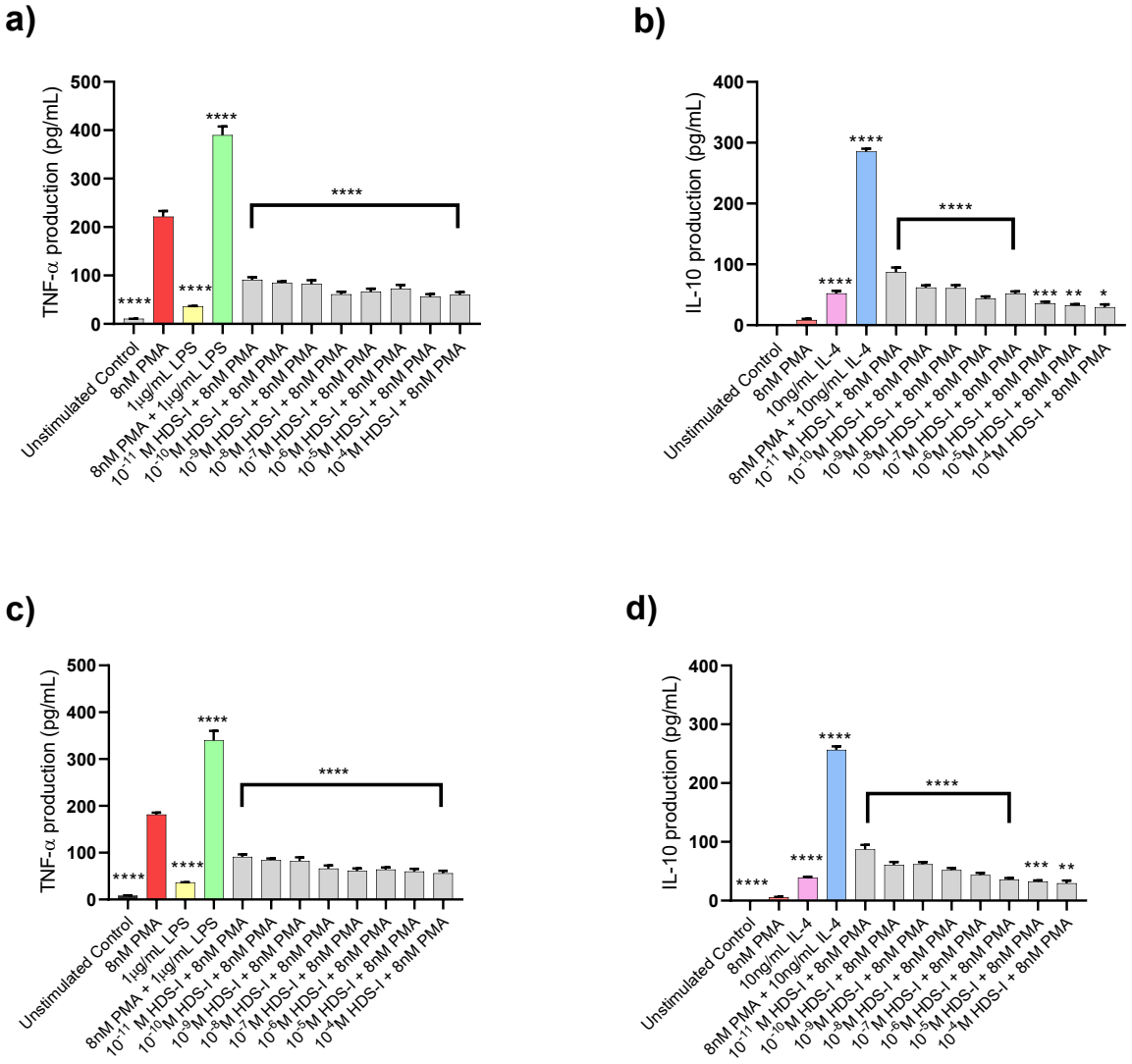


**Figure 6. 4.** ***Impact of HDS-I on TNF-α and IL-10 synthesis when given 2 h before PMA.***

*The U937 (a,b) and THP-1 (c,d) were pre-incubated with HDS-I at concentrations of $10^{-11}$ M to $10^{-4}$ M for 2 hour prior 8 nM PMA stimulation for 48 h (followed by 72 h rest). PMA-induced M0 macrophages were considered as a control to compare HDS-I + PMA macrophages TNF-α and IL-10 production. In this study, cells were not stimulated with LPS or IL-4. ANOVA followed by Dunnett's Test, mean ± SEM (n=3), ****p<0.001 vs. PMA. TNF-α and IL-10 production was assessed by ELISA.*

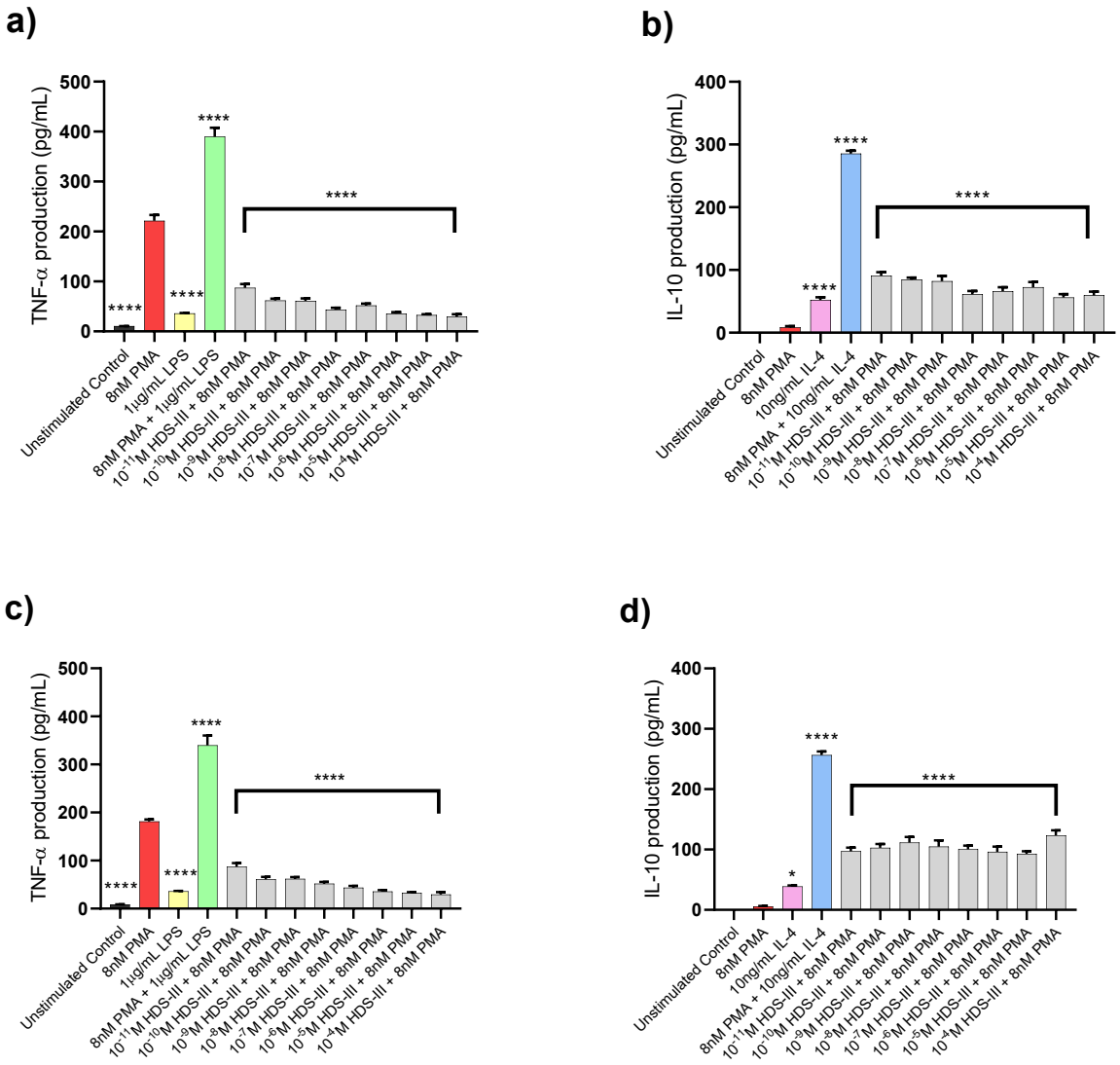


**Figure 6. 5*. Impact of HDS-III on TNF-α and IL-10 synthesis when given 2 h before PMA.***

*The U937 (a,b) and THP-1 (c,d) were pre-incubated with HDS-III at concentrations of $10^{-11}$ M to $10^{-4}$ M for 2 hour prior 8 nM PMA stimulation for 48 h (followed by 72 h rest). PMA-induced M0 macrophages were considered as a control to compare HDS-III + PMA macrophages TNF-α and IL-10 production. In this study, cells were not stimulated with LPS or IL-4. ANOVA followed by Dunnett's Test, mean ± SEM (n=3), ****p<0.001, *p<0.05 vs. PMA. TNF-α and IL-10 production was assessed by ELISA.*

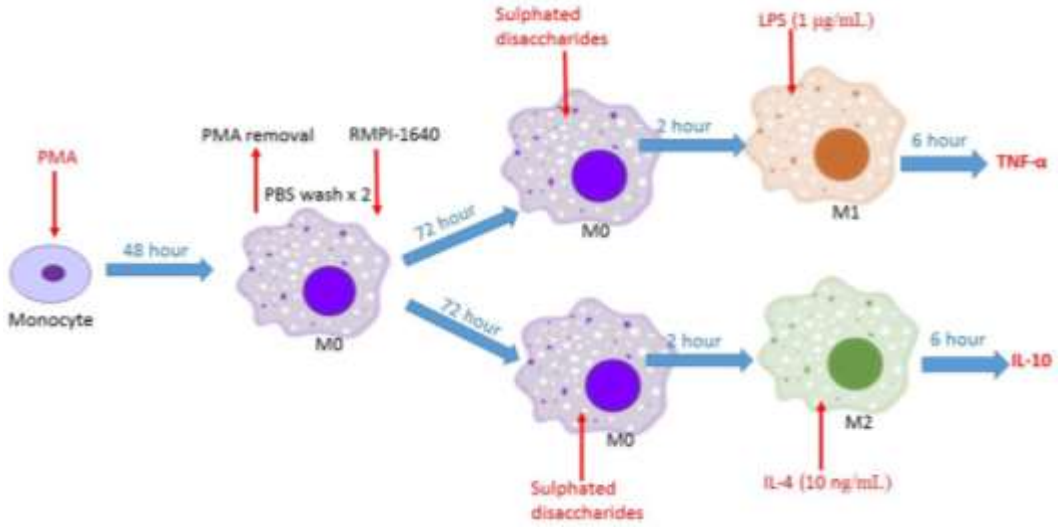


**Figure 6. 6*. In vitro study design 2 - Sulphated disaccharides given 2 h before LPS or IL-4.***

*To study the impact of sulphated disaccharides on LPS or IL-4 stimulated TNF-α and IL10 production. In this study, U937 and THP-1 cells were stimulated with 8 nM PMA for 48 h at 37 $^{0}$C with 5% $CO_2$. After 48 h PMA stimulus, the PMA -containing media was removed; cells were washed twice with cold PBS and rested in fresh PMA-free RPMI-1640 media for a further 72 h. SOS, DOS, HDS-I and HDS-III at a concentration of $10^{-11}$ to $10^{-4}$ M were given 2 h before 1 µg/mL LPS and 10 ng/mL IL-4 treatment for 6 h.*

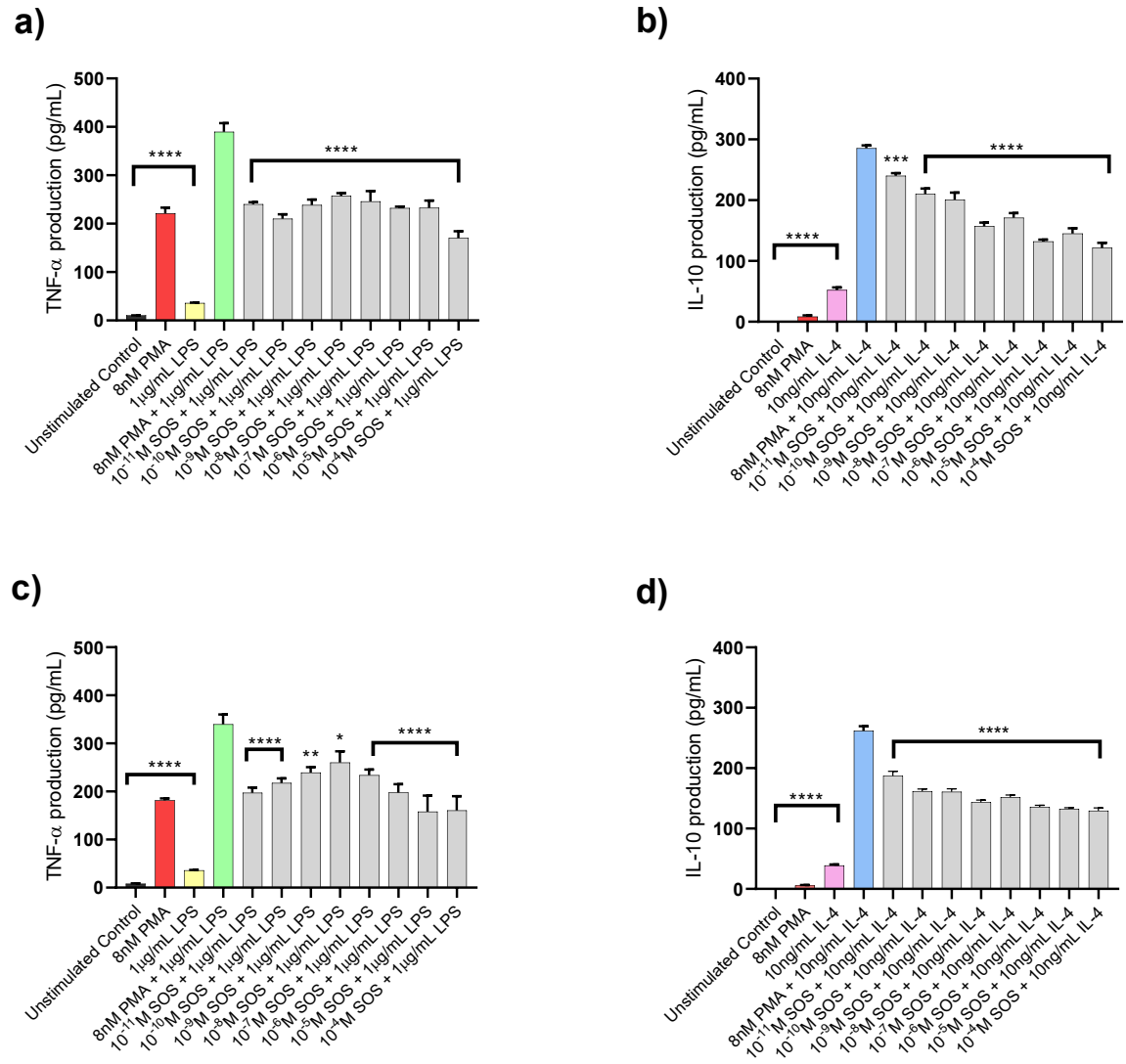


**Figure 6. 7*. Impact of SOS on TNF-α and IL-10 synthesis when given 2 h before LPS or IL-4.***

*The U937 (a,b) and THP-1 (c,d) were pre-incubated with 8 nM PMA for 48 h (followed by 72 h rest). Cells were treated with SOS at concentrations of $10^{-11}$ M to $10^{-4}$ M for 2 hour prior to 1 µg/mL LPS and 10 ng/mL IL-4 treatment for 6 h. LPS-induced or IL-4 macrophages were considered as a control to compare SOS + PMA macrophages TNF-α and IL-10 production. ANOVA followed by Dunnett's Test, mean ± SEM (n=3), *=p<0.05, **=p<0.01, ****=p<0.0001 vs. PMA+LPS/IL-4. TNF-α and IL-10 production was assessed by ELISA.*

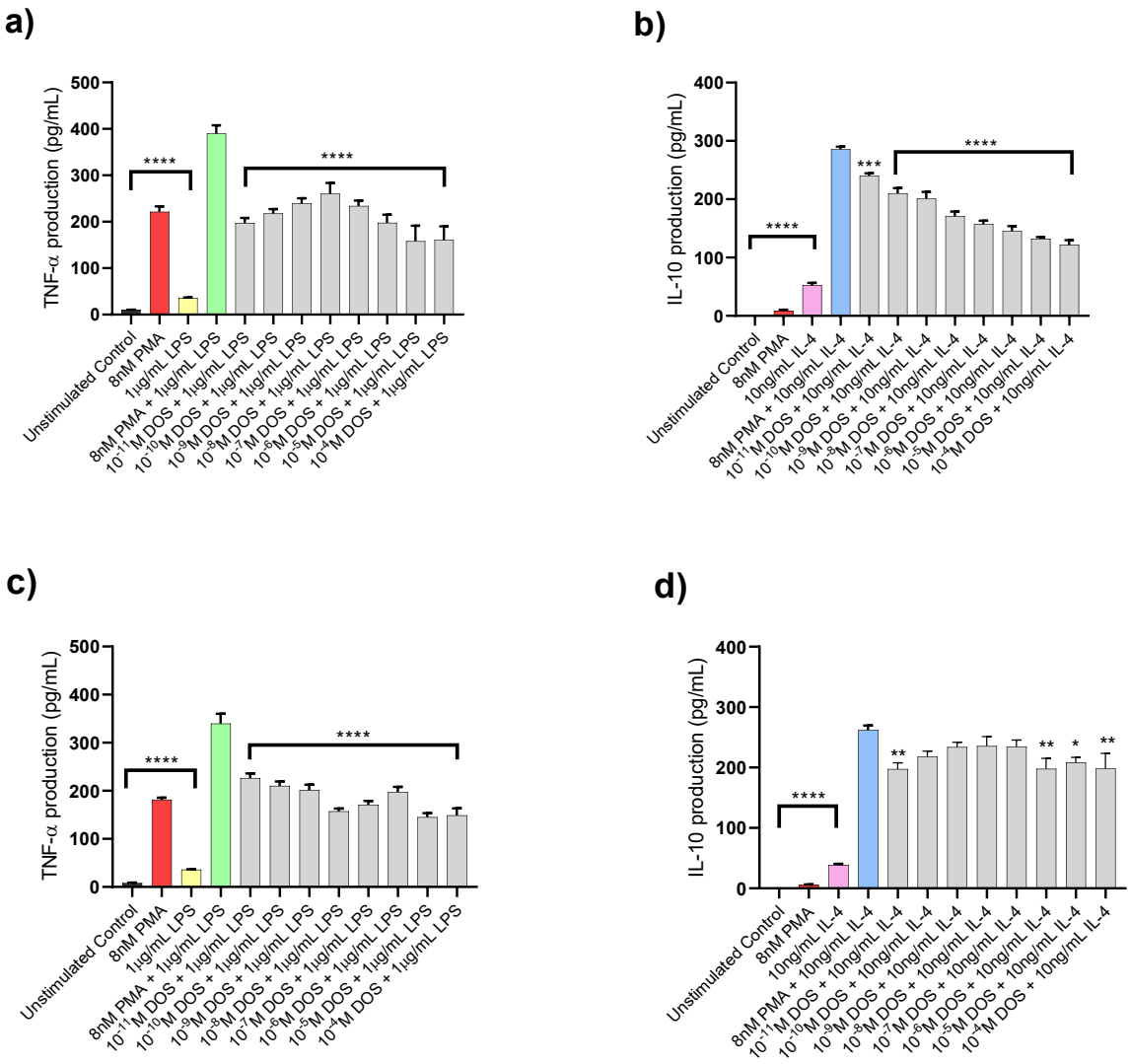


**Figure 6. 8*. Impact of DOS on TNF-α and IL-10 synthesis when given 2 h before LPS or IL-4.***

*The U937 (a,b) and THP-1 (c,d) were pre-incubated with 8 nM PMA for 48 h (followed by 72 h rest). Cells were treated with DOS at concentrations of $10^{-11}$ M to $10^{-4}$ M for 2 hour prior to 1 µg/mL LPS and 10 ng/mL IL-4 treatment for 6 h. LPS-induced or IL-4 macrophages were considered as a control to compare DOS + PMA macrophages TNF-α and IL-10 production. ANOVA followed by Dunnett's Test, mean ± SEM (n=3), *=p<0.05, **=p<0.01, ***=p<0.001, ****=p<0.0001 vs. PMA+LPS/IL-4. TNF-α and IL-10 production was assessed by ELISA.*

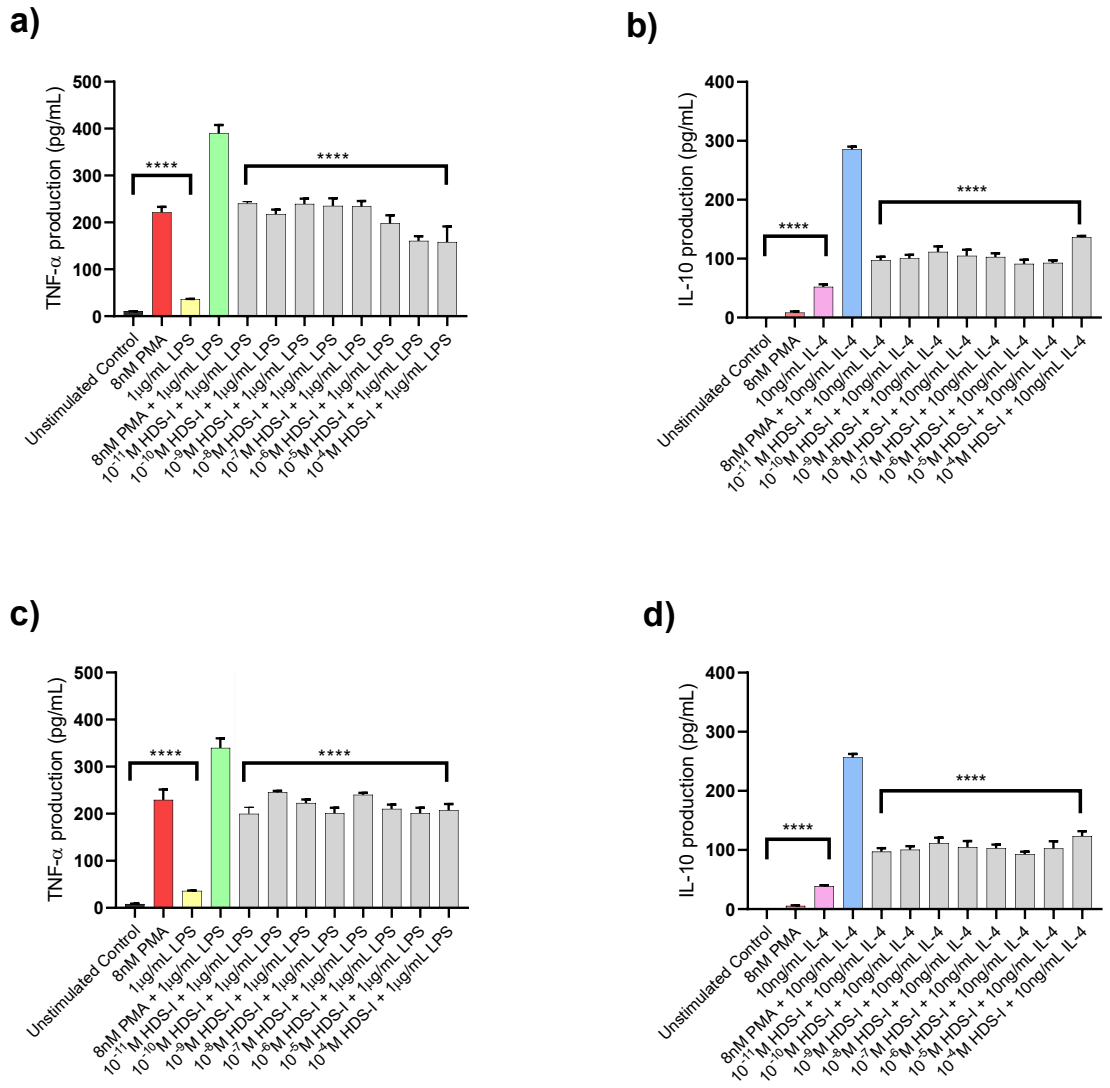


**Figure 6. 9*. Impact of HDS-I on TNF-α and IL-10 synthesis when given 2 h before LPS or IL-4.***

*The U937 (a,b) and THP-1 (c,d) were pre-incubated with 8 nM PMA for 48 h (followed by 72 h rest). Cells were treated with HDS-I at concentrations of $10^{-11}$ M to $10^{-4}$ M for 2 hour prior to 1 µg/mL LPS and 10 ng/mL IL-4 treatment for 6 h. LPS-induced or IL-4 macrophages were considered as a control to compare HDS-I + PMA macrophages TNF-α and IL-10 production. ANOVA followed by Dunnett's Test, mean ± SEM (n=3), ****=p<0.0001 vs. PMA+LPS/IL-4. TNF-α and IL-10 production was assessed by ELISA.*

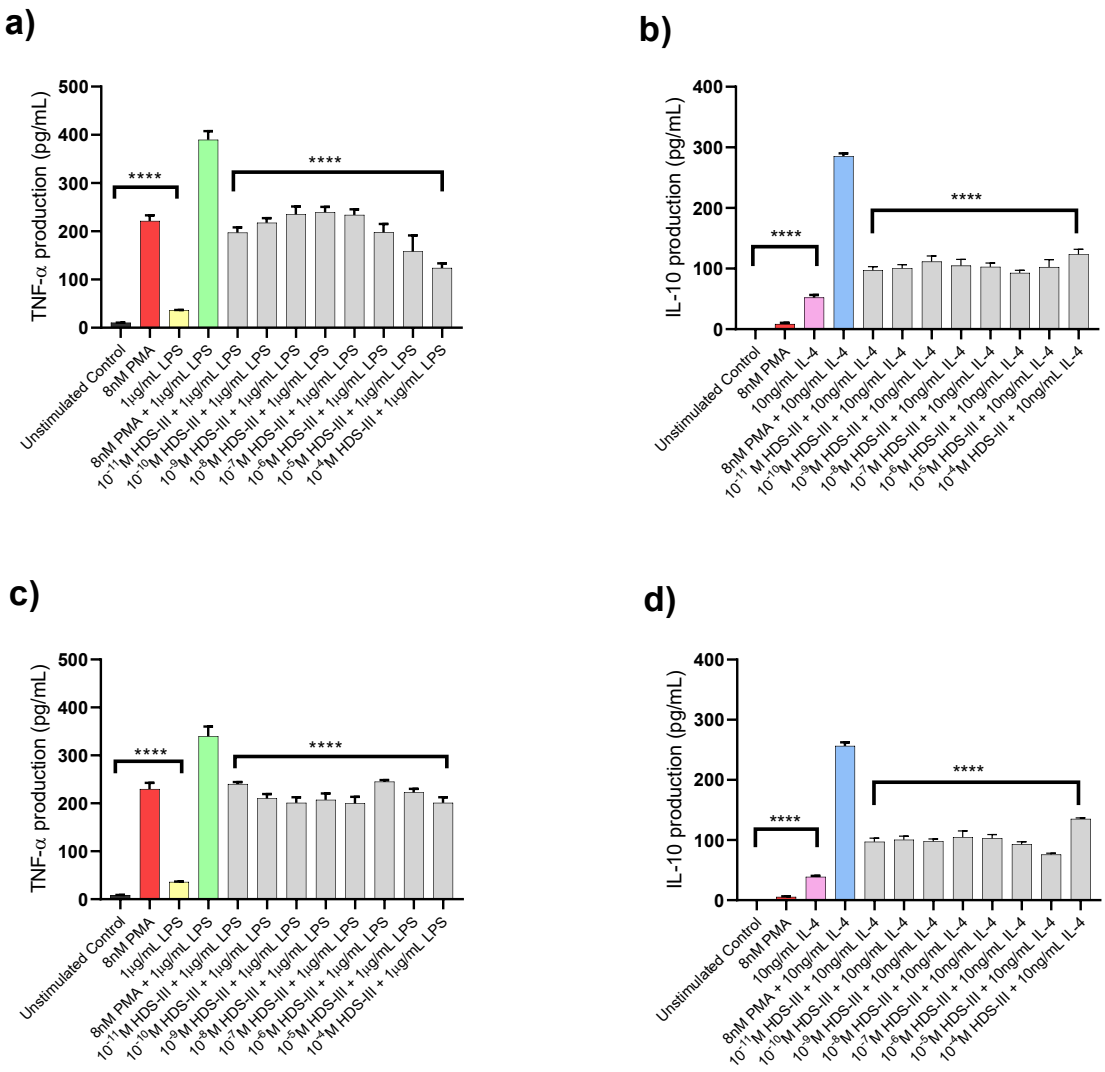


**Figure 6. 10*. Impact of HDS-III on TNF-α and IL-10 synthesis when given 2 h before LPS or IL-4.***

*The U937 (a,b) and THP-1 (c,d) were pre-incubated with 8 nM PMA for 48 h (followed by 72 h rest). Cells were treated with HDS-III at concentrations of $10^{-11}$ M to $10^{-4}$ M for 2 hour prior 1 µg/mL LPS and 10 ng/mL IL-4 treatment for 6 h. LPS-induced or IL-4 macrophages were considered as a control to compare HDS-III + PMA macrophages TNF-α and IL-10 production. ANOVA followed by Dunnett's Test, mean ± SEM (n=3), ****=p<0.0001 vs. PMA+LPS/IL-4. TNF-α and IL-10 production was assessed by ELISA.*

### 6.3.2 Sulphated disaccharides impact on CD206, CD163 and CD86

In this study, the impact of sulphated disaccharides on U937 cells was assessed for M2 (CD206 and CD163) and M1 (CD86) cell surface marker expression (Fig.6.11). In this study, CD206 and CD163 M2 cell surface markers were used because M2 macrophages express high levels of CD206 a mannose receptor C type 1 (MRC1), and CD163 (a scavenger receptor, a member of the cysteine-rich family, a monocyte/macrophage-specific membrane) surface markers (Duluc *et al.*, 2007 and Roszer *et al.,* 2015). As CD163 is considered a marker of alternatively activated or anti-inflammatory macrophages and CD206 is considered to be expressed on the M2 but not the M1 subtype, CD206 and CD163 were used as useful markers to identify the M2 phenotype. In this study, cells were treated with sulphated disaccharides, collected, stained (with CD206, CD163, and CD86 antibodies), and acquired and analysed by flow cytometry as described in materials and methods section 2.4 (Appendix Fig.106 to Appendix Fig.113).


**Figure 6. 11*. In vitro study design 4 - The impact of sulphated disaccharides on CD206, CD163 and CD86 expression on PMA differentiated U937 cells.***

*In this study, U937 ($2x10^5$ cells/mL per well) were cultured in 24-well tissue culture plates and were incubated with SOS, DOS, HDS-I and HDS-III at concentrations of $10^{-11}$ M-$10^{-4}$ M for 2 h prior to 8 nM PMA. After 48 h PMA stimulus, the non-adherent cells were removed from wells and discarded. The adherent cells were washed twice with cold 1X PBS and were rested in fresh PMA-free RPMI-1640 supplemented media for 72 h incubation. Subsequently, the cells were washed twice in 1X PBS, collected using 0.25% EDTA/cell scrapers and cells were re-suspended in 1X PBS, counted and stained for M2 (CD206, CD163) and M1 (CD86) cell surface markers. LPS or IL-4 was used as controls to test the model (Appendix Fig.106).*

In this study, PMA-induced M0 macrophages were considered as control it was observed that PMA-induced U937 M0 cells were found to be more $CD206^+$, $CD163^+$ compared to unstimulated control monocyte cells, IL-4-stimulated monocyte cells and less positive compared to PMA + IL-4 polarized M2 cells. In addition, PMA-stimulated U937 M0 cells were more $CD86^+$ compared to unstimulated control monocyte cells and LPS-stimulated monocyte cells. However, PMA-stimulated M0 cells were less $CD86^+$ compared to PMA + LPS-polarized M1 (Fig.6.12-Fig.6.15).

SOS + PMA-stimulated U937 cells expressed more $CD206^+$ (Fig.6.12a), $CD163^+$ (Fig.6.12c) cells compared to PMA stimulated cells. In addition, SOS + PMA cells were less $CD86^+$ (Fig.6.12e) compared to PMA-stimulated cells. There was no significant difference between DOS + PMA-stimulated U937 cells and PMA-stimulated $CD206^+$ (Fig.6.13a). DOS + PMA-stimulated U937 cells were less $CD163^+$ (Fig.6.13c) and $CD86^+$ (Fig.6.13e) compared to PMA-stimulated cells.

HDS-I + PMA-stimulated U937 cells were more $CD206^+$ (except at concentrations of $10^{-11}$ M and $10^{-8}$ M) compared to PMA-stimulated cells (Fig.6.14a). At concentration of $10^{-6}$ M HDS-I + PMA-stimulated cells were more $CD163^+$ (Fig.6.14c) and $CD86^+$ (Fig.6.14e) compared to PMA-stimulated. HDS-III + PMA-stimulated U937 cells expressed more $CD206^+$ (Fig.6.15a), $CD86^+$ (Fig.6.15e) and less $CD163^+$ (Fig.6.15c) cells compared to PMA-stimulated cells.

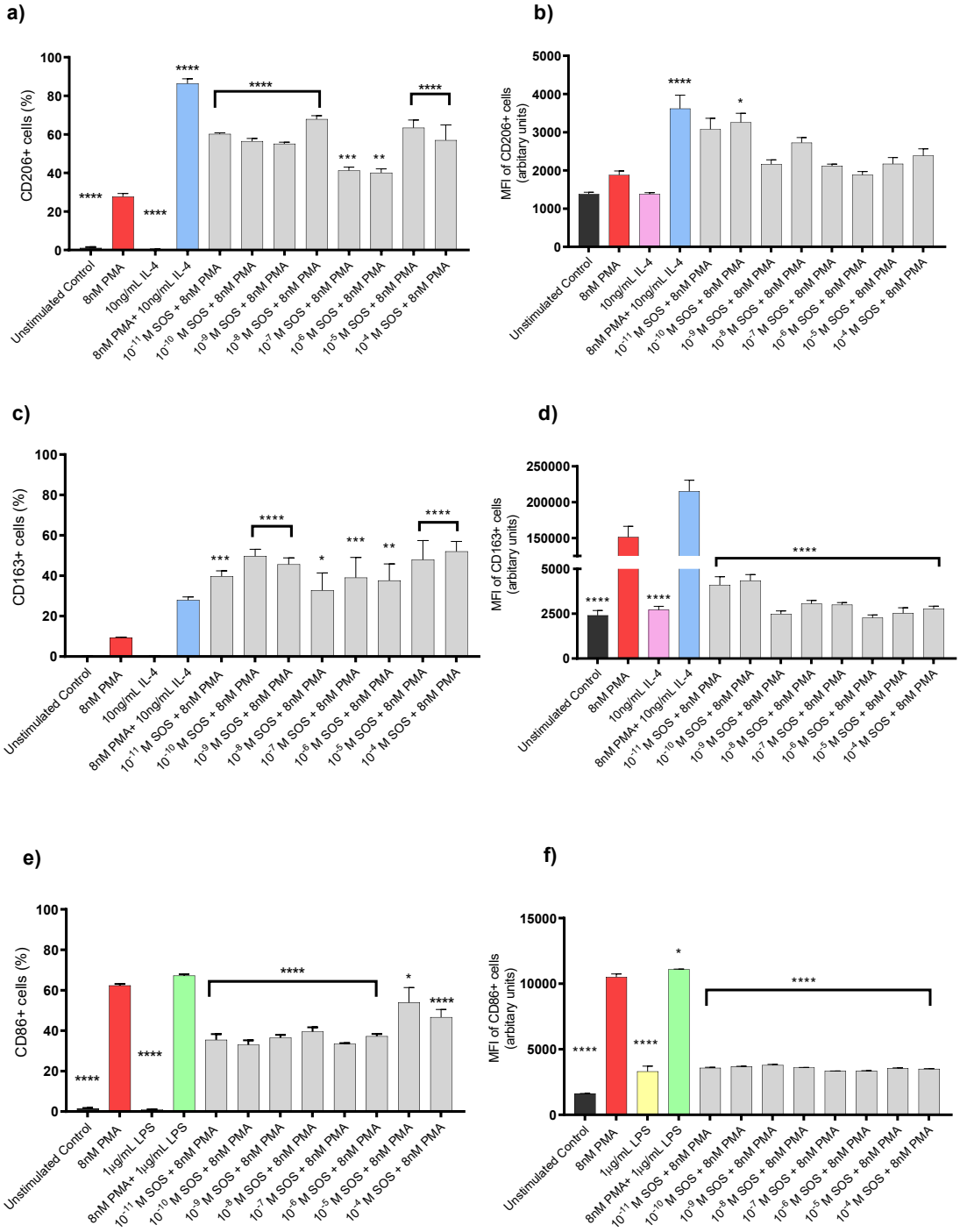


**Figure 6. 12.** ***SOS stimulated CD206, CD163 and inhibited CD86 expression in PMA-induced U937 cells.***

*Data are presented as the percentage of positive cells for marker and mean fluorescence intensity. Bar graphs represents (a, b) CD206⁺% cells, MFI, (c, d) CD163⁺% cells, MFI*

*and (e, f) $CD86^+$% cells, MFI by U937 cells, as assessed by FACS. U937 cells were pre-treated with SOS at a concentration of $10^{-11}$ to $10^{-4}$ M 2 h before with 8 nM PMA for 48 h. After 48 h PMA stimulus, the PMA -containing media was removed; cells were washed twice with cold PBS and rested in fresh PMA-free RPMI-1640 media for a further 72 h. LPS (1 μg/mL) and IL-4 (10ng/mL) were used as controls to test the model. *=p<0.05, **=p<0.01, ***=p<0.001, ****=p<0.0001 vs. PMA control, ANOVA followed by post hoc Dunnett's test, mean ± SEM (n=3).*

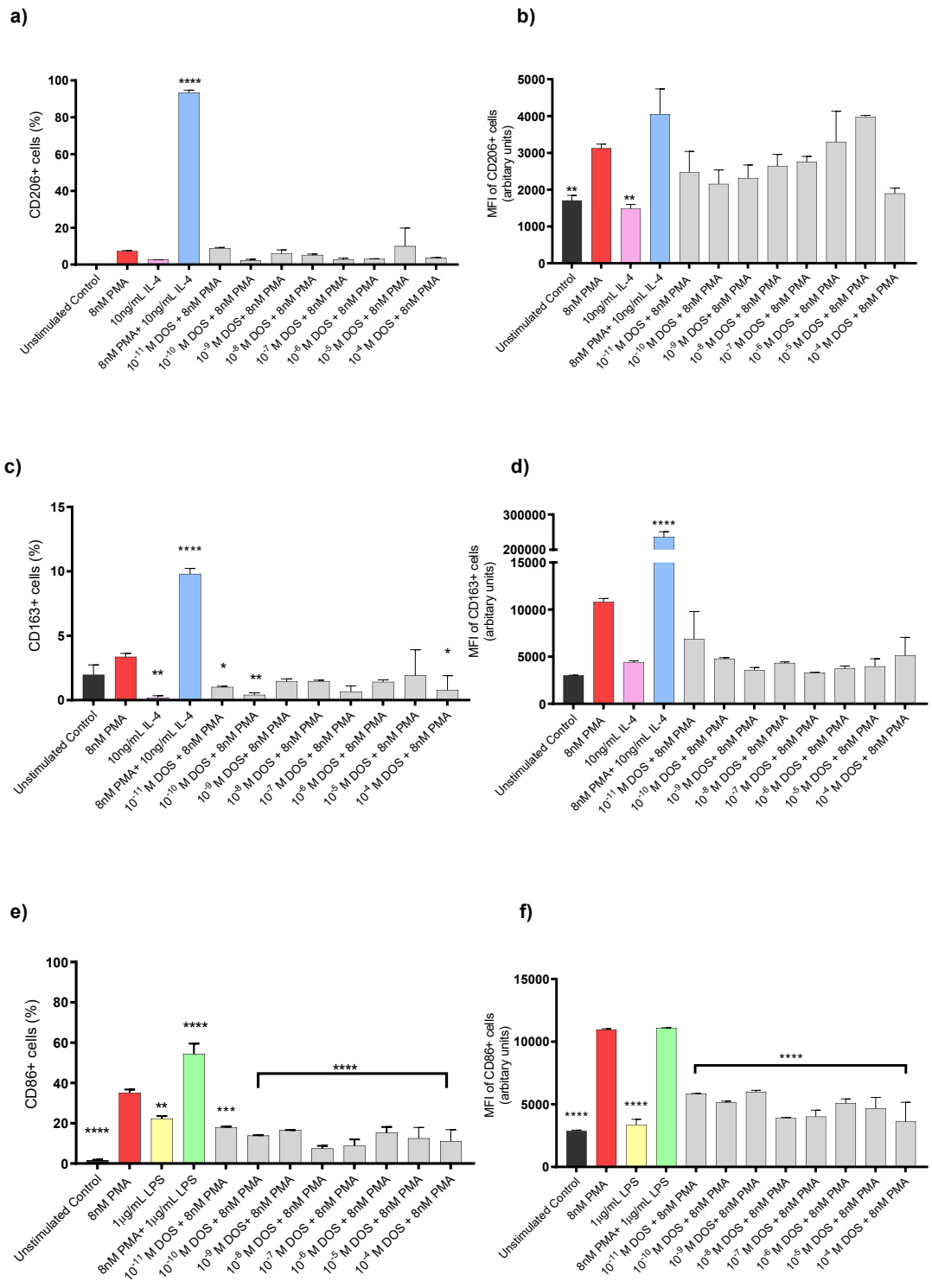


**Figure 6. 13.** ***DOS impact on CD206, CD163 and CD86 expression in PMA-induced U937 cells.***

*Data are presented as the percentage of positive cells for marker and mean fluorescence intensity. Bar graphs represents (a, b) $CD206^{+}$% cells, MFI, (c, d) $CD163^{+}$% cells, MFI and (e, f) $CD86^{+}$% cells, MFI by U937 cells, as assessed by FACS. U937 cells were pre-treated with DOS at a concentration of $10^{-11}$ to $10^{-4}$ M 2 h before with 8 nM PMA for 48 h. After 48 h PMA stimulus, the PMA -containing media was removed; cells were washed twice with cold PBS and rested in fresh PMA-free RPMI-1640 media for a further 72 h. LPS (1 µg/mL) and IL-4 (10ng/mL) were used as controls to test the model. *=p<0.05, **=p<0.01, ***=p<0.001, ****=p<0.0001 vs. PMA control, ANOVA followed by post hoc Dunnett's test, mean ± SEM (n=3).*

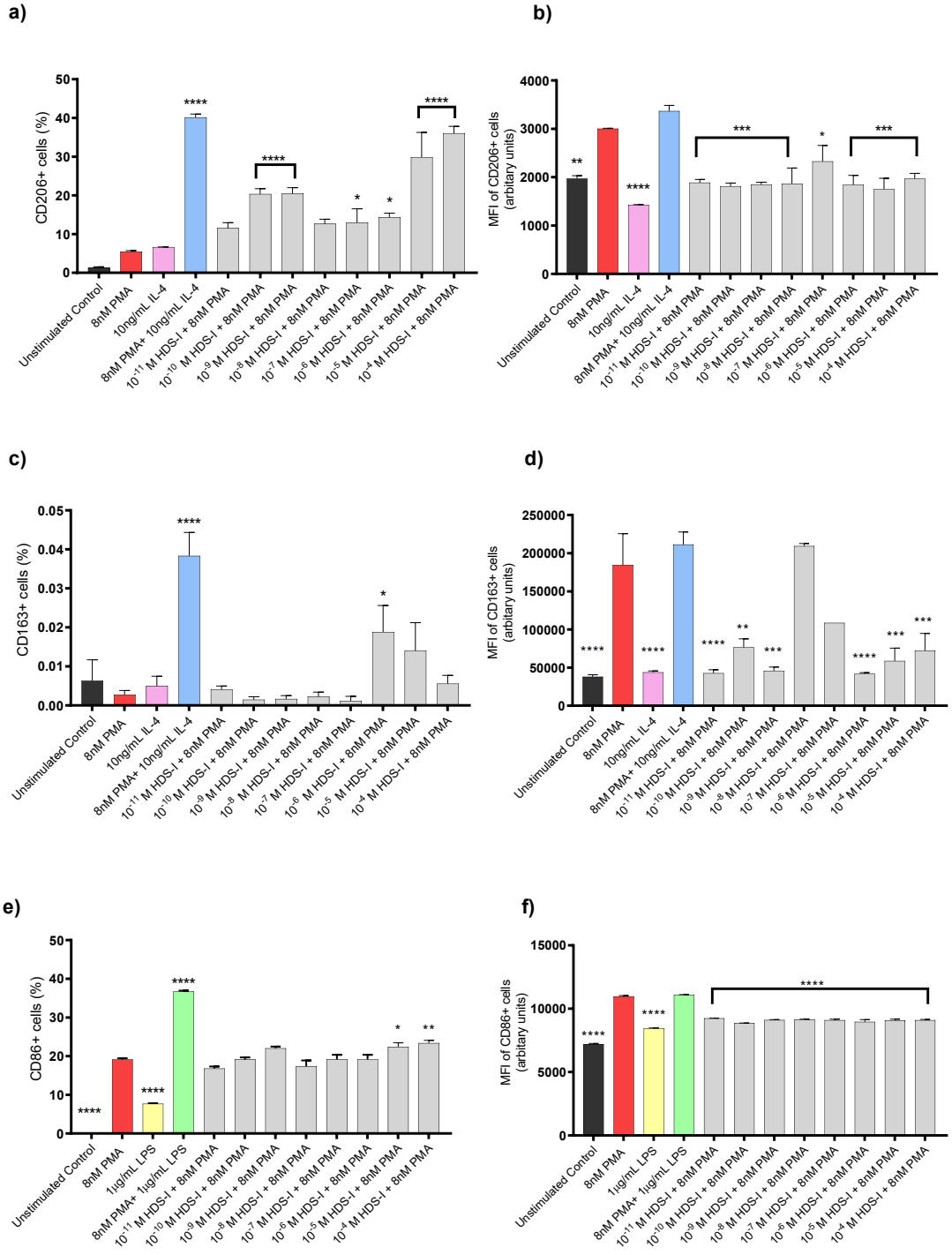


**Figure 6. 14*. HDS-I impact on CD206, CD163 and CD86 expression in PMA-induced U937 cells.***

*Data are presented as the percentage of positive cells for marker and mean fluorescence intensity. Bar graphs represents (a, b) CD206⁺% cells, MFI, (c, d) CD163⁺% cells, MFI*

*and (e, f) $CD86^+$% cells, MFI by U937 cells, as assessed by FACS. U937 cells were pre-treated with HDS-I at a concentration of $10^{-11}$ to $10^{-4}$ M 2 h before with 8 nM PMA for 48 h. After 48 h PMA stimulus, the PMA -containing media was removed; cells were washed twice with cold PBS and rested in fresh PMA-free RPMI-1640 media for a further 72 h. LPS (1 µg/mL) and IL-4 (10ng/mL) were used as controls to test the model. *=p<0.05, **=p<0.01, ***=p<0.001, ****=p<0.0001 vs. PMA control, Dunnett's test, mean ± SEM (n=3).*

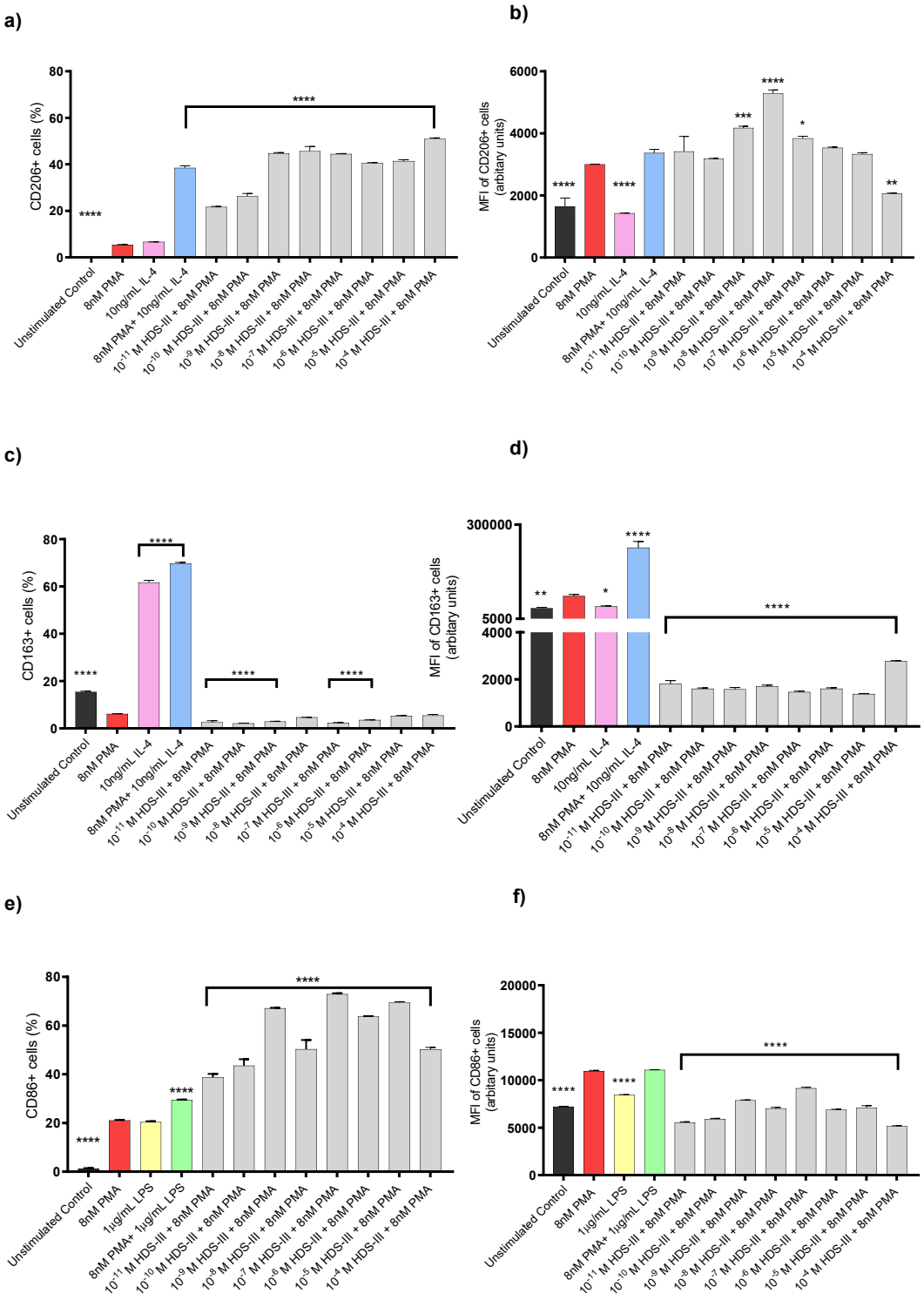


**Figure 6. 15*. HDS-III impact on CD206, CD163 and CD86 expression in PMA-induced U937 cells.***

*Data are presented as the percentage of positive cells for marker and mean fluorescence intensity. Bar graphs represents (a, b) $CD206^{+}$% cells, MFI, (c, d) $CD163^{+}$% cells, MFI and (e, f) $CD86^{+}$% cells, MFI by U937 cells, as assessed by FACS. U937 cells were pre-treated with HDS-III at a concentration of $10^{-11}$ to $10^{-4}$ M 2 h before with 8 nM PMA for 48 h. After 48 h PMA stimulus, the PMA -containing media was removed; cells were washed twice with cold PBS and rested in fresh PMA-free RPMI-1640 media for a further 72 h. LPS (1 µg/mL) and IL-4 (10ng/mL) were used as controls to test the model. *=p<0.05, **=p<0.01, ***=p<0.001, ****=p<0.0001 vs. PMA control, Dunnett's test, mean ± SEM (n=3).*

### 6.3.3 Gene expression analysis of PMA-induced M1 and M2 macrophages by Reverse transcriptase PCR

In addition, to study the expression of p21, CD14, CD200R and Arginase-1 at the transcriptional level, cell density of 2 x $10^5$ U937 were grown in monolayer in 6-well plates. U937 cells were pre-incubated with SOS and DOS at concentrations of $10^{-11}$ to $10^{-4}$ M for 2 h prior addition of 8 nM PMA at 48 h.

Total RNA was isolated by using Trizol reagent as described in the materials and methods section 2.9 and reverse transcribed for gene expression of CD14, CD206, CD200R, Arginase 1, $p21^{WAF1/Cip1}$ and cyclin D1 and using RT-PCR analysis as described in the materials and methods section 2.9. β-actin control was used as a control to normalise the samples. Bands intensity was measured using ImageJ.

Stimulation with PMA resulted in high expression of p21 and CD14 compared to unstimulated control U937 cells (Fig.6.16b,c- Fig.6.17b,c). SOS up-regulated CD200R (Fig.6.16d) and Arginase-1 (Fig.6.16e) gene expression in PMA-stimulated U937 cells at 48 h. But did not inhibit PMA stimulated p21 (Fig.6.16b) and CD14 (Fig.6.16c) gene expression. DOS in the presence of PMA down-regulated expression of p21 in PMA-stimulated U937 cells at concentrations of $10^{-11}$ M, $10^{-8}$ M to $10^{-4}$ M (Fig.6.17b) and down-regulated CD14 at concentrations of $10^{-11}$ M, $10^{-7}$ M to $10^{-4}$ M (Fig.6.17c). However, DOS up-regulated Arginase-1 (Fig.6.17e) gene expression at a concentration of $10^{-4}$ M. No inhibition was seen in the expression of CD200R (Fig.6.17d).

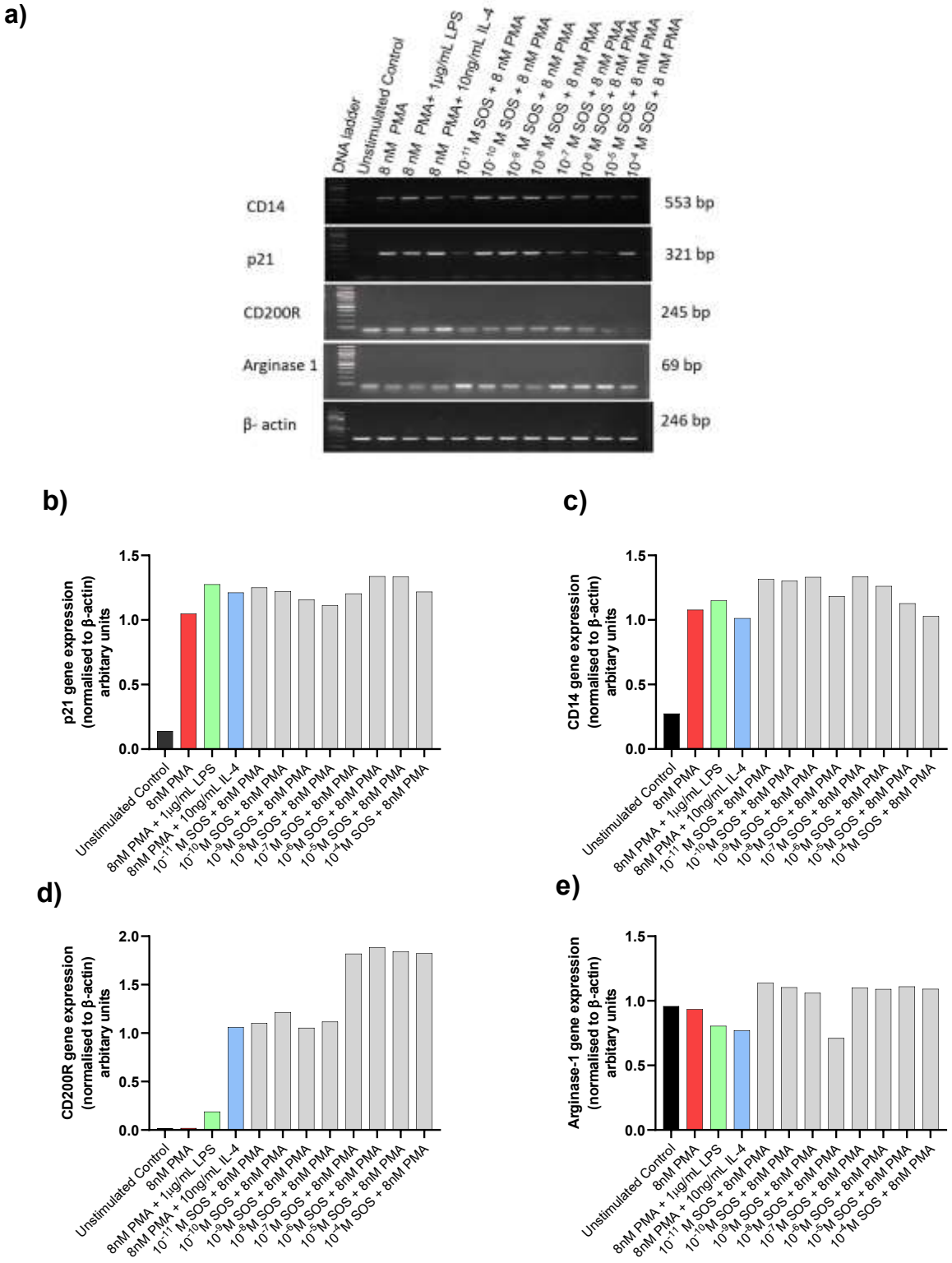


**Figure 6. 16*. SOS impact on PMA-induced gene expression.***

*(a) Data shown are representative agarose gel electrophoresis (2% agarose) of PCR amplified products using species-specific PCR primer sets. Normalised RNA expression of (b) p21, (c) CD14, (d) CD200R and (e) Arginase-1. Gene expression of PMA differentiated U937 differentiated assessed by RT-PCR. The cells were stimulated with PMA (8nM) for 48 hours and stimulated with LPS or IL-4, or SOS ($10^{-11}$M – $10^{-4}$M). The U937 cells were pre-treated with SOS for 2 h before PMA stimulation. Representative of two independent experiments. Quantification of the protein bands was performed by densitometry Image J and the signals were then normalised to β control, and the results are expressed in arbitrary units.*

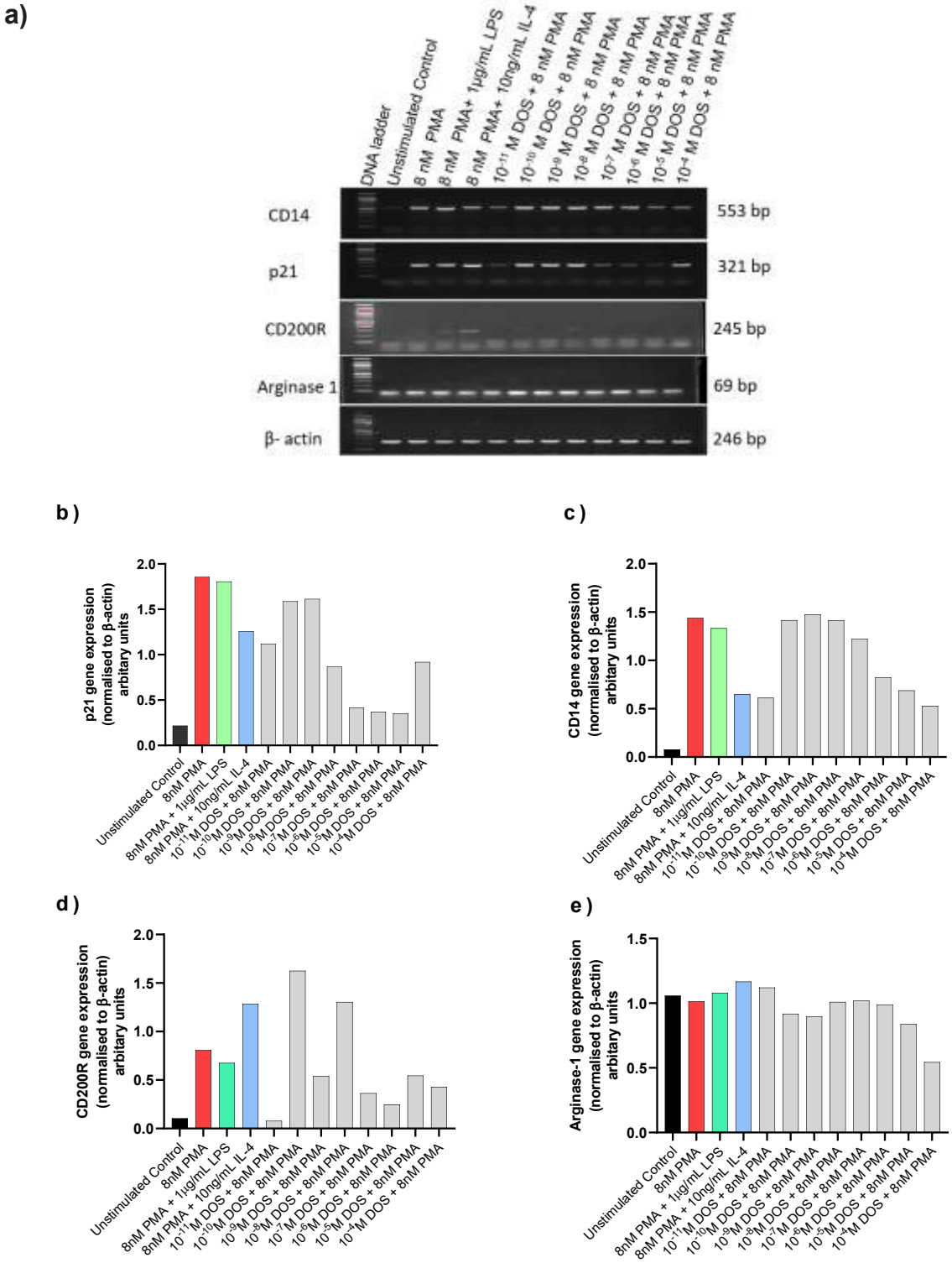


**Figure 6. 17.** ***DOS impact on PMA-induced gene expression.***

*(a) Data shown are representative agarose gel electrophoresis (2% agarose) of PCR amplified products using species-specific PCR primer sets. Normalised RNA expression of (b) p21, (c) CD14, (d) CD200R and (e) Arginase-1. Gene expression of PMA differentiated U937 differentiated assessed by RT-PCR. The cells were stimulated with PMA (8nM) for 48 hours and stimulated with LPS or IL-4, or DOS ($10^{-11}$M – $10^{-4}$M). The U937 cells were pre-treated with DOS for 2 h before PMA stimulation. Representative of two independent experiments. Quantification of the protein bands was performed by densitometry Image J and the signals were then normalised to β control, and the results are expressed in arbitrary units.*

## 6.4 Discussion

As outlined in chapter 1, macrophages are key sources of pro-inflammatory TNF-α and anti-inflammatory IL-10 cytokines production that play an important role in the progression and resolution of inflammation. In this chapter, it was asked whether inhibition of PMA-induced monocyte-macrophages by sulphated disaccharides is correlated with cytokines production. This study investigated the impact of sulphated disaccharide compounds on macrophage polarization from M0 to M1 and M2 and M1 to M2 phenotypes using TNF-α or IL-10 cytokine production, surface marker and gene expression. The optimal concentrations of LPS and IL-4 were determined at different time points (Appendix Fig.105 to Appendix Fig.106).

Mantovani *et al.,* (2002), described M1 and M2 phenotypes as extremes of a continuum of functional states. A study by Biswas *et* al., (2011) stated that in sites of chronic inflammation where a tumour may develop, macrophages have an M1 phenotype. M1 macrophages are cytotoxic for pathogens and tumour cells. Van Ginderachter *et al.,* (2006) reported that their tumoricidal activity was related to their ability to secrete reactive nitrogen and oxygen species and pro-inflammatory cytokines. Several studies reported that macrophages exhibit predominantly an M2-like phenotype in malignant tumours (Mantovani *et al*., 2002; Biswas *et al*., 2006 and Saccani *et al*., 2006).

In this chapter's results, the *in vitro* monocyte-macrophage differentiation model demonstrated that PMA alone induced TNF-α and IL-10 production compared to unstimulated control cells, but PMA + LPS or PMA + IL-4 induced expression to a much greater extent indicating differentiation from M0 to M1, and from M0 to M2 macrophages respectively. Sulphated disaccharides inhibited PMA driven TNF-α production and up-regulated IL-10 production in a concentration-dependent manner, and inhibited LPS stimulated TNF-α along with IL-4 induced IL-10.

The increased CD14 expression in PMA-differentiated cells (Chapter 3) partly explains why PMA differentiated M0 cells respond well to LPS. However, the addition of sulphated disaccharides after PMA stimulation resulted in lower maximal inhibition of both cytokines, suggesting different mechanisms of action between the two protocols. Sulphated

disaccharides decreased PMA-induced M1 TNF-α cytokine production and decreased IL-10 production when given with IL-4. Sulphated disaccharides increased TNF-α and reduced IL-10 in M0 cells when given before differentiation. They thus skewed the M0 into behaving more like M1 cells.

Lees *et al*., (2008), reported inhibition of phytohaemagglututinin (PHA)-stimulated IL-1α, IL-1β, IL-2, IL-4, IL-5, IL-6, IL-17, IL-13, IFNy, GCSF, GM-CSF and TNF-α synthesis by 0.01 μM SOS in human whole blood. *In vitro,* PMA (5 μg/mL) simulated U937 human macrophage TNF-α synthesis was also inhibited by SOS at the concentrations of 0.10 μM to 100 μM. In addition, Lees *et al*., (2008), investigated the anti-TNF and anti-rheumatic activity of DOS (as outlined in chapter 1). DOS hydrolyses to monoglucosylamine sulphate and glucose sulphate, which is prevented by N-acetylation (NAcdiGA). The results of this study reported that TNF synthesis and 24 h antigen-induced arthritis were inhibited by diosamine™ (diglucopyranosylamine, 1 μM). Diosamine™ at 100mg/kg reduced antigen-induced arthritis when administered intravenously ($p<0.05$) and intraperitoneal ($p<0.05$), but is hydrolysed by oral administration (non-significant). Polysulphated diosamine™ is stabilised by N-acetylation, to give DOS. TNF synthesis was potently inhibited by both diosamine™ and DOS (IC50 < 0.1 μM). DOS (100mg/kg) inhibited antigen-induced arthritis when given by administrated orally. DOS with lower degrees of sulphation inhibited the development of mouse collagen-induced arthritis as assessed by clinical score. A study by Lees *et al*., (2008), proposed that sulphated n-acetyl di-glucopyranosylamine represent a new class of heparinoid that are potent inhibitors of TNF synthesis and possess oral anti-rheumatic activity. DOS was found to be less potent compared to SOS when given orally (Fig.1.20 and Fig.1.21 in Chapter 1).

In addition, in this chapter, the impact of sulphated disaccharides on M2 macrophages was also assessed. M1 macrophages were identified as $CD86^+$ and M2 macrophages were identified as $CD206^+$ and $CD163^+$ by flow cytometry. Sulphated disaccharides reduced PMA-induced $CD86^+$ M1 cells and up-regulated mannose receptor $CD206^+$ and scavenger receptor type A $CD163^+$ M2 cells, indicating polarization of M1 macrophages to M2 macrophages. Also, they revert PMA-induced M1 cells to the M2 phenotype.

However, SOS, DOS, HDS-I, and HDS-III showed different patterns (Fig.6.17). SOS, HDS-I and HDS-III enhanced the expression of CD206 more potently than DOS. Therefore, in future work, it would be interesting to assess these compounds structure in more detail as structural-functional mechanisms could be at play.

To assess the impact of PMA and sulphated disaccharides (SOS and DOS) on gene expression, in this study p21, CD14, CD200R, and Arginase-1 were used as M1 and M2 macrophages genes to characterise a gene expression in PMA-induced U937 cells. The results suggest that the differentiation of U937 cells was controlled by transcription factors and directed cells to M1 and M2 phenotypes (Fig.6.18).

Altogether, these results showed that M1 and M2 macrophages differentiated and polarized. The findings of this study suggest that sulphated disaccharides inhibitory action was not cell specific.

The results of this chapter suggest that inhibition of TNF-α production by sulphated disaccharides is correlated with inhibition of cell differentiation (chapter 4 and chapter 5). Sulphated disaccharides may inhibit PMA-induced monocyte-macrophage differentiation by inhibiting NF-κB activation, thereby reducing the number of M0 polarized M1 macrophages available to produce TNF-α, resulting in inhibition of pro-inflammatory TNF-α cytokine production. This also indicates that the low level of IL-10 production could be due to the reduced number of available macrophages to be polarized to M2 to produce IL-10.

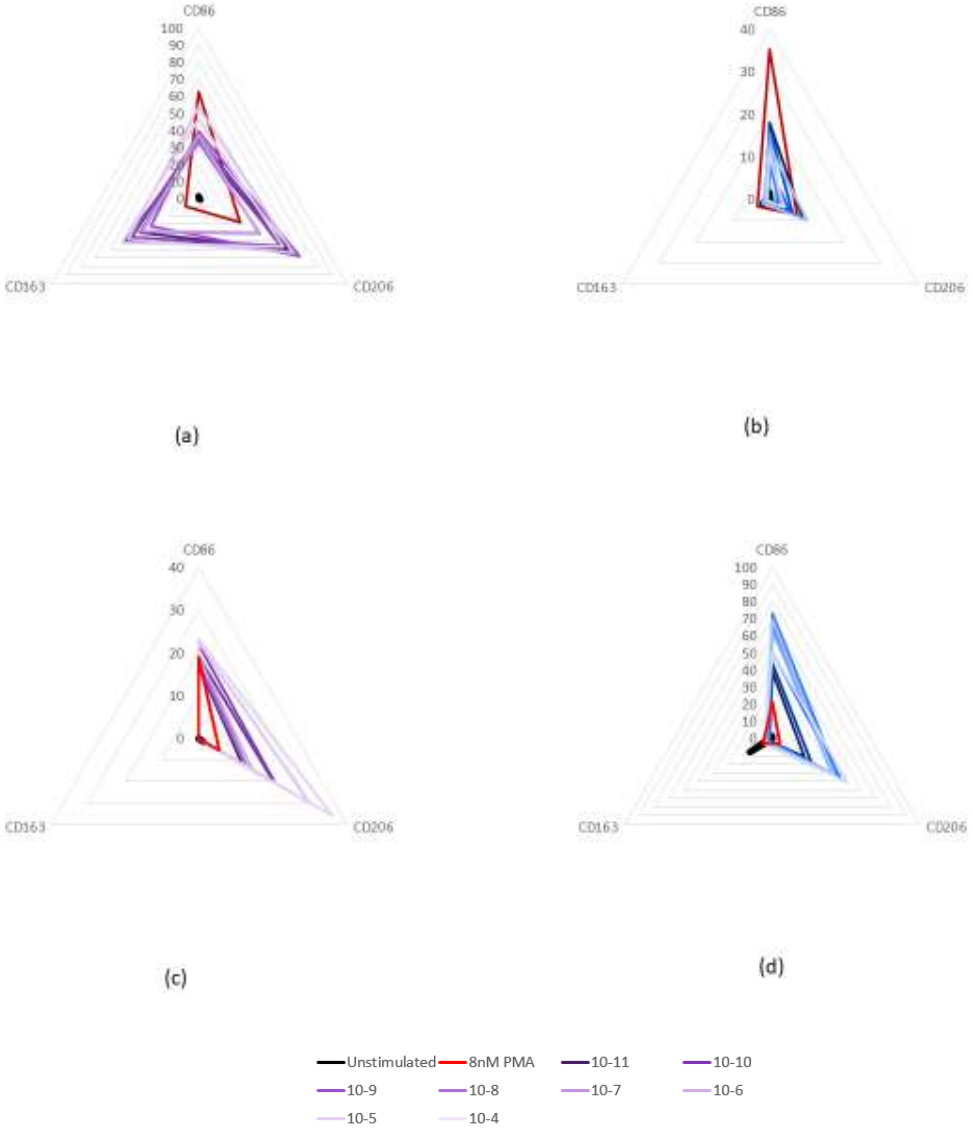


**Figure 6. 18.** ***Radar charts representing the summary of M1/M2 CD expression on PMA differentiated U937 cells in the presence of SOS (a), DOS (b), HDS-I (c), HDS-III (d) (findings of Fig.6.12 – Fig.6.15).***

*Sulphated disaccharides down-regulated PMA-induced cell surface markers percentage of positive U937 cells and their expression. Radar charts used for seeing which surface marker expression upregulated or downregulated within a dataset. Radar plots were used to plot CD206, CD163 and CD86 surface markers over sulphated disaccharide concentrations or MFI by giving an axis for each variable, and these axes were arranged radially around a central point and spaced equally. The data from a single observation*

*(average of triplicates) are plotted along each axis and connected to form a polygon. The grid lines were used to connect the axes and are used as a guideline to facilitate interpretation of the data.*

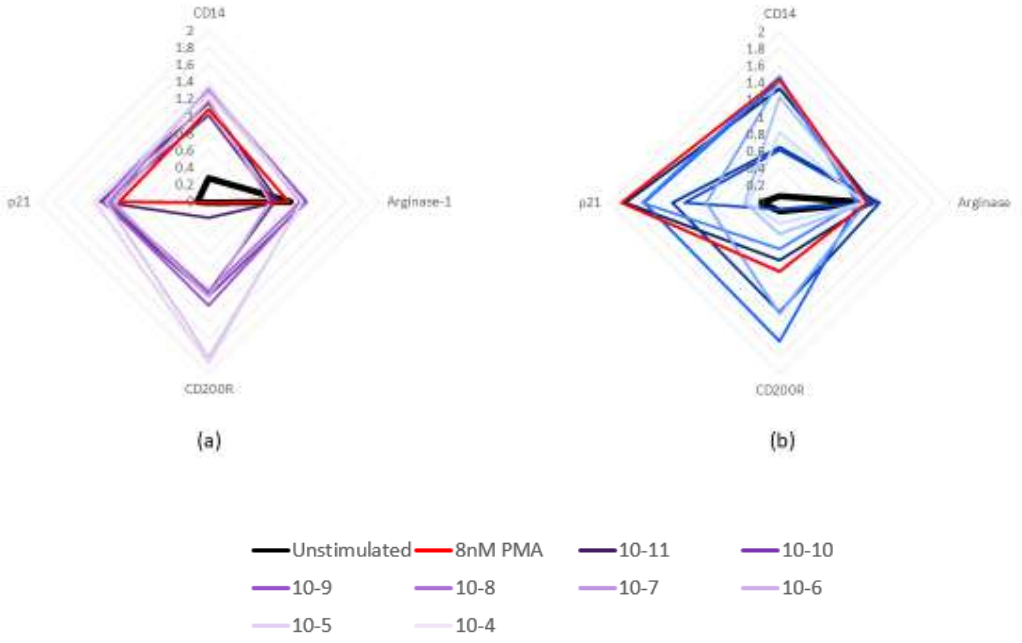


**Figure 6. 19*. Radar charts representing the summary of gene expression on PMA differentiated U937 cells in the presence of (a) SOS and (b) DOS (findings of Fig.6.16 – Fig.6.17).***

*Sulphated disaccharides down-regulated PMA-induced cell surface markers percentage of positive U937 cells and their expression. Radar charts used for seeing which surface marker expression upregulated or downregulated within a dataset. Radar plots were used to plot CD14, CD200R, Arginase-1 and p21 gene expression over sulphated disaccharide concentrations or MFI by giving an axis for each variable, and these axes were arranged radially around a central point and spaced equally. The data from a single observation (average of triplicates) are plotted along each axis and connected to form a polygon. The grid lines were used to connect the axes and are used as a guideline to facilitate interpretation of the data.*

## 6.5 Conclusion

The present study provides an in-depth understanding of PMA-induced macrophage polarization by sulphated disaccharides and confirms that inhibition of PMA-induced monocyte-macrophage differentiation lead to macrophage polarization. This shift from M0 to M2 and M1 to M2 phenotype by sulphated disaccharides confirmed that balance of pro-inflammatory and anti-inflammatory macrophages is required for inflammation resolution.

The down-regulation of TNF-α and up-regulation of IL-10 synthesis explains the anti-inflammatory effect of sulphated disaccharides on arthritis and hypersensitivity. Hence, the anti-inflammatory activity of sulphated disaccharides could be explained by its anti-adhesive activity (inhibition of cell adhesion).

The results of this chapter suggest that there is a possibility sulphated disaccharides could inhibit PMA-induced TNF-α production due to inhibition of NF-kB activation, which leads to reduced translocation of the p65-NF-kB subunit to the nucleus from the cytoplasm in activated U937 or THP-1 differentiated cells. Therefore, as future work, it would be interesting to assess sulphated disaccharides impact on NF-kB in the nucleus and cytoplasm.

The finding of this chapter indicates that degraded products of heparan sulphate have positive feedback on macrophage polarization and provide insight into sulphated disaccharides inhibitory mechanism to enable the design of therapeutic interventions for chronic inflammatory diseases.

# CHAPTER 7: FINAL DISCUSSION & FUTURE WORK

## 7.1 Final discussion

### 7.1.1 Can sulphated disaccharides inhibit monocyte-macrophage differentiation?

Sulphated disaccharides are generated during inflammation by heparanase enzyme activity and are located within inflamed (Cahalon *et al.,* 1997). Lees *et al.*, (2009) reported that orally active sulphated disaccharides may provide the basis for new oral anti-rheumatic therapeutics. These compounds have been suggested to play an important role in the inhibition of arthritis and hypersensitivity *in vitro* models through an unknown mechanism. This research aimed to elucidate the molecular mechanism of these compounds by using an *in vitro* model of macrophage differentiation and function. Therefore, different experimental approaches were used to investigate the sulphated disaccharides mechanism as described in Chapter 2.

The findings of this study indicate that sulphate disaccharide compounds exhibit their inhibitory action even at very low concentrations especially the oligosulphated compounds acting at $10^{-11}$ M. In agreement with this study data, it has been previously reported by others that these compounds act at low concentrations demonstrating inhibitory effects in a concentration-dependent manner (Cahalon *et al,* 1997). Thus, suggesting a novel molecular mechanism for these as a new generation of small molecule inhibitors for the treatment of chronic inflammatory diseases.

The present study objectives and key findings were:

**1. To identify the impact of sulphated disaccharides on differentiated macrophage cell surface markers and whether this impact contributes to inhibition of surface markers expression outcome.**

**Findings:** Sulphated disaccharides inhibited PMA-induced human monocytes differentiation into macrophages *in vitro.* Sulphated disaccharides prevented U937 and THP-1 monocytes from developing morphological characteristics of the macrophage-like phenotype. This, in turn, leads to downregulation of adhesion cell surface marker

expression (CD11a & CD11b), as well as CD14, a marker of non-specific TLR immune function, and CD68, a marker of inflammatory macrophages. This study showed that sulphated disaccharides inhibited the induction of cell arrest in U937 and THP-1 cells by PMA at very low concentrations that do not affect cell viability or baseline metabolism. SOS potently inhibited the maturation of non-adherent cells to adherent macrophage-like cells. DOS mimicked SOS, preventing PMA induced differentiation to viable adherent cells.

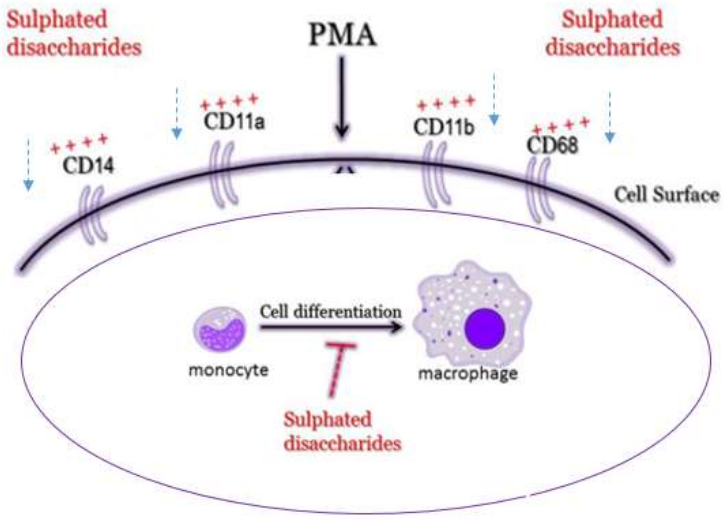


**Figure 7. 1*. Diagram representation for the surface markers expression outcome from targeting monocytes with sulphated disaccharides in vitro.***

*Targeting U937 and THP-1 monocyte cells in vitro with sulphated disaccharides inhibited PMA-induced cell surface markers expression (arrow indicate reduced surface markers expression) and inhibited PMA-induced cell differentiation.*

**2. To study the possibility of cell differentiation inhibition by targeting p38 and ERK1/2 MAPK signalling pathways with sulphated disaccharides.**

**Findings:** Sulphated disaccharides modulated intracellular signalling pathways in PMA-differentiated cells. The phosphorylation of p38 at Thr180 and Tyr182 was inhibited by SOS, DOS and HDS-I. The phosphorylation of ERK1/2 at Thr202 and Tyr204 of Erk1 and Thr185 and Tyr187 of Erk2 was inhibited by SOS, DOS, HDS-III and HDS-I.

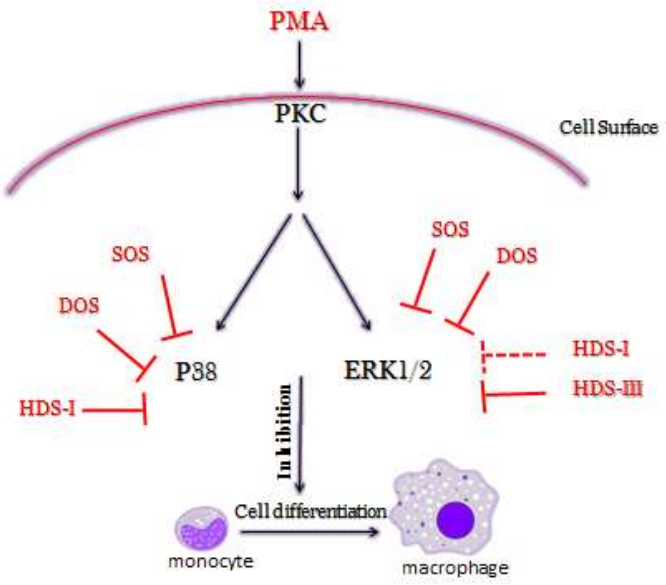


**Figure 7. 2.** ***Diagram representation for the p38 and ERK1/2 expression outcome from targeting monocytes with sulphated disaccharides in vitro.***

*Targeting U937 monocyte cells in vitro with sulphated disaccharides inhibited PMA-induced p38 and ERK1/2 expression. The results indicated that inhibitory action of SOS and DOS is p38 and ERK1/2 dependent, HDS-I is p38 and partial ERK1/2, HDS-III is ERK1/2 dependent.*

### 3. To study the impact of sulphated disaccharides on intracellular calcium mobilisation.

**Findings:** Sulphated disaccharides inhibited PMA-induced calcium mobilisation in human monocytes. The results suggest that sulphated disaccharides may penetrate the cell within 10 minutes pre-incubation period and directly interacts with G-protein coupled receptors which regulate mobilisation of calcium and thus affect PKC downstream signalling pathways. SOS, DOS, HDS-I and HDS-III inhibited PMA-induced intracellular $Ca^{2+}$ in a similar inhibition pattern. This study suggests that the concentration of intracellular calcium is critical to the regulation of cell differentiation.

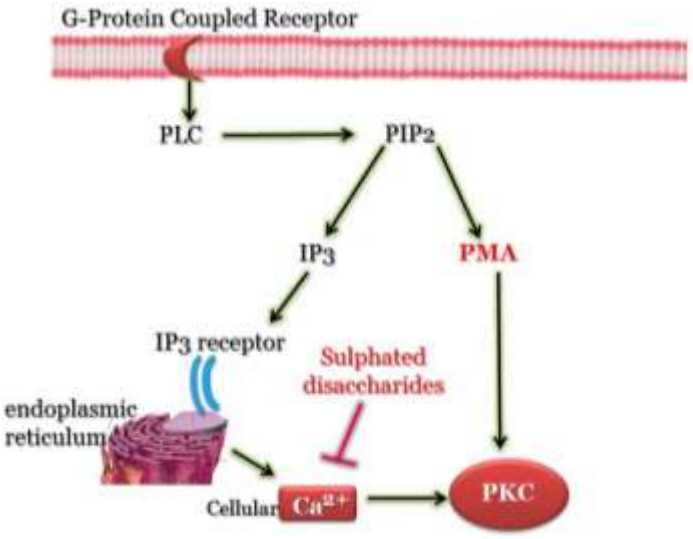


**Figure 7. 3*. Diagram representation for the calcium mobilisation outcome from targeting calcium mobilisation with sulphated disaccharide.***

*Targeting U937 and THP-1 cells with sulphated disaccharides inhibit PMA-induced calcium mobilisation when given 10 minutes before PMA.*

**4. To determine whether sulphated disaccharides induce a phenotypic switch of differentiated macrophage (M0) phenotype into activated pro-inflammatory (M1) phenotype macrophage or anti-inflammatory (M2) phenotype macrophage or switch from M1 phenotype into M2 phenotype.**

**Findings:** Sulphated disaccharides affected phenotypic and functional features of PMA-induced macrophages. They downregulated M1 macrophage TNF-α production and surface marker CD86 and up-regulated IL-10 production and macrophage surface marker CD206. Based on results it has been suggested that the ability of sulphated disaccharides to inhibit cell differentiation might result from their direct interaction with the cytokines, thus affecting the TNF-α and IL-10 production. The findings hypothesised that sulphate disaccharides are involved in macrophage skewing from differentiated macrophage to an anti-inflammatory macrophage phenotype. The inhibition of CD14 expression of those cells that have adhered will also affect LPS responses, CD14 being a co-receptor for TLR-4, which is the receptor mediating LPS activation of the MAPK pathway that leads to TNFα action and release. Overall findings indicate that sulphated disaccharides polarize PMA-induced inflammatory macrophage to an anti-inflammatory phenotype through inhibition of monocyte-macrophage differentiation.

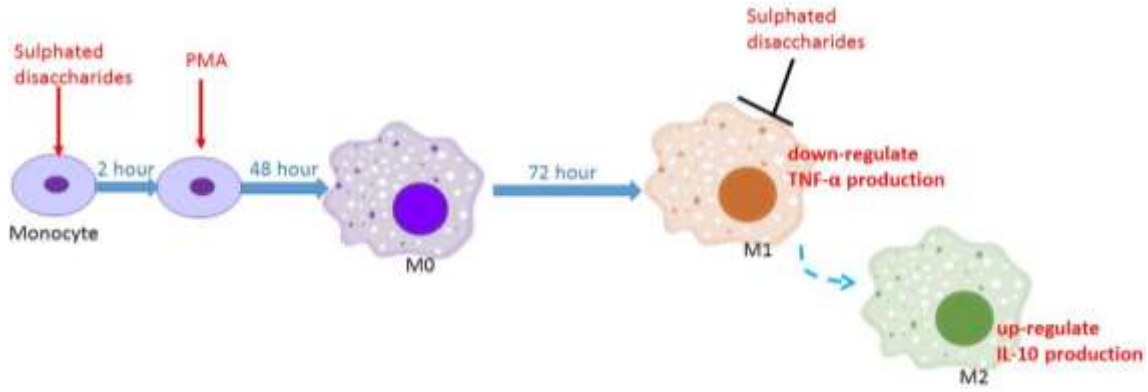


**Figure 7. 4.** ***Diagram representation for the cytokine outcome from targeting monocytes with sulphated disaccharides in vitro.***

*Treatment of U937 and THP-1 cells in vitro with sulphated disaccharides inhibit TNF-α production from PMA-induced macrophages and polarize pro-inflammatory macrophages to anti-inflammatory macrophages.*

As Shriver *et al*., (2012) suggest that due to the structural diversity exhibited by heparin and heparan sulphate molecules, it is believed that possibly unique (in some cases) or most likely an ensemble of structural motifs might be responsible for different interactions. Therefore, it has become increasingly important to interpret the structural information represented in sulphated disaccharides to enable a better understanding of their structure-function relationships. Sulphated disaccharides inhibited cell differentiation and with a maximal inhibition seen at $10^{-11}$ M. The results indicate that a single sulphate on each sugar is required for potent activity, as HDS-IIIS containing one sulphate group resulted in a great reduction in PMA-induced activity. Based on a different pattern of responses of SOS, DOS, HDS-I and HDS-III this has been concluded that the specificity of sulphated disaccharides inhibitory potential is related to the distribution and conformation of the backbone of iduronic acid or glucuronic acid and a glucosamine moieties, as well as the position of glycosidic -O-linkage sulphation of the glycosyl and furanyl moieties and -N-linkage sulphate groups in glucuronic acid and glucosamine moieties. A specific sequence of sulphated disaccharides can favour the interaction of these molecules with intracellular proteins and not with others. In addition, DOS could inhibit intracellular protein activity through the N-acetylated region of DOS, which is rich in β-D-GlcA residues.

DiGa (diosamine™) is a low potency inhibitor of β-glucosidase (Kolorova *et al*, 1995), and as such may inhibit other glycosylation enzymes that may affect immune responses. However, N-acetylation of di-Ga renders this molecule inactive, but still inhibits TNFα synthesis. In addition, di-Ga has two mannose-binding motifs, but such motifs of mono- and disaccharides are only active in the high μMolar, low mMolar range. The inhibition of TNF synthesis occurs at much lower concentrations. TNF inhibition explains the anti-keratitic activity of di-Ga (Roberts *et al.,* 1990). Sulphation thus dramatically enhances potency of this scaffold. As regards SOS, sulphated carbohydrates are highly anionic and thus bind a wide variety of cationic proteins (Jones et al., 2004). SOS or heparin di-saccharides interact with RANTES, bFGF, or CXCL2 for example, each of which will affect the inflammatory disease. RANTES inhibition for example prevents adjuvant-induced arthritis. However, these widespread actions for sulphated disaccharides, including SOS, often occur at concentrations higher than those reported here for TNF

synthesis inhibition (<0.1μM). Orally administered sulphated heparinoid disaccharides (Lider, 1995) are also anti-rheumatic and inhibit TNF synthesis. In addition, they also inhibit T-cell adhesion to CXCL12 (Hecht *et al,* 2004) and MIP1α. This indicates that these effects may involve NFkB inhibition and Giα protein activation (Hecht *et al.,* 2004). It should be noted that cell membranes are impermeable to highly charged molecules such as the sulphated sugar (Yang & Hinner 2015), so if they do become available intracellularly, it is likely to be via an active process. However, despite a wide variety of molecules being substrate for transporters, sulphated disaccharides are not reported to be among them. Indeed, being highly charged these molecules do not conform to the Lipinsky Rule of 5 that predicts cell permeability. The fact that DOS and SOS are orally active *in vivo*, and that SOS is absorbed, demonstrates that there is an ability to cross membranes such as the gut epithelium.

In this context, Cahalon *et al.,* (1997), reported that the inhibitory action of sulphate disaccharides is dependent on the structural-functional activity relationship between synthetic and natural sulphate disaccharides. Little is known of the mechanism of action of the non-sulphated scaffold/backbone, DiGa, or its anti-rheumatic activity. Considering the structural-functional relationship of these compounds it can be proposed that the sulphur group provides a molecular determinant for enhanced activity, as the attachment of the sulphur group on the glycosidic -O-linkage or -N-linkage rings of such molecules is important for their ability to inhibit intracellular $Ca^{2+}$ mobilisation to inhibit p38, ERK1/2 activation and eventually cell differentiation. The presence of sulphates gives these compounds a strong acidic character. The negative charges of these compounds may have provided a tendency to interact with calcium and other proteins. Therefore, as future work, it would be interesting to assess the structural conformation of these compounds to shed light on the negative charge of these compounds. It would also be interesting to assess whether $Ca^{2+}$ can form bridging interactions between negatively charged sulphate groups of sulphated disaccharides.

As outlined in chapter 1 that cAMP regulates the pro-inflammatory and anti-inflammatory activities of the cells. The drugs that elevate intracellular cAMP levels reduce the production of pro-inflammatory mediators and increase the production of anti-

inflammatory factors. In the context of this, the results of this study have shown that sulphated disaccharides inhibited TNF-α production and up-regulated IL-10 production. Thus, it postulates that sulphated disaccharides influence cAMP levels. It would be interesting to shed light on the molecular mechanism by which sulphated disaccharides impact cAMP using an enzyme-linked immunoassay. As outlined in chapter 5, cGMP can reduce intracellular calcium levels (Lincoln *et al*., 1993). Therefore, this study's findings also hypothesises that sulphated disaccharides may act via a feedback loop within cells whereby they could have stimulated NO production, which may have inhibited calcium levels through the generation of cGMP.

### 7.1.2. Future work

Given the potential signalling mechanism of sulphated disaccharides for the inhibition of cell differentiation in *in vitro* model, investigation of the assimilation of this mechanism in *in vivo* models will enable the functionality of this mechanism. In addition, this will improve the understanding in-depth and how these compounds can be utilised by the inflammatory cells as signals to modify their function, and as a result, end the inflammatory reaction. Since cGMP and cGMP signalling controls very different processes in different cells, a better understanding of the sulphated disaccharides on cAMP-mediated or cGMP-mediated activities in primary cells or synovial cell types could advance the search for new therapies for inflammatory diseases. Further research is required to elucidate possible mechanism pathways of sulphated disaccharides. The findings of this study open doors for further research in this field.

Studies by Krysan *et al*., 2004 and Sheng *et al*., 1998 have shown that NF-$_k$B induced COX-2 (Nakao *et al*., 2002 and Toledo *et at*., 2004) is involved in cell survival by modulation of its anti-apoptotic protein expression. Therefore in future work, it would be interesting to assess the NF-$_k$B-mediated anti-apoptotic function of the COX-2 pathway which may be closely involved in the function of sulphated disaccharides to inhibit PMA-induced cell apoptosis in U937 and THP-1 cells.

## 7.2. Final conclusion

The study was conducted to enhance the current knowledge of the possible endogenous roles of sulphated disaccharides in inflammation in the context of monocyte-macrophage differentiation and their potential for the treatment of inflammatory diseases in the context of RA.

Overall, this thesis has demonstrated for the first time insight into the mechanism of sulphated disaccharides. The signalling mechanism of sulphated disaccharides has been elucidated utilising *in vitro* model that leads to inhibition of human monocytes differentiation and established a possible molecular link between sulphated disaccharides and monocyte response. This thesis has provided a link that has not been shown until the present research.

The current study provides an insight into the possibility of targeting inhibition of cell-differentiation through inhibition of calcium mobilisation, leading to de-activation of p38 and ERK1/2 MAPK expression, TNF-α production and eventually inhibition of cell-differentiation induced cell surface adhesion markers expression. In addition, sulphated disaccharides promote macrophage divergence towards an anti-inflammatory phenotype. The findings of this study hypothesised that sulphated disaccharides act via the cAMP pathway to exhibit their inhibitory action or there is a possibility that they act via a feedback loop within cells to stimulate NO production, which may have inhibited calcium levels through the generation of cGMP. Thus, this study provides a molecular mechanism by which sulphated disaccharides may inhibit cell differentiation (Fig.7.5).

The findings of this thesis could contribute to new anti-inflammatory therapeutics for the treatment of inflammatory diseases. This thesis has overall suggested that targeting monocytes with sulphated disaccharides can promote inhibition of cell differentiation. A more complete picture of the molecular mechanism pathways of sulphated disaccharides is beginning to emerge and it should now be possible to apply this new knowledge to explore in more detail for further research.

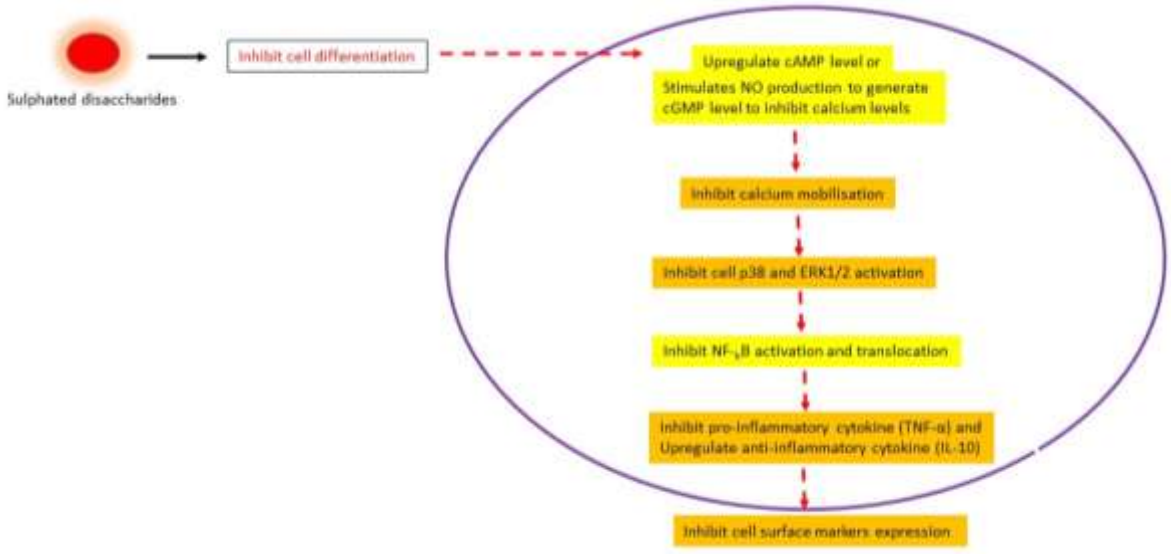


**Figure 7. 5*. A molecular mechanism by which sulphated disaccharides may inhibit cell differentiation.***

*Treatment of U937 and THP-1 monocyte cells with 8 nM PMA for 48 hours induced monocyte-macrophage differentiation in association with upregulation of $Ca^{2+}$ mobilisation, activation of p38 and p42/p45ERK MARK signalling pathways. As literature evident that p38 and ERK1/2 activation result in NF-$_k$B activation and translocation to the nucleus and then surface markers are upregulated. There is a possibility that sulphated disaccharides act via cAMP/cGMP - $Ca^{2+}$ pathway to inhibit cell differentiation.*

## REFERENCES


Aarvak, T., Chabaud, M., Miossec, P. and Natvig, J.B., 1999. IL-17 is produced by some proinflammatory Th1/Th0 cells but not by Th2 cells. *The Journal of Immunology*, *162*(3), pp.1246-1251.

Abbas, A.K., Murphy, K.M. and Sher, A., 1996. Functional diversity of helper T lymphocytes. *Nature*, *383*(6603), pp.787-793.

Abbott, S.G. and Denton, M.F., 1992. Catalytic combustion of solvent vapours from adhesives. *International Journal of Adhesion and Adhesives*, *12*(3), pp.211-214.

Abrahams, V.M., Kim, Y.M., Straszewski, S.L., Romero, R. and Mor, G., 2004. Macrophages and apoptotic cell clearance during pregnancy. *American journal of reproductive immunology*, *51*(4), pp.275-282.

Agadir, A., Chen, G.Q., Bost, F., Li, Y., Mercola, D. and Zhang, X.K., 1999. Differential effect of retinoic acid on growth regulation by phorbol ester in human cancer cell lines. *Journal of Biological Chemistry*, *274*(42), pp.29779-29785.

Aggarwal, B.B., 2003. Signalling pathways of the TNF superfamily: a double-edged sword. *Nature reviews immunology*, *3*(9), pp.745-756.

Alcorn, N., Saunders, S. and Madhok, R., 2009. Benefit-risk assessment of leflunomide. *Drug safety*, *32*(12), pp.1123-1134.

Alessi, D.R., Cuenda, A., Cohen, P., Dudley, D.T. and Saltiel, A.R., 1995. PD 098059 is a specific inhibitor of the activation of mitogen-activated protein kinase kinase in vitro and in vivo. *Journal of Biological Chemistry*, *270*(46), pp.27489-27494.

Allen, C.A., Highton, J. and Palmer, D.G., 1989. Increased expression of p150, 95 and CR3 leukocyte adhesion molecules by mononuclear phagocytes in rheumatoid synovial membranes. Comparison with osteoarthritic and normal synovial membranes. *Arthritis & Rheumatism: Official Journal of the American College of Rheumatology*, *32*(8), pp.947-954.

Allen, J.B., Wong, H.L., Costa, G.L., Bienkowski, M.J. and Wahl, S.M., 1993. Suppression of monocyte function and differential regulation of IL-1 and IL-1ra by IL-4 contribute to resolution of experimental arthritis. *The Journal of Immunology*, *151*(8), pp.4344-4351.

Almog, T. and Naor, Z., 2008. Mitogen activated protein kinases (MAPKs) as regulators of spermatogenesis and spermatozoa functions. *Molecular and cellular endocrinology*, *282*(1-2), pp.39-44.

Ambarus, C.A., Noordenbos, T., de Hair, M.J., Tak, P.P. and Baeten, D.L., 2012. Intimal lining layer macrophages but not synovial sublining macrophages display an IL-10 polarized-like phenotype in chronic synovitis. *Arthritis research & therapy*, *14*(2), pp.1-14.

Ammari, M., Presumey, J., Ponsolles, C., Roussignol, G., Roubert, C., Escriou, V., Toupet, K., Mausset-Bonnefont, A.L., Cren, M., Robin, M. and Georgel, P., 2018. Delivery of miR-146a to Ly6Chigh monocytes inhibits pathogenic bone erosion in inflammatory arthritis. *Theranostics*, *8*(21), p.5972.

Andrews, D.A., Yang, L. and Low, P.S., 2002. Phorbol ester stimulates a protein kinase C–mediated agatoxin-TK–sensitive calcium permeability pathway in human red blood cells. *Blood, The Journal of the American Society of Hematology*, *100*(9), pp.3392-3399.

Aquino, R.S., Hayashida, A. and Park, P.W., 2020. Host syndecan-1 promotes listeriosis by inhibiting intravascular neutrophil extracellular traps. *PLoS Pathogens*, *16*(5), p.e1008497.

Arden, G.P., Taylor, A.R. and Ansell, B.M., 1970. Total hip replacement using the McKee-Farrar prosthesis. In rheumatoid arthritis, Still's disease, and ankylosing spondylitis. *Annals of the rheumatic diseases*, *29*(1), p.1.

Arnold, K., Liao, Y.E. and Liu, J., 2020. Potential Use of Anti-Inflammatory Synthetic Heparan Sulphate to Attenuate Liver Damage. *Biomedicines*, *8*(11), p.503.

Babinchak, W.M., Dumm, B.K., Venus, S., Boyko, S., Putnam, A.A., Jankowsky, E. and Surewicz, W.K., 2020. Small molecules as potent biphasic modulators of protein liquid-liquid phase separation. *Nature communications*, *11*(1), pp.1-15.

Bacher, N., Raker, V., Hofmann, C., Graulich, E., Schwenk, M., Baumgrass, R., Bopp, T., Zechner, U., Merten, L., Becker, C. and Steinbrink, K., 2013. Interferon-α suppresses cAMP to disarm human regulatory T cells. *Cancer research*, *73*(18), pp.5647-5656.

Baek, Y.S., Haas, S., Hackstein, H., Bein, G., Hernandez-Santana, M., Lehrach, H., Sauer, S. and Seitz, H., 2009. Identification of novel transcriptional regulators involved in macrophage differentiation and activation in U937 cells. *BMC immunology*, *10*(1), pp.1-15.

Baeuerle, P.A. and Baltimore, D., 1988. I kappa B: a specific inhibitor of the NF-kappa B transcription factor. *Science*, *242*(4878), pp.540-546.

Baird, L. and Dinkova-Kostova, A.T., 2011. The cytoprotective role of the Keap1–Nrf2 pathway. *Archives of toxicology*, *85*(4), pp.241-272.

Bajwa, P., Seed, M., 2015. Sulphated disaccharides inhibit the differentiation of U937 cells in response to phorbol myristate acetate to the adherent phenotype, pA2 online: E-journal of the British Pharmacology Society, 327P Queen Elizabeth II Conference Centre London Pharmacology 2015.

Baker, P.F., Hodgkin, A.L. and Ridgway, E.B., 1971. Depolarization and calcium entry in squid giant axons. *The Journal of physiology*, *218*(3), pp.709-755.

Barrera, P., Blom, A., Van Lent, P.L., Van Bloois, L., Beijnen, J.H., Van Rooijen, N., De Waal Malefijt, M.C., Van De Putte, L.B., Storm, G. and Van Den Berg, W.B., 2000. Synovial macrophage depletion with clodronate-containing liposomes in rheumatoid arthritis. *Arthritis & Rheumatism: Official Journal of the American College of Rheumatology*, *43*(9), pp.1951-1959.

Bas, S., Gauthier, B.R., Spenato, U., Stingelin, S. and Gabay, C., 2004. CD14 is an acute-phase protein. *The Journal of Immunology*, *172*(7), pp.4470-4479.

Beavo, J.A. and Brunton, L.L., 2002. Cyclic nucleotide research—still expanding after half a century. *Nature reviews Molecular cell biology*, *3*(9), pp.710-717.

Bell, J.K., Mullen, G.E., Leifer, C.A., Mazzoni, A., Davies, D.R. and Segal, D.M., 2003. Leucine-rich repeats and pathogen recognition in Toll-like receptors. *Trends in immunology*, *24*(10), pp.528-533.

Berridge, M.J. and Irvine, R.F., 1984. Inositol trisphosphate, a novel second messenger in cellular signal transduction. *Nature*, *312*(5992), pp.315-321.

Berridge, M.J., 2006. Calcium microdomains: organization and function. *Cell calcium*, *40*(5-6), pp.405-412.

Bessis, N., Boissier, M.C., Ferrara, P., Blankenstein, T., Fradelizi, D. and Fournier, C., 1996. Attenuation of collagen-induced arthritis in mice by treatment with vector cells engineered to secrete interleukin-13. *European journal of immunology*, *26*(10), pp.2399-2403.

Beyaert, R., Cuenda, A., Vanden Berghe, W., Plaisance, S., Lee, J.C., Haegeman, G., Cohen, P. and Fiers, W., 1996. The p38/RK mitogen-activated protein kinase pathway regulates interleukin-6 synthesis response to tumour necrosis factor. *The EMBO journal*, *15*(8), pp.1914-1923.

Bezouška, K., Yuen, C.T., O'Brien, J., Childs, R.A., Chai, W., Lawson, A.M., Drbal, K., Fišerová, A., Posíšil, M. and Feizi, T., 1994. Oligosaccharide ligands for NKR-P1 protein activate NK cells and cytotoxicity. *Nature*, *372*(6502), pp.150-157.

Bhat, N.R., Zhang, P. and Mohanty, S.B., 2007. p38 MAP kinase regulation of oligodendrocyte differentiation with CREB as a potential target. *Neurochemical research*, *32*(2), pp.293-302.

Biswas, S.K., Chittezhath, M., Shalova, I.N. and Lim, J.Y., 2012. Macrophage polarization and plasticity in health and disease. *Immunologic research*, *53*(1), pp.11-24.

Biswas, S.K., Gangi, L., Paul, S., Schioppa, T., Saccani, A., Sironi, M., Bottazzi, B., Doni, A., Vincenzo, B., Pasqualini, F. and Vago, L., 2006. A distinct and unique transcriptional program expressed by tumour-associated macrophages (defective NF-κB and enhanced IRF-3/STAT1 activation). *Blood*, *107*(5), pp.2112-2122.

Biswas, S.K., Sica, A. and Lewis, C.E., 2008. Plasticity of macrophage function during tumour progression: regulation by distinct molecular mechanisms. *The Journal of Immunology*, *180*(4), pp.2011-2017.

Bocci, V. and Valacchi, G., 2015. Nrf2 activation as target to implement therapeutic treatments. *Frontiers in chemistry*, *3*, p.4.

Bonder, C.S., Finlay-Jones, J.J. and Hart, P.H., 1999. Interleukin-4 regulation of human monocyte and macrophage interleukin-10 and interleukin-12 production. Role of a functional interleukin-2 receptor γ-chain. *Immunology*, *96*(4), p.529.

---

Bondeson, J., Foxwell, B., Brennan, F. and Feldmann, M., 1999. Defining therapeutic targets by using adenovirus: blocking NF-κB inhibits both inflammatory and destructive mechanisms in rheumatoid synovium but spares anti-inflammatory mediators. *Proceedings of the National Academy of Sciences*, *96*(10), pp.5668-5673.

Bopp, T., Becker, C., Klein, M., Klein-Heßling, S., Palmetshofer, A., Serfling, E., Heib, V., Becker, M., Kubach, J., Schmitt, S. and Stoll, S., 2007. Cyclic adenosine monophosphate is a key component of regulatory T cell–mediated suppression. *The Journal of experimental medicine*, *204*(6), pp.1303-1310.

Bopp, T., Dehzad, N., Reuter, S., Klein, M., Ullrich, N., Stassen, M., Schild, H., Buhl, R., Schmitt, E. and Taube, C., 2009. Inhibition of cAMP degradation improves regulatory T cell-mediated suppression. *The Journal of Immunology*, *182*(7), pp.4017-4024.

Bradford, M.M., 1976. A rapid and sensitive method for the quantitation of microgram quantities of protein utilizing the principle of protein-dye binding. *Analytical biochemistry*, *72*(1-2), pp.248-254

Bröker, B., Smith, M.D., Moretta, L., Ciccone, E., Grossi, C.E., Edwards, J.C.W., Yüksel, F., Colaco, B., Worman, C., Mackenzie, L. and Kinne, R., 1990. Tγδ cells and their

subsets in blood and synovial tissue from rheumatoid arthritis patients. *Scandinavian journal of immunology*, *32*(6), pp.585-593.

Brown, P.M., Pratt, A.G. and Isaacs, J.D., 2016. Mechanism of action of methotrexate in rheumatoid arthritis, and the search for biomarkers. *Nature Reviews Rheumatology*, *12*(12), pp.731-742.

Bruckmeier, M., Kuehnl, A., Culmes, M., Pelisek, J. and Eckstein, H.H., 2012. Impact of oxLDL and LPS on C-type natriuretic peptide system is different between THP-1 cells and human peripheral blood monocytic cells. *Cellular Physiology and Biochemistry*, *30*(1), pp.199-209.

Bryne, M., 1991. Prognostic value of various molecular and cellular features in oral squamous cell carcinomas: a review. *Journal of oral pathology & medicine*, *20*(9), pp.413-420.

Buch, M., and Emery, P., 2002. Treating rheumatoid arthritis with tumour necrosis factor α blockade: May be a giant therapeutic leap or a small expensive step. *Bmj*, *324*(7333), pp.312-313.

Buchanan, S.G.S.C. and Gay, N.J., 1996. Structural and functional diversity in the leucine-rich repeat family of proteins. *Progress in biophysics and molecular biology*, *65*(1-2), pp.1-44.

Burmester, G.R., McInnes, I.B., Kremer, J., Miranda, P., Korkosz, M., Vencovsky, J., Rubbert-Roth, A., Mysler, E., Sleeman, M.A., Godwood, A. and Sinibaldi, D., 2017. A randomised phase IIb study of mavrilimumab, a novel GM–CSF receptor alpha monoclonal antibody, in the treatment of rheumatoid arthritis. *Annals of the rheumatic diseases*, *76*(6), pp.1020-1030.

Butcher, E.C. and Picker, L.J., 1996. Lymphocyte homing and homeostasis. *Science*, *272*(5258), pp.60-67.

Cahalon, L., Lider, O., Schor, H., Avron, A., Gilat, D., Hershkoviz, R., Margalit, R., Eshel, A., Shoseyev, O. and Cohen, I.R., 1997. Heparin disaccharides inhibit tumour necrosis factor-alpha production by macrophages and arrest immune inflammation in rodents. *International immunology*, *9*(10), pp.1517-1522.

Cam, A. and de Mejia, E.G., 2012. RGD-peptide lunasin inhibits Akt-mediated NF-κB activation in human macrophages through interaction with the αVβ3 integrin. *Molecular nutrition & food research*, *56*(10), pp.1569-1581.

Campanero, M.R., Del Pozo, M.A., Arroyo, A.G., Sánchez-Mateos, P., Hernández-Caselles, T., Craig, A., Pulido, R. and Sánchez-Madrid, F., 1993. ICAM-3 interacts with

LFA-1 and regulates the LFA-1/ICAM-1 cell adhesion pathway. *The Journal of cell biology*, *123*(4), pp.1007-1016.

Cao, W., Daniel, K.W., Robidoux, J., Puigserver, P., Medvedev, A.V., Bai, X., Floering, L.M., Spiegelman, B.M. and Collins, S., 2004. p38 mitogen-activated protein kinase is the central regulator of cyclic AMP-dependent transcription of the brown fat uncoupling protein 1 gene. *Molecular and cellular biology*, *24*(7), pp.3057-3067.

Careau, E. and Bissonnette, E.Y., 2004. Adoptive transfer of alveolar macrophages abrogates bronchial hyperresponsiveness. *American journal of respiratory cell and molecular biology*, *31*(1), pp.22-27.

Carlos, T., Kovach, N., Schwartz, B., Rosa, M., Newman, B., Wayner, E., Benjamin, C., Osborn, L., Lobb, R. and Harlan, J., 1991. Human monocytes bind to two cytokine-induced adhesive ligands on cultured human endothelial cells: endothelial-leukocyte adhesion molecule-1 and vascular cell adhesion molecule-1.

Carlos, T., Kovach, N., Schwartz, B., Rosa, M., Newman, B., Wayner, E., Benjamin, C., Osborn, L., Lobb, R. and Harlan, J., 1991. Human monocytes bind to two cytokine-induced adhesive ligands on cultured human endothelial cells: endothelial-leukocyte adhesion molecule-1 and vascular cell adhesion molecule-1.

Carlos, T.M. and Harlan, J.M., 1994. Leukocyte-endothelial adhesion molecules

Carmichael, L., 1954. Manual of child psychology.

Cavalli, G. and Dinarello, C.A., 2015. Treating rheumatological diseases and co-morbidities with interleukin-1 blocking therapies. *Rheumatology*, *54*(12), pp.2134-2144.

Cavender, D.E., Edelbaum, D. and Welkovich, L., 1991. Effects of inflammatory cytokines and phorbol esters on the adhesion of U937 cells, a human monocyte-like cell line, to endothelial cell monolayers and extracellular matrix proteins. *Journal of leukocyte biology*, *49*(6), pp.566-578.

Cekic, C., Sag, D., Day, Y.J. and Linden, J., 2013. Extracellular adenosine regulates naive T cell development and peripheral maintenance. *Journal of Experimental Medicine*, *210*(12), pp.2693-2706.

Chanput, W., Peters, V. and Wichers, H., 2015. THP-1 and U937 Cells. *The impact of food bioactives on health*, pp.147-159.

Chanput, Wasaporn, Jurriaan J. Mes, and Harry J. Wichers. "THP-1 cell line: an in vitro cell model for immune modulation approach." *International immunopharmacology* 23, no. 1 (2014): 37-45.

Chanput, Wasaporn, Jurriaan J. Mes, and Harry J. Wichers. "THP-1 cell line: an in vitro cell model for immune modulation approach." *International immunopharmacology* 23, no. 1 (2014): 37-45.

Chen, Qiuyan, and A. Catharine Ross. "Retinoic acid regulates cell cycle progression and cell differentiation in human monocytic THP-1 cells." *Experimental cell research* 297, no. 1 (2004): 68-81.

Chen, X., Wen, Z., Xu, W. and Xiong, S., 2013. Granulin exacerbates lupus nephritis via enhancing macrophage M2b polarization. *PLoS One*, *8*(6), p.e65542.

Chiu, R., Imagawa, M., Imbra, R.J., Bockoven, J.R. and Karin, M., 1987. Multiple cis-and trans-acting elements mediate the transcriptional response to phorbol esters. *Nature*, *329*(6140), pp.648-651

Choi, S.C., Kim, B.S., Song, M.Y., Choi, E.Y., Oh, H.M., Lyou, J.H., Han, W.C., Moon, H.B., Kim, T.H., Oh, J.M. and Chung, H.T., 2003. Downregulation of p38 kinase pathway by cAMP response element-binding protein protects HL-60 cells from iron chelator-induced apoptosis. *Free Radical Biology and Medicine*, *35*(10), pp.1171-1184.

Chowers, Y., Lider, O., Schor, H., Barsnack, I., Tal, R., Ariel, A., Bar-Meir, S., Cohen, I.R. and Cahalon, L., 2001. Disaccharides derived from heparin or heparan sulphate regulate IL-8 and IL-1β secretion by intestinal epithelial cells. *Gastroenterology*, *120*(2), pp.449-459

Ciabattini, A., Cuppone, A.M., Pulimeno, R., Iannelli, F., Pozzi, G. and Medaglini, D., 2006. Stimulation of human monocytes with the gram-positive vaccine vector Streptococcus gordonii. *Clinical and vaccine immunology*, *13*(9), pp.1037-1043.

Cobb, M.H., Boulton, T.G. and Robbins, D.J., 1991. Extracellular signal-regulated kinases: ERKs in progress. *Cell regulation*, *2*(12), pp.965-978.

Colin, S., Chinetti-Gbaguidi, G. and Staels, B., 2014. Macrophage phenotypes in atherosclerosis. *Immunological reviews*, *262*(1), pp.153-166.

Collart, M.A., Baeuerle, P. and Vassalli, P., 1990. Regulation of tumour necrosis factor alpha transcription in macrophages: involvement of four kappa B-like motifs and of constitutive and inducible forms of NF-kappa B. *Molecular and cellular biology*, *10*(4), pp.1498-1506.

Collins, L.E. and Troeberg, L., 2019. Heparan sulphate as a regulator of inflammation and immunity. *Journal of leukocyte biology*, *105*(1), pp.81-92.

Coppock, D.L., Buffolino, P., Kopman, C. and Nathanson, L., 1995. Inhibition of the melanoma cell cycle and regulation at the G1/S transition by 12-O-tetradecanoylphorbol-

13-acetate (TPA) by modulation of CDK2 activity. *Experimental cell research*, *221*(1), pp.92-102.

Crijns, H., Vanheule, V. and Proost, P., 2020. Targeting chemokine—glycosaminoglycan interactions to inhibit inflammation. *Frontiers in immunology*, *11*, p.483.

Cruz, C.D., Neto, F.L., Castro-Lopes, J., McMahon, S.B. and Cruz, F., 2005. Inhibition of ERK phosphorylation decreases nociceptive behaviour in monoarthritic rats. *Pain*, *116*(3), pp.411-419.

Cuenda, A., Rouse, J., Doza, Y.N., Meier, R., Cohen, P., Gallagher, T.F., Young, P.R. and Lee, J.C., 1995. SB 203580 is a specific inhibitor of a MAP kinase homologue which is stimulated by cellular stresses and interleukin-1. *FEBS letters*, *364*(2), pp.229-233.

Cutolo, M., Sulli, A., Barone, A., Seriolo, B. and Accardo, S., 1993. Macrophages, synovial tissue and rheumatoid arthritis. *Clinical and experimental rheumatology*, *11*(3), pp.331-339.

Cutolo, M., Trombetta, A.C. and Soldano, S., 2018. Monocyte and macrophage phenotypes: a look beyond systemic sclerosis. Response to:'M1/M2 polarization state of M-CSF blood-derived macrophages in systemic sclerosis' by Lescoat et al. *Annals of the rheumatic diseases*, *78*(11), pp.e128-e128.

Daha, N.A., Banda, N.K., Roos, A., Beurskens, F.J., Bakker, J.M., Daha, M.R. and Trouw, L.A., 2011. Complement activation by (auto-) antibodies. *Molecular immunology*, *48*(14), pp.1656-1665.

Daigneault, M., Preston, J.A., Marriott, H.M., Whyte, M.K. and Dockrell, D.H., 2010. The identification of markers of macrophage differentiation in PMA-stimulated THP-1 cells and monocyte-derived macrophages. *PloS one*, *5*(1), p.e8668.

Daigneault, M., Preston, J.A., Marriott, H.M., Whyte, M.K. and Dockrell, D.H., 2010. The identification of markers of macrophage differentiation in PMA-stimulated THP-1 cells and monocyte-derived macrophages. *PloS one*, *5*(1), p.e8668.

Das, D., Pintucci, G. and Stern, A., 2000. MAPK-dependent expression of p21WAF and p27kip1 in PMA-induced differentiation of HL60 cells. *FEBS letters*, *472*(1), pp.50-52.

Dayer, J.M. and Choy, E., 2010. Therapeutic targets in rheumatoid arthritis: the interleukin-6 receptor. *Rheumatology*, *49*(1), pp.15-24.

de Fougerolles, A.R. and Springer, T.A., 1992. Intercellular adhesion molecule 3, a third adhesion counter-receptor for lymphocyte function-associated molecule 1 on resting lymphocytes. *Journal of Experimental Medicine*, *175*(1), pp.185-190.

de Fougerolles, A.R., Stacker, S.A., Schwarting, R. and Springer, T.A., 1991. Characterization of ICAM-2 and evidence for a third counter-receptor for LFA-1. *The Journal of experimental medicine*, *174*(1), pp.253-267

Deleuran, B.W., Chu, C.Q., Field, M., Brennan, F.M., Katsikis, P., Feldmann, M. and Maini, R.N., 1992. Localization of interleukin-1α, type 1 interleukin-1 receptor and interleukin-1 receptor antagonist in the synovial membrane and cartilage/pannus junction in rheumatoid arthritis. *Rheumatology*, *31*(12), pp.801-809.

Dent, G., Giembycz, M.A., Rabe, K.F., Wolf, B., Barnes, P.J. and Magnussen, H., 1994. Theophylline suppresses human alveolar macrophage respiratory burst through phosphodiesterase inhibition. *American journal of respiratory cell and molecular biology*, *10*(5), pp.565-572.

Derksen, V.F.A.M., Huizinga, T.W.J. and Van Der Woude, D., 2017, June. The role of autoantibodies in the pathophysiology of rheumatoid arthritis. In *Seminars in immunopathology* (Vol. 39, No. 4, pp. 437-446). Springer Berlin Heidelberg.

Di Giovine, F., Eastgate, J., Wood, N., Symons, J., Grinlinton, F. and Duff, G., 1988. Correlation of plasma interleukin 1 levels with disease activity in rheumatoid arthritis. *The Lancet*, *332*(8613), pp.706-709.

Dinarello, C.A., 1999. Interleukin-18. *Methods*, *19*(1), pp.121-132.

Ding, J., Lin, L., Hang, W. and Yan, X., 2009. Beryllium uptake and related biological effects studied in THP-1 differentiated macrophages. *Metallomics*, *1*(6), pp.471-478.

Dobrovolskaia, M.A. and Vogel, S.N., 2002. Toll receptors, CD14, and macrophage activation and deactivation by LPS. *Microbes and Infection*, *4*(9), pp.903-914.

Donahue, K.E., Gartlehner, G., Jonas, D.E., Lux, L.J., Thieda, P., Jonas, B.L., Hansen, R.A., Morgan, L.C. and Lohr, K.N., 2008. Systematic review: comparative effectiveness and harms of disease-modifying medications for rheumatoid arthritis. *Annals of internal medicine*, *148*(2), pp.124-134.

Drouet, C., Shakhov, A.N. and Jongeneel, C.V., 1991. Enhancers and transcription factors controlling the inducibility of the tumour necrosis factor-alpha promoter in primary macrophages. *The Journal of Immunology*, *147*(5), pp.1694-1700.

Dufourny, B., Alblas, J., van Teeffelen, H.A., van Schaik, F.M., van der Burg, B., Steenbergh, P.H. and Sussenbach, J.S., 1997. Mitogenic signalling of insulin-like growth factor I in MCF-7 human breast cancer cells requires phosphatidylinositol 3-kinase and is independent of mitogen-activated protein kinase. *Journal of Biological Chemistry*, *272*(49), pp.31163-31171.

Duhe, R.J., Nielsen, M.D., Dittman, A.H., Villacres, E.C., Choi, E.J. and Storm, D.R., 1994. Oxidation of critical cysteine residues of type I adenylyl cyclase by o-iodosobenzoate or nitric oxide reversibly inhibits stimulation by calcium and calmodulin. *Journal of Biological Chemistry*, *269*(10), pp.7290-7296.

Duluc, D., Delneste, Y., Tan, F., Moles, M.P., Grimaud, L., Lenoir, J., Preisser, L., Anegon, I., Catala, L., Ifrah, N. and Descamps, P., 2007. Tumour-associated leukemia inhibitory factor and IL-6 skew monocyte differentiation into tumour-associated macrophage-like cells. *Blood, The Journal of the American Society of Hematology*, *110*(13), pp.4319-4330.

Dustin, M.L., Rothlein, R., Bhan, A.K., Dinarello, C.A. and Springer, T.A., 1986. Induction by IL 1 and interferon-gamma: tissue distribution, biochemistry, and function of a natural adherence molecule (ICAM-1). *The Journal of Immunology*, *137*(1), pp.245-254.

Economou, J.S., Rhoades, K.R.I.S.T.I.N.A., Essner, R.I.C.H.A.R.D., McBride, W.H., Gasson, J.C. and Morton, D.L., 1989. Genetic analysis of the human tumour necrosis factor alpha/cachectin promoter region in a macrophage cell line. *The Journal of experimental medicine*, *170*(1), pp.321-326.

Edilova, M.I., Akram, A. and Abdul-Sater, A.A., 2020. Innate immunity drives pathogenesis of rheumatoid arthritis. *biomedical journal*, *44*(2), pp.172-182.

Edwards, J.C.W., Cambridge, G. and Abrahams, V.M., 1999. Do self-perpetuating B lymphocytes drive human autoimmune disease?. *Immunology*, *97*(2), p.188

El Gabalawy, H. and Wilkins, J., 1993. Beta 1 (CD29) integrin expression in rheumatoid synovial membranes: an immunohistologic study of distribution patterns. *The Journal of rheumatology*, *20*(2), pp.231-237.

El-Gabalawy, H., Gallatin, M., Vazeux, R., Peterman, G. and Wilkins, J., 1994. Expression of ICAM-R (ICAM-3), a novel counter-receptor for LFA-1, in rheumatoid and nonrheumatoid synovium. *Arthritis & Rheumatism: Official Journal of the American College of Rheumatology*, *37*(6), pp.846-854.

Elices, M.J., Osborn, L., Takada, Y., Crouse, C., Luhowskyj, S., Hemler, M.E. and Lobb, R.R., 1990. VCAM-1 on activated endothelium interacts with the leukocyte integrin VLA-4 at a site distinct from the VLA-4/fibronectin binding site. *Cell*, *60*(4), pp.577-584.

Endo, H., Akahoshi, T., Takagishi, K., Kashiwazaki, S. and Matsushima, K., 1991. Elevation of interleukin-8 (IL-8) levels in joint fluids of patients with rheumatoid arthritis and the induction by IL-8 of leukocyte infiltration and synovitis in rabbit joints. *Lymphokine and cytokine research*, *10*(4), pp.245-252.

Epstein, F. and Harris, E.,1990. Rheumatoid Arthritis. New England Journal of Medicine, 322(18), pp.1277-1289.

Eun, S.Y., Jin, H., Lee, J.S., Park, S.W., Lee, J.H., Chang, K.C. and Kim, H.J., 2014. P2Y 2 receptor activation by nucleotides released from highly metastatic breast cancer cells increases tumour growth and invasion via crosstalk with endothelial cells. *Breast Cancer Research*, *16*(5), pp.1-14.

Eymard, F., Pigenet, A., Citadelle, D., Tordjman, J., Foucher, L., Rose, C., Lachaniette, C.H.F., Rouault, C., Clément, K., Berenbaum, F. and Chevalier, X., 2017. Knee and hip intra-articular adipose tissues (IAATs) compared with autologous subcutaneous adipose tissue: a specific phenotype for a central player in osteoarthritis. *Annals of the rheumatic diseases*, *76*(6), pp.1142-1148.

Falzoni, S., Munerati, M., Ferrari, D., Spisani, S., Moretti, S. and Di Virgilio, F., 1995. The purinergic P2Z receptor of human macrophage cells. Characterization and possible physiological role. *The Journal of clinical investigation*, *95*(3), pp.1207-1216.

Fan, H.C., Fernández-Hernando, C. and Lai, J.H., 2014. Protein kinase C isoforms in atherosclerosis: pro-or anti-inflammatory?. *Biochemical pharmacology*, *88*(2), pp.139-149

Fannon, M., Forsten-Williams, K., Nugent, M.A., Gregory, K.J., Chu, C.L., Goerges-Wildt, A.L., Panigrahy, D., Kaipainen, A., Barnes, C., Lapp, C. and Shing, Y., 2008. Sucrose octasulphate regulates fibroblast growth factor-2 binding, transport, and activity: Potential for regulation of tumour growth. *Journal of cellular physiology*, *215*(2), pp.434-441.

Fassio, A., Rossini, M., Viapiana, O., Idolazzi, L., Vantaggiato, E., Benini, C. and Gatti, D., 2017. New strategies for the prevention and treatment of systemic and local bone loss; from pathophysiology to clinical application. *Current pharmaceutical design*, *23*(41), pp.6241-6250.

Fawcett, J., Holness, C.L., Needham, L.A., Turley, H., Gattert, K.C., Mason, D.Y. and Simmons, D.L., 1992. Molecular cloning of ICAM-3, a third ligand for LFA-1, constitutively expressed on resting leukocytes. *Nature*, *360*(6403), pp.481-484.

Feldmann, M., Brennan, F.M. and Maini, R.N., 1996. Role of cytokines in rheumatoid arthritis. *Annual review of immunology*, *14*(1), pp.397-440.

Feldmann, M., Brennan, F.M., Foxwell, B.M. and Maini, R.N., 2001. The role of TNF-a and IL-1 in rheumatoid arthritis. *Curr Dir Autoimmun*, *3*, pp.188-99.

Feng, G.J., Goodridge, H.S., Harnett, M.M., Wei, X.Q., Nikolaev, A.V., Higson, A.P. and Liew, F.Y., 1999. Extracellular signal-related kinase (ERK) and p38 mitogen-activated protein (MAP) kinases differentially regulate the lipopolysaccharide-mediated induction of inducible nitric oxide synthase and IL-12 in macrophages: Leishmania phosphoglycans subvert macrophage IL-12 production by targeting ERK MAP kinase. *The Journal of Immunology*, *163*(12), pp.6403-6412.

Feng, W.G., Wang, Y.B., Zhang, J.S., Wang, X.Y., Li, C.L. and Chang, Z.L., 2002. cAMP elevators inhibit LPS-induced IL-12 p40 expression by interfering with phosphorylation of p38 MAPK in murine peritoneal macrophages. *Cell research*, *12*(5), pp.331-337.

Ferrante, C.J. and Leibovich, S.J., 2012. Regulation of macrophage polarization and wound healing. *Advances in wound care*, *1*(1), pp.10-16.

Ferrante, C.J., Pinhal-Enfield, G., Elson, G., Cronstein, B.N., Hasko, G., Outram, S. and Leibovich, S.J., 2013. The adenosine-dependent angiogenic switch of macrophages to an M2-like phenotype is independent of interleukin-4 receptor alpha (IL-4Rα) signalling. *Inflammation*, *36*(4), pp.921-931.

Feuerstein, N., Monos, D.S. and Cooper, H.L., 1985. Phorbol ester effect in platelets, lymphocytes, and leukemic cells (HL-60) is associated with enhanced phosphorylation of class I HLA antigens: Coprecipitation of myosin light chain. *Biochemical and biophysical research communications*, *126*(1), pp.206-213.

Firestein, G.S., 2003. Evolving concepts of rheumatoid arthritis. *Nature*, *423*(6937), pp.356-361.

Fleit, H.B. and Kobasiuk, C.D., 1991. The human monocyte-like cell line THP-1 expresses FcγRI and FCγRII. *Journal of leukocyte biology*, *49*(6), pp.556-565.

Foey, A.D., Parry, S.L., Williams, L.M., Feldmann, M., Foxwell, B.M. and Brennan, F.M., 1998. Regulation of monocyte IL-10 synthesis by endogenous IL-1 and TNF-α: role of the p38 and p42/44 mitogen-activated protein kinases. *The Journal of Immunology*, *160*(2), pp.920-928.

Foster, N., Cheetham, J., Taylor, J.J. and Preshaw, P.M., 2005. VIP inhibits Porphyromonas gingivalis LPS-induced immune responses in human monocytes. *Journal of dental research*, *84*(11), pp.999-1004.

Fridman, R., Lider, O., Naparstek, Y., Fuks, Z., Vlodavsky, I. and Cohen, I.R., 1987. Soluble antigen induces T lymphocytes to secrete an endoglycosidase that degrades the heparan sulphate moiety of subendothelial extracellular matrix. *Journal of cellular physiology*, *130*(1), pp.85-92.

Fukui, S., Iwamoto, N., Takatani, A., Igawa, T., Shimizu, T., Umeda, M., Nishino, A., Horai, Y., Hirai, Y., Koga, T. and Kawashiri, S.Y., 2018. M1 and M2 monocytes in rheumatoid arthritis: a contribution of imbalance of M1/M2 monocytes to osteoclastogenesis. *Frontiers in immunology*, *8*, p.1958.

Gaudino, S.J. and Kumar, P., 2019. Cross-talk between antigen presenting cells and T cells impacts intestinal homeostasis, bacterial infections, and tumourigenesis. *Frontiers in immunology*, *10*, p.360.

Ge, Y.C., Li, J.N., Ni, X.T., Guo, C.M., Wang, W.S., Duan, T. and Sun, K., 2011. Cross talk between cAMP and p38 MAPK pathways in the induction of leptin by hCG in human placental syncytiotrophoblasts. *Reproduction*, *142*(2), p.369.

Gennaro, R., Florio, C. and Romeo, D., 1985. Activation of protein kinase C in neutrophil cytoplasts: Localization of protein substrates and possible relationship with stimulus-response coupling. *FEBS letters*, *180*(2), pp.185-190.

Gennaro, R., Florio, C. and Romeo, D., 1986. Co-activation of protein kinase C and NADPH oxidase in the plasma membrane of neutrophil cytoplasts. *Biochemical and biophysical research communications*, *134*(1), pp.305-312.

Genot, E.M., Parker, P.J. and Cantrell, D.A., 1995. Analysis of the Role of Protein Kinase C-α,-ε, and-ζ in T Cell Activation (∗). *Journal of Biological Chemistry*, *270*(17), pp.9833-9839.

Giasson, E., Servant, M.J. and Meloche, S., 1997. Cyclic AMP-mediated inhibition of angiotensin II-induced protein synthesis is associated with suppression of tyrosine phosphorylation signalling in vascular smooth muscle cells. *Journal of Biological Chemistry*, *272*(43), pp.26879-26886.

Gilbert, K.M. and Hoffmann, M.K., 1985. cAMP is an essential signal in the induction of antibody production by B cells but inhibits helper function of T cells. *The Journal of Immunology*, *135*(3), pp.2084-2089.

Gillies, P.J., Bhatia, S.K., Belcher, L.A., Hannon, D.B., Thompson, J.T. and Heuvel, J.P.V., 2012. Regulation of inflammatory and lipid metabolism genes by eicosapentaenoic acid-rich oil [S]. *Journal of lipid research*, *53*(8), pp.1679-1689.

Goodridge, H.S., Harnett, W., Liew, F.Y. and Harnett, M.M., 2003. Differential regulation of interleukin-12 p40 and p35 induction via Erk mitogen-activated protein kinase-dependent and-independent mechanisms and the implications for bioactive IL-12 and IL-23 responses. *Immunology*, *109*(3), pp.415-425.

Gordon, S. and Martinez, F.O., 2010. Alternative activation of macrophages: mechanism and functions. *Immunity*, *32*(5), pp.593-604.

Goudot, C., Coillard, A., Villani, A.C., Gueguen, P., Cros, A., Sarkizova, S., Tang-Huau, T.L., Bohec, M., Baulande, S., Hacohen, N. and Amigorena, S., 2017. Aryl hydrocarbon receptor controls monocyte differentiation into dendritic cells versus macrophages. *Immunity*, *47*(3), pp.582-596.

Gouze, J.N., Gouze, E., Popp, M.P., Bush, M.L., Dacanay, E.A., Kay, J.D., Levings, P.P., Patel, K.R., Saran, J.P.S., Watson, R.S. and Ghivizzani, S.C., 2006. Exogenous glucosamine globally protects chondrocytes from the arthritogenic effects of IL-1β. *Arthritis research & therapy*, *8*(6), pp.1-14.

Gracie, J.A., Forsey, R.J., Chan, W.L., Gilmour, A., Leung, B.P., Greer, M.R., Kennedy, K., Carter, R., Wei, X.Q., Xu, D. and Field, M., 1999. A proinflammatory role for IL-18 in rheumatoid arthritis. *The Journal of clinical investigation*, *104*(10), pp.1393-1401.

Graves, L.M., Bornfeldt, K.E., Raines, E.W., Potts, B.C., Macdonald, S.G., Ross, R. and Krebs, E.G., 1993. Protein kinase A antagonizes platelet-derived growth factor-induced signalling by mitogen-activated protein kinase in human arterial smooth muscle cells. *Proceedings of the National Academy of Sciences*, *90*(21), pp.10300-10304.

Grijalva, C.G., Chen, L., Delzell, E., Baddley, J.W., Beukelman, T., Winthrop, K.L., Griffin, M.R., Herrinton, L.J., Liu, L., Ouellet-Hellstrom, R. and Patkar, N.M., 2011. Initiation of tumour necrosis factor-α antagonists and the risk of hospitalization for infection in patients with autoimmune diseases. *Jama*, *306*(21), pp.2331-2339.

Hahnenberger, R., Jakobson, Å.M., Ansari, A., Wehler, T., Svahn, C.M. and Lindahl, U., 1993. Low-sulphated oligosaccharides derived from heparan sulphate inhibit normal angiogenesis. *Glycobiology*, *3*(6), pp.567-573.

Hammaker, D. and Firestein, G.S., 2010. “Go upstream, young man”: lessons learned from the p38 saga. *Annals of the rheumatic diseases*, *69*(Suppl 1), pp.i77-i82.

Han, J., Lee, J.D., Tobias, P.S. and Ulevitch, R.J., 1993. Endotoxin induces rapid protein tyrosine phosphorylation in 70Z/3 cells expressing CD14. *Journal of Biological Chemistry*, *268*(33), pp.25009-25014.

Harris Jr, E.D., 1990. Rheumatoid arthritis: pathophysiology and implications for therapy. *New England Journal of Medicine*, *322*(18), pp.1277-1289.

Harris, P. and Ralph, P., 1985. Human leukemic models of myelomonocytic development: a review of the HL-60 and U937 cell lines. *Journal of leukocyte biology*, *37*(4), pp.407-422.

Hart, P.H., Hunt, E.K., Bonder, C.S., Watson, C.J. and Finlay-Jones, J.J., 1996. Regulation of surface and soluble TNF receptor expression on human monocytes and synovial fluid macrophages by IL-4 and IL-10. *The Journal of Immunology*, *157*(8), pp.3672-3680.

Hashimoto, A., Okada, H., Jiang, A., Kurosaki, M., Greenberg, S., Clark, E.A. and Kurosaki, T., 1998. Involvement of guanosine triphosphatases and phospholipase C-γ2 in extracellular signal–regulated kinase, c-Jun NH2-terminal kinase, and p38 mitogen-activated protein kinase activation by the B cell antigen receptor. *Journal of Experimental Medicine*, *188*(7), pp.1287-1295.

Hatano, S. and Watanabe, H., 2020. Regulation of macrophage and dendritic cell function by chondroitin sulphate in innate to antigen-specific adaptive immunity. *Frontiers in immunology*, *11*, p.232.

Hayakawa, T., Kawasaki, S., Hirayama, Y., Tsutsui, T., Sugiyama, E., Adachi, K., Kon, R., Suematsu, M. and Sugiura, Y., 2019. A thin layer of sucrose octasulphate protects the oesophageal mucosal epithelium in reflux oesophagitis. *Scientific reports*, *9*(1), pp.1-10.

Hayashida, K., Chen, Y., Bartlett, A.H. and Park, P.W., 2008. Syndecan-1 is an in vivo suppressor of Gram-positive toxic shock. *Journal of Biological Chemistry*, *283*(29), pp.19895-19903.

Hecht, I., Hershkoviz, R., Shivtiel, S., Lapidot, T., Cohen, I.R., Lider, O. and Cahalon, L., 2004. Heparin-disaccharide affects T cells: inhibition of NF-κB activation, cell migration, and modulation of intracellular signalling. *Journal of leukocyte biology*, *75*(6), pp.1139-1146.

Hedrich, C.M., Crispin, J.C., Rauen, T., Ioannidis, C., Apostolidis, S.A., Lo, M.S., Kyttaris, V.C. and Tsokos, G.C., 2012. cAMP response element modulator α controls IL2 and IL17A expression during CD4 lineage commitment and subset distribution in lupus. *Proceedings of the National Academy of Sciences*, *109*(41), pp.16606-16611.

Heldin, C.H., Lu, B., Evans, R. and Gutkind, J.S., 2016. Signals and receptors. *Cold Spring Harbor Perspectives in Biology*, *8*(4), p.a005900.

Helfman, D.M., Appelbaum, B.D., Vogler, W.R. and Kuo, J.F., 1983. Phospholipid-sensitive Ca2+-dependent protein kinase and its substrates in human neutrophils. *Biochemical and biophysical research communications*, *111*(3), pp.847-853.

Henderson, B., Edwards, J.G. and Pettipher, E.R. eds., 1995. *Mechanisms and models in rheumatoid arthritis*. Academic Press.

Hershkoviz, R., Schor, H., Ariel, A., Hecht, I., Cohen, I.R., Lider, O. and Cahalon, L., 2000. Disaccharides generated from heparan sulphate or heparin modulate chemokine-induced T-cell adhesion to extracellular matrix. *Immunology*, *99*(1), pp.87-93.

Hiebert, L.M., Wice, S.M., Ping, T., Hileman, R.E., Polat, T. and Linhardt, R.J., 2002. Tissue Distribution of [14 C] Sucrose Octasulphate following Oral Administration to Rats. *Pharmaceutical research*, *19*(6), pp.838-844.

Hijiya, N., Miyake, K., Akashi, S., Matsuura, K., Higuchi, Y. and Yamamoto, S., 2002. Possible involvement of toll-like receptor 4 in endothelial cell activation of larger vessels in response to lipopolysaccharide. *Pathobiology*, *70*(1), pp.18-25.

Hiraoki, T. and Vogel, H.J., 1987. Structure and function of calcium-binding proteins. *Journal of cardiovascular pharmacology*, *10*, pp.S14-31.

Hjort, M.R., Brenyo, A.J., Finkelstein, J.N., Frampton, M.W., LoMonaco, M.B., Stewart, J.C., Johnston, C.J. and D'Angio, C.T., 2003. Alveolar epithelial cell-macrophage interactions affect oxygen-stimulated interleukin-8 release. *Inflammation*, *27*(3), pp.137-145.

Hofkens, W., Schelbergen, R., Storm, G., van den Berg, W.B. and van Lent, P.L., 2013. Liposomal targeting of prednisolone phosphate to synovial lining macrophages during experimental arthritis inhibits M1 activation but does not favor M2 differentiation. *PloS one*, *8*(2), p.e54016.

Holness, C.L. and Simmons, D.L., 1993. Molecular cloning of CD68, a human macrophage marker related to lysosomal glycoproteins.

Hopewood, J.J., 1989. Enzymes that degrade heparin and heparan sulphate. *Heparin. Chemical and Biological Properties, Clinical Applications*, *191*.

Hopkins, A.L. and Groom, C.R., 2002. The druggable genome. *Nature reviews Drug discovery*, *1*(9), pp.727-730.

Howe, L.R., Leevers, S.J., Gómez, N., Nakielny, S., Cohen, P. and Marshall, C.J., 1992. Activation of the MAP kinase pathway by the protein kinase raf. *Cell*, *71*(2), pp.335-342.

Hunter, T., 1995. Protein kinases and phosphatases: the yin and yang of protein phosphorylation and signalling. *Cell*, *80*(2), pp.225-236

Idzko, M., la Sala, A., Ferrari, D., Panther, E., Herouy, Y., Dichmann, S., Mockenhaupt, M., Di Virgilio, F., Girolomoni, G. and Norgauer, J., 2002. Expression and function of histamine receptors in human monocyte-derived dendritic cells. *Journal of allergy and clinical immunology*, *109*(5), pp.839-846.

Ishai-Michaeli, R., Svahn, C.M., Weber, M., Chajek-Shaul, T., Korner, G., Ekre, H.P. and Vlodavsky, I., 1992. Importance of size and sulphation of heparin in release of basic fibroblast growth factor from the vascular endothelium and extracellular matrix. *Biochemistry*, *31*(7), pp.2080-2088.

Isomäki, P., Luukkainen, R., Saario, R., Toivanen, P. and Punnonen, J., 1996. Interleukin-10 functions as an antiinflammatory cytokine in rheumatoid synovium. *Arthritis & Rheumatism: Official Journal of the American College of Rheumatology*, *39*(3), pp.386-395.

Isomäki, P., Luukkainen, R., Toivanen, P. and Punnonen, J., 1996. The presence of interleukin-13 in rheumatoid synovium and its antiinflammatory effects on synovial fluid macrophages from patients with rheumatoid arthritis. *Arthritis & Rheumatism: Official Journal of the American College of Rheumatology*, *39*(10), pp.1693-1702.

Itoh, T., Kusaka, K., Kawaura, K., Kashimura, K., Yamakawa, J., Takahashi, T. and Kanda, T., 2004. Selective binding of sucralfate to endoscopic mucosal resection-induced gastric ulcer: evaluation of aluminium adherence. *Journal of international medical research*, *32*(5), pp.520-529.

---

Jablonski, K.A., Amici, S.A., Webb, L.M., Ruiz-Rosado, J.D.D., Popovich, P.G., Partida-Sanchez, S. and Guerau-de-Arellano, M., 2015. Novel markers to delineate murine M1 and M2 macrophages. *PloS one*, *10*(12), p.e0145342.

Jackson, V.M., Trout, S.J., Brain, K.L. and Cunnane, T.C., 2001. Characterization of action potential-evoked calcium transients in mouse postganglionic sympathetic axon bundles. *The Journal of Physiology*, *537*(1), pp.3-16.

Jacob, F., Novo, C.P., Bachert, C. and Van Crombruggen, K., 2013. Purinergic signalling in inflammatory cells: P2 receptor expression, functional effects, and modulation of inflammatory responses. *Purinergic signalling*, *9*(3), pp.285-306.

Jacobs, M. and Harrison, S., 1998. Structure of an IκBα/NF-κB complex. *Cell*, *95*, pp.749-758.

Jacquel, A., Herrant, M., Legros, L., Belhacene, N., Luciano, F., Pages, G., Hofman, P. and Auberger, P., 2003. Imatinib induces mitochondria-dependent apoptosis of the Bcr-Abl-positive K562 cell line and its differentiation toward the erythroid lineage. *The FASEB journal*, *17*(14), pp.2160-2162.

Jaffee, B.D., Manos, E.J., Collins, R.J., Czerniak, P.M., Favata, M.F., Magolda, R.L., Scherle, P.A. and Trzaskos, J.M., 2000. Inhibition of MAP kinase kinase (MEK) results in

an anti-inflammatory response in vivo. *Biochemical and biophysical research communications*, *268*(2), pp.647-651.

Jiang, Y. and Fleet, J.C., 2012. Effect of phorbol 12-myristate 13-acetate activated signalling pathways on 1α, 25 dihydroxyvitamin D3 Regulated Human 25-hydroxyvitamin D3 24-hydroxylase Gene Expression in Differentiated Caco-2 Cells. *Journal of cellular biochemistry*, *113*(5), pp.1599-1607.

Jin, M., Iwamoto, T., Yamada, K., Satsu, H., Totsuka, M. and Shimizu, M., 2011. Effects of chondroitin sulphate and its oligosaccharides on toll-like receptor-mediated IL-6 secretion by macrophage-like J774. 1 cells. *Bioscience, biotechnology, and biochemistry*, *75*(7), pp.1283-1289.

Jomphe, C., Gabriac, M., Hale, T.M., Héroux, L., Trudeau, L.É., Deblois, D., Montell, E., Vergés, J. and Du Souich, P., 2008. Chondroitin Sulphate Inhibits the Nuclear Translocation of Nuclear Factor-κB in Interleukin-1β-Stimulated Chondrocytes. *Basic & clinical pharmacology & toxicology*, *102*(1), pp.59-65.

Jones, D.T., Jäger, N., Kool, M., Zichner, T., Hutter, B., Sultan, M., Cho, Y.J., Pugh, T.J., Hovestadt, V., Stütz, A.M. and Rausch, T., 2012. Dissecting the genomic complexity underlying medulloblastoma. *Nature*, *488*(7409), pp.100-105.

Jones, L.S., Yazzie, B. and Middaugh, C.R., 2004. Polyanions and the proteome. *Molecular & Cellular Proteomics*, *3*(8), pp.746-769.

Jovanovic, D.V., Di Battista, J.A., Martel-Pelletier, J., Jolicoeur, F.C., He, Y., Zhang, M., Mineau, F. and Pelletier, J.P., 1998. IL-17 stimulates the production and expression of proinflammatory cytokines, IL-β and TNF-α, by human macrophages. *The Journal of Immunology*, *160*(7), pp.3513-3521.

Juliet, P.A., Hayashi, T., Iguchi, A. and Ignarro, L.J., 2003. Concomitant production of nitric oxide and superoxide in human macrophages. *Biochemical and biophysical research communications*, *310*(2), pp.367-370.

Jung, K.A., Choi, B.H., Nam, C.W., Song, M., Kim, S.T., Lee, J.Y. and Kwak, M.K., 2013. Identification of aldo-keto reductases as NRF2-target marker genes in human cells. *Toxicology letters*, *218*(1), pp.39-49.

Kang, J.H., 2014. Protein kinase C (PKC) isozymes and cancer. *New Journal of Science*, *2014*.

Kasarełło, K., Cudnoch-Jędrzejewska, A., Członkowski, A. and Mirowska-Guzel, D., 2017. Mechanism of action of three newly registered drugs for multiple sclerosis treatment. *Pharmacological Reports*, *69*(4), pp.702-708.

Kawamura, K., Shibata, T., Saget, O., Peel, D. and Bryant, P.J., 1999. A new family of growth factors produced by the fat body and active on Drosophila imaginal disc cells. *Development*, *126*(2), pp.211-219.

Keadle, T.L., Usui, N., Laycock, K.A., Miller, J.K., Pepose, J.S. and Stuart, P.M., 2000. IL-1 and TNF-α are important factors in the pathogenesis of murine recurrent herpetic stromal keratitis. *Investigative ophthalmology & visual science*, *41*(1), pp.96-102.

Keffer, J., Probert, L., Cazlaris, H., Georgopoulos, S., Kaslaris, E., Kioussis, D. and Kollias, G., 1991. Transgenic mice expressing human tumour necrosis factor: a predictive genetic model of arthritis. *The EMBO journal*, *10*(13), pp.4025-4031.

Kennedy, A., Fearon, U., Veale, D.J. and Godson, C., 2011. Macrophages in synovial inflammation. *Frontiers in Immunology*, *2*, p.52.

Kharbanda, S., Saleem, A., Emoto, Y., Stone, R., Rapp, U. and Kufe, D., 1994. Activation of Raf-1 and mitogen-activated protein kinases during monocytic differentiation of human myeloid leukemia cells. *Journal of Biological Chemistry*, *269*(2), pp.872-878.

Kim, E.K., Kwon, J.E., Lee, S.Y., Lee, E.J., Kim, D.S., Moon, S.J., Lee, J., Kwok, S.K., Park, S.H. and Cho, M.L., 2018. IL-17-mediated mitochondrial dysfunction impairs apoptosis in rheumatoid arthritis synovial fibroblasts through activation of autophagy. *Cell Death & Disease*, *8*(1), pp.e2565-e2565.

Kim, E.Y. and Moudgil, K.D., 2017. Immunomodulation of autoimmune arthritis by pro-inflammatory cytokines. *Cytokine*, *98*, pp.87-96.

Kim, H.K., Kim, S.H., Kang, Y.W., Kim, B., Rhee, K.J. and Kim, Y.S., 2016. Triglyceride Regulates the Expression of M1 and M2 Macrophage-specific Markers in THP-1 Monocytes. *Biomedical Science Letters*, *22*(4), pp.220-226.

Kinne, R.W., Kunisch, E., Winter, R. and Roth, A., 2002, February. Differential influence of IL-1-β, TNF-α, and PDGF-BB on the expression of matrix-metalloproteinases (MMPs) and'total'-MMP activity in early-passage RA-and OA-synovial fibroblasts (SFB). In *Arthritis Research & Therapy* (Vol. 4, No. 1, pp. 1-38). BioMed Central.

Kiyotaki, C. and Bloom, B.R., 1984. Activation of murine macrophage cell lines. Possible involvement of protein kinases in stimulation of superoxide production. *The Journal of Immunology*, *133*(2), pp.923-931.

Kjellen, L. and Lindahl, U., 1991. Proteoglycans: structures and interactions. *Annual review of biochemistry*, *60*(1), pp.443-475.

Klein, M., Vaeth, M., Scheel, T., Grabbe, S., Baumgrass, R., Berberich-Siebelt, F., Bopp, T., Schmitt, E. and Becker, C., 2012. Repression of cyclic adenosine monophosphate

upregulation disarms and expands human regulatory T cells. *The Journal of Immunology*, *188*(3), pp.1091-1097.

Koch, A.E., Burrows, J.C., Haines, G.K., Carlos, T.M., Harlan, J.M. and Leibovich, S.J., 1991. Immunolocalization of endothelial and leukocyte adhesion molecules in human rheumatoid and osteoarthritic synovial tissues. *Laboratory investigation; a journal of technical methods and pathology*, *64*(3), pp.313-320.

Kolarova, N., Trgiňa, R., Linek, K. and Farkaš, V., 1995. Inhibitory effect of diglucosylamines on two β-glucosidases. *Carbohydrate research*, *273*(1), pp.109-113.

Kolarova, N., Trgiňa, R., Linek, K. and Farkaš, V., 1995. Inhibitory effect of diglucosylamines on two β-glucosidases. *Carbohydrate research*, *273*(1), pp.109-113.

König, B., Di Nitto, P.A. and Blumberg, P.M., 1985. Phospholipid and Ca++ dependency of phorbol ester receptors. *Journal of cellular biochemistry*, *27*(3), pp.255-265.

Korb, A., Tohidast-Akrad, M., Cetin, E., Axmann, R., Smolen, J. and Schett, G., 2006. Differential tissue expression and activation of p38 MAPK α, β, γ, and δ isoforms in rheumatoid arthritis. *Arthritis & Rheumatism*, *54*(9), pp.2745-2756.

Kosako, H., Yamaguchi, N., Aranami, C., Ushiyama, M., Kose, S., Imamoto, N., Taniguchi, H., Nishida, E. and Hattori, S., 2009. Phosphoproteomics reveals new ERK MAP kinase targets and links ERK to nucleoporin-mediated nuclear transport. *Nature structural & molecular biology*, *16*(10), pp.1026-1035.

Kotake, S., Udagawa, N., Takahashi, N., Matsuzaki, K., Itoh, K., Ishiyama, S., Saito, S., Inoue, K., Kamatani, N., Gillespie, M.T. and Martin, T.J., 1999. IL-17 in synovial fluids from patients with rheumatoid arthritis is a potent stimulator of osteoclastogenesis. *The Journal of clinical investigation*, *103*(9), pp.1345-1352.

Kraan, M.C., Reece, R.J., Barg, E.C., Smeets, T.J., Farnell, J., Rosenburg, R., Veale, D.J., Breedveld, F.C., Emery, P. and Tak, P.P., 2000. Modulation of inflammation and metalloproteinase expression in synovial tissue by leflunomide and methotrexate in patients with active rheumatoid arthritis: findings in a prospective, randomized, double-blind, parallel-design clinical trial in thirty-nine patients at two centers. *Arthritis & Rheumatism: Official Journal of the American College of Rheumatology*, *43*(8), pp.1820-1830.

Kramer, P.R. and Wray, S., 2002. 17-β-Estradiol regulates expression of genes that function in macrophage activation and cholesterol homeostasis. *The Journal of steroid biochemistry and molecular biology*, *81*(3), pp.203-216.

Krysan, K., Dalwadi, H., Sharma, S., Põld, M. and Dubinett, S., 2004. Cyclooxygenase 2-dependent expression of survivin is critical for apoptosis resistance in non-small cell lung cancer. *Cancer research*, *64*(18), pp.6359-6362.

Kuhn, A.M., Tzieply, N., Schmidt, M.V., Von Knethen, A., Namgaladze, D., Yamamoto, M. and Brüne, B., 2011. Antioxidant signalling via Nrf2 counteracts lipopolysaccharide-mediated inflammatory responses in foam cell macrophages. *Free Radical Biology and Medicine*, *50*(10), pp.1382-1391.

Kumar, S., Boehm, J. and Lee, J.C., 2003. p38 MAP kinases: key signalling molecules as therapeutic targets for inflammatory diseases. *Nature reviews Drug discovery*, *2*(9), pp.717-726.

Kunisch, E., Fuhrmann, R., Roth, A., Winter, R., Lungershausen, W. and Kinne, R.W., 2004. Macrophage specificity of three anti-CD68 monoclonal antibodies (KP1, EBM11, and PGM1) widely used for immunohistochemistry and flow cytometry. *Annals of the rheumatic diseases*, *63*(7), pp.774-784.

Kunisch, E., Jansen, A., Kojima, F., Löffler, I., Kapoor, M., Kawai, S., Rubio, I., Crofford, L.J. and Kinne, R.W., 2009. Prostaglandin E2 differentially modulates proinflammatory/prodestructive effects of TNF-α on synovial fibroblasts via specific E prostanoid receptors/cAMP. *The Journal of Immunology*, *183*(2), pp.1328-1336.

Kyriakis, J.M. and Avruch, J., 1996. Protein kinase cascades activated by stress and inflammatory cytokines. *Bioessays*, *18*(7), pp.567-577.

Kyriakis, J.M. and Avruch, J., 2001. Mammalian mitogen-activated protein kinase signal transduction pathways activated by stress and inflammation. *Physiological reviews*, *81*(2), pp.807-869.

Laemmli, U.K., 1970. Cleavage of structural proteins during the assembly of the head of bacteriophage T4. *nature*, *227*(5259), pp.680-685.

Lawrence, T. and Natoli, G., 2011. Transcriptional regulation of macrophage polarization: enabling diversity with identity. *Nature reviews immunology*, *11*(11), pp.750-761.

Lawrence, T., Willoughby, D.A. and Gilroy, D.W., 2002. Anti-inflammatory lipid mediators and insights into the resolution of inflammation. *Nature Reviews Immunology*, *2*(10), pp.787-795.

Lederberg, J., Hamburg, M.A. and Smolinski, M.S. eds., 2003. Microbial threats to health: emergence, detection, and response.

Lee, J.C. and Young, P.R., 1996. Role of CSBP/p38/RK stress response kinase in LPS and cytokine signalling mechanisms. *Journal of Leukocyte Biology*, *59*(2), pp.152-157.

Lee, J.C., Kassis, S., Kumar, S., Badger, A. and Adams, J.L., 1999. p38 mitogen-activated protein kinase inhibitors—mechanisms and therapeutic potentials. *Pharmacology & therapeutics*, *82*(2-3), pp.389-397.

Lee, J.C., Laydon, J.T., McDonnell, P.C., Gallagher, T.F., Kumar, S., Green, D., McNulty, D., Blumenthal, M.J., Keys, J.R., Strickler, J.E. and McLaughlin, M.M., 1994. A protein kinase involved in the regulation of inflammatory cytokine biosynthesis. *Nature*, *372*(6508), pp.739-746.

Lees, M., Dugo, L., Ganiyu-dada, Z., Mancini, J., Burnet, J., Seed, M., 2008. 'Anti-rheumatic activity and cytokine synthesis inhibition by the oligosulphated disaccharide sucrose octasulphate', *Inflammaopharmacology* 9th International Conference, Queens' College, Cambridge. 8-10 September, pp. 318 - 319.

Lever, R. and Page, C., 2001. Glycosaminoglycans, airways inflammation and bronchial hyperresponsiveness. *Pulmonary pharmacology & therapeutics*, *14*(3), pp.249-254.

Levy, F.O., Rasmussen, A.M., Taskén, K., Skålhegg, B.S., Huitfeldt, H.S., Funderud, S., Smeland, E.B. and Hansson, V., 1996. Cyclic AMP-dependent protein kinase (cAK) in human B cells: co-localization of type I cAK (RIα2C2) with the antigen receptor during anti-immunoglobulin-induced B cell activation. *European journal of immunology*, *26*(6), pp.1290-1296.

Li, J.X., Shen, Y.Q., Cai, B.Z., Zhao, J., Bai, X., Lu, Y.J. and Li, X.Q., 2009. Arsenic trioxide induces the apoptosis in vascular smooth muscle cells via increasing intracellular calcium and ROS formation. *Molecular biology reports*, *37*(3), pp.1569-1576.

Li, S.N., Wang, W., Fu, S.P., Wang, J.F., Liu, H.M., Xie, S.S., Liu, B.R., Li, Y., Lv, Q.K., Li, Z.Q. and Xue, W.J., 2013. IL-21 modulates release of proinflammatory cytokines in LPS-stimulated macrophages through distinct signalling pathways. *Mediators of inflammation*, *2013*.

Li, W. and Kong, A.N., 2009. Molecular mechanisms of Nrf2-mediated antioxidant response. *Molecular Carcinogenesis: Published in cooperation with the University of Texas MD Anderson Cancer Center*, *48*(2), pp.91-104.

Liang, F., Seyrantepe, V., Landry, K., Ahmad, R., Ahmad, A., Stamatos, N.M. and Pshezhetsky, A.V., 2006. Monocyte differentiation up-regulates the expression of the lysosomal sialidase, Neu1, and triggers its targeting to the plasma membrane via major histocompatibility complex class II-positive compartments. *Journal of Biological Chemistry*, *281*(37), pp.27526-27538.

Lider, O., Baharav, E., Mekori, Y.A., Miller, T., Naparstek, Y., Vlodavsky, I. and Cohen, I.R., 1989. Suppression of experimental autoimmune diseases and prolongation of allograft survival by treatment of animals with low doses of heparins. *The Journal of clinical investigation*, *83*(3), pp.752-756.

Lider, O., Cahalon, L., Gilat, D., Hershkoviz, R., Siegel, D., Margalit, R., Shoseyov, O. and Cohen, I.R., 1995. A disaccharide that inhibits tumour necrosis factor alpha is formed from the extracellular matrix by the enzyme heparanase. *Proceedings of the National Academy of Sciences*, *92*(11), pp.5037-5041.

Linares, V., Alonso, V. and Domingo, J.L., 2011. Oxidative stress as a mechanism underlying sulfasalazine-induced toxicity. *Expert opinion on drug safety*, *10*(2), pp.253-263.

Lincoln, T.M. and Cornwell, T.L., 1993. Intracellular cyclic GMP receptor proteins. *The FASEB journal*, *7*(2), pp.328-338.

Liopeta, K., Boubali, S., Virgilio, L., Thyphronitis, G., Mavrothalassitis, G., Dimitracopoulos, G. and Paliogianni, F., 2009. cAMP regulates IL-10 production by normal human T lymphocytes at multiple levels: a potential role for MEF2. *Molecular immunology*, *46*(3), pp.345-354.

Liote, F., Boval-Boizard, B., Weill, D., Kuntz, D. and WAUTIER, J.L., 1996. Blood monocyte activation in rheumatoid arthritis: increased monocyte adhesiveness, integrin expression, and cytokine release. *Clinical & Experimental Immunology*, *106*(1), pp.13-19.

Liu, C., Li, Y., Yu, J., Feng, L., Hou, S., Liu, Y., Guo, M., Xie, Y., Meng, J., Zhang, H. and Xiao, B., 2013. Targeting the shift from M1 to M2 macrophages in experimental autoimmune encephalomyelitis mice treated with fasudil. *PloS one*, *8*(2), p.e54841.

Liu, L., Zubik, L., Collins, F.W., Marko, M. and Meydani, M., 2004. The antiatherogenic potential of oat phenolic compounds. *Atherosclerosis*, *175*(1), pp.39-49.

MacNaul, K.L., Hutchinson, N.I., Parsons, J.N., Bayne, E.K. and Tocci, M.J., 1990. Analysis of IL-1 and TNF-alpha gene expression in human rheumatoid synoviocytes and normal monocytes by in situ hybridization. *The Journal of Immunology*, *145*(12), pp.4154-4166.

Maddison, J.E., Page, S.W. and Church, D.B. eds., 2008. *Small animal clinical pharmacology* (Vol. 5). Elsevier Health Sciences.

Makarov, S.S., 2000. NF-κB as a therapeutic target in chronic inflammation: recent advances. *Molecular medicine today*, *6*(11), pp.441-448.

Mantovani, A., Sica, A. and Locati, M., 2007. New vistas on macrophage differentiation and activation. *European journal of immunology*, *37*(1), pp.14-16.

Mantovani, A., Sica, A., Sozzani, S., Allavena, P., Vecchi, A. and Locati, M., 2004. The chemokine system in diverse forms of macrophage activation and polarization. *Trends in immunology*, *25*(12), pp.677-686.

Mantovani, A., Sozzani, S., Locati, M., Allavena, P. and Sica, A., 2002. Macrophage polarization: tumour-associated macrophages as a paradigm for polarized M2 mononuclear phagocytes. *Trends in immunology*, *23*(11), pp.549-555.

Marlin, S.D. and Springer, T.A., 1987. Purified intercellular adhesion molecule-1 (ICAM-1) is a ligand for lymphocyte function-associated antigen 1 (LFA-1). *Cell*, *51*(5), pp.813-819.

Marshall, M.S., 1995. Ras target proteins in eukaryotic cells. *The FASEB Journal*, *9*(13), pp.1311-1318.

Martinez, F.O. and Gordon, S., 2014. The M1 and M2 paradigm of macrophage activation: time for reassessment. *F1000prime reports*, *6*.

Martinez, F.O., Gordon, S., Locati, M. and Mantovani, A., 2006. Transcriptional profiling of the human monocyte-to-macrophage differentiation and polarization: new molecules and patterns of gene expression. *The Journal of Immunology*, *177*(10), pp.7303-7311.

Martinez, F.O., Sica, A., Mantovani, A. and Locati, M., 2008. Macrophage activation and polarization. *Front Biosci*, *13*(1), pp.453-461.

Maskrey, B.H., Megson, I.L., Whitfield, P.D. and Rossi, A.G., 2011. Mechanisms of resolution of inflammation: a focus on cardiovascular disease. *Arteriosclerosis, thrombosis, and vascular biology*, *31*(5), pp.1001-1006.

Matsumoto, E., Hatanaka, M., Bohgaki, M. and Maeda, S., 2006. PKC pathway and ERK/MAPK pathway are required for induction of cyclin D1 and p21Waf1 during 12-o-tetradecanoylphorbol 13-acetate-induced differentiation of myeloleukemia cells. *Kobe Journal of Medical Sciences*, *52*(6), p.181.

May, W.S., Jacobs, S. and Cuatrecasas, P., 1984. Association of phorbol ester-induced hyperphosphorylation and reversible regulation of transferrin membrane receptors in HL60 cells. *Proceedings of the National Academy of Sciences*, *81*(7), pp.2016-2020.

McInnes, I.B. and Schett, G., 2007. Cytokines in the pathogenesis of rheumatoid arthritis. *Nature Reviews Immunology*, *7*(6), pp.429-442.

McKenzie, F.R. and Pouysségur, J., 1996. cAMP-mediated growth inhibition in fibroblasts is not mediated via mitogen-activated protein (MAP) kinase (ERK) inhibition: cAMP-dependent protein kinase induces a temporal shift in growth factor-stimulated MAP kinases. *Journal of Biological Chemistry*, *271*(23), pp.13476-13483.

McLachlan, J., 1985. Macroalgae (seaweeds): industrial resources and their utilization. In *Biosalinity in action: bioproduction with saline water* (pp. 137-157). Springer, Dordrecht.

McPhail, L.C. and Snyderman, R., 1983. Activation of the respiratory burst enzyme in human polymorphonuclear leukocytes by chemoattractants and other soluble stimuli. Evidence that the same oxidase is activated by different transductional mechanisms. *The Journal of clinical investigation*, *72*(1), pp.192-200.

Mellado, M., Martínez-Muñoz, L., Cascio, G., Lucas, P., Pablos, J.L. and Rodríguez-Frade, J.M., 2015. T cell migration in rheumatoid arthritis. *Frontiers in immunology*, *6*, p.384.

Microbiology. (2021). *Major Histocompatibility Complexes and Antigen-Presenting Cells*. [online] Available at: https://courses.lumenlearning.com/microbiology/chapter/major-histocompatibility-complexes-and-antigen-presenting-cells/.

Mills, C.D., Kincaid, K., Alt, J.M., Heilman, M.J. and Hill, A.M., 2000. M-1/M-2 macrophages and the Th1/Th2 paradigm. *The Journal of immunology*, *164*(12), pp.6166-6173.

Minta, J.O. and Pambrun, L., 1985. In vitro induction of cytologic and functional differentiation of the immature human monocytelike cell line U-937 with phorbol myristate acetate. *The American journal of pathology*, *119*(1), p.111.

Miossec, P., Naviliat, M., D'Angeac, A.D., Sany, J. and Banchereau, J., 1990. Low levels of interleukin-4 and high levels of transforming growth factor β in rheumatoid synovitis. *Arthritis & rheumatism*, *33*(8), pp.1180-1187.

Mochly-Rosen, D., Das, K. and Grimes, K.V., 2012. Protein kinase C, an elusive therapeutic target?. *Nature reviews Drug discovery*, *11*(12), pp.937-957.

Morales-Ducret, J., Wayner, E., Elices, M.J., Alvaro-Gracia, J.M., Zvaifler, N.J. and Firestein, G.S., 1992. Alpha 4/beta 1 integrin (VLA-4) ligands in arthritis. Vascular cell adhesion molecule-1 expression in synovium and on fibroblast-like synoviocytes. *the Journal of Immunology*, *149*(4), pp.1424-1431.

Moreno-Navarrete, J.M., Ortega, F.J., Bassols, J., Ricart, W. and Fernández-Real, J.M., 2009. Decreased circulating lactoferrin in insulin resistance and altered glucose tolerance as a possible marker of neutrophil dysfunction in type 2 diabetes. *The Journal of Clinical Endocrinology & Metabolism*, *94*(10), pp.4036-4044.

Morrison, D.K., 2012. MAP kinase pathways. *Cold Spring Harbor perspectives in biology*, *4*(11), p.a011254.

Mosior, M. and Newton, A.C., 1996. Calcium-independent binding to interfacial phorbol esters causes protein kinase C to associate with membranes in the absence of acidic lipids. *Biochemistry*, *35*(5), pp.1612-1623.

Mosmann, T., 1983. Rapid colorimetric assay for cellular growth and survival: application to proliferation and cytotoxicity assays. *Journal of immunological methods*, *65*(1-2), pp.55-63.

Mosser, D.M. and Edwards, J.P., 2008. Exploring the full spectrum of macrophage activation. *Nature reviews immunology*, *8*(12), pp.958-969.

Mosser, D.M. and Edwards, J.P., 2008. Exploring the full spectrum of macrophage activation. *Nature reviews immunology*, *8*(12), pp.958-969.

Mota, P., Reddy, V. and Isenberg, D., 2017. Improving B-cell depletion in systemic lupus erythematosus and rheumatoid arthritis. *Expert review of clinical immunology*, *13*(7), pp.667-676.

Mulherin, D., Fitzgerald, O. and Bresnihan, B., 1996. Synovial tissue macrophage populations and articular damage in rheumatoid arthritis. *Arthritis & Rheumatism: Official Journal of the American College of Rheumatology*, *39*(1), pp.115-124.

Murphy, A., Vines, A. and McBean, G.J., 2009. Stimulation of EAAC1 in C6 glioma cells by store-operated calcium influx. *Biochimica et Biophysica Acta (BBA)-Biomembranes*, *1788*(2), pp.551-558.

Murphy, R.A. and Walker, J.S., 1998. Inhibitory mechanisms for cross-bridge cycling: the nitric oxide-cGMP signal transduction pathway in smooth muscle relaxation. *Acta physiologica scandinavica*, *164*(4), pp.373-380.

Murray, P.J. and Wynn, T.A., 2011. Obstacles and opportunities for understanding macrophage polarization. *Journal of leukocyte biology*, *89*(4), pp.557-563.

Murray, P.J., Allen, J.E., Biswas, S.K., Fisher, E.A., Gilroy, D.W., Goerdt, S., Gordon, S., Hamilton, J.A., Ivashkiv, L.B., Lawrence, T. and Locati, M., 2014. Macrophage activation and polarization: nomenclature and experimental guidelines. *Immunity*, *41*(1), pp.14-20.

Murthy, P.K., Dennis, V.A., Lasater, B.L. and Philipp, M.T., 2000. Interleukin-10 modulates proinflammatory cytokines in the human monocytic cell line THP-1 stimulated with Borrelia burgdorferi lipoproteins. *Infection and immunity*, *68*(12), pp.6663-6669.

---

Nader, H.B., Chavante, S.F., Dos-Santos, E.A., Oliveira, F.W., De-Paiva, J.F., Jerônimo, S.M.B., Medeiros, G.F.D., De-Abreu, L.R.D., Leite, E.L., de-Sousa-Filho, J.F. and Castro, R.A.B., 1999. Heparan sulphates and heparins: similar compounds performing the same

functions in vertebrates and invertebrates?. *Brazilian Journal of Medical and Biological Research*, *32*(5), pp.529-538.

Nagarkatti, D.S. and Ramadan, I.S., 1998. Role of p38 MAP kinase in myocardial stress. *Journal of molecular and cellular cardiology*, *30*(8), pp.1651-1664.

Nagashima, R., 1980. Selective binding of sucralfate to ulcer lesion. I: Experiments in rats with acetic acid-induced gastric ulcer receiving unlabelled sucralfate.

Nagashima, R., Hinohara, Y., Hirano, T.E., Tohira, Y. and Kamiyama, H., 1980. Selective binding of sucralfate to ulcer lesion. II. Experiments in rats with gastric ulcer receiving 14C-sucralfate or potassium 14C-sucrose sulphate. *Arzneimittel-forschung*, *30*(1), pp.84-88.

Nakao, S., Ogtata, Y., Shimizu, E., Yamazaki, M., Furuyama, S. and Sugiya, H., 2002. Tumour necrosis factor α (TNF-α)-induced prostaglanding E 2 release is mediated by the activation of cyclooxygenase-2 (COX-2) transcription via NFκB in human gingival fibroblasts. *Molecular and cellular biochemistry*, *238*(1), pp.11-18.

Nakazawa, S., Nagashima, R. and Samloff, I.M., 1981. Selective binding of sucralfate to gastric ulcer in man. *Digestive diseases and sciences*, *26*(4), pp.297-300.

Nalbandian, A., Crispin, J.C. and Tsokos, G.C., 2009. Interleukin-17 and systemic lupus erythematosus: current concepts. *Clinical & Experimental Immunology*, *157*(2), pp.209-215.

Nam, E.J. and Park, P.W., 2012. Shedding of cell membrane-bound proteoglycans. *Proteoglycans*, pp.291-305.

Nathan, C., 1992. Nitric oxide as a secretory product of mammalian cells. *The FASEB journal*, *6*(12), pp.3051-3064.

Nelson, R.M., Cecconi, O., Roberts, W.G., Aruffo, A., Linhardt, R.J. and Bevilacqua, M.P., 1993. Heparin oligosaccharides bind L-and P-selectin and inhibit acute inflammation.

Newell, C.L., Deisseroth, A.B. and Lopez-Berestein, G., 1994. Interaction of nuclear proteins with an AP-1/CRE-like promoter sequence in the human TNF-α gene. *Journal of Leukocyte Biology*, *56*(1), pp.27-35.

Newton, A.C., 2001. Protein kinase C: structural and spatial regulation by phosphorylation, cofactors, and macromolecular interactions. *Chemical reviews*, *101*(8), pp.2353-2364.

Newton, A.C., Bootman, M.D. and Scott, J.D., 2016. Second messengers. *Cold Spring Harbor perspectives in biology*, *8*(8), p.a005926.

Nishimura, N., Harada-Shiba, M., Tajima, S., Sugano, R., Yamamura, T., Qiang, Q.Z. and Yamamoto, A., 1998. Acquisition of secretion of transforming growth factor-β1 leads to autonomous suppression of scavenger receptor activity in a monocyte-macrophage cell line, THP-1. *Journal of Biological Chemistry*, *273*(3), pp.1562-1567.

Nishizuka, Y., 1995. Protein kinase C and lipid signalling for sustained cellular responses. *The FASEB journal*, *9*(7), pp.484-496.

Nomura, N., Nomura, M., Sugiyama, K. and Hamada, J.I., 2007. Phorbol 12-myristate 13-acetate (PMA)-induced migration of glioblastoma cells is mediated via p38MAPK/Hsp27 pathway. *Biochemical pharmacology*, *74*(5), pp.690-701.

Nussler, A.K. and Billiar, T.R., 1993. Inflammation, immunoregulation, and inducible nitric oxide synthase. *Journal of leukocyte biology*, *54*(2), pp.171-178.

Nutchey, B.K., Kaplan, J.S., Dwivedi, P.P., Omdahl, J.L., Ferrante, A., May, B.K. and Hii, C.S., 2005. Molecular action of 1, 25-dihydroxyvitamin D3 and phorbol ester on the activation of the rat cytochrome P450C24 (CYP24) promoter: role of MAP kinase activities and identification of an important transcription factor binding site. *Biochemical Journal*, *389*(3), pp.753-762.

O'Brian, C.A. and Ward, N.E., 1989. Biology of the protein kinase C family. *Cancer and Metastasis Reviews*, *8*(3), pp.199-214.

Oduah, E.I., Linhardt, R.J. and Sharfstein, S.T., 2016. Heparin: past, present, and future. *Pharmaceuticals*, *9*(3), p.38.

Orlando, R.C. and Tobey, N.A., 1990. Why Does Sucralfate Improve Healing in Reflux Esophagitis?: The Role of Sucrose Octasulphate. *Scandinavian Journal of Gastroenterology*, *25*(sup173), pp.17-21.

Orlando, R.C., 1987. Cytoprotection by sucralfate in acid-exposed esophagus: a review. *Scandinavian Journal of Gastroenterology*, *22*(sup127), pp.97-100.

Orlando, R.C., Turjman, N.A., Tobey, N.A., Schreiner, V.J. and Powell, D.W., 1987. Mucosal protection by sucralfate and its components in acid-exposed rabbit esophagus. *Gastroenterology*, *93*(2), pp.352-361.

Osiri, M., Shea, B., Robinson, V., Suarez-Almazor, M., Strand, V., Tugwell, P. and Wells, G., 2003. Leflunomide for the treatment of rheumatoid arthritis: a systematic review and metaanalysis. *The Journal of rheumatology*, *30*(6), pp.1182-1190.

Paleolog, E.M., 2002. Angiogenesis in rheumatoid arthritis. *Arthritis Research & Therapy*, *4*(3), pp.1-10.

Panayi, G.S., Mackay, J.M., Neill, W.A., McCormick, J.N., Marmion, B.P. and Duthie, J.J., 1974. Cytology of rheumatoid synovial cells in culture. II. Association of polykarocytes with rheumatoid and other forms of arthritis. *Annals of the rheumatic diseases*, *33*(3), p.234.

Parish, C.R., 2006. The role of heparan sulphate in inflammation. *Nature Reviews Immunology*, *6*(9), pp.633-643.

Park, E.K., Jung, H.S., Yang, H.I., Yoo, M.C., Kim, C. and Kim, K.S., 2007. Optimized THP-1 differentiation is required for the detection of responses to weak stimuli. *Inflammation research*, *56*(1), pp.45-50.

Parrillo, J.E., 1993. Pathogenetic mechanisms of septic shock. *New England Journal of Medicine*, *328*(20), pp.1471-1477.

Pearlman, E., Jiwa, A.H., Engleberg, N.C. and Eisenstein, B.I., 1988. Growth of Legionella pneumophila in a human macrophage-like (U937) cell line. *Microbial pathogenesis*, *5*(2), pp.87-95.

Pearson, G., Robinson, F., Beers Gibson, T., Xu, B.E., Karandikar, M., Berman, K. and Cobb, M.H., 2001. Mitogen-activated protein (MAP) kinase pathways: regulation and physiological functions. *Endocrine reviews*, *22*(2), pp.153-183.

Pedrinaci, S., Ruiz-Cabello, F., Gomez, O., Collado, A. and Garrido, F., 1990. Protein kinase C-mediated regulation of the expression of CD14 and CD11/CD18 in U937 cells. *International journal of cancer*, *45*(2), pp.294-298.

Pelletier, J.P., Fernandes, J.C., Brunet, J., Moldovan, F., Schrier, D., Flory, C. and Martel-Pelletier, J., 2003. In vivo selective inhibition of mitogen-activated protein kinase kinase 1/2 in rabbit experimental osteoarthritis is associated with a reduction in the development of structural changes. *Arthritis & Rheumatism: Official Journal of the American College of Rheumatology*, *48*(6), pp.1582-1593.

Pierce, K.L., Premont, R.T. and Lefkowitz, R.J., 2002. Seven-transmembrane receptors. *Nature reviews Molecular cell biology*, *3*(9), pp.639-650.

Pincus, T., Marcum, S.B. and Callahan, L.F., 1992. Longterm drug therapy for rheumatoid arthritis in seven rheumatology private practices: II. Second line drugs and prednisone. *The Journal of rheumatology*, *19*(12), pp.1885-1894.

Pitzalis, C., Humby, F., Seed, M. P., 2014. Synovial Pathology - Oxford Textbook of Rheumatology. 4th edn. London: Oxford. pp. 386 - 397.

Pollard, L., Choy, E.H. and Scott, D.L., 2005. The consequences of rheumatoid arthritis: quality of life measures in the individual patient. *Clinical and experimental rheumatology*, *23*(5), p.S43.

Pouliot, M., Baillargeon, J., Lee, J.C., Cleland, L.G. and James, M.J., 1997. Inhibition of prostaglandin endoperoxide synthase-2 expression in stimulated human monocytes by inhibitors of p38 mitogen-activated protein kinase. *The Journal of Immunology*, *158*(10), pp.4930-4937.

Press, N.J. and Banner, K.H., 2009. 2 PDE4 inhibitors–a review of the current field. *Progress in medicinal chemistry*, *47*, pp.37-74.

Przygodzki, T., Sokal, A. and Bryszewska, M., 2005. Calcium ionophore A23187 action on cardiac myocytes is accompanied by enhanced production of reactive oxygen species. *Biochimica et Biophysica Acta (BBA)-Molecular Basis of Disease*, *1740*(3), pp.481-488.

Qin, Z., 2012. The use of THP-1 cells as a model for mimicking the function and regulation of monocytes and macrophages in the vasculature. *Atherosclerosis*, *221*(1), pp.2-11.

Quero, L., Hanser, E., Manigold, T., Tiaden, A.N. and Kyburz, D., 2017. TLR2 stimulation impairs anti-inflammatory activity of M2-like macrophages, generating a chimeric M1/M2 phenotype. *Arthritis research & therapy*, *19*(1), pp.1-13.

Rahman, A., Anwar, K.N., Minhajuddin, M., Bijli, K.M., Javaid, K., True, A.L. and Malik, A.B., 2004. cAMP targeting of p38 MAP kinase inhibits thrombin-induced NF-κB activation and ICAM-1 expression in endothelial cells. *American Journal of Physiology-Lung Cellular and Molecular Physiology*, *287*(5), pp.L1017-L1024.

Raimondo, M.G., Biggioggero, M., Crotti, C., Becciolini, A. and Favalli, E.G., 2017. Profile of sarilumab and its potential in the treatment of rheumatoid arthritis. *Drug design, development and therapy*, *11*, p.1593.

Raingeaud, J., Whitmarsh, A.J., Barrett, T., Derijard, B. and Davis, R.J., 1996. MKK3-and MKK6-regulated gene expression is mediated by the p38 mitogen-activated protein kinase signal transduction pathway. *Molecular and cellular biology*, *16*(3), pp.1247-1255.

Rainsford, K.D., Parke, A.L., Clifford-Rashotte, M. and Kean, W.F., 2015. Therapy and pharmacological properties of hydroxychloroquine and chloroquine in treatment of systemic lupus erythematosus, rheumatoid arthritis and related diseases. *Inflammopharmacology*, *23*(5), pp.231-269.

Raker, V.K., Becker, C. and Steinbrink, K., 2016. The cAMP pathway as therapeutic target in autoimmune and inflammatory diseases. *Frontiers in immunology*, *7*, p.123.

Razin, S., 1981. *Organization of Prokaryotic Cell Membranes* (B. K. Ghosh, ed.), Vol. I, pp. 180–273, CRC Press, Boca Raton, Fla.

Rey, A., Manen, D., Rizzoli, R., Ferrari, S.L. and Caverzasio, J., 2007. Evidences for a role of p38 MAP kinase in the stimulation of alkaline phosphatase and matrix mineralization induced by parathyroid hormone in osteoblastic cells. *Bone*, *41*(1), pp.59-67.

Reyes, L., Davidson, M.K., Thomas, L.C. and Davis, J.K., 1999. Effects of Mycoplasma fermentans incognitus on differentiation of THP-1 cells. *Infection and immunity*, *67*(7), pp.3188-3192.

Rice, K.G., Kim, Y.S., Grant, A.C., Merchant, Z.M. and Linhardt, R.J., 1985. High-performance liquid chromatographic separation of heparin-derived oligosaccharides. *Analytical biochemistry*, *150*(2), pp.325-331.

Righi, M., 1993. Modulation of cytokine expression by cAMP analogs in myc-immortalized microglial cell lines. *Functional neurology*, *8*(5), pp.359-363.

Roberts, S.M., Collins, J.E, Severin, G.A., 1990. Safe anti-inflammatory therapy for feline herpesvirus conjunctivitis/keratitis. XXI Annual Meeting ACVO, October 11-14.

Robidoux, J., Cao, W., Quan, H., Daniel, K.W., Moukdar, F., Bai, X., Floering, L.M. and Collins, S., 2005. Selective activation of mitogen-activated protein (MAP) kinase kinase 3 and p38α MAP kinase is essential for cyclic AMP-dependent UCP1 expression in adipocytes. *Molecular and Cellular Biology*, *25*(13), pp.5466-5479.

Robinson, M.J. and Cobb, M.H., 1997. Mitogen-activated protein kinase pathways. *Current opinion in cell biology*, *9*(2), pp.180-186.

Ronca, F., Palmieri, L., Panicucci, P. and Ronca, G., 1998. Anti-inflammatory activity of chondroitin sulphate. *Osteoarthritis and Cartilage*, *6*, pp.14-21.

Ropes, M.W., 1958. 1958 revision of diagnostic criteria for rheumatoid arthritis. *Bull Rheum Dis*, *9*, pp.175-176.

Rőszer, T., 2015. Understanding the mysterious M2 macrophage through activation markers and effector mechanisms. *Mediators of inflammation*, *2015*.

Ryoo, I.G., Shin, D.H., Kang, K.S. and Kwak, M.K., 2015. Involvement of Nrf2-GSH signalling in TGFβ1-stimulated epithelial-to-mesenchymal transition changes in rat renal tubular cells. *Archives of pharmacal research*, *38*(2), pp.272-281.

Saccani, A., Schioppa, T., Porta, C., Biswas, S.K., Nebuloni, M., Vago, L., Bottazzi, B., Colombo, M.P., Mantovani, A. and Sica, A., 2006. p50 nuclear factor-κB overexpression

in tumour-associated macrophages inhibits M1 inflammatory responses and antitumour resistance. *Cancer research*, *66*(23), pp.11432-11440.

Sakamoto, H., Aikawa, M., Hill, C.C., Weiss, D., Taylor, W.R., Libby, P. and Lee, R.T., 2001. Biomechanical strain induces class a scavenger receptor expression in human monocyte/macrophages and THP-1 cells: a potential mechanism of increased atherosclerosis in hypertension. *Circulation*, *104*(1), pp.109-114.

Salisbury, A.K., Duke, O. and Poulter, L.W., 1987. Macrophage-like cells of the pannus area in rheumatoid arthritic joints. *Scandinavian journal of rheumatology*, *16*(4), pp.263-272.

Salliot, C. and van der Heijde, D., 2009. Long-term safety of methotrexate monotherapy in patients with rheumatoid arthritis: a systematic literature research. *Annals of the rheumatic diseases*, *68*(7), pp.1100-1104.

Salmivirta, M., Lidholt, K. and Lindahl, U.L.F., 1996. Heparan sulphate: a piece of information. *The FASEB Journal*, *10*(11), pp.1270-1279.

Sánchez-Reyes, K., Bravo-Cuellar, A., Hernández-Flores, G., Lerma-Díaz, J.M., Jave-Suárez, L.F., Gómez-Lomelí, P., de Celis, R., Aguilar-Lemarroy, A., Domínguez-Rodríguez, J.R. and Ortiz-Lazareno, P.C., 2014. Cervical cancer cell supernatants induce a phenotypic switch from U937-derived macrophage-activated M1 state into M2-like suppressor phenotype with change in Toll-like receptor profile. *BioMed research international*, *2014*.

Saraiva, M. and O'garra, A., 2010. The regulation of IL-10 production by immune cells. *Nature reviews immunology*, *10*(3), pp.170-181.

Sato, H., Ogata, H. and De Luca, L.M., 2000. Annexin V inhibits the 12-O-tetradecanoylphorbol-13-acetate-induced activation of Ras/extracellular signal-regulated kinase (ERK) signalling pathway upstream of Shc in MCF-7 cells. *Oncogene*, *19*(25), pp.2904-2912.

Satoh, T., Kidoya, H., Naito, H., Yamamoto, M., Takemura, N., Nakagawa, K., Yoshioka, Y., Morii, E., Takakura, N., Takeuchi, O. and Akira, S., 2013. Critical role of Trib1 in differentiation of tissue-resident M2-like macrophages. *Nature*, *495*(7442), pp.524-528.

Schett, G., Tohidast-Akrad, M., Smolen, J.S., Schmid, B.J., Steiner, C.W., Bitzan, P., Zenz, P., Redlich, K., Xu, Q. and Steiner, G., 2000. Activation, differential localization, and regulation of the stress-activated protein kinases, extracellular signal–regulated kinase, c-Jun N-terminal kinase, and p38 mitogen-activated protein kinase, in synovial tissue and cells in rheumatoid arthritis. *Arthritis & Rheumatism: Official Journal of the American College of Rheumatology*, *43*(11), pp.2501-2512.

Schett, G., Tohidast-Akrad, M., Smolen, J.S., Schmid, B.J., Steiner, C.W., Bitzan, P., Zenz, P., Redlich, K., Xu, Q. and Steiner, G., 2000. Activation, differential localization, and regulation of the stress-activated protein kinases, extracellular signal–regulated kinase, c-Jun N-terminal kinase, and p38 mitogen-activated protein kinase, in synovial tissue and cells in rheumatoid arthritis. *Arthritis & Rheumatism: Official Journal of the American College of Rheumatology*, *43*(11), pp.2501-2512.

Schett, G., Zwerina, J. and Firestein, G., 2008. The p38 mitogen-activated protein kinase (MAPK) pathway in rheumatoid arthritis. *Annals of the rheumatic diseases*, *67*(7), pp.909-916.

Schildberger, A., Rossmanith, E., Eichhorn, T., Strassl, K. and Weber, V., 2013. Monocytes, peripheral blood mononuclear cells, and THP-1 cells exhibit different cytokine expression patterns following stimulation with lipopolysaccharide. *Mediators of inflammation*, *2013*.

Schwende, H., Fitzke, E., Ambs, P. and Dieter, P., 1996. Differences in the state of differentiation of THP-1 cells induced by phorbol ester and 1, 25-dihydroxyvitamin D3. *Journal of leukocyte biology*, *59*(4), pp.555-561.

Scott, D.L., Wolfe, F. and Huizinga, T.W., 2010. Rheumatoid arthritis. *The Lancet*, *376*(9746), pp.1094-1108.

SD, W., 1990. Ramos RA, Tobias PS, Ulevitch RJ, Mathison JC. CD14, a receptor for complexes of lipopolysaccharide (LPS) and LPS binding protein. *Science*, *249*(4975), pp.1431-1433.

Seger, R. and Krebs, E.G., 1995. The MAPK signalling cascade. *The FASEB journal*, *9*(9), pp.726-735.

Sengupta, N., Vinod, P.K. and Venkatesh, K.V., 2007. Crosstalk between cAMP-PKA and MAP kinase pathways is a key regulatory design necessary to regulate FLO11 expression. *Biophysical chemistry*, *125*(1), pp.59-71.

Serezani, C.H., Ballinger, M.N., Aronoff, D.M. and Peters-Golden, M., 2008. Cyclic AMP: master regulator of innate immune cell function. *American journal of respiratory cell and molecular biology*, *39*(2), pp.127-132.

Shackelford, D.A. and Trowbridge, I.S., 1984. Induction of expression and phosphorylation of the human interleukin 2 receptor by a phorbol diester. *Journal of Biological Chemistry*, *259*(19), pp.11706-11712.

Shakhov, A.N., Collart, M.A., Vassalli, P., Nedospasov, S.A. and Jongeneel, C.V., 1990. Kappa B-type enhancers are involved in lipopolysaccharide-mediated transcriptional

activation of the tumour necrosis factor alpha gene in primary macrophages. *The Journal of experimental medicine*, *171*(1), pp.35-47.

Shalom-Barak, T., Quach, J. and Lotz, M., 1998. Interleukin-17-induced gene expression in articular chondrocytes is associated with activation of mitogen-activated protein kinases and NF-κB. *Journal of Biological Chemistry*, *273*(42), pp.27467-27473.

Sheng, H., Shao, J., Morrow, J.D., Beauchamp, R.D. and DuBois, R.N., 1998. Modulation of apoptosis and Bcl-2 expression by prostaglandin E2 in human colon cancer cells. *Cancer research*, *58*(2), pp.362-366.

Shi, J., van Veelen, P.A., Mahler, M., Janssen, G.M., Drijfhout, J.W., Huizinga, T.W., Toes, R.E. and Trouw, L.A., 2014. Carbamylation and antibodies against carbamylated proteins in autoimmunity and other pathologies. *Autoimmunity reviews*, *13*(3), pp.225-230.

Shi, Z., Zhang, X., Chen, Z., Liebeskind, D.S. and Lou, M., 2014. Elevated thyroid autoantibodies and intracranial stenosis in stroke at an early age. *International Journal of Stroke*, *9*(6), pp.735-740.

Shimo, T., Matsumura, S., Ibaragi, S., Isowa, S., Kishimoto, K., Mese, H., Nishiyama, A. and Sasaki, A., 2007. Specific inhibitor of MEK-mediated cross-talk between ERK and p38 MAPK during differentiation of human osteosarcoma cells. *Journal of cell communication and signalling*, *1*(2), pp.103-111.

Shindo, K., Iizuka, M., Sasaki, K., Konno, S., Itou, H., Horie, Y. and Watanabe, S., 2006. Sucralfate prevents the delay of wound repair in intestinal epithelial cells by hydrogen peroxide through NF-κB pathway. *Journal of gastroenterology*, *41*(5), pp.450-461.

Shinjo, S.K., Tersariol, I.L., Oliveira, V., Nakaie, C.R., Oshiro, M.E., Ferreira, A.T., Santos, I.A., Dietrich, C.P. and Nader, H.B., 2002. Heparin and Heparan Sulphate Disaccharides Bind to the Exchanger Inhibitor Peptide Region of Na+/Ca2+ Exchanger and Reduce the Cytosolic Calcium of Smooth Muscle Cell Lines: REQUIREMENT OF C4-C5 UNSATURATION AND 1→ 4 GLYCOSIDIC LINKAGE FOR ACTIVITY. *Journal of Biological Chemistry*, *277*(50), pp.48227-48233.

Shriver, Z., Capila, I., Venkataraman, G. and Sasisekharan, R., 2012. Heparin and heparan sulphate: analyzing structure and microheterogeneity. *Heparin-A Century of Progress*, pp.159-176.

Shriver, Z., Capila, I., Venkataraman, G. and Sasisekharan, R., 2012. Heparin and heparan sulphate: analyzing structure and microheterogeneity. *Heparin-A Century of Progress*, pp.159-176.

Sica, A. and Bronte, V., 2007. Altered macrophage differentiation and immune dysfunction in tumour development. *The Journal of clinical investigation*, *117*(5), pp.1155-1166.

Sierra-Filardi, E., Puig-Kröger, A., Blanco, F.J., Nieto, C., Bragado, R., Palomero, M.I., Bernabéu, C., Vega, M.A. and Corbí, A.L., 2011. Activin A skews macrophage polarization by promoting a proinflammatory phenotype and inhibiting the acquisition of anti-inflammatory macrophage markers. *Blood, The Journal of the American Society of Hematology*, *117*(19), pp.5092-5101.

Sintiprungrat, K., Singhto, N., Sinchaikul, S., Chen, S.T. and Thongboonkerd, V., 2010. Alterations in cellular proteome and secretome upon differentiation from monocyte to macrophage by treatment with phorbol myristate acetate: insights into biological processes. *Journal of Proteomics*, *73*(3), pp.602-618.

Smolen, J.S. and Steiner, G., 2003. Therapeutic strategies for rheumatoid arthritis. *Nature reviews Drug discovery*, *2*(6), pp.473-488.

Soeder, K.J., Snedden, S.K., Cao, W., Della Rocca, G.J., Daniel, K.W., Luttrell, L.M. and Collins, S., 1999. The β3-adrenergic receptor activates mitogen-activated protein kinase in adipocytes through a Gi-dependent mechanism. *Journal of Biological Chemistry*, *274*(17), pp.12017-12022.

Soler Palacios, B., Estrada-Capetillo, L., Izquierdo, E., Criado, G., Nieto, C., Municio, C., González-Alvaro, I., Sánchez-Mateos, P., Pablos, J.L., Corbí, A.L. and Puig-Kröger, A., 2015. Macrophages from the synovium of active rheumatoid arthritis exhibit an activin A-dependent pro-inflammatory profile. *The Journal of pathology*, *235*(3), pp.515-526.

Song, J.W. and Choi, B.S., 2013. Mercury induced the accumulation of amyloid beta (Aβ) in PC12 cells: the role of production and degradation of Aβ. *Toxicological research*, *29*(4), pp.235-240.

Song, M.G., Ryoo, I.G., Choi, H.Y., Choi, B.H., Kim, S.T., Heo, T.H., Lee, J.Y., Park, P.H. and Kwak, M.K., 2015. NRF2 signalling negatively regulates phorbol-12-myristate-13-acetate (PMA)-induced differentiation of human monocytic U937 cells into pro-inflammatory macrophages. *PLoS One*, *10*(7), p.e0134235.

Spector, W.G., Lykke, A.W.J. and Willoughby, D.A., 1967. A quantitative study of leucocyte emigration in chronic inflammatory granulomata. *The Journal of pathology and bacteriology*, *93*(1), pp.101-107.

Stanbridge, E. J., and Reff, M. E. (1979) in The Mycoplasmas (Barile, M. F., and Razin, S., eds.) Vol. 1, pp. 159- 185, Academic Press, New York.

Stankov, K., Bogdanovic, G., Stankov, S., Draskovic, D., Grubor-Lajsic, G., Spasic, M. and Blagojevic, D., 2012. Expression analysis of genes involved in apoptosis, proliferation and endoplasmic reticulum stress in ionomycin/PMA treated Jurkat cells. *Journal of BU ON.: official journal of the Balkan Union of Oncology*, *17*(2), pp.369-376.

Steiner, K., Bühring, K.U., Faro, H.P., Garbe, A. and Nowak, H., 1982. Sucralfate: pharmacokinetics, metabolism and selective binding to experimental gastric and duodenal ulcers in animals. *Arzneimittel-forschung*, *32*(5), pp.512-518.

---

Steinman, R.A., Huang, J., Yaroslavskiy, B., Goff, J.P., Ball, E.D. and Nguyen, A., 1998. Regulation of p21 (WAF1) expression during normal myeloid differentiation. *Blood, The Journal of the American Society of Hematology*, *91*(12), pp.4531-4542.

Steinman, R.M., 1991. The dendritic cell system and its role in immunogenicity. *Annual review of immunology*, *9*(1), pp.271-296.

Storey, G.O., Comer, M. and Scott, D.L., 1994. Chronic arthritis before 1876: early British cases suggesting rheumatoid arthritis. *Annals of the rheumatic diseases*, *53*(9), p.557.

Stork, P.J. and Schmitt, J.M., 2002. Crosstalk between cAMP and MAP kinase signalling in the regulation of cell proliferation. *Trends in cell biology*, *12*(6), pp.258-266.

Straub, R.H. and Kalden, J.R., 2009. Stress of different types increases the proinflammatory load in rheumatoid arthritis. *Arthritis research & therapy*, *11*(3), pp.1-2.

Strobl, H., Scheinecker, C., Csmarits, B., Majdic, O. and Knapp, W., 1995. Flow cytometric analysis of intracellular CD6 8 molecule expression in normal and malignant haemopoiesis. *British journal of haematology*, *90*(4), pp.774-782.

Suarez-Almazor, M.E., Belseck, E., Shea, B., Tugwell, P. and Wells, G.A., 1998. Methotrexate for treating rheumatoid arthritis. *Cochrane Database of Systematic Reviews*, (2).

Sugden, P.H. and Clerk, A., 1997. Regulation of the ERK subgroup of MAP kinase cascades through G protein-coupled receptors. *Cellular signalling*, *9*(5), pp.337-351.

Sugibayashi, R., Shimizu, T., Suzuki, T., Yamamoto, N., Hamada, H. and Takeda, K., 2001. Upregulation of p21 WAF1/CIP1 leads to morphologic changes and esterase activity in TPA-mediated differentiation of human prostate cancer cell line TSU-Pr1. *Oncogene*, *20*(10), pp.1220-1228.

Sundström, C. and Nilsson, K., 1976. Establishment and characterization of a human histiocytic lymphoma cell line (U-937). *International journal of cancer*, *17*(5), pp.565-577.

Sutherland, E.W. and Rall, T.W., 1958. Fractionation and characterization of a cyclic adenine ribonucleotide formed by tissue particles. *Journal of Biological Chemistry*, *232*(2), pp.1077-1092.

Sweeney, S.E. and Firestein, G.S., 2006. Mitogen activated protein kinase inhibitors: where are we now and where are we going?. *Annals of the rheumatic diseases*, *65*(suppl 3), pp.iii83-iii88.

Szabo, S. and Brown, A., 1987. Prevention of ethanol-induced vascular injury and gastric mucosal lesions by sucralfate and its components: possible role of endogenous sulfhydryls. *Proceedings of the society for Experimental Biology and Medicine*, *185*(4), pp.493-497.

---

Tak, P.P., Smeets, T.J., Daha, M.R., Kluin, P.M., Meijers, K.A., Brand, R., Meinders, A.E. and Breedveld, F.C., 1997. Analysis of the synovial cell infiltrate in early rheumatoid synovial tissue in relation to local disease activity. *Arthritis & Rheumatism: Official Journal of the American College of Rheumatology*, *40*(2), pp.217-225.

Takashiba, S., Van Dyke, T.E., Amar, S., Murayama, Y., Soskolne, A.W. and Shapira, L., 1999. Differentiation of monocytes to macrophages primes cells for lipopolysaccharide stimulation via accumulation of cytoplasmic nuclear factor κB. *Infection and immunity*, *67*(11), pp.5573-5578.

Takashiba, S., Van Dyke, T.E., Shapira, L. and Amar, S., 1995. Lipopolysaccharide-inducible and salicylate-sensitive nuclear factor (s) on human tumour necrosis factor alpha promoter. *Infection and Immunity*, *63*(4), pp.1529-1534.

Takeda, N., O'Dea, E.L., Doedens, A., Kim, J.W., Weidemann, A., Stockmann, C., Asagiri, M., Simon, M.C., Hoffmann, A. and Johnson, R.S., 2010. Differential activation and antagonistic function of HIF-α isoforms in macrophages are essential for NO homeostasis. *Genes & development*, *24*(5), pp.491-501.

Tanaka, C. and Nishizuka, Y., 1994. The protein kinase C family for neuronal signalling. *Annual review of neuroscience*, *17*(1), pp.551-567.

Taraballi, F., Corradetti, B., Minardi, S., Powel, S., Cabrera, F., Van Eps, J.L., Weiner, B.K. and Tasciotti, E., 2016. Biomimetic collagenous scaffold to tune inflammation by targeting macrophages. *Journal of tissue engineering*, *7*, p.2041731415624667.

Tarique, A.A., Logan, J., Thomas, E., Holt, P.G., Sly, P.D. and Fantino, E., 2015. Phenotypic, functional, and plasticity features of classical and alternatively activated human macrophages. *American journal of respiratory cell and molecular biology*, *53*(5), pp.676-688.

Tárnok, A., 1996. Improved kinetic analysis of cytosolic free calcium in pressure-sensitive neuronal cells by fixed-time flow cytometry. *Cytometry: The Journal of the International Society for Analytical Cytology*, *23*(1), pp.82-89.

Tárnok, A., 1997. Rare-event sorting by fixed-time flow cytometry based on changes in intracellular free calcium. *Cytometry: The Journal of the International Society for Analytical Cytology*, *27*(1), pp.65-70.

Taylor, P.R., Martinez-Pomares, L., Stacey, M., Lin, H.H., Brown, G.D. and Gordon, S., 2005. Macrophage receptors and immune recognition. *Annu. Rev. Immunol.*, *23*, pp.901-944.

Ten Broeke, T., Wubbolts, R. and Stoorvogel, W., 2013. MHC class II antigen presentation by dendritic cells regulated through endosomal sorting. *Cold Spring Harbor perspectives in biology*, *5*(12), p.a016873.

Thimmulappa, R.K., Scollick, C., Traore, K., Yates, M., Trush, M.A., Liby, K.T., Sporn, M.B., Yamamoto, M., Kensler, T.W. and Biswal, S., 2006. Nrf2-dependent protection from LPS induced inflammatory response and mortality by CDDO-Imidazolide. *Biochemical and biophysical research communications*, *351*(4), pp.883-889.

Tibbles, L.A. and Woodgett, J.R., 1999. The stress-activated protein kinase pathways. *Cellular and Molecular Life Sciences CMLS*, *55*(10), pp.1230-1254.

Tobey, N.A., Orlando, R.C., Schreiner, V.J. and Powell, D.W., 1986. Cytoprotective effect of sulphate ions in acid-exposed rabbit esophagus. *American Journal of Physiology-Gastrointestinal and Liver Physiology*, *251*(6), pp.G866-G869.

---

Tobias, P.S., Soldau, K., Kline, L., Lee, J.D., Kato, K., Martin, T.P. and Ulevitch, R.J., 1993. Cross-linking of lipopolysaccharide (LPS) to CD14 on THP-1 cells mediated by LPS-binding protein. *The Journal of Immunology*, *150*(7), pp.3011-3021.

Toledo-Pereyra, L.H., Toledo, A.H., Walsh, J. and Lopez-Neblina, F., 2004. Molecular signalling pathways in ischemia/reperfusion. *Exp Clin Transplant*, *2*(1), pp.174-177.

Torphy, T.J., 1998. Phosphodiesterase isozymes: molecular targets for novel antiasthma agents. *American Journal of Respiratory and Critical Care Medicine*, *157*(2), pp.351-370.

Torphy, T.J., Zhou, H.L. and Cieslinski, L.B., 1992. Stimulation of beta adrenoceptors in a human monocyte cell line (U937) up-regulates cyclic AMP-specific phosphodiesterase activity. *Journal of Pharmacology and Experimental Therapeutics*, *263*(3), pp.1195-1205.

Torsteinsdóttir, I., Arvidson, N.G., Hällgren, R. and Håkansson, L., 1999. Monocyte activation in rheumatoid arthritis (RA): increased integrin, Fcγ and complement receptor

expression and the effect of glucocorticoids. *Clinical and experimental immunology*, *115*(3), p.554.

Touqui, L., Rothhut, B., Shaw, A.M., Fradin, A., Vargaftig, B.B. and Russo-Marie, F., 1986. Platelet activation—a role for a 40K anti-phospholipase A 2 protein indistinguishable from lipocortin. *Nature*, *321*(6066), pp.177-180.

Trede, N.S., Tsytsykova, A.V., Chatila, T., Goldfeld, A.E. and Geha, R.S., 1995. Transcriptional activation of the human TNF-alpha promoter by superantigen in human monocytic cells: role of NF-kappa B. *The Journal of Immunology*, *155*(2), pp.902-908.

Triggiani, M., Granata, F., Oriente, A., Gentile, M., Petraroli, A., Balestrieri, B. and Marone, G., 2002. Secretory phospholipases A2 induce cytokine release from blood and synovial fluid monocytes. *European journal of immunology*, *32*(1), pp.67-76.

Trombetta, A.C., Soldano, S., Contini, P., Tomatis, V., Ruaro, B., Paolino, S., Brizzolara, R., Montagna, P., Sulli, A., Pizzorni, C. and Smith, V., 2018. A circulating cell population showing both M1 and M2 monocyte/macrophage surface markers characterizes systemic sclerosis patients with lung involvement. *Respiratory research*, *19*(1), pp.1-12.

Trouw, L.A., Haisma, E.M., Levarht, E.W.N., Van Der Woude, D., Ioan-Facsinay, A., Daha, M.R., Huizinga, T.W.J. and Toes, R.E., 2009. Anti–cyclic citrullinated peptide antibodies from rheumatoid arthritis patients activate complement via both the classical and alternative pathways. *Arthritis & Rheumatism: Official Journal of the American College of Rheumatology*, *60*(7), pp.1923-1931.

Trouw, L.A., Rispens, T. and Toes, R.E., 2017. Beyond citrullination: other post-translational protein modifications in rheumatoid arthritis. *Nature Reviews Rheumatology*, *13*(6), pp.331-339.

Trushin, S.A., Pennington, K.N., Algeciras-Schimnich, A. and Paya, C.V., 1999. Protein kinase C and calcineurin synergize to activate IκB kinase and NF-κB in T lymphocytes. *Journal of Biological Chemistry*, *274*(33), pp.22923-22931.

Tsuchiya, S., Kobayashi, Y., Goto, Y., Okumura, H., Nakae, S., Konno, T. and Tada, K., 1982. Induction of maturation in cultured human monocytic leukemia cells by a phorbol diester. *Cancer research*, *42*(4), pp.1530-1536.

Tsuchiya, S., Yamabe, M., Yamaguchi, Y., Kobayashi, Y., Konno, T. and Tada, K., 1980. Establishment and characterization of a human acute monocytic leukemia cell line (THP-1). *International journal of cancer*, *26*(2), pp.171-176.

Tsutsumi, M., Inoue, K., Denda, S., Ikeyama, K., Goto, M. and Denda, M., 2009. Mechanical-stimulation-evoked calcium waves in proliferating and differentiated human keratinocytes. *Cell and tissue research*, *338*(1), pp.99-106.

Udalova, I.A., Mantovani, A. and Feldmann, M., 2016. Macrophage heterogeneity in the context of rheumatoid arthritis. *Nature Reviews Rheumatology*, *12*(8), pp.472-485.

Ueda, Y., Hirai, S.I., Osada, S.I., Suzuki, A., Mizuno, K. and Ohno, S., 1996. Protein kinase C δ activates the MEK-ERK pathway in a manner independent of Ras and dependent on Raf. *Journal of Biological Chemistry*, *271*(38), pp.23512-23519.

Ueki, K., Tabeta, K., Yoshie, H. and Yamazaki, K., 2002. Self-heat shock protein 60 induces tumour necrosis factor-α in monocyte-derived macrophage: possible role in chronic inflammatory periodontal disease. *Clinical & Experimental Immunology*, *127*(1), pp.72-77.

Umino, T., Skold, C.M., Pirruccello, S.J. and Rennard, S.I., 1999. Two-colour flow-cytometric analysis of pulmonary alveolar macrophages from smokers. *European Respiratory Journal*, *13*(4), pp.894-899.

Vahl, J.C., Drees, C., Heger, K., Heink, S., Fischer, J.C., Nedjic, J., Ohkura, N., Morikawa, H., Poeck, H., Schallenberg, S. and Rieß, D., 2014. Continuous T cell receptor signals maintain a functional regulatory T cell pool. *Immunity*, *41*(5), pp.722-736.

Van Ginderachter, J.A., Movahedi, K., Ghassabeh, G.H., Meerschaut, S., Beschin, A., Raes, G. and De Baetselier, P., 2006. Classical and alternative activation of mononuclear phagocytes: picking the best of both worlds for tumour promotion. *Immunobiology*, *211*(6-8), pp.487-501.

van Laar, M., Pergolizzi Jr, J.V., Mellinghoff, H.U., Merchante, I.M., Nalamachu, S., O'Brien, J., Perrot, S. and Raffa, R.B., 2012. Pain treatment in arthritis-related pain: beyond NSAIDs. *The open rheumatology journal*, *6*, p.320.

Vang, T., Torgersen, K.M., Sundvold, V., Saxena, M., Levy, F.O., Skålhegg, B.S., Hansson, V., Mustelin, T. and Taskén, K., 2001. Activation of the COOH-terminal Src kinase (Csk) by cAMP-dependent protein kinase inhibits signalling through the T cell receptor. *The Journal of experimental medicine*, *193*(4), pp.497-508.

Vang, T., Torgersen, K.M., Sundvold, V., Saxena, M., Levy, F.O., Skålhegg, B.S., Hansson, V., Mustelin, T. and Taskén, K., 2001. Activation of the COOH-terminal Src kinase (Csk) by cAMP-dependent protein kinase inhibits signalling through the T cell receptor. *The Journal of experimental medicine*, *193*(4), pp.497-508.

Vasanthi, P., Nalini, G. and Rajasekhar, G., 2007. Role of tumour necrosis factor-alpha in rheumatoid arthritis: a review. *APLAR Journal of Rheumatology*, *10*(4), pp.270-274.

Vig, M., George, A., Sen, R., Durdik, J., Rath, S. and Bal, V., 2002. Commitment of activated T cells to secondary responsiveness is enhanced by signals mediated by cAMP-dependent protein kinase AI. *Molecular pharmacology*, *62*(6), pp.1471-1481.

Vorherr, T., Knoepfel, L., Hofmann, F., Mollner, S., Pfeuffer, T. and Carafoli, E., 1993. The calmodulin binding domain of nitric oxide synthase and adenylyl cyclase. *Biochemistry*, *32*(23), pp.6081-6088.

Waksman, S.A., 1953. Streptomycin: background, isolation, properties, and utilization. *Science*, *118*(3062), pp.259-266.

Wall, E.A., Zavzavadjian, J.R., Chang, M.S., Randhawa, B., Zhu, X., Hsueh, R.C., Liu, J., Driver, A., Bao, X.R., Sternweis, P.C. and Simon, M.I., 2009. Suppression of LPS-induced TNF-α production in macrophages by cAMP is mediated by PKA-AKAP95-p105. *Science signalling*, *2*(75), pp.ra28-ra28.

Wang, K.Y., Arima, N., Higuchi, S., Shimajiri, S., Tanimoto, A., Murata, Y., Hamada, T. and Sasaguri, Y., 2000. Switch of histamine receptor expression from H2 to H1 during differentiation of monocytes into macrophages. *FEBS letters*, *473*(3), pp.345-348.

Wang, Q., Ni, H., Lan, L., Wei, X., Xiang, R. and Wang, Y., 2010. Fra-1 protooncogene regulates IL-6 expression in macrophages and promotes the generation of M2d macrophages. *Cell research*, *20*(6), pp.701-712.

Wang, S., Yan, L., Wesley, R.A. and Danner, R.L., 1997. Nitric oxide increases tumour necrosis factor production in differentiated U937 cells by decreasing cyclic AMP. *Journal of Biological Chemistry*, *272*(9), pp.5959-5965.

Webb, L., Ehrengruber, M.U., Clark-Lewis, I., Baggiolini, M. and Rot, A., 1993. Binding to heparan sulphate or heparin enhances neutrophil responses to interleukin 8. *Proceedings of the National Academy of Sciences*, *90*(15), pp.7158-7162.

West, A.P., Koblansky, A.A. and Ghosh, S., 2006. Recognition and signalling by toll-like receptors. *Annu. Rev. Cell Dev. Biol.*, *22*, pp.409-437.

Wettschureck, N. and Offermanns, S., 2005. Mammalian G proteins and their cell type specific functions. *Physiological reviews*, *85*(4), pp.1159-1204.

Whitehurst, A.W., Wilsbacher, J.L., You, Y., Luby-Phelps, K., Moore, M.S. and Cobb, M.H., 2002. ERK2 enters the nucleus by a carrier-independent mechanism. *Proceedings of the National Academy of Sciences*, *99*(11), pp.7496-7501.

Wiktor-Jedrzejczak, W. and Gordon, S., 1996. Cytokine regulation of the macrophage (M phi) system studied using the colony stimulating factor-1-deficient op/op mouse. *Physiological reviews*, *76*(4), pp.927-947.

Wilkinson, L.S., Edwards, J.C., Poston, R.N. and Haskard, D.O., 1993. Expression of vascular cell adhesion molecule-1 in normal and inflamed synovium. *Laboratory investigation; a journal of technical methods and pathology*, *68*(1), pp.82-88.

Wilson, C.H., Ali, E.S., Scrimgeour, N., Martin, A.M., Hua, J., Tallis, G.A., Rychkov, G.Y. and Barritt, G.J., 2015. Steatosis inhibits liver cell store-operated Ca2+ entry and reduces ER Ca2+ through a protein kinase C-dependent mechanism. *Biochemical Journal*, *466*(2), pp.379-390.

Winthrop, K.L., Wouters, A.G., Choy, E.H., Soma, K., Hodge, J.A., Nduaka, C.I., Biswas, P., Needle, E., Passador, S., Mojcik, C.F. and Rigby, W.F., 2017. The safety and immunogenicity of live zoster vaccination in patients with rheumatoid arthritis before starting tofacitinib: a randomized phase II trial. *Arthritis & Rheumatology*, *69*(10), pp.1969-1977.

Wolf, M., LeVine, H., May, W.S., Cuatrecasas, P. and Sahyoun, N., 1985. A model for intracellular translocation of protein kinase C involving synergism between Ca 2+ and phorbol esters. *Nature*, *317*(6037), pp.546-549.

Wolfe, F., Mitchell, D.M., Sibley, J.T., Fries, J.F., Bloch, D.A., Williams, C.A., Spitz, P.W., Haga, M., Kleinheksel, S.M. and Cathey, M.A., 1994. The mortality of rheumatoid arthritis. *Arthritis & Rheumatism*, *37*(4), pp.481-494.

Wong, P., Cuello, C., Bertouch, J.V., Roberts-Thomson, P.J., Ahern, M.J., Smith, M.D. and Youssef, P.P., 2000. The effects of pulse methylprednisolone on matrix metalloproteinase and tissue inhibitor of metalloproteinase-1 expression in rheumatoid arthritis. *Rheumatology*, *39*(10), pp.1067-1073.

Woods, M.L. and Shimizu, Y., 2001. Signalling networks regulating β1 integrin-mediated adhesion of T lymphocytes to extracellular matrix. *Journal of leukocyte biology*, *69*(6), pp.874-880.

Wortis, H.H., Teutsch, M., Higer, M., Zheng, J. and Parker, D.C., 1995. B-cell activation by crosslinking of surface IgM or ligation of CD40 involves alternative signal pathways and results in different B-cell phenotypes. *Proceedings of the National Academy of Sciences*, *92*(8), pp.3348-3352.

Wrenshall, L.E., Cerra, F.B., Singh, R.K. and Platt, J.L., 1995. Heparan sulphate initiates signals in murine macrophages leading to divergent biologic outcomes. *The Journal of Immunology*, *154*(2), pp.871-880.

Wright, S.D., Ramos, R.A., Tobias, P.S., Ulevitch, R.J. and Mathison, J.C., 1990. CD14, a receptor for complexes of lipopolysaccharide (LPS) and LPS binding protein. *Science*, *249*(4975), pp.1431-1433.

Wu, J., Dent, P., Jelinek, T., Wolfman, A., Weber, M.J. and Sturgill, T.W., 1993. Inhibition of the EGF-activated MAP kinase signalling pathway by adenosine 3', 5'-monophosphate. *Science*, *262*(5136), pp.1065-1069.

Wu-Zhang, A.X. and Newton, A.C., 2013. Protein kinase C pharmacology: refining the toolbox. *Biochemical Journal*, *452*(2), pp.195-209.

Xu, C., Wyman, A.R., Alaamery, M.A., Argueta, S.A., Ivey, F.D., Meyers, J.A., Lerner, A., Burdo, T.H., Connolly, T., Hoffman, C.S. and Chiles, T.C., 2016. Anti-inflammatory effects of novel barbituric acid derivatives in T lymphocytes. *International immunopharmacology*, *38*, pp.223-232.

Xu, C.X., Jin, H., Chung, Y.S., Shin, J.Y., Woo, M.A., Lee, K.H., Palmos, G.N., Choi, B.D. and Cho, M.H., 2008. Chondroitin sulphate extracted from the Styela clava tunic suppresses TNF-α-induced expression of inflammatory factors, VCAM-1 and iNOS by blocking Akt/NF-κB signal in JB6 cells. *Cancer letters*, *264*(1), pp.93-100.

Yamaguchi, K., Ogita, K., Nakamura, S.I. and Nishizuka, Y., 1995. The protein kinase C isoforms leading to MAP-kinase activation in CHO cells. *Biochemical and biophysical research communications*, *210*(3), pp.639-647.

Yamaoka, K., 2016. Janus kinase inhibitors for rheumatoid arthritis. *Current opinion in chemical biology*, *32*, pp.29-33.

Yang, N.J. and Hinner, M.J., 2015. Getting across the cell membrane: an overview for small molecules, peptides, and proteins. *Site-specific protein labeling*, pp.29-53.

Yanni, G., Whelan, A., Feighery, C. and Bresnihan, B., 1994. Synovial tissue macrophages and joint erosion in rheumatoid arthritis. *Annals of the rheumatic diseases*, *53*(1), pp.39-44.

Yip, L., Woehrle, T., Corriden, R., Hirsh, M., Chen, Y., Inoue, Y., Ferrari, V., Insel, P.A. and Junger, W.G., 2009. Autocrine regulation of T-cell activation by ATP release and P2X7 receptors. *The FASEB Journal*, *23*(6), pp.1685-1693.

Yoon, C.H., Cho, M.L., Hwang, S.Y., Park, M.K., Min, S.Y., Lee, S.H., Park, S.H. and Kim, H.Y., 2004. Effector function of type II collagen–stimulated T cells from rheumatoid arthritis patients: Cross-talk between T cells and synovial fibroblasts. *Arthritis & Rheumatism*, *50*(3), pp.776-784.

Young, E., 2008. The anti-inflammatory effects of heparin and related compounds. *Thrombosis research*, *122*(6), pp.743-752.

Yu, S., Nakashima, N., Xu, B.H., Matsuda, T., Izumihara, A., Sunahara, N., Nakamura, T., Tsukano, M. and Matsuyama, T., 1998. Pathological significance of elevated soluble CD14 production in rheumatoid arthritis: in the presence of soluble CD14, lipopolysaccharides at low concentrations activate RA synovial fibroblasts. *Rheumatology international*, *17*(6), pp.237-243.

Zamani, N., Russell, P., Lantz, H., Hoeppner, M.P., Meadows, J.R., Vijay, N., Mauceli, E., di Palma, F., Lindblad-Toh, K., Jern, P. and Grabherr, M.G., 2013. Unsupervised genome-wide recognition of local relationship patterns. *BMC genomics*, *14*(1), pp.1-11.

Zhang, J., Bui, T.N., Xiang, J. and Lin, A., 2006. Cyclic AMP inhibits p38 activation via CREB-induced dynein light chain. *Molecular and cellular biology*, *26*(4), pp.1223-1234.

Zhang, W., Xu, W. and Xiong, S., 2010. Blockade of Notch1 signalling alleviates murine lupus via blunting macrophage activation and M2b polarization. *The Journal of Immunology*, *184*(11), pp.6465-6478.

Zhang, Y., Lian, F., Zhu, Y., Xia, M., Wang, Q., Ling, W. and Wang, X.D., 2010. Cyanidin-3-O-β-glucoside inhibits LPS-induced expression of inflammatory mediators through decreasing IκBα phosphorylation in THP-1 cells. *Inflammation research*, *59*(9), pp.723-730.

Zhao, J., Yuan, W., Tao, C., Sun, P., Yang, Z. and Xu, W., 2017. M2 polarization of monocytes in ankylosing spondylitis and relationship with inflammation and structural damage. *Apmis*, *125*(12), pp.1070-1075.

Zhong, W.W., Burke, P.A., Drotar, M.E., Chavali, S.R. and Forse, R.A., 1995. Effects of prostaglandin E2, cholera toxin and 8-bromo-cyclic AMP on lipopolysaccharide-induced gene expression of cytokines in human macrophages. *Immunology*, *84*(3), p.446.

Ziff, M., 1989, August. Role of endothelium in chronic inflammation. In *Springer seminars in immunopathology* (Vol. 11, No. 2, pp. 199-214). Springer-Verlag.

Zwerina, J., Hayer, S., Redlich, K., Bobacz, K., Kollias, G., Smolen, J.S. and Schett, G., 2006. Activation of p38 MAPK is a key step in tumour necrosis factor–mediated inflammatory bone destruction. *Arthritis & Rheumatism: Official Journal of the American College of Rheumatology*, *54*(2), pp.463-472.

# APPENDIX

**List of Appendix Tables**

**List of Appendix Figures**

**Appendix Table 1.** *The DNase I (endonuclease) digestion reaction for RNA samples prior to RT-PCR*

| Component | Volume |
|---|---|
| RNA sample in nuclease-free water | 1- 8 µL per µg RNA |
| RQ1 RNase-Free DNase 10X reaction buffer (400 Mm Tris-HCl (pH 8.0, 100 Mm $MgSO_4$ and 10 mM $CaCl_2$) | 1 µL per µg RNA |
| RQ1 RNase-Free DNase (1000 units) | 1 unit/µg RNA |
| Nuclease-free water to a final volume of | 10 µL |

**Appendix Table 2.** *GoScript™ reverse transcription reaction mix for positive controls.*

| Component | Volume |
|---|---|
| Nuclease-Free water | 4 µL |
| GoScript™ reaction buffer, random primers | 4 µL |
| GoScript™ Enzyme mix | 2 µL |
| Final Volume | 10 µL |

**Appendix Table 3.** *GoScript™ reverse transcription reaction mix for negative controls.*

| Component | Volume |
|---|---|
| Nuclease-Free water | 6 µL |
| GoScript™ reaction buffer, random primers | 4 µL |
| Final Volume | 10 µL |

**Appendix Table 4.** *The reverse transcription reaction mix for cDNA preparation.*

| Component | Volume |
|---|---|
| GoScript™ reverse transcription mix | 10 µL |
| Experimental RNA | ___µL |
| Nuclease-Free water | to final volume of 20 µL |
| Final Volume | 20 µL |

**Appendix Table 5.** *The PCR parameters for reverse transcription reaction mix.*

| Step | Temperature | Time | Number of Cycles |
|---|---|---|---|
| Anneal primer | 25 $^0$C | 5 min | 1 cycle |
| Extension | 42 $^0$C | 60 min | 1 cycle |
| Inactivation | 70 $^0$C | 15 min | 1 cycle |
| Hold | 4 $^0$C | ∞ | 1 cycle |

**Appendix Table 6.** *RT-PCR reaction mix for cDNA amplification.*

| Component | Volume | Final Concentration |
|---|---|---|
| PCR Master Mix; 2X | 12.5 µL | 1X |
| Forward primer; 10X | 2.5 µL | 1 µM |
| Reverse primer; 10X | 2.5 µL | 1 µM |
| cDNA template | 2.0 µL | <250 ng |
| Nuclease- Free water | 5.5 µL | N.A. |

**Appendix Table 7.** *PCR amplification parameters for β-actin with total number of 30 cycles and for CD14, CD206, CD200R and Arginase 1 with total number of 34 cycles.*

| Step | Temperature | Time |
|---|---|---|
| Initial denaturation | 95 $^0$C | 3 min |
| Denaturation | 95 $^0$C | 1 min |
| Annealing | 95 $^0$C | 1 min |
| Extension | 60 $^0$C | 1 min |
| Final extension | 72 $^0$C | 7 min |
| Hold | 4 $^0$C | ∞ |

**Appendix Table 8.** *PCR amplification parameters for p21WAF1/Cip1 with total number of 30 cycles.*

| Step | Temperature | Time |
|---|---|---|
| Initial denaturation | 95 $^0$C | 3 min |
| Denaturation | 94 $^0$C | 1 min |
| Annealing | 58 $^0$C | 1 min |
| Extension | 72 $^0$C | 2 min |
| Final extension | 72 $^0$C | 5 min |
| Hold | 4 $^0$C | ∞ |

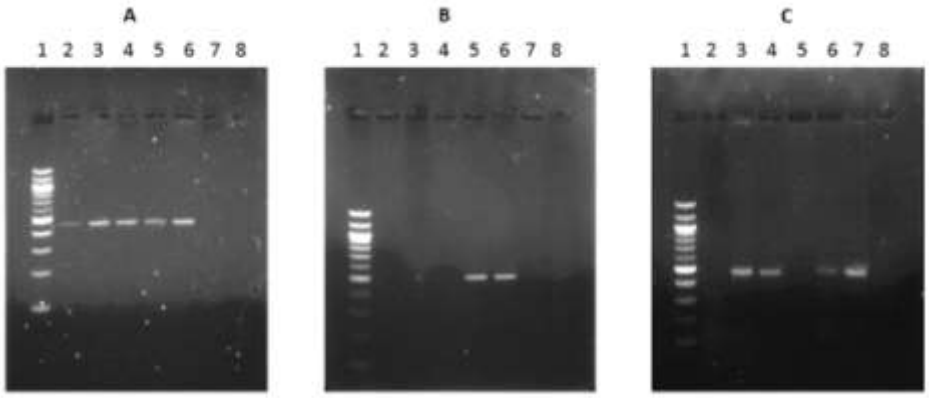


**Appendix Figure 1.** ***Mycoplasma testing for U937 and THP-1 cells.***

*Routine testing of U937 and THP-1 cell cultures was carried out for bacterial, yeast, or fungal contamination under a microscope. The cells were tested for Mycoplasma (quarterly) for contamination free cell culture by using the American Type Culture Collection Universal Mycoplasma detection kit. Mycoplasma contamination was tested in U937 and THP-1 cell cultures by resolving PCR products on 2% TAE agarose gel. The cell cultures were free from Mycoplasma contamination. The DNA ladder in the first lane was used as a guide, it includes fragments ranging from 100 bp to 1,517 bp. 100 bp DNA Ladder visualized by SYBER safe staining on a 2% TAE agarose gel. Total load of DNA and samples per gel lane was 10 µl. The 500 and 1,000 bp bands had increased intensity which was served as reference band. The bands of the test samples of cell culture were determined comparing the positive control bands in the 434 bp to 468 bp range for the presence of Mycoplasma. No visible band detected in the negative control lane as accepted. For U937 and THP-1 test samples bands were outside the 434 to 468 bp range, indicating test samples do not contain Mycoplasma contamination. Representative image of 2% agarose gel indicate U937 and THP-1 cell culture samples Mycoplasma contaminated (A) and Mycoplasma contamination free (B). A. Lane 1 represents DNA ladder, lane 2 and 3 represents test samples of U937 and THP-1, lanes 4 represents positive control, lane 5 and 6 represents test samples containing positive control, lane 7 represents negative control. B Lane 1 represents DNA ladder, lane 3 represents test samples of U937, lanes 5 represents positive control, lane 6 represents test samples containing positive control, and lane 8 represents negative control. C Lane 1 represents DNA ladder, lane 2 represents test samples of THP-1, lanes 3 and 7 represents positive*

*control, lane 4 and 6 represents test samples containing positive control, lane 8 represents negative control. As per manufacture's instruction the positive control samples exhibited a 464-bp band. There was no visible band in the negative control lane. Bands outside the 434 to 468 bp range were observed in the U937 and THP-1 samples, this indicate samples were free from Mycoplasma.*

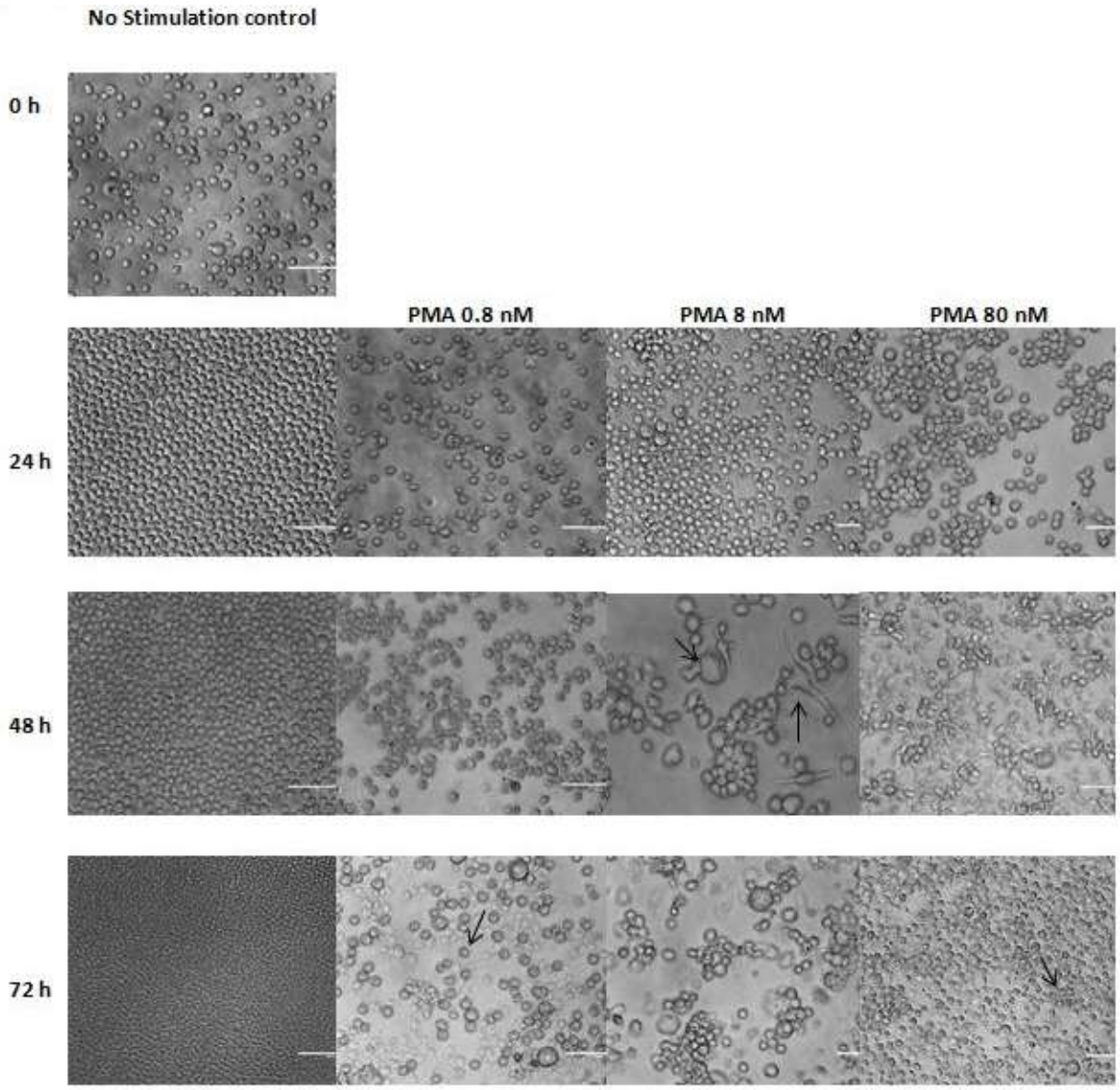


**Appendix Figure 2.** ***PMA induced differentiation of U937 monocyte cells to macrophages.***

*Representative figure of three independent experiments demonstrates PMA concentration dependent change in morphology of U937 cells at 24 h, 48 h and 72 h). U937 monocytic cells morphological characteristics were changed from a shape floating cells after treatment with 0.8 nM PMA, 8 nM PMA, 80 nM PMA to adherent cells with pseudopodia. Arrow indicates morphological change. Magnification x40. Scale bar - 100µm.*

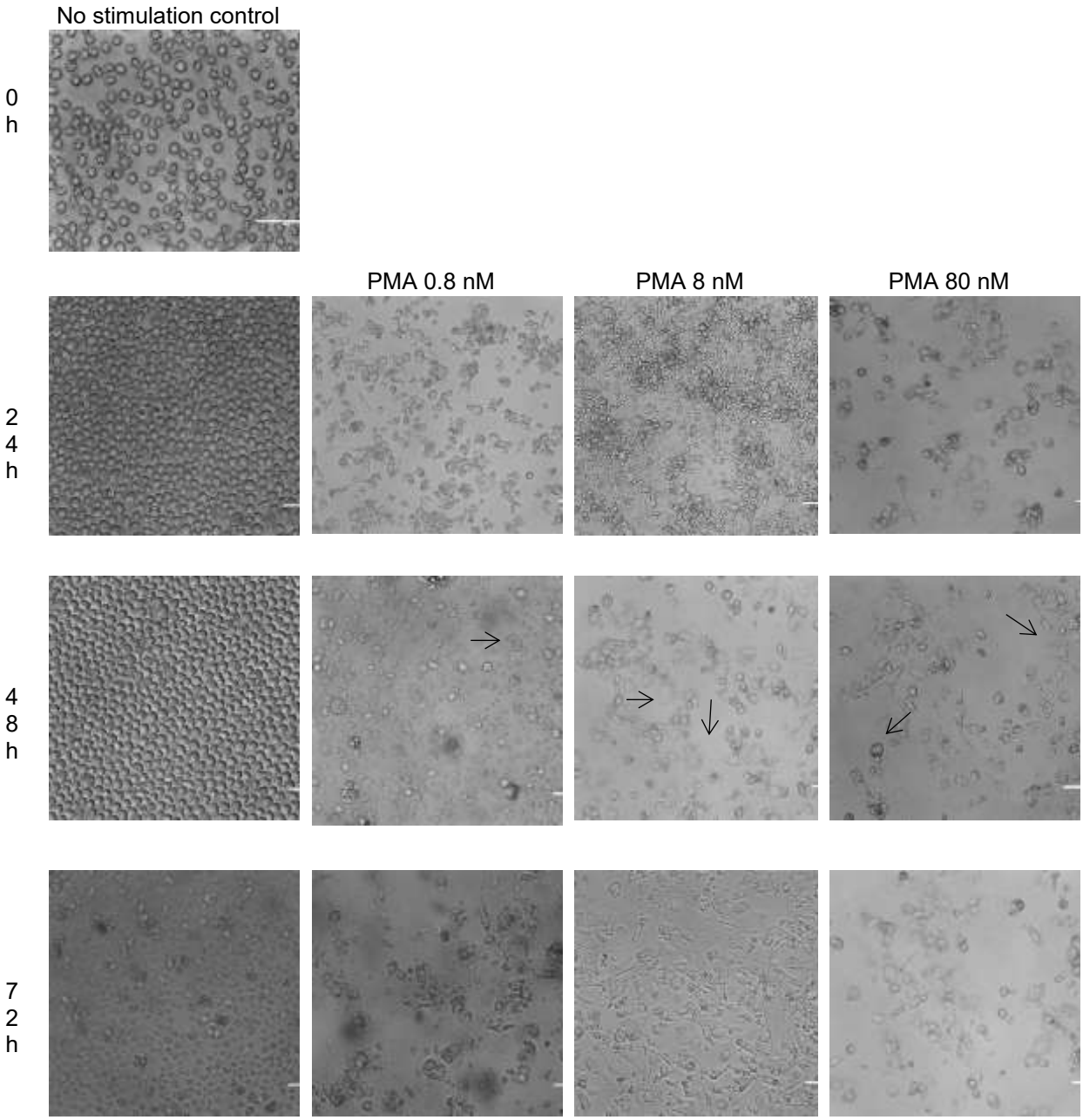


**Appendix Figure 3*. PMA induced THP-1 monocyte cells differentiation to macrophages.***

*Representative figure of three independent experiments demonstrates PMA concentration dependent change in morphology of THP-1 cells at 24 h, 48 h and 72 h. THP-1 monocytic cells morphological characteristics were changed from a shape floating cells after treatment with 0.8 nM PMA, 8 nM PMA, 80 nM PMA to adherent cells with*

*pseudopodia. Arrow indicates morphological change. Magnification x40. Scale bar - 100µm.*

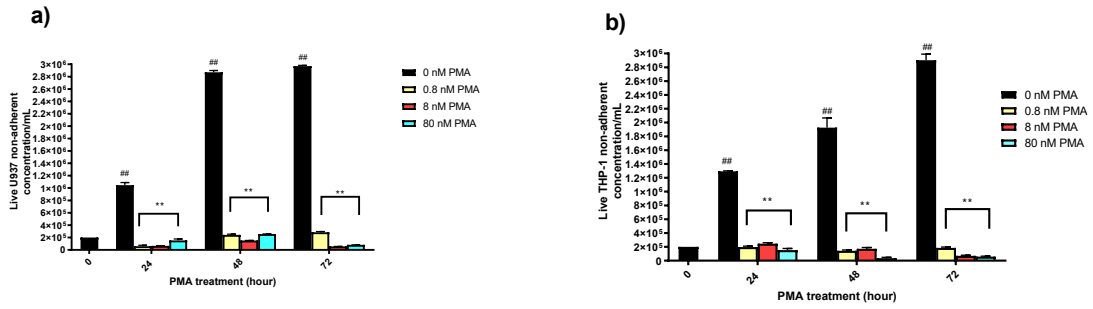


**Appendix Figure 4. Number of non-adherent U937 and THP-1 cells in the PMA cultures.**

*Number of non-adherent of (a) U937 and (b) THP-1 cells reduced in PMA treated groups. The data was analysed by Cell countess as described on section 2.2 and one-way ANOVA with post hoc Dunnett's test and is presented as mean ± SEM of viable cells (viability analysed by trypan blue exclusion) of three independent experiments. Two hashtags (##) indicates significant difference between unstimulated U937 cells at 0 h to 24 h, 48 h and 72 h ($p < 0.01$). The existence of non-adherent cells that were obtained from the PMA cultures during cell count in the above studies raised questions. Therefore, it was asked in this study whether non-adherent cells of PMA cultures phenotype is similar to the adherent cells. Does non-adherent cells of PMA cultures exhibit a different or similar potential compared to adherent cells? Therefore, in the present study, the phenotypic characteristics of non-adherent cells of PMA cultures were compared with that of unstimulated control cells by cell count and flow cytometry (Appendix Fig.8).*

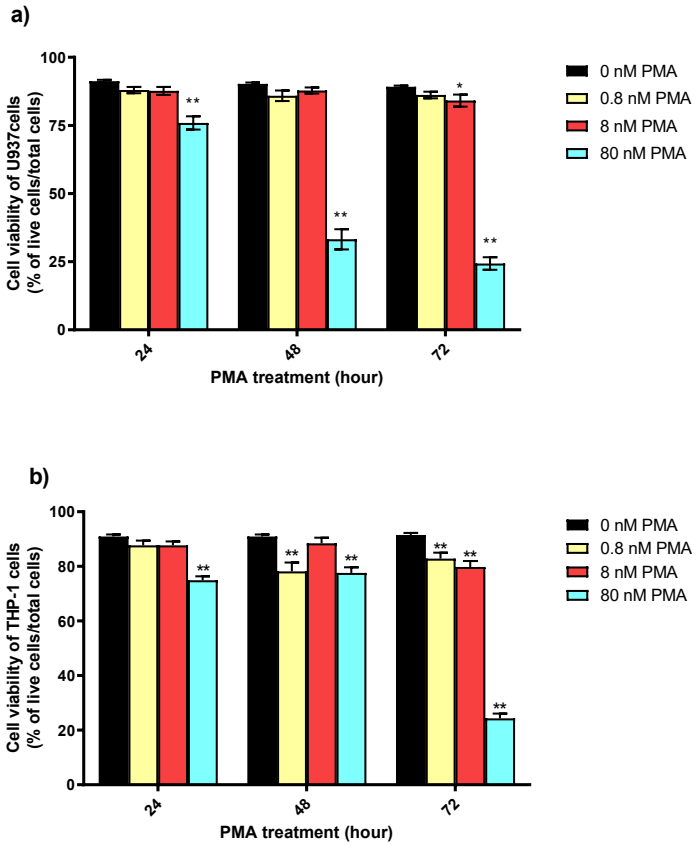


**Appendix Figure 5**. ***PMA impact on cell viability of U937 and THP-1 cells.***

*PMA induced cytotoxicity in U937 (b) and THP-1 (a) cells in a concentration (0.8 nM, 8 nM and 80 nM) and time dependent manner (24, 48 and 72 h). The concentration of 80 nM PMA at 24 h, 48 and 72 h was significantly toxic compared to 0.8 nM PMA and 80 nM PMA. MTT is dependent on cell proliferation means if cells are in cycle arrest these will have a lower MTT than control unstimulated cells because the unstimulated have continued to proliferate. The reduction of MTT was measured by mitochondrial succinate dehydrogenase in active U937 and THP-1 cells. Therefore, the level of activity was proportional to measure of the metabolic activity of the cells. The data was analysed by one-way ANOVA with post hoc Dunnett's test and is presented as mean ± SEM of viable cells (viability analysed by MTT assay see methods section 2.5) of three independent experiments. The asterisk * in indicates significant differences between unstimulated U937 cells to PMA stimulated cells with different concentrations at 24 h, 48 h, 72 h ($p < 0.05$ and $p < 0.01$).*

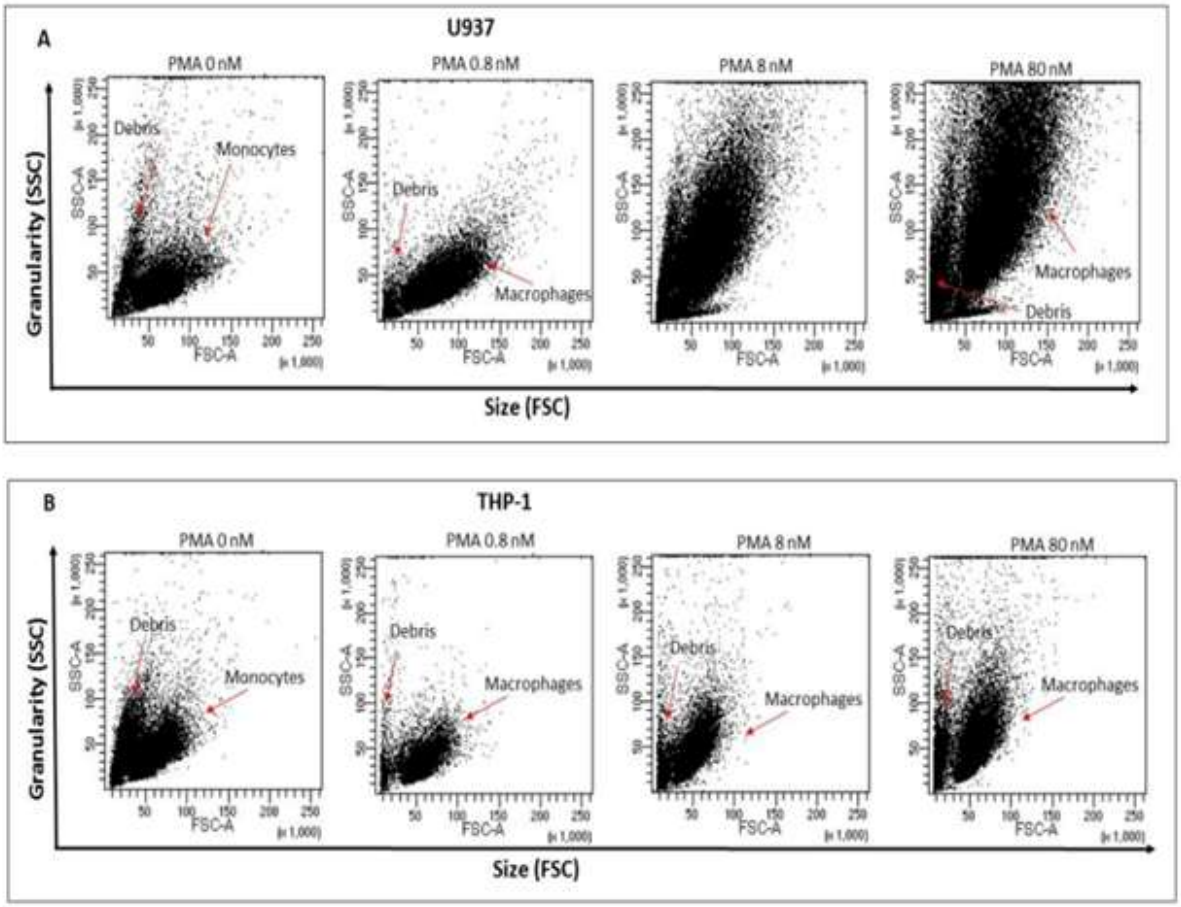


**Appendix Figure 6**. ***Effect of PMA on size and granularity of differentiated U937 and THP-1 cells.***

*To optimise the PMA concentration, PMA-differentiated cells at 48 h were analysed to identify the cell population (monocytes and macrophages). As described in section 2.2 U937 and THP-1 cells were stimulated with different concentrations of PMA at 48 h. Representative dot plot of two independent experiments showing the increase in size (FSC) and granularity (SSC) of U937 (A) and THP-1 (B) cells at baseline (0 nM) and in the presence of PMA (0.8nM, 8nM and 80nM) after 48 h of treatment. The results are the representative of three independent experiments showing similar results. This study was undertaken to analyse further PMA-differentiated adherent cells for their size and complexity. The U937 and THP-1 cells were cultured with 0.8 nM PMA, 8 nM PMA and 80 nM PMA for 48 h. The unstained PMA differentiated cells were acquired to identify cell*

*population and to measure the size and internal complexity of U937/THP-1 monocyte and PMA-induced adherent cells by using glow cytometry forward side scatter (FSC) and side scatter (SSC). It was observed that PMA-induced U937 and THP-1 adherent cells were larger and granular in comparison to unstimulated control U937 and THP-1 monocytes. This indicated that adherent cells acquired the phenotypic characteristics of macrophages. The number of cells detected in the non-adherent population was reduced after PMA treatment, whilst the number of adherent cells was increased and as they adhere they displayed a larger size and granularity. In addition, consistent with the higher size and complexity that characterizes adherent cells in comparison with non-adherent cells, the adherent population of U937 and THP-1 cells after PMA treatment displayed a higher FSC (size) and SSC (complexity) than the non-adherent cells. PMA induced U937 and THP-1 cells differentiation into phenotypic characteristics of macrophages compared to non-treated cells. The different phenotypic characteristics are indicated by red arrow. The samples were analysed by BD Accuri C6 software.*

(a) U937 cells

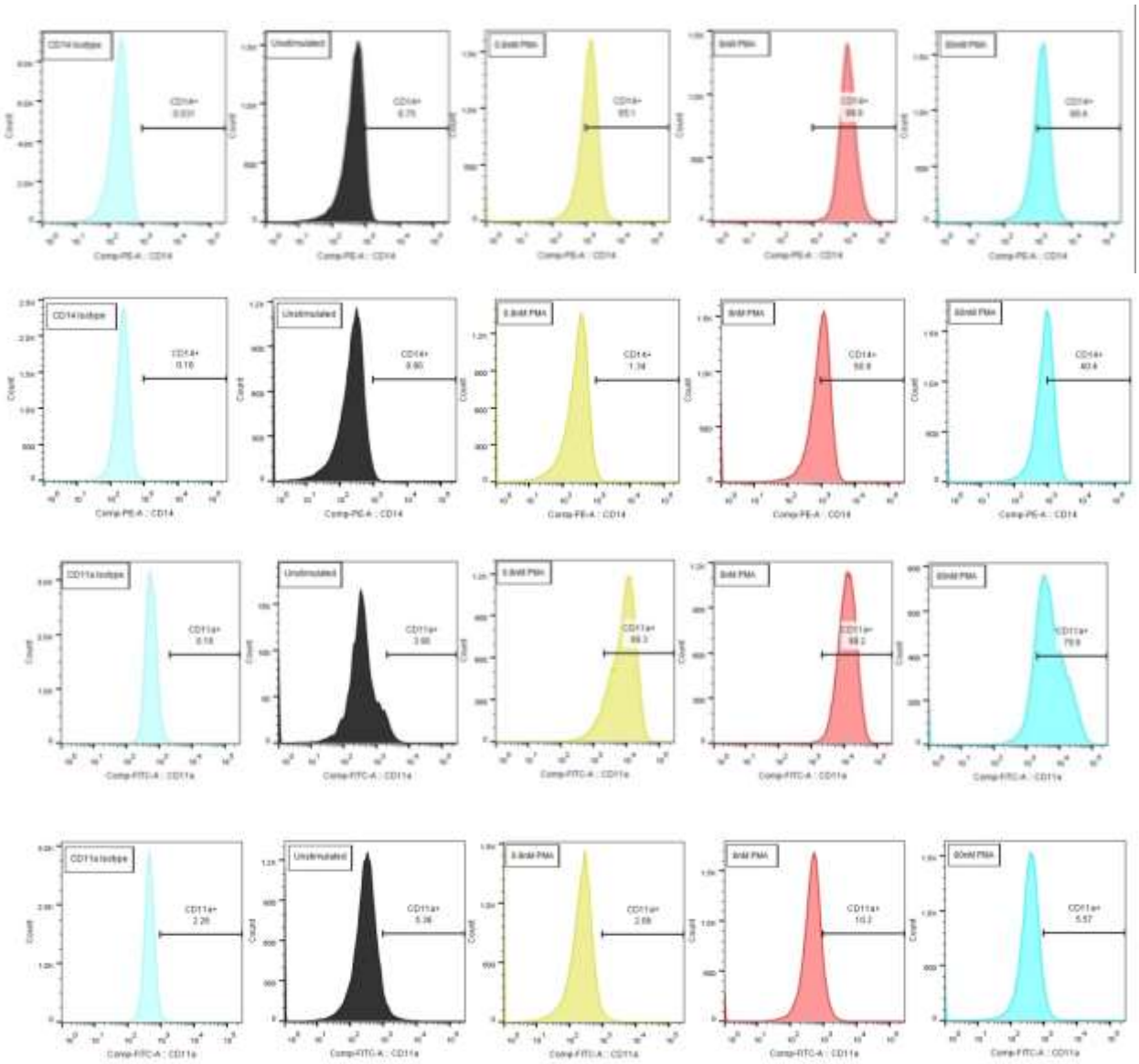

(b) THP-1 cells

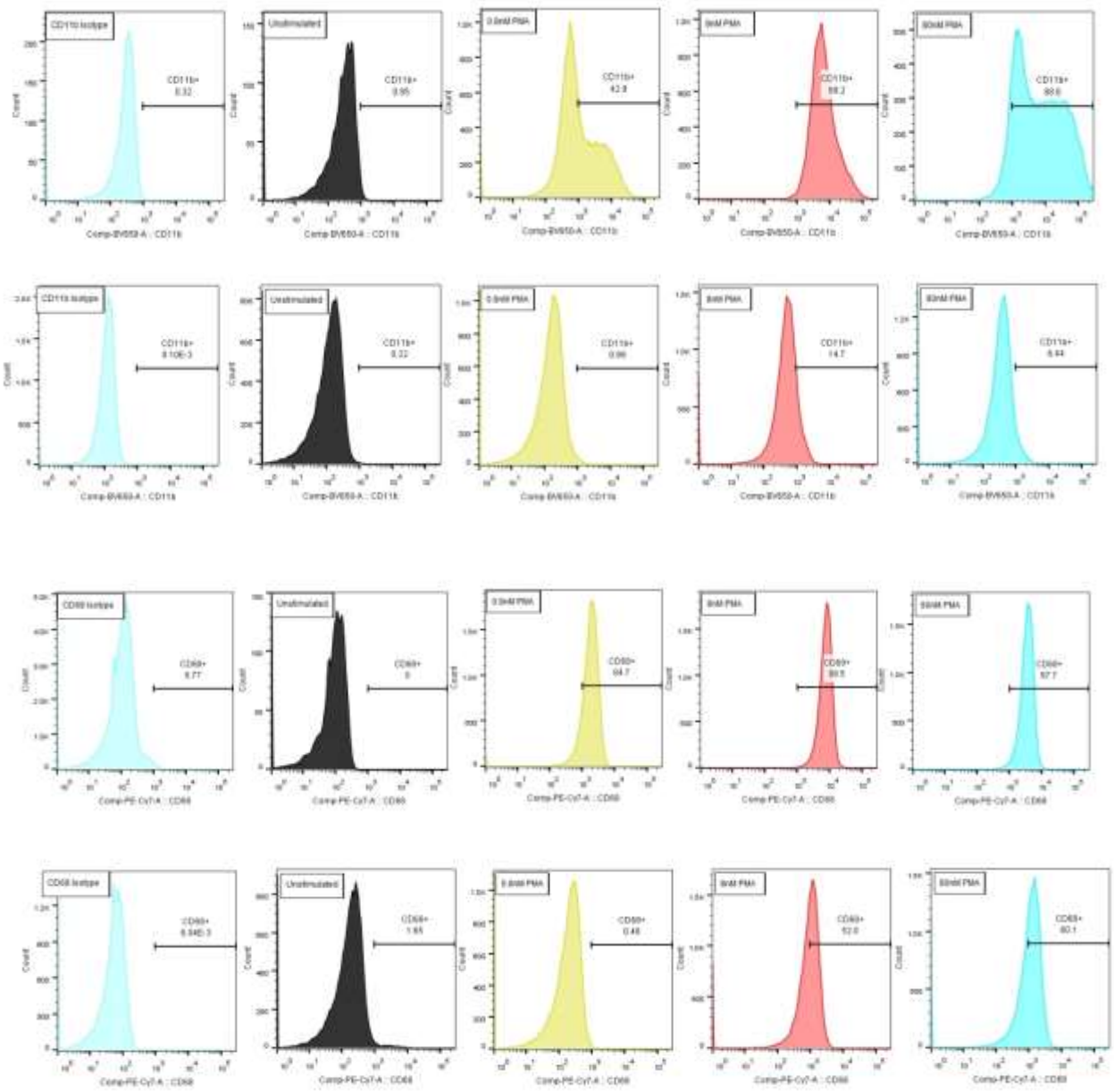

**Appendix Figure 7**. ***(a) U937 and (b) THP-1 cells. Histogram fluorescence images of CD14, CD11a, CD11b and CD68 analysed by flow cytometry.***

## (i) U937 cells

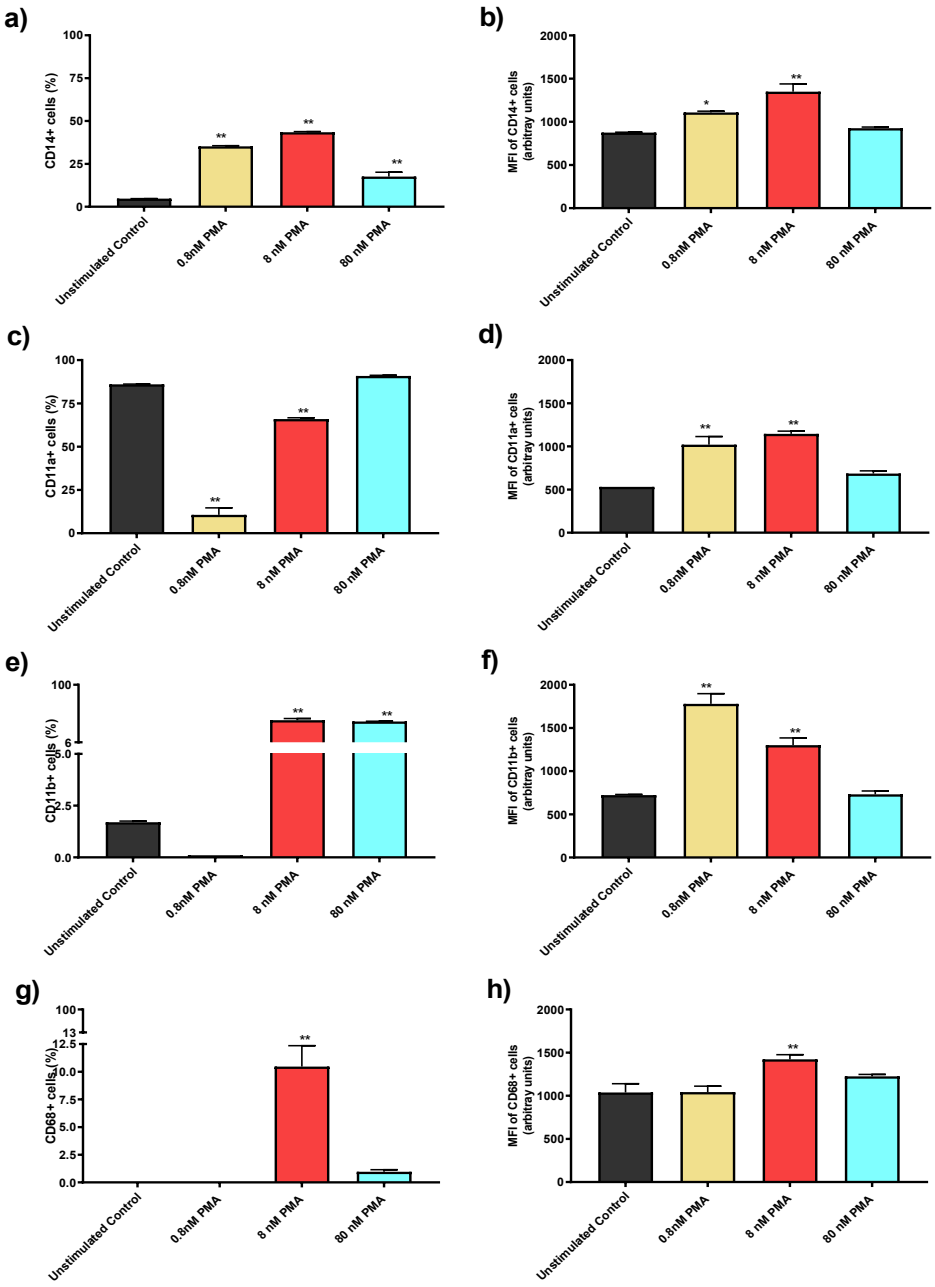
a)
CD14+ cells (%)
b)
MFI of CD14+ cells (arbitray units)
c)
CD11a+ cells (%)
d)
MFI of CD11a+ cells (arbitray units)
e)
CD11b+ cells (%)
f)
MFI of CD11b+ cells (arbitray units)
g)
CD68+ cells (%)
h)
MFI of CD68+ cells (arbitray units)
Unstimulated Control
0.8nM PMA
8 nM PMA
80 nM PMA

## (ii) THP-1 cells

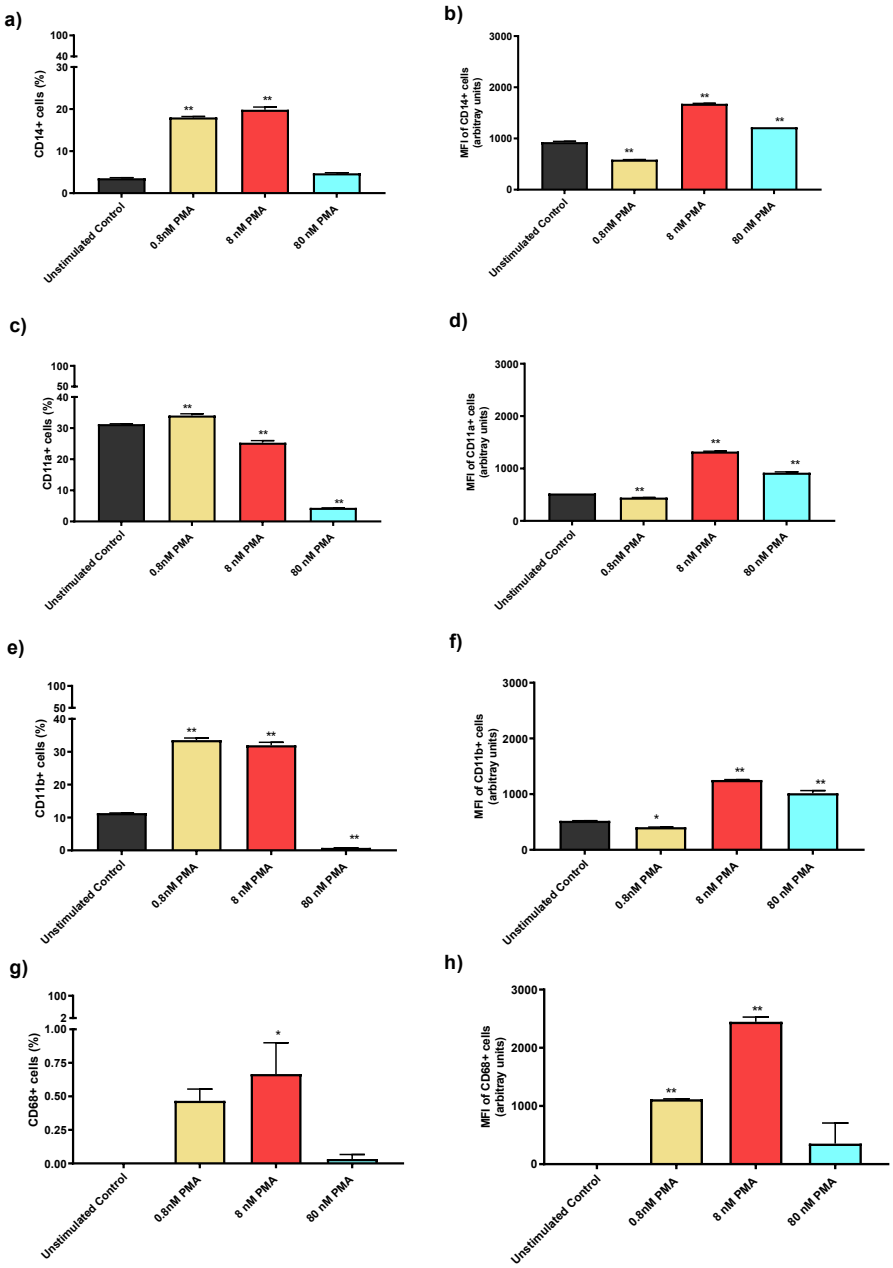


**Appendix Figure 8.** ***Expression of non-adherent (i) U937 and (ii) Thp-1 cells from PMA cultures.***

*Effect of PMA on surface markers expression during U937 differentiation analysed by flow cytometry. To determine U937 cell differentiation, PMA treated non-adherent cells were analysed by flow cytometry to measure the expression of CD14, CD11a, CD11b and CD68. Bar graphs (right panel-a, c, e, g) indicates comparison between non-adherent from the PMA cultures and unstimulated control cells for positive cells and MFI of live cells (left panel) in CD14-PE (b), CD11a-FITC (d), CD11b-BV650 (f) and CD68-Cyanine-7 (h) channels. ANOVA with post hoc Dunnett's test, mean ± SEM (n=3), **p < 0.01 vs unstimulated control U937 and THP-1 cells. The percentage of $CD14^+$ (0.8 nM PMA, 8 nM PMA, 80 nM PMA; p<0.01), $CD11a^+$ (0.8 nM PMA, 8 nM PMA; p<0.01), $CD11b^+$ (8 nM PMA, 80 nM PMA; p<0.01) and $CD68^+$ (8 nM PMA p<0.01) cells in non-adherent U937 cells of PMA culture was higher compared to unstimulated control U937 cells. Similarly, the percentage of $CD14^+$ (0.8 nM PMA, 8 nM PMA; p<0.01), $CD11a^+$ (0.8 nM PMA, 8 nM PMA, 80 nM PMA; p<0.01), $CD11b^+$ (0.8 nM PMA, 8 nM PMA, 80 nM PMA; p<0.01) and $CD68^+$ (8 nM PMA p<0.05) cells in non-adherent THP-1 cells of PMA culture was higher compared to unstimulated control THP-1 cells.*

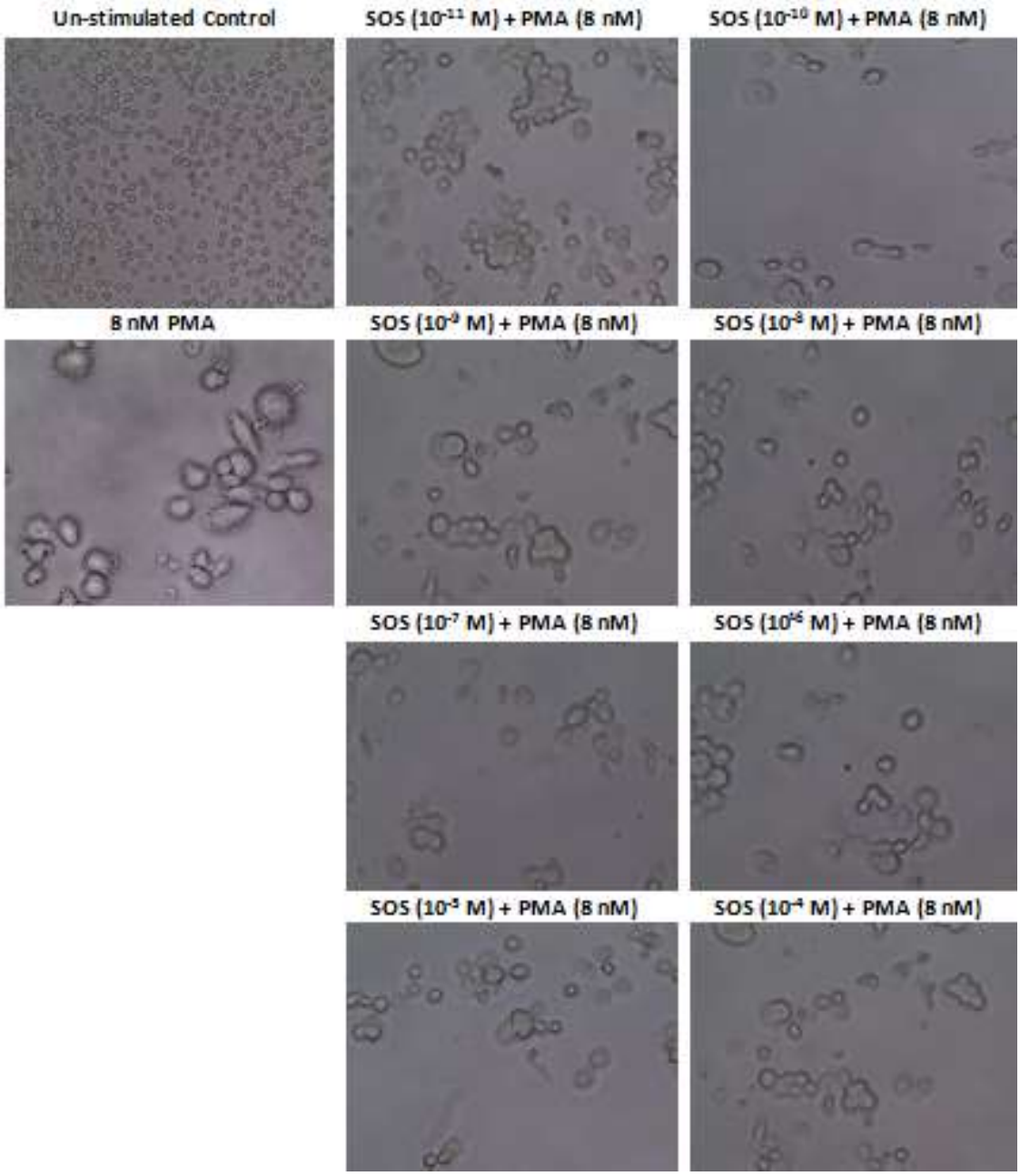


**Appendix Figure 9**. ***SOS impact on U937 cell morphology in the presence of PMA.***

*Representative image of three independent experiments where U937 cells were treated with SOS ($10^{-11}$ to $10^{-4}$ M) for 48 h in the presence of 8 nM PMA and analysed by inverted phase-contrast microscope with an original magnification power of 40x. Scale 100µm.*

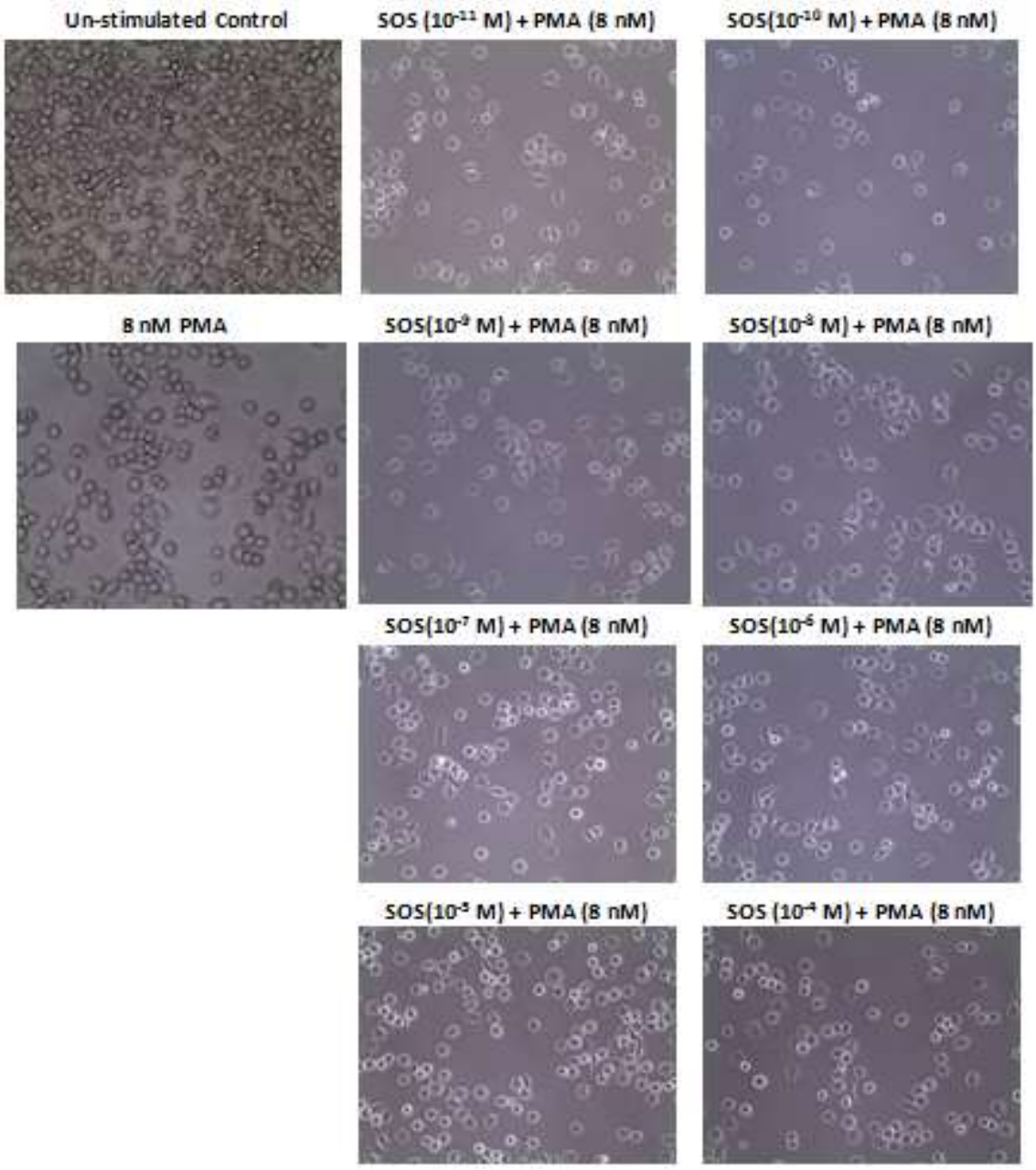


**Appendix Figure 10.** ***SOS impact on THP-1 cell morphology in the presence of PMA.***

*Representative image of three independent experiments where THP-1 cells were treated with SOS ($10^{-11}$ to $10^{-4}$ M) for 48 h in the presence of 8 nM PMA (see methods section 2.6) and analysed by inverted phase-contrast microscope with an original magnification power of 40x. Scale bar - 100µm.*

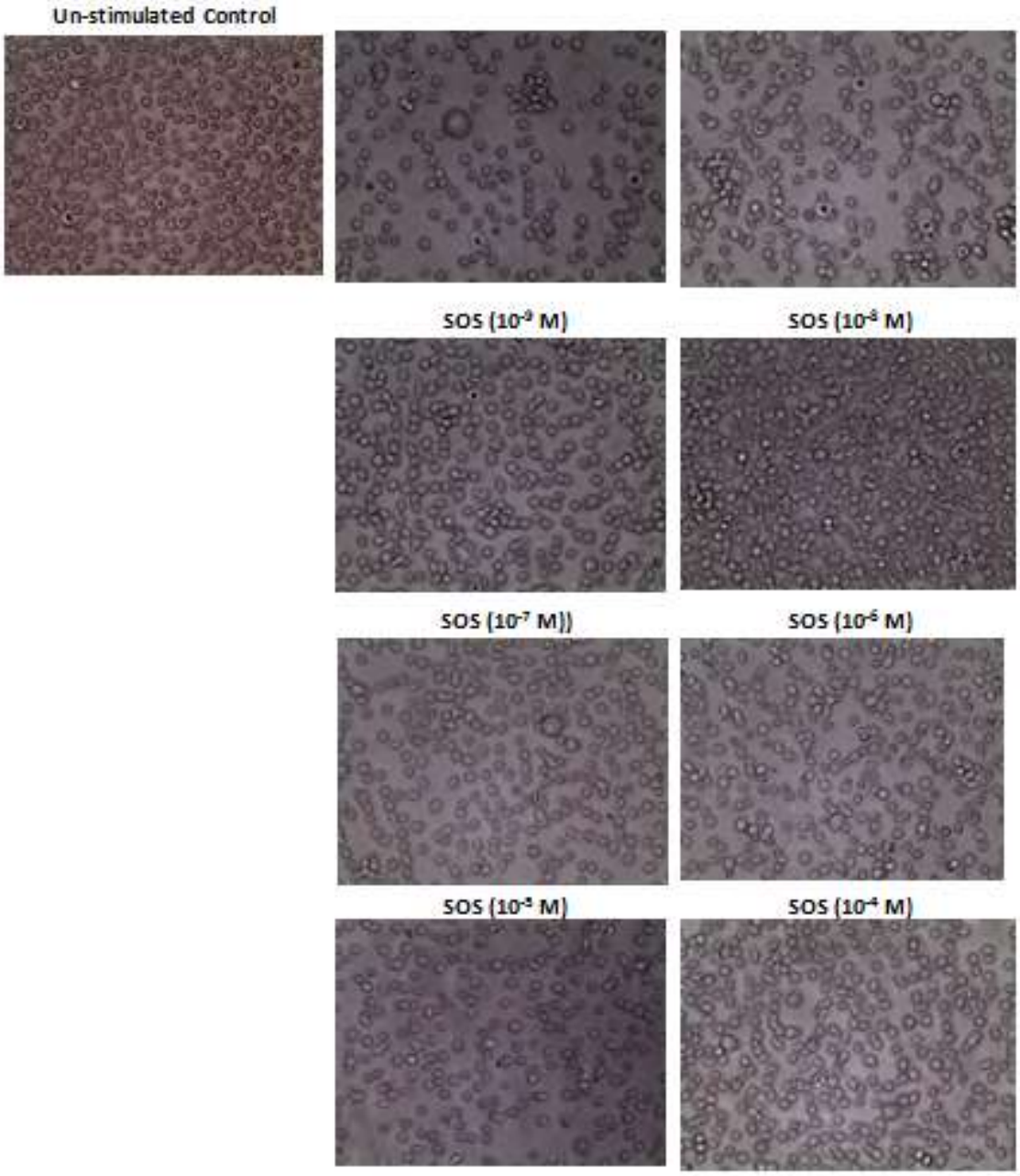


**Appendix Figure 11**. ***SOS impact on U937 cell morphology in the absence of PMA.***

*Representative image of three independent experiments where U937 cells were treated with SOS ($10^{-11}$ to $10^{-4}$ M) for 48 h in the absence of 8 nM PMA (see methods section 2.6) and analysed by inverted phase-contrast microscope with original magnification power of 40x. Scale bar - 100µm.*

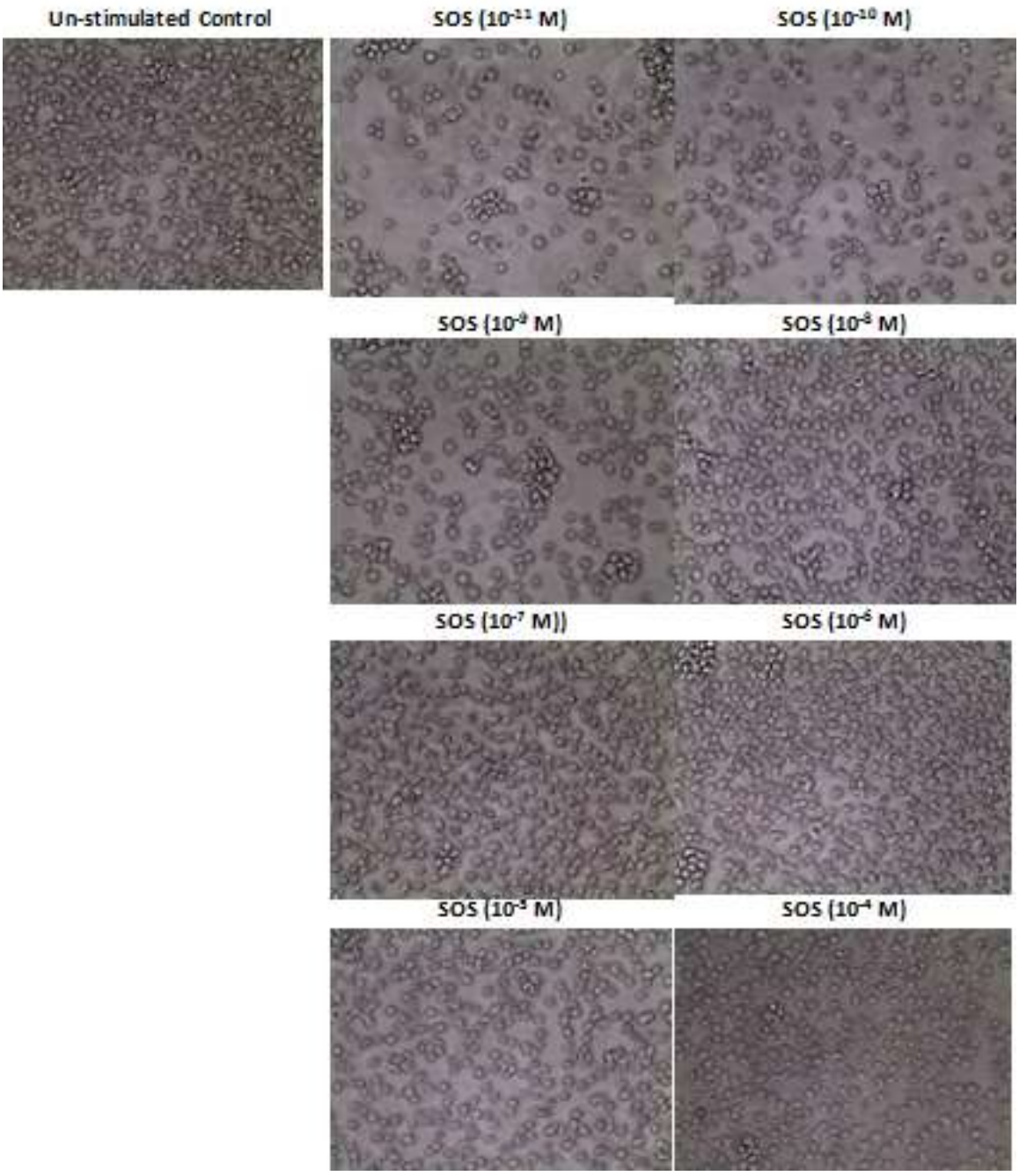


**Appendix Figure 12**. ***SOS impact on THP-1 cell morphology in the absence of PMA.***

*Representative image of three independent experiments where THP-1 cells were treated with SOS ($10^{-11}$ to $10^{-4}$ M) for 48 h in the absence of 8 nM PMA (see methods section 2.6) and analysed by inverted phase-contrast microscope with original magnification power of 40x. Scale bar - 100µm.*

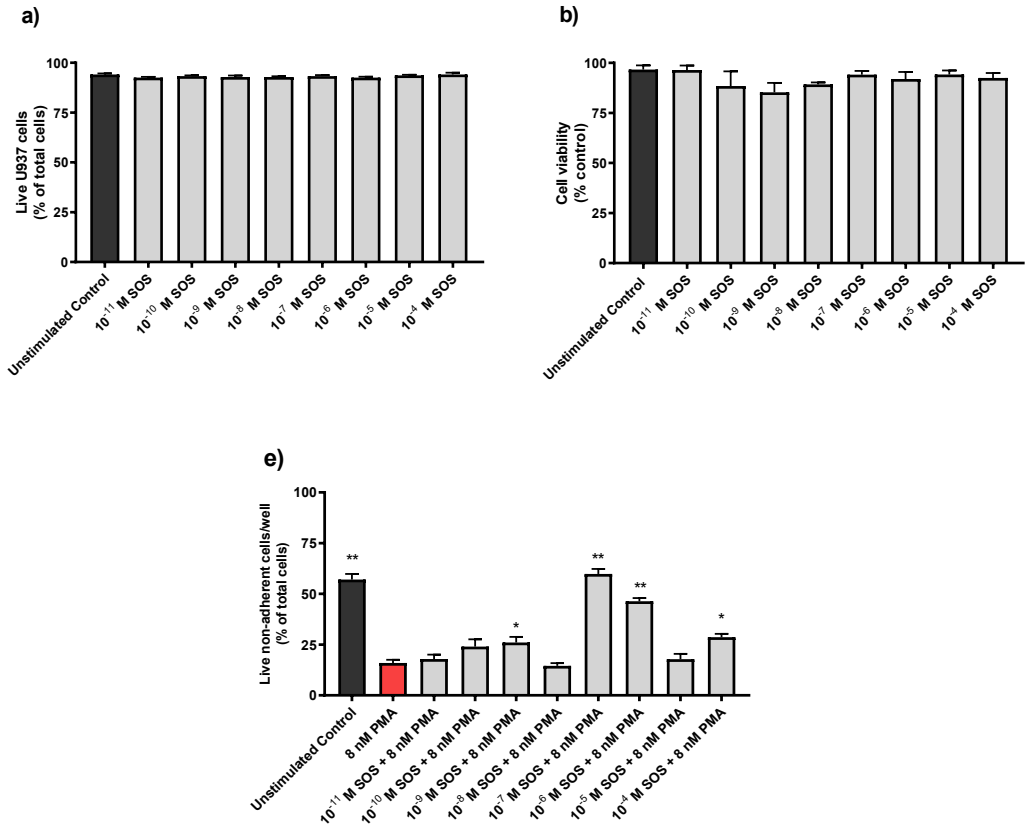


**Appendix Figure 13**. ***SOS impact on U937 cell count in the absence of PMA.***

*U937 cells were treated with SOS ($10^{-11}$ to $10^{-4}$ M) for 48 h in (a,b) absence of 8 nM PMA (given 2 h before PMA). Cell count (presented as live cells/mL and percentage of control) for non-adherent cells in the absence of PMA. (e) Cell viability was determined by MTT assay. Dunnett's post hoc test, means± SEM (n =3), *p<0.05, **p<0.01 vs unstimulated control or PMA.*

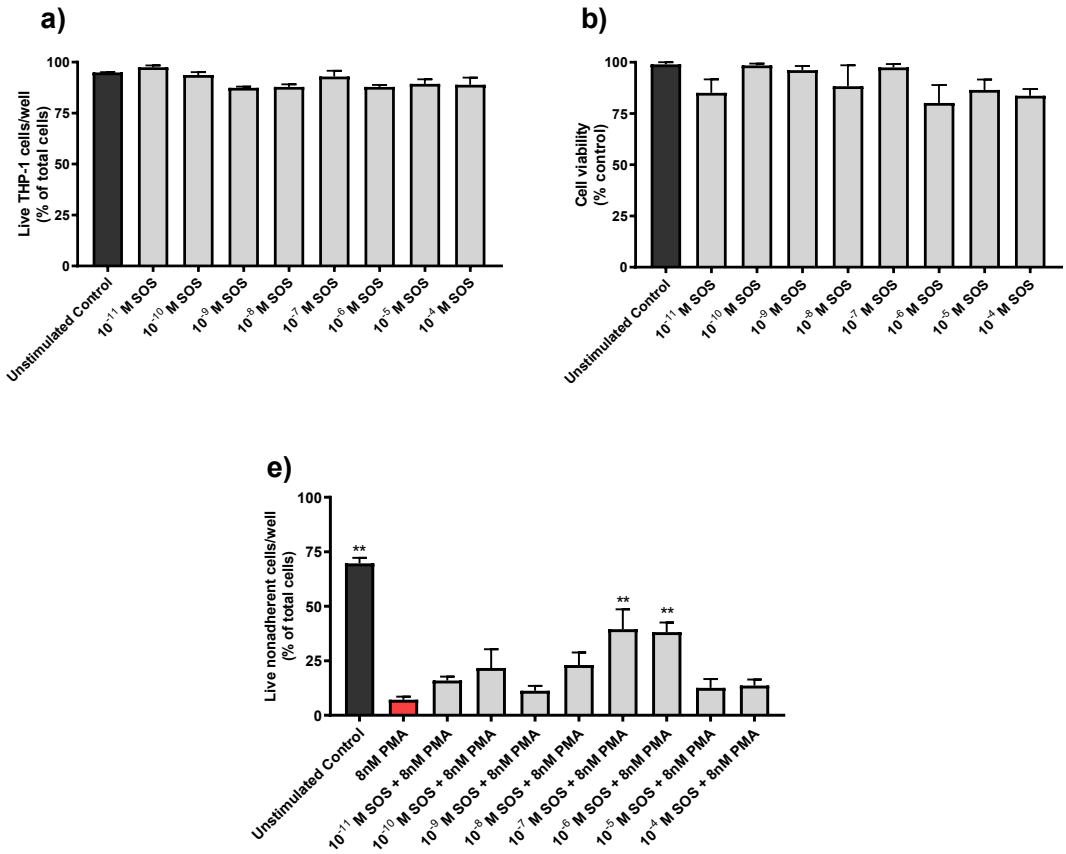


**Appendix Figure 14*. SOS impact on THP-1 cell count in the absence of PMA.***

*U937 cells were treated with SOS ($10^{-11}$ to $10^{-4}$ M) for 48 h in (a,b) absence of 8 nM PMA (given 2 h before PMA). Cell count (presented as live cells/mL and percentage of control) for non-adherent cells in the absence of PMA. (e) Cell viability was determined by MTT assay. Dunnett's post hoc test, means± SEM (n =3), *p<0.05, **p<0.01 vs unstimulated control or PMA.*

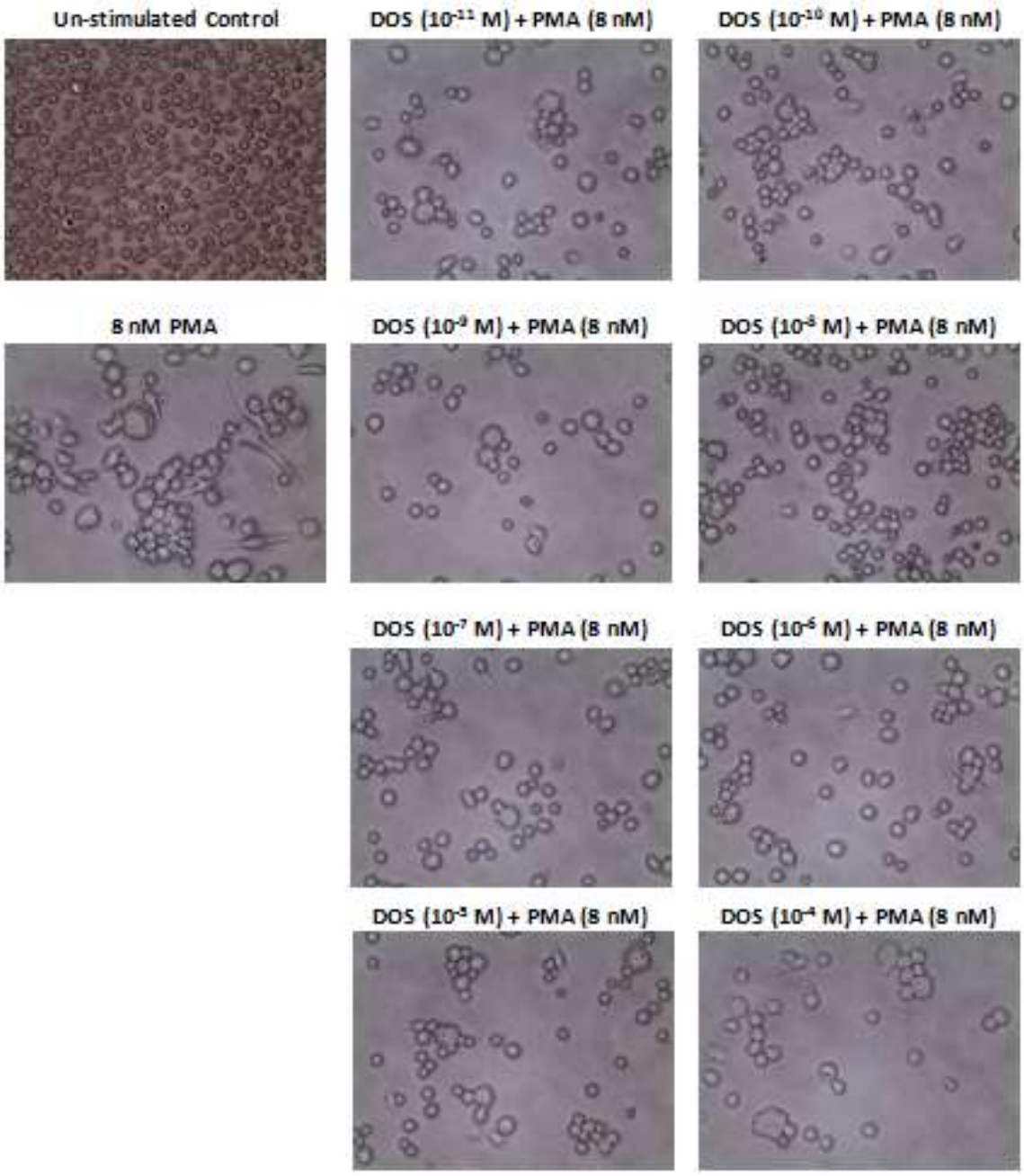


**Appendix Figure 15.** ***DOS impact on U937 cell morphology in the presence of PMA.***

*Representative image of three independent experiments where U937 cells were treated with DOS ($10^{-11}$ to $10^{-4}$ M) for 48 h in the presence of 8 nM PMA and analysed by inverted phase-contrast microscope with original magnification power of 40x. Scale bar - 100µm.*

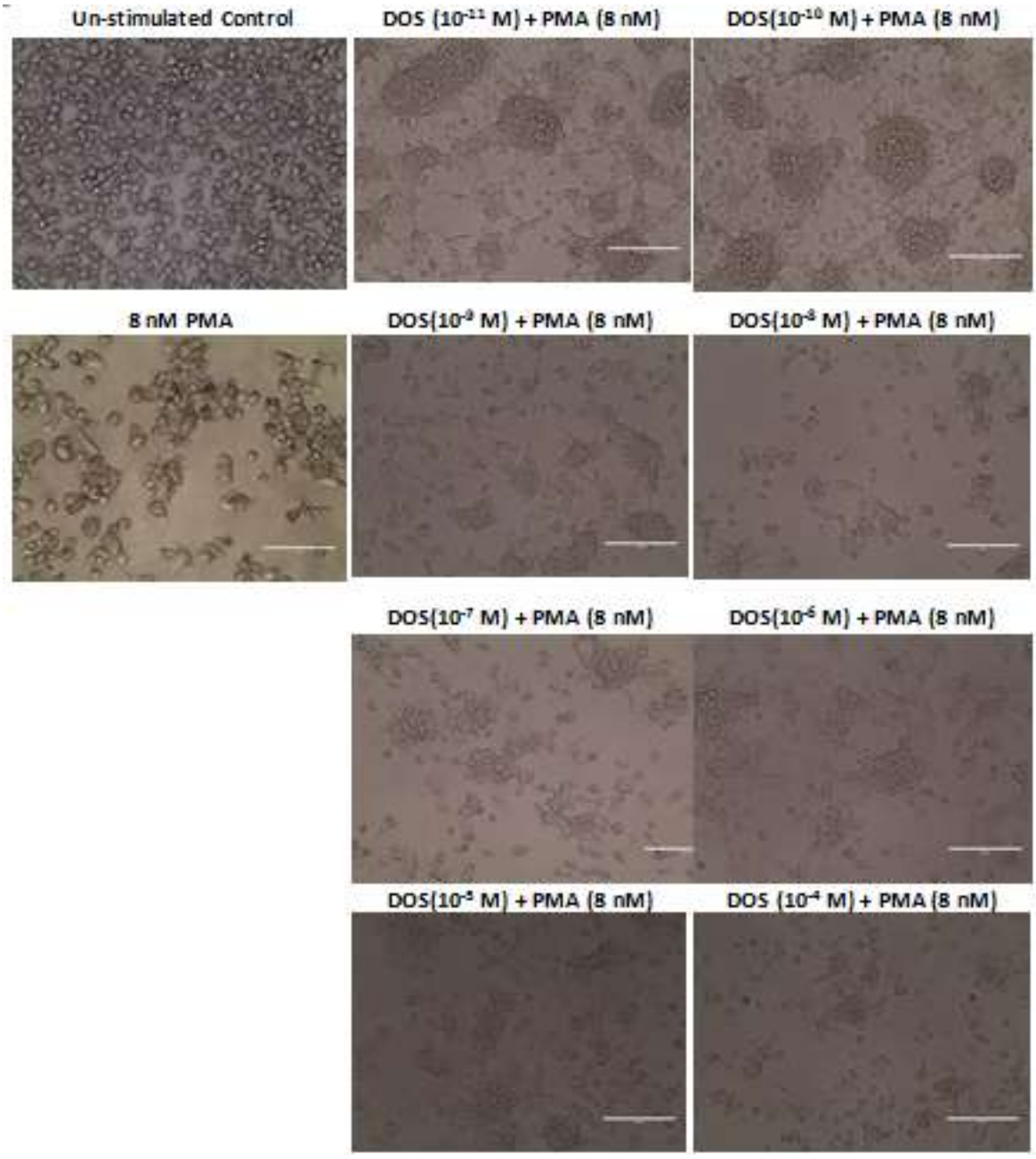


**Appendix Figure 16.** ***DOS impact on THP-1 cell morphology in the presence of PMA.***

*Representative image of three independent experiments where THP-1 cells were treated with DOS ($10^{-11}$ to $10^{-4}$ M) for 48 h in the presence of 8 nM PMA and analysed by inverted phase-contrast microscope with original magnification power of 40x. Scale bar - 100µm.*

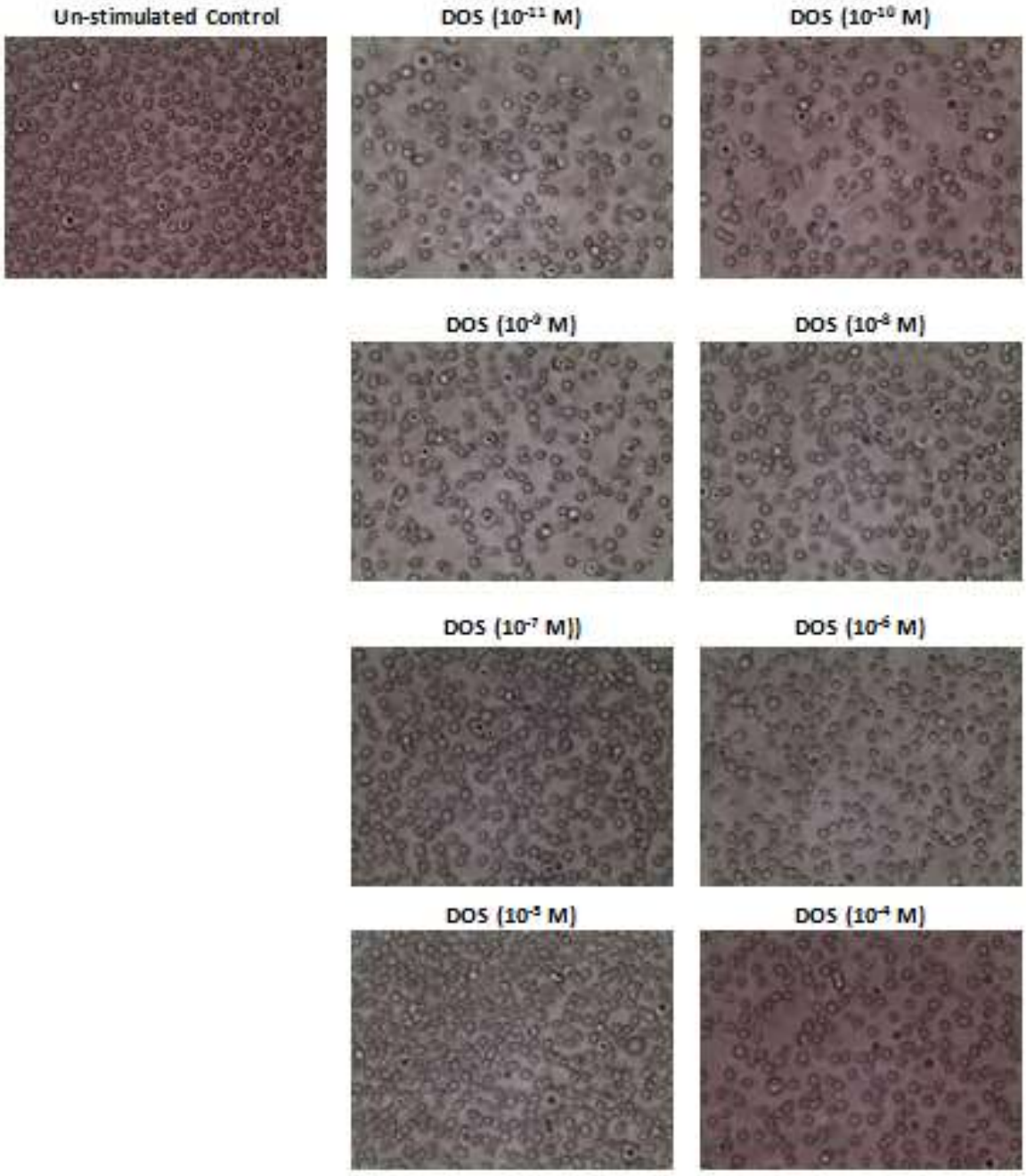


**Appendix Figure 17.** ***DOS impact on U937 cell morphology the absence of PMA.***

*Representative image of three independent experiments where U937 cells were treated with DOS ($10^{-11}$ to $10^{-4}$ M) for 48 h in the absence of 8 nM PMA and analysed by inverted phase-contrast microscope with original magnification power of 40x. Scale bar - 100µm.*

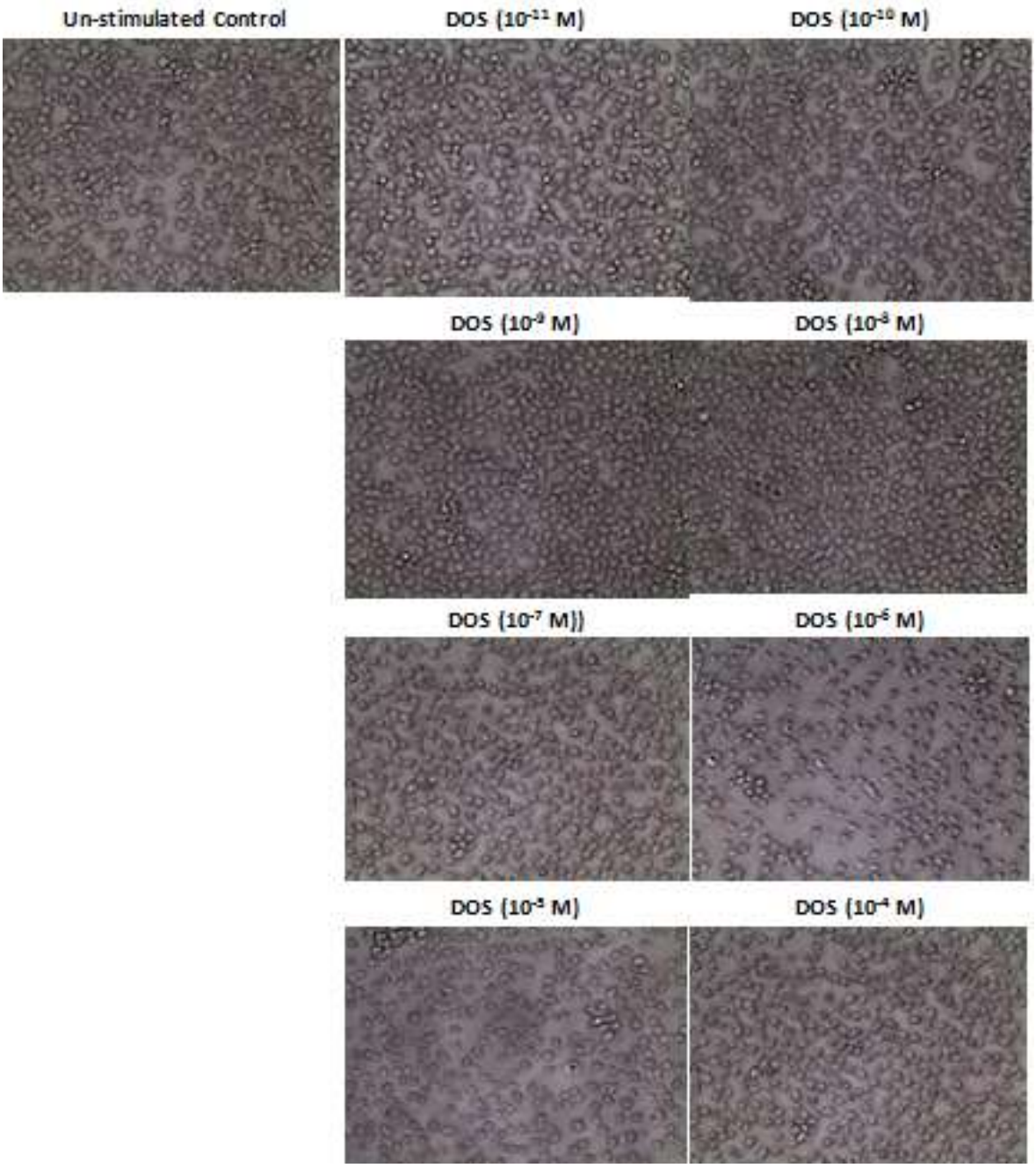


**Appendix Figure 18.** ***DOS impact on THP-1 cell morphology in the absence of PMA.***

*Representative image of three independent experiments where THP-1 cells were treated with DOS ($10^{-11}$ to $10^{-4}$ M) for 48 h in the absence of 8 nM PMA and analysed by inverted phase-contrast microscope with original magnification power of 40x. Scale bar - 100µm.*

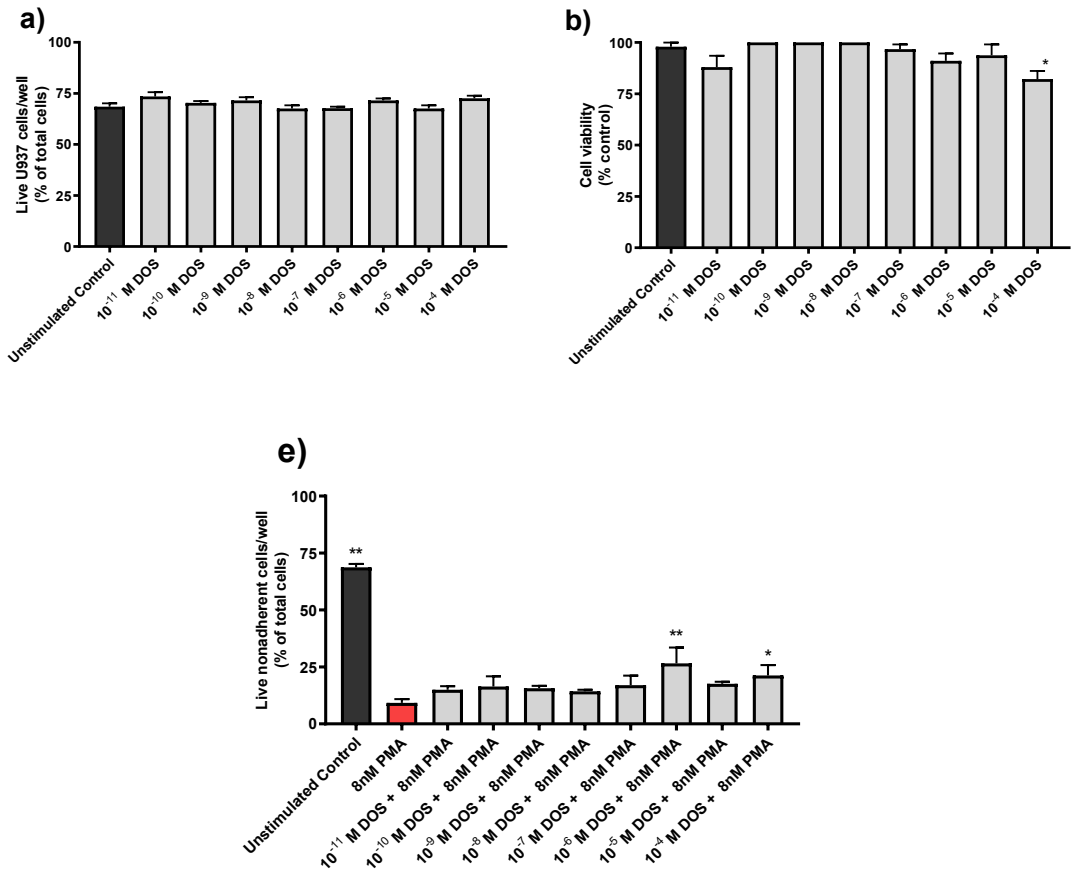


**Appendix Figure 19. DOS impact on U937 cell count in the absence of PMA.**

*U937 cells were treated with DOS ($10^{-11}$ to $10^{-4}$ M) for 48 h in (a,b) absence of 8 nM PMA (given 2 h before PMA). Cell count (presented as live cells/mL and percentage of control) for non-adherent cells in the absence of PMA. (e) Cell viability was determined by MTT assay. Dunnett's post hoc test, means± SEM (n =3), *p<0.05, **p<0.01 vs unstimulated control or PMA. MTT assay results revealed that the cell viability was reduced significantly in the presence of DOS and PMA at concentrations of $10^{-6}$ M to $10^{-4}$ M (p <0.01) in U937 cells and at concentrations of $10^{-10}$ M to $10^{-4}$ M (p <0.05, p <0.01) in THP-1 cells. DOS at concentration of $10^{-4}$ M in the absence of PMA also showed significant (p <0.05) cell death in U937 cells whereas in THP-1 cells DOS at concentrations of $10^{-11}$ M to $10^{-4}$ M had no significant effect on cell viability compared to unstimulated control cells.*

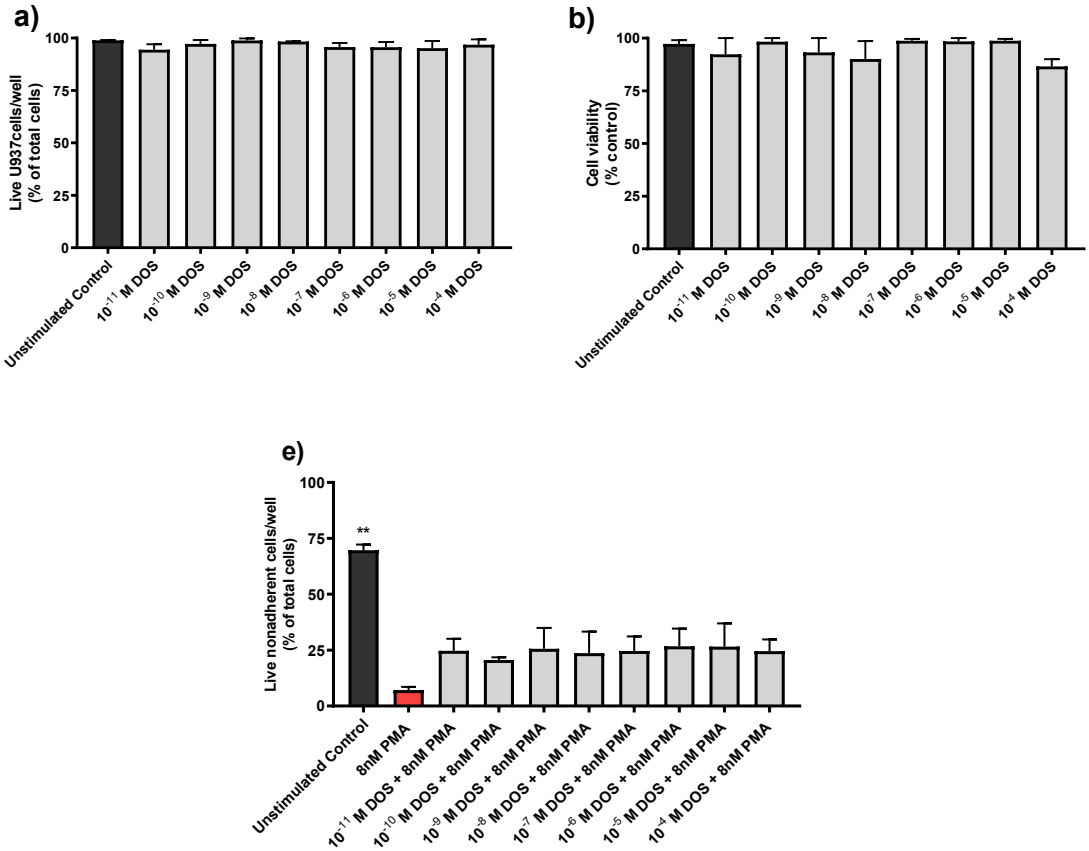


**Appendix Figure 20**. ***DOS impact on THP-1 cell count in the absence of PMA.***

*THP-1 cells were treated with DOS ($10^{-11}$ to $10^{-4}$ M) for 48 h in (a,b) absence of 8 nM PMA (given 2 h before PMA). Cell count (presented as live cells/mL and percentage of control) for non-adherent cells in the absence of PMA. (e) Cell viability was determined by MTT assay. Dunnett's post hoc test, means± SEM (n =3), *p<0.05, **p<0.01 vs unstimulated control or PMA.*

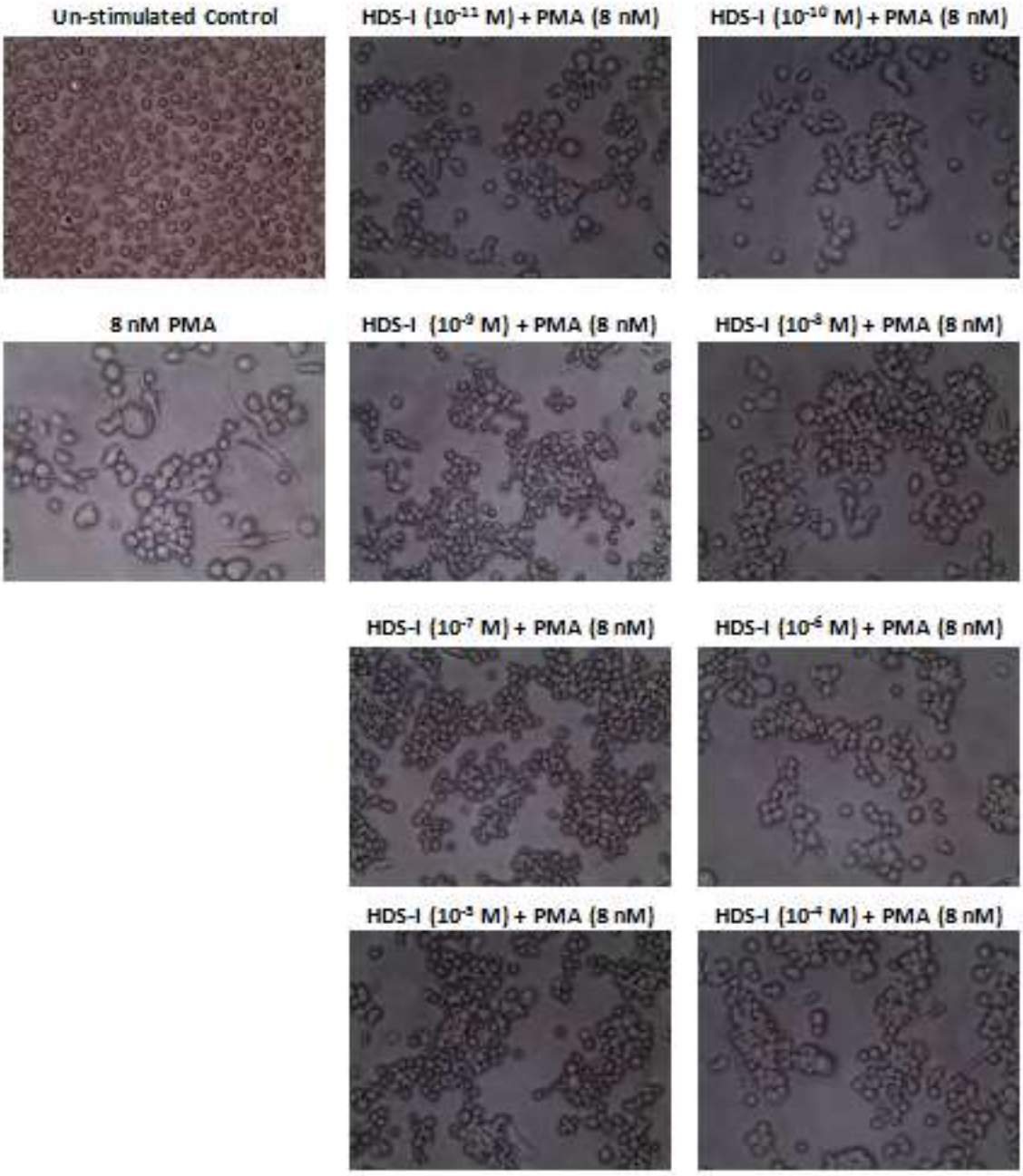


**Appendix Figure 21.** ***HDS-I impact on U937 cell morphology in the presence of PMA.***

*Representative image of three independent experiments where U937 cells were treated with HDS-I ($10^{-11}$ to $10^{-4}$ M) for 48 h in the presence of 8 nM PMA and analysed by inverted phase-contrast microscope with original magnification power of 40x. Scale bar - 100µm.*


**Appendix Figure 22.** ***HDS-I impact on THP-1 cell morphology in the presence of PMA.***

*Representative image of three independent experiments where THP-1 cells were treated with HDS-I ($10^{-11}$ to $10^{-4}$ M) for 48 h in the presence of 8 nM PMA and analysed by inverted phase-contrast microscope with original magnification power of 40x. Scale bar - 100µm.*

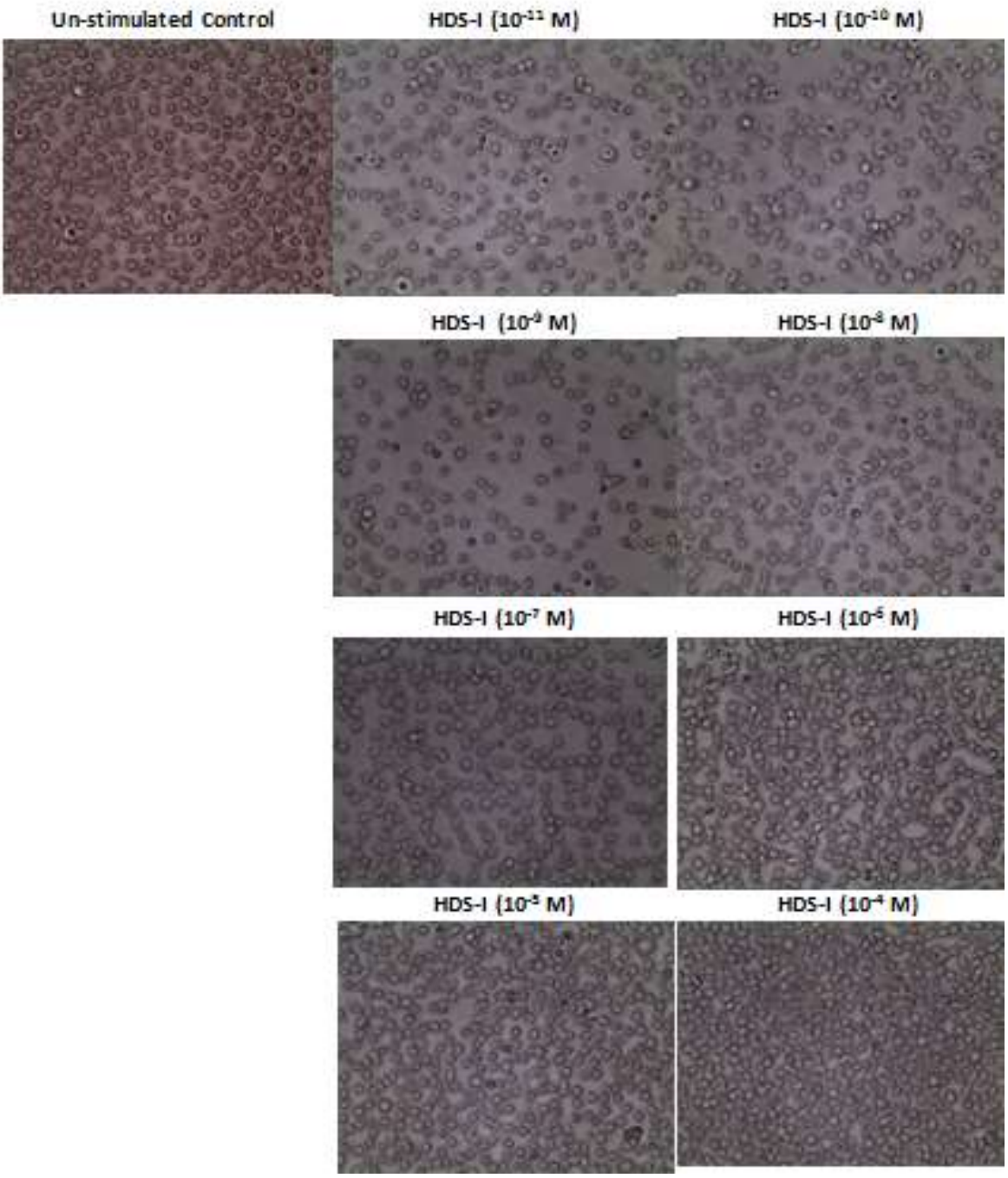


**Appendix Figure 23.** ***HDS-I impact on U937 cell morphology in the absence of PMA.***

*Representative image of three independent experiments where U937 cells were treated with HDS-I ($10^{-11}$ to $10^{-4}$ M) for 48 h in the absence of 8 nM PMA and analysed by inverted phase-contrast microscope with original magnification power of 40x. Scale bar - 100µm.*

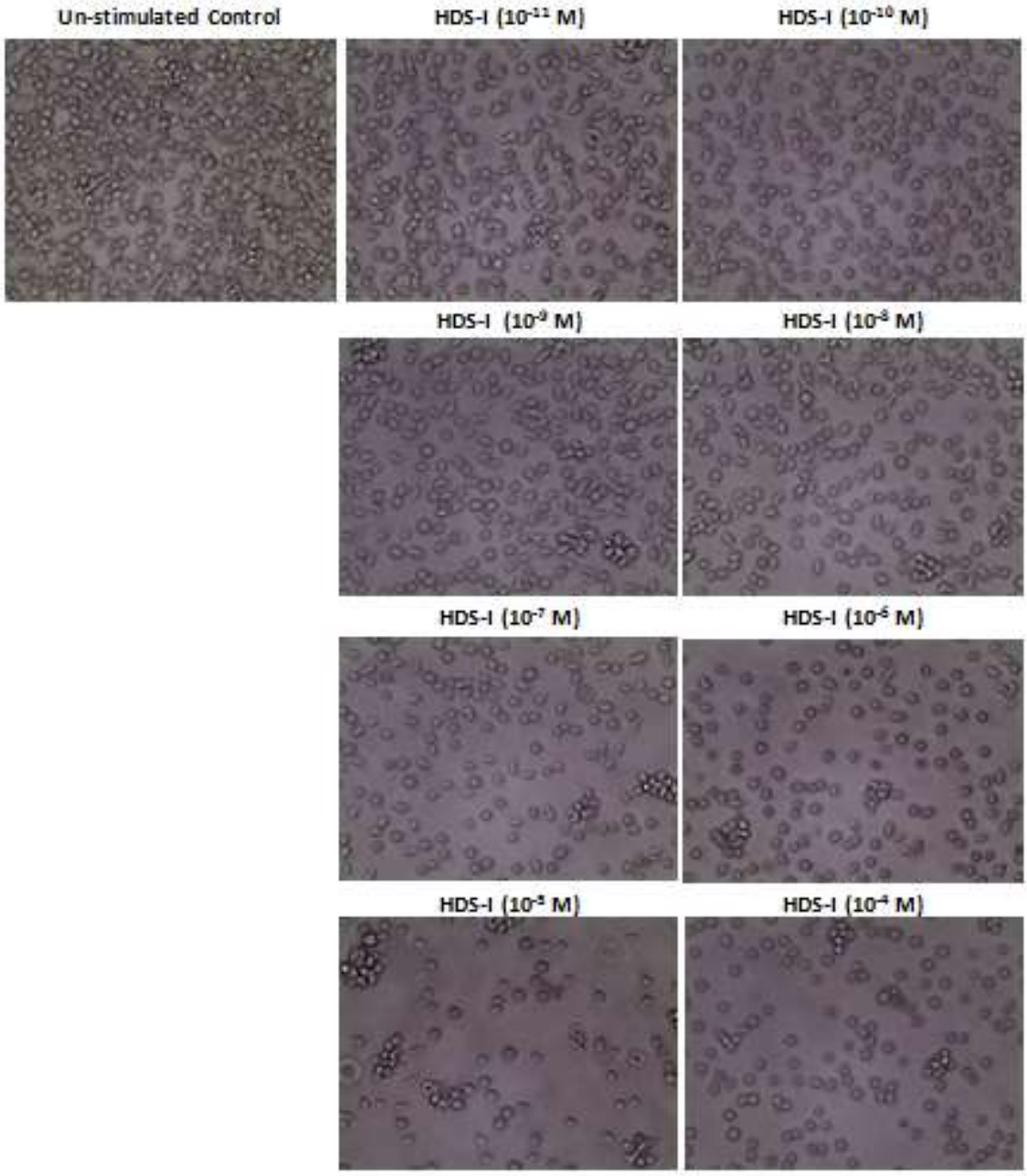


**Appendix Figure 24.** ***HDS-I impact on THP-1 cell morphology in the absence of PMA.***

*Representative image of three independent experiments where THP-1 cells were treated with HDS-I ($10^{-11}$ to $10^{-4}$ M) for 48 h in the absence of 8 nM PMA and analysed by inverted phase-contrast microscope with original magnification power of 40x. Scale bar - 100µm.*

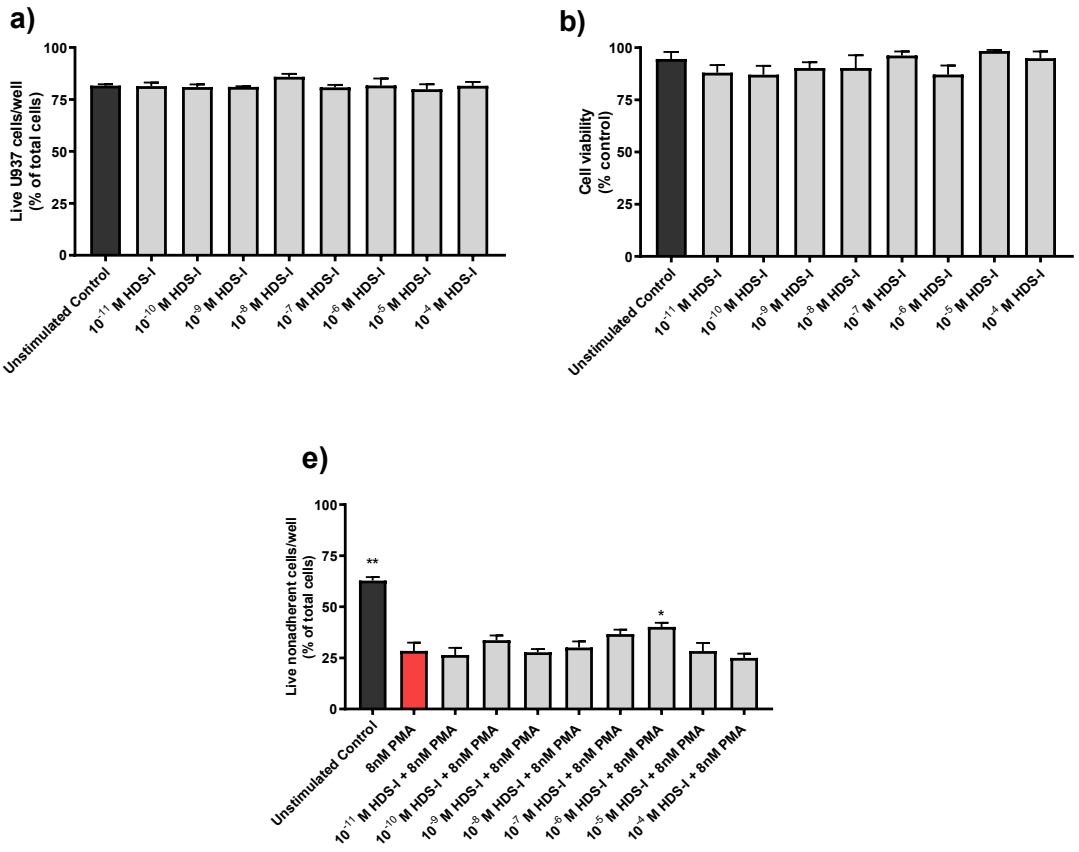


**Appendix Figure 25**. **HDS-I impact on U937 cell count in the absence of PMA.**

*U937 cells were treated with HDS-I ($10^{-11}$ to $10^{-4}$ M) for 48 h in (a,b) absence of 8 nM PMA (given 2 h before PMA). Cell count (presented as live cells/mL and percentage of control) for non-adherent cells in the absence of PMA. (e) Cell viability was determined by MTT assay. Dunnett's post hoc test, means± SEM (n =3), *p<0.05, **p<0.01 vs unstimulated control or PMA. No significant differences in cell morphology, monocyte cell count and cell viability (MTT assay) were seen between HDS-I treated U937 or THP-1 cells at concentrations of $10^{-11}$ M to $10^{-4}$ M and unstimulated control U937 or THP-1 cells.*

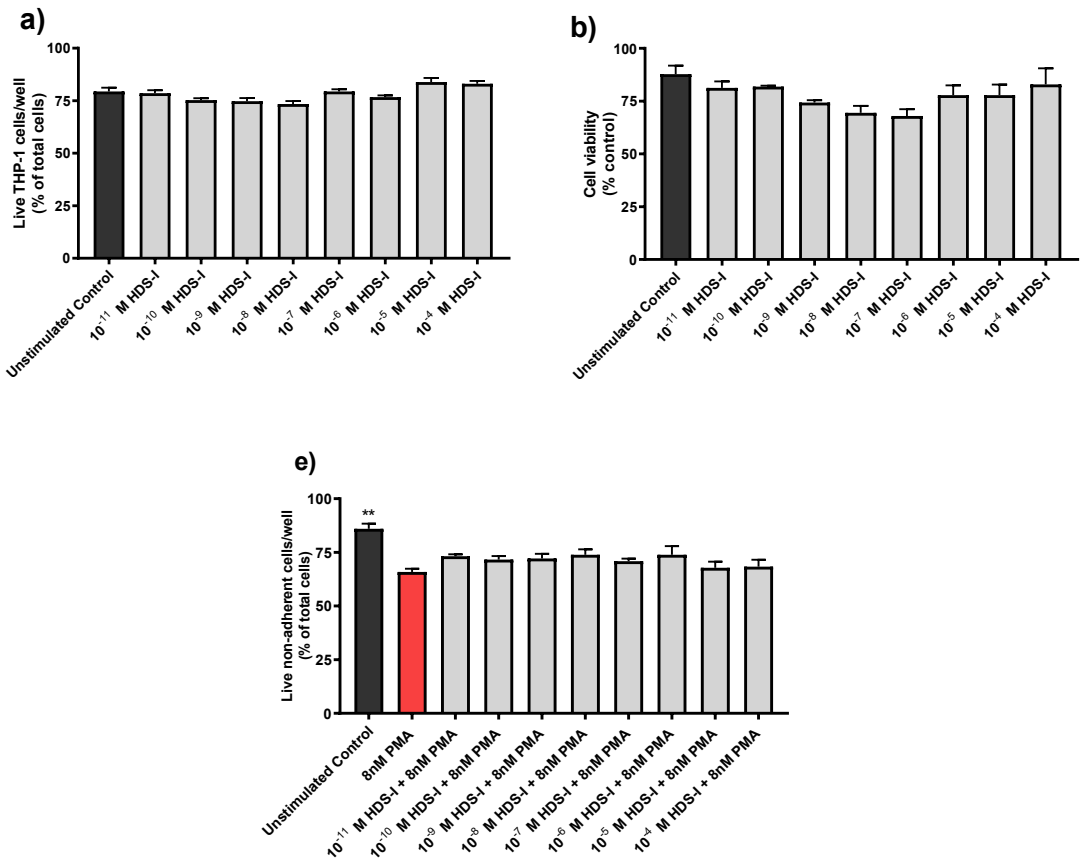


**Appendix Figure 26*. HDS-I impact on THP-1 cell count in the absence of PMA.***

*THP-1 cells were treated with SOS ($10^{-11}$ to $10^{-4}$ M) for 48 h in (a,b) absence of 8 nM PMA (given 2 h before PMA). Cell count (presented as live cells/mL and percentage of control) for non-adherent cells in the absence of PMA. (e) Cell viability was determined by MTT assay. Dunnett's post hoc test, means± SEM (n =3), *p<0.05, **p<0.01 vs unstimulated control or PMA.*

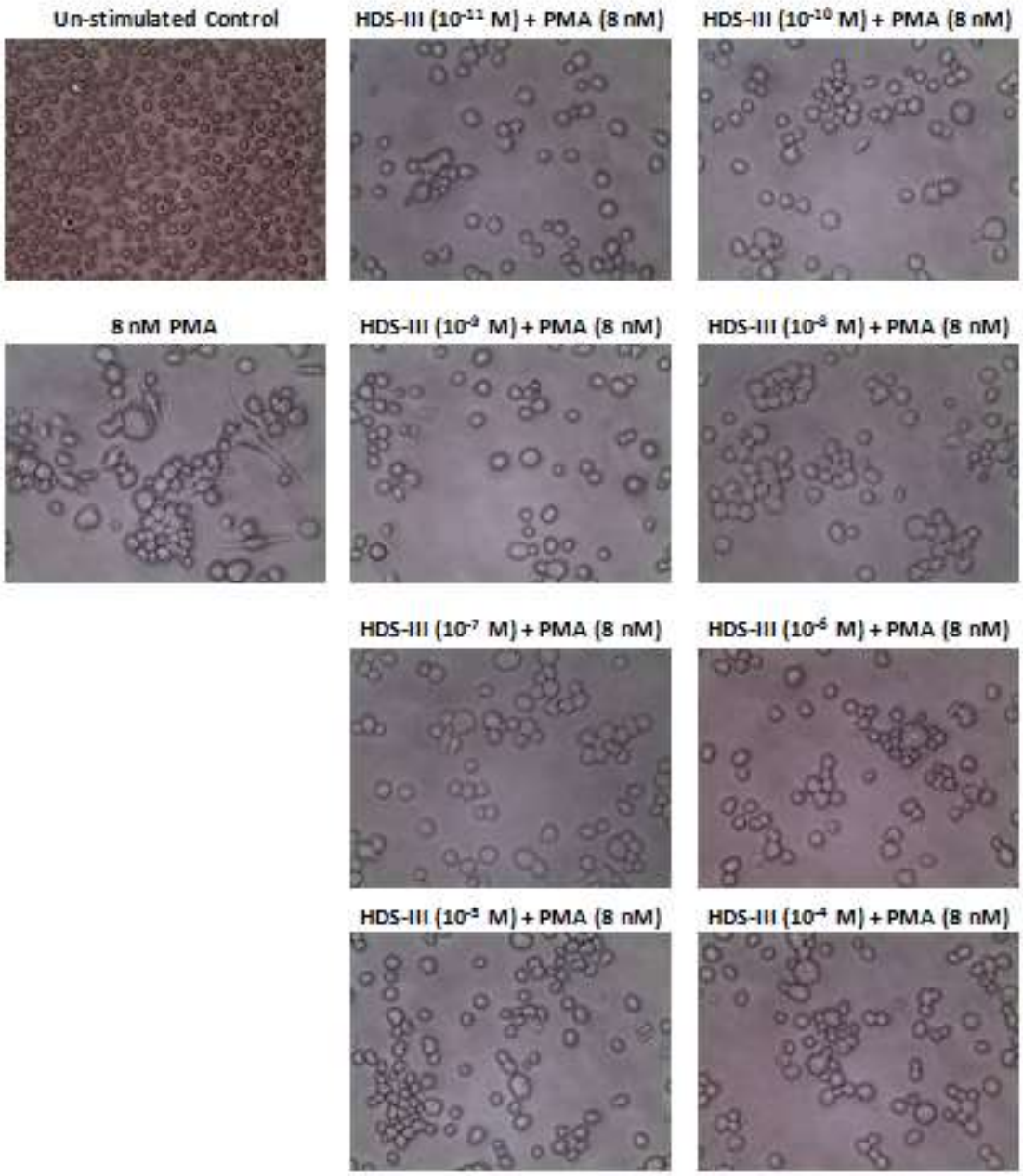


**Appendix Figure 27**. ***HDS-III impact on U937 cell morphology in the presence of PMA.***

*Representative image of three independent experiments where U937 cells were treated with HDS-III ($10^{-11}$ to $10^{-4}$ M) for 48 h in the presence of 8 nM PMA and analysed by inverted phase-contrast microscope with original magnification power of 40x. Scale bar - 100µm.*

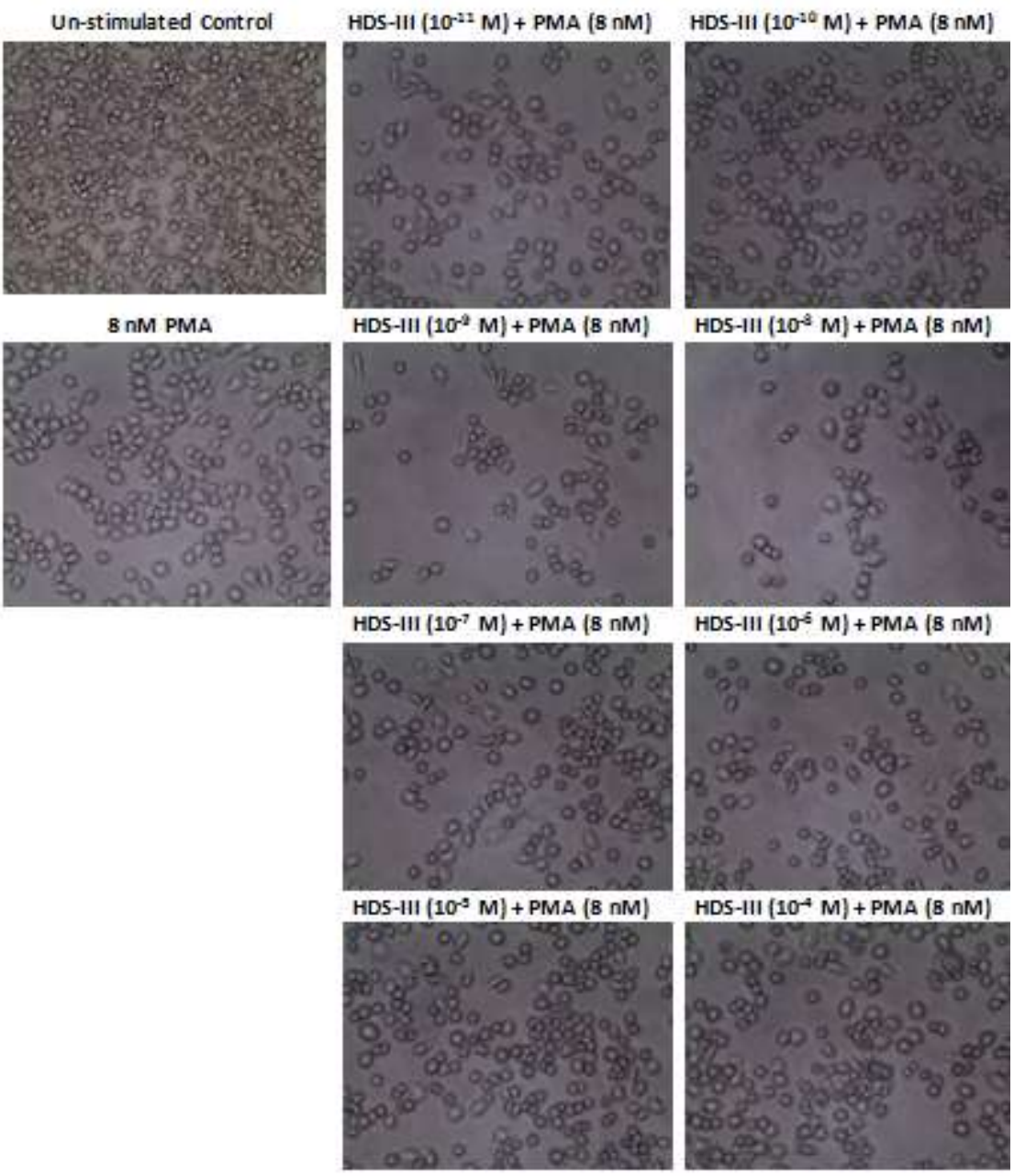


**Appendix Figure 28**. ***HDS-III impact on THP-1 cell morphology in the presence of PMA.***

*Representative image of three independent experiments where THP-1 cells were treated with HDS-III ($10^{-11}$ to $10^{-4}$ M) for 48 h in the presence of 8 nM PMA and analysed by inverted phase-contrast microscope with original magnification power of 40x. Scale bar - 100µm.*

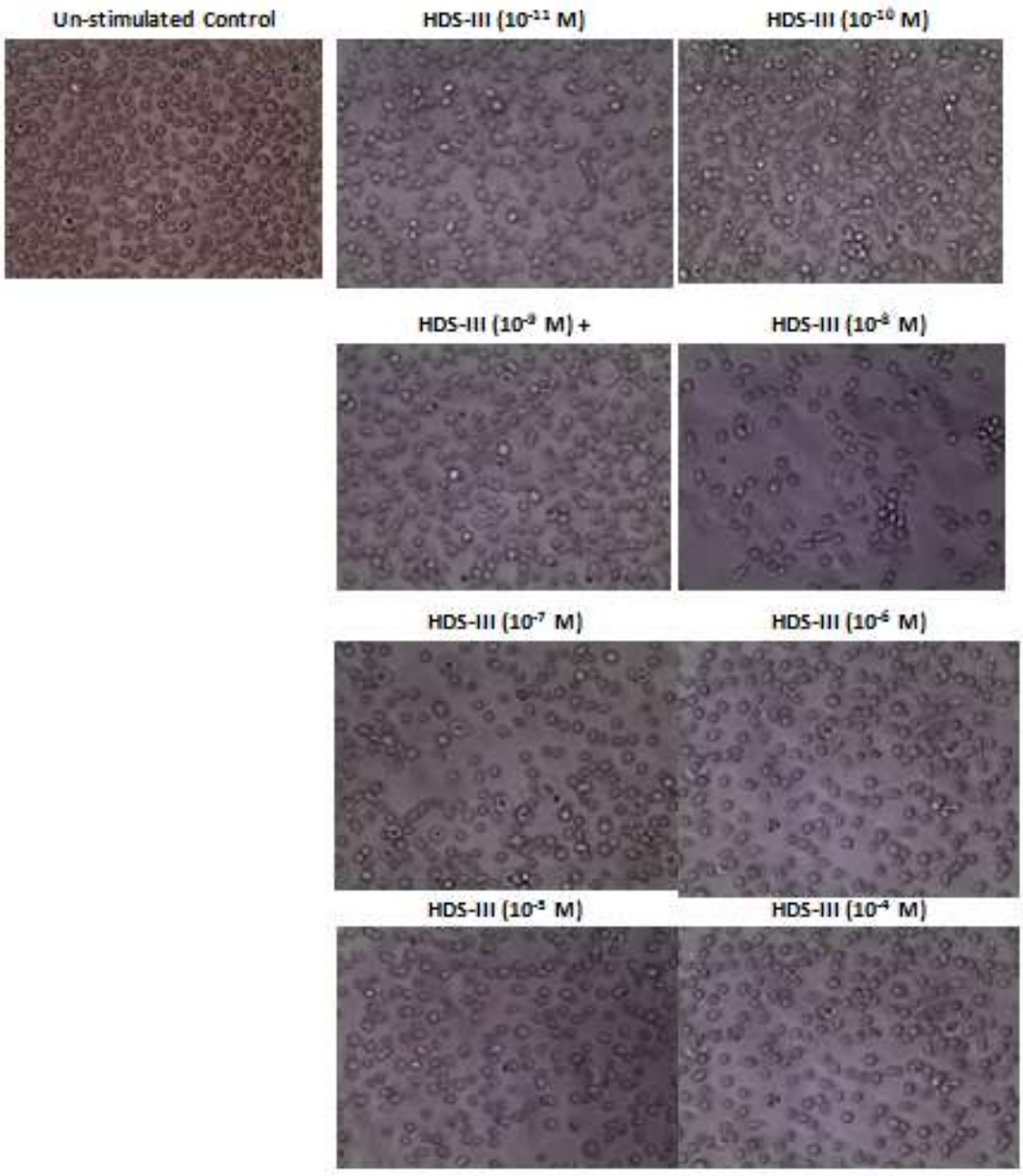


**Appendix Figure 29*. HDS-III impact on U937 cell morphology in the absence of PMA.***

*Representative image of three independent experiments where U937 cells were treated with HDS-III ($10^{-11}$ to $10^{-4}$ M) for 48 h in the absence of 8 nM PMA and analysed by inverted phase-contrast microscope with original magnification power of 40x. Scale bar - 100µm.*

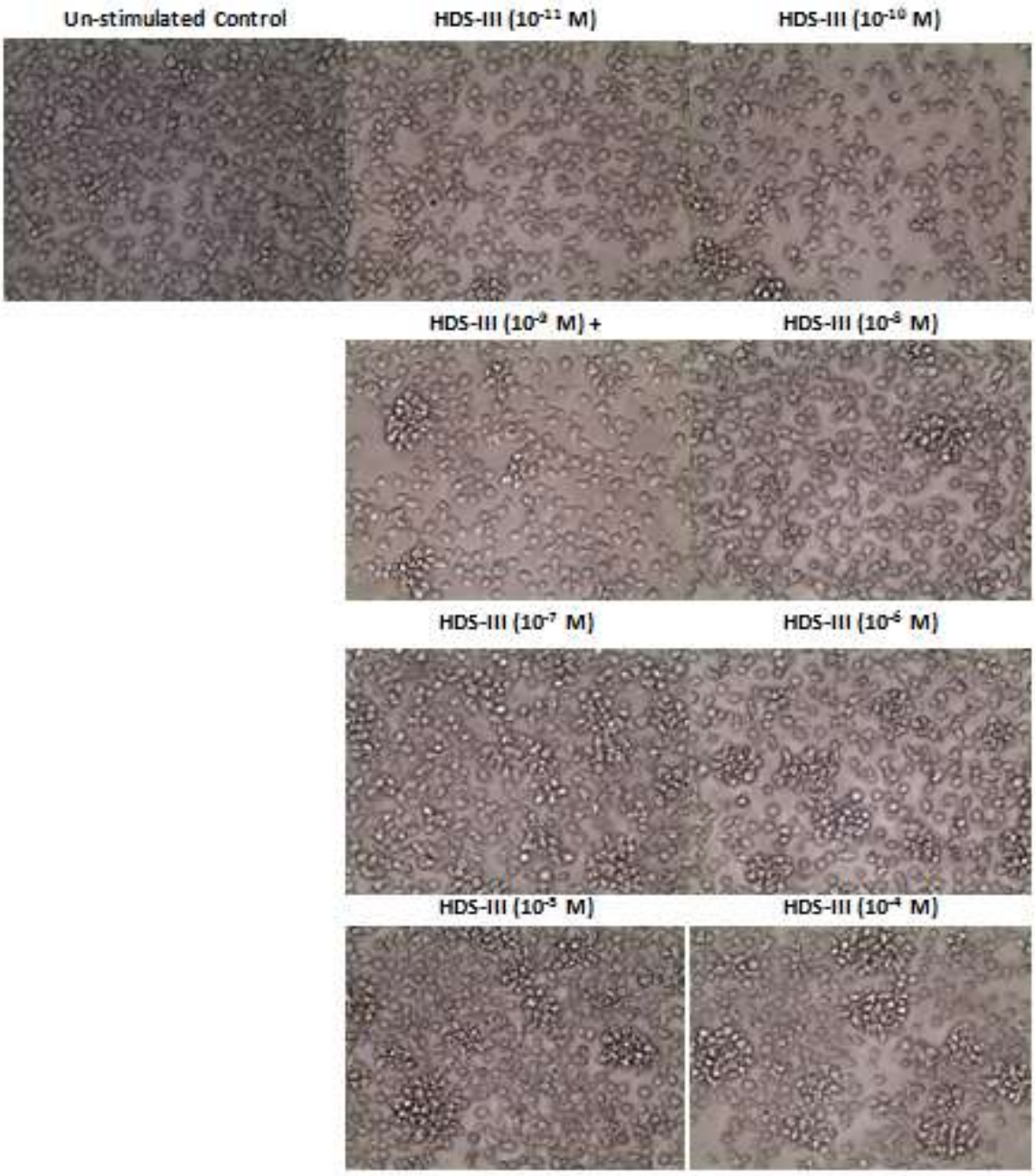


**Appendix Figure 30**. ***HDS-III impact on THP-1 cell morphology in the absence of PMA.***

*Representative image of three independent experiments where THP-1 cells were treated with HDS-III ($10^{-11}$ to $10^{-4}$ M) for 48 h in the absence of 8 nM PMA and analysed by inverted phase-contrast microscope with original magnification power of 40x. Scale bar - 100µm.*

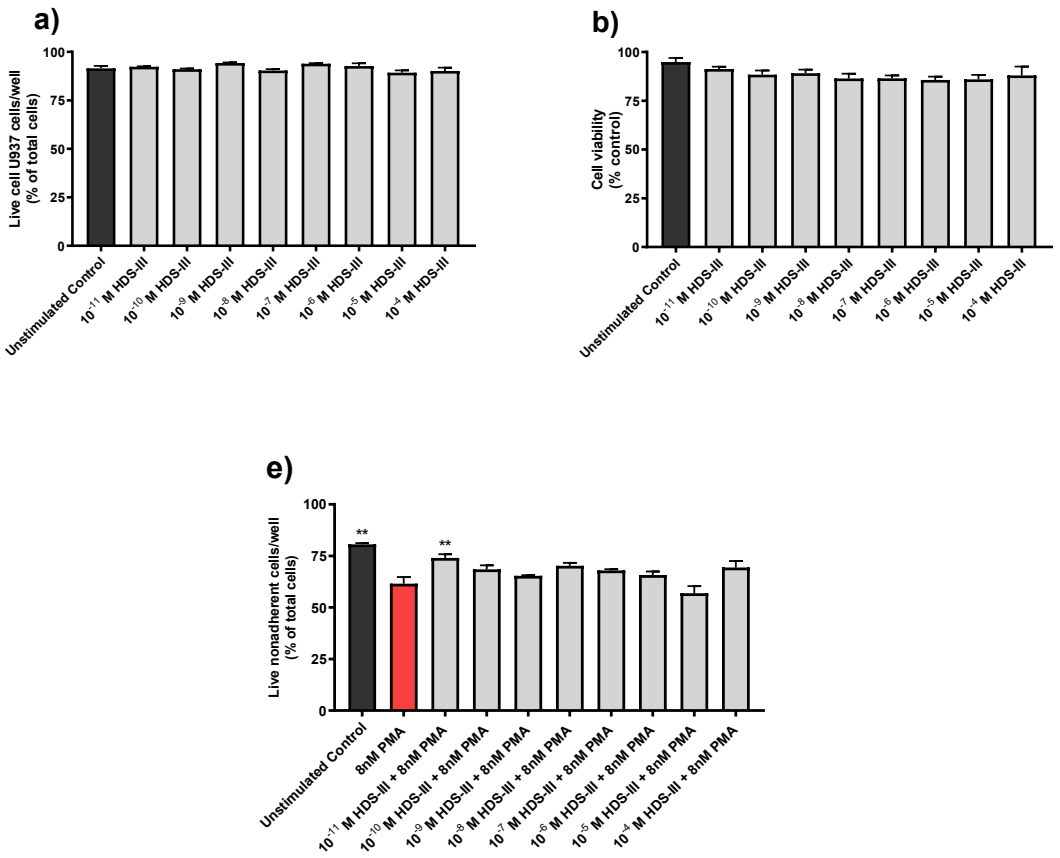


**Appendix Figure 31**. ***HDS-III impact on U937 cell count in the absence of PMA.***

*U937 cells were treated with SOS ($10^{-11}$ to $10^{-4}$ M) for 48 h in (a,b) absence of 8 nM PMA (given 2 h before PMA). Cell count (presented as live cells/mL and percentage of control) for non-adherent cells in the absence of PMA. (e) Cell viability was determined by MTT assay. Dunnett's post hoc test, means± SEM (n =3), *p<0.05, **p<0.01 vs unstimulated control or PMA. MTT assay analysis indicated that the cell viability of U937 cells in the presence of HDS-III and PMA was considerably higher at concentrations of $10^{-11}$ M, $10^{-9}$ M, $10^{-5}$ M (<0.01) and $10^{-7}$ M (p <0.05) compared to PMA. In contrast, in THP-1 cell cultured with HDS-III at concentrations of $10^{-11}$ M and $10^{-8}$ M to $10^{-4}$ M (p<0.01) was found to be significantly toxic in the presence of PMA.*

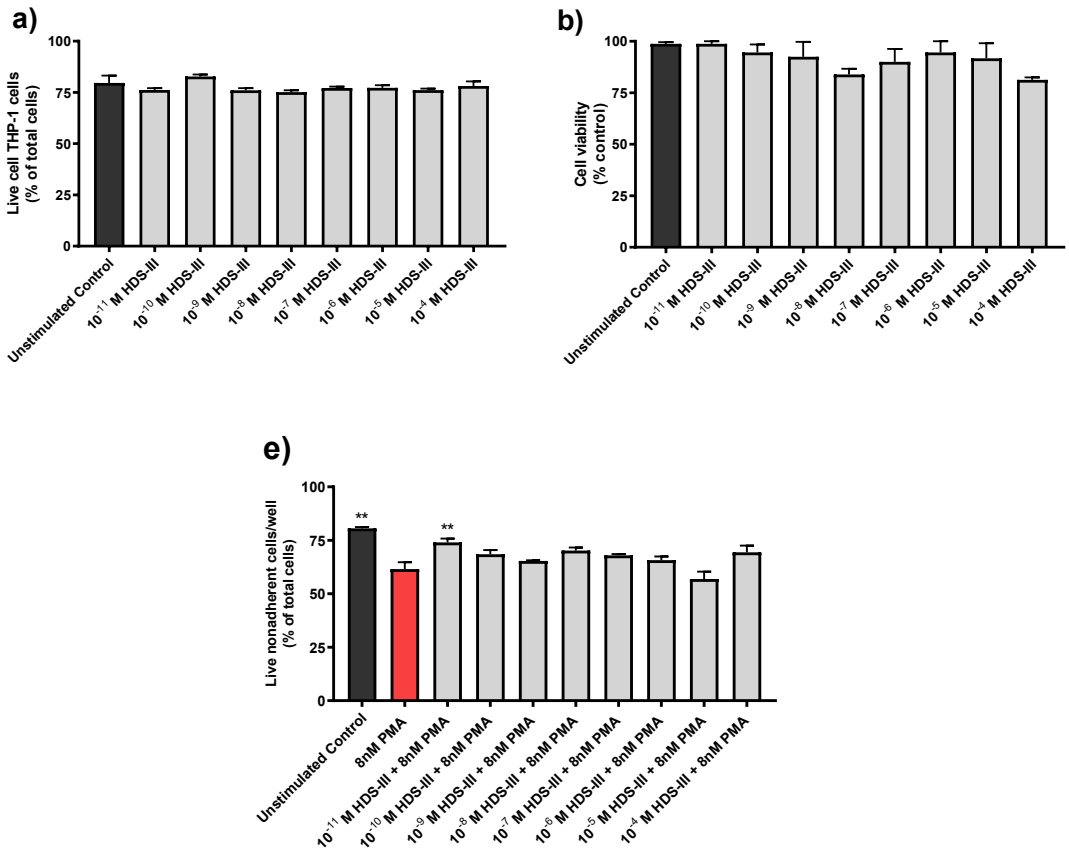


**Appendix Figure 32**. **HDS-III impact on THP-1 cell count in the absence of PMA.**

*THP-1 cells were treated with SOS ($10^{-11}$ to $10^{-4}$ M) for 48 h in (a,b) absence of 8 nM PMA (given 2 h before PMA). Cell count (presented as live cells/mL and percentage of control) for non-adherent cells in the absence of PMA. (e) Cell viability was determined by MTT assay. Dunnett's post hoc test, means± SEM (n =3), *p<0.05, **p<0.01 vs unstimulated control or PMA.*

The results indicate that cell death was due to PMA as sulphated disaccharides alone at concentrations of $10^{-11}$ M to $10^{-4}$ M did not cause any toxicity to U937 and THP-1 cells. The impact of sulphated disaccharides on U937 and THP-1 cells morphology and cell adhesion was examined in the absence of PMA. There was no significant difference in monocyte cell count of SOS, DOS treated U937 or THP-1 cells in comparison to unstimulated control U937 and THP-1 cells.

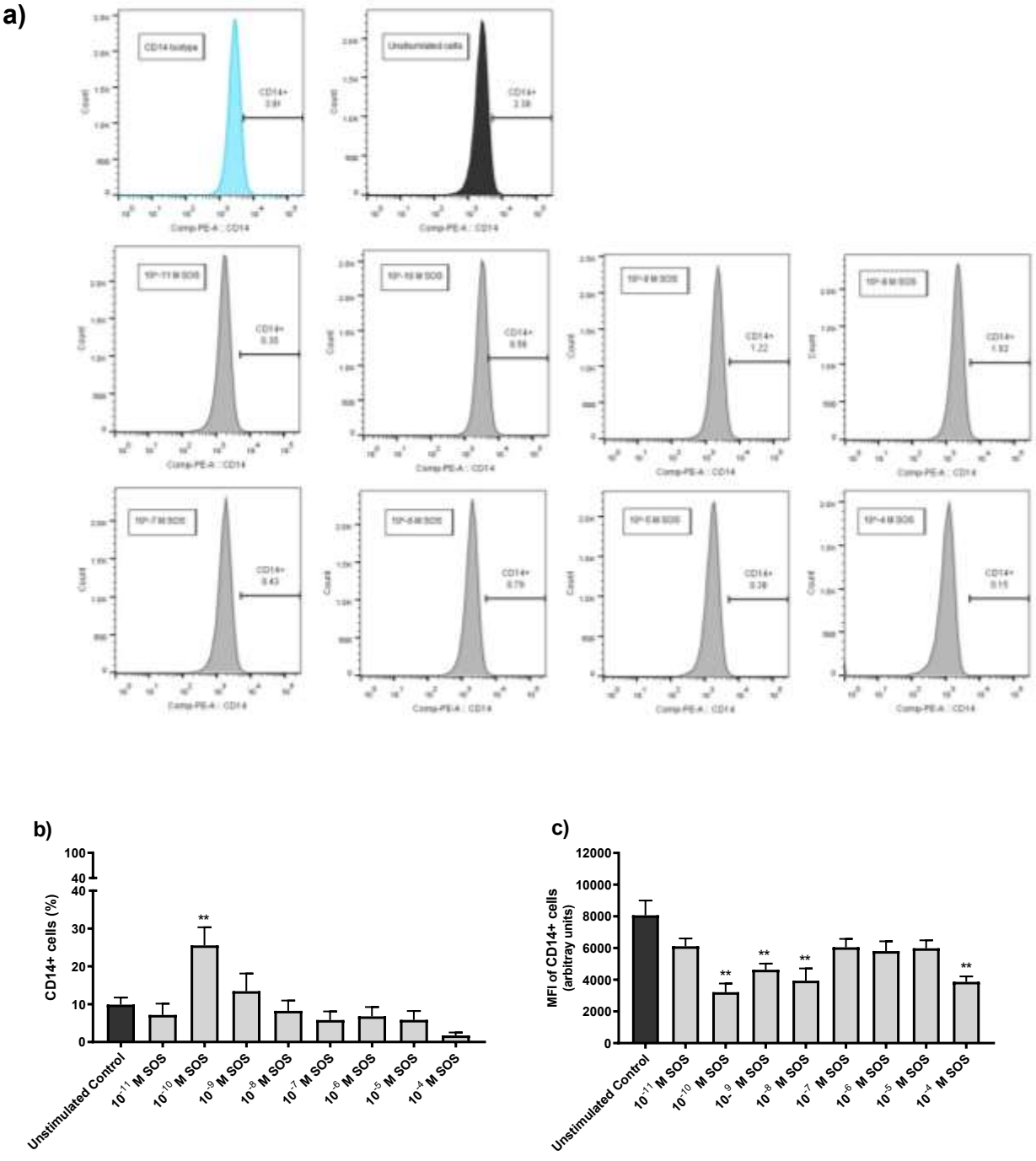


**Appendix Figure 33*. The impact of SOS on U937 CD14 expression in the absence of PMA.***

*a) Histograms represent the overlays comparison of SOS ($10^{-11}$ to $10^{-4}$ M) treated cells at 48 h in the absence of PMA compared to unstimulated control cells against isotype control on CD14-PE channel analysed by flow cytometry. Bar graphs (b) positive cells and (c)*

*MFI of positive cells. ANOVA with post hoc Dunnett's test, mean ± SEM (n=3), **p < 0.01 vs unstimulated control.*

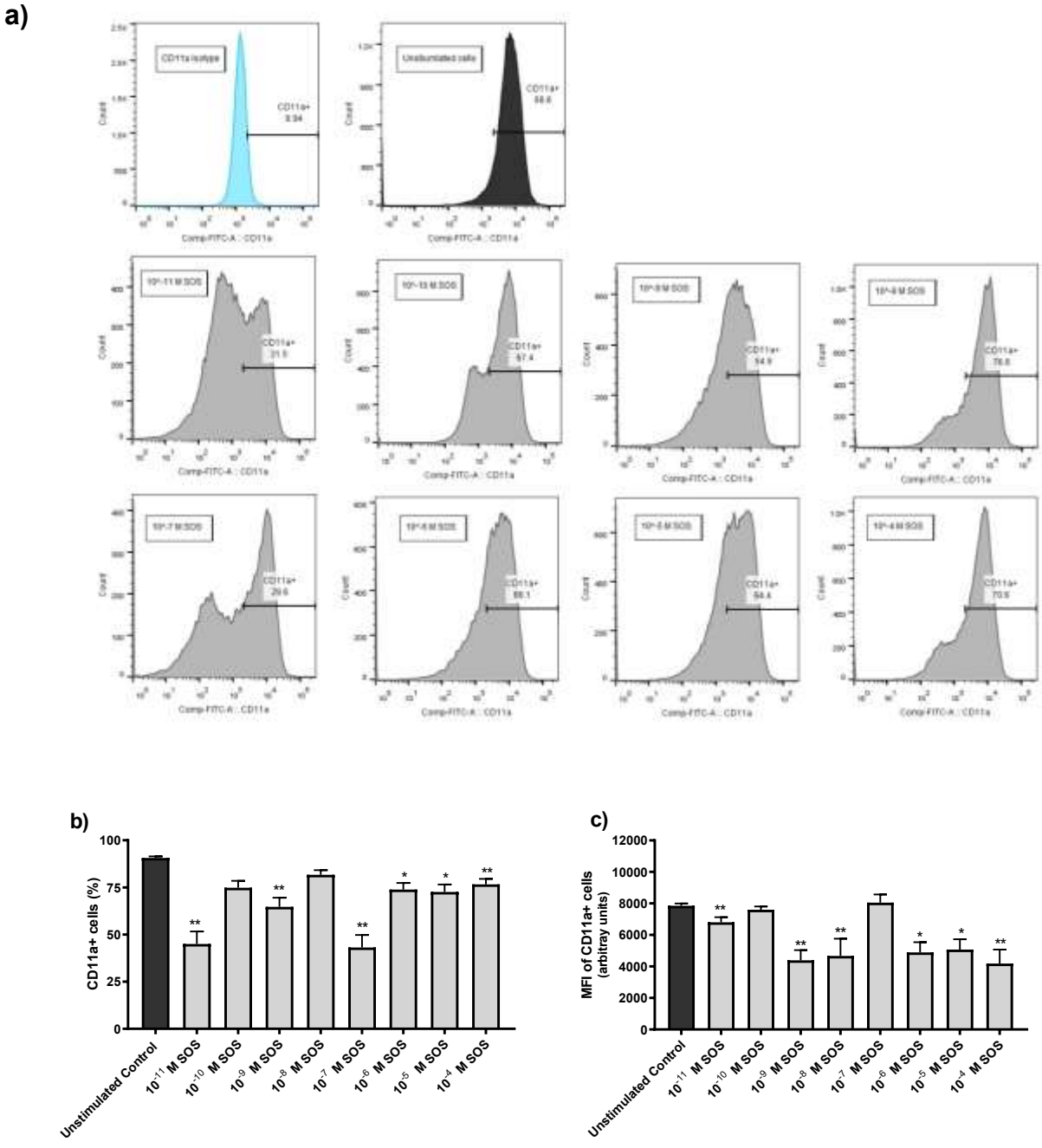


**Appendix Figure 34.** ***The impact of SOS on CD11a expression in the absence of PMA.***

*a) Histograms represent the overlays comparison of SOS ($10^{-11}$ to $10^{-4}$ M) treated cells at 48 h in the absence of PMA compared to unstimulated control cells against isotype control on CD11a-FITC channel analysed by flow cytometry. Bar graphs: (b) positive cells and (c) MFI of positive cells. ANOVA with post hoc Dunnett's test, mean ± SEM (n=3), *p<0.5, **p < 0.01 vs unstimulated control.*

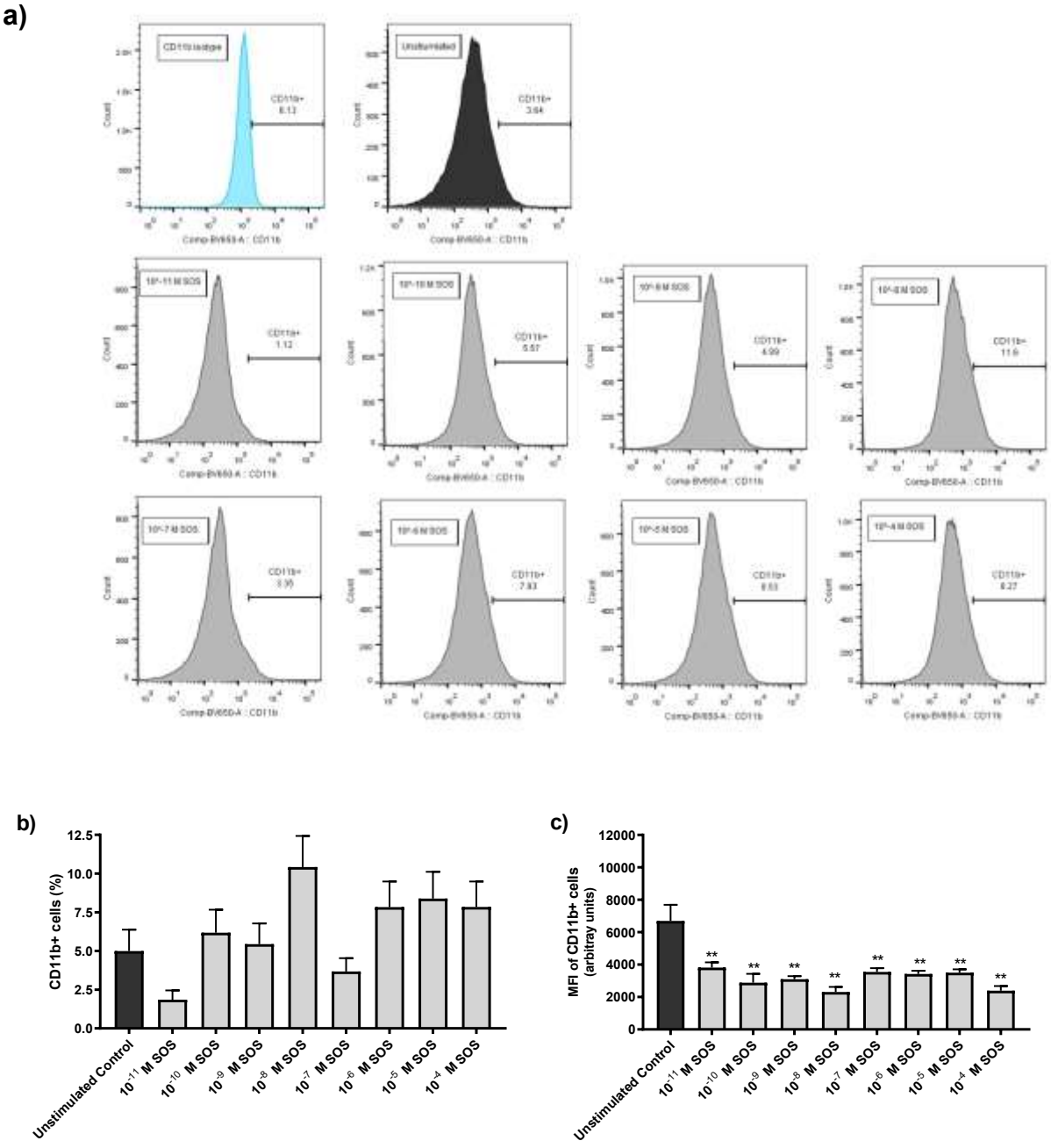


**Appendix Figure 35.** ***The impact of SOS on U937 CD11b expression in the absence of PMA.***

*a) Histograms represent the overlays comparison of SOS ($10^{-11}$ to $10^{-4}$ M) treated cells at 48 h in the absence of PMA compared to unstimulated control cells against isotype control on CD11b-BV650 channel analysed by flow cytometry. Bar graphs: (b) positive cells and*

*(c) MFI of positive cells. ANOVA with post hoc Dunnett's test, mean ± SEM (n=3), **p < 0.01 vs unstimulated control.*

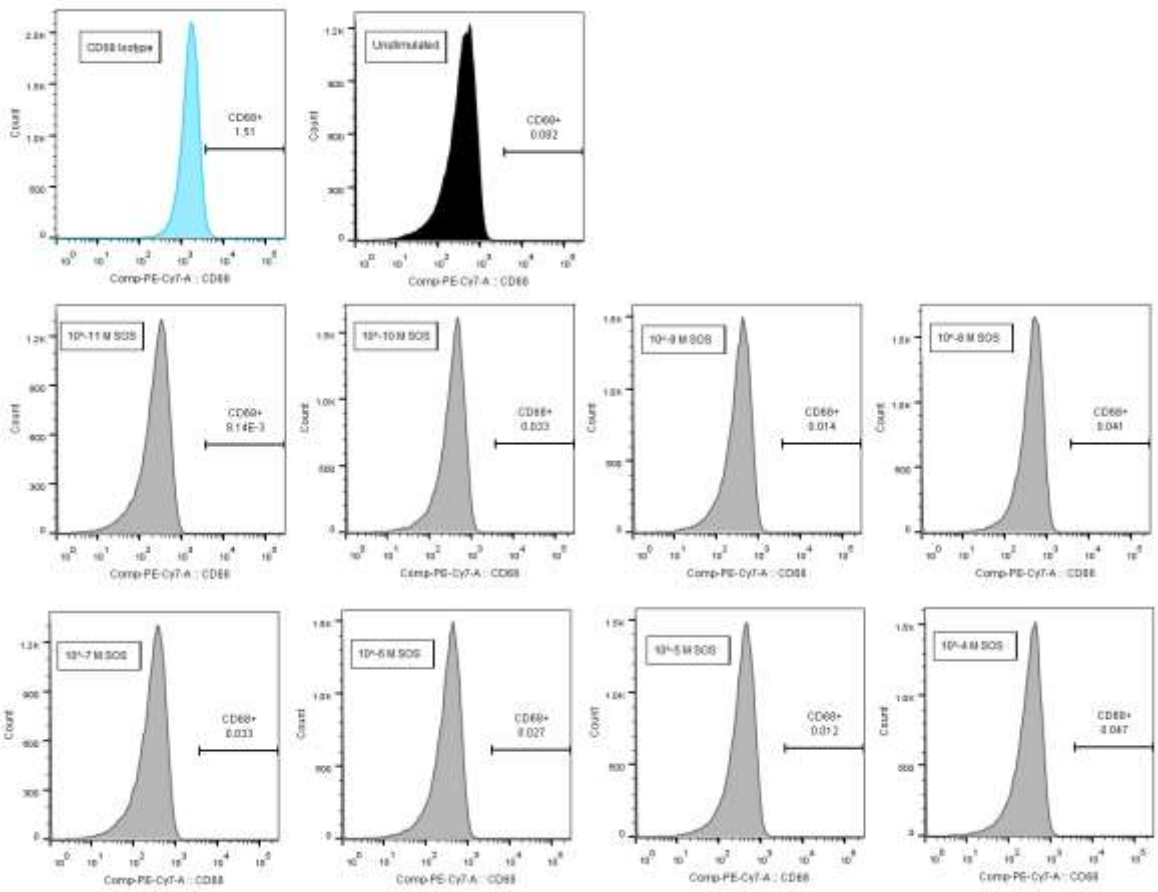


**Appendix Figure 36.** ***The impact of SOS on U937 CD68 expression in the absence of PMA.***

*Histograms represent (n =3) the overlays comparison of SOS ($10^{-11}$ to $10^{-4}$ M) treated cells at 48 h in the absence of PMA compared to unstimulated control cells against isotype control analysed by flow cytometry. No CD68 positive cells found in cultures.*

**a)**

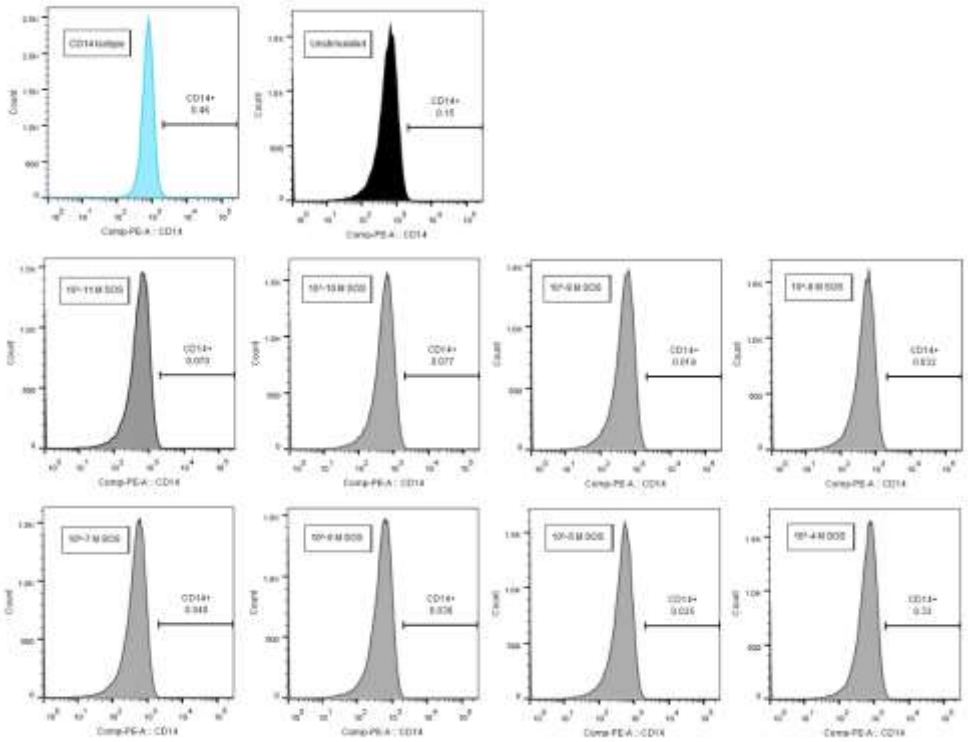

**b)**

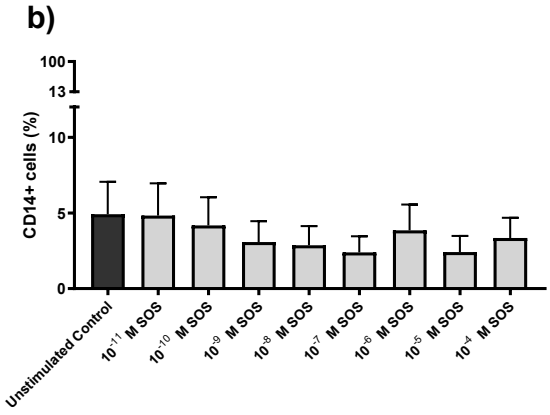


**c)**

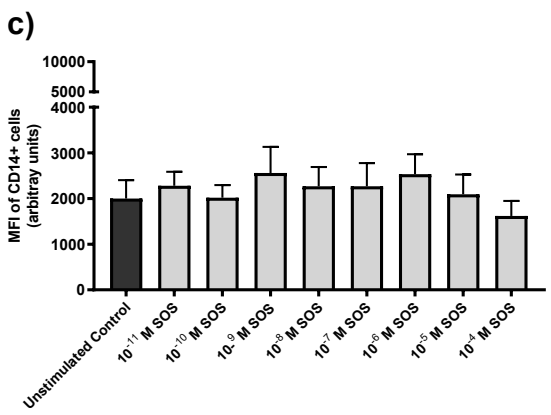


**Appendix Figure 37**. ***The impact of SOS on THP-1 CD14 expression in the absence of PMA.***

*a) Histograms represent the overlays comparison of SOS ($10^{-11}$ to $10^{-4}$ M) treated cells at 48 h in the absence of PMA compared to unstimulated control cells against isotype control on CD14-PE channel analysed by flow cytometry . Bar graphs: (b) positive cells and (c)*

*MFI of positive cells. ANOVA with post hoc Dunnett's test, mean ± SEM (n=3), non-significant p value vs unstimulated control.*

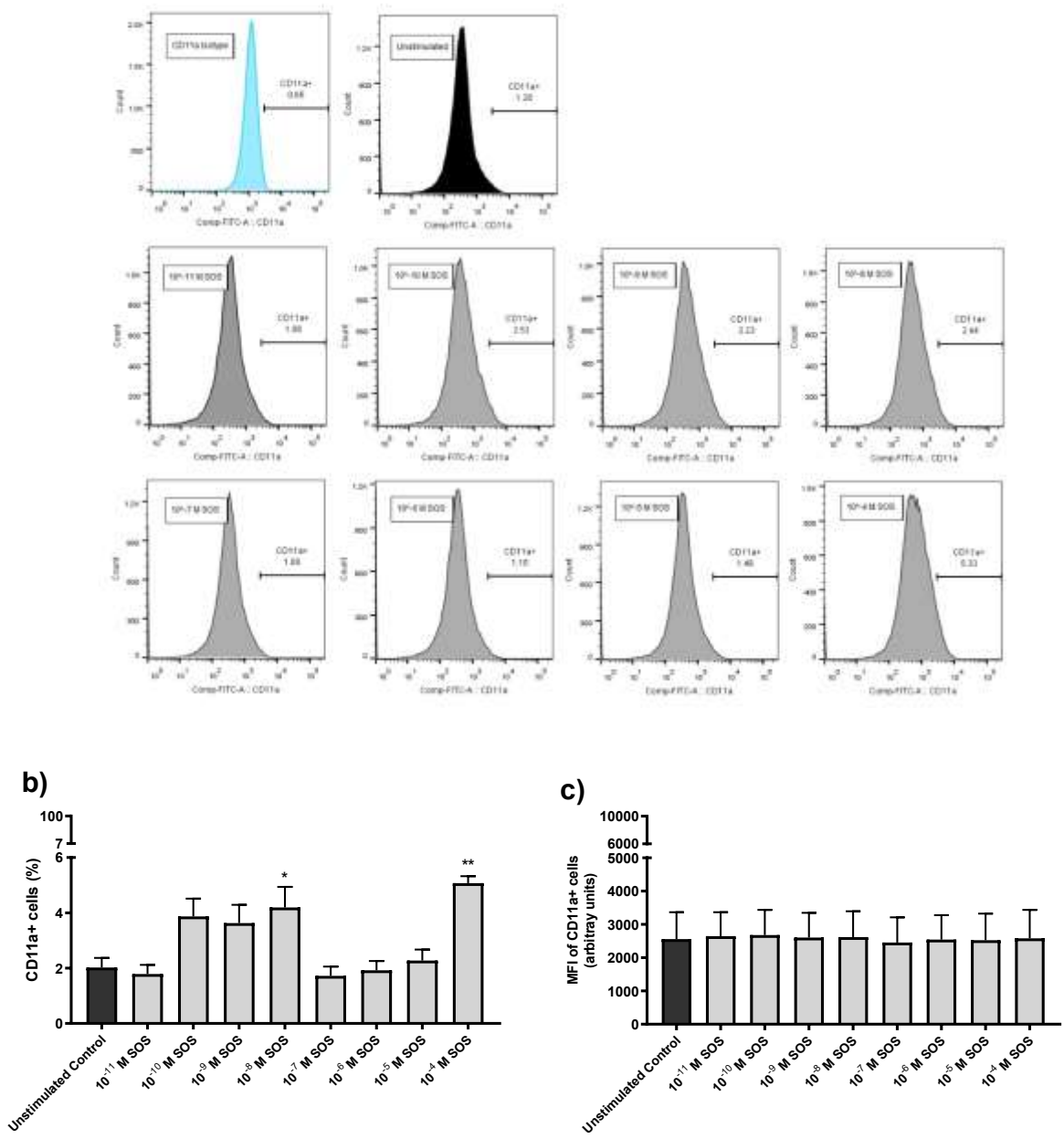


**Appendix Figure 38**. ***The impact of SOS on THP-1 CD11a expression in the absence of PMA.***

*a) Histograms represent the overlays comparison of SOS ($10^{-11}$ to $10^{-4}$ M) treated cells at 48 h in the absence of PMA compared to unstimulated control cells against isotype control on CD14-PE channel analysed by flow cytometry . Bar graphs (b) positive cells and (c)*

*MFI of positive cells. ANOVA with post hoc Dunnett's test, mean ± SEM (n=3), *p<0.5, **p < 0.01 vs unstimulated control.*

**a)**

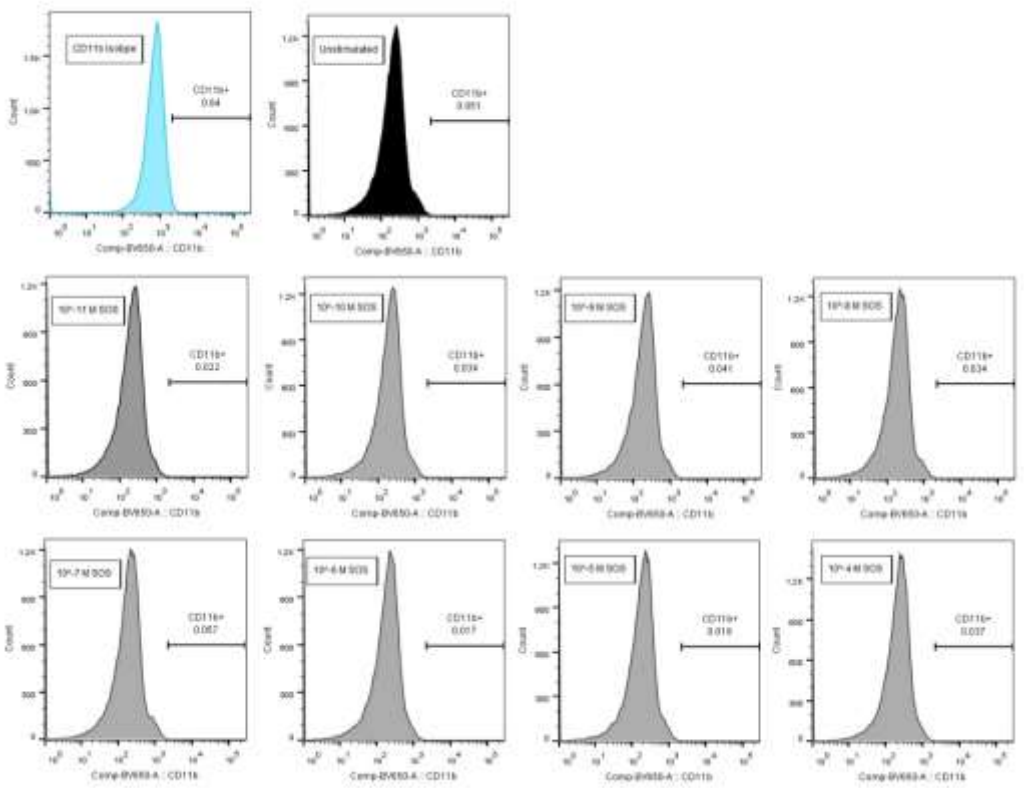

**b)**

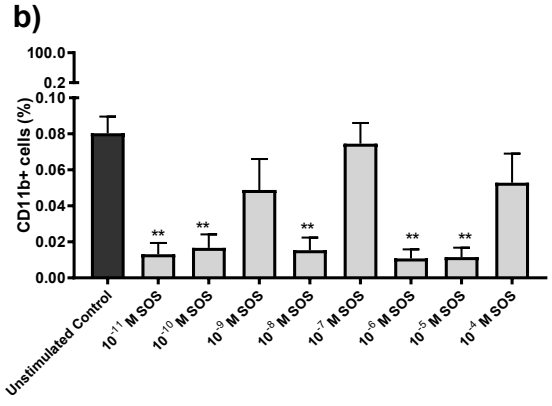


**c)**

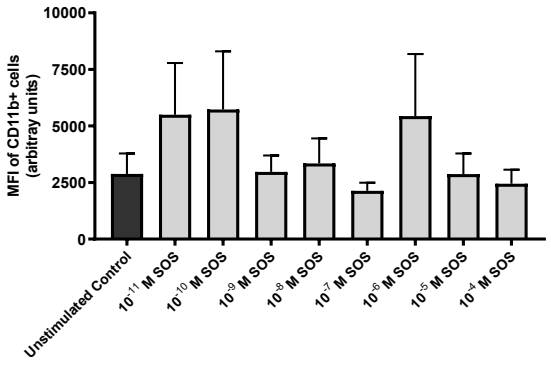


**Appendix Figure 39**. ***SOS: The impact of SOS on THP-1 CD11b expression in the absence of PMA.***

*a) Histograms represent the overlays comparison of SOS ($10^{-11}$ to $10^{-4}$ M) treated cells at 48 h in the absence of PMA compared to unstimulated control cells against isotype control on CD11b-BV650 channel analysed by flow cytometry . Bar graphs (b) positive cells and (c) MFI of positive cells. ANOVA with post hoc Dunnett's test, mean ± SEM (n=3), **p < 0.01 vs unstimulated control.*

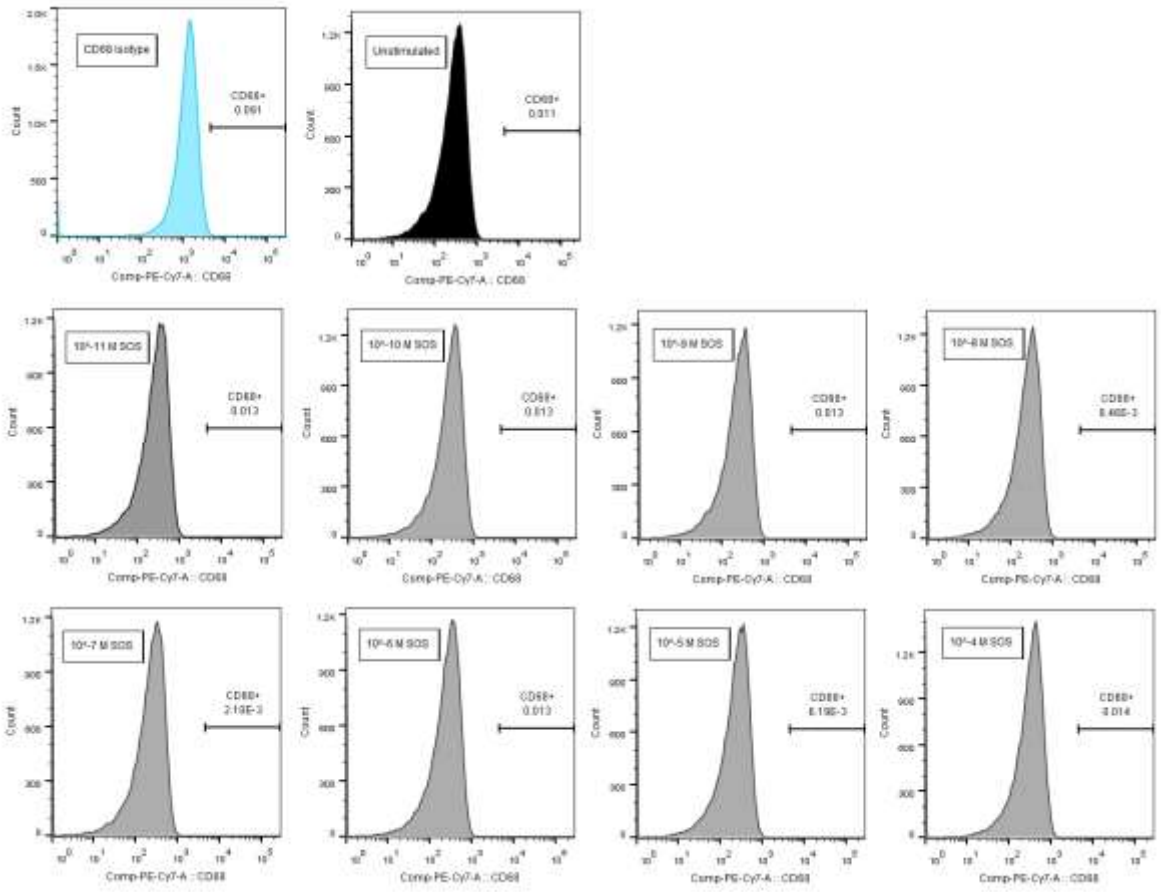


**Appendix Figure 40**. ***The impact of SOS on THP-1 CD68 expression in the absence of PMA.***

*Histograms represent (n =3) the overlays comparison of SOS ($10^{-11}$ to $10^{-4}$ M) treated cells at 48 h in the absence of PMA compared to unstimulated control cells against isotype control analysed by flow cytometry . No CD68 positive found in cell cultures.*

The impact of sulphated disaccharides was studied in the absence of PMA. The U937 and THP-1 cells were cultured in a 24-well tissue culture plates at an initial density of $2x10^5$ cells/mL per well. Cells were then incubated with SOS, DOS, HDS-I and HDS-III at concentrations of $10^{-11}$ M to $10^{-4}$ M for 48 h at 37 $^0$C with 5% $CO_2$. Following incubation period, cells were harvested, subsequently washed twice in ice-cold (4 $^0$C) PBS and cells were counted and stained for CD14, CD11a, CD11b, CD68 cell surface markers and analysed using flow cytometry.

SOS in the absence of PMA in U937 cell cultures was found to be more positive for $CD14^+$ cells at $10^{-10}$ M SOS ($p < 0.01$) compared to unstimulated control U937 cultures. However, decrease in intensity of $CD14^+$ cells was observed at concentrations of $10^{-10}$ M to $10^{-8}$ M and $10^{-4}$ M ($p < 0.01$). In contrast, there was no significant difference in percentage of $CD14^+$ cells and the degree of marker expression in SOS-THP-1 cultures and unstimulated control THP-1 cultures. SOS reduced the percentage of $CD11a^+$ cells at concentrations of $10^{-11}$ M, $10^{-9}$ M, $10^{-7}$ M, $10^{-4}$ M ($p < 0.01$) and $10^{-6}$ M, $10^{-5}$M ($p < 0.05$) and of $CD11a^+$ expressing cells at concentrations of $10^{-11}$ M, $10^{-9}$ M, $10^{-8}$ M, $10^{-4}$ M ($p < 0.01$) and $10^{-6}$ M, $10^{-5}$ M ($p < 0.05$) in SOS – U937 cultures compared to unstimulated control U937 cultures. In SOS-THP-1 cultures the percentage of $CD11a^+$ cells at concentrations of $10^{-8}$ M ($p < 0.05$) and $10^{-4}$ M ($p < 0.01$) was higher with no significant difference in their intensity compared to unstimulated control THP-1 cells. $CD11b^+$ cells mean fluorescence intensity was reduced in SOS-U937 cultures by SOS at concentrations of $10^{-11}$ M to $10^{-4}$ M ($p < 0.01$) with no significant difference in percentage of $CD11b^+$ cells compared to unstimulated control U937 cells. In contrast, $CD11b^+$cells were reduced in SOS-THP-1 cultures by SOS at concentrations of $^{11}$ M, $10^{-10}$ M, $10^{-8}$ M, $10^{-6}$ M, $10^{-5}$ M ($p < 0.01$) with no significant difference in their intensity compared to unstimulated control THP-1 cells. Negligible percentage of $CD68^+$cells was seen in SOS-U937 and SOS-THP-1 cultures when compared to unstimulated control U937 and THP-1 cultures.

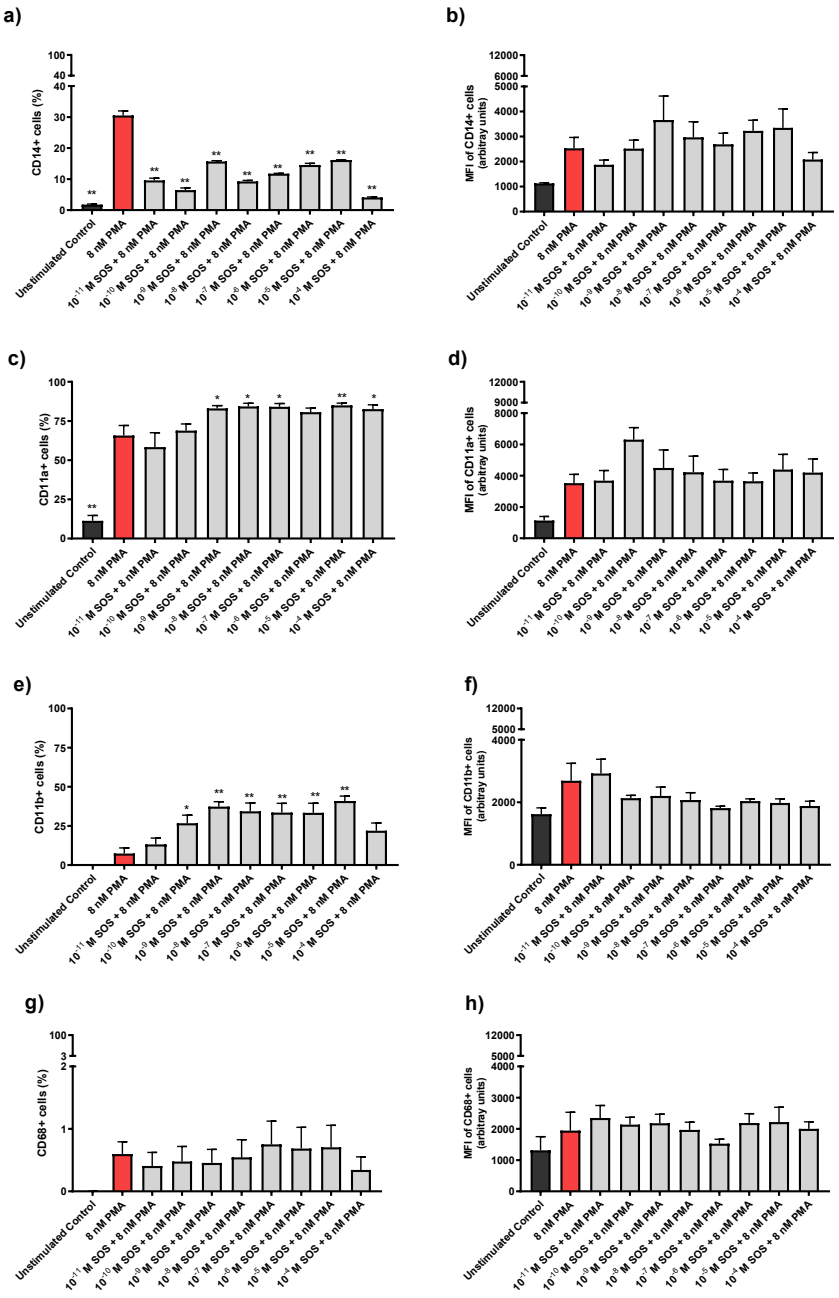


**Appendix Figure 41**. ***The impact of SOS on non-adherent U937 cells surface markers expression of SOS and PMA cultures.***

*Non-adherent cells from SOS ($10^{-11}$ to $10^{-4}$ M) + PMA cultures compared to non-adherent cells from PMA control cells, analysed by flow cytometry. Bar graph represents positive cells (a, c, e, g) MFI of positive cells (b, d, f, h). ANOVA with post hoc Dunnett's test, mean ± SEM (n=3), *p<0.05, **p < 0.01 vs PMA.*

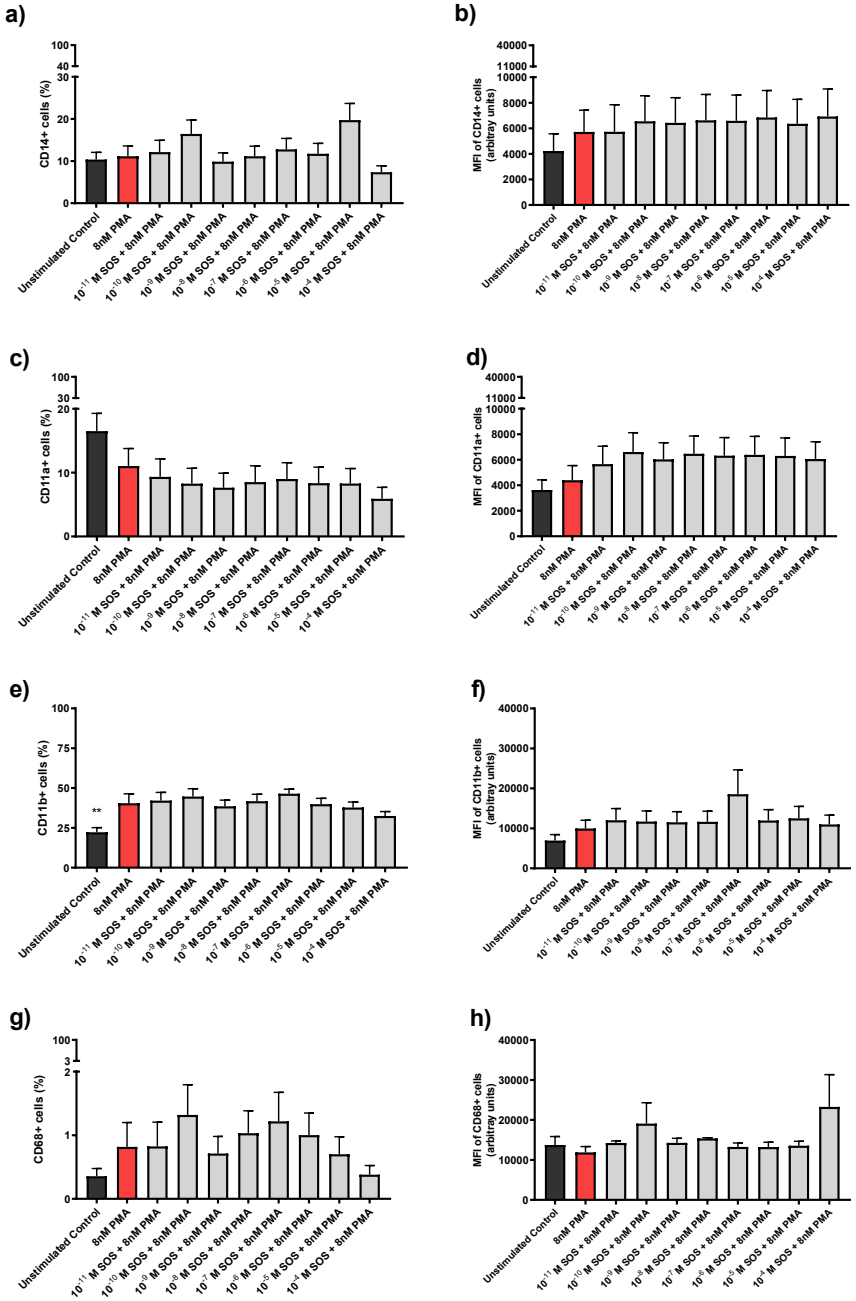


**Appendix Figure 42.** ***The impact of SOS on non-adherent THP-1 cells surface markers expression of SOS and PMA cultures.***

*Non-adherent cells from SOS ($10^{-11}$ to $10^{-4}$ M) + PMA cultures compared to non-adherent cells from PMA control cells by flow cytometry. Bar graph represents positive cells (a, c,*

*e, g) MFI of positive cells (b, d, f, h). ANOVA with post hoc Dunnett's test, mean ± SEM (n=3), no significant p value vs PMA. SOS reduced $CD14^+$at concentrations of $10^{-11}$ M to $10^{-4}$ M ($p<0.01$) , $CD11a^+$ at concentrations of $10^{-9}$ M, $10^{-7}$ M, $10^{-4}$ M($p <0.05$), $10^{-5}$ M ($p <0.01$), $CD11b^+$at concentrations of $10^{-10}$ M ($p <0.05$), $10^{-9}$ M to $10^{-4}$ M ($p <0.01$) and non-significantly $CD68^+$cells in non-adherent SOS + PMA U937 cultures with no significant difference in their expression (MFI) compared to PMA- non-adherent U937 cultures (Fig.41). However no significant difference in $CD14^+$, $CD11a^+$, $CD11b^+$, $CD68^+$ numbers and their marker expression in SOS + PMA-THP-1 non-adherent cultures compared to PMA-THP-1 cultures.*

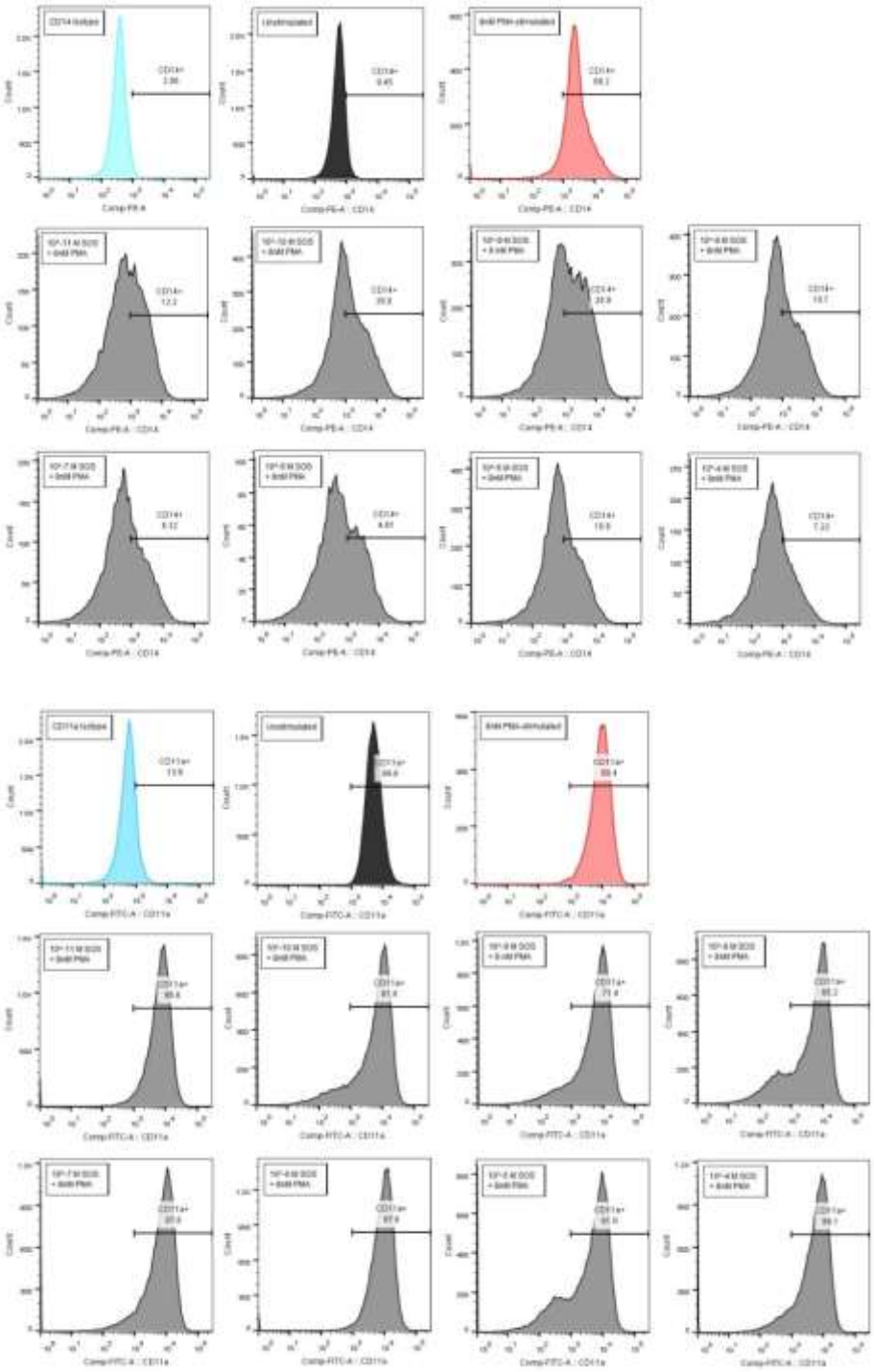

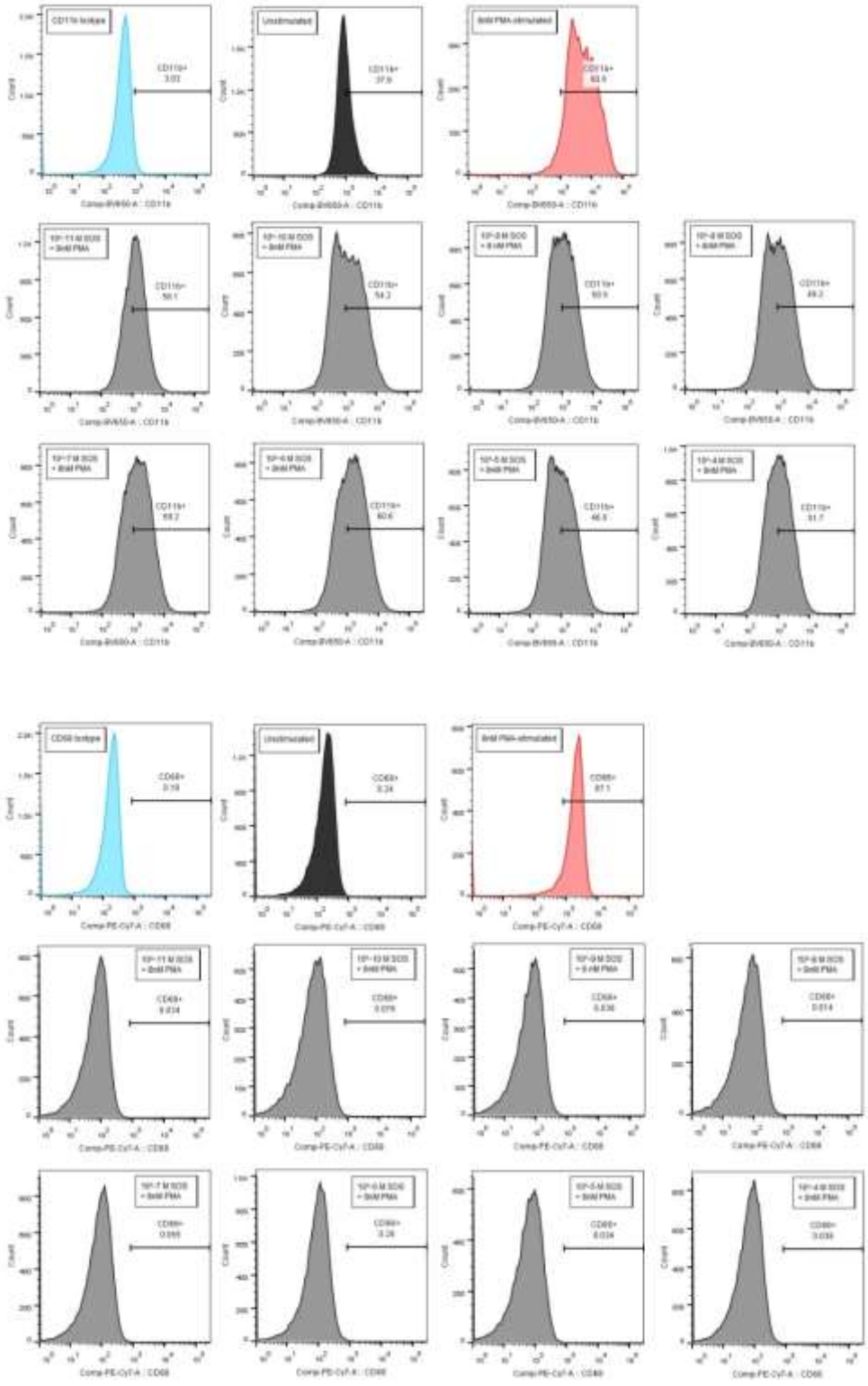

**Appendix Figure 43.** ***The impact of SOS on U937 CD14, CD11a, CD11b, CD68 expression in the presence of PMA.***

*Histograms represent the overlays comparison of SOS ($10^{-11}$ to $10^{-4}$ M) treated cells at 48 h in the presence of 8 nM PMA (given 2 h before PMA) compared to PMA control cells against isotype control analysed by flow cytometry.*

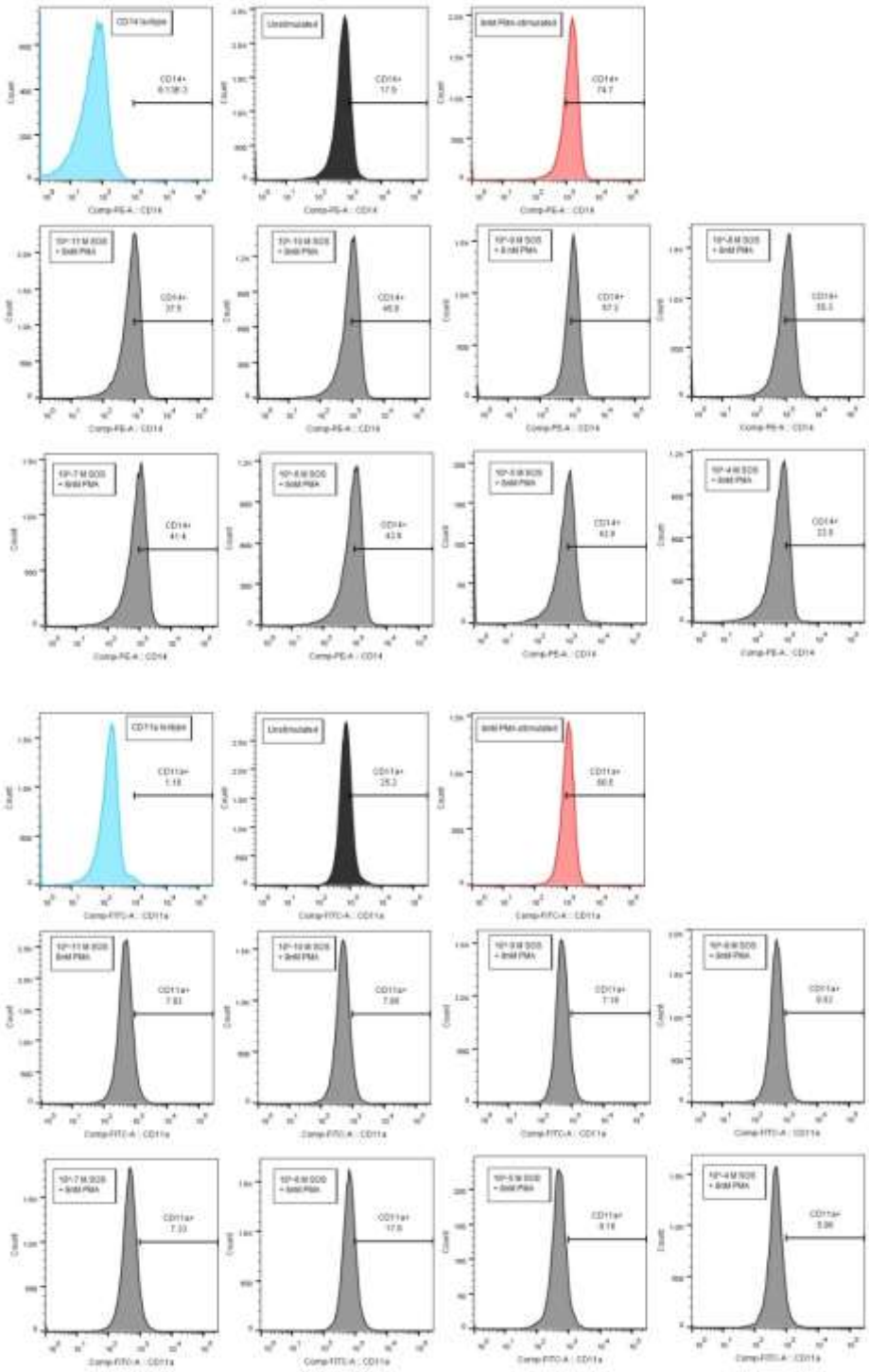

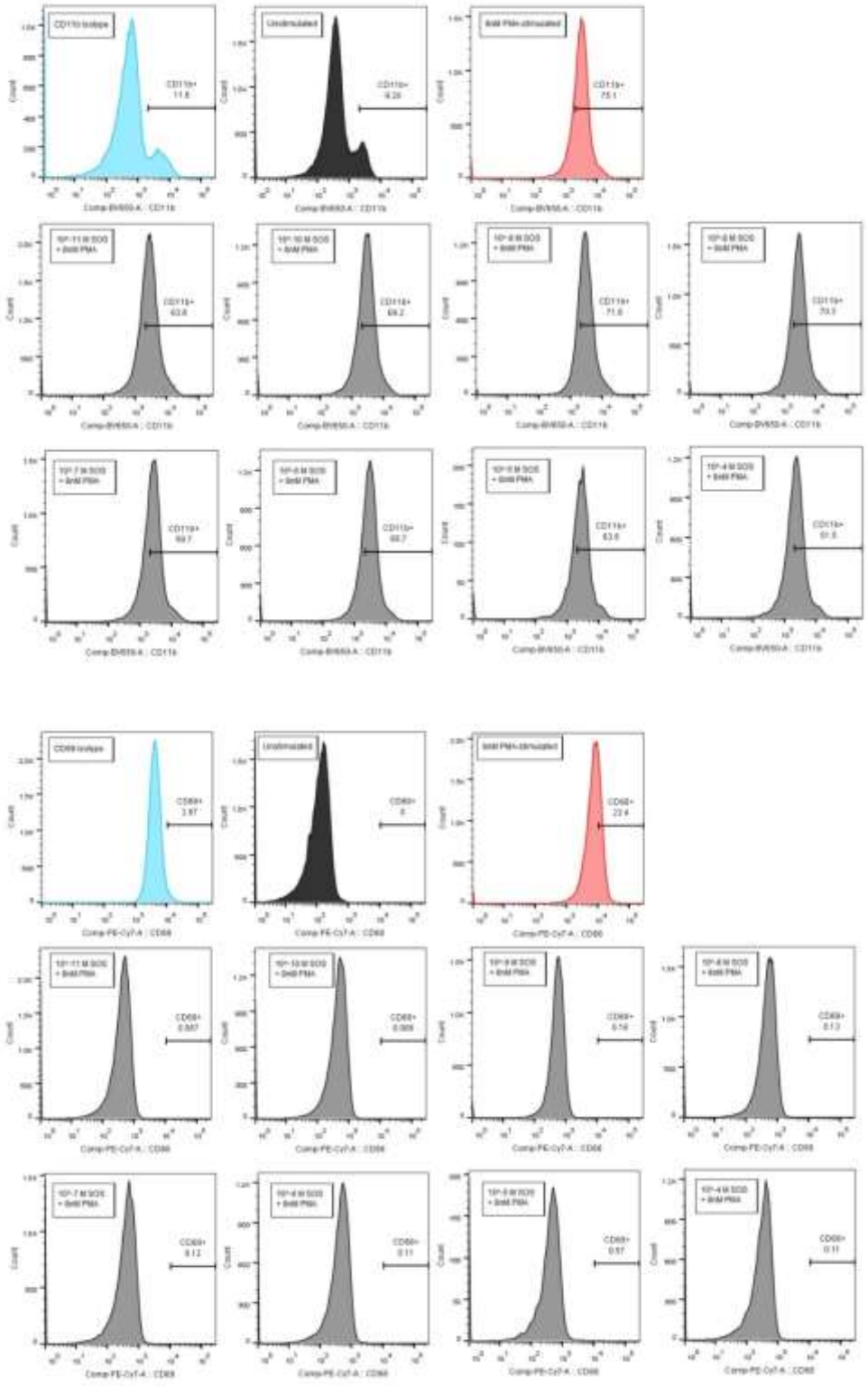

**Appendix Figure 44**. ***The impact of SOS on THP-1 CD14, CD11a, CD11b, CD68 expression in the presence of PMA.***

*Histograms represent the overlays comparison of SOS ($10^{-11}$ to $10^{-4}$ M) treated cells at 48 h in the presence of 8 nM PMA (given 2 h before PMA) compared to PMA control cells against isotype control analysed by flow cytometry.*

**a)**

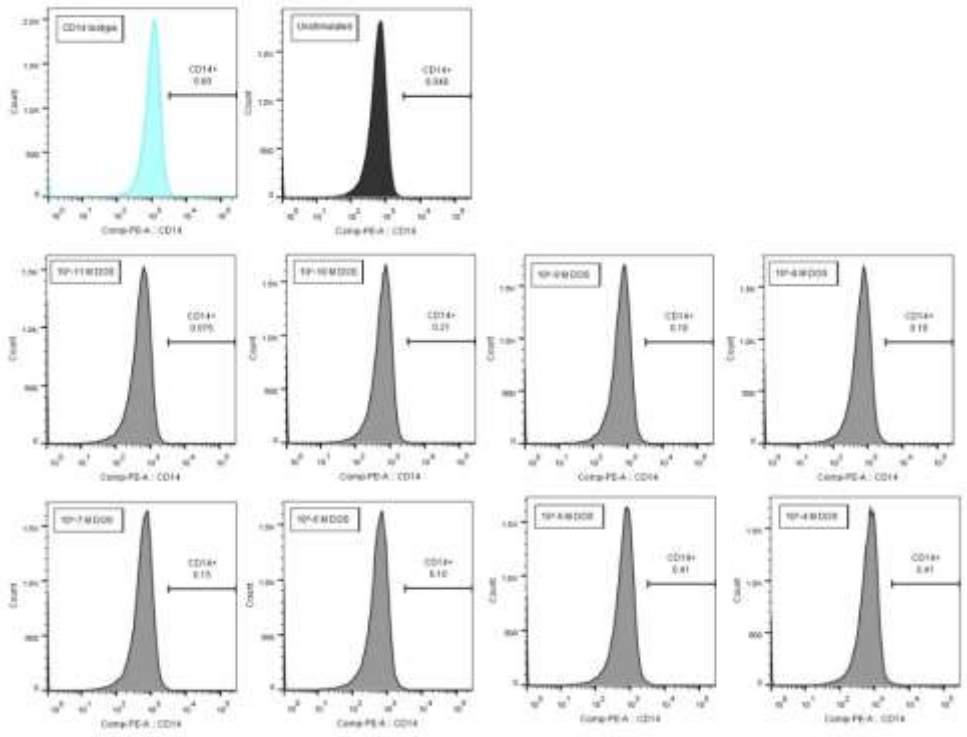

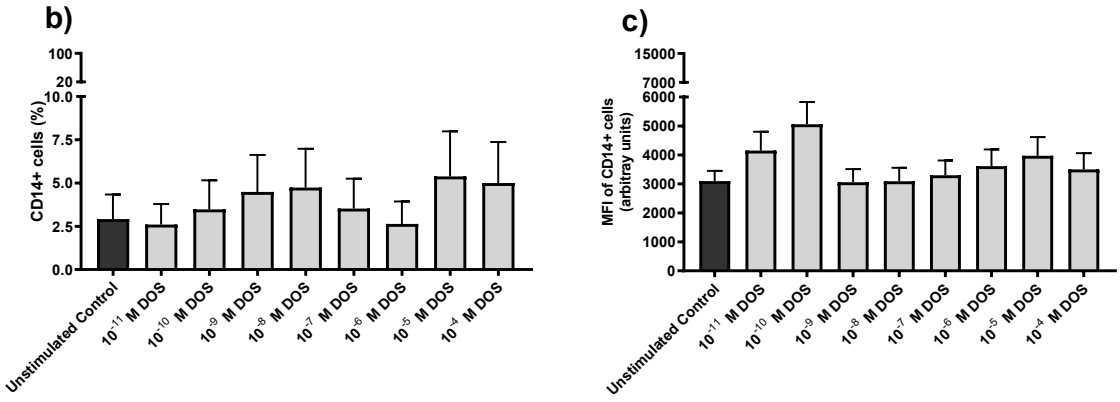


**Appendix Figure 45.** ***The impact of DOS on U937 CD14 expression in the absence of PMA***.

*a) Histograms represent the overlays comparison of DOS ($10^{-11}$ to $10^{-4}$ M) treated cells at 48 h in the absence of PMA compared to unstimulated control cells against isotype control on CD14-PE, channel analysed by flow cytometry. Bar graphs represents (b)*

*positive cells and (c) MFI of positive cells. ANOVA with post hoc Dunnett's test, mean ± SEM (n=3), no significant p value vs unstimulated control.*

**a)**

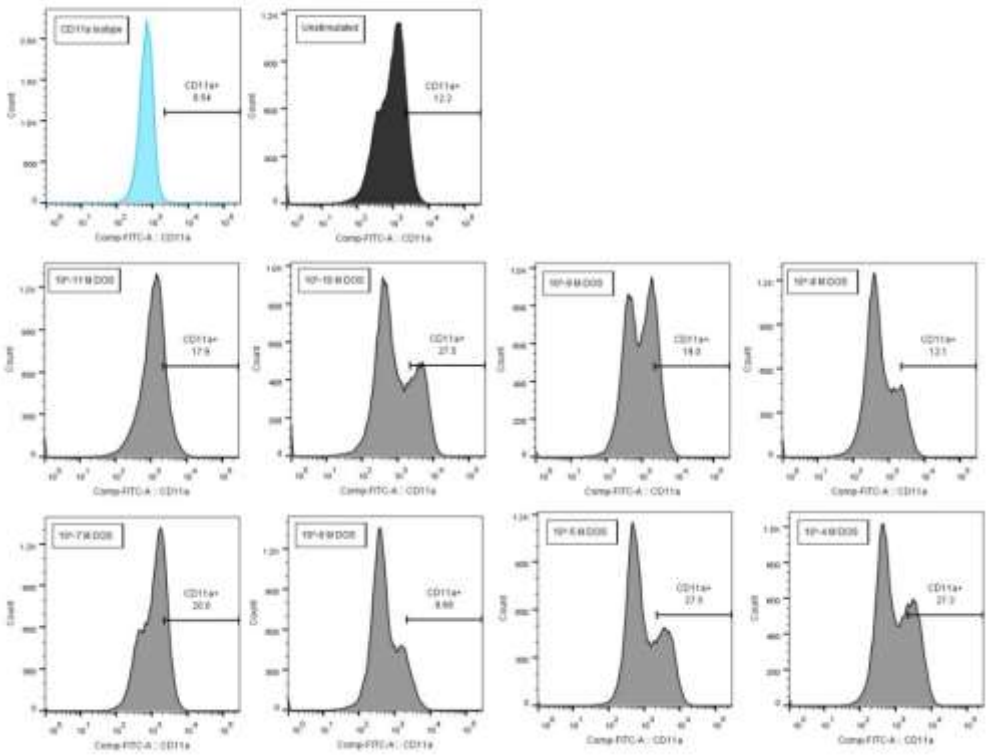

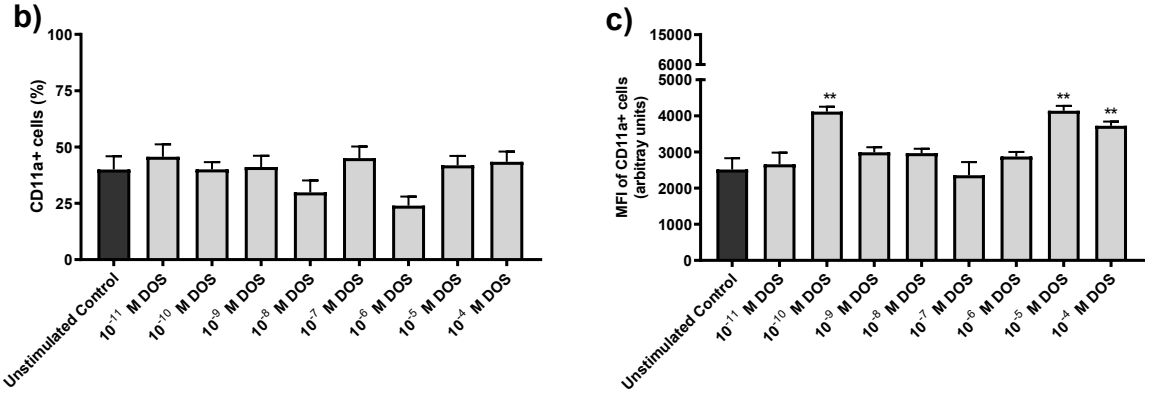


**Appendix Figure 46**. ***The impact of DOS on U937 CD11a expression in the absence of PMA.***

*a) Histograms represent the overlays comparison of DOS ($10^{-11}$ to $10^{-4}$ M) treated cells at 48 h in the absence of PMA compared to unstimulated control cells against isotype control on CD11a-FITC, channel analysed by flow cytometry. Bar graph represents (b)*

*positive cells and (c) MFI of positive cells. ANOVA with post hoc Dunnett's test, mean ± SEM (n=3), **p < 0.01 vs unstimulated control.*

a)

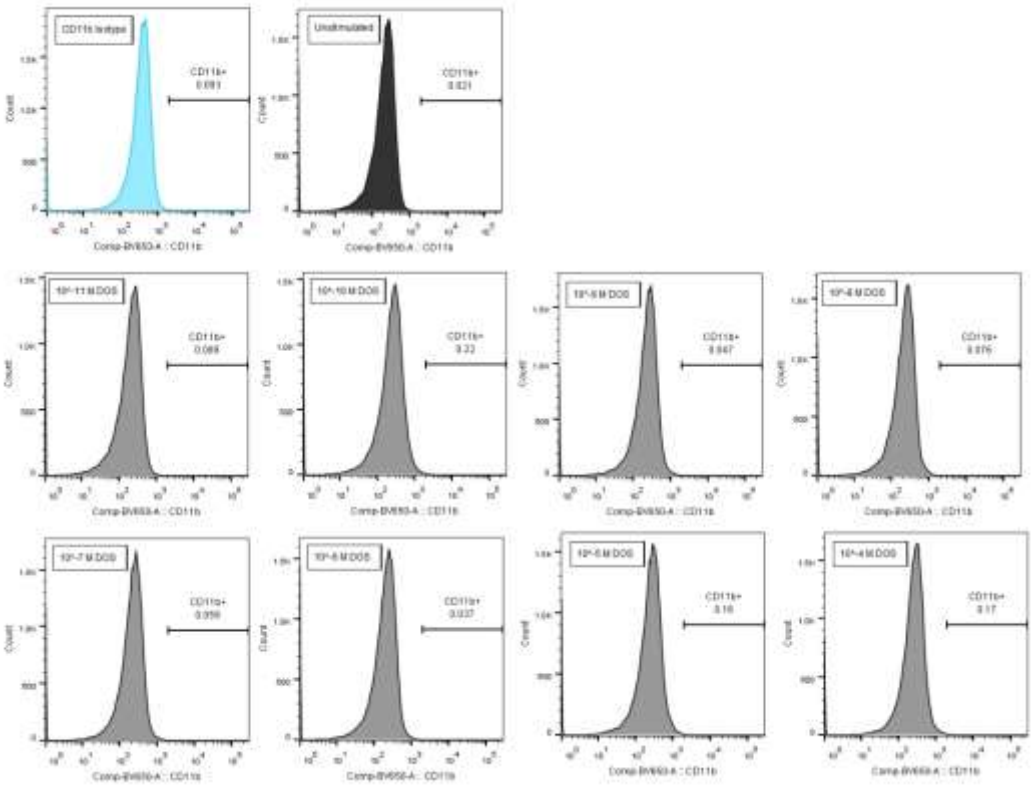

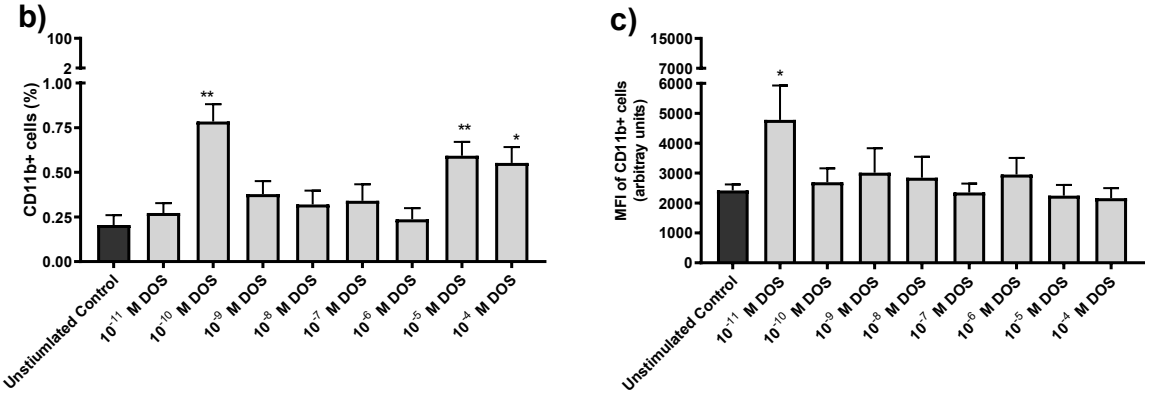


**Appendix Figure 47*. The impact of DOS on U937 CD11b expression in the absence of PMA.***

*a) Histograms represent the overlays comparison of DOS ($10^{-11}$ to $10^{-4}$ M) treated cells at 48 h in the absence of PMA compared to unstimulated control cells against isotype control on CD11b-BV650 channel analysed by flow cytometry . Bar graph represents (b)*

*positive cells and (c) MFI of positive cells. ANOVA with post hoc Dunnett's test, mean ± SEM (n=3), *p<0.05, **p < 0.01 vs unstimulated control.*

**a)**

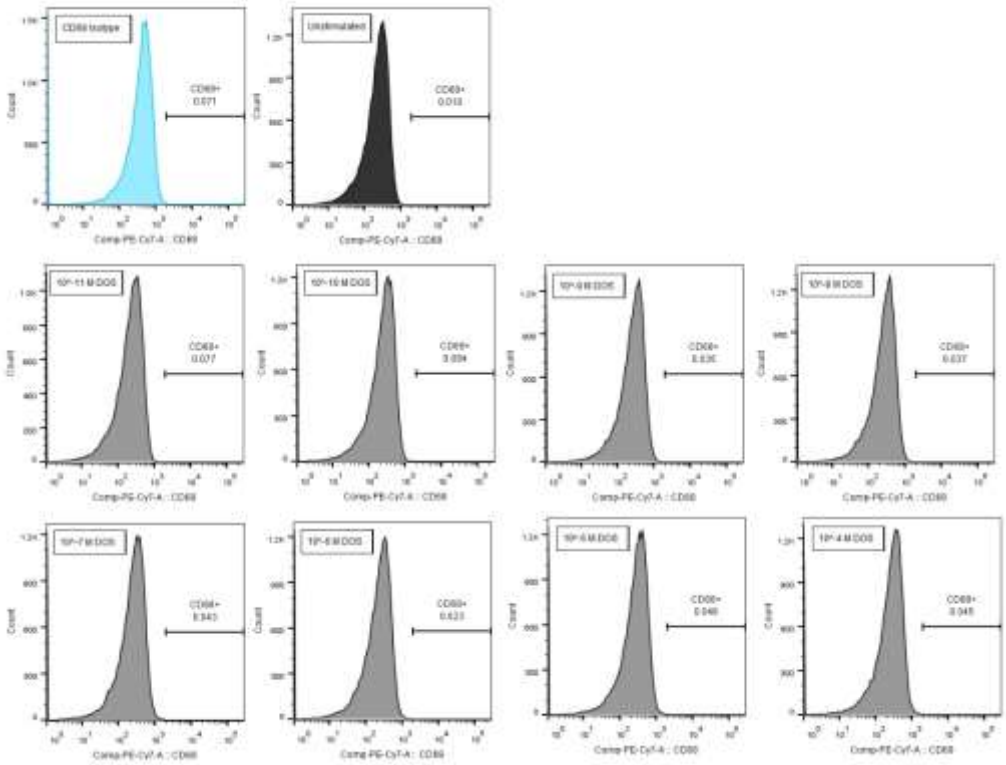

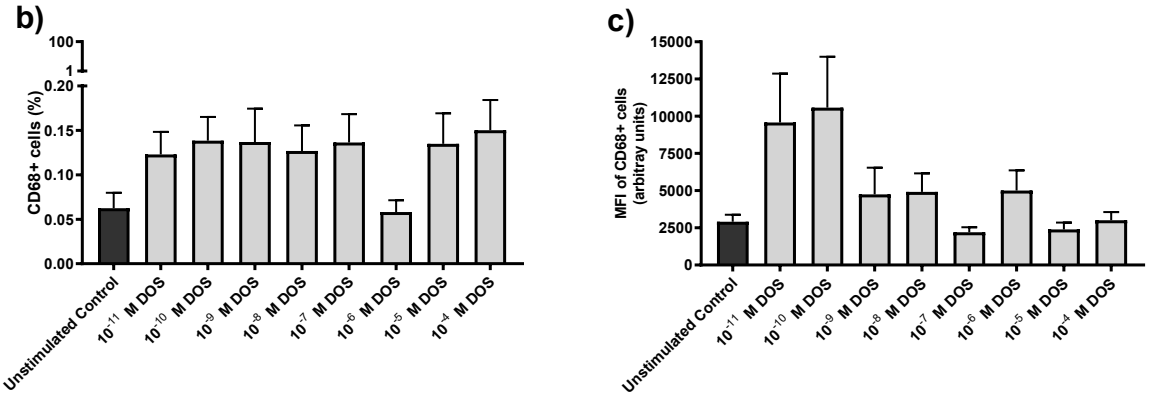


**Appendix Figure 48*. The impact of DOS on U937 CD68 expression in the absence of PMA.***

*a) Histograms represent the overlays comparison of DOS ($10^{-11}$ to $10^{-4}$ M) treated cells at 48 h in the absence of PMA compared to unstimulated control cells against isotype*

*control analysed by flow cytometry . Bar represents graphs (b) positive cells and (c) MFI of positive cells. ANOVA with post hoc Dunnett's test, mean ± SEM (n=3), no significant p value vs unstimulated control.*

DOS in the absence of PMA in U937 cell cultures had no significant effect on the percentage of $CD14^+$and $CD68^+$cells and their expression at concentrations of $10^{-11}$ M and $10^{-4}$ M compared to unstimulated control U937 cultures. However, DOS treated U937 cells had higher MFI for $CD11a^+$ cells at concentration of $10^{-10}$ M, $10^{-5}$ M and $10^{-4}$ M ($p < 0.01$) with no significant difference in percentage of $CD11a^+$cells compared to unstimulated control U937 cells.

The percentage of $CD11b^+$ cells in DOS- U937 cultures was higher at concentrations of $10^{-10}$ M, $10^{-5}$ M and $10^{-4}$ M ($p < 0.01$) compared to unstimulated control U937 cells. Also, the mean intensity of $CD11b^+$ cells at concentration of $10^{-11}$ M ($p < 0.05$) was higher compared to unstimulated control U937 cells.

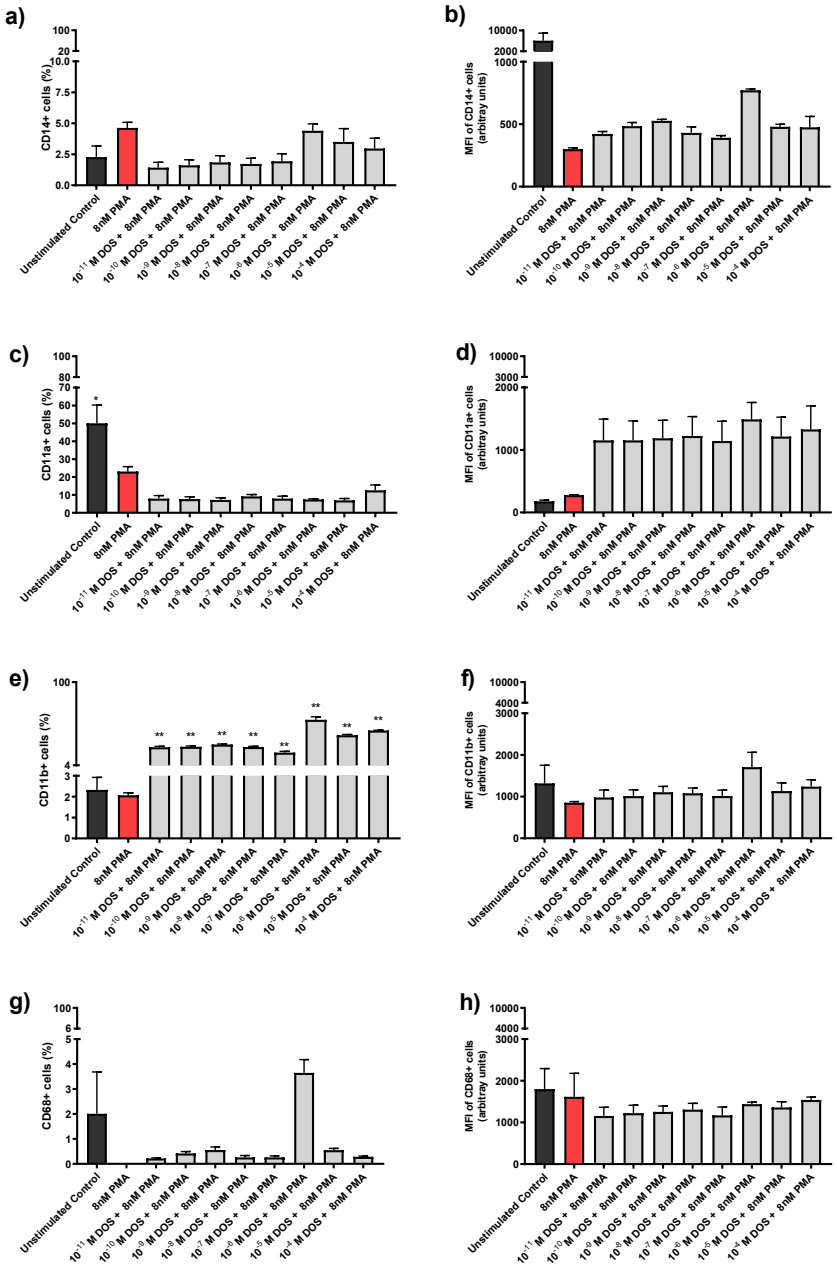


**Appendix Figure 49.** ***The impact of DOS on non-adherent U937 cells surface markers expression of DOS and PMA cultures.***

*Non-adherent cells from DOS ($10^{-11}$ to $10^{-4}$ M) + PMA cultures compared to non-adherent cells from PMA control cells analysed by flow cytometry . Bar graph represents positive cells (a, c, e, g) MFI of positive cells (b, d, f, h). ANOVA with post hoc Dunnett's test, mean ± SEM (n=3), *P<0.05, **p < 0.01 vs PMA.*

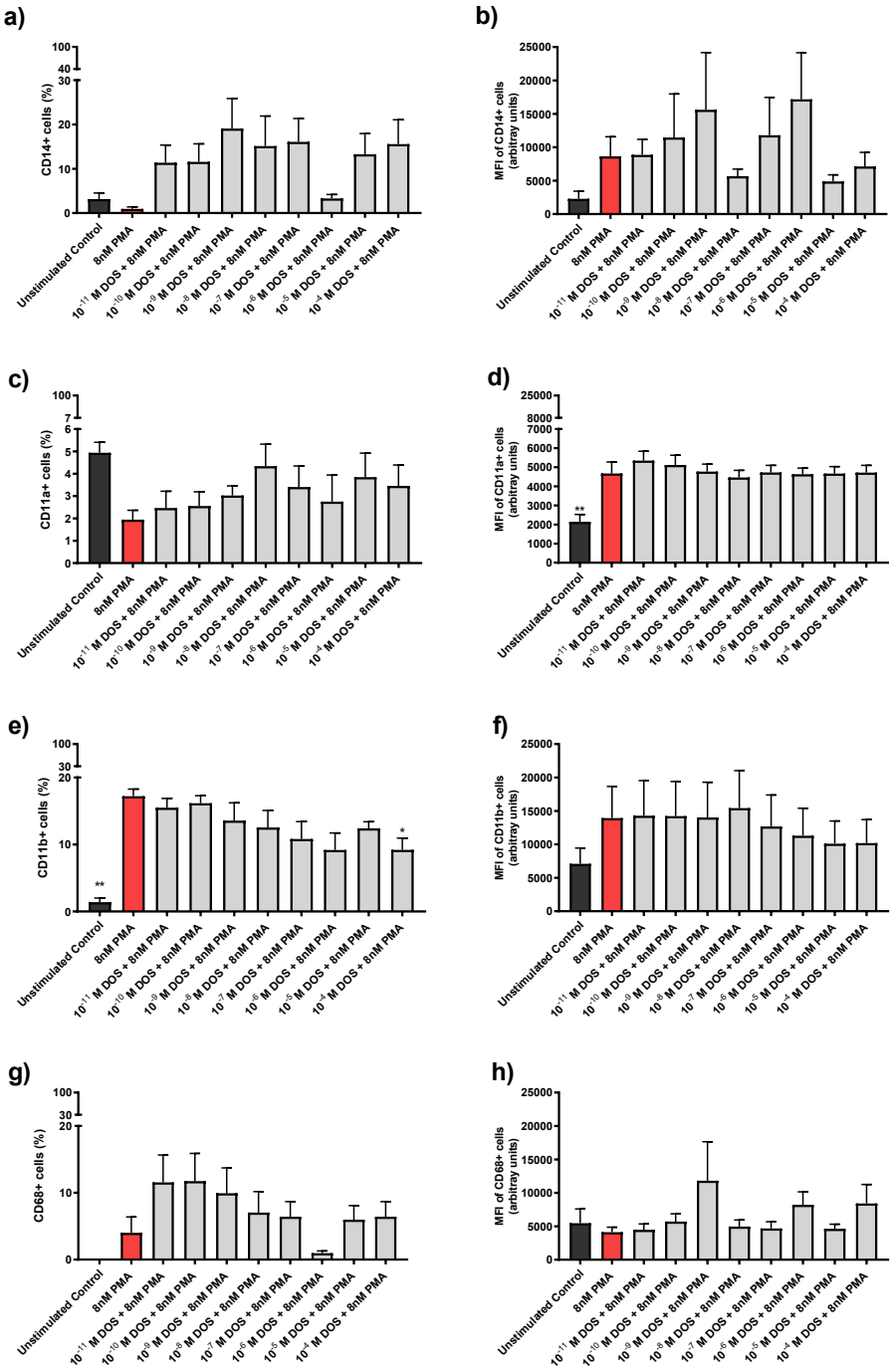


**Appendix Figure 50.** ***The impact of DOS on non-adherent THP-1 cells surface markers expression of DOS and PMA cultures.***

*Non-adherent cells from DOS ($10^{-11}$ to $10^{-4}$ M) + PMA cultures compared to non-adherent cells from PMA control cells analysed by flow cytometry. Bar graph represents positive cells (a, c, e, g) MFI of positive cells (b, d, f, h). ANOVA with post hoc Dunnett's test, mean ± SEM (n=3), no significant difference in p-value vs PMA.*

DOS at concentrations of $10^{-11}$ M to $10^{-4}$ M had no significant difference on the percentage of $CD14^+$, $CD11a^+$and $CD68^+$cells and nor intensity of expression in DOS + PMA U937 non-adherent cultures and DOS + PMA THP-1 non-adherent cultures compared to PMA non-adherent U937 and THP-1 cultures. A higher percentage of $CD11b^+$ cells was observed at DOS concentrations of $10^{-11}$ M to $10^{-4}$ M ($p < 0.01$) with no significant difference in their MFI in DOS + PMA U937 non-adherent cultures compared to PMA-U937 non-adherent cultures. No significant difference was seen in DOS + PMA THP-1 non-adherent cultures at DOS concentrations of $10^{-11}$ M to $10^{-4}$ M compared to PMA-THP-1 non-adherent cultures.

**a)**

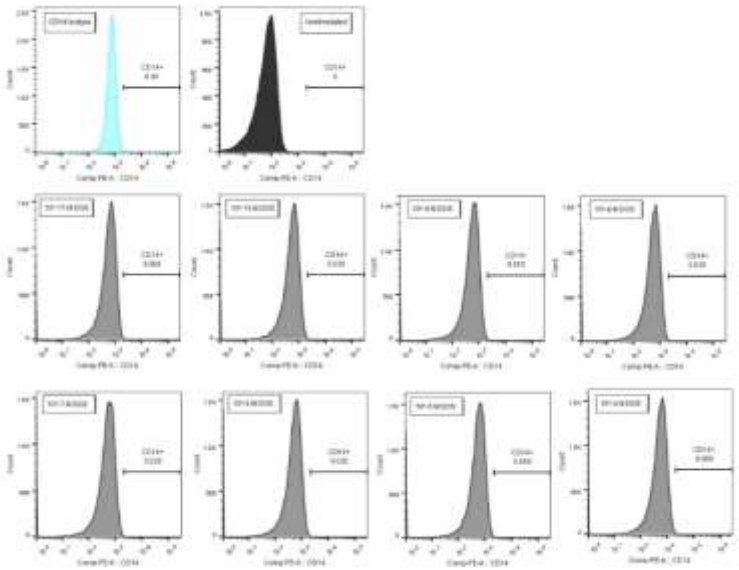

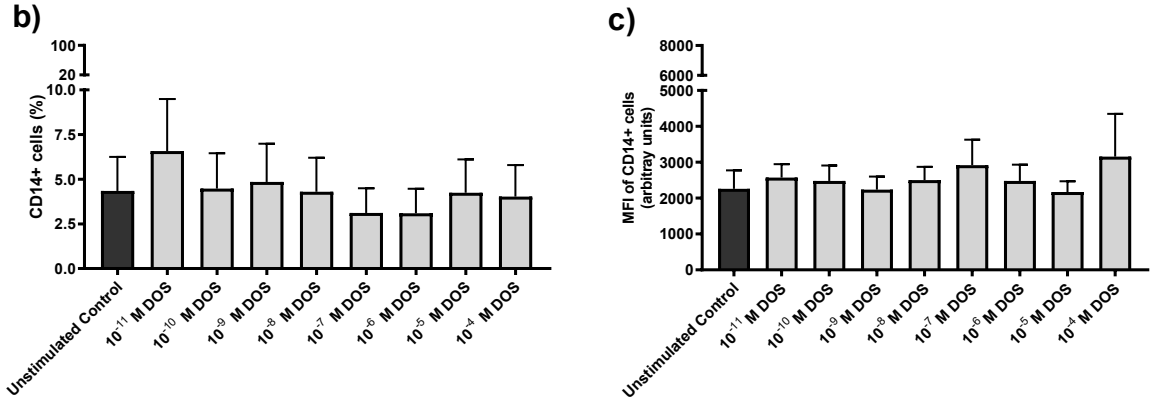


**Appendix Figure 51*. The impact of DOS on THP-1 CD14 expression in the absence of PMA.***

*a) Histograms represent the overlays comparison of DOS ($10^{-11}$ to $10^{-4}$ M) treated cells at 48 h in the absence of PMA compared to unstimulated control cells against isotype control on CD14-PE, channel analysed by flow cytometry. Bar graphs represents (b) positive cells and (c) MFI of positive cells. ANOVA with post hoc Dunnett's test, mean ± SEM (n=3), no significant p-value vs unstimulated control.*

**a)**

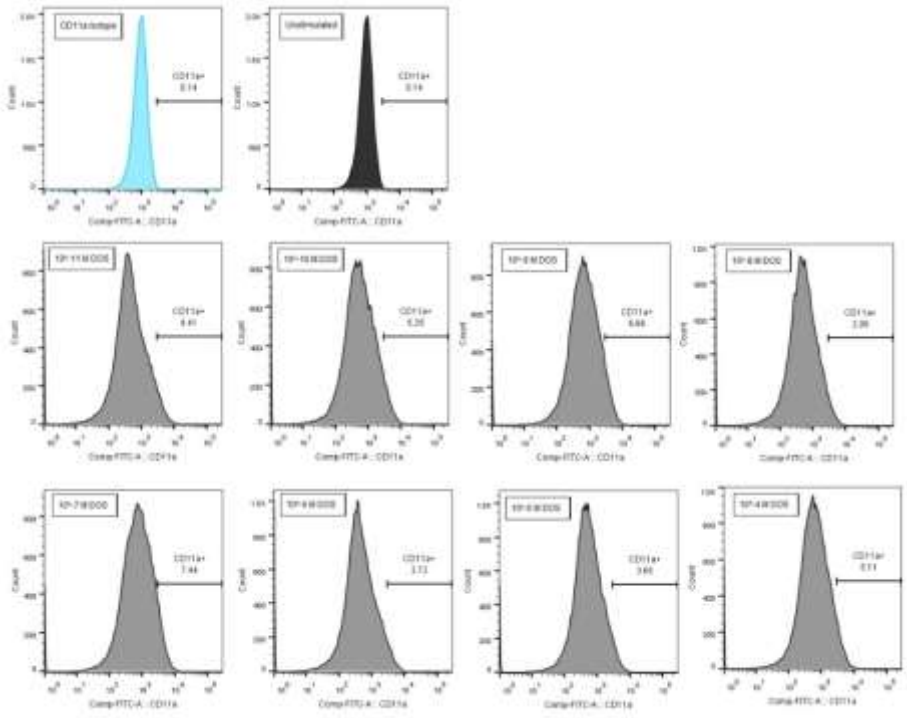

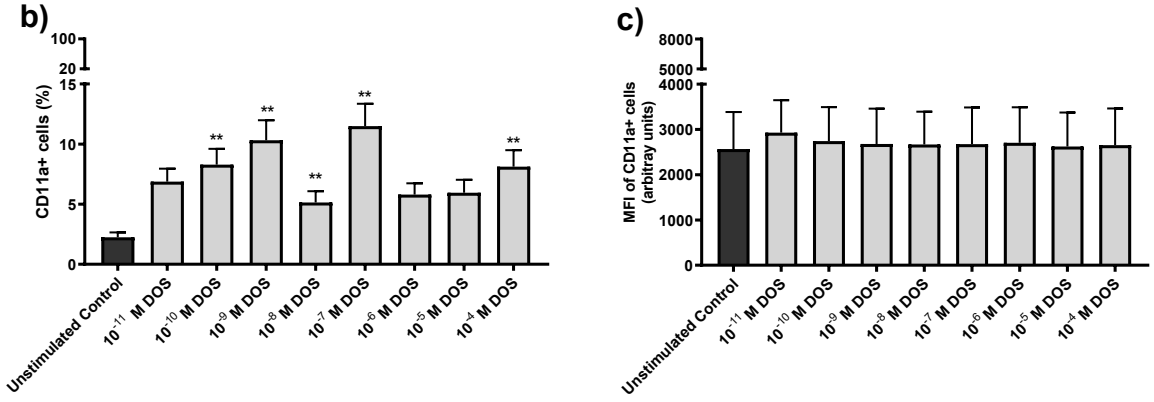


**Appendix Figure 52.** ***The impact of DOS on U937 THP-1 CD11a expression in the absence of PMA.***

*a) Histograms represent the overlays comparison of DOS ($10^{-11}$ to $10^{-4}$ M) treated cells at 48 h in the absence of PMA compared to unstimulated control cells against isotype control on CD11a-FITC, channel analysed by flow cytometry. Bar graph represents (b) positive cells and (c) MFI of positive cells. ANOVA with post hoc Dunnett's test, mean ± SEM (n=3), **p < 0.01 vs unstimulated control.*

**a)**

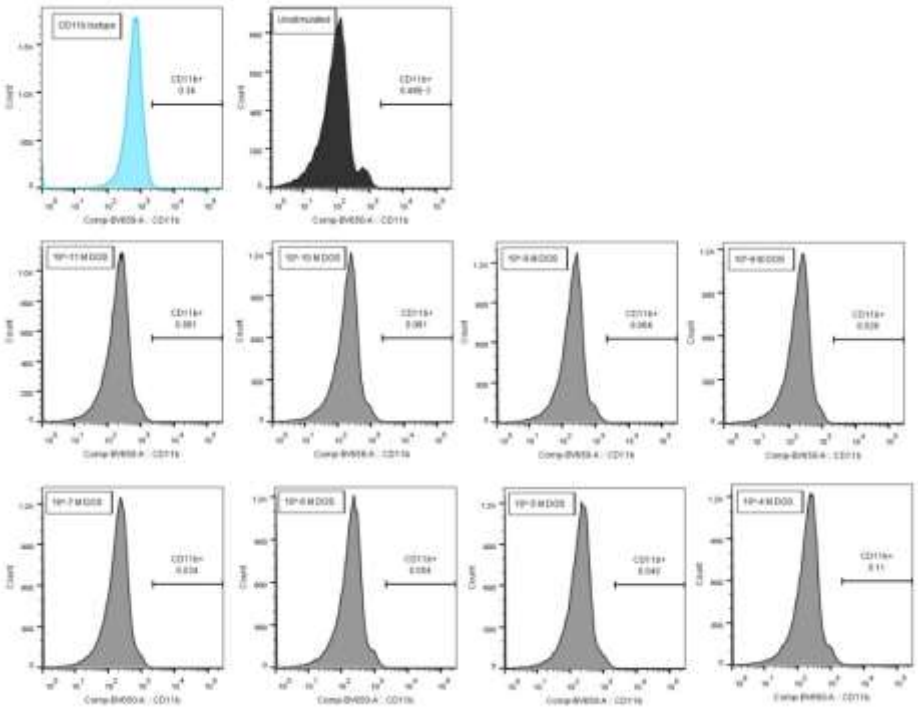

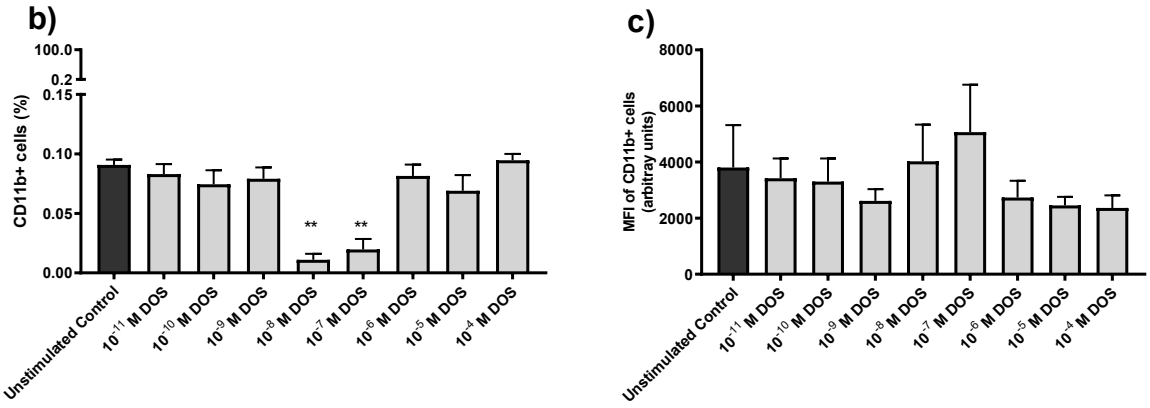


**Appendix Figure 53.** ***The impact of DOS on THP-1 CD11b expression in the absence of PMA.***

*a) Histograms represent the overlays comparison of DOS ($10^{-11}$ to $10^{-4}$ M) treated cells at 48 h in the absence of PMA compared to unstimulated control cells against isotype control on CD11b-BV650 channel analysed by flow cytometry. Bar graphs represents (b) positive cells and (c) MFI of positive cells. ANOVA with post hoc Dunnett's test, mean ± SEM (n=3), **p < 0.01 vs unstimulated control.*

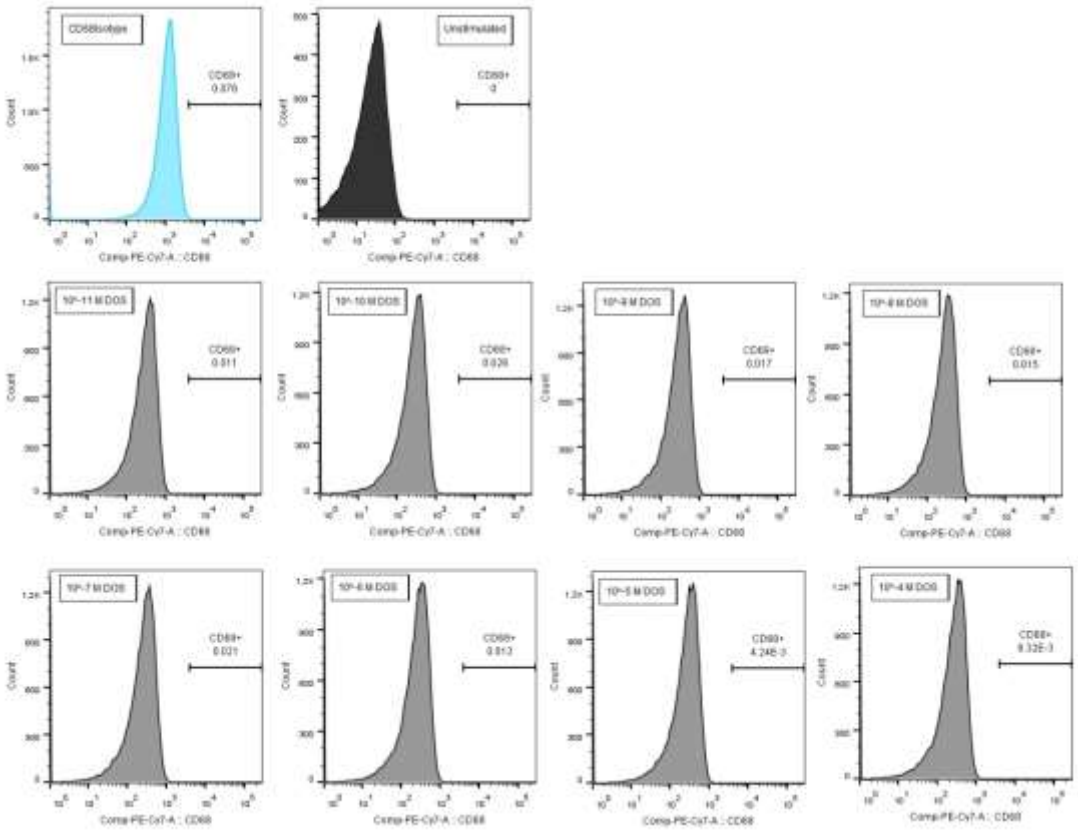

**Appendix Figure 54*. The impact of DOS on THP-1 CD68 expression in the absence of PMA.***

*Histograms represent (n =3) the overlays comparison of DOS ($10^{-11}$ to $10^{-4}$ M) treated cells at 48 h in the absence of PMA compared to unstimulated control cells against isotype control analysed by flow cytometry. No CD68 positive cells found in cultures.*

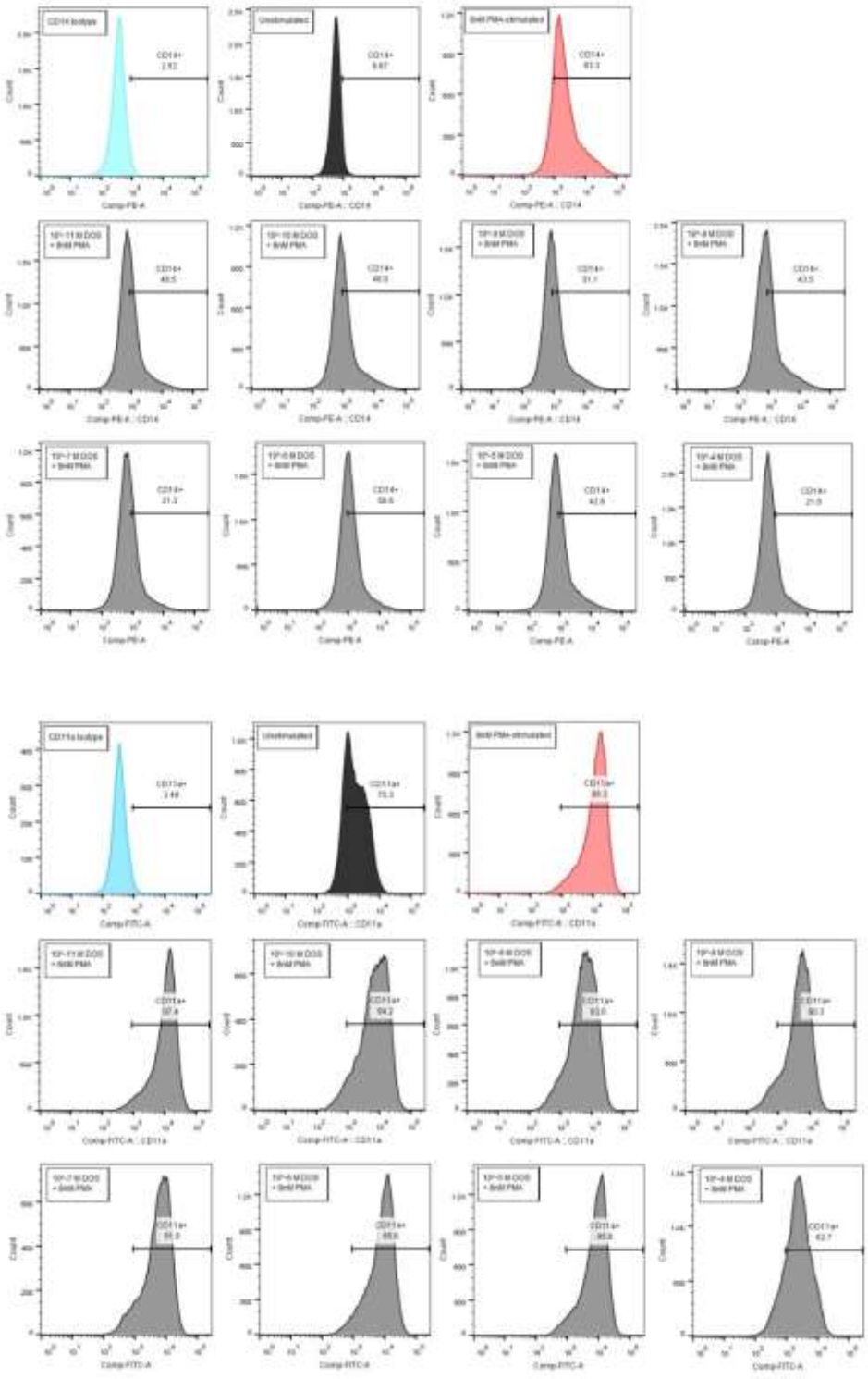

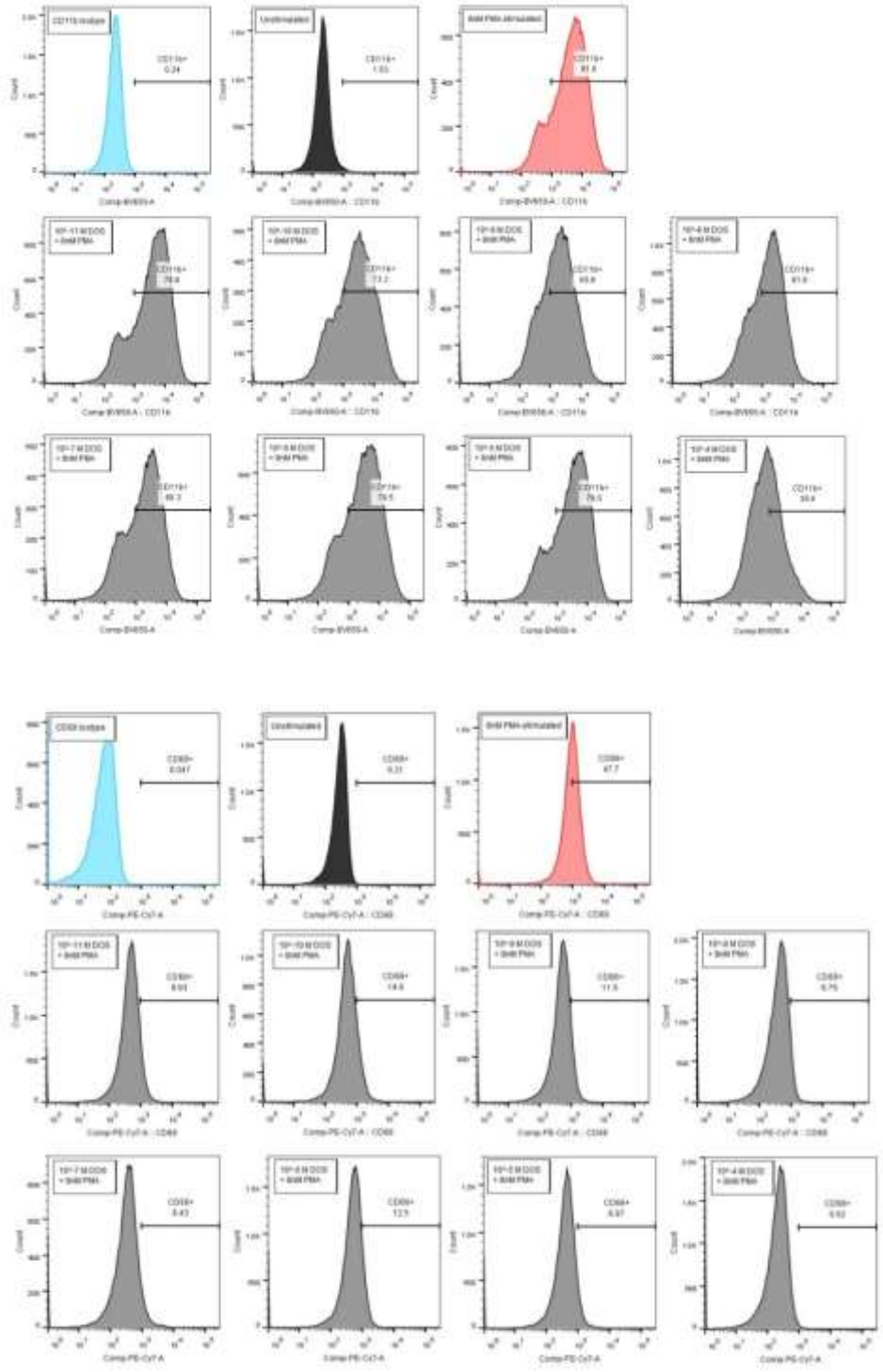

**Appendix Figure 55.** ***The impact of DOS on U937 CD68 expression in the presence of PMA.***

*a) Histograms represent the overlays comparison of DOS ($10^{-11}$ to $10^{-4}$ M) treated cells at 48 h in the presence of 8 nM PMA (given 2 h before PMA) compared to PMA control cells against isotype control analysed by flow cytometry.*

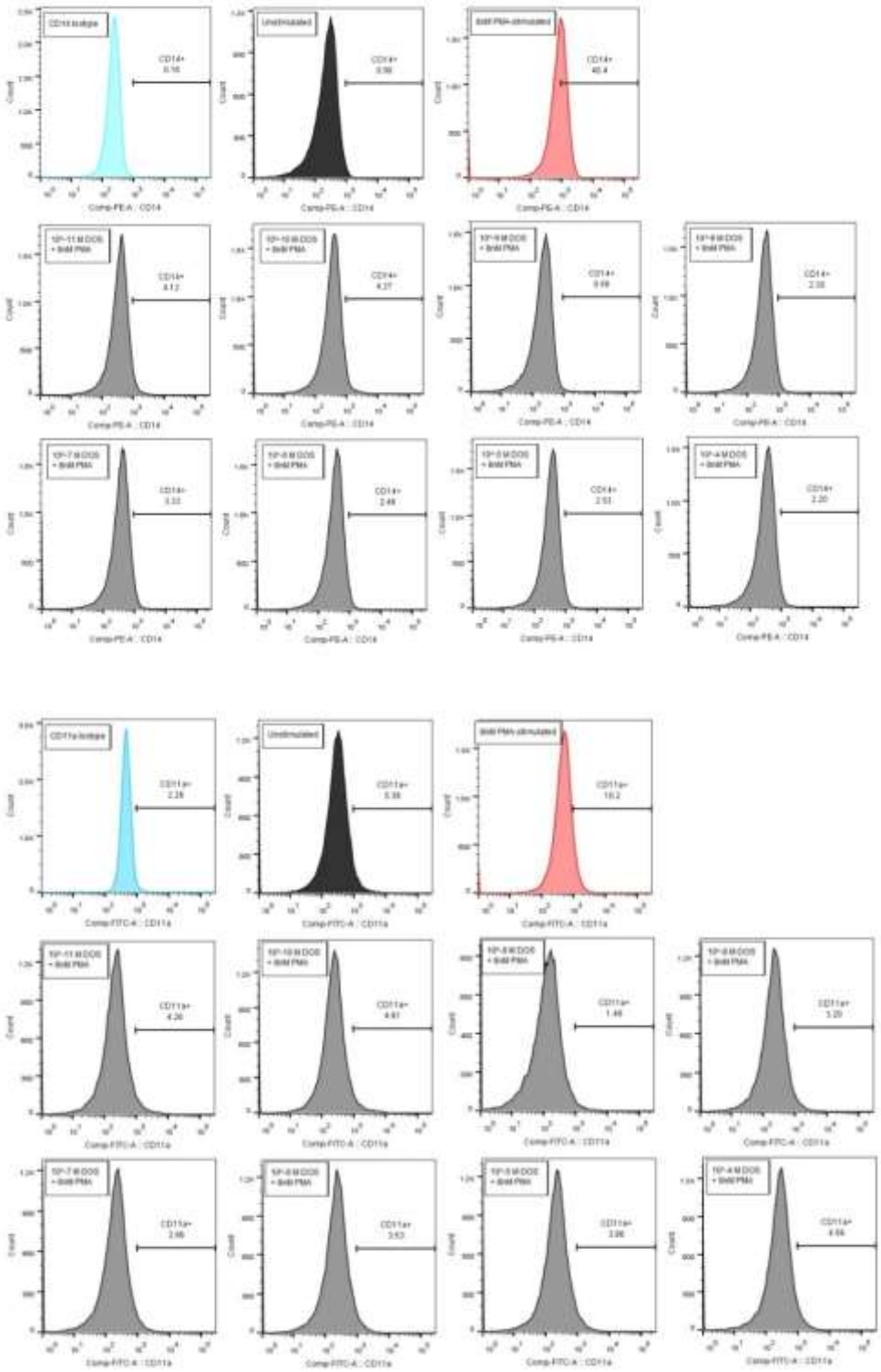

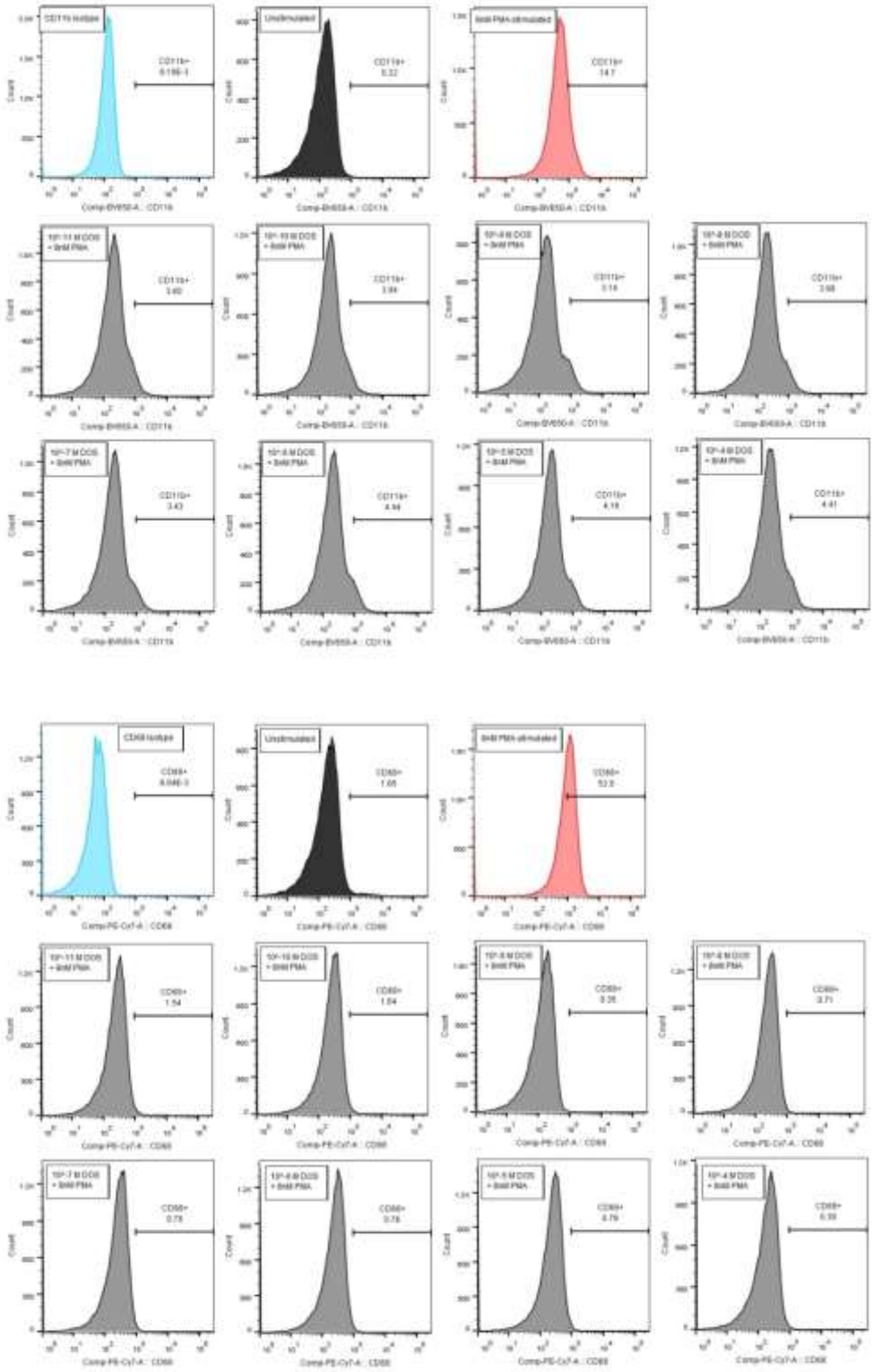

**Appendix Figure 56.** ***The impact of DOS on THP-1 CD68 expression in the presence of PMA.***

*a) Histograms represent the overlays comparison of DOS ($10^{-11}$ to $10^{-4}$ M) treated cells at 48 h in the presence of 8 nM PMA (given 2 h before PMA) compared to PMA control cells against isotype control analysed by flow cytometry.*

**a)**

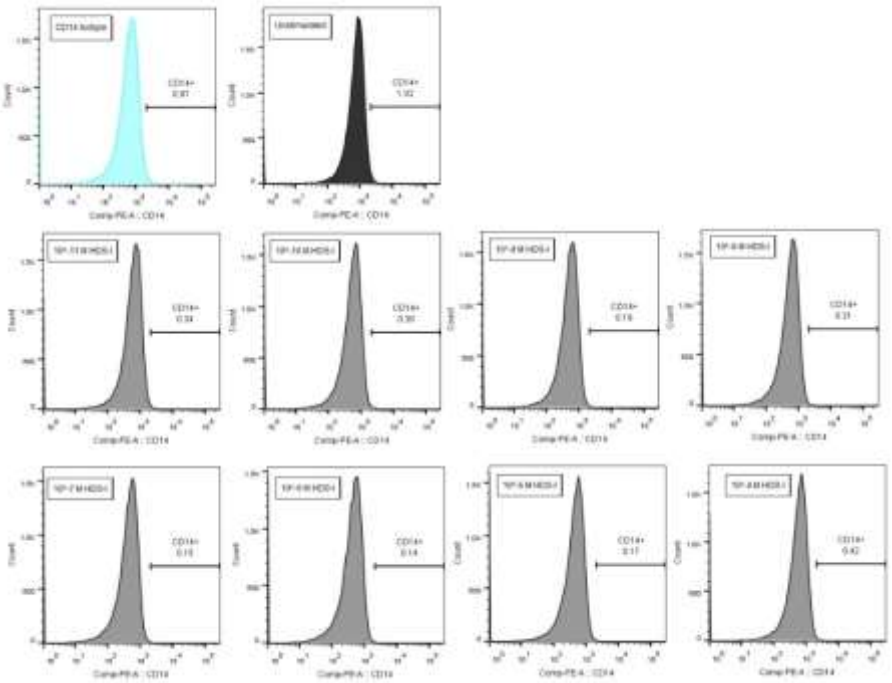

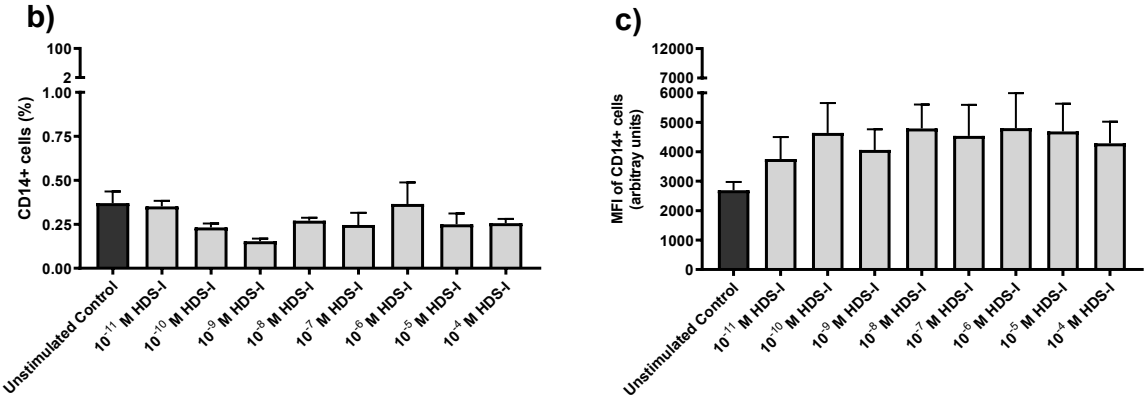


**Appendix Figure 57*. The impact of HDS-I on U937 CD14 expression in the absence of PMA.***

*a) Histograms represent the overlays comparison of HDS-I ($10^{-11}$ to $10^{-4}$ M) treated cells at 48 h in the absence of PMA compared to unstimulated control cells against isotype control on CD14-PE, channel analysed by flow cytometry. Bar graphs represent (b) positive cells and (c) MFI of positive cells. ANOVA with post hoc Dunnett's test, mean ± SEM (n=3), no significant difference vs unstimulated control.*

**a)**

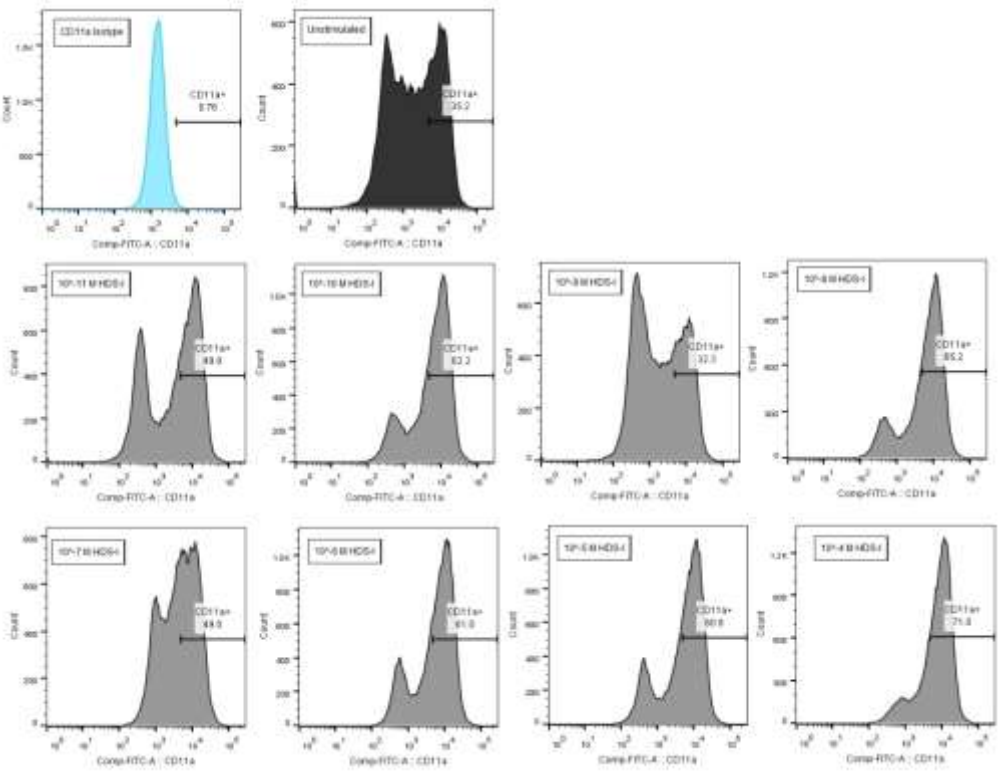

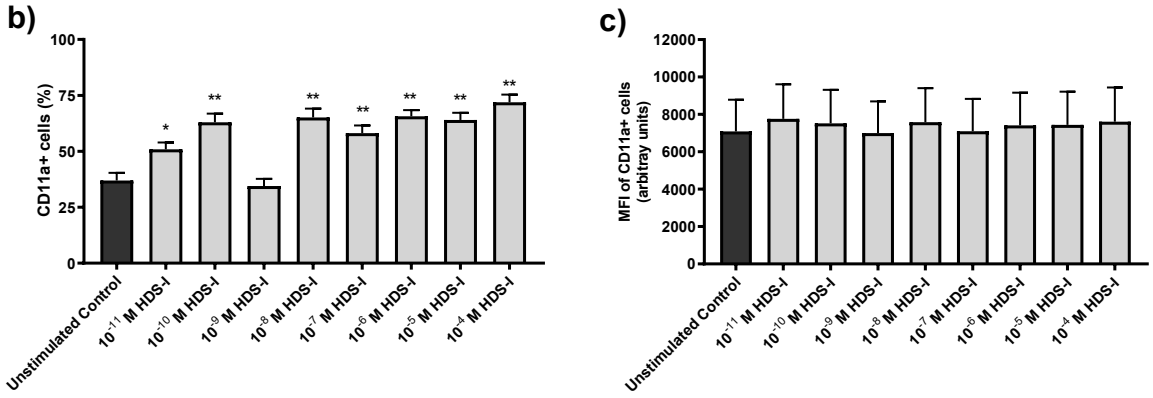


**Appendix Figure 58.** ***The impact of HDS-I on U937 CD11a expression in the absence of PMA.***

*a) Histograms represent the overlays comparison of HDS-I ($10^{-11}$ to $10^{-4}$ M) treated cells at 48 h in the absence of PMA compared to unstimulated control cells against isotype control on CD11a-FITC, channel analysed by flow cytometry . Bar graph represents (b)*

*positive cells and (c) MFI of positive cells. ANOVA with post hoc Dunnett's test, mean ± SEM (n=3), *p<0.05, **p < 0.01 vs unstimulated control.*

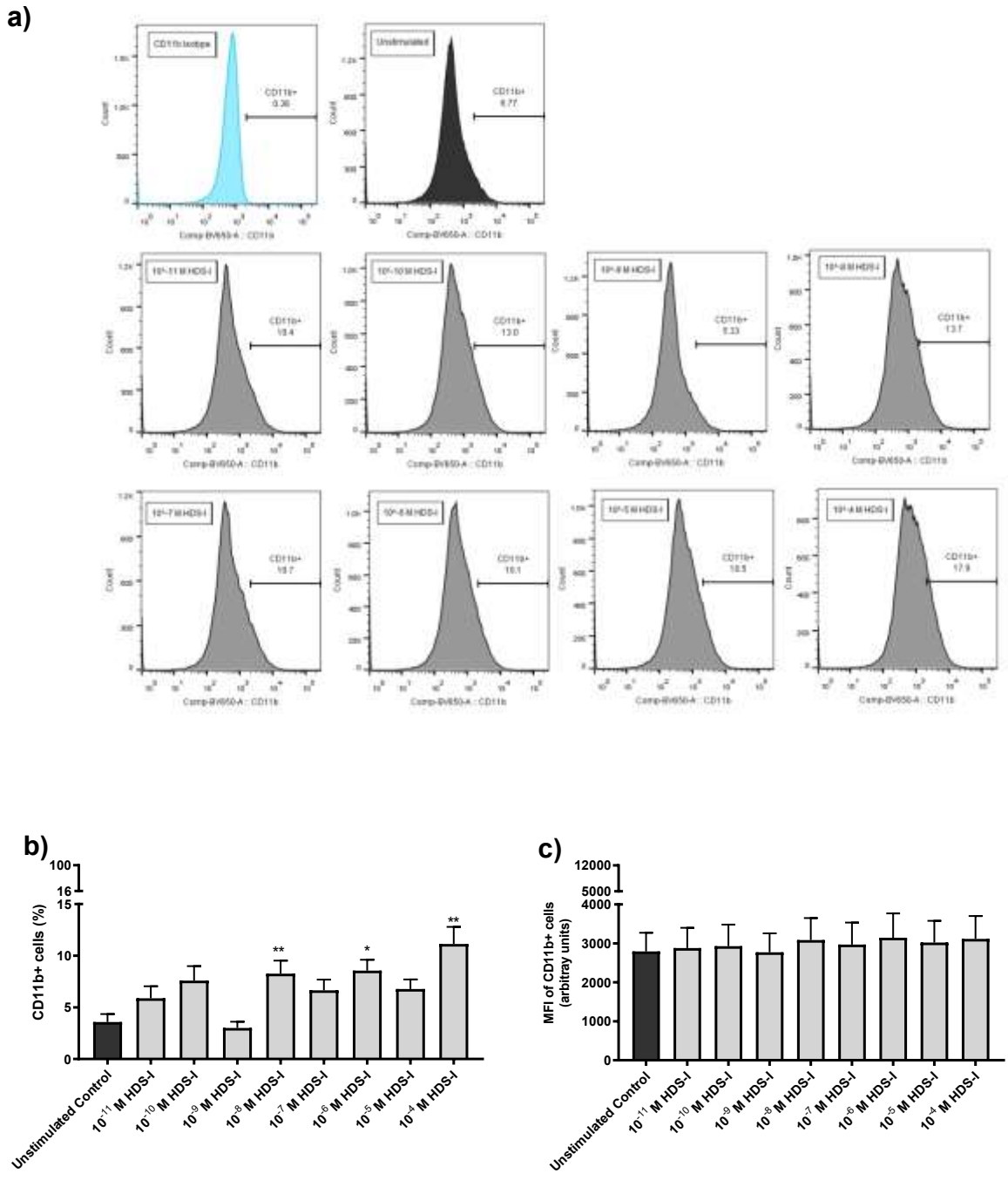


**Appendix Figure 59. The impact of HDS-I on U937 CD11b expression in the absence of PMA.**

*a) Histograms represent the overlays comparison of HDS-I ($10^{-11}$ to $10^{-4}$ M) treated cells at 48 h in the absence of PMA compared to unstimulated control cells against isotype control on CD11b-BV650 channel analysed by flow cytometry . Bar graphs represents*

*(b) positive cells and (c) MFI of positive cells. ANOVA with post hoc Dunnett's test, mean ± SEM (n=3), *p<0.05, **p < 0.01 vs unstimulated control.*

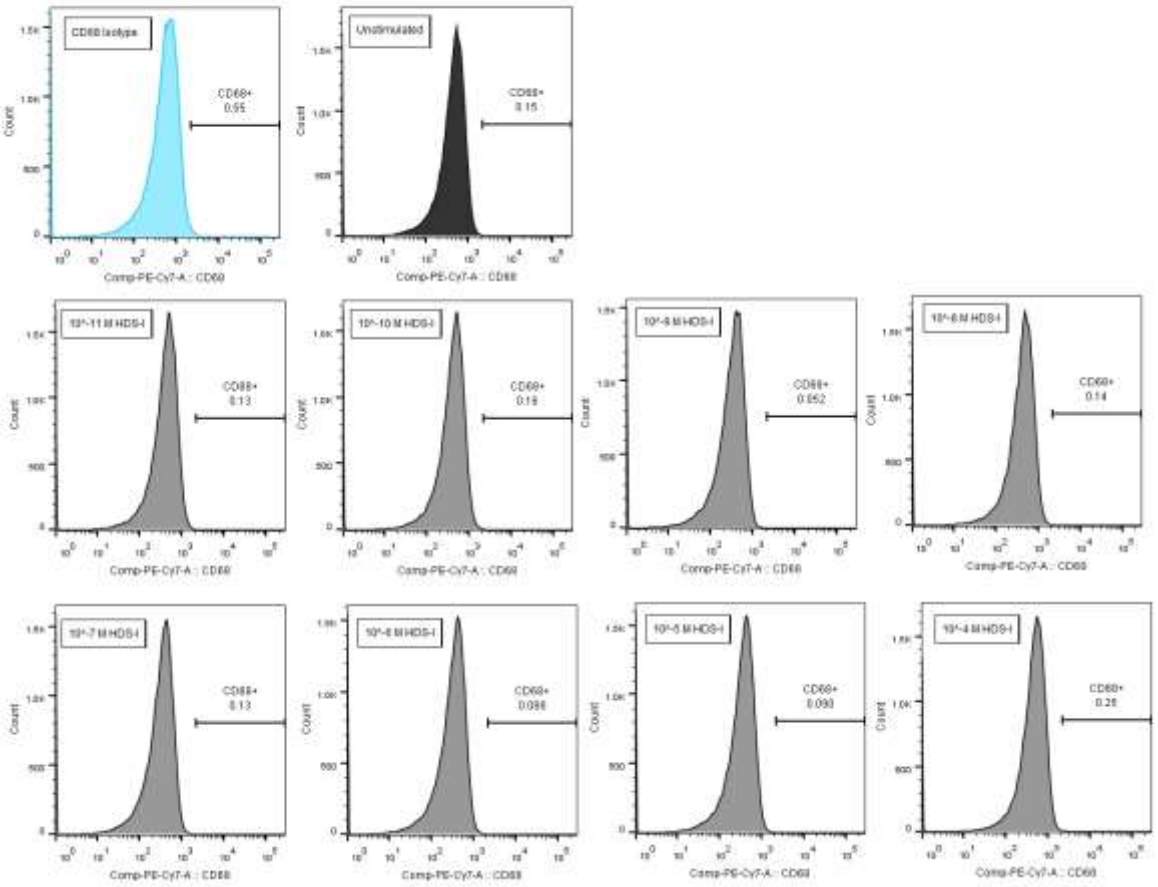

**Appendix Figure 60.** ***The impact of HDS-I on U937 CD68 expression in the absence of PMA.***

*Histograms represent the overlays comparison of HDS-I ($10^{-11}$ to $10^{-4}$ M) treated cells at 48 h in the absence of PMA compared to unstimulated control cells against isotype control on CD68-Cyanine-7 channel analysed by flow cytometry. No CD68 positive cells found in cultures.*

HDS-I at concentrations of $10^{-11}$ M to $10^{-4}$ M had no significant impact on expression of $CD14^+$ and $CD68^+$ cells in HDS-I-U937 cell cultures compared to unstimulated control U937 cells at 48 h. But HDS-I-U937 cell cultures had significantly ($p < 0.05$, $p < 0.01$) higher percentage of $CD11a^+$ cells at HDS-I concentrations of $10^{-11}$ M, $10^{-10}$ M,$10^{-8}$ M, $10^{-4}$ M and $CD11b^+$ cells at HDS-I concentrations of $10^{-8}$ M,$10^{-6}$ M, $10^{-4}$ M compared to unstimulated control U937 cultures. However, no significant differences for $CD14^+$, $CD11a^+$, $CD11b^+$ and $CD68^+$ cells were found in HDS-I THP-1 cell cultures compared to unstimulated-THP-1 cultures at 48 h.

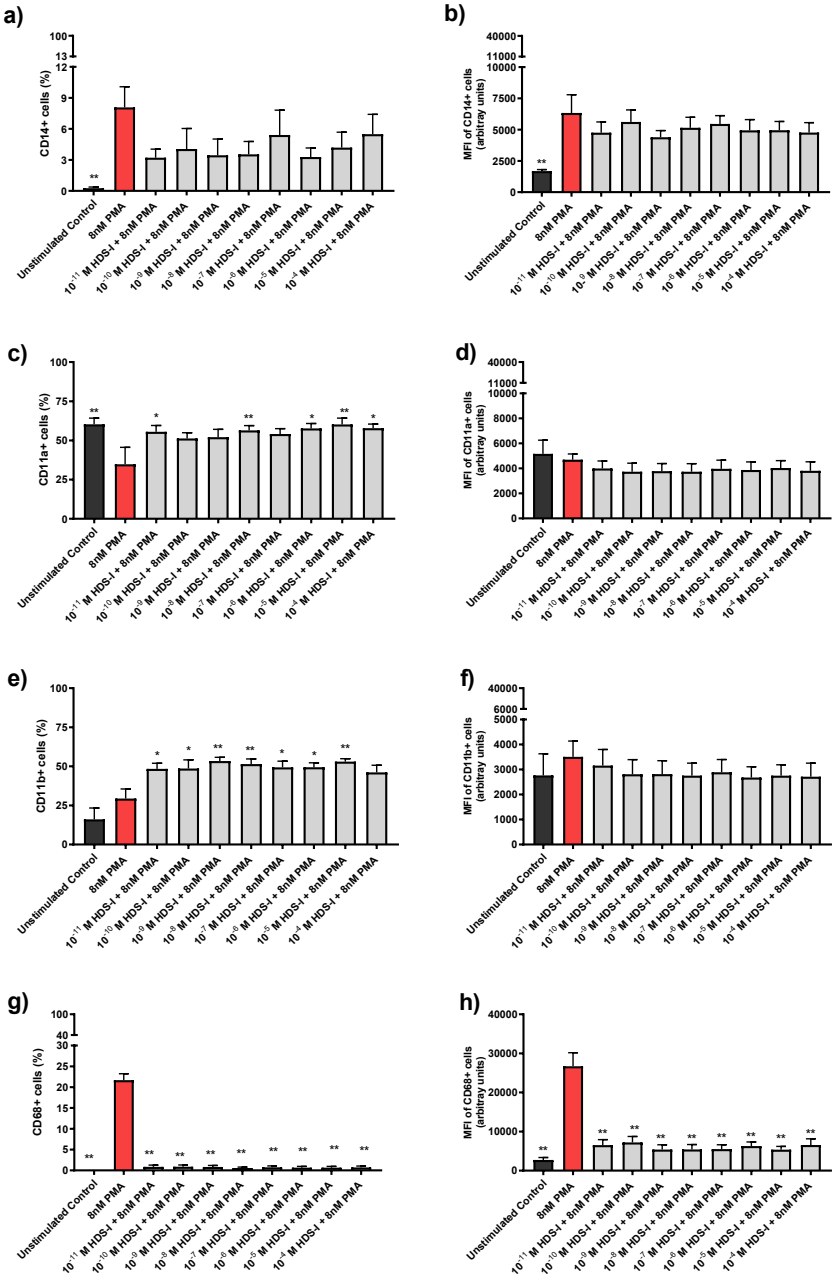


**Appendix Figure 61.** ***The impact of HDS-I on non-adherent U937 cells surface markers expression of HDS-I and PMA cultures.***

*Non-adherent cells from HDS-I ($10^{-11}$ to $10^{-4}$ M) + PMA cultures compared to non-adherent cells from PMA control cells, analysed by flow cytometry . Bar graph represents*

*positive cells (a, c, e, g) MFI of positive cells (b, d, f, h). ANOVA with post hoc Dunnett's test, mean ± SEM (n=3), *p<0.05, **p < 0.01 vs PMA.*

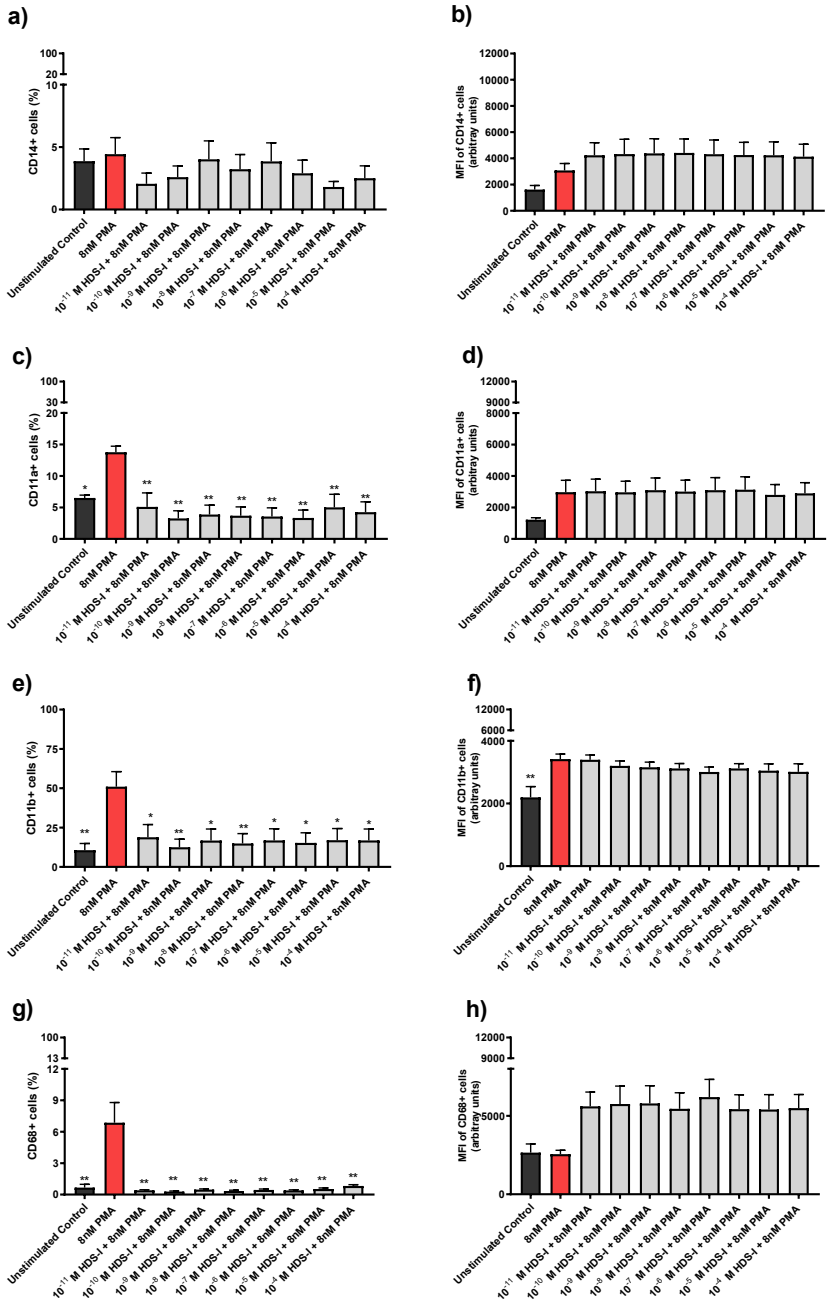


**Appendix Figure 62.** ***The impact of HDS-I on non-adherent THP-1 cells surface markers expression of HDS-I and PMA cultures.***

*Non-adherent cells from HDS-I ($10^{-11}$ to $10^{-4}$ M) + PMA cultures compared to non-adherent cells from PMA control cells, analysed by flow cytometry. Bar graph represents positive cells (a, c, e, g) MFI of positive cells (b, d, f, h). ANOVA with post hoc Dunnett's test, mean ± SEM (n=3), *p<0.05, **p < 0.01 vs PMA.*

HDS-I at concentrations of $10^{-11}$ M to $10^{-4}$ M had no significant effect on the percentage of $CD14^+$ cells and their CD14 expression in HDS-I + PMA U937 non-adherent cultures compared to PMA non-adherent U937 cultures. Significantly higher percentages of $CD11a^+$ cells were observed at HDS-I concentrations of $10^{-11}$ M, $10^{-6}$M, $10^{-4}$ M ($p < 0.05$) and $10^{-8}$M, $10^{-5}$M ($p < 0.01$). There was no significant differences in MFI of $CD14^+$, $CD11a^+$, $CD11b^+$ and $CD68^+$ cells in HDS-I + PMA non-adherent U937 cultures compared to PMA non-adherent U937 cultures. Also, significantly higher percentages of $CD11b^+$ were found in HDS-I + PMA non-adherent cultures at HDS-I concentrations of $10^{-11}$ M, $10^{-10}$ M, $10^{-7}$M, $10^{-6}$ M ($p < 0.05$), $10^{-9}$ M, $10^{-8}$M, $10^{-5}$ ($p < 0.01$) with no significant difference in their MFI in HDS-I + PMA non-adherent U937 cultures compared to PMA non-adherent U937 cultures.

In HDS-I + PMA non-adherent THP-1 cultures HDS-I at concentrations of $10^{-11}$ M to $10^{-4}$ M had no significant difference on percentage of $CD14^+$ and their expression compared to PMA non-adherent THP-1 cultures. But HDS-I at concentrations of $10^{-11}$ M to $10^{-4}$ M reduced percentage of $CD11a^+$ and $CD11b^+$ cells were significantly ($p < 0.05$, $p < 0.01$) reduced in HDS-I + PMA non-adherent THP-1 cultures compared to PMA non-adherent THP-1 cultures. HDS-I reduced significantly ( $p < 0.01$) percentage of $CD68^+$ cells and their MFI in HDS-I + PMA non-adherent U937 cultures compared to PMA non-adherent U937 cultures at concentrations of $10^{-11}$ M to $10^{-4}$ M. Similarly, the percentage of $CD68^+$ cells was reduced in HDS-I + PMA non-adherent THP-1 cultures by HDS-I at concentrations of $10^{-11}$ M to $10^{-4}$ M ( $p < 0.01$) but with no significant difference in their MFI compared to PMA non-adherent THP-1 cultures.

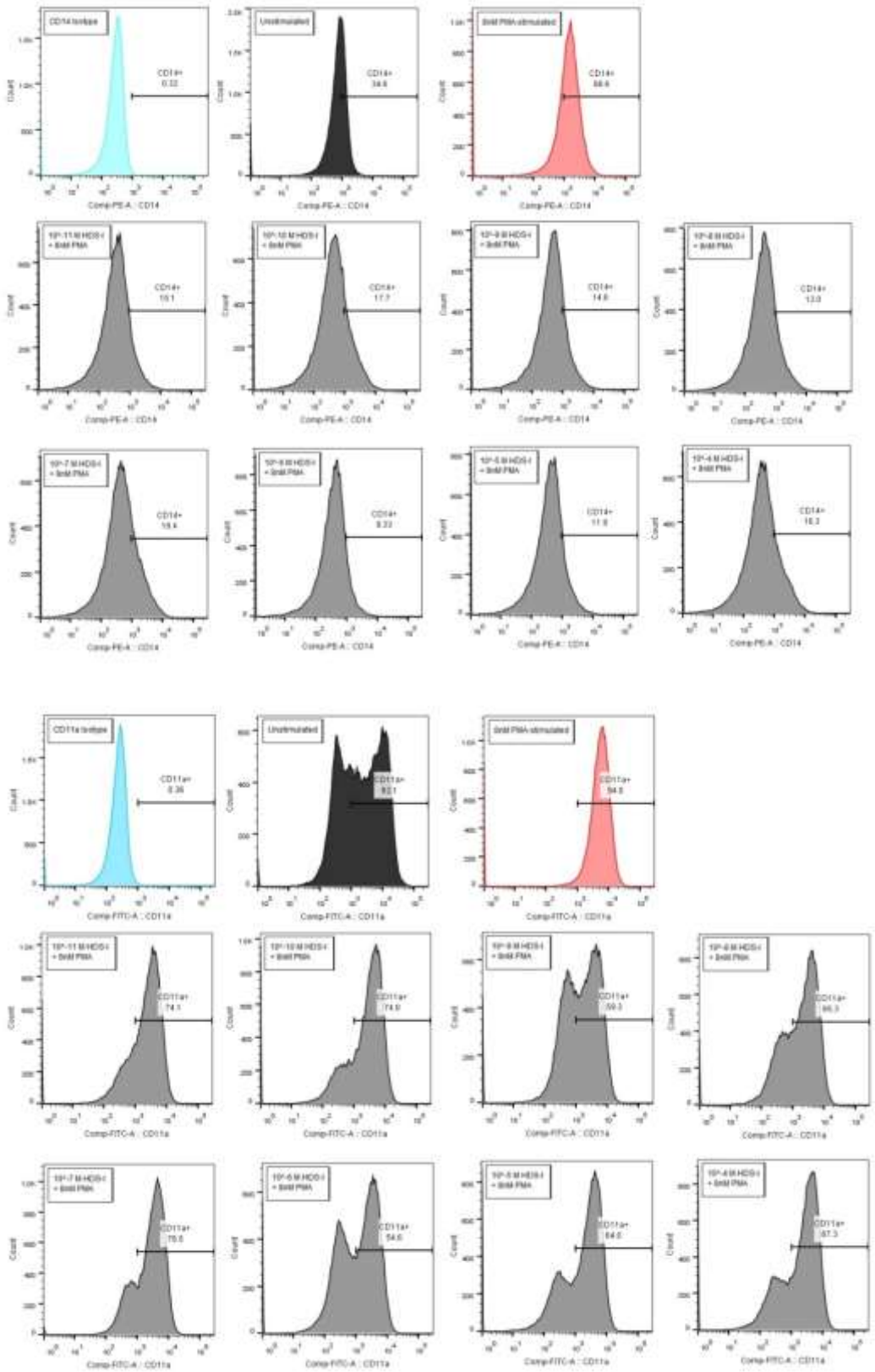

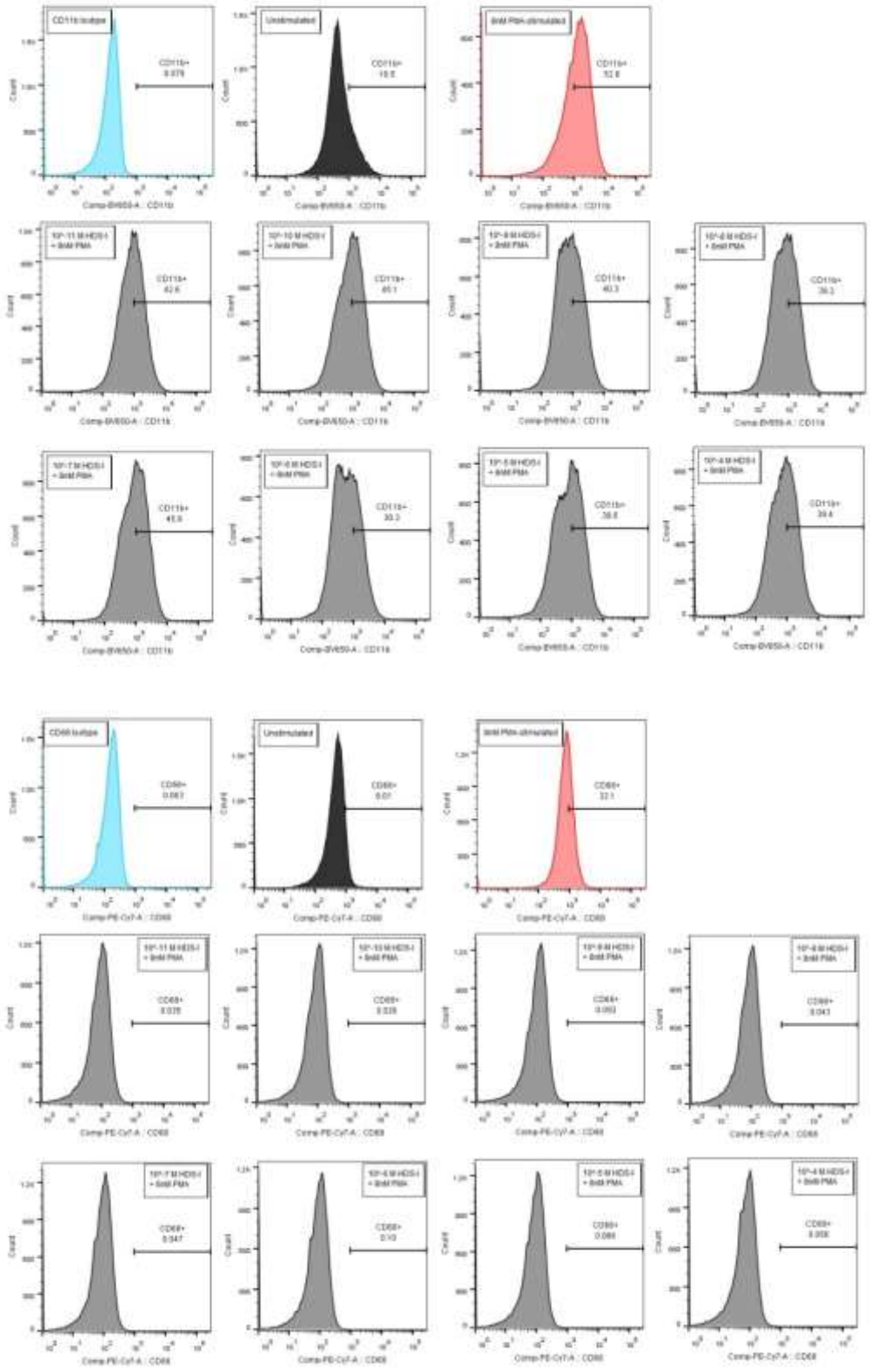

**Appendix Figure 63**. ***The impact of HDS-I on U937 CD68 expression in the presence of PMA.***

*a) Histograms represent the overlays comparison of HDS-I ($10^{-11}$ to $10^{-4}$ M) treated cells at 48 h in the presence of 8 nM PMA (given 2 h before PMA) compared to PMA control cells against isotype control analysed by flow cytometry .*

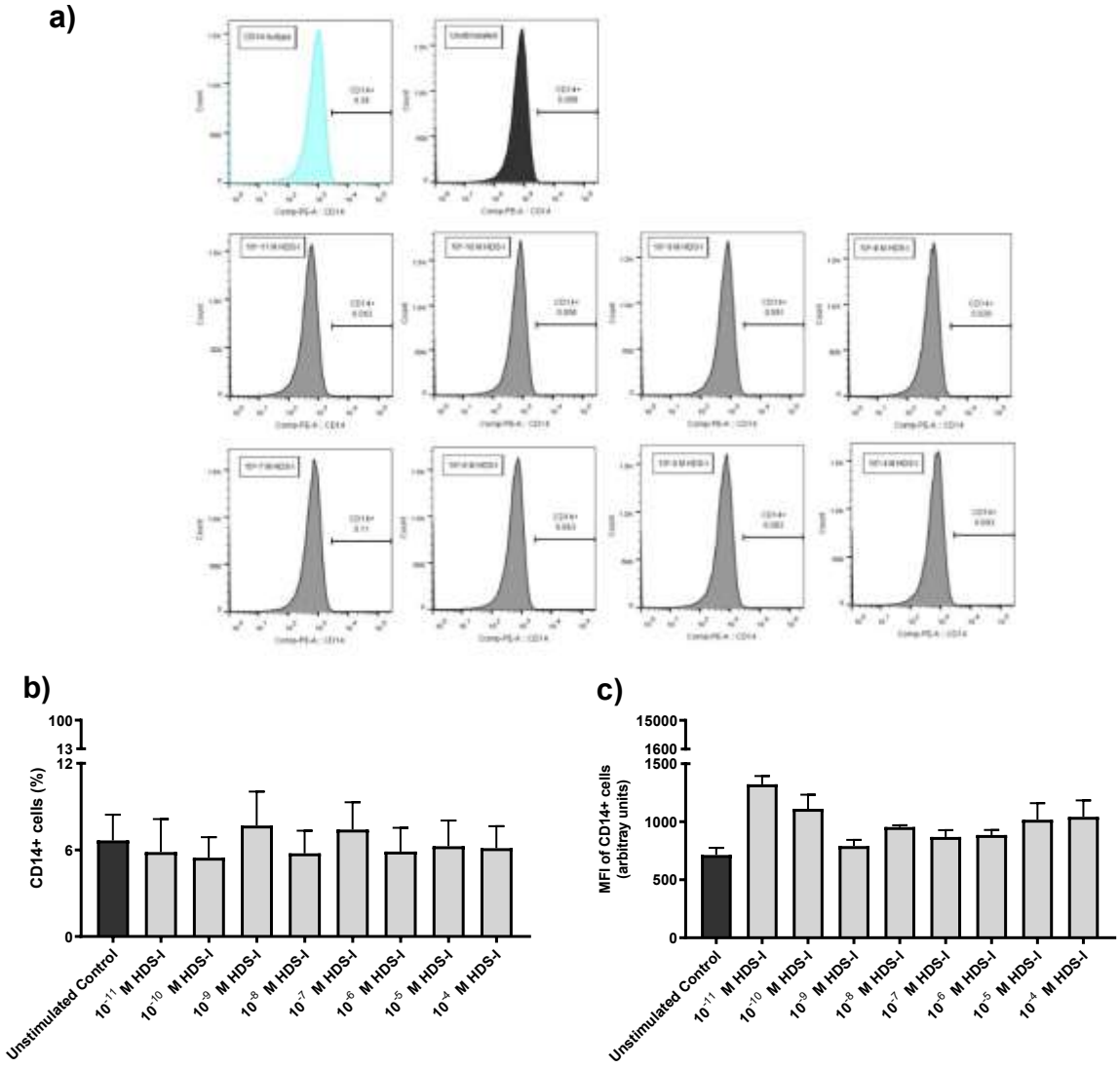


**Appendix Figure 64.** ***The impact of HDS-I on THP-1 CD14 expression in the absence of PMA.***

*a) Histograms represent the overlays comparison of HDS-I ($10^{-11}$ to $10^{-4}$ M) treated cells at 48 h in the absence of PMA compared to unstimulated control cells against isotype control on CD14-PE, channel analysed by flow cytometry. Bar graphs represent (b) positive cells and (c) MFI of positive cells. ANOVA with post hoc Dunnett's test, mean ± SEM (n=3), no significant differences vs unstimulated control.*

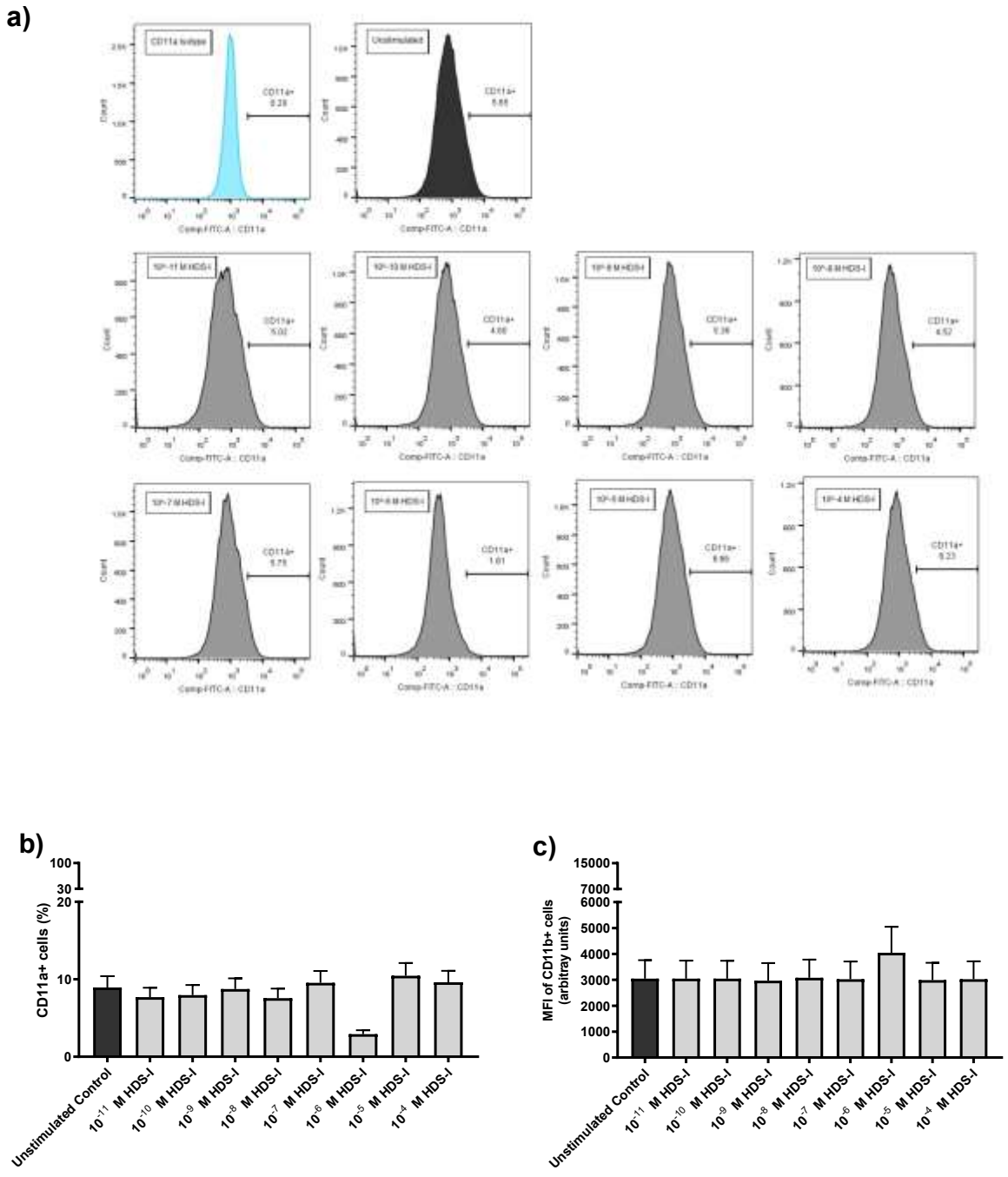


**Appendix Figure 65. The impact of HDS-I on THP-1 CD11a expression in the absence of PMA.**

*a) Histograms represent the overlays comparison of HDS-I ($10^{-11}$ to $10^{-4}$ M) treated cells at 48 h in the absence of PMA compared to unstimulated control cells against isotype control on CD11a-FITC, channel analysed by flow cytometry . Bar graph represents (b)*

*positive cells and (c) MFI of positive cells. ANOVA with post hoc Dunnett's test, mean ± SEM (n=3), no significant differences vs unstimulated control.*

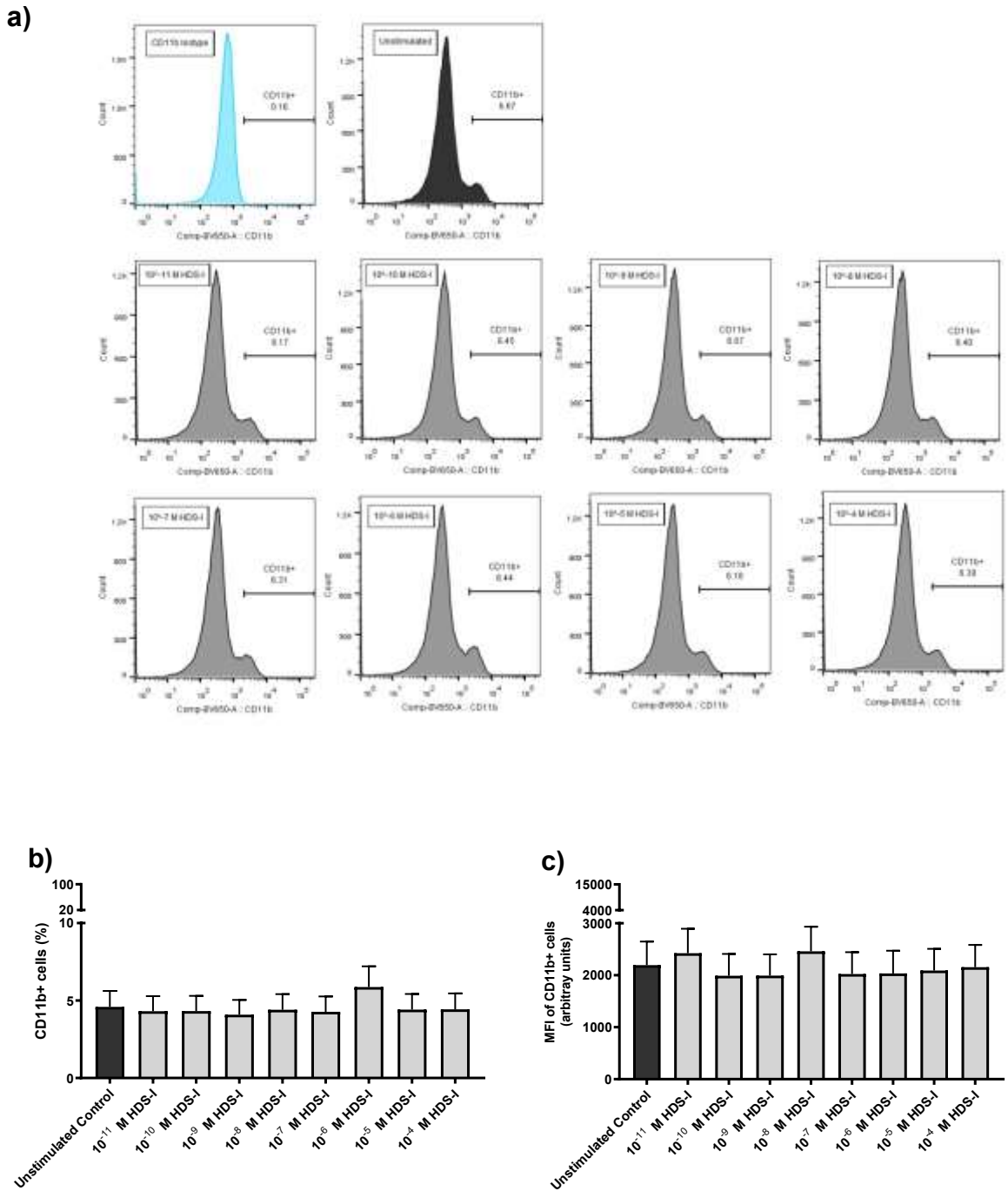


**Appendix Figure 66.** ***The impact of HDS-I on THP-1 CD11b expression in the absence of PMA.***

*a) Histograms represent the overlays comparison of HDS-I ($10^{-11}$ to $10^{-4}$ M) treated cells at 48 h in the absence of PMA compared to unstimulated control cells against isotype*

*control on CD11b-BV650 channel analysed by flow cytometry . Bar graphs represents (b) positive cells and (c) MFI of positive cells. ANOVA with post hoc Dunnett's test, mean ± SEM (n=3), no significant differences vs unstimulated control.*

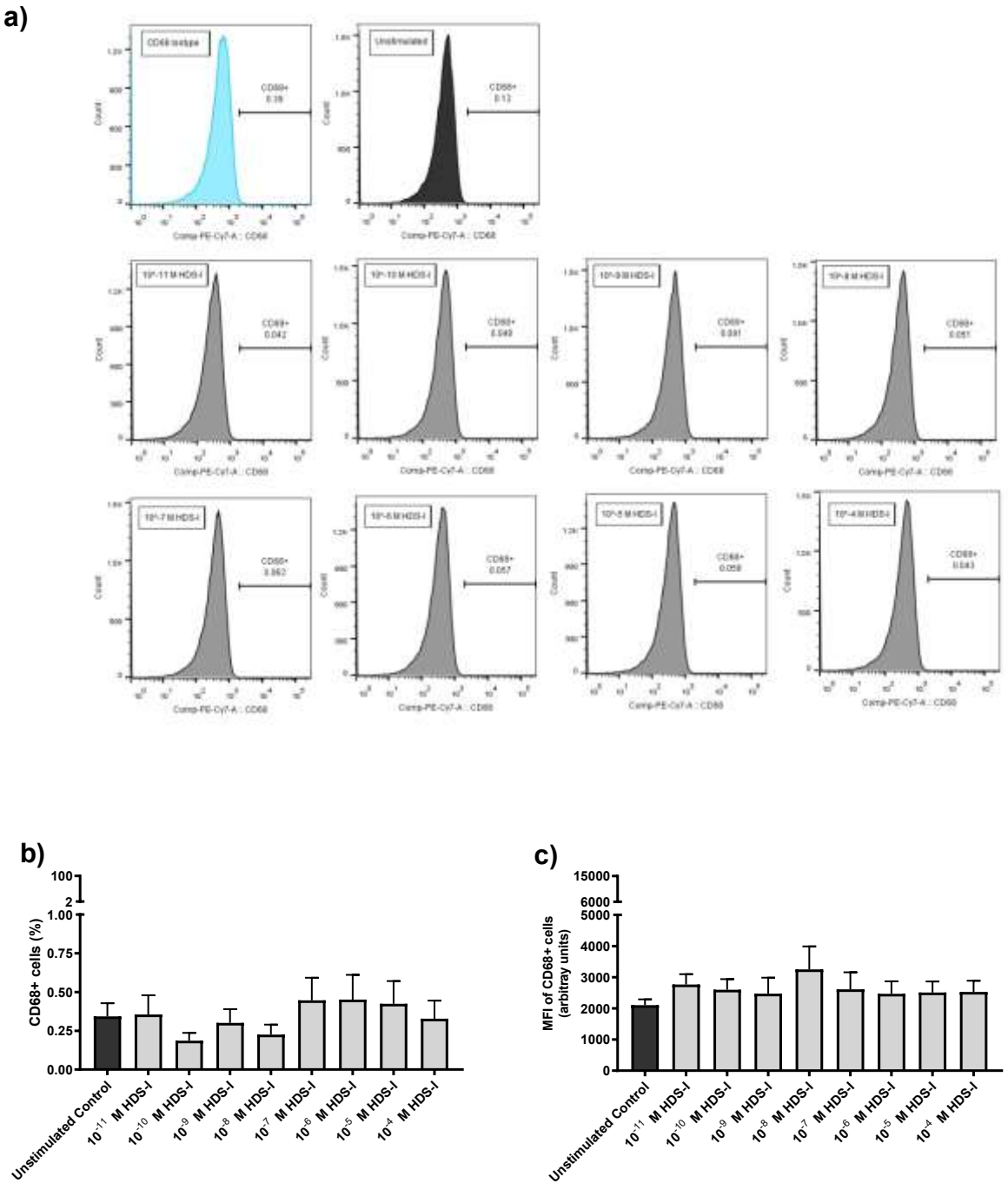


**Appendix Figure 67.** ***The impact of HDS-I on THP-1 CD68 expression in the absence of PMA.***

*a) Histograms represent the overlays comparison of HDS-I ($10^{-11}$ to $10^{-4}$ M) treated cells at 48 h in the absence of PMA compared to unstimulated control cells against isotype control analysed by flow cytometry . Bar represents graphs (b) positive cells and (c) MFI*

*of positive cells. ANOVA with post hoc Dunnett's test, mean ± SEM (n=3), no significant differences vs unstimulated control.*

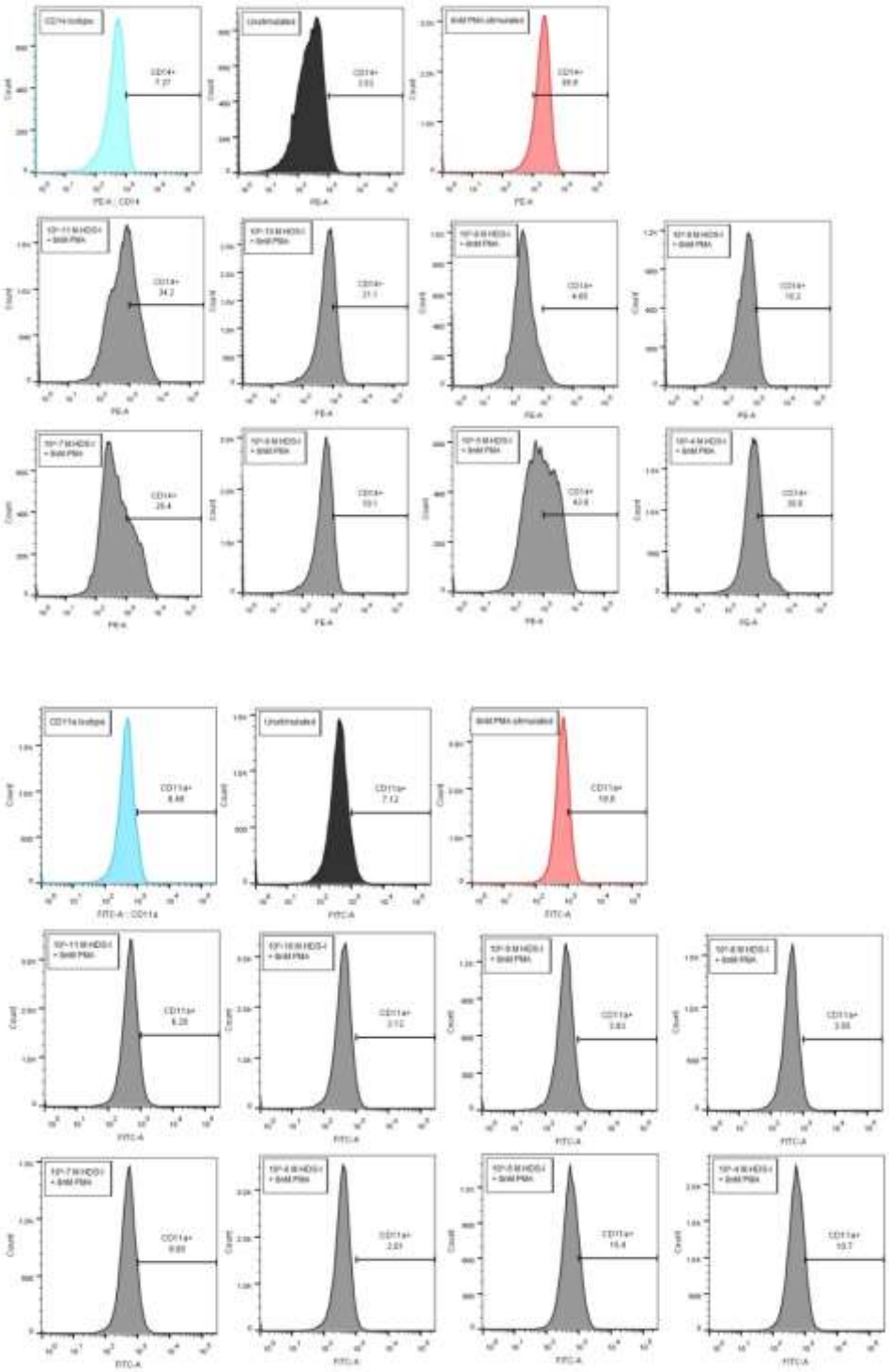

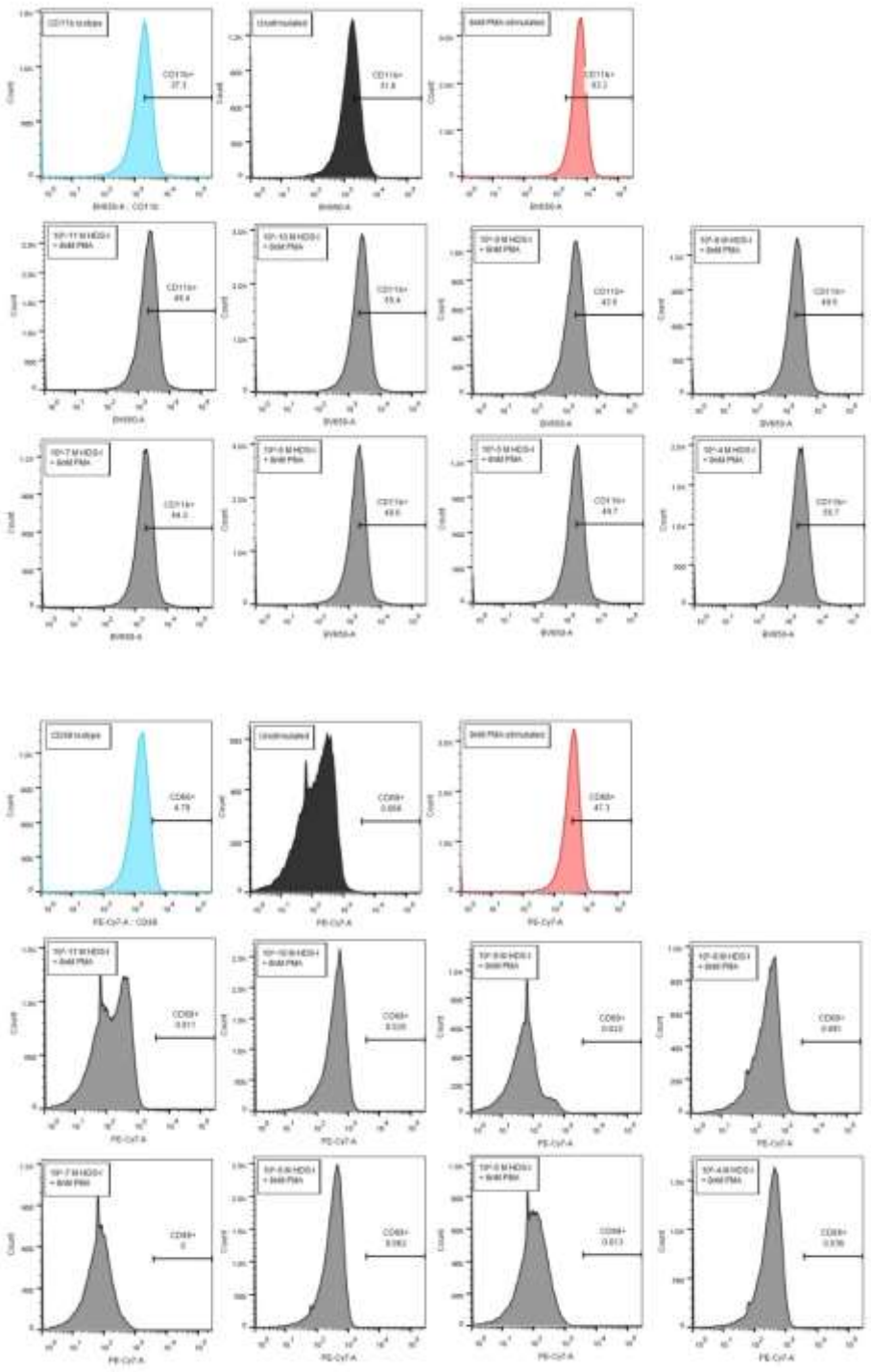

**Appendix Figure 68.** ***The impact of HDS-I on THP-1 CD14 expression in the presence of PMA.***

*a) Histograms represent the overlays comparison of HDS-I ($10^{-11}$ to $10^{-4}$ M) treated cells at 48 h in the presence of 8 nM PMA (given 2 h before PMA) compared to PMA control cells against isotype control analysed by flow cytometry .*

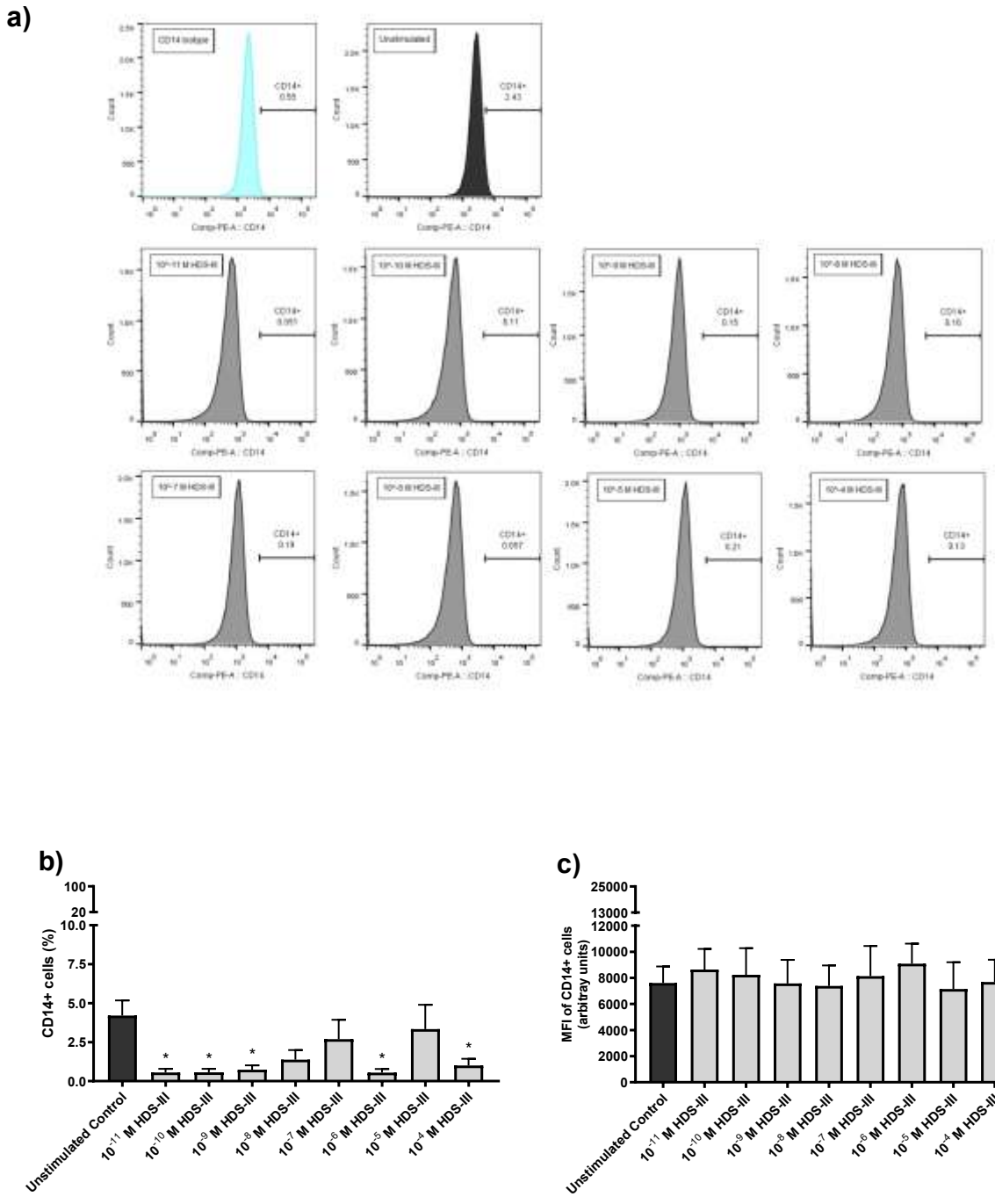


**Appendix Figure 69.** ***The impact of HDS-III on U937 CD14 expression in the absence of PMA.***

*a) Histograms represent the overlays comparison of HDS-III ($10^{-11}$ to $10^{-4}$ M) treated cells at 48 h in the absence of PMA compared to unstimulated control cells against isotype control on CD14-PE, channel analysed by flow cytometry . Bar graphs represent (b)*

*positive cells and (c) MFI of positive cells. ANOVA with post hoc Dunnett's test, mean ± SEM (n=3), *p < 0.05 vs unstimulated control.*

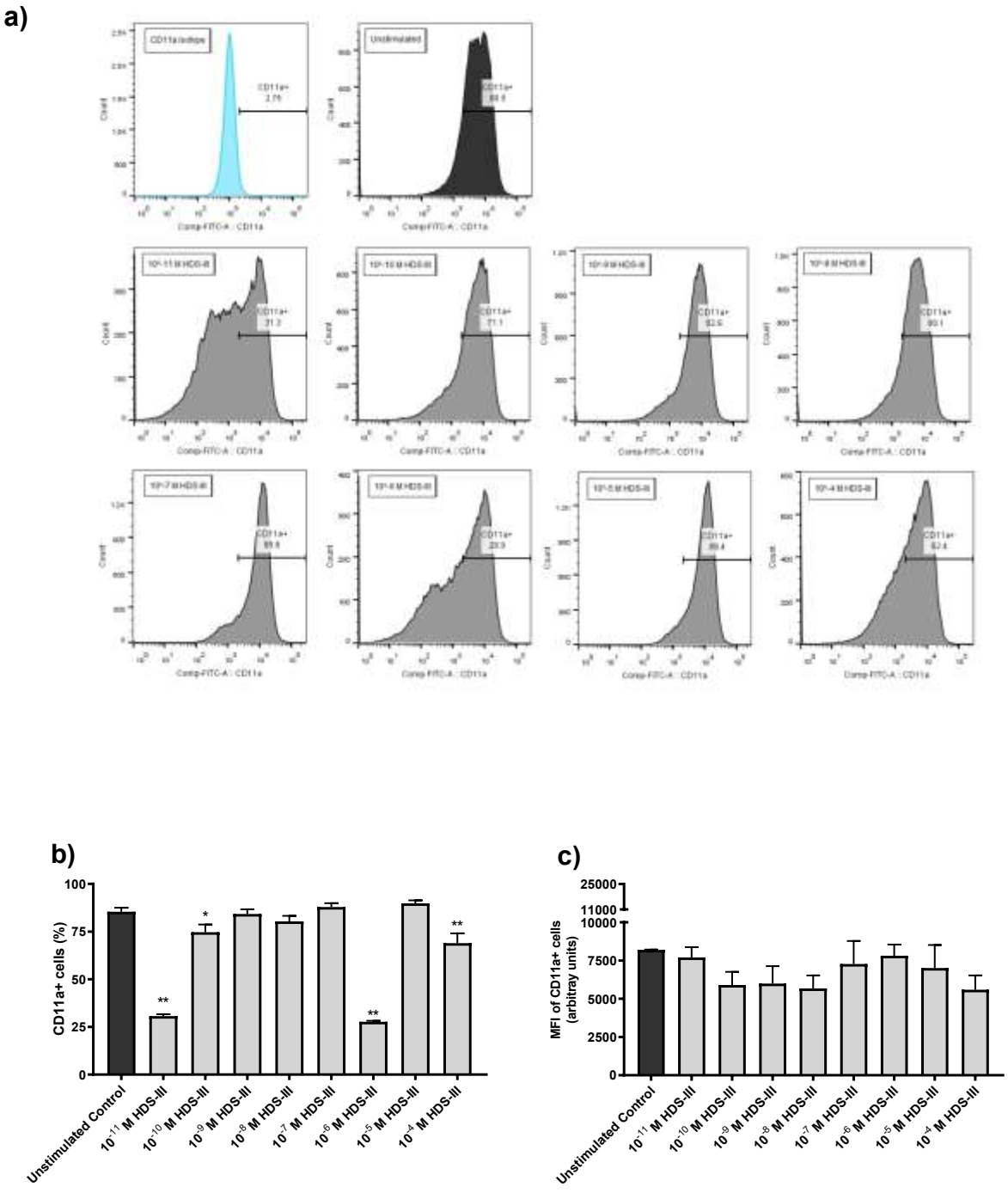


**Appendix Figure 70.** ***The impact of HDS-III on U937 CD11a expression in the absence of PMA.***

*a) Histograms represent the overlays comparison of HDS-III ($10^{-11}$ to $10^{-4}$ M) treated cells at 48 h in the absence of PMA compared to unstimulated control cells against isotype control on CD11a-FITC, channel analysed by flow cytometry . Bar graph represents (b)*

*positive cells and (c) MFI of positive cells. ANOVA with post hoc Dunnett's test, mean ± SEM (n=3), *P<0.05, **p < 0.01 vs unstimulated control.*

**a)**

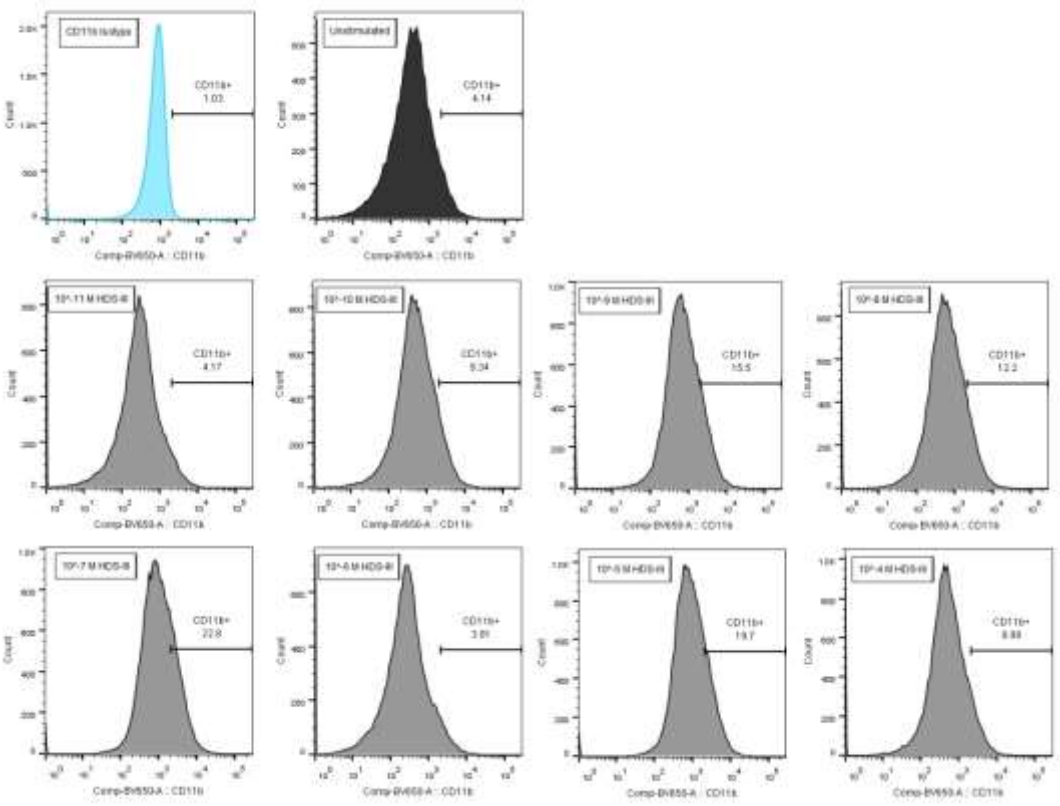

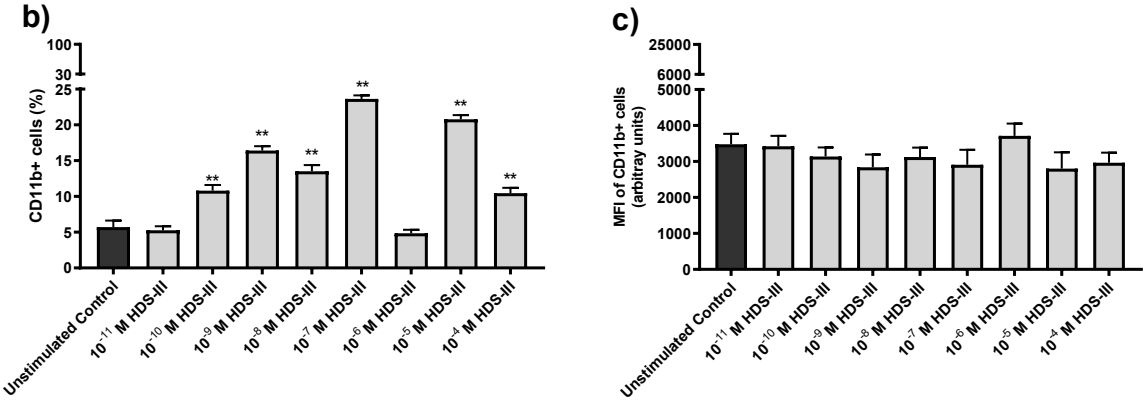


**Appendix Figure 71*. The impact of HDS-III on U937 CD11b expression in the absence of PMA.***

*a) Histograms represent the overlays comparison of HDS-III ($10^{-11}$ to $10^{-4}$ M) treated cells at 48 h in the absence of PMA compared to unstimulated control cells against isotype*

*control on CD11b-BV650 channel analysed by flow cytometry . Bar graphs represents (b) positive cells and (c) MFI of positive cells. ANOVA with post hoc Dunnett's test, mean ± SEM (n=3), **p < 0.01 vs unstimulated control.*

**a)**

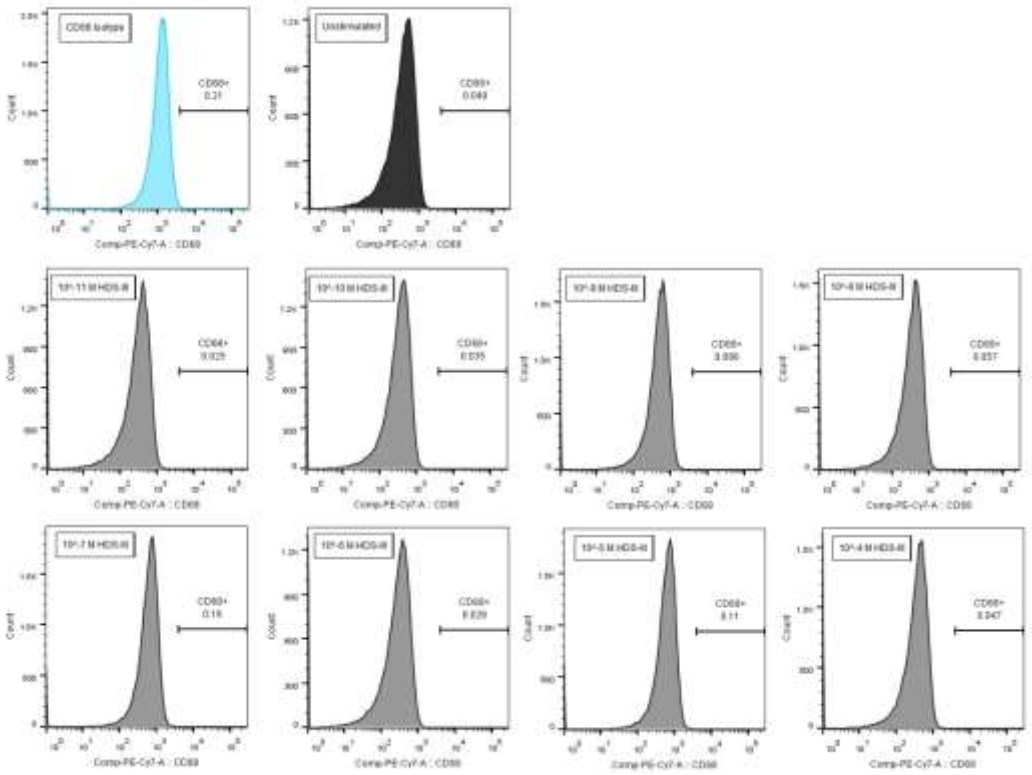

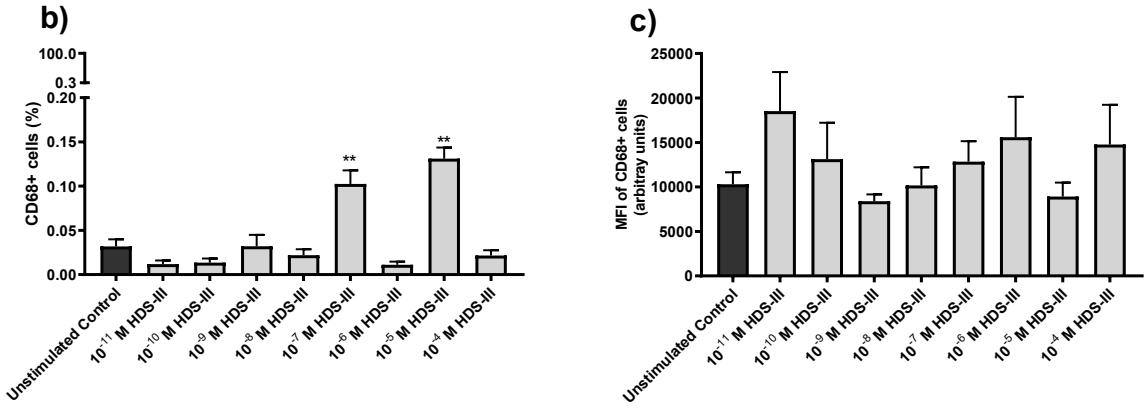


**Appendix Figure 72.** ***The impact of HDS-III on U937 CD68 expression in the absence of PMA.***

*a) Histograms represent the overlays comparison of HDS-III ($10^{-11}$ to $10^{-4}$ M) treated cells at 48 h in the absence of PMA compared to unstimulated control cells against isotype control analysed by flow cytometry . Bar represents graphs (b) positive cells and (c) MFI*

*of positive cells. ANOVA with post hoc Dunnett's test, mean ± SEM (n=3), **p < 0.01 vs unstimulated control.*

HDS-III reduced significantly ( $p < 0.05$, $p < 0.01$) percentage of $CD14^+$ cells (at concentrations $10^{-11}$ M, $10^{-9}$M, $10^{-6}$ M), $10^{-4}$ M, $CD11a^+$ cells (at concentrations $10^{-11}$ M, $10^{-10}$ M, $10^{-6}$ M, $10^{-4}$ M), $CD11b^+$ cells (at concentrations $10^{-10}$ M to $10^{-7}$ M and $10^{-5}$ M to $10^{-4}$ M) and increased percentage of $CD68^+$ cells (at concentrations of $10^{-7}$ M and $10^{-5}$ M). HDS-III at concentrations of $10^{-11}$ M to $10^{-4}$ M had no significant differences in MFI of $CD14^+$, $CD11a^+$, $CD11b^+$ and $CD68^+$ cells in HDS-III-U937 cell cultures compared to unstimulated U937 cells at 48 h. In comparison in THP-1 cultures in the absence of PMA no significant difference was observed for $CD14^+$, $CD11a^+$, $CD11b^+$ and $CD68^+$ cells and their MFI at concentrations of HDS-III ($10^{-11}$ M to $10^{-4}$ M) compared to unstimulated control THP-1 cells.

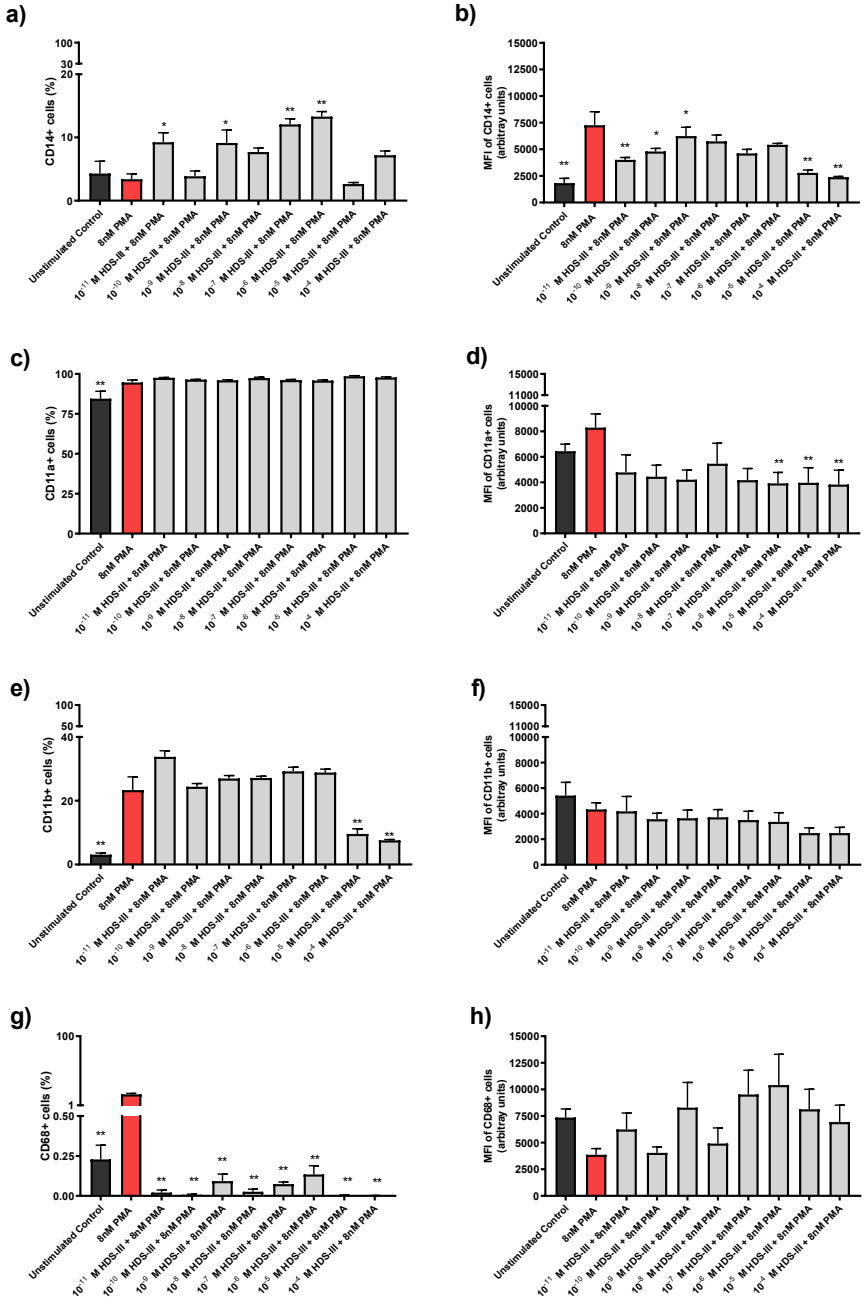


**Appendix Figure 73.** ***The impact of HDS-III on non-adherent U937 cells surface markers expression of HDS-III and PMA cultures.***

*Non-adherent cells from HDS-III ($10^{-11}$ to $10^{-4}$ M) + PMA cultures compared to non-adherent cells from PMA control cells, analysed by flow cytometry . Bar graph represents*

*positive cells (a, c, e, g) MFI of positive cells (b, d, f, h). ANOVA with post hoc Dunnett's test, mean ± SEM (n=3), **p < 0.01 vs PMA.*

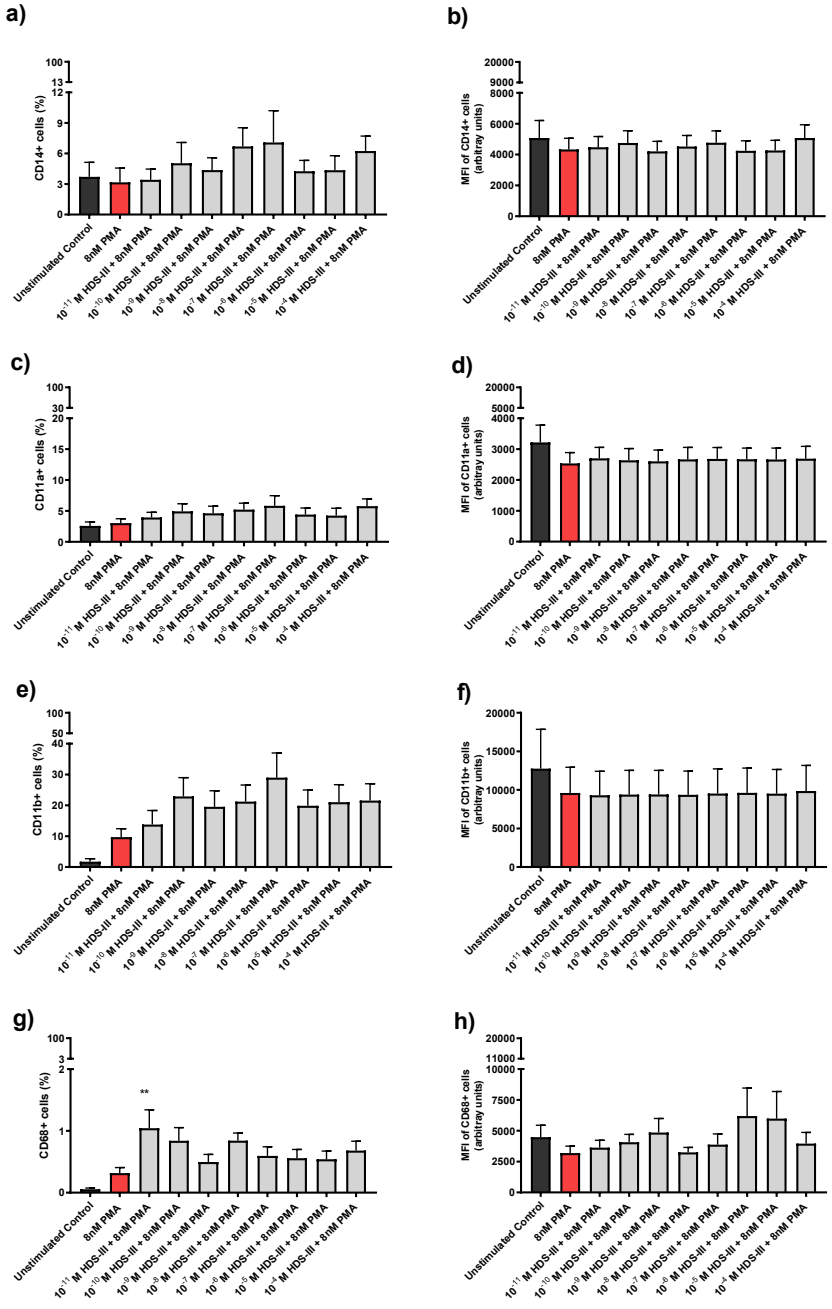


**Appendix Figure 74.** ***The impact of HDS-III on non-adherent THP-1 cells surface markers expression of HDS-III and PMA cultures.***

*Non-adherent cells from HDS-III ($10^{-11}$ to $10^{-4}$ M) + PMA cultures compared to non-adherent cells from PMA control cells analysed by flow cytometry . Bar graph represents*

*positive cells (a, c, e, g) MFI of positive cells (b, d, f, h). ANOVA with post hoc Dunnett's test, mean ± SEM (n=3), **p < 0.01 vs PMA.*

HDS-III at concentrations of $10^{-11}$ M, $10^{-9}$ M, $10^{-7}$ M, $10^{-6}$M reduced the percentage of $CD14^+$ cells significantly ($p < 0.05$, $p < 0.01$) and it reduced CD14 expression at concentrations of $10^{-11}$ M to $10^{-9}$ M, $10^{-5}$M to $10^{-4}$M in HDS-III + PMA non-adherent U937 cultures compared to PMA non-adherent U937 cultures. HDS-III at concentrations of $10^{-11}$ M to $10^{-4}$ M had no significant impact on percentage the expression of CD11a in HDS-III + PMA non-adherent U937 cultures compared to PMA non-adherent U937 cultures. HDS-III reduced percentage of $CD11b^+$cells (at concentrations of $10^{-5}$ M to $10^{-4}$ M) and $CD68^+$ cells (at concentrations of $10^{-11}$ M to $10^{-4}$ M) with no significant difference in their MFI in HDS-III + PMA non-adherentU937 cultures compared to PMA non-adherent U937 cultures. HDS-III at concentrations of $10^{-11}$ M to $10^{-4}$ M exhibited no significant difference for $CD14^+$, $CD11a^+$ and $CD11b^+$ cells and heir degree of expression in HDS-III + PMA THP-1 cultures compared to PMA-THP-1 cultures. The percentage of $CD68^+$ cells was reduced by HDS-III at concentrations of $10^{-5}$ M and $10^{-4}$ M in HDS-III + PMA non-adherent THP-1 cultures but with no significant difference in CD68 expression compared to PMA non-adherent THP-1 cultures.

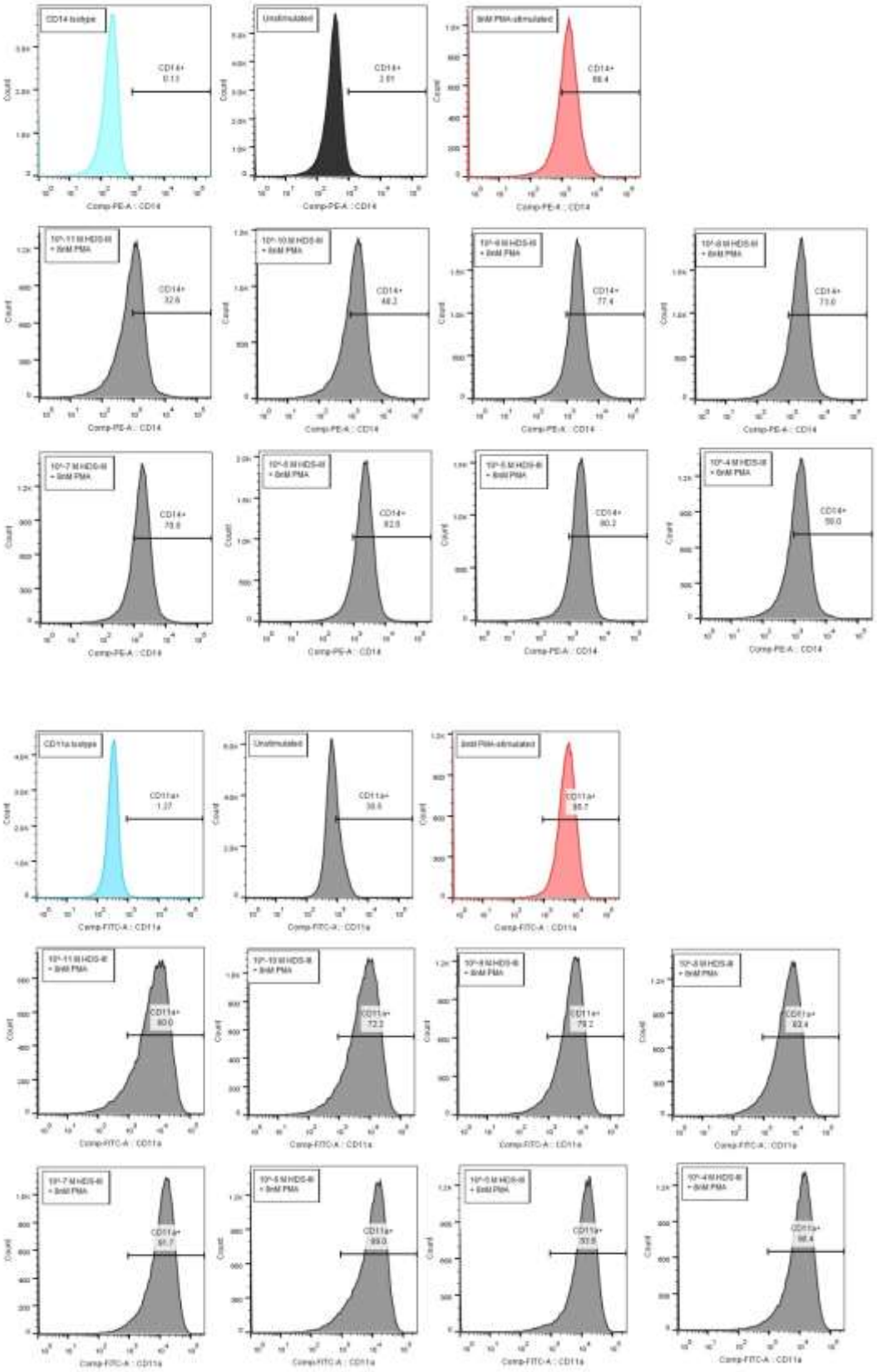

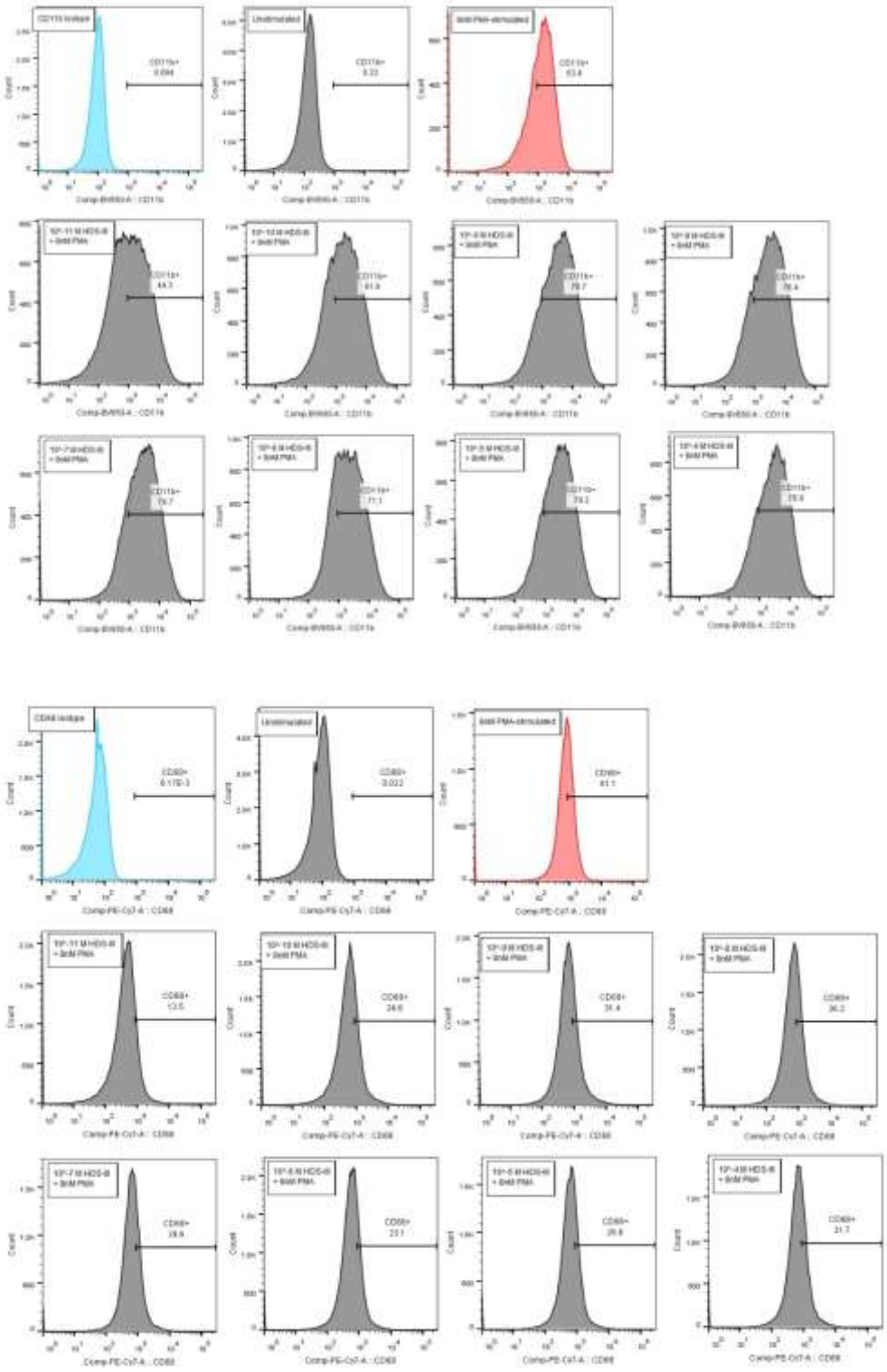

**Appendix Figure 75.** ***The impact of HDS-III on U937 CD14, CD11a, CD11b and CD68 expression in the presence of PMA.***

*Histograms represent the overlays comparison of HDS-III ($10^{-11}$ to $10^{-4}$ M) treated cells at 48 h in the presence of 8 nM PMA (given 2 h before PMA) compared to PMA control cells against isotype control analysed by flow cytometry.*

**a)**

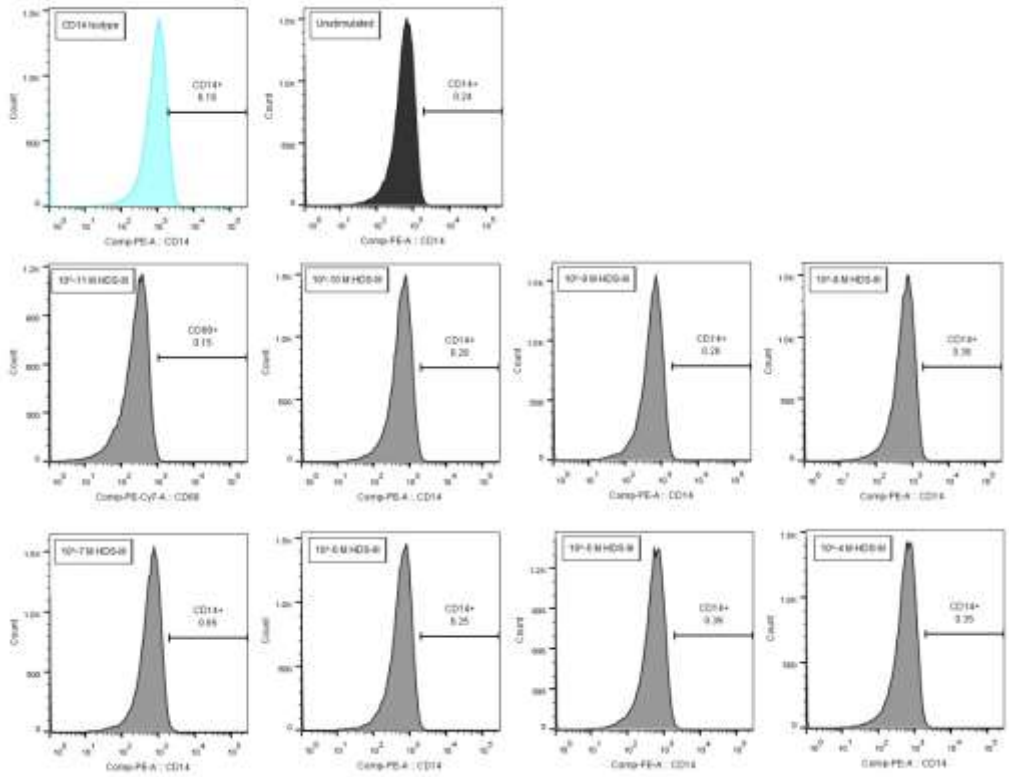

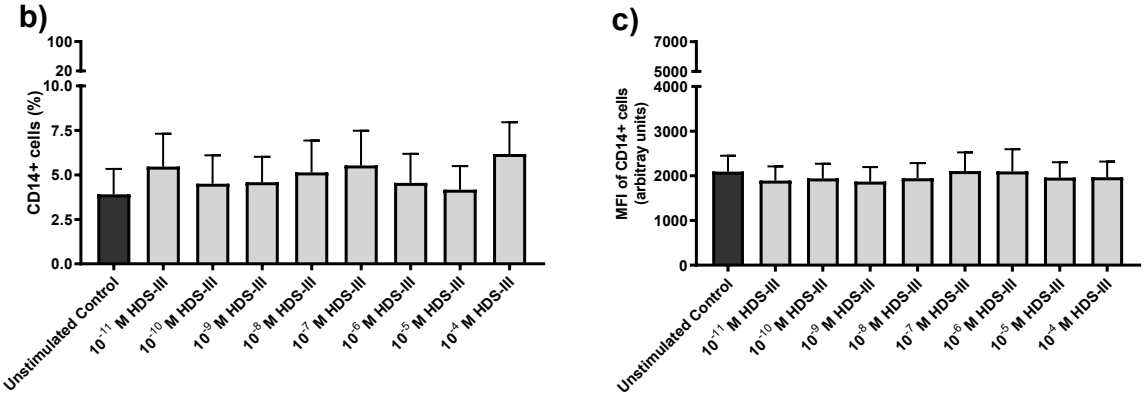


**Appendix Figure 76.** ***The impact of HDS-III on THP-1 CD14 expression in the absence of PMA.***

*a) Histograms represent the overlays comparison of HDS-III ($10^{-11}$ to $10^{-4}$ M) treated cells at 48 h in the absence of PMA compared to unstimulated control cells against isotype control on CD14-PE, channel analysed by flow cytometry . Bar graphs represent (b)*

*positive cells and (c) MFI of positive cells. ANOVA with post hoc Dunnett's test, mean ± SEM (n=3), no significant differences vs unstimulated control.*

**a)**

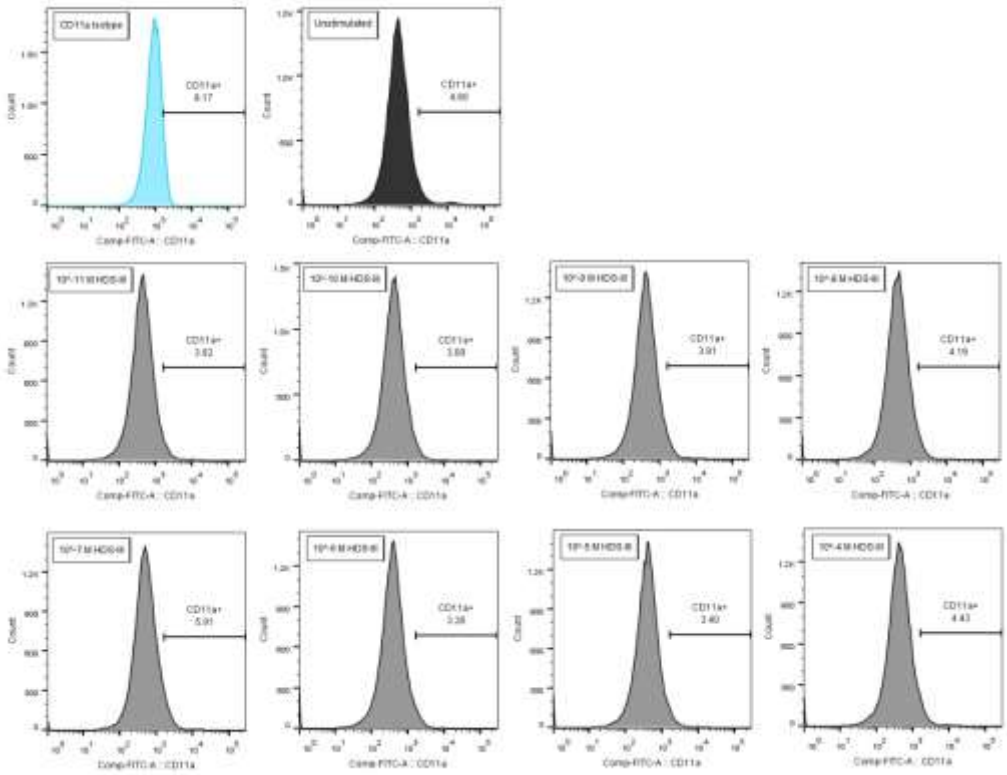

**b)**

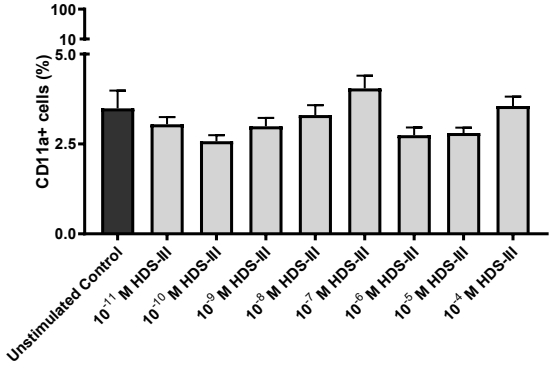


**c)**

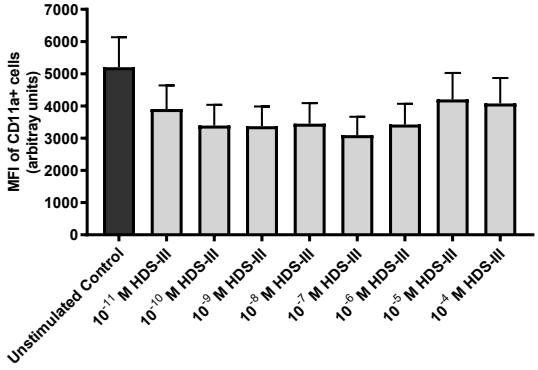


**Appendix Figure 77*. The impact of HDS-III on THP-1 CD11a expression in the absence of PMA.***

*a) Histograms represent the overlays comparison of HDS-III ($10^{-11}$ to $10^{-4}$ M) treated cells at 48 h in the absence of PMA compared to unstimulated control cells against isotype control on CD11a-FITC, channel analysed by flow cytometry . Bar graph represents (b)*

*positive cells and (c) MFI of positive cells. ANOVA with post hoc Dunnett's test, mean ± SEM (n=3), no significant differences vs unstimulated control.*

**a)**

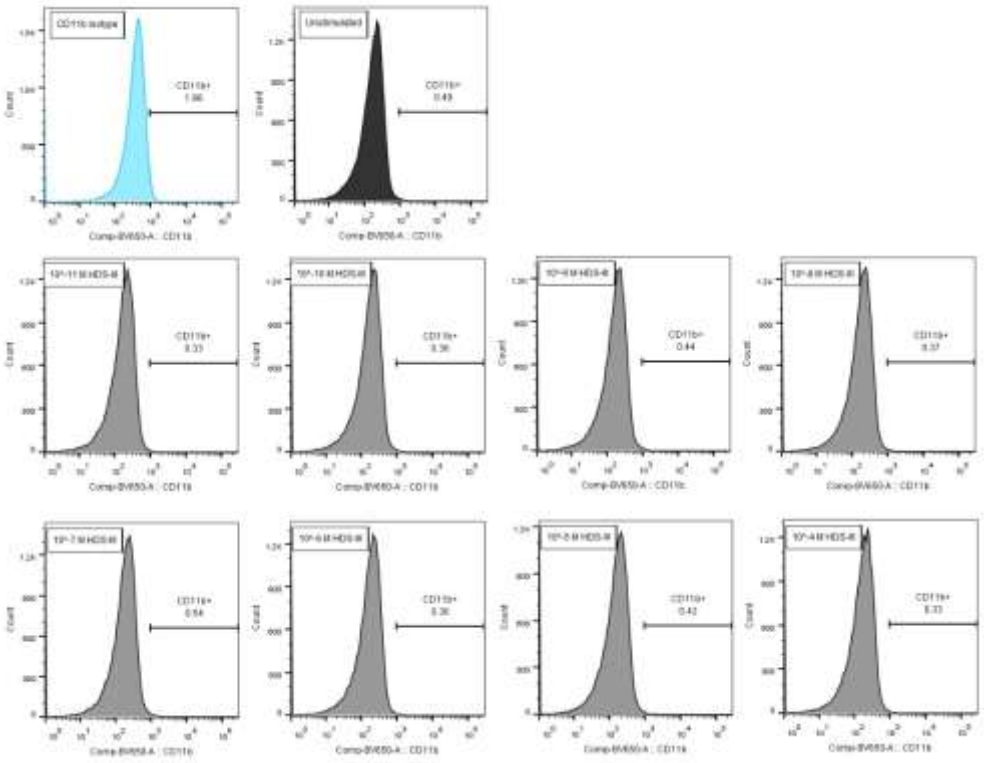

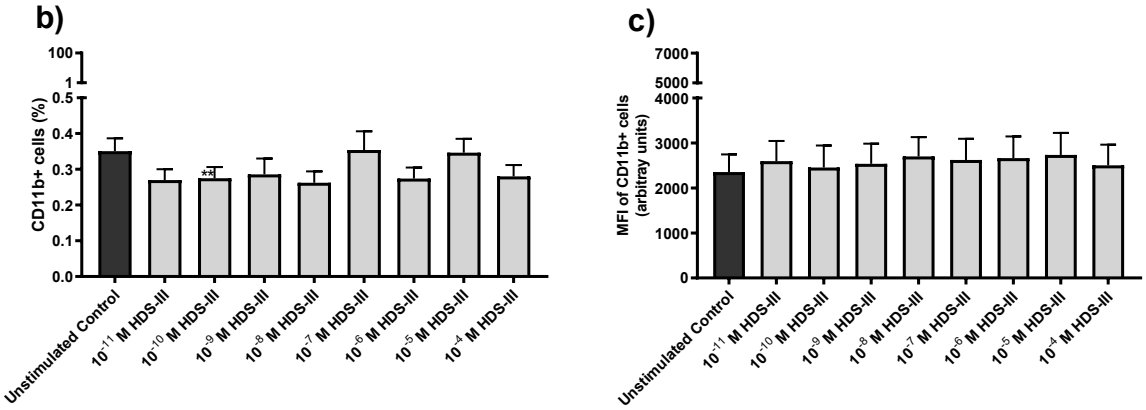


**Appendix Figure 78.** ***The impact of HDS-III on THP-1 CD11b expression in the absence of PMA.***

*a) Histograms represent the overlays comparison of HDS-III ($10^{-11}$ to $10^{-4}$ M) treated cells at 48 h in the absence of PMA compared to unstimulated control cells against isotype control on CD11b-BV650 channel analysed by flow cytometry . Bar graphs represents (b) positive cells and (c) MFI of positive cells. ANOVA with post hoc Dunnett's test, mean ± SEM (n=3), no significant differences vs unstimulated control.*

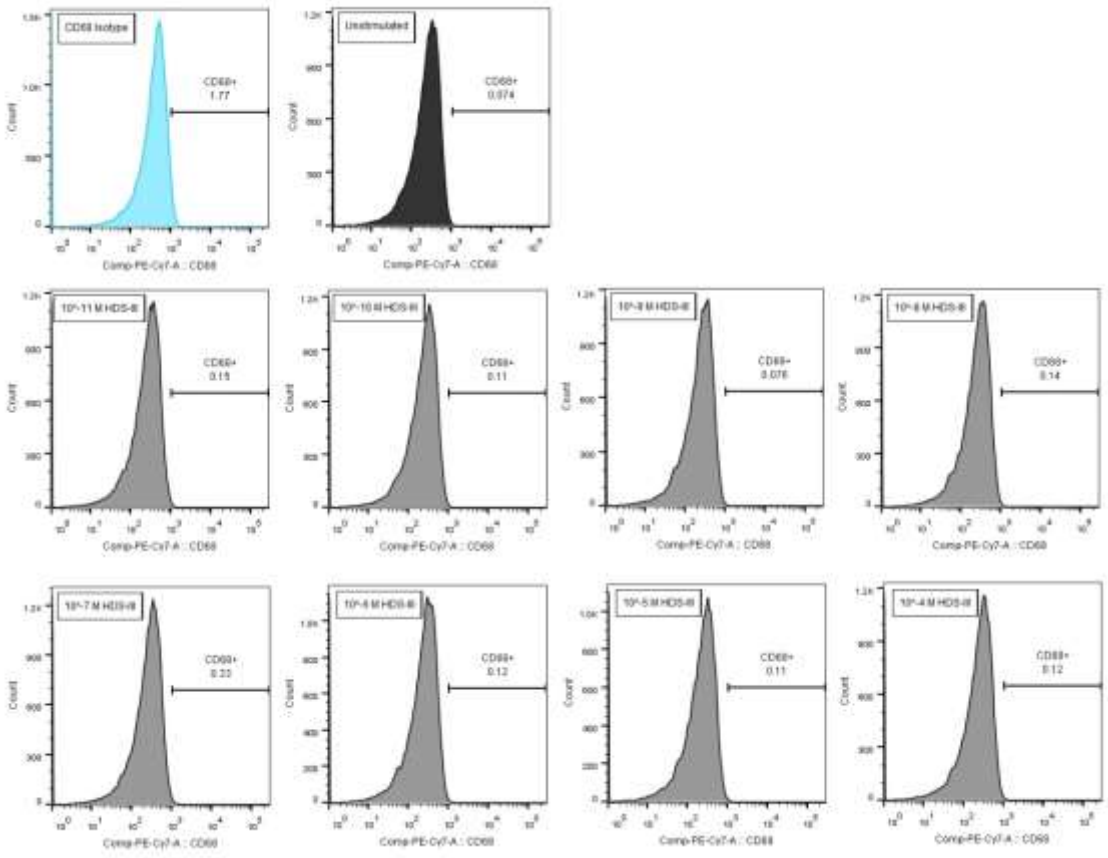

**Appendix Figure 79.** ***The impact of HDS-III on THP-1 CD68 expression in the absence of PMA.***

*Histograms represent the overlays comparison of HDS-III ($10^{-11}$ to $10^{-4}$ M) treated cells at 48 h in the absence of PMA compared to unstimulated control cells against isotype control analysed by flow cytometry . No CD68 positive stained cells found in cultures.*

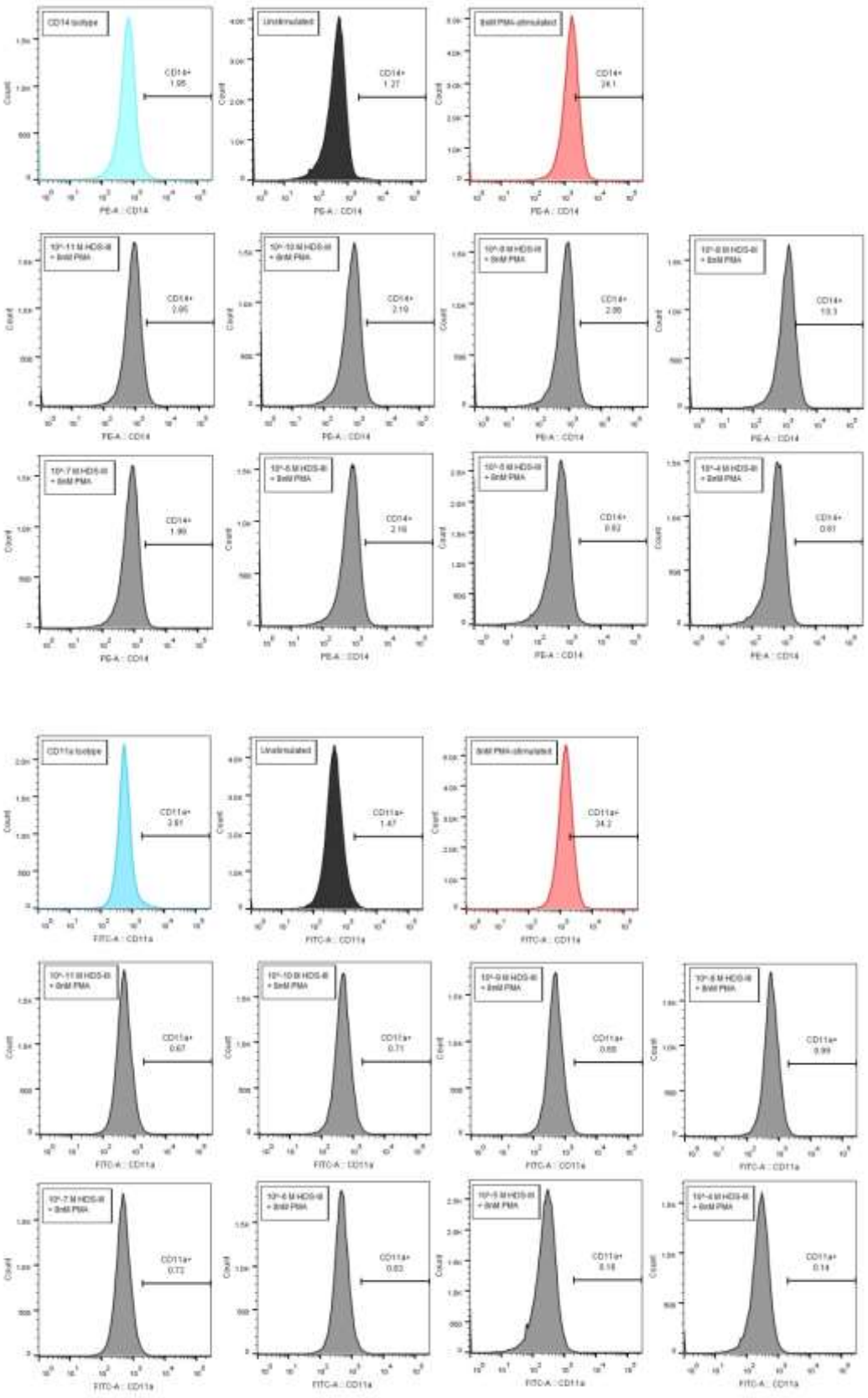

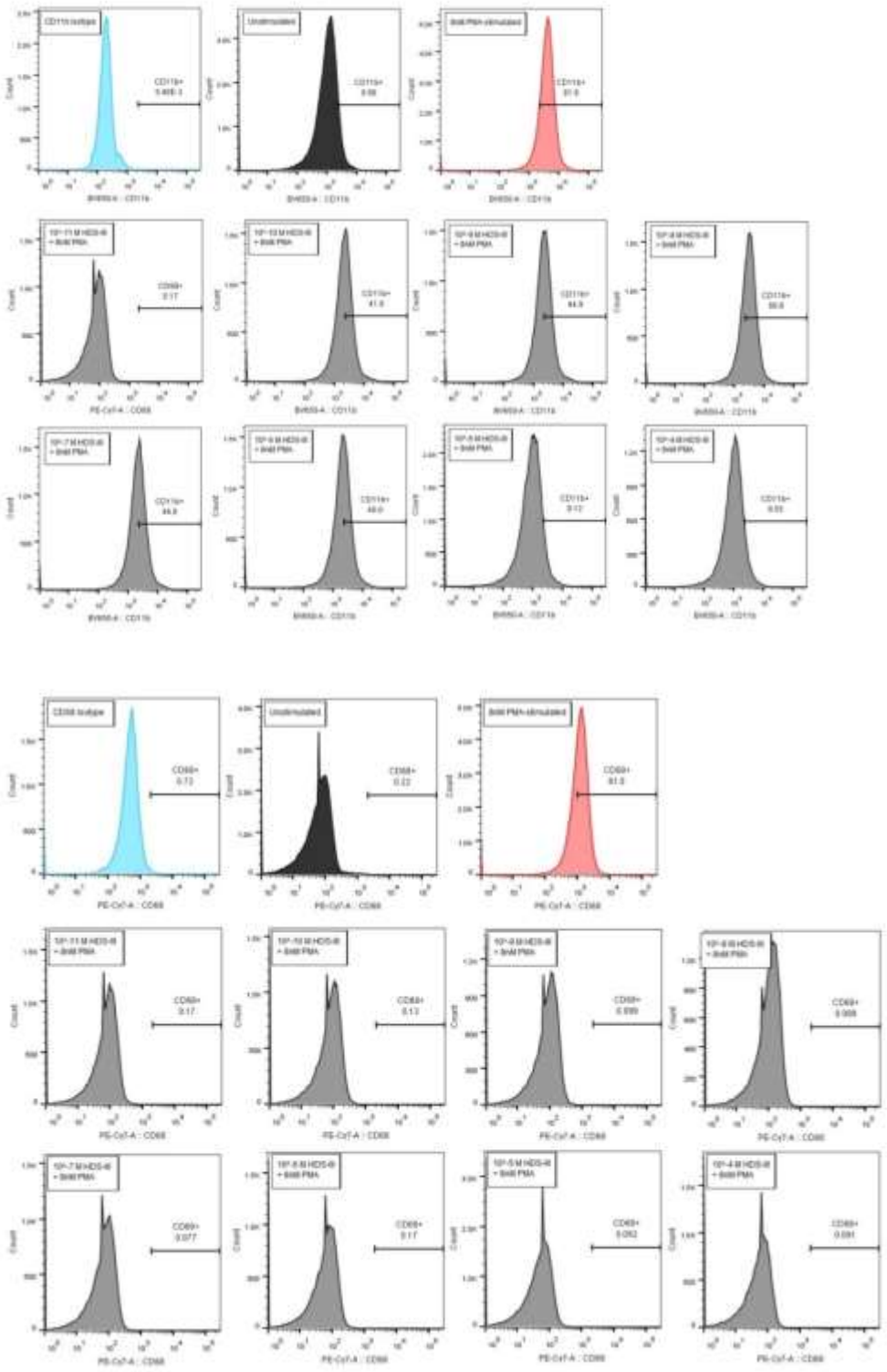

**Appendix Figure 80.** ***The impact of HDS-III on THP-1 CD14, CD11a, CD11b, CD68 expression in the presence of PMA.***

*Histograms represent the overlays comparison of HDS-III ($10^{-11}$ to $10^{-4}$ M) treated cells at 48 h in the presence of 8 nM PMA (given 2 h before PMA) compared to PMA control cells against isotype control analysed by flow cytometry .*

Results indicated that sulphated disaccharides had no significant impact on the expression of CD14, CD11a, CD11b, CD68 positive cells when given in the absence of PMA.

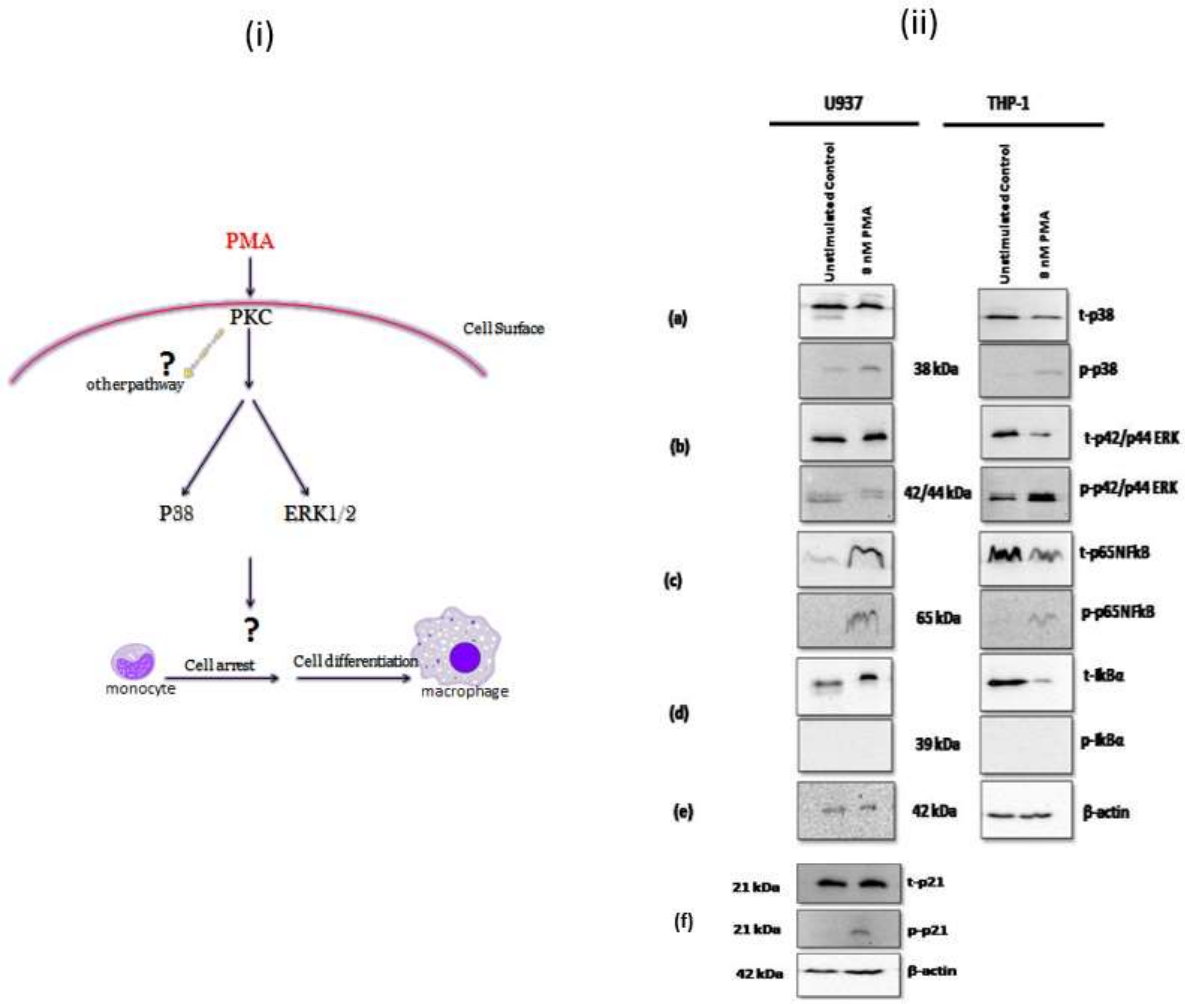


**Appendix Figure 81**. ***(i) A model to study impact of PMA on intracellular signalling pathways during monocyte macrophage differentiation. (ii) PMA induced phosphorylation of p38, p24/p44ERK, p65-NF-kB and p21 $^{WAF1/Cip1}$ in U937 and THP-1 cells.***

*To understand the PMA-induced signalling pathways involved at PKC downstream level and p38/ERK1/2 MAPK downstream level in U937 and THP-1 cells as proposed in (i) was studied by analysing the phosphorylation of p38, ERK1/2 MAPK, IkBα, p65NFkB, p21$^{WAF1/Cip1}$in unstimulated control (10% RPMI-1640 media) U937 and THP-1 cells and 8 nM PMA-stimulated U937 and THP-1 cells at 48 h. The protein lysates were extracted using cell lysis kit and quantified using Bradford assay. Protein was extracted using cell lysis kit. The 20 µg protein of untreated and PMA-treated U937 was separated by SDS-*

*PAGE on 12% gel. Protein was transferred onto nitrocellulose membrane and immunoblotted with total and phospho-rabbit monoclonal primary antibodies (dilution, 1:1000). The nitrocellulose membranes were probed with total protein (t-p38, t-ERK1/2, t-IkBα, t-p65NF-kB, t-p21$^{WAF1/Cip1}$) and phosphorylated (p-p38,p-ERK1/2, p-IkBα, p-p65NF-kB, p- p21$^{WAF1/Cip1}$) antibodies as described in section 2.7. β-actin was used as a control to test the consistency of the sample loading between all wells. Endogenous level of total and phosphorylated p38 MAPK (panel a), p42/p44 ERK MAPK (panel b), p65NF-kB (panel c) was detected at a molecular weight of 38 kDa, 42/44 kDa and 65 kDa respectively in U937 and THP-1 cells. No visible band was detected in p-IkBα, but total IkBα endogenous level was detected at a molecular weight of 39 kDa (panel d). The shape of bands in p65NF-kB could be gel composition but clear activation of p65NF-kB was detected in PMA-treated U937 and THP-1 cells. Endogenous level of (panel f) t-p2 $^{WAF1/Cip1}$ and p-p2 $^{WAF1/Cip1}$ 1 was detected at a molecular weight of 21 kDa, in U937 cells. It was observed that 8nM PMA induced p38 and ERK1/2 MAPK phosphorylation. The phosphorylation level of p38 and ERK1/2 was increased after PMA treatment compared to unstimulated control U937 and THP-1 cells (Fig.2.19a & Fig.2.19b). The phosphorylation of p38 and ERK1/2 in differentiated cells indicated that the activity of p38 MAPK and ERK1/2 MAPK was associated with the monocytic differentiation of U937 and THP-1 cells induced by PMA. One specific band of about 38 kDa in size (Fig.2.19a), corresponding to the size of p38, was detected while two bands of similar size and intensity (~p42 kDa and ~p44 kDa, corresponding to ERK1/2 were detected. p38 and p42/p44 ERK phosphorylation revealed that PMA induced activation of p38 and ERK1/2 at 48 h treatment. In contrast, the total protein of p38 and p42/44 ERK detected using total antibody revealed that PMA did not affect the cellular levels of these proteins (Fig.2.19b). The results suggested that PMA-induced NF-kB phosphorylation at Ser536 in PMA-treated U937 and THP-1 cells, indicating NF-kB degradation from IkBα subunit, followed by nuclear translocation from cytoplasm where it is sequestered in an inactive form by association with inhibitory IkBα. The expression of the phosphorylated form of IkBα (band of about 39 kDa) was not detected (Fig.2.19d); however, p65NFkB expression was phosphorylated in the presence of PMA (Fig.2.19c), indicating that activity of p65NFkB was associated with the differentiation of U937 and THP-1 cells*

*induced by PMA. One specific band of about 65 kDa in size (Fig.2.19c), corresponding to the size of p65NF-kB) was detected while no band of size and intensity (~p39 kDa, corresponding to IkBα was not detected (Fig.2.19d). The Total antibody was used to determine endogenous levels of total p65NF-kB protein and IkBα. In addition as shown in Fig.2.19a, one specific band of about 21 kDa in size (corresponding to the size of p21) was detected in 8 nM PMA treated U937 cells at 48 h, indicating the activity of $p21^{WAF1/Cip1}$ is associated with the monocytic-macrophage differentiation. The total protein of $p21^{WAF1/Cip1}$ was detected using total antibody (Fig.2.19f). Assessment and validation of primary and secondary antibodies - The primary and secondary antibody positive controls were performed to assess and validate their specificity to the target protein of interest. The unstimulated and PMA stimulated samples of U937 cells were subjected to primary antibody for overnight at $4^0C$ or with secondary antibody for 1 hour at room temperature. The primary antibody control for phosphorylated form (p-p38,p-ERK1/2, p-IkBα, p-p65NF-kB, p- $p21^{WAF1/Cip1}$) and total protein (t-p38, t-ERK1/2, t-IkBα, t-p65NF-kB, t-$p21^{WAF1/Cip1}$, β- actin) was performed in the absence of secondary antibody. The secondary antibody control for anti-mouse IgG/HRP antibody and anti-rabbit IgG/HRP antibody was performed in the absence of primary antibody. No protein expression (absence of visible bands) in primary antibodies positive control for phosphorylated form (p-p38,p-ERK1/2, p-IkBα, p- p65NF-kB, p- $p21^{WAF1/Cip1}$) and total protein(t-p38, t-ERK1/2, t-IkBα, t-p65NF-kB, t-$p21^{WAF1/Cip1}$, β- actin) was detected in the absence of secondary antibodies. Similarly, secondary antibodies positive control for anti-mouse IgG/HRP antibody and anti-rabbit IgG/HRP antibody did not recognise the protein in the tested samples of U937 cells in the absence of primary antibody. This resulted in no protein expression in U937 cells. Absence of protein expression confirmed that the secondary antibody's specificity and compatibility to primary antibodies (data not presented).*

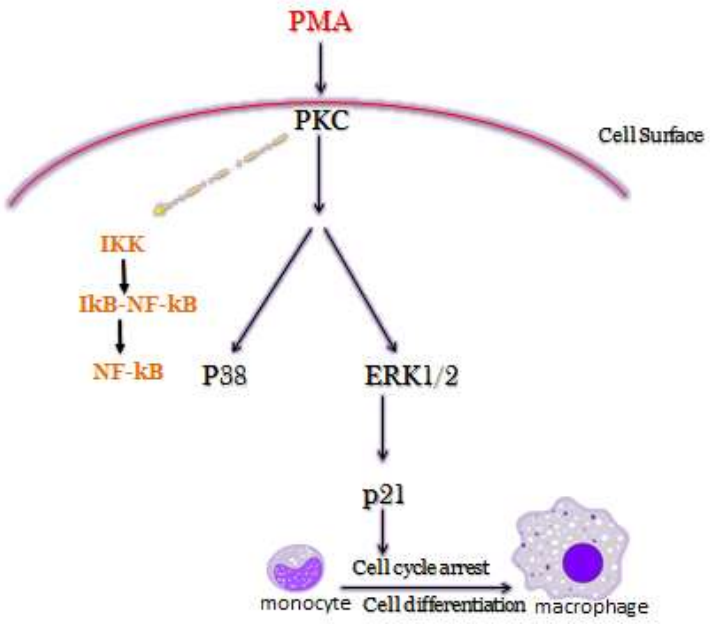


**Appendix Figure 82**. ***Diagram to conclude study 1. p38, ERK1/2 MAPK, p65NFkB and p21WAF1/Cip1 are involved in PMA induced macrophage differentiation and activation.***

*The focus of this study was to explore possible protein signalling pathways involved during macrophage differentiation using U937 and THP-1 cells as a model system. The phosphorylation of p65NFkB and p21$^{WAF1/Cip1}$ in PMA-stimulated cells compared to unstimulated control cells revealed that these proteins are also activated during macrophage differentiation.*

The protein expression analysis of p38, p42/44 ERK, p65NFkB and p21WAF1/Cip1 phosphorylation and de-phosphorylation of IkBα revealed that PMA induced activation of p38, ERK1/2, p65NFkB and p21WAF1/Cip1 at 48 h treatment. The result showed only a marginal increased activation to p-p38, p-p42/44 ERK, p-p65NFkB and p-p21WAF1/Cip1 in PMA -treated U937 and THP-1 cells compared to that of the undifferentiated cells.

The level of p-p38, p-ERK1/2, p-p65NFkB and p- p21WAF1/Cip1 was less intense but showed sustained activation at 48 h. The total protein of p38, p42/44 ERK, IkBα, p65NFkB and p21WAF1/Cip1 was detected using total antibody. The basal level of p38 MAPK, p42/44 ERK, IkBα, p65NFkB and p21WAF1/Cip1 decreased in the PMA-treated THP-1 cells, indicating that p38, p42/44 ERK, p65NFkB and p21WAF1/Cip1 are expressed and activated in PMA-treated cells, which did not affect the cellular levels of p38, p42/44 ERK, IkBα, p65NFkB and p21WAF1/Cip1.

The phosphorylation of ERK1/2 was observed in unstimulated control U937 and THP-1 cells as free ERK1/2 has potential to enter and exit the nucleus of cell in the absence of ERK1/2 pathway activation because of interaction with nuclear pore proteins (Kosako*et al*., 2009 and Whitehurst *et al*., 2002). However, double bands corresponding 42 kDa ERK1/2 and 44 kDa ERK1/2 were observed in PMA-stimulated U937 and THP-1 cells, suggesting that ERK1/2 was fully activated by PMA. ERK1/2 required two phosphorylation events for full activation, the first on a tyrosine residue and second on a proximal threonine residue. But it can also act either as a single switch via rapid double phosphorylation or can act via mono-phosphorylation (Boulton *et al*., 1991; Huang and Ferrell, 1996; Robbins and Cobb, 1992).

The results demonstrate that the mechanism through which U937 and THP-1 cells respond to PMA treatment, which involves cell cycle arrest at the G1-phase by up-regulation of p21W$^{AF1/Cip1}$ in the cells.

a)

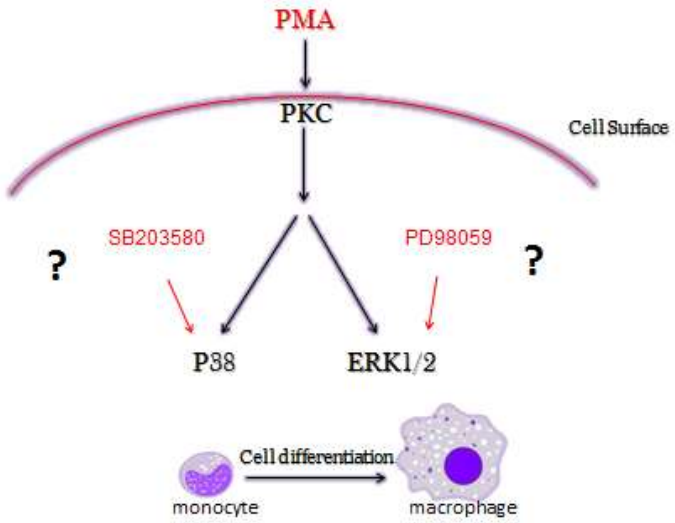


b)

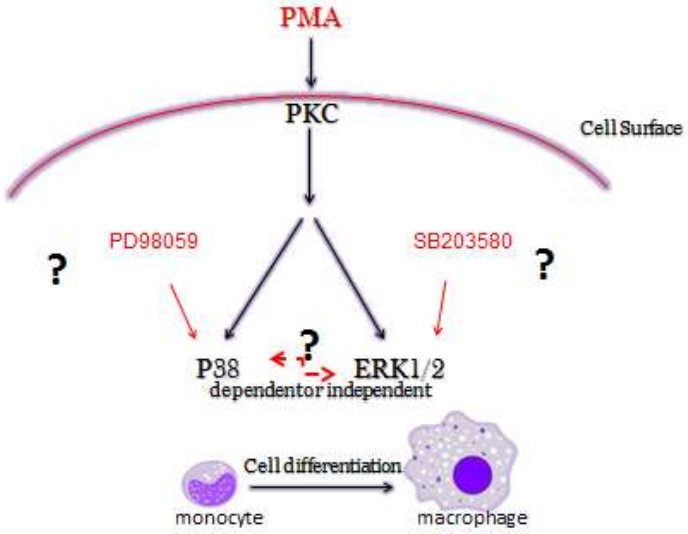


**Appendix Figure 83*. Experimental model to study SB203580 and PD98059 impact on p38 and ERK1/2 signalling in PMA induced U937 cells.***

*After 48 h, the protein lysates were extracted using the cell lysis kit followed by protein quantification using the Bradford assay. Protein (20 µg/lane) was electrophoresed on 12% SDS/PAGE gels and transferred to nitrocellulose membranes to probe with specific antibodies. β-actin was used as a control to test the uniformity of the sample loading between all wells. In the first experimental protocol (a), the nitrocellulose membranes of SB203580 treated samples were probed with t-p38, p-p38antibodies and PD98059 treated samples were probed with t-ERK1/2, p-ERK1/2 antibodies to study the specificity of these inhibitors to inhibit p38 and ERK1/2 MAPK activation and thus to confirm*

*inhibition of PMA-induced cell differentiation. In the second experimental protocol (b), the nitrocellulose membranes of SB203580 treated samples were probed with t-ERK1/2, p-ERK1/2 antibodies and PD98059 treated samples were probed with t-p38, p-p38 antibodies to study the cross-talk relationship between p38 and ERK1/2 MAPK in PMA-induced cell differentiation. Taken together, the study results indicated that the p38 inhibitor SB203580 increased the phosphorylation of ERK1/2, and ERK1/2 inhibitor PD98059 increased the phosphorylation of p38. Therefore, p38 and ERK1/2 MAPK signalling pathways have a cross-talk relationship meaning activated p38 pathway can activate ERK1/2 similarly, activated ERK1/2 pathway can activate p38 pathway for monocyte-macrophage differentiation.*

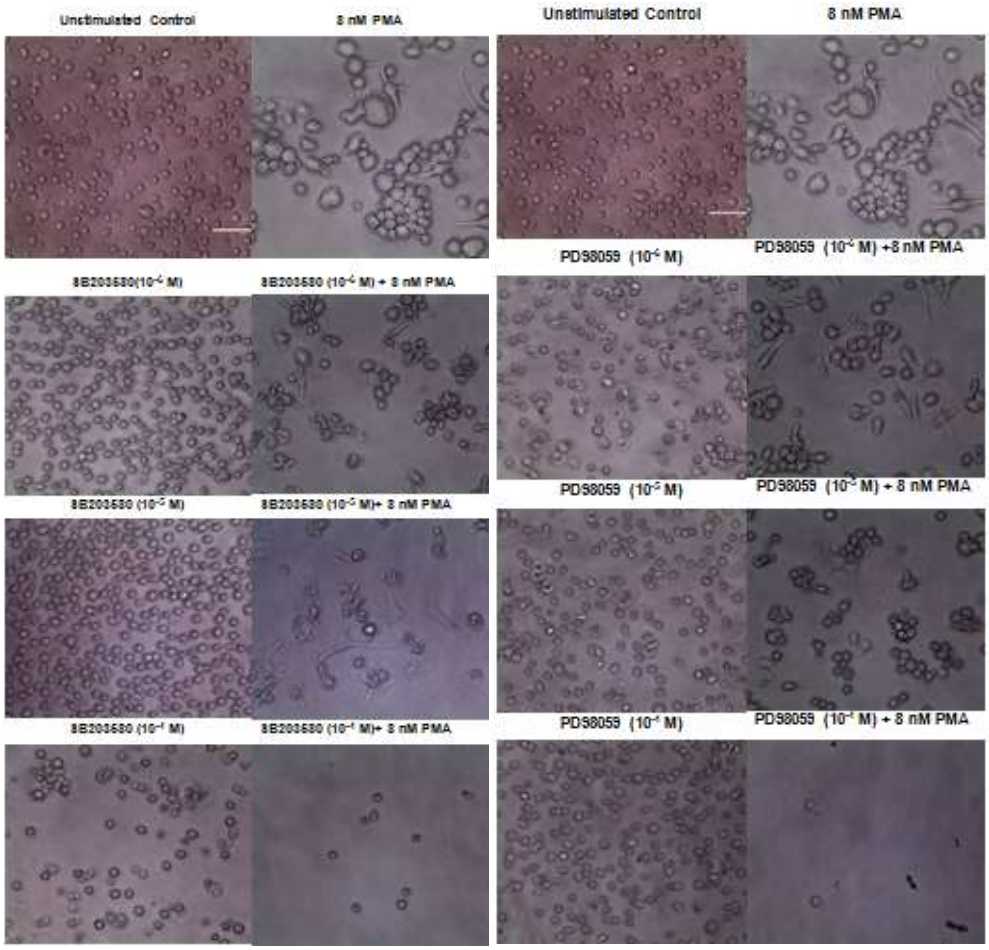


**Appendix Figure 84**. ***The impact of SB203580 and PD98059 on U937 cell morphology in the absence and presence of PMA.***

*As demonstrated in chapter 3 it has been established that PMA can lead to the activation of p38 and ERK1/2 MAPK signalling pathways. To further determine the importance of p38 and ERK1/2 in U937 cell differentiation, the U937 cells were incubated in 10% RPMI-1640 media and stimulated with 8 nM PMA in the presence and absence of the p38 specific inhibitor SB203580 and ERK1/2 MAPK specific inhibitor PD98059 at concentrations of $10^{-6}$ M, $10^{-5}$M and $10^{-4}$M for 48 h in 24-well plates. The cellular morphology of U937 cells was observed at 48. The adherence of PMA-treated U937 cells was inhibited in the presence of SB203580 and PD98059 demonstrating inhibition of PMA-induced cell-differentiation. Representative image of three independent experiments of U937 cells treated with SB203580 and PD98059 for 48 h in the absence and presence of 8 nM PMA to study their impact on cell morphology and analysed by*

*inverted phase-contrast microscope with original magnification power of 40x. Scale 100µm. SB203580 and PD98059 inhibited PMA induced cell differentiation of U937 cells at 48 h.*

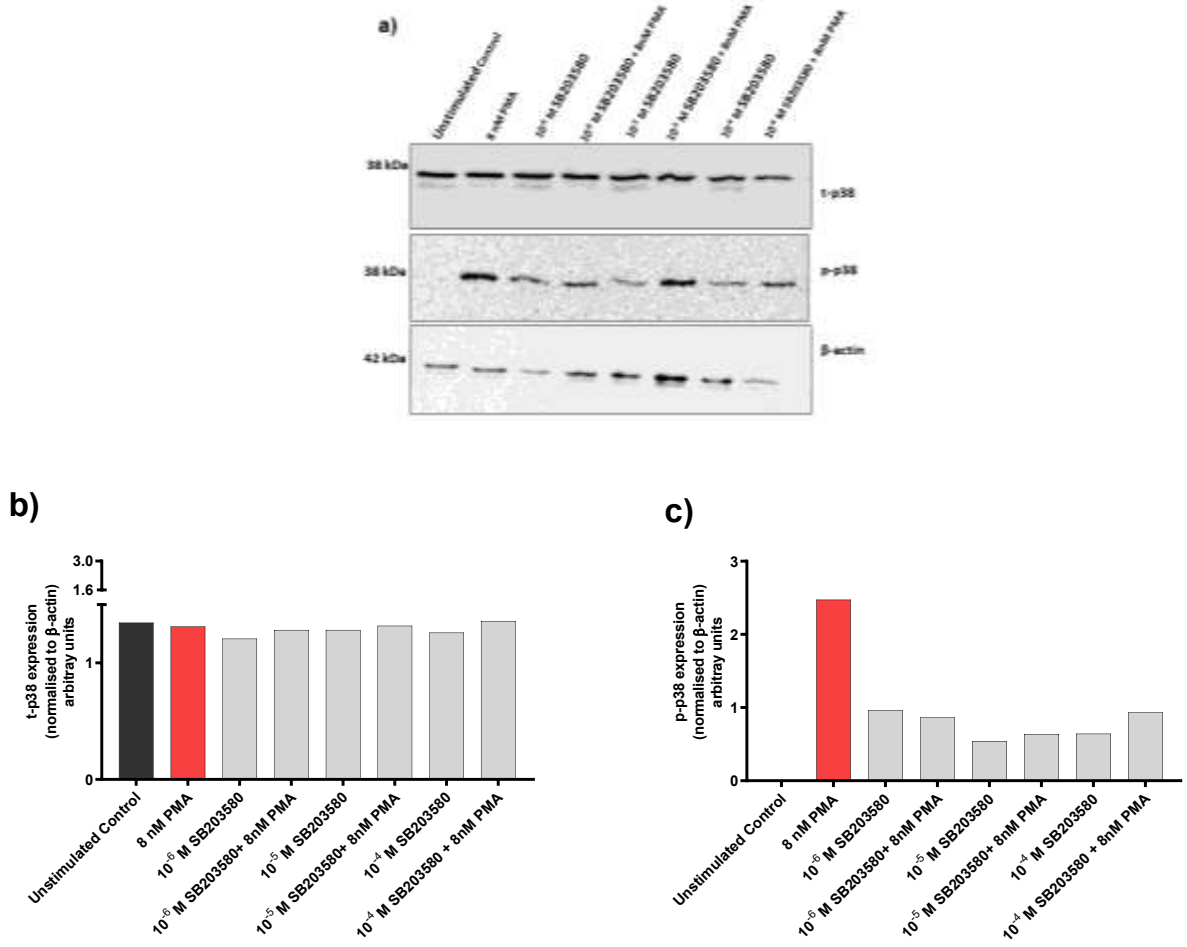


**Appendix Figure 85**. ***SB205380 impact on p38 expression.***

*Expression and phosphorylation of p38 in U937 cells in control unstimulated and PMA (8nM, 48 hours) stimulated cells with and without p38 inhibition with SB205380 ($10^{-6}$ M, $10^{-5}$ M, $10^{-4}$ M). (a), Western blots showing total p38 (t-p38), phosphorylated p38 (p-p38) and β-actin. The observation of the visible bands of 38 kDa in PMA-stimulated U937 cells suggested activation and phosphorylation of p38 at 48 h compared to unstimulated control cells. Treatment of U937 cells with SB203580 inhibited PMA-induced p38 phosphorylation in a concentration-dependent manner. (b, c) Densitometric results controlled for β-actin for t-p38 and p-p38 respectively.*

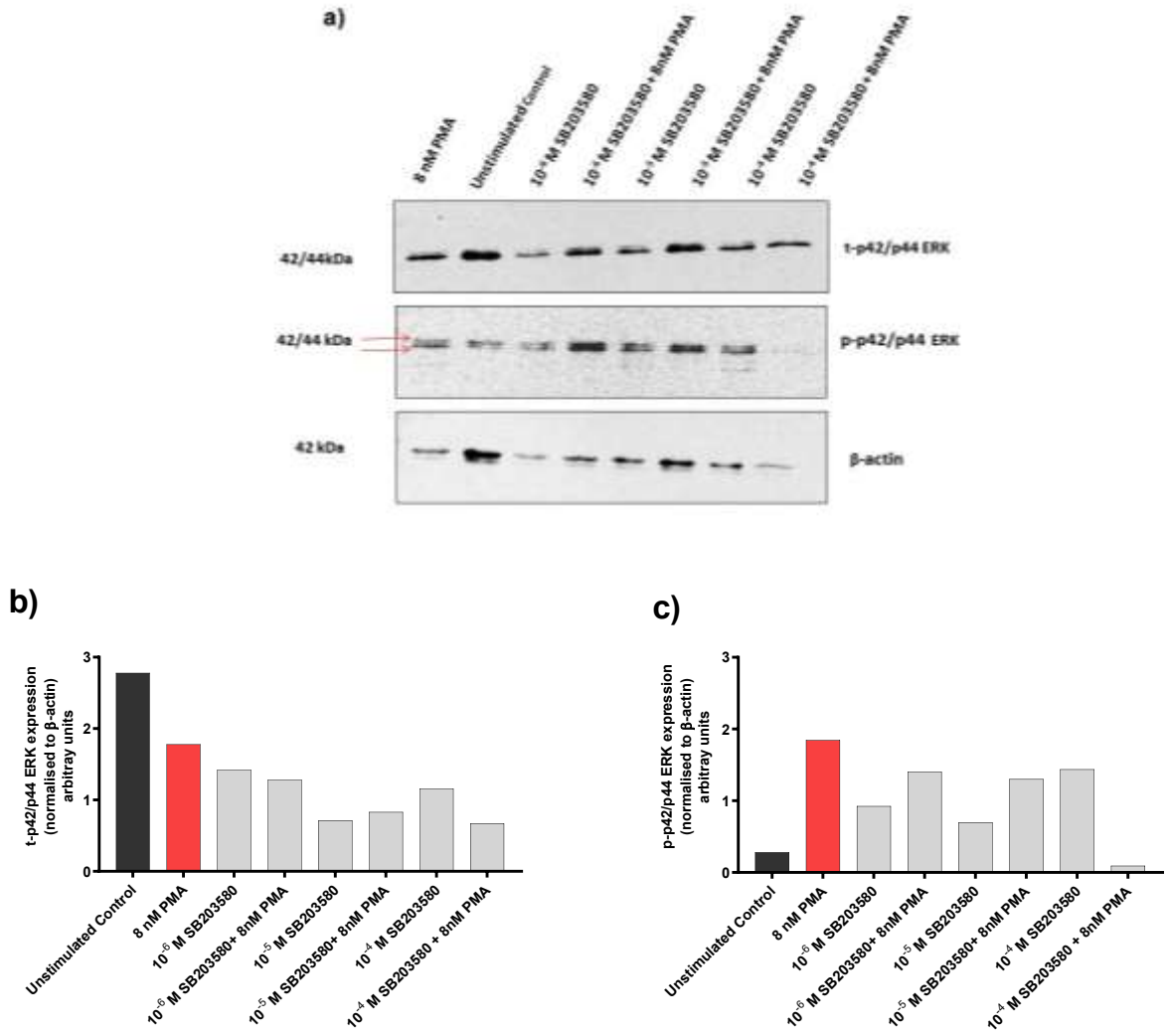


**Appendix Figure 86.** ***SB205380 impact on ERK1/2 expression.***

*Expression and phosphorylation of ERK1/2 in U937 cells in control unstimulated and PMA (8nM, 48 hours) stimulated cells with and without p38 inhibition with SB205380 ($10^{-6}$ M, $10^{-5}$ M, $10^{-4}$ M). (a), Western blots showing total ERK1/2 (t-p42/p44 ERK), phosphorylated ERK1/2 (p-t-p42/p44 ERK) and β-actin. PMA-induced phosphorylation of ERK1/2 was up-regulated by SB203580. The decrease in ERK1/2 phosphorylation was observed at SB203580 $10^{-4}$ M. On the other hand, the phosphorylation of ERK1/2 MAPK was increased in PMA-stimulated U937 cells compared to unstimulated control cells at 48 h. (b, c) Densitometric results controlled for β-actin for t-p42/p44 ERK and t-p42/p44 ERK respectively.*

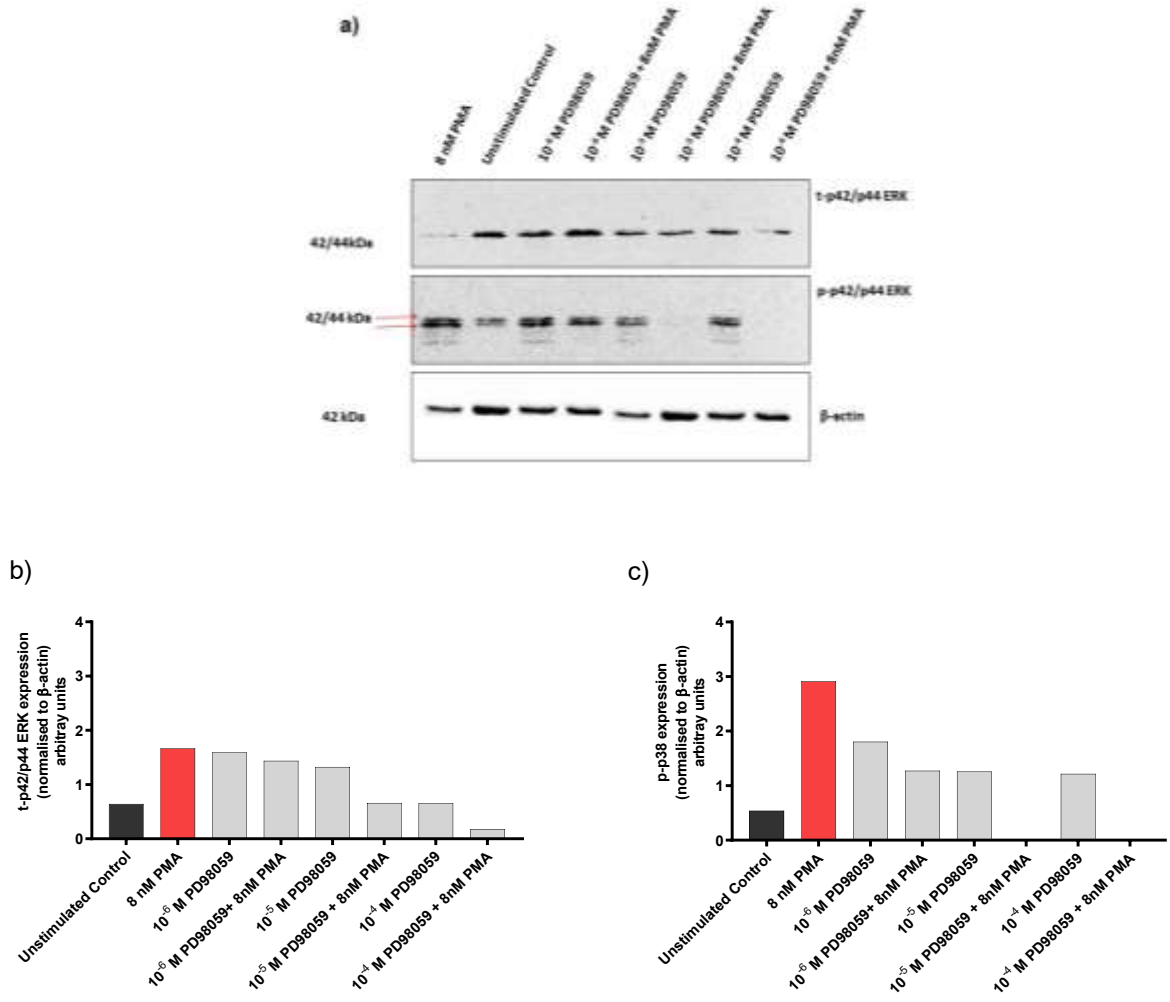


**Appendix Figure 87*. PD98059 impact on ERK1/2 MAPK expression.***

*Expression and phosphorylation of ERK1/2 in U937 cells in control unstimulated and PMA (8nM, 48 hours) stimulated cells with and without ERK1/2 inhibition with PD98059 ($10^{-6}$ M, $10^{-5}$ M, $10^{-4}$ M). (a), Western blots showing total ERK1/2 (t-ERK1/2), phosphorylated ERK1/2 (p-ERK1/2) and β-actin. PD98059 significantly inhibited PMA-induced phosphorylation of ERK1/2 MAPK in U937 cells in a concentration-dependent manner at 48 h. Total inhibition of 8 nM PMA-induced ERK1/2 MAPK phosphorylation was observed at $10^{-5}$ M PD98059 and $10^{-4}$ M PD98059. (b, c) Densitometric results controlled for β-actin for t-ERK1/2 and p-ERK1/2 respectively.*

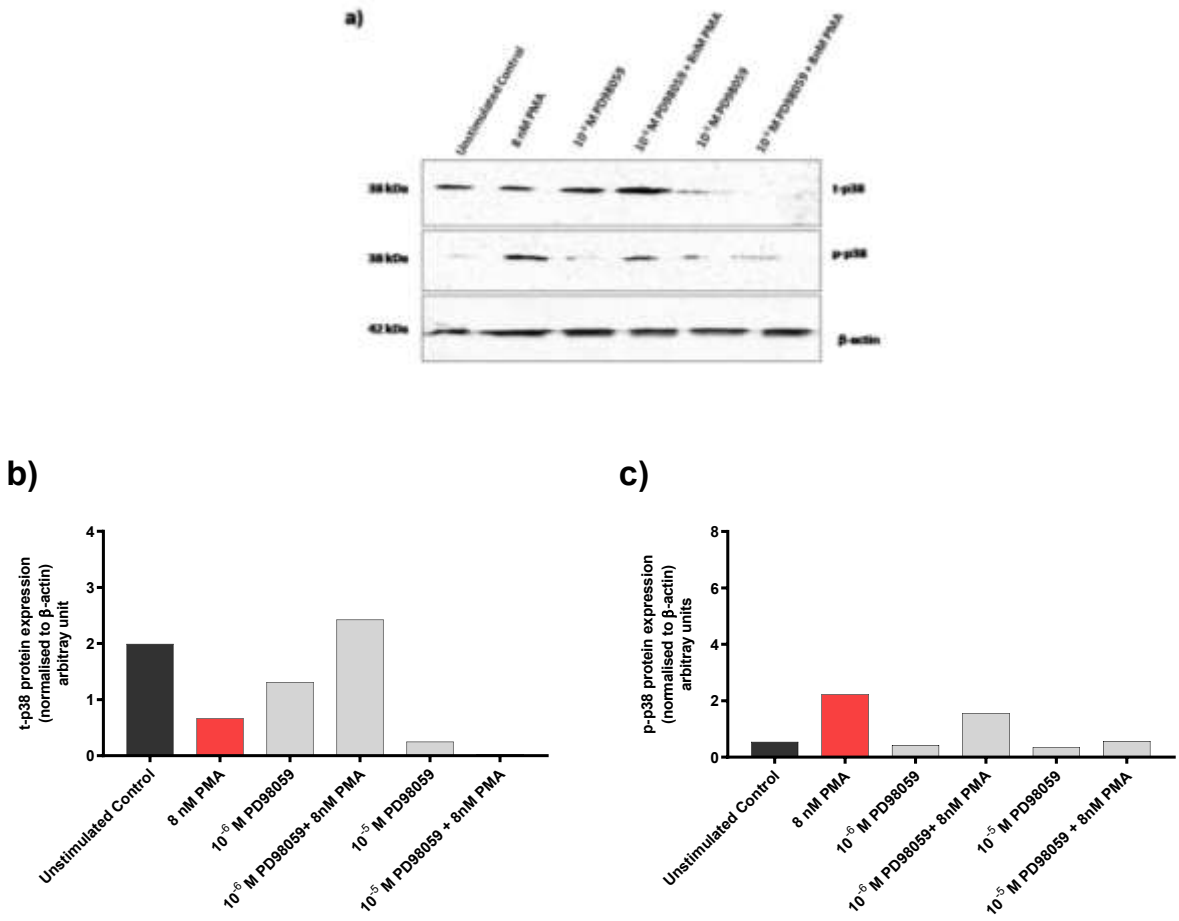


**Appendix Figure 88.** ***PD98059 impact on p38.***

*Expression and phosphorylation of p38 in U937 cells in control unstimulated and PMA (8nM, 48 hours) stimulated cells with and without ERK1/2 inhibition with PD98059 ($10^{-6}$ M, $10^{-5}$ M). (a), Western blots showing total p38 (t-p38), phosphorylated p38 (p-p38) and β-actin. The phosphorylation of p38 was up-regulated in the presence of PD98059in a concentration dependent manner. (b, c) Densitometric results controlled for β-actin for t-p38 and p-p38 respectively.*

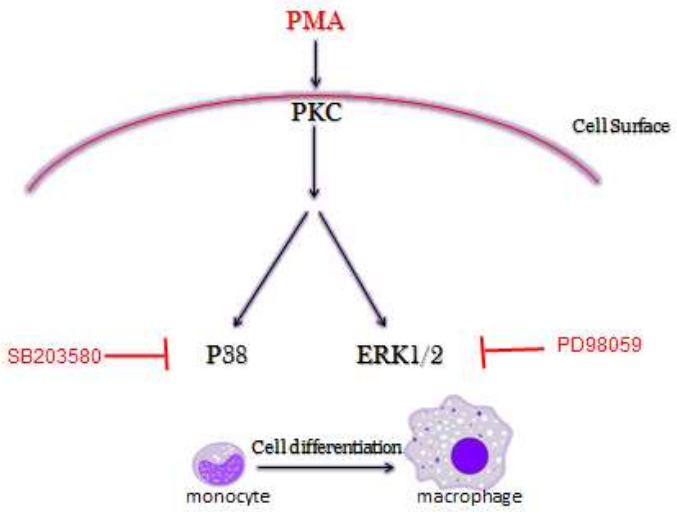


**Appendix Figure 89**. ***Diagram to conclude study a). p38 and ERK1/2 MAPK signalling is inhibited by using SB203580 and PD98059 in PMA-induced U937 cells.***

*To examine the importance of the p38 and ERK1/2 MAP kinase pathways in PMA-induced monocyte differentiation the low molecular weight potent and specific inhibitors SB203580 for the blockage of p38 and PD98059 for the blockage of ERK1/2 MAPK pathways activation were used in a concentration-dependent manner. Western blot analysis revealed that PMA-induced phosphorylation level of p38 and ERK1/2 was significantly inhibited after the blockage of p38 and ERK1/2 using SB203580 and PD98059, respectively. Taken together, it can be strongly suggested that p38 and ERK1/2 MAPK play an important role in monocyte-macrophage differentiation as inhibition of these pathways by selective inhibitors inhibits cell differentiation.*

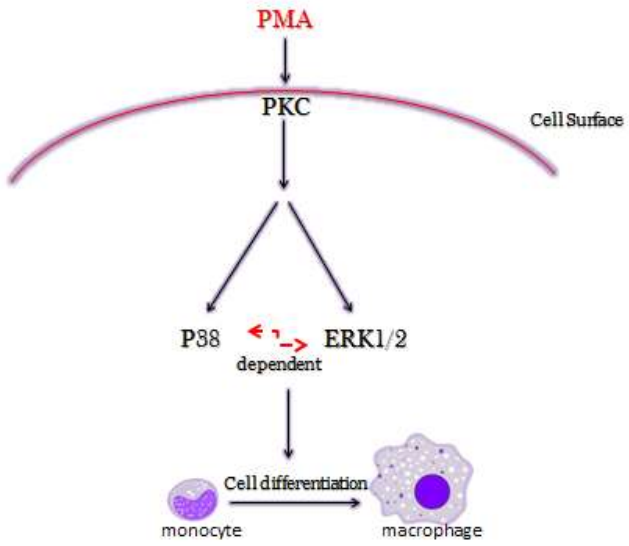


**Appendix Figure 90**. ***Diagram to conclude study b). p38 and ERK1/2 MAPK cross-talk to induce monocyte-macrophage differentiation.***

*In this study, the impact of p38 and ERK1/2 inhibition on the PMA-induced cell differentiation of U937 cells was investigated using Western blot analysis. The expression of p38 and ERK1/2 was significantly increased in the presence of PMA, whereas the p38 inhibitor SB203580 inhibited PMA-induced p38 expression and increased PMA-induced ERK1/2 expression. Similarly, PD98059 inhibited PMA-induced ERK1/2 expression and increased PMA-induced p38 expression. The results suggest that there is a possibility that SB203580 and PD98059 act through a positive feedback mechanism on ERK1/2 and p38 pathways respectively. Others have reported similar results (Shimo et al., 2007 and New et al., 2001). The results of this study revealed that p38 and ERK1/2 signalling pathways are dependent on each other and balanced p38 and ERK1/2 MAPK signalling pathways are required for PMA-induced U937 cell-differentiation.*

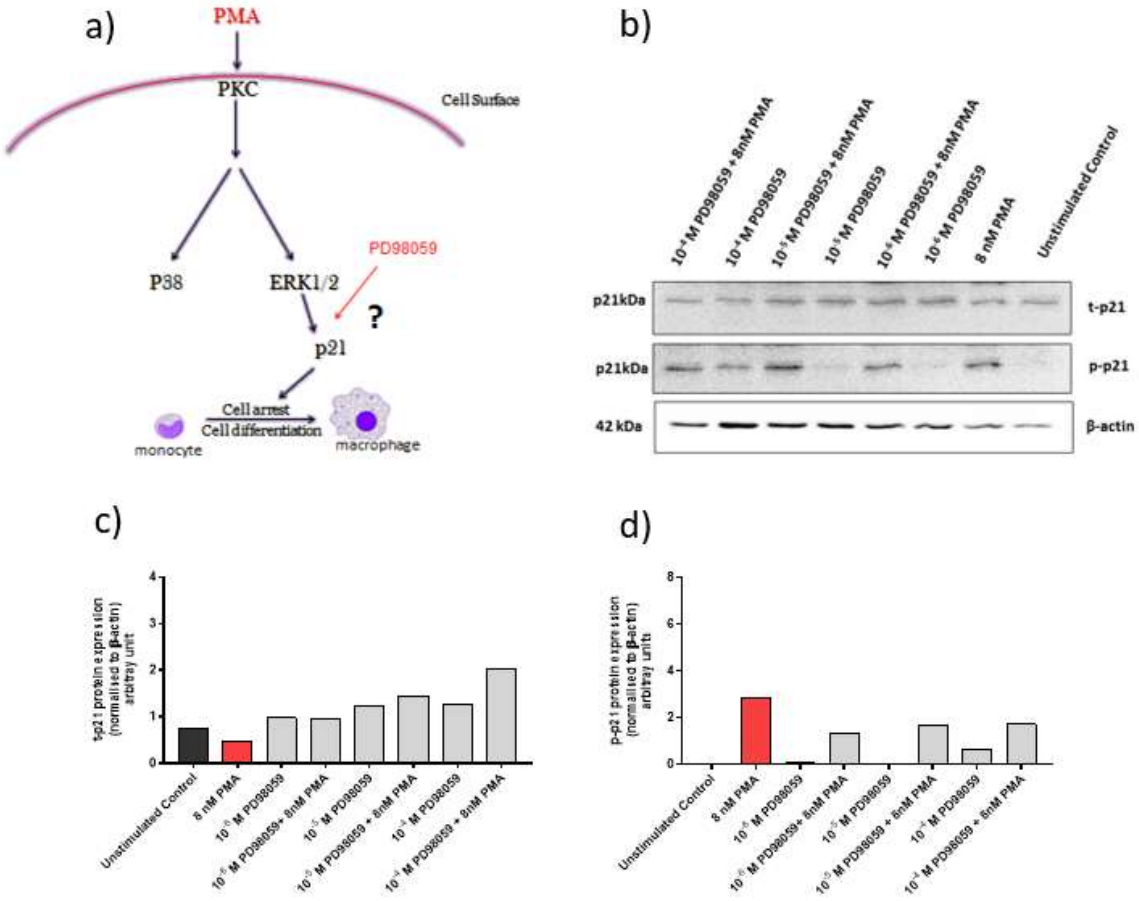


**Appendix Figure 91**. ***PD98059 impact on p21 $^{WAF1/Cip1}$ expression. (a) A model to investigate PD98059 impact on p21 expression in U937 cells***.

*In this study, the impact of ERK1/2 inhibitor PD98059 at concentrations of $10^{-6}$ M, $10^{-5}$ and $10^{-4}$ M on the PMA-induced p21$^{WAF1/Cip1}$ phosphorylation in U937 cells at 48 h was investigated in the absence and presence of PMA. The nitrocellulose membranes of PD98059 treated samples in the presence and absence of PMA were probed with t-p21$^{WAF1/Cip1}$ and p-p21$^{WAF1/Cip1}$ antibodies. Expression and phosphorylation of p21$^{WAF1/Cip1}$ in U937 cells in control unstimulated and PMA (8nM, 48 hours) stimulated cells with and without ERK1/2 inhibition with PD98059 ($10^{-6}$ M, $10^{-5}$ M, $10^{-4}$ M). (b), Western blots showing total p21$^{WAF1/Cip1}$ (t-p21), phosphorylated p21$^{WAF1/Cip1}$ (p-p21) and β-actin. PMA-induced p21$^{WAF1/Cip1}$ phosphorylation in U937 cells compared to unstimulated control U937 cells and it was inhibited by PD98059 in a concentration dependent manner in U937 cells, suggesting the involvement of ERK1/2 MAPK signalling pathway in p21$^{WAF1/Cip1}$*

*expression* (Agadir *et al*., 1999, Das *et al*., 2000, Dufourny*et al*., 1997 and Sato *et al*., 2000). *(c, d) Densitometric results controlled for β-actin for t-p21 and p-p21 respectively.*

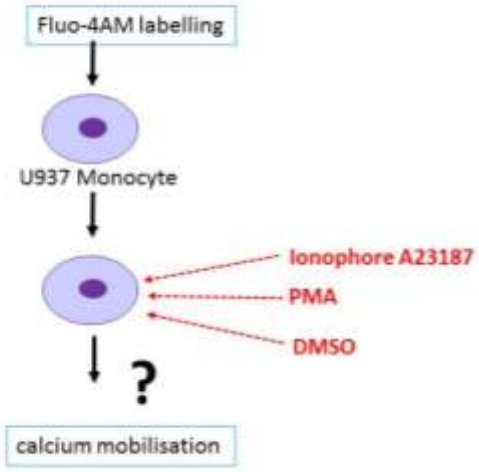


**Appendix Figure 92*. Study design for determination of calcium by flow cytometry.***

*To investigate the impact of Ionophore A23187, PMA and DMSO in intracellular calcium of U937 and THP-1 monocyte cells were labelled with Flou-4AM for 60 minutes at 37°C. The unstimulated Fluo-4M labelled U937/THP-1 cells were stimulated with 1µM A23187 calcium ionophore and 8 nM PMA while acquiring the sample on flow cytometry (BD Accuri C6) using FL1-A FITC channel filters to measure the fluorescence intensity. In addition, Ionophore and PMA were dissolved in DMSO therefore, in this study, DMSO was also assessed for its ability to mobilise intracellular calcium in THP-1 cells. The no-cell control Flou-4AM buffer was acquired for background correction. Calcium determination was also assessed by Fluorescence spectroscopy. In this protocol, U937 cells were labeled with Fluo-4AM dye in 96-well plate. The samples were incubated with $10^{-11}$ M SOS, $10^{-4}$ M SOS, $10^{-11}$ M DOS, $10^{-4}$ M DOS in the absence and presence of with 8 nM PMA for 24 hour. The cells treated with PMA were used as positive control and unstimulated cells were used as negative control. The fluorescence intensity of Flou-4 AM labelled U937 cells was measured for 24 hour (intervals of 15 minutes) using filter having excitation at 485 nm and emission at 518 nm. The kinetics of appearance of the fluorescent cleavage product of the Fluo-4 AM was monitored to determine the intra $Ca^{2+}$. Fluorescence intensity of U937 cells was calculated in relative fluorescent units (RFU) as*

*the maximum response minus the minimum response divided by the minimum response (data not presented). In this study, PMA failed to induce significant intracellular $Ca^{2+}$ mobilisation compared to unstimulated control cells, SOS and DOS stimulated U937 cells. Failure to PMA to mobilise calcium does not reflect an inability to activate PKC since PMA, is able to activate PKC in an analogous manner to DAG. Therefore, intracellular $Ca^{2+}$ was further determined by flow cytomtery method to establish an effective study model.*

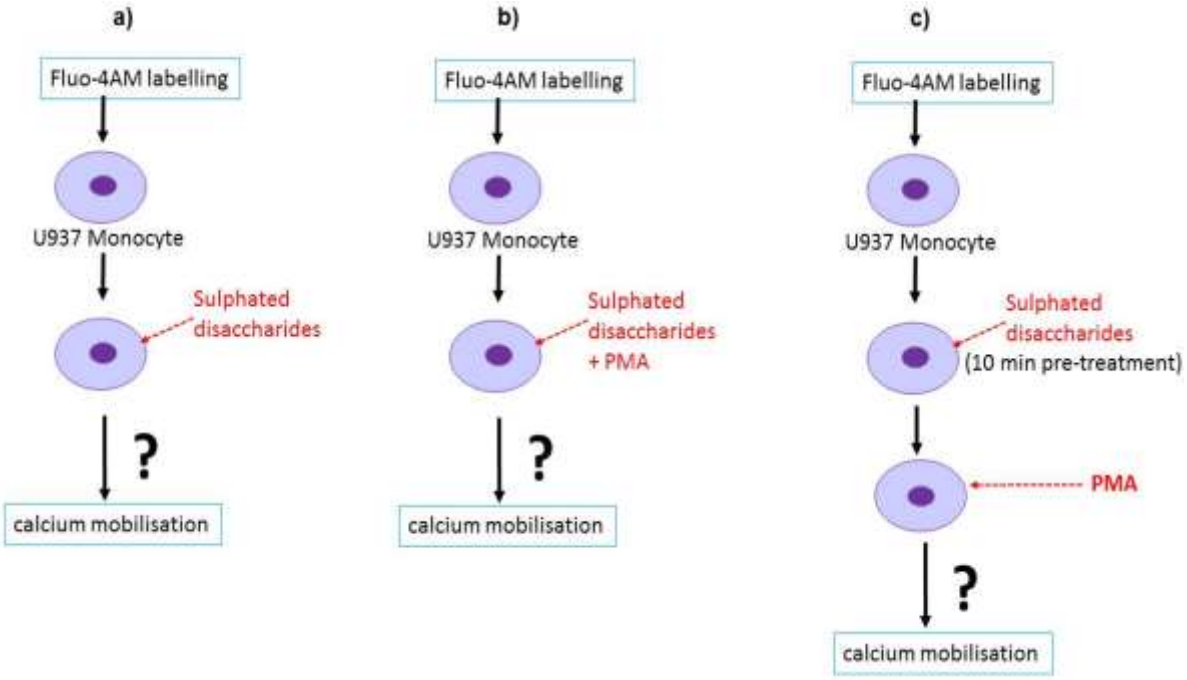


**Appendix Figure 93**. ***Study designs for optimisation.***

*To find the optimal time point for sulphated disaccharides impact on PMA induced intracellular calcium changes in U937/THP-1 monocyte cell lines. In this protocol, THP-1 cells were labelled with Flou-4 AM in Eppendorf tubes. Flou-4 AM labelled THP-1 cell fluorescence intensity was measured using BD Accuri C6 flow cytometry settings appropriate for dye excitation at 494 nm and emission at 516 nm. The unstimulated Fluo-4 M labelled THP-1 cells were stimulated with 1 μM calcium ionophore A23187, 8 nM PMA, $10^{-7}$ M SOS, $10^{-4}$ M SOS, $10^{-7}$ M DOS and $10^{-4}$ M DOS. SOS and DOS were given at 1 min in the absence of PMA, co-administered with PMA and 10 minutes before PMA.*

a)

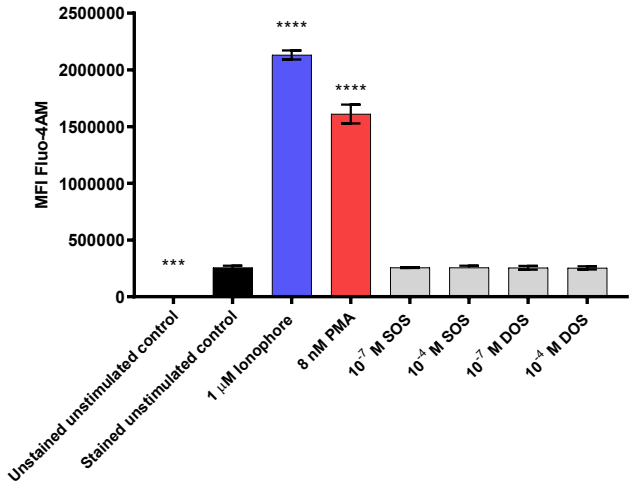


b)

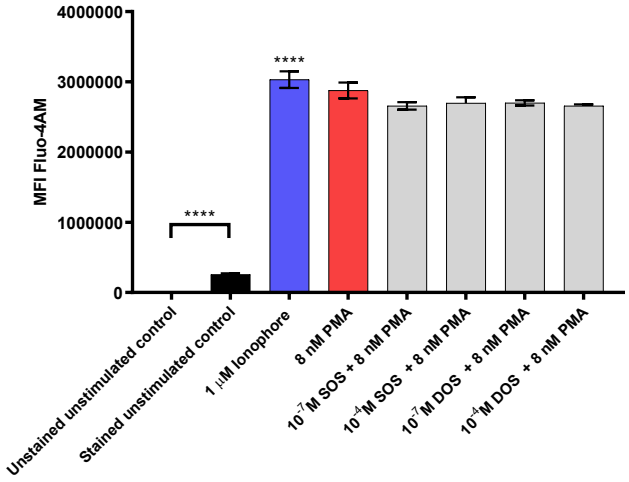


c)

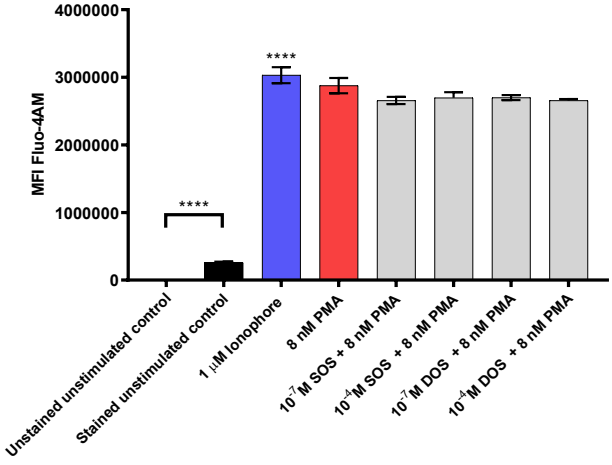


**Appendix Figure 94.** ***SOS and DOS impact on calcium, when given in the absence of PMA (a), at the same time as PMA (b) and when given before PMA (c).***

*The mean fluorescence intensity of Fluo-4AM (Fig. 2.13) was plotted to determine the statistical SOS and DOS effect was compared to PMA. PMA effect was compared to ionophore A23187 and unstimulated THP-1 cells. Mean ± SEM (replicates=3) ANOVA followed by Dunnett's post hoc analysis. ***p<0.001, ****p<0.0001 vs unstained unstimulated control (a), ****p<0.0001 vs PMA (b), ****p<0.0001, ***p<0.001 vs PMA (c). PMA induced intracellular $Ca^{2+}$ mobilisation was compared with calcium ionophore A23187. THP-1 cells treated with PMA induced significant mobilisation of intra-cellular $Ca^{2+}$ when compared to unstimulated cells (p<0.01). THP-1 cells treated with 1 μM A23187 induced a dramatically larger mobilisation of $Ca^{2+}$ into the cytosol. However, SOS and DOS at concentrations $10^{-7}$ M and $10^{-4}$ M had no effect on calcium influx when given alone (Fig.2.11a). PMA induced intracellular calcium mobilisation was significantly inhibited (p<0.05) when SOS and DOS were co-administrated (Fig.2.11b). The PMA-induced calcium influx was also significantly downregulated (p<0.01) when THP-1 cell suspensions were pre-treated with SOS, DOS for 10 minutes at 37 $^{0}$C prior to PMA (Fig.2.11c). At concentration $10^{-7}$ M SOS had no significance difference (p>0.05) compared to $10^{-4}$ M SOS whereas, $10^{-7}$ M DOS had more significant difference (p<0.01) compared to $10^{-4}$ M DOS. There was also no significance difference (p>0.05) between $10^{-7}$ M and $10^{-4}$ M concentrations of SOS and DOS. The results indicate that PMA opens a calcium influx pathway and sulphated disaccharides can inhibits PMA elicited response when given before PMA. The 10 minutes pre-incubation is important for sulphated disaccharides inhibitory action as they were ineffective when given alone or at the same time of PMA. (Also see Fig. 2.12 and Fig.2.13).*

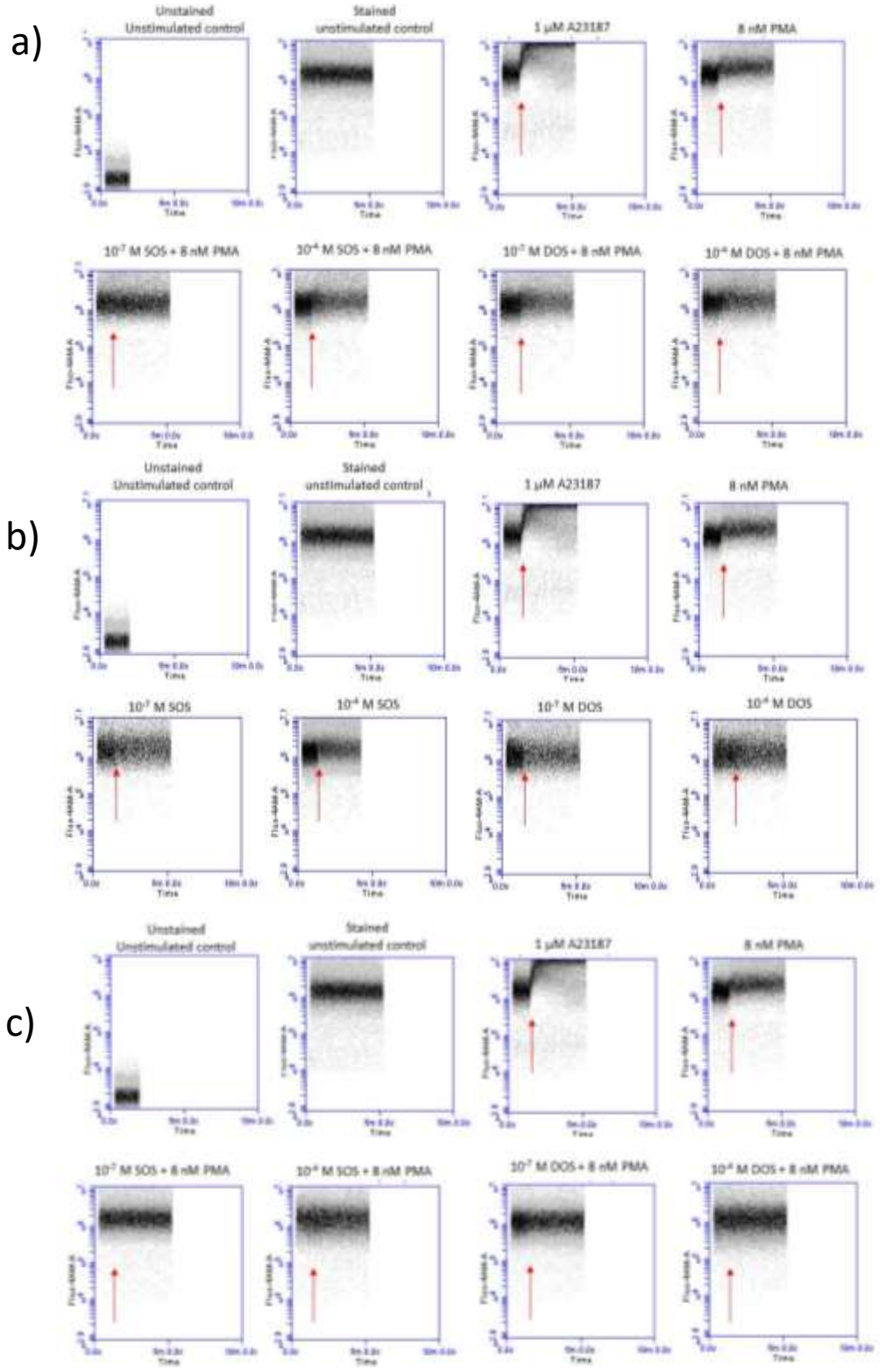


**Appendix Figure 95.** ***Tracings representative of a preliminary experiment study 1-3 data (Fig.2.12).***

*Arrow indicates addition of (1μM A23187, 8 nM PMA) and (SOS, DOS $10^{-7}$ M and $10^{-4}$ M) stimulus in the (a) absence and presence of PMA (co-administration (b) or pre-incubation for 10 min (c)) at 1 minute in Fluo-4AM loaded THP-1 cells (see overlays Fig. 2.13).*

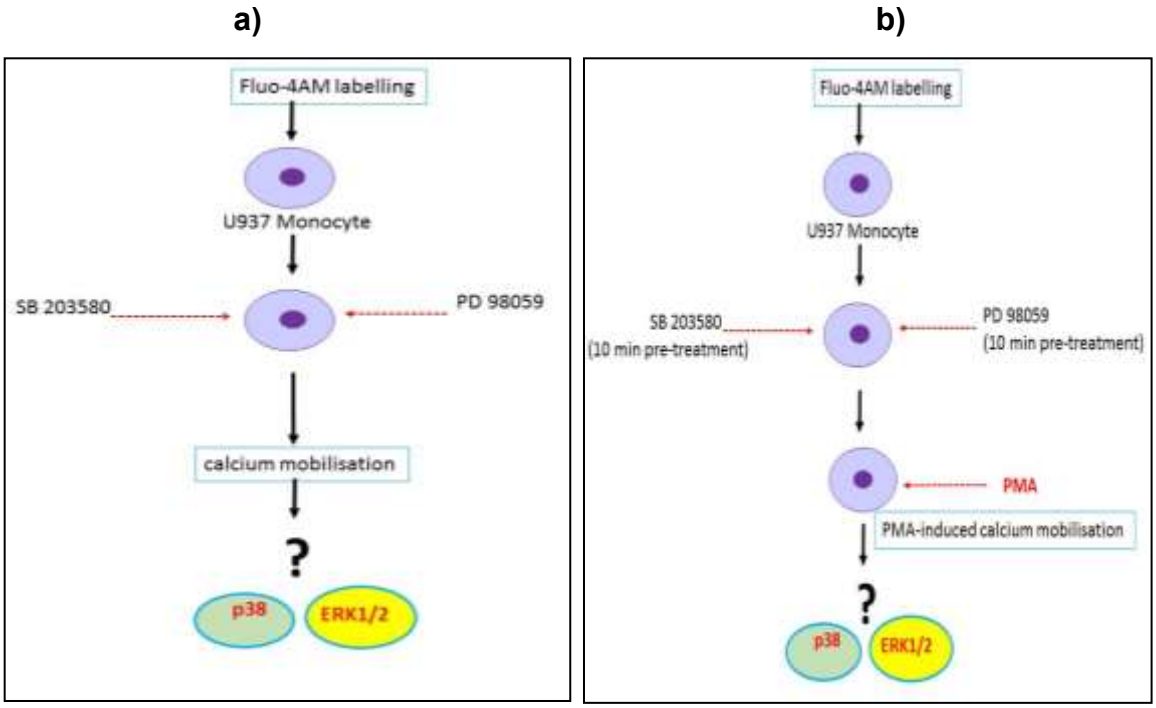


**Appendix Figure 96**. ***Study design to investigate the impact of SB203580 and PD98059 on Intracellular $Ca^{2+}$***.

*In this study, the impact of p38 inhibitor SB203580 and ERK ½ inhibitor PD98059 was studied on PMA-induced intracellular $Ca^{2+}$ mobilisation in the absence and presence of PMA to explore the relationship between $Ca^{2+}$ mobilisation and activation of p38 or ERK ½ pathways. Flou-4 AM labelled U937 cells were stimulated with SB203580 and PD98059 at concentrations of $10^{-6}$ M, $10^{-5}$ M, $10^{-4}$ M in the absence of 8 nM PMA (Fig.2.14a) and pre-incubated with SB203580 and PD98059 at concentrations of $10^{-6}$ M, $10^{-5}$ M, $10^{-4}$ M for 10 minutes at 37°C prior to 8 nM PMA stimulus (Fig.2.14b) at 1 minute and samples were acquired for 5 minutes for calcium response on flow cytometry.*

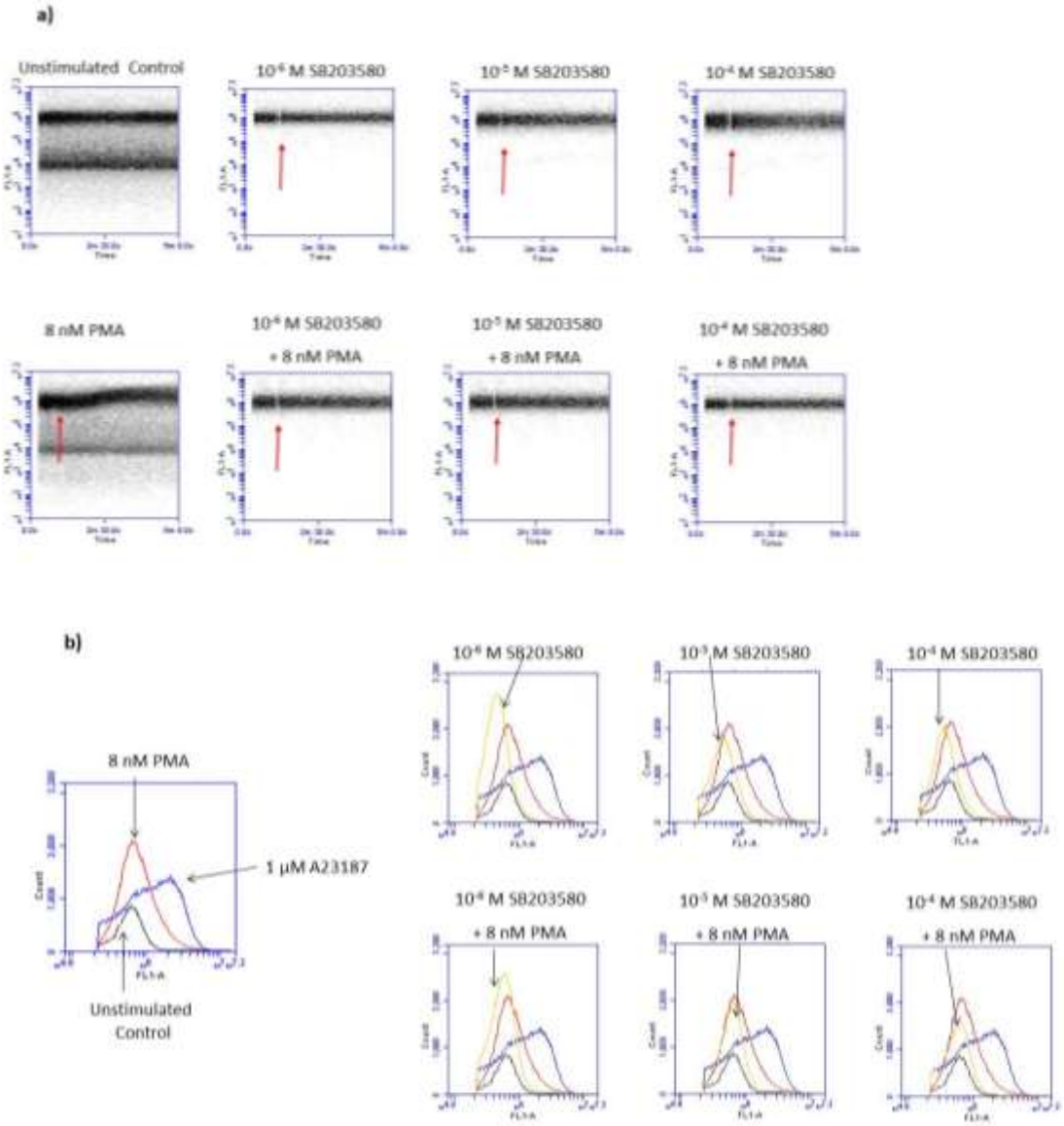


**Appendix Figure 97**. ***SB203580 impact on intracellular $Ca^{2+}$ mobilisation in U937 cells.***

*a) Fluo-4AM loaded U937 cells were treated with SB203580 ($10^{-6}$ M, $10^{-5}$ M and $10^{-4}$ M) in the absence and presence of PMA (pre-treated with SB203580 for 10 min following PMA stimulation at 1 min) and analysed for calcium response for 5 min. The red arrows indicate addition of SB203580 and PMA. b) The panel of histograms of SB203580 in the absence and presence of PMA indicates the changes produced on FL1-fluorescence of Fluo-4AM of U937 cells. The overlays are created by using the BD Accuri C6 analysis*

*tool and are displayed using the plus zoom tool. Arrows indicate SB203580 to show the shift compared to PMA stimulated U937 cells.*

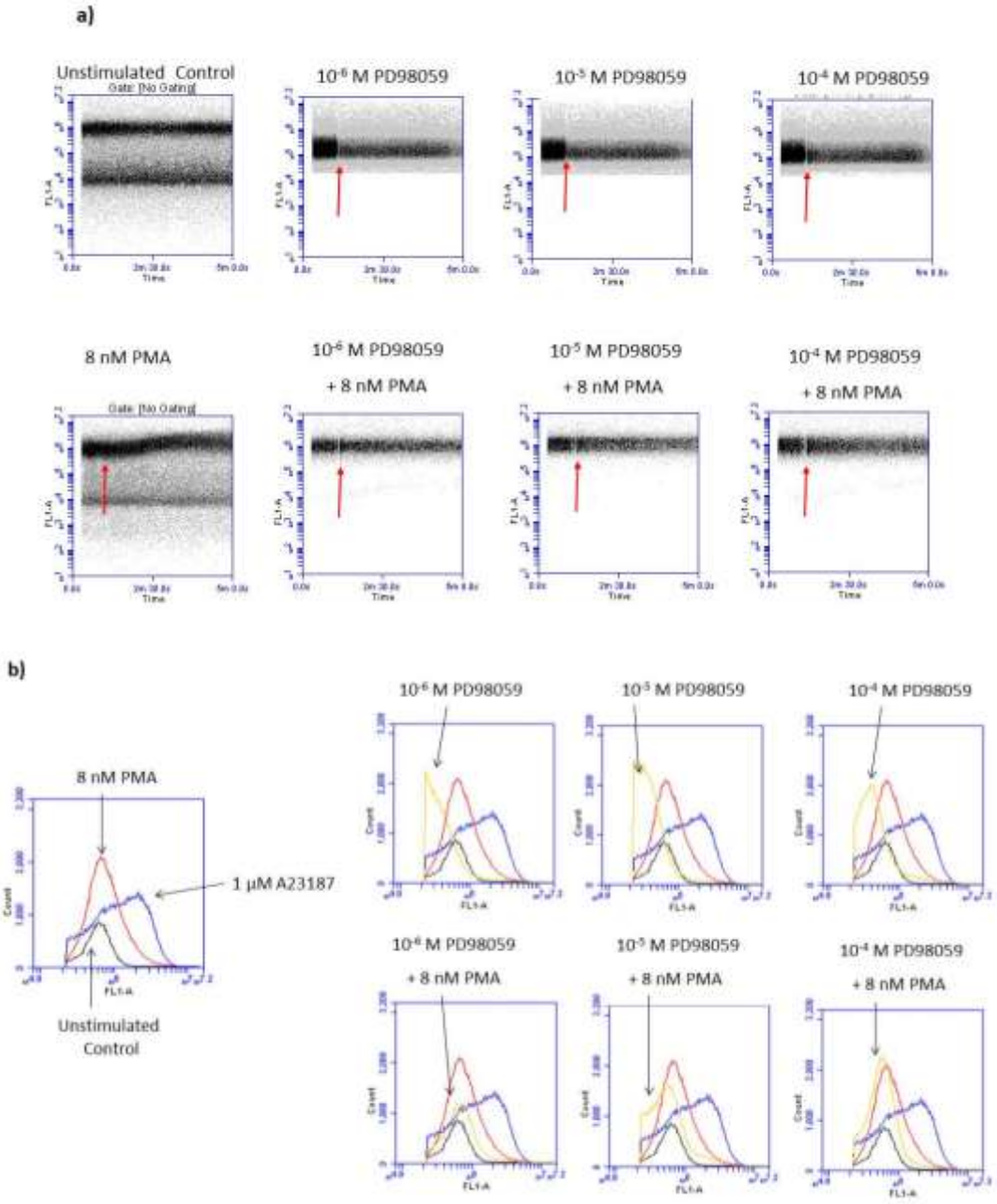


**Appendix Figure 98**. ***PD98059 impact on intracellular $Ca^{2+}$ mobilisation in U937 cells***.

*a) Fluo-4AM loaded U937 cells were treated with PD98059 ($10^{-6}$ M, $10^{-5}$ M and $10^{-4}$ M) in the absence and presence of PMA (pre-treated with PD98059 for 10 min following PMA*

*stimulation at 1 min) and analysed for calcium response for 5 min. The red arrows indicate addition of PD98059 and PMA. b) The panel of histograms of SB203580 in the absence and presence of PMA indicates the changes produced on FL1-channel. Arrows indicate PD98059 to show the shift compared to PMA stimulated U937 cells.*

a)

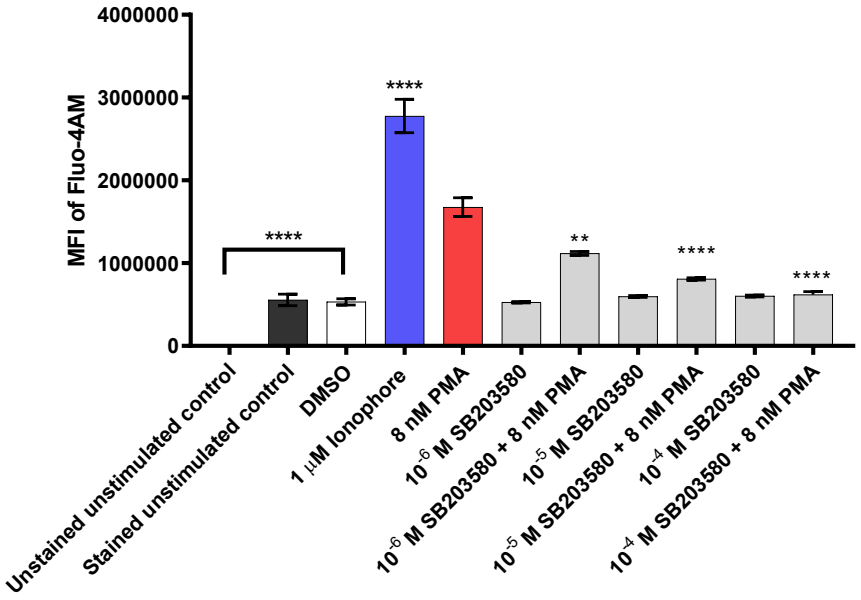


b)

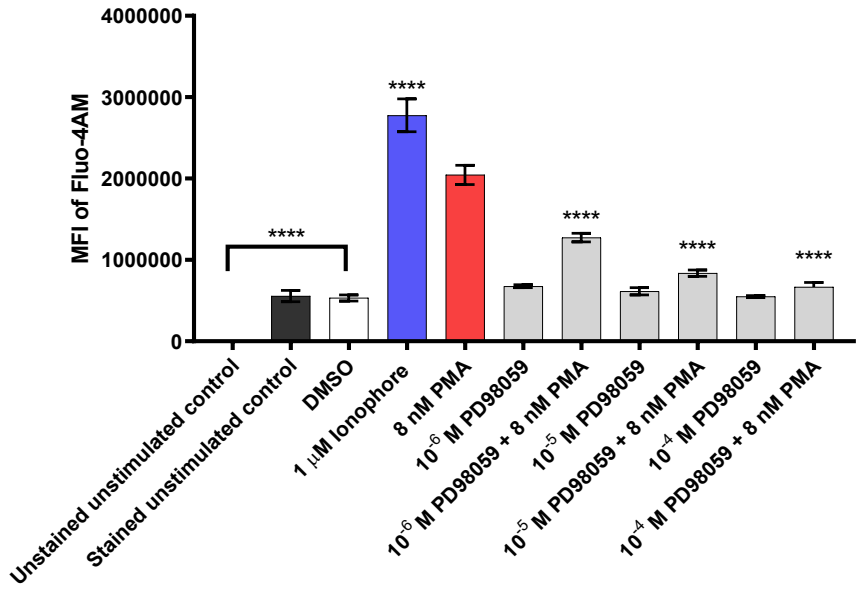


**Appendix Figure 99**. ***SB203580 and PD98059 inhibited intracellular $Ca^{2+}$ mobilisation in U937 cells.***

*The Mean fluorescence intensity (MFI) of Fluo-4 AM of U937 cells (Fig.2.14 and Fig.2.15) in the presence of (a) SB203580 or (b) PD98059 ($10^{-6}$ M, $10^{-5}$ M and $10^{-4}$ M) and presence of (a) SB203580 + PMA or (b) PD98059 + PMA was measured using FL1-fluorescence channel of BD Accuri flow cytometry. The MFI is represented as mean ± SEM, *p<0.01, ****p<0.0001 vs PMA. Dunnett's test (n=3). It was observed that in U937 cells, there was no effect of SB203580 and PD98059 on intracellular calcium ion mobilisation in the absence of PMA compared to unstimulated control U937 cells for 5 minute. In contrast, the 10 minute pre-treatment of SB203580 and PD98059 prior to addition of 8 nM PMA, significantly inhibited PMA-induced $Ca^{2+}$ mobilisation for 5 minutes in a concentration dependent manner.*

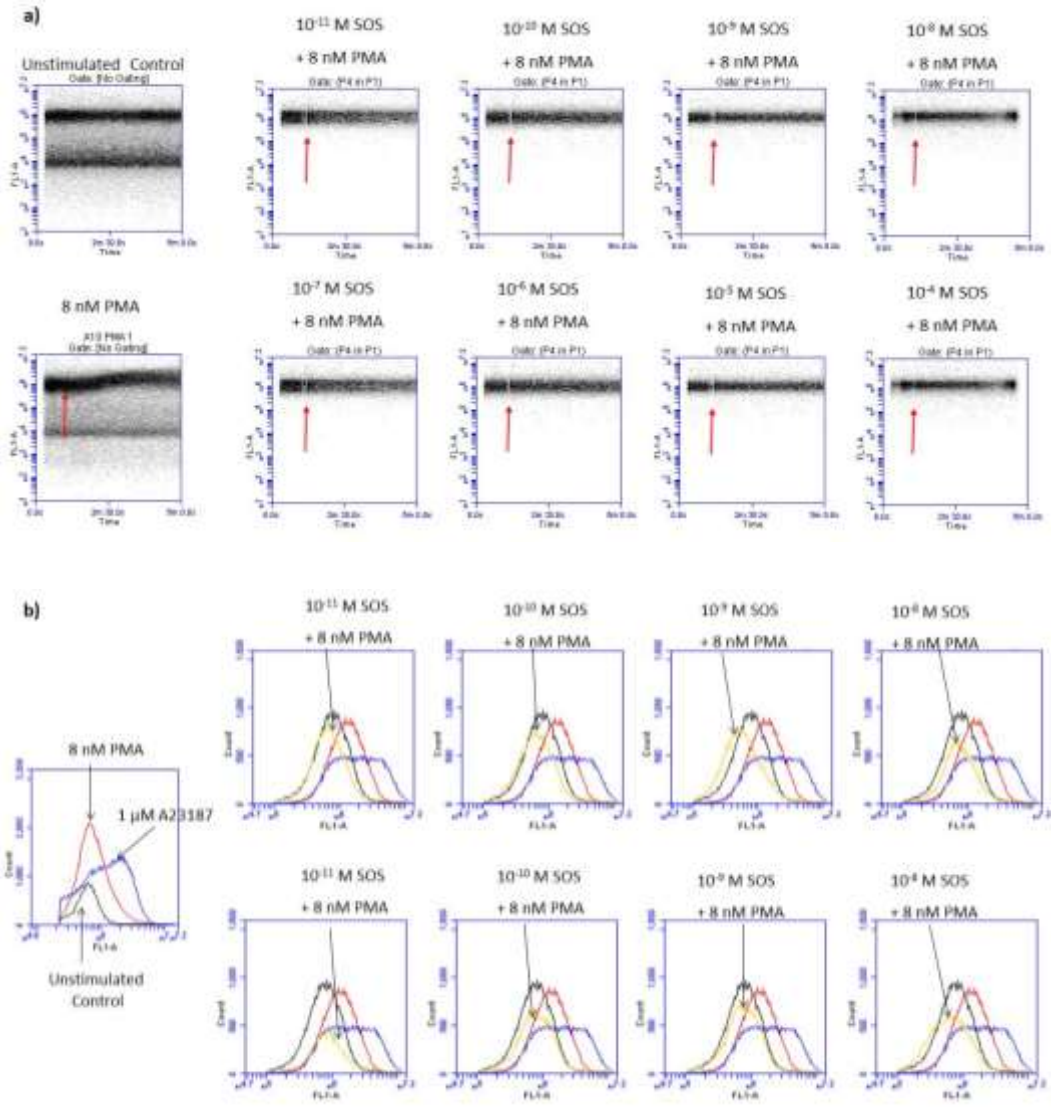


**Appendix Figure 100.** ***Impact of SOS on PMA-induced intracellular $Ca^{2+}$ mobilisation.***

*a) Representative (of three independent experiments) cytograms of fluorescence of Fluo-4AM (585/40) indicates the fluorescence of the ungated population. Addition of PMA (8nM) is indicated by red arrow, SOS compound was given 10 minutes prior to PMA (8 nM) addition at different concentrations ($10^{-11}$ to $10^{-4}$ M). b) Histograms indicates the changes produced on fluorescence of Fluo-4AM of cells by gating cells after the addition of PMA at 1minute (Region 6), where SOS (yellow line) showed shift to left compared to unstimulated cells (black line), PMA (red line) and inophore A23187 (blue line). SOS significantly inhibited PMA -induced calcium intracellular mobilisation in U937 cells.*

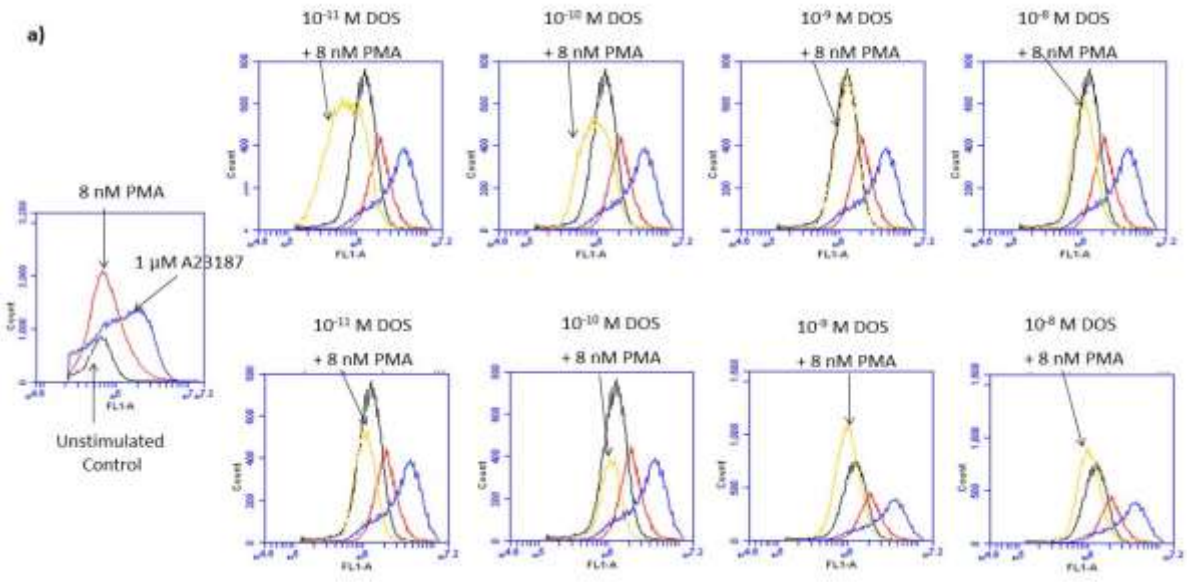


**Appendix Figure 101*. Impact of DOS on PMA-induced intracellular $Ca^{2+}$ mobilisation.***

*Panel of histograms indicates the changes produced on fluorescence (mean fluorescent intensity of Fluo-4AM) of cells by gating cells after the addition of PMA at 1minute (Region 6), where DOS (yellow line) showed shift to left compared to unstimulated cells (black line), PMA (red line) and inophore A23187 (blue line). DOS significantly inhibited PMA -induced calcium intracellular mobilisation in U937 cells. Overlay can be accurately displayed by using the Cflow Plus zoom tool. Panel C. MFI of Fluo-4AM labelled U937 cells on FL1-A FITC channel.*

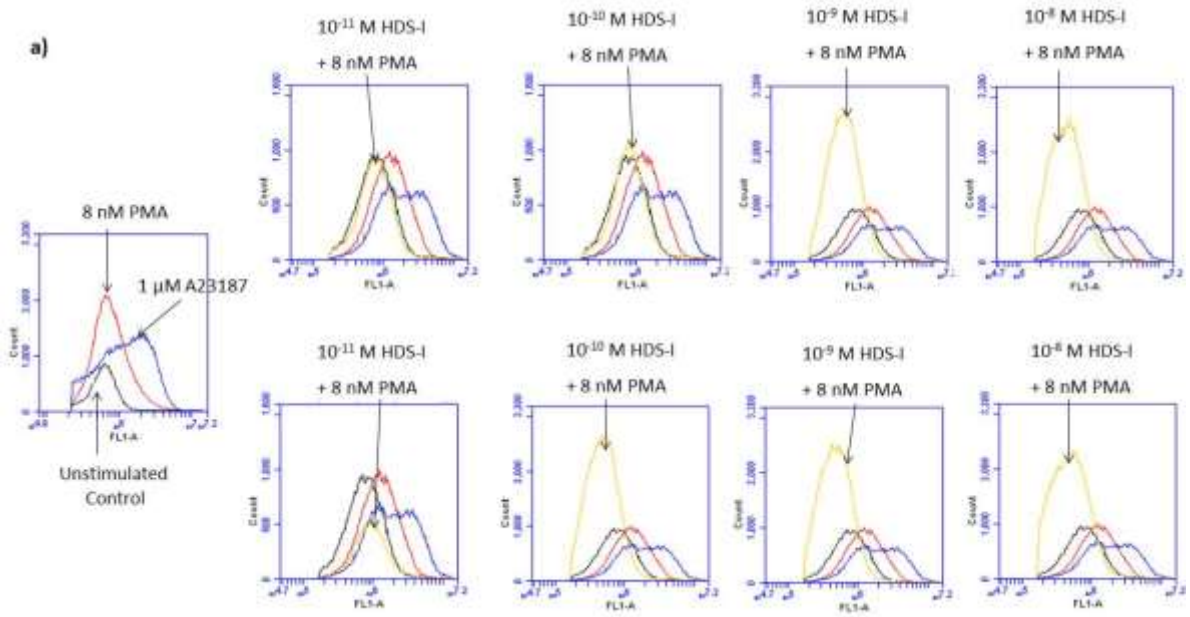


**Appendix Figure 102**. ***Impact of HDS-I on PMA-induced intracellular $Ca^{2+}$ mobilisation.***

*Panel of histograms indicates the changes produced on fluorescence (mean fluorescent intensity of Fluo-4AM) of cells by gating cells after the addition of PMA at 1minute (Region 6), where HDS-I (yellow line) showed shift to left compared to unstimulated cells (black line), PMA (red line) and inophore A23187 (blue line). HDS-I significantly inhibited PMA - induced calcium intracellular mobilisation in U937 cells. Overlay can be accurately displayed by using the Cflow Plus zoom tool. Panel C. MFI of Fluo-4AM labelled U937 cells on FL1-A FITC channel.*

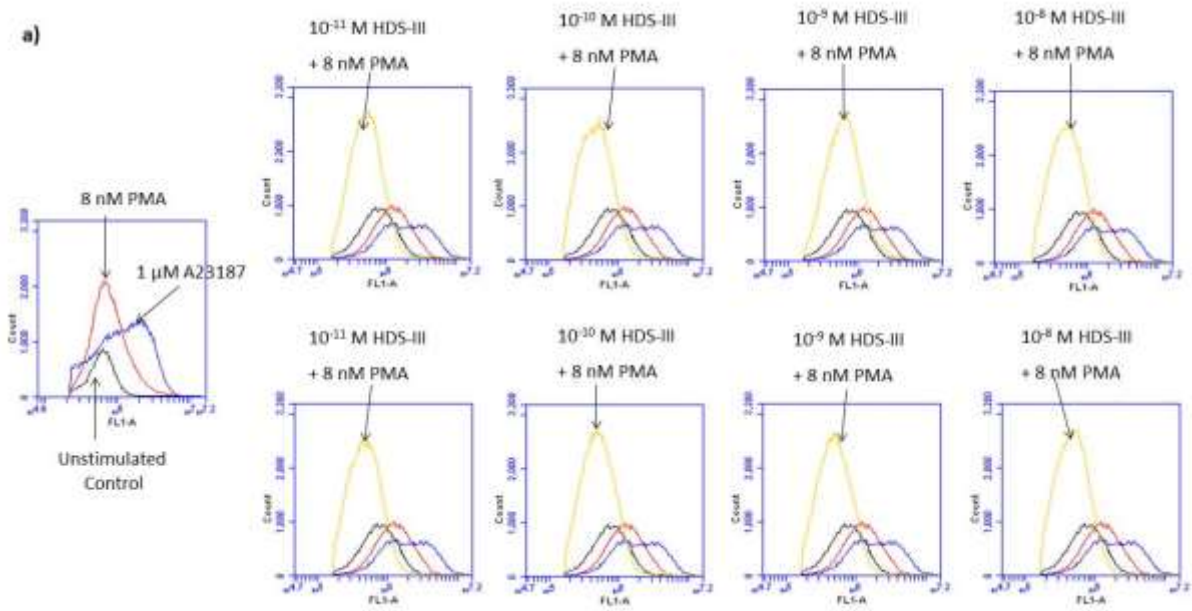


**Appendix Figure 103.** ***Impact of HDS-III on PMA-induced intracellular $Ca^{2+}$ mobilisation.***

*Panel of histograms indicates the changes produced on fluorescence (mean fluorescent intensity of Fluo-4AM) of cells by gating cells after the addition of PMA at 1minute (Region 6), where HDS-III (yellow line) showed shift to left compared to unstimulated cells (black line), PMA (red line) and inophore A23187 (blue line). HDS-III significantly inhibited PMA -induced calcium intracellular mobilisation in U937 cells. Overlay can be accurately displayed by using the Cflow Plus zoom tool. Panel C. MFI of Fluo-4AM labelled U937 cells on FL1-A FITC channel.*

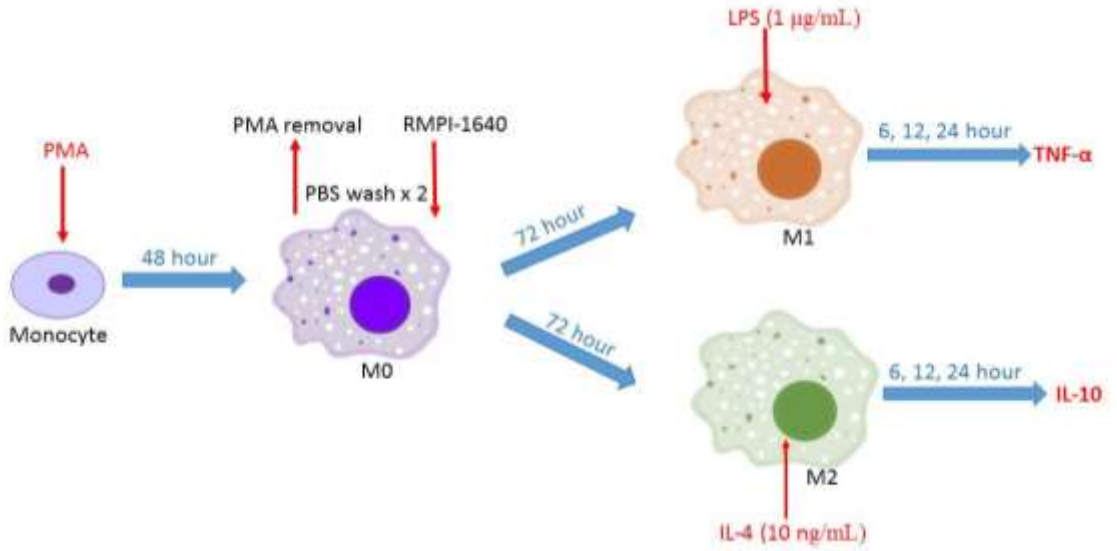


**Appendix Figure 104**. ***In vitro study design for the determination of TNF-α and IL10 by PMA differentiated U937 cells stimulated with LPS or IL-4.***

*To establish an in vitro macrophage polarization model, U937 cells at a density of 2x10$^5$ cells/ml per well were grown as confluent monolayer overnight on a 24-well tissue culture plate. Cells were treated with or without 8 nM PMA for 48 h at 37 $^0$C with 5% $CO_2$. After 48 h PMA stimulus, the PMA-containing medium was removed, cells were washed twice with cold PBS and rested in fresh PMA-free RPMI-1640 media for further 72 h. PMA differentiated U937 cells were stimulated with 1 µg/mL LPS and 10 ng/mL IL-4 for 6 h, 12 h and 24. Subsequently, cell culture supernatants were collected and to analyse TNF-α and IL-10 production by using ELISA. In this study, PMA-induced M0 macrophages were considered as a control to compare PMA + LPS and PMA + IL-4 macrophages cytokine production.*

**a)**

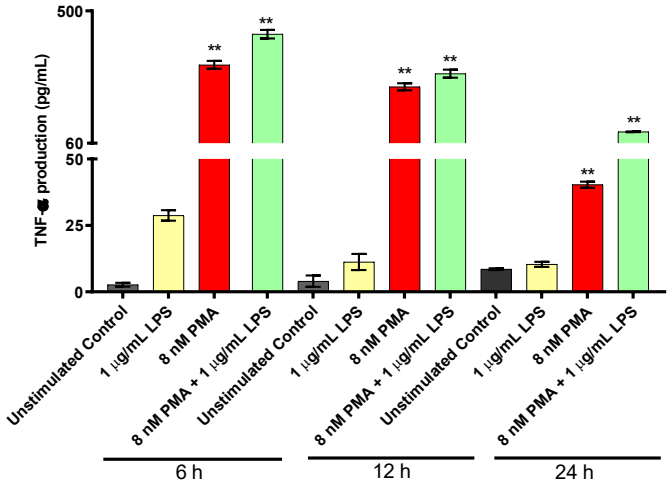


**b)**

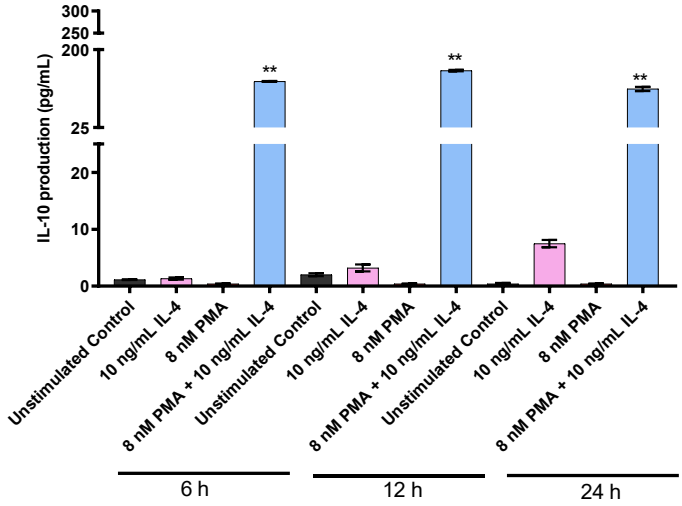


**Appendix Figure 105**. ***LPS and IL-4 stimulates PMA-differentiated cell TNF-α and IL-10 synthesis.***

*LPS and IL-4 induced (a) TNF-α synthesis and (b) IL-10 from differentiated and undifferentiated U937 cells (lower panel). Differentiation to macrophages was induced by incubation of the cells with 8 nM PMA for 48 h following a 72 h maturation period. LPS (1 μg/ml) and IL-4 (10 ng/ml) were added to the culture medium and harvested for TNF-α synthesis and IL-10 analysis by ELISA after 6 h, 12, 24h of incubation. Upon exposure to*

*PMA, U937 or THP-1 differentiated cells exhibited M0 and M1 phenotype, PMA + LPS treatment stimulated cells exhibited M1 phenotype and PMA + IL-4 treatment stimulated cells exhibited M2 phenotype. PMA and PMA + LPS-treated cells exhibited highest M1 cytokine TNF-α production compared to unstimulated control U937 cells at 6 h, 24 h and 24 h. However, TNF-α production by PMA and PMA + LPS was decreased in a time dependent manner. The TNF-α production was higher at 6h compared to 12 h and 24 h (Fig.2.04a). Similarly, PMA + IL-4-treated cells showed highest M2 cytokine IL-10 production compared to unstimulated control U937 cells at 6 h, 12 h and 24 h. There was slight increase in IL-10 production at 12 h compared to 6 h but IL-10 production was decreased at 24 h compared to 12 h (Fig.2.04b). Therefore, 6 h treatment was optimal for TNF-α and IL-10 production in vitro. Results are presented as Dunnett's Test mean± standard errors (n = 3), **=p<0.01 vs. unstimulated control.*

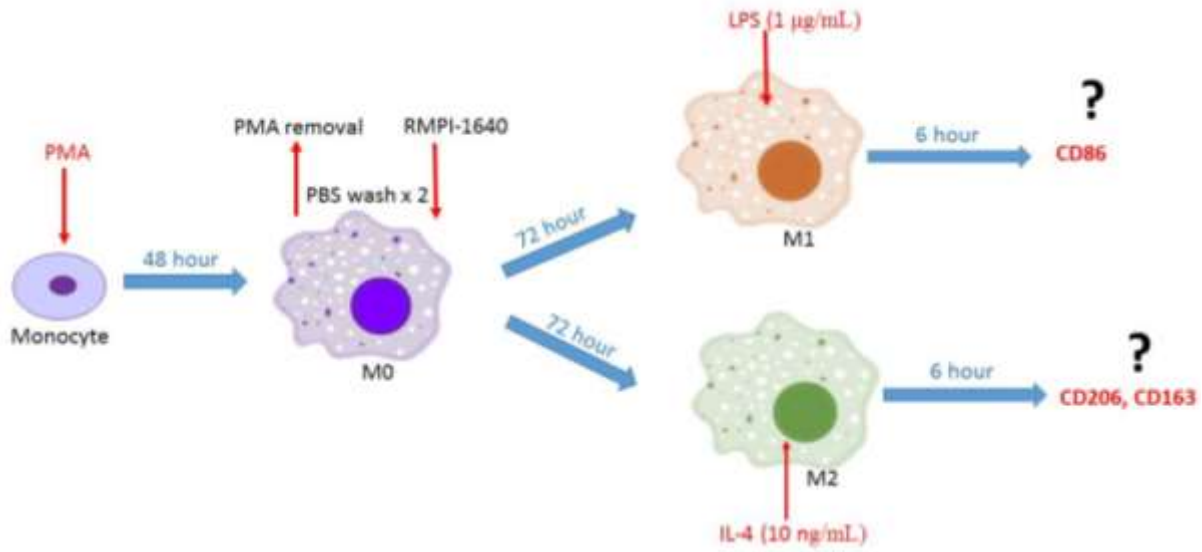


**Appendix Figure 106**. ***In vitro study design 3 to study the impact of PMA on differentiated macrophages markers: CD86 (M1), CD206 and CD163 (M2) expression. LPS or IL-4 was used as controls to test the model.***

*To study the cell surface CD phenotypes of PMA-induced M1 and M2 macrophages, THP-1 cells (2x10$^5$ cells/mL per well) were cultured in 24-well tissue culture plates in the absence or presence of PMA. Duplicate sets of triplicates for negative (unstimulated) and positive (PMA-stimulated alone) controls were prepared. Following the incubation period, PMA-containing media was removed, cells were washed twice with PBS and left in fresh PMA-free RPMI-1640 supplemented media for further 72 h. The cells were treated with 1 µg/mL LPS or 10 ng/mL IL-4 for 6 h in set of triplicates of negative and positive control wells. The cells were harvested, subsequently washed twice with 1X PBS and stained with CD86, CD206 and CD163 surface markers and analysed using flow cytometry. The unstimulated control U937 cells were used as a negative control and 8 nM PMA-stimulated U937 cells were used as a positive control. In addition, 8 nM PMA + 1 µg/mL LPS stimulated U937 cells and 8 nM PMA + 10 ng/mL IL-4 stimulated cells were used to compare PMA induced M1 and M2 profiles.*

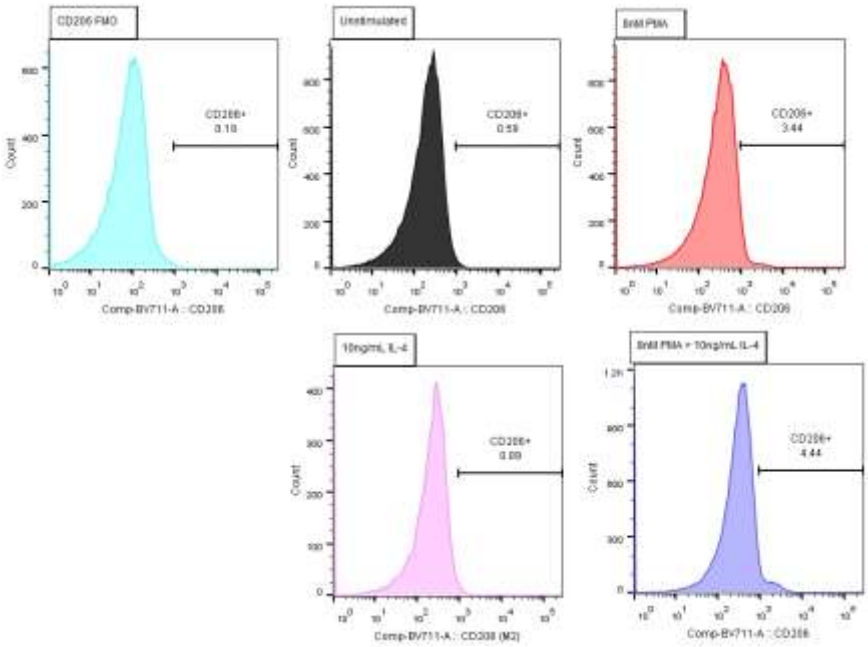


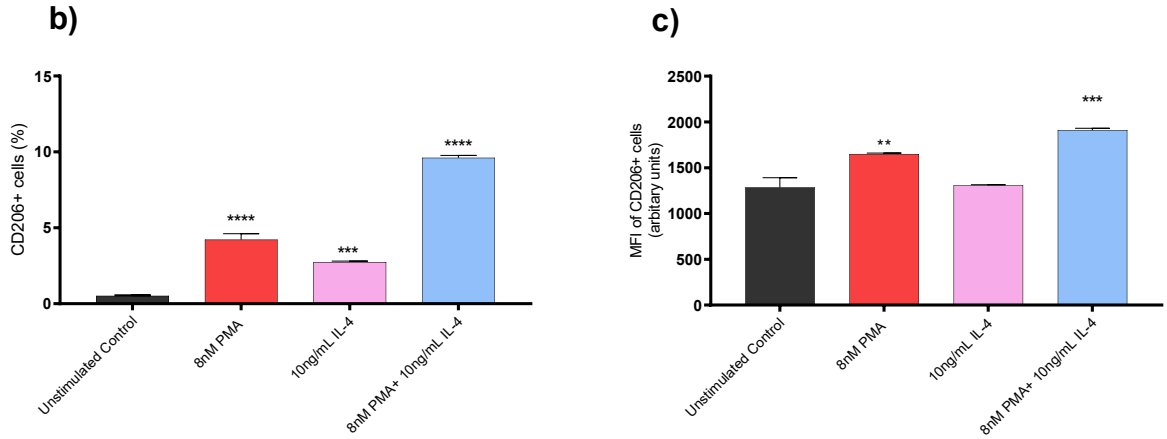


**Appendix Figure 107*. PMA impact on CD206 expression.***

*CD206 expression (% cells, and MFI) by THP-1 cells, as assessed by FACS (see methods in section 2.3.3). Cells were treated with either IL-4 (10ng/mL), PMA (8 nM) for 48 hours, or PMA + IL-4. ****=p<0.0001 vs. untreated control, Dunnett's test.*

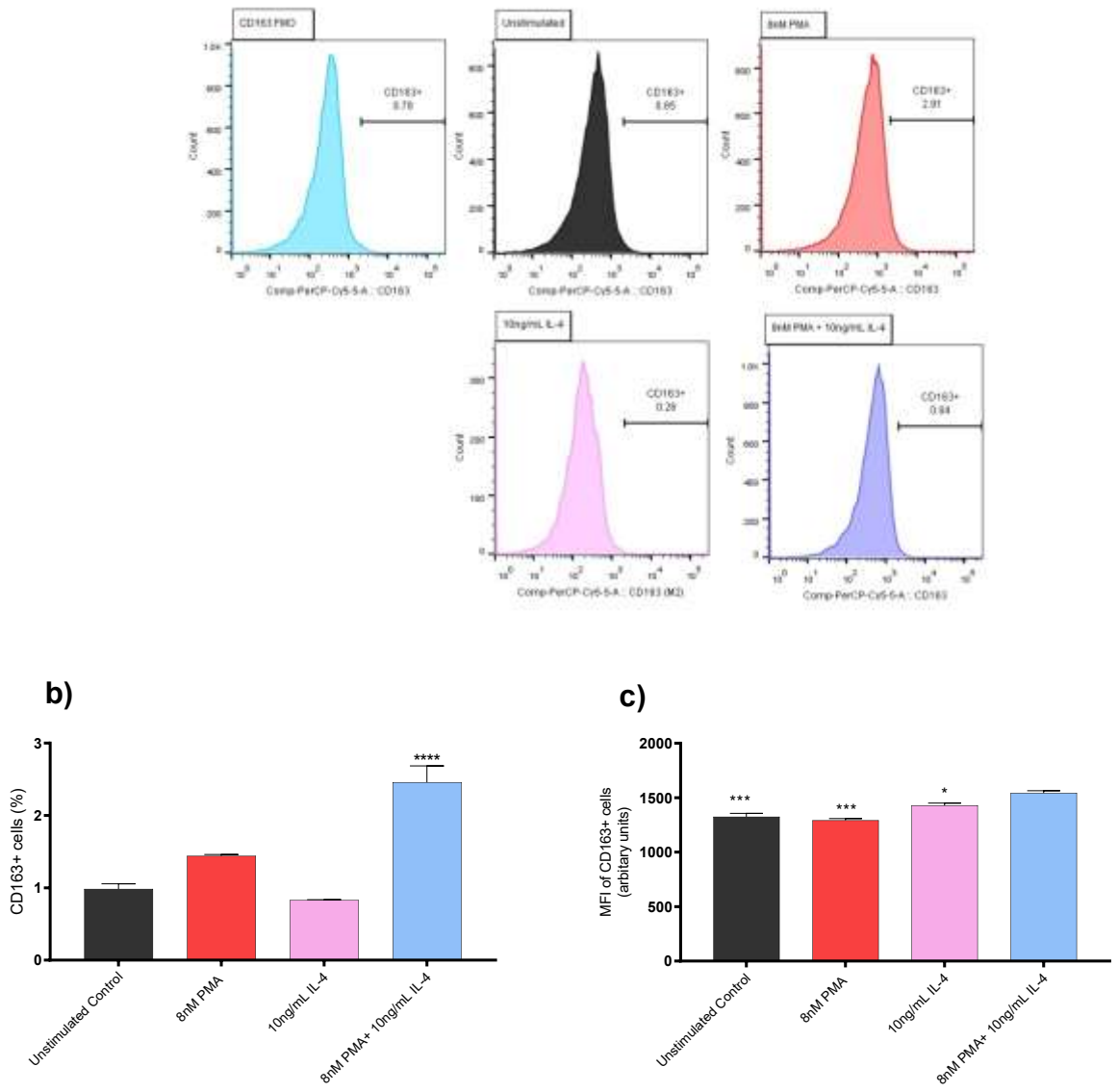


**Appendix Figure 108*. PMA impact on CD163 expression.***

*CD163 expression (% cells, and MFI) by THP-1 cells, as assessed by FACS (see methods). Cells were treated with either IL-4 (10ng/mL), PMA (8 nM) for 48 hours, or PMA + IL-4. *=p<0.05, ***=p<0.001, ****=p<0.0001 vs. untreated control, Dunnett's test.*

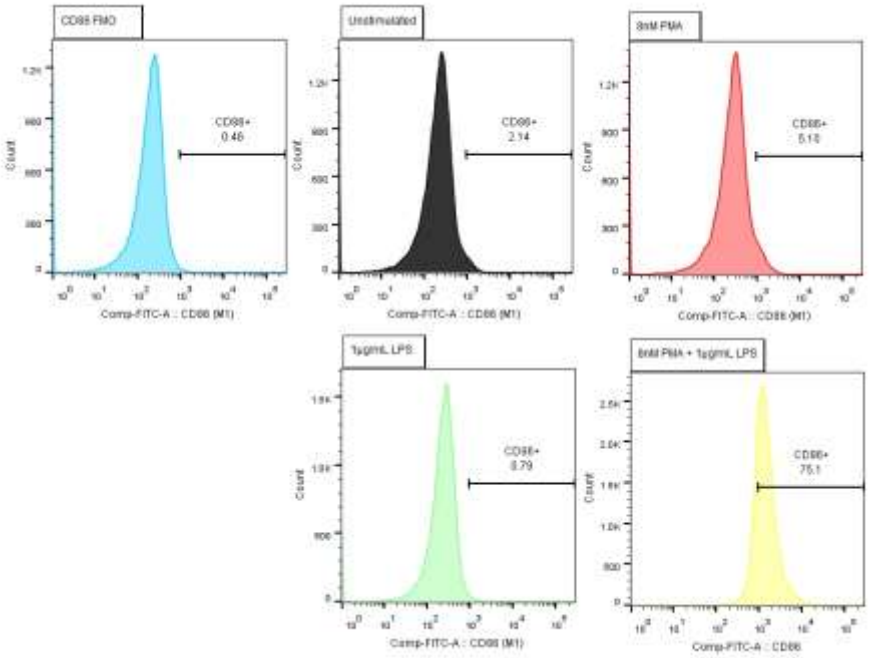


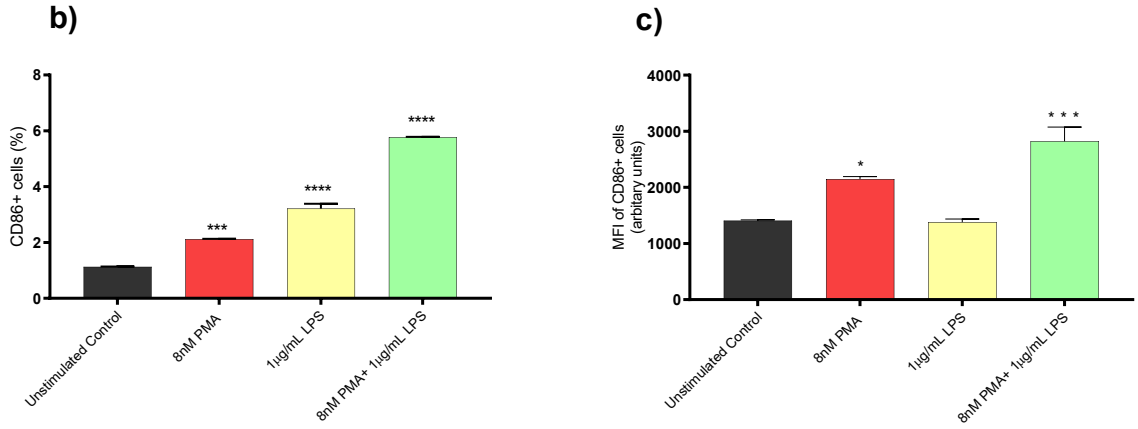


**Appendix Figure 109.** ***PMA impact on CD86 expression.***

*CD86 expression (% cells, and MFI) by THP-1 cells, as assessed by FACS (see methods). Cells were treated with either IL-4 (10ng/mL), PMA (8 nM) for 48 hours, or PMA + IL-4. *=p<0.05, **=p<0.01, ****=p<0.0001 vs. untreated control, Dunnett's test. As shown in Fig.108 - 109, It was observed that PMA-differentiated THP-1 M0 cells were more CD206⁺ (3.44%), CD163⁺ (2.91%) compared to unstimulated control monocyte cells (0.59 % CD206⁺, 0.85 % CD163⁺), IL-4-stimulated monocyte cells (0.89 % CD206⁺, 0.26% CD163⁺) and less positive compared to 8 nM PMA + 10 ng/mL IL-4-stimulated M2*

*cells (4.44% CD206$^{+}$, 0.84% CD163$^{+}$). PMA-differentiated THP-1 M0 cells were more CD86$^{+}$ (5.10%) compared to unstimulated control monocyte cells (2.14% CD86$^{+}$) and LPS-stimulated monocyte cells (0.79% CD86$^{+}$). However, PMA-stimulated U937 M0 cells were less CD86$^{+}$ compared to 8 nM PMA + 1 µg/mL LPS-stimulated M1 cells (75.1% CD86$^{+}$). The percentage of CD206$^{+}$, CD163$^{+}$ and CD86$^{+}$ cells was very low in THP-1 cells. Therefore, U937 cells were employed to determine sulphated disaccharides impact on CD206, CD163 and CD86.*

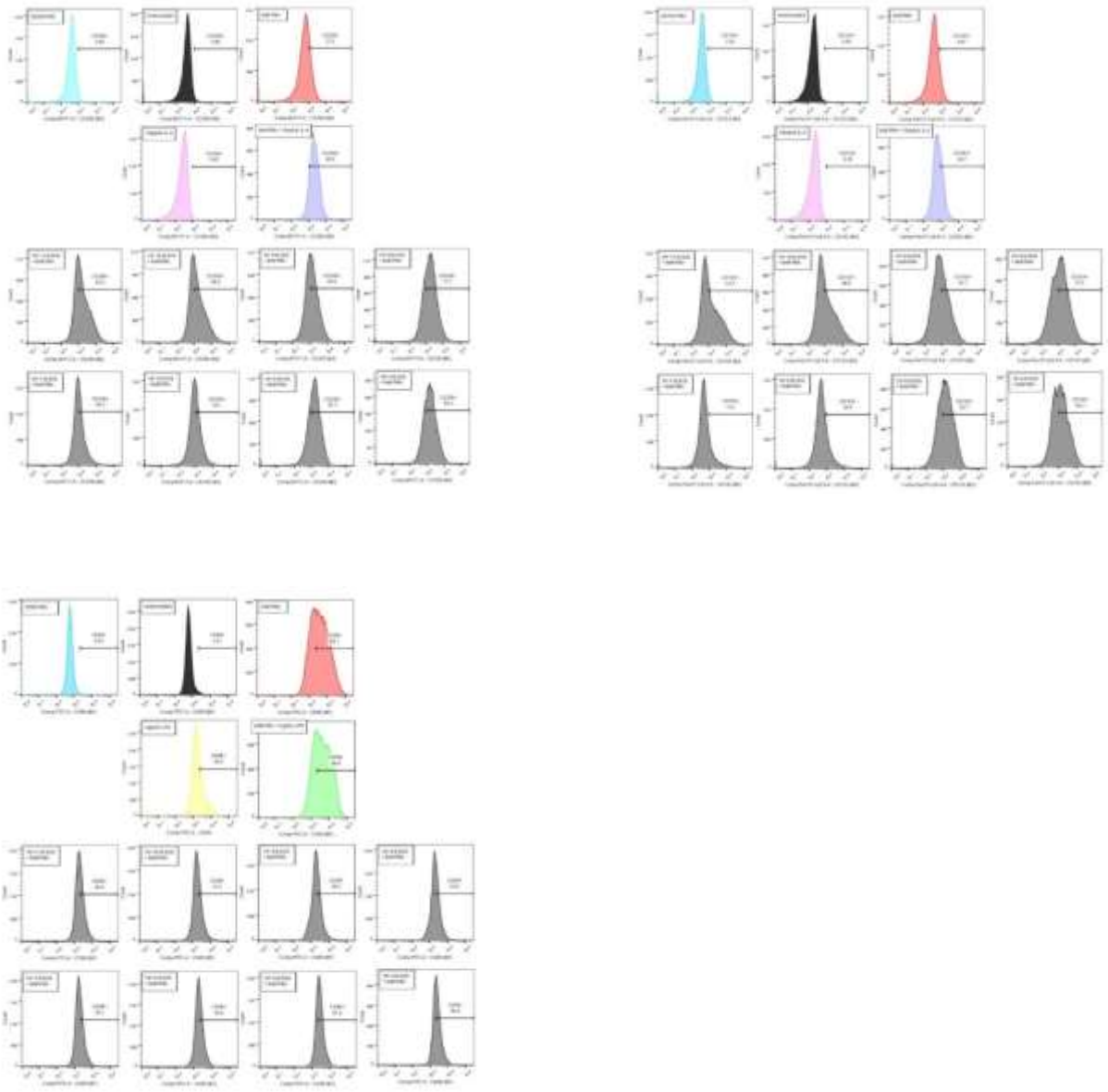

**Appendix Figure 110.** ***SOS impact on CD206, CD163 and CD86 expression in PMA-induced U937 cells.***

*Histograms represent the overlays of CD206, CD163 and CD86 comparison of SOS different concentration. Cells were treated with either IL-4 (10ng/mL), PMA (8 nM) for 48 hours, or SOS ($10^{-11}$ – $10^{-4}$M) PMA + IL-4.*

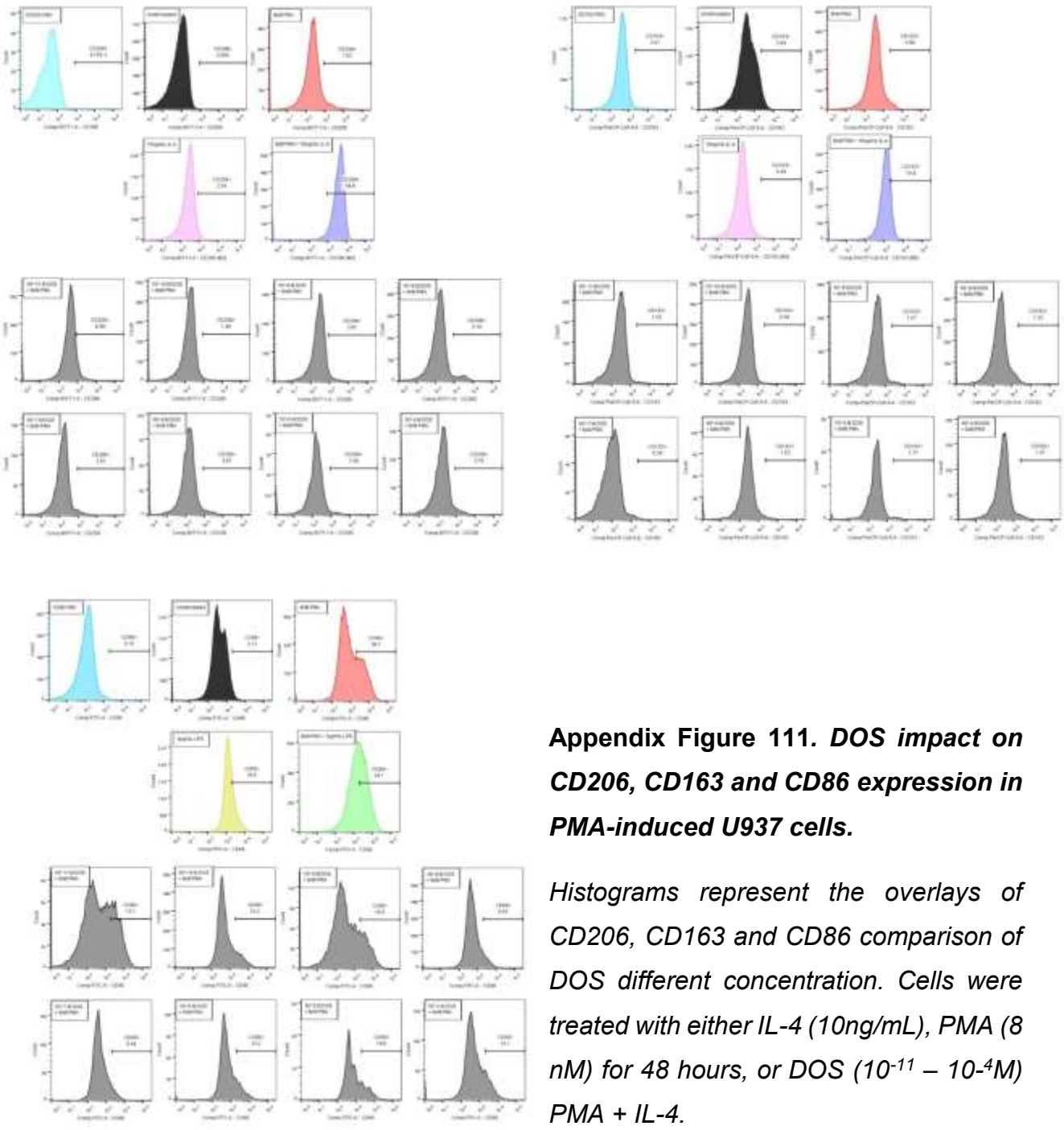

**Appendix Figure 111.** ***DOS impact on CD206, CD163 and CD86 expression in PMA-induced U937 cells.***

*Histograms represent the overlays of CD206, CD163 and CD86 comparison of DOS different concentration. Cells were treated with either IL-4 (10ng/mL), PMA (8 nM) for 48 hours, or DOS ($10^{-11}$ – $10^{-4}$M) PMA + IL-4.*

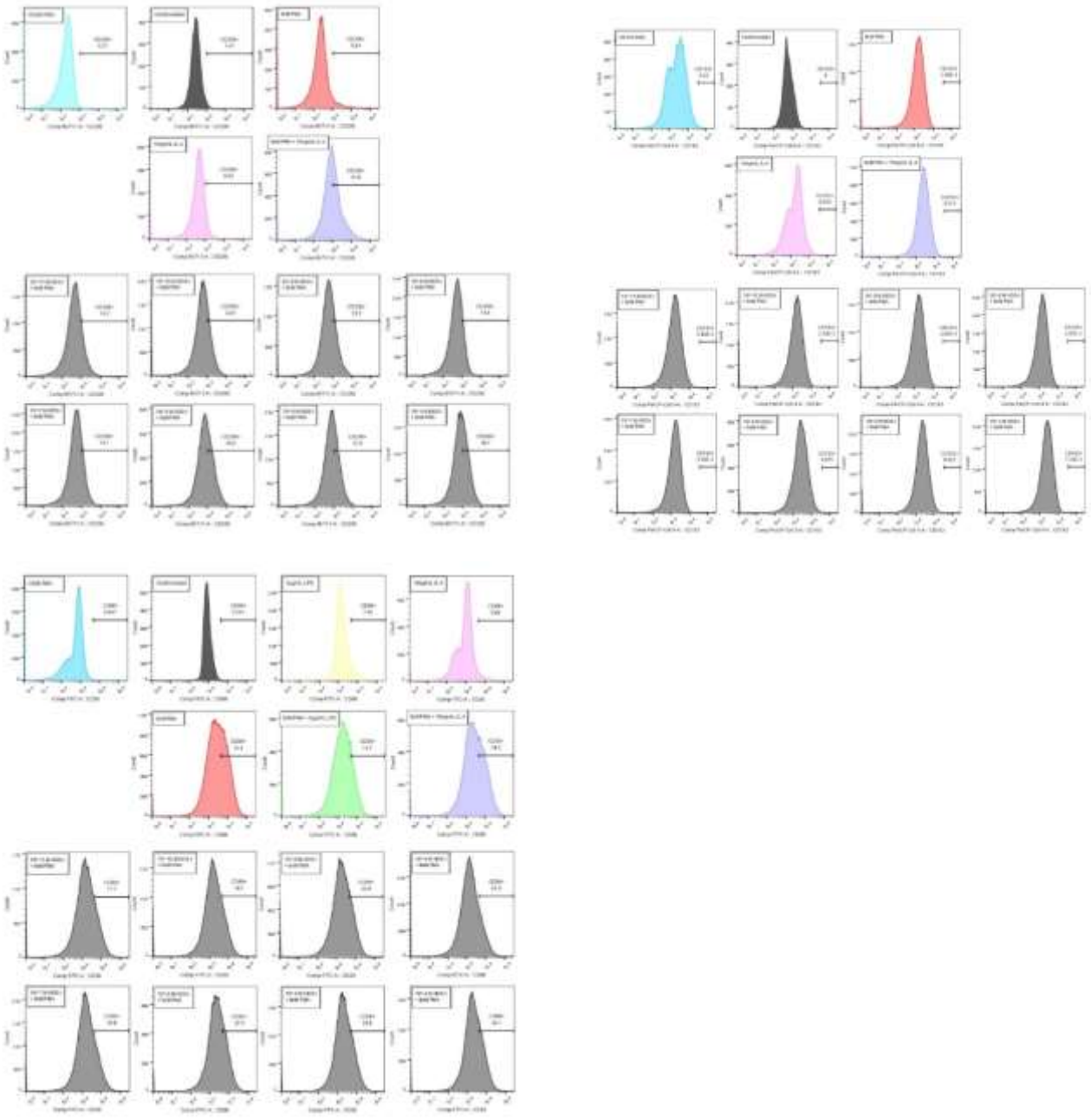

**Appendix Figure 112*. HDS-I impact on CD206, CD163 and CD86 expression in PMA-induced U937 cells.***

*Histograms represent the overlays of CD206, CD163 and CD86 comparison of HDS-I different concentration. Cells were treated with either IL-4 (10ng/mL), PMA (8 nM) for 48 hours, or HDS-I ($10^{-11}$ – $10^{-4}$M) PMA + IL-4.*

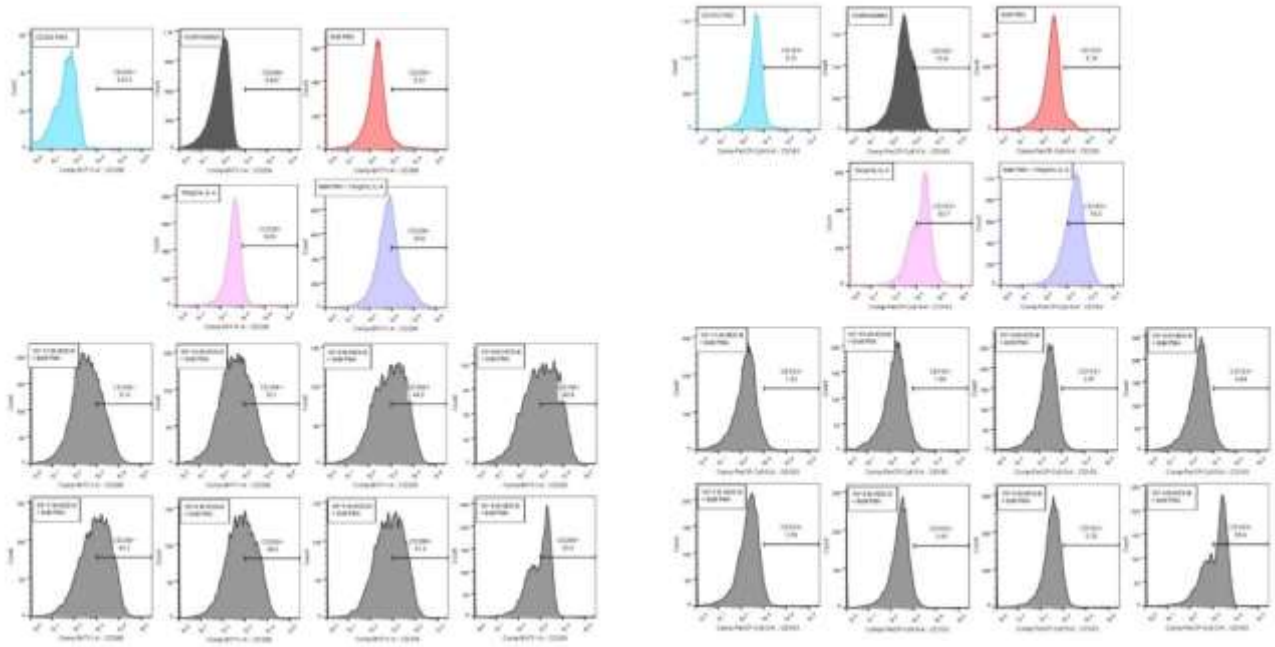

**Appendix Figure 113.** ***HDS-III impact on CD206, CD163 and CD86 expression in PMA-induced U937 cells.***

*Histograms represent the overlays of CD206, CD163 and CD86 comparison of HDS-III different concentration. Cells were treated with either IL-4 (10ng/mL), PMA (8 nM) for 48 hours, or HDS-III ($10^{-11}$ – $10^{-4}$M) PMA + IL-4.*